frontiers | Research Topics

Advances in mast cell physiology and mast cell-driven diseases

Edited by
Carlo Pucillo and Ulrich Blank

Published in
Frontiers in Immunology

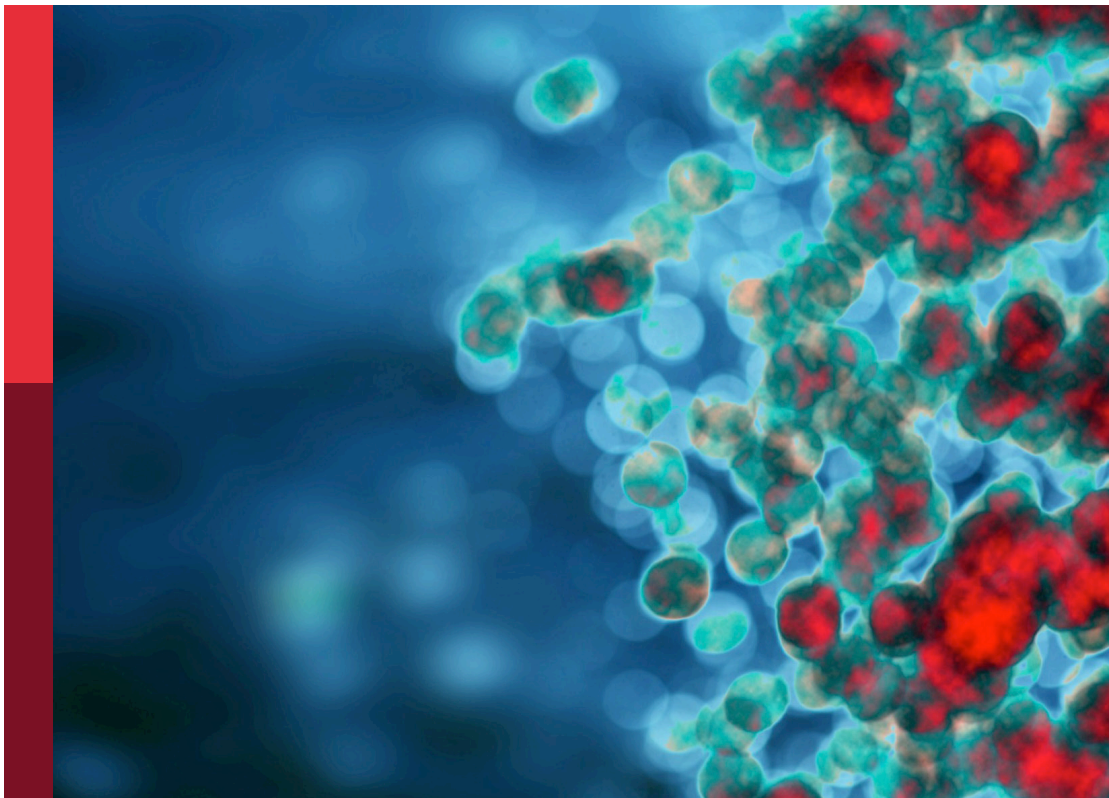

ISSN 1664-8714
ISBN 978-2-8325-3854-8
DOI 10.3389/978-2-8325-3854-8

About Frontiers

Frontiers is more than just an open access publisher of scholarly articles: it is a pioneering approach to the world of academia, radically improving the way scholarly research is managed. The grand vision of Frontiers is a world where all people have an equal opportunity to seek, share and generate knowledge. Frontiers provides immediate and permanent online open access to all its publications, but this alone is not enough to realize our grand goals.

Frontiers journal series

The Frontiers journal series is a multi-tier and interdisciplinary set of open-access, online journals, promising a paradigm shift from the current review, selection and dissemination processes in academic publishing. All Frontiers journals are driven by researchers for researchers; therefore, they constitute a service to the scholarly community. At the same time, the *Frontiers journal series* operates on a revolutionary invention, the tiered publishing system, initially addressing specific communities of scholars, and gradually climbing up to broader public understanding, thus serving the interests of the lay society, too.

Dedication to quality

Each Frontiers article is a landmark of the highest quality, thanks to genuinely collaborative interactions between authors and review editors, who include some of the world's best academicians. Research must be certified by peers before entering a stream of knowledge that may eventually reach the public - and shape society; therefore, Frontiers only applies the most rigorous and unbiased reviews. Frontiers revolutionizes research publishing by freely delivering the most outstanding research, evaluated with no bias from both the academic and social point of view. By applying the most advanced information technologies, Frontiers is catapulting scholarly publishing into a new generation.

What are Frontiers Research Topics?

Frontiers Research Topics are very popular trademarks of the *Frontiers journals series*: they are collections of at least ten articles, all centered on a particular subject. With their unique mix of varied contributions from Original Research to Review Articles, Frontiers Research Topics unify the most influential researchers, the latest key findings and historical advances in a hot research area.

Find out more on how to host your own Frontiers Research Topic or contribute to one as an author by contacting the Frontiers editorial office: frontiersin.org/about/contact

Advances in mast cell physiology and mast cell-driven diseases

Topic editors

Carlo Pucillo — University of Udine, Italy

Ulrich Blank — Institut National de la Santé et de la Recherche Médicale (INSERM), France

Citation

Pucillo, C., Blank, U., eds. (2023). *Advances in mast cell physiology and mast cell-driven diseases*. Lausanne: Frontiers Media SA.

doi: 10.3389/978-2-8325-3854-8

Table of contents

frontiers | Frontiers in Immunology

TYPE Editorial
PUBLISHED 19 October 2023
DOI 10.3389/fimmu.2023.1303726

OPEN ACCESS

EDITED AND REVIEWED BY
Francesca Granucci,
University of Milano-Bicocca, Italy

*CORRESPONDENCE
Ulrich Blank
ulrich.blank@inserm.fr
Carlo Pucillo
carlo.pucillo@uniud.it

RECEIVED 28 September 2023
ACCEPTED 05 October 2023
PUBLISHED 19 October 2023

CITATION
Blank U and Pucillo C (2023) Editorial: Advances in mast cell physiology and mast cell-driven diseases. *Front. Immunol.* 14:1303726. doi: 10.3389/fimmu.2023.1303726

Editorial: Advances in mast cell physiology and mast cell-driven diseases

Ulrich Blank[1,2]* and Carlo Pucillo[3]*

[1]Université Paris Cité, Centre de Recherche sur l'Inflammation, Institut National de la Santé et de la Recherche Médicale (INSERM) Unité Mixte de Recherche (UMR)1149, Centre National de la Recherche Scientifique (CNRS) Equipe Mixte de Recherche (EMR)-8252, Faculté de Médecine site Bichat, Paris, France, [2]Université Paris Cité, Laboratoire d'Excellence INFLAMEX, Paris, France, [3]Department of Medicine, University of Udine, Udine, Italy

KEYWORDS

mast cell, inflammation, allergies, pseudo-allergies, inflammatory mediators, mastocytosis

Editorial on the Research Topic
Advances in mast cell physiology and mast cell-driven diseases

Mast cells (MCs) are long-lived tissue-resident immune cells occupying their final residence in several locations, including the fetal liver during fetal development. In adults, they arise from bone marrow–derived progenitors, which, after a short passage in the blood, migrate to their final destination and differentiate into mature MCs (1). They are predominant in tissues that are in close contact with the external environment, such as the skin or at mucosal surfaces, but can be found in virtually every organ, often increasing during an inflammatory process (2).

They are well-known effectors of IgE-mediated immune responses protecting against parasitic infections and toxins such as snake venoms but are also key effectors of allergies. When activated through IgE receptors (FcεRI), they release a whole set of inflammatory mediators stored in cytoplasmic granules, including histamine and various MC-specific proteases (3). This is followed by a wave of newly synthesized lipid mediators, such as prostaglandins and leukotrienes, and a large variety of chemokines and cytokines, thereby perpetuating and regulating the initiated inflammatory response. Besides FcεRI, MCs express a large set of other receptors (4) empowering them to respond to IgE-independent stimuli in various physiological settings, implicating them as contributors to IgE-independent autoimmune diseases, various chronic inflammatory disorders, and cancers including mastocytosis. A recently described receptor, MRPRX2, has received great attention due to its ability to interact with a large variety of positively charged chemical compound and peptides, being responsible for the development of so-called pseudo-allergic reactions as well as the crosstalk with the peripheral nervous system, releasing neuropeptides (5).

This Research Topic assembles 10 original research articles and one review article with a large majority (five) devoted to the recently discovered MC-specific receptor MRGPRX2. Two articles analyze MCs in the context of transformation and mastocytosis, and the remaining articles seek to further characterize and describe the physiology/pathophysiology of MCs in different contexts. Concerning the study of MRGPRX2, Thapaliya et al. investigate the effect of various inhibitors of G protein-coupled receptor

(GPCR) kinase 2 (GRK2) on IgE- and MRGPRX2-initiated MC responses. The authors show that while these inhibitors readily inhibit IgE-induced anaphylactic responses, they have a contrary activating role on human MRGBRX2-induced responses and its murine counterpart MRGPRB2. Conversely, Bawazir et al. show that two inverse MRGPRX2 agonists, while inhibiting the MRGBRX2 agonist responses, did not do so when using the murine equivalent MRGPRP2 or FcεRI-induced responses, setting a framework for selective treatment of IgE-independent MC-mediated drug hypersensitivity and cutaneous disorders. The study by Guo et al. describes a novel signaling pathway initiated by MRGPRX2 and involving nuclear translocation of the moonlighting protein lysyl t-RNA synthetase (LysRS), thereby activating the microphthalmia-associated transcription factor (MITF) involved in various MRGPRX2-initiated MC responses. Raj et al. perform a structural study examining the ability of certain analogs of Substance P to activate MRGPRX2 based on computational studies. The authors confirm the importance of basic residues for full-blown activation, although some responses, such as CCL2 chemokine secretion, can still be detected. Another study by Thapaliya and Ali on the role of GRK2, a Serine/Threonine kinase that promotes desensitization and internalization of GPCRs. Using MCs where this kinase has been specifically knocked out, the authors show that certain but not all FcεRI-initiated responses are inhibited, while, on the contrary, MRGPRB2-initated responses are enhanced, although this was dependent on the nature of the ligand, supporting a role in GPCR receptor desensitization. The authors also reveal a GRK2-independent crosstalk between FcεRI and MRGPRP2. Concerning mastocytosis, Bandara et al. investigate the role of two oncogenic mutations (D816V and V560G) of the KIT receptor by engineering a human MC line, HMC-1.2 cells, with a single D816V-KIT mutation and comparing it to the parent cell line bearing both mutations. The authors reveal several differences and suggest that the cell line with the single D816V-KIT mutation, which is the mutation present in most mastocytosis cases, represents an improved clinical mastocytosis model. Capellmann et al. characterize a new spontaneously developed transformed murine peritoneal MC line with accelerated cell cycle progression, called PMC-306, although the culture was still dependent on the presence of the growth factors IL-3 and SCF. Transformation was accompanied by the loss of the critical cell cycle regulators Cdkn2a and Arf expression that involves the activation of Kit. This new cell line represents a new tool to study MC biology and MC tumorigenic processes. Concerning MC functions, Herrera-Heredia et al. present a study on the physiological role of heparin stored in cytoplasmic granules. Generating a novel experimental model of Heparin deficiency in connective tissue type MCs, the authors present a variety of results highlighting the role of heparin in secretory granule formation and various physiological responses. The role of microgravity, i.e., the complete or near-complete absence of the sensation of weight, on MC functions was studied by Kim et al. using a rotary culture system that simulates microgravity. The authors reveal a variety of negative regulatory functions contributing to the understanding of immune system function/dysfunction in space medicine research. Rönnberg et al. investigate the heterogeneity of sorted human lung MCs implicated in airway inflammatory diseases, such as asthma, using single cell RNA sequencing. The authors reveal a high expression of classical MC markers. Although variable expression of several individual genes could be detected, no specific subpopulation could be detected by unbiased clustering. Finally, Schulman et al. review the role of P2 purinergic cell-surface receptors (P2R) interacting with extracellular adenosine 5′-triphosphate (ATP). ATP is a component of the damage-associated molecular patterns that can potently enhance FcεRI-induced degranulation. Potential therapeutic approaches targeting this interaction are discussed.

Taken as a whole, this Research Topic of original articles gives us new insights into MC functions. A large proportion of the articles concerns the role of MRGPRX2 specifically expressed by MC. They also provide new data on MC biology and models to study MC transformation. We hope that these new insights will contribute to a better understanding of MC physiology/pathophysiology and will, at least partly, also provide new ideas for therapeutic interventions of MC driven diseases.

Author contributions

UB: Writing – original draft. CP: Writing – original draft.

Funding

The author(s) declare that no financial support was received for the research, authorship, and/or publication of this article.

Conflict of interest

The authors declare that the research was conducted in the absence of any commercial or financial relationships that could be construed as a potential conflict of interest.

The author(s) declared that they were an editorial board member of Frontiers, at the time of submission. This had no impact on the peer review process and the final decision

Publisher's note

References

1. Chia SL, Kapoor S, Carvalho C, Bajenoff M, Gentek R. Mast cell ontogeny: From fetal development to life-long health and disease. *Immunol Rev* (2023) 315(1):31–53. doi: 10.1111/imr.13191

2. Levi-Schaffer F, Gibbs BF, Hallgren J, Pucillo C, Redegeld F, Siebenhaar F, et al. Selected recent advances in understanding the role of human mast cells in health and disease. *J Allergy Clin Immunol* (2022) 149(6):1833–44. doi: 10.1016/j.jaci.2022.01.030

3. Blank U, Huang H, Kawakami T. The high affinity IgE receptor: a signaling update. *Curr Opin Immunol* (2021) 72:51–8. doi: 10.1016/j.coi.2021.03.015

4. Redegeld FA, Yu Y, Kumari S, Charles N, Blank U. Non-IgE mediated mast cell activation. *Immunol Rev* (2018) 282(1):87–113. doi: 10.1111/imr.12629

5. Roy S, Chompunud Na Ayudhya C, Thapaliya M, Deepak V, Ali H. Multifaceted MRGPRX2: New insight into the role of mast cells in health and disease. *J Allergy Clin Immunol* (2021) 148(2):293–308. doi: 10.1016/j.jaci.2021.03.049

frontiers | Frontiers in Immunology

TYPE Original Research
PUBLISHED 06 October 2022
DOI 10.3389/fimmu.2022.1032497

OPEN ACCESS

EDITED BY
Ulrich Blank,
Institut National de la Santé et de la Recherche Médicale (INSERM), France

REVIEWED BY
Kosuke Nishi,
Ehime University, Japan
Michael Huber,
RWTH Aachen University, Germany

*CORRESPONDENCE
Hydar Ali
alih@upenn.edu

SPECIALTY SECTION
This article was submitted to Molecular Innate Immunity, a section of the journal Frontiers in Immunology

RECEIVED 30 August 2022
ACCEPTED 21 September 2022
PUBLISHED 06 October 2022

CITATION
Thapaliya M, Amponnawarat A, Tesmer JJG and Ali H (2022) GRK2 inhibitors, paroxetine and CCG258747, attenuate IgE-mediated anaphylaxis but activate mast cells *via* MRGPRX2 and MRGPRB2.
Front. Immunol. 13:1032497.
doi: 10.3389/fimmu.2022.1032497

GRK2 inhibitors, paroxetine and CCG258747, attenuate IgE-mediated anaphylaxis but activate mast cells *via* MRGPRX2 and MRGPRB2

Monica Thapaliya[1], Aetas Amponnawarat[1,2], John J. G. Tesmer[3] and Hydar Ali[1]*

[1]Department of Basic and Translational Sciences, University of Pennsylvania, School of Dental Medicine, Philadelphia, PA, United States, [2]Department of Family and Community Dentistry, Faculty of Dentistry, Chiang Mai University, Chiang Mai, Thailand, [3]Departments of Biological Sciences and of Medicinal Chemistry and Molecular Pharmacology, Purdue University, West Lafayette, IN, United States

G protein-coupled receptor (GPCR) kinase 2 (GRK2), which phosphorylates agonist-occupied GPCRs to promote their desensitization, has been investigated as an attractive therapeutic target for cardiovascular and metabolic diseases. Several GRK2-targeted inhibition strategies have been reported including the use of direct pharmacological inhibitors such as paroxetine (a widely prescribed antidepressant) and its analogs such as compound CCG258747. Cross-linking of high affinity IgE receptor (FcεRI) on mast cells (MCs) and the resulting degranulation causes anaphylaxis and allergic asthma. Using gene silencing strategy, we recently showed that GRK2 contributes to FcεRI signaling and MC degranulation. The purpose of this study was to determine if the GRK2 inhibitors paroxetine and CCG258747 modulate FcεRI-mediated MC responses *in vitro* and *in vivo*. Utilizing rat basophilic leukemia (RBL-2H3) cells and primary mouse lung MCs (LMCs), we found that paroxetine and CCG258747 inhibit FcεRI-mediated calcium mobilization and degranulation. Furthermore, intravenous administration of paroxetine and CCG258747 in mice resulted in substantial reduction of IgE-mediated passive cutaneous anaphylaxis. Unlike LMCs, human cutaneous MCs abundantly express a novel GPCR known as MRGPRX2 (mouse; MRGPRB2). We found that in contrast to their inhibitory effects on FcεRI-mediated MC responses, both paroxetine and CCG258747 induce calcium mobilization and degranulation in RBL-2H3 cells stably expressing MRGPRX2 but not in untransfected cells. Furthermore, paroxetine and CCG258747 induced degranulation in peritoneal MCs from Wild-type (WT) mice *in vitro* and caused increased cutaneous vascular permeability *in vivo*, but these responses were substantially reduced in *Mrgprb2*$^{-/-}$ mice. Additionally, upon intradermal injection, paroxetine also induced neutrophil recruitment in WT but not *Mrgprb2*$^{-/-}$ mice. These findings suggest that in addition to their potential therapeutic utility against cardiovascular and metabolic disorders, paroxetine-based GRK2-inhibitors may serve to modulate IgE-mediated anaphylaxis and to

10.3389/fimmu.2022.1032497

enhance cutaneous host defense by harnessing MC's immunomodulatory property through the activation of MRGPRX2/MRGPRB2.

KEYWORDS

GRK2, paroxetine, mast cells, MRGPRX2, FcεRI, anaphylaxis, MRGPRB2

Introduction

G protein-coupled receptors (GPCRs) are extensively studied pharmacological targets which account for ~34% of all drugs approved by the US Food and Drug Administration (FDA) (1). Functions of GPCRs are regulated by a process known as desensitization, in which agonist-occupied receptors undergo phosphorylation by GPCR kinases (GRKs) to attenuate the effects of sustained signaling. However, dysregulated GRK2 levels and enhanced desensitization are the main drivers of pathology involved in cardiovascular, renal, metabolic, cancer, and neurodegenerative diseases (2, 3). Extensive efforts have been made to target GRK2 *via* different inhibition strategies that include genetic inhibition, RNA-based aptameric molecules, peptides, and the use of small molecular inhibitors (3).

Paroxetine (Paxil), a widely prescribed FDA-approved selective serotonin reuptake inhibitor (SSRI)-based antidepressant, has been identified as a direct inhibitor of GRK2. It prevents GPCR desensitization by binding to the active site of GRK2 (4), and has been extensively reported to have benefits in osteoarthritis, cardiac hypertrophy, myocardial infarction, and heart failure (4–9). Thus, efforts have been made to develop GRK2-specific inhibitors based on the paroxetine scaffold (10). Compound CCG258747, which has an added indazole ring, has recently been shown to have high selectivity and potency against GRK2 (11).

In contrast to its role in GPCR desensitization, GRK2 contributes to the activation of signaling *via* receptors that do not couple to G proteins. For example, GRK2 is upregulated in human asthmatic lungs (12), it associates with T cell receptors, and T-cell-specific deletion of GRK2 attenuates airway inflammation and hyperresponsiveness in mouse model of allergic asthma (12, 13). Mast cells (MCs) play a central role in the manifestation of allergic responses such as life-threatening anaphylaxis *via* the aggregation of the high affinity IgE receptor (FcεRI) by allergen (14). One *in vitro* study showed that GRK2 contributes to FcεRI signaling and mediator release in MCs (15). However, the possibility that paroxetine and CCG258747 can modulate IgE-mediated anaphylaxis has not been tested.

Abbreviations: MCs, Mast cells; GPCR, G protein-coupled receptor; GRK2, GPCR kinase 2; MRGPRX2, Mas-related GPCR X2; MRGPRB2, Mas-related GPCR B2; RBL, Rat Basophilic Leukemia; WT, Wild type.

While MCs are characterized by the presence of cell surface FcεRI, a subtype present in the human skin also expresses a novel GPCR, Mas-related GPCR X2 (MRGPRX2; mouse orthologue MRGPRB2) (16–18). Our lab was the first to show that host defense peptides activate MCs *via* this receptor (19) and recent evidence suggests that MRGPRB2-mediated local MC activation plays a crucial role in clearing bacterial infection *via* neutrophil recruitment (20, 21). Additionally, this receptor also contributes to hypersensitivity reactions in response to multiple clinically used FDA-approved peptidergic drugs (22–24). McNeil et al. (16), showed that the presence of a common tetrahydroisoquinoline (THIQ) motif in these drugs contributes to their ability to activate MRGPRX2 and MRGPRB2. Additionally, Wolf et al. (25), showed that cationic tricyclic compounds with hydrophobic center and a halogen substituent such as paroxetine activates MRGPRX2/MRGPRB2. The main purpose of the present study was to determine if paroxetine and CCG258747 inhibit IgE/FcεRI-mediated MC degranulation and anaphylaxis. We found that both paroxetine and CCG258747 inhibit IgE/FcεRI-mediated MC responses *in vitro* and intravenous administration of these compounds in mice results in significant reduction of IgE-mediated anaphylaxis. However, intradermal injection of the compounds activates cutaneous MCs to enhance host defense by harnessing immunomodulatory property through the activation of MRGPRX2/MRGPRB2.

Materials and methods

Reagents

All cell culture reagents, 2,4-dinitrophenyalted Bovine Serum Albumin (DNP-BSA; Cat # A23018) and DNP-specific mouse IgE (SPE-7) were purchased from Invitrogen (Gaithersburg, MD, USA). Recombinant mouse interleukin-3 (IL-3) and stem cell factor (SCF) were purchased from Peprotech (Rocky Hill, NJ). 2-Mercaptoethanol (Cat #M7522), p-nitrophenyl-N-acetyl-β-D-glucosamine (PNAG) and Evans blue dye were obtained from Sigma-Aldrich (St. Louis, MO). Fura-2 acetoxymethyl ester was purchased from Abcam (Cambridge, MA, USA). Compound 48/80 was obtained from AnaSpec (Fremont, CA). Phycoerythrin (PE)- conjugated c-kit

and Allophycocyanin (APC)-conjugated FcεRI antibodies were acquired from eBiosciences (San Diego, CA) Paroxetine hydrochloride hemihydrate (CAS RN: 110429-35-1, Product Number: P1977, solvent PBS) was obtained from TCI chemicals, paroxetine analog CCG258747 (solvent DMSO) was kindly provided by Dr. John J. G. Tesmer, Purdue University.

Mice

All mice were housed in pathogen-free cages on autoclaved hardwood bedding. C57BL/6 (Wild type; WT) mice were purchased from the Jackson Laboratory (Bar Harbor, ME, USA). MRGPRB2 deficient mice (*Mrgprb2*$^{-/-}$) in the C57BL/6 background were generated by the CRISPR-Cas9 core facility of the University of Pennsylvania. Eight-12 weeks mice were used for entire studies. The experiments were approved by the Institutional Animal Care and Use Committee at The University of Pennsylvania.

Cells

Rat Basophilic Leukemia (RBL-2H3) were cultured in Eagle's medium (DMEM) supplemented with 10% FBS, L-glutamine (2 mM), penicillin (100 IU/mL), and streptomycin (100 μg/mL) and maintained in monolayer at 37°C with 5% CO_2. Same culture conditions were used for RBL-2H3 cells stably expressing MRGPRX2 (RBL-MRGPRX2) in the presence of G-418 (1 mg/mL).

Peritoneal MCs (PMCs)

PMCs from WT and *Mrgprb2*$^{-/-}$ mice were isolated and purified as described (26). Briefly, Hank's Balanced Salt Solution (HBSS) supplemented with 3% fetal bovine serum (FBS) and 1mM HEPES in a 10 mL volume was used to lavage the cells. Cells were then cultured in Gibco Roswell Park Memorial Institute (RPMI) 1640 media with GlutaMAX and 25mM HEPES supplemented with 10% FBS, 5% Non-Essential Amino Acid (NEAA), penicillin (100 IU/mL) and streptomycin (100 μg/mL), 2-mercaptoethanol (45.6 μM), murine IL-3 (10 ng/mL), and murine SCF (30 ng/mL). Non-adherent cells were removed after 48 h and cultured in fresh medium for 4-8 weeks. After 4 weeks of culture > 90% of cells were PMCs as confirmed by alcian safranin staining as described (27).

Lung MCs (LMCs)

LMCs were obtained from *ex-vivo* differentiation of fresh lung tissue isolated from WT mice as described (28). Briefly, lungs were excised and chopped into fine pieces with scissors. Chopped lungs were then cultured in complete media same as media for PMCs culture, supplemented with 10 ng/mL murine SCF and 10 ng/mL of murine IL-3. Cells coming out from the tissue gets dispersed into the media and after 7-10 days the tissue disappears leaving fat like droplets behind which was strained, and the cells were further cultured for 4-6 weeks with continuous removal of adherent cells 1-2 times a week. The purity LMCs was > 90% as determined by flow cytometry (BD LSR II flow cytometer, BD Biosciences) using anti-c-kit-PE and anti-FcεRI-FITC antibodies.

Degranulation

RBL-2H3 cells (5×10^4), LMCs (4×10^4), *Mrgprb2*$^{-/-}$ PMCs (1×10^4) were sensitized with DNP-specific mouse IgE (SPE-7) (1 μg/mL). After 16 h, cells were washed with HEPES-buffered saline containing 0.1% BSA, seeded in 96-well clear flat bottom plates, and incubated with different concentrations of paroxetine or CCG258747 (1-30 μM) at 37°C for 30 min and stimulated with antigen (DNP-BSA, 30 ng/mL) at 37°C for another 30 min. For total β-hexosaminidase release, unstimulated cells were lysed in 50 μL of 0.1% Triton X-100. Aliquots (20 μL) of supernatant or cell lysates were incubated with 20 μL of 1 mM p-nitrophenyl-N-acetyl-β-D-glucosamine for 1 h at 37°C. The reaction was stopped by adding 250 μL of a 0.1 M Na_2CO_3/0.1 M $NaHCO_3$ buffer and absorbance was measured at 405 nm using Versamax microplate spectrophotometer (San Jose, CA, USA). Degranulation in RBL-2H3 cells stably expressing MRGPRX2, WT and *Mrgprb2*$^{-/-}$ PMCs was performed similarly with direct stimulation with paroxetine and CCG258747 (0-30 μM) for 30 min.

Calcium mobilization

RBL-2H3 (1.5×10^6) were sensitized with DNP-specific mouse IgE (1 μg/mL, 16 h). Cells were washed in HEPES-buffered saline containing 0.1% BSA and loaded with 1 μM Fura-2 acetoxymethyl ester for 30 min at 37°C, followed by de-esterification in the buffer for additional 15 min at room temperature. Cells were then incubated with paroxetine or compound CCG258747 (30 μM) for 30 min at 37°C and stimulated with 30 ng/mL of DNP-BSA at 100 sec. For experiments involving RBL-2H3 and RBL-MRGPRX2 cells where the compounds were tested as agonists, cells were stimulated with paroxetine (30 μM) or compound CCG258747 (10 μM) at 100 sec. Calcium mobilization was determined using a Hitachi F-2700 Fluorescence Spectrophotometer with dual excitation wavelength of 340 and 380 nm, and an emission wavelength of 510 nm.

Evans blue dye extravasation

For IgE-mediated cutaneous anaphylaxis, mice were sensitized *via* intradermal injection with DNP-specific mouse

IgE (SPE-7) (20 ng, 30 µL) into the right hind paw or vehicle (PBS, 30 µL) in the left hind paw. After 24 h, mice were given intravenous injection of paroxetine (100 µg, 100 µL, 5 mg/kg) or vehicle (PBS); CCG258747 (100 µg, 100 µL, 5 mg/kg) or vehicle (1% DMSO in PBS) and after 30 min, mice were challenged with an intravenous injection of 100 µg DNP-BSA in 200 µL PBS containing 1% Evans blue for another 30 min. For experiments with paroxetine and CCG758747 mediated cutaneous anaphylaxis, WT and *Mrgprb2*$^{-/-}$ mice were intravenously injected with 1% Evans blue in PBS (200 µL) followed by paroxetine (30 µL of 100 µg/mL) or CCG758747 (20 µL of 100 µg/mL) in right hind paw or with respective vehicles (PBS or 1% DMSO) in left hind paw for 30 min. For IgE-mediated anaphylaxis response in *Mrgprb2*$^{-/-}$ mice, passively sensitized mice were intradermally injected with same dose of paroxetine and challenged by antigen (20 µg, 200 µL in 1% Evans blue dye in PBS) or vehicle (200 µL in 1% Evans blue dye in PBS) intravenously for 30 min. Mice were then euthanized; paws were removed, weighed, dried overnight, dissolved in 500 µL formamide and incubated at 55˚C overnight. Supernatant was collected and Evans blue dye extravasation was determined by measuring the absorbance at 650 nm.

Cutaneous neutrophil recruitment

WT and *Mrgprb2*$^{-/-}$ mice were intradermally injected with paroxetine (30 µL of 100 µg/mL, 0.1 mg/kg) in right hind paw and vehicle control in the left hind paw. After 3 h, mice were sacrificed and skin tissue from the injection site was harvested for flow cytometric analyses.

Flow cytometry

To measure the neutrophil recruitment, single cell suspension was prepared from the skin harvested by digesting the skin using the previously published protocol with slight modifications (29). Briefly, the tissues were chopped and digested using digestion buffer (RPMI 1640 containing 0.8% FBS, DNase I (0.15 mg/mL; Roche), collagenase type IV (3.2 mg/mL; Gibco-Life Technologies), and Dispase II (2.6 U/mL; Sigma-Aldrich) for 1 h at 37°C with constant agitation. Further, cells were strained with a 70-µm strainer and red blood cells were lysed with ammonium-chloride-potassium (ACK) buffer and washed with dPBS supplemented with 2% FBS and 10 mM EDTA. Fc receptors were blocked with anti-CD16/32 IgG (BioLegend), and dead cells were detected using a Zombie Yellow Fixable Viability Kit (BioLegend). Cells were then stained with fluorochrome-tagged antibodies to CD45, CD11b, Ly-6G (BioLegend) for measuring neutrophils. Cells stained with FMO were used as needed. Cells were analyzed by a BD LSR II flow cytometer (San Jose, CA) and FlowJo software version 10.7.2 (Tree Star Inc., Ashland, OR).

Systemic anaphylaxis

Systemic anaphylaxis was performed as previously described (16). Paroxetine (5 mg/kg, 100 µL) or PBS control was injected intraperitoneal in WT mice. Core body temperature was measured with a rectal thermometer (physitemp) every 10 min for 90 min and mice were euthanized after 90 min, and temperature drop from the baseline was calculated.

Statistical analysis

To ensure scientific rigor and reproducibility, all *in vivo* experiments were performed with 6-10 mice per experiment. All *in vitro* experiments were at least repeated 3-4 times with different batches of cells ran in triplicates. Statistical significance was determined by two-way ANOVA or ordinary one way-ANOVA with multiple comparison test. Significant differences were set at *$p \leq 0.05$, **$p \leq 0.01$, ***$p \leq 0.001$ and ****$p \leq 0.0001$ and analyzed by GraphPad Prism version 9.

Results

Paroxetine and CCG258747 inhibit FcεRI-mediated calcium mobilization and degranulation in RBL-2H3 cells

RBL-2H3 cells have been extensively used to study the regulation of FcεRI signaling in MCs. Thus, we initially utilized this cell line to determine if GRK2 inhibitor, paroxetine (Figure 1A) inhibits FcεRI-mediated signaling and degranulation. We found that paroxetine at 30 µM inhibits antigen (DNP-BSA)-induced calcium mobilization in cells sensitized with DNP-specific IgE (Figure 1B). Next, the inhibitory dose response of paroxetine (0 – 30 µM) on antigen-induced degranulation was measured using a β-hexosaminidase release assay. We found that compared to the control, there was a dose-dependent inhibition of degranulation in paroxetine-treated cells (Figure 1C). Likewise, treatment of RBL-2H3 cells with CCG258747 (Figure 1D) also resulted in inhibition of IgE-mediated calcium mobilization (Figure 1E) and degranulation (Figure 1F). These data demonstrate that both paroxetine and CCG258747 inhibit FcεRI-mediated signaling in RBL-2H3 cells.

Paroxetine and CCG258747 inhibit IgE-mediated degranulation in primary LMCs *in vitro* and cutaneous anaphylaxis *in vivo*

Next, we wanted to test if these findings can be translated into a physiologically relevant cell system. For this, we generated murine LMCs and found that paroxetine caused a significant reduction in IgE-mediated degranulation (Figure 2A). Treatment of LMCs with CCG258747 also caused a significant reduction of

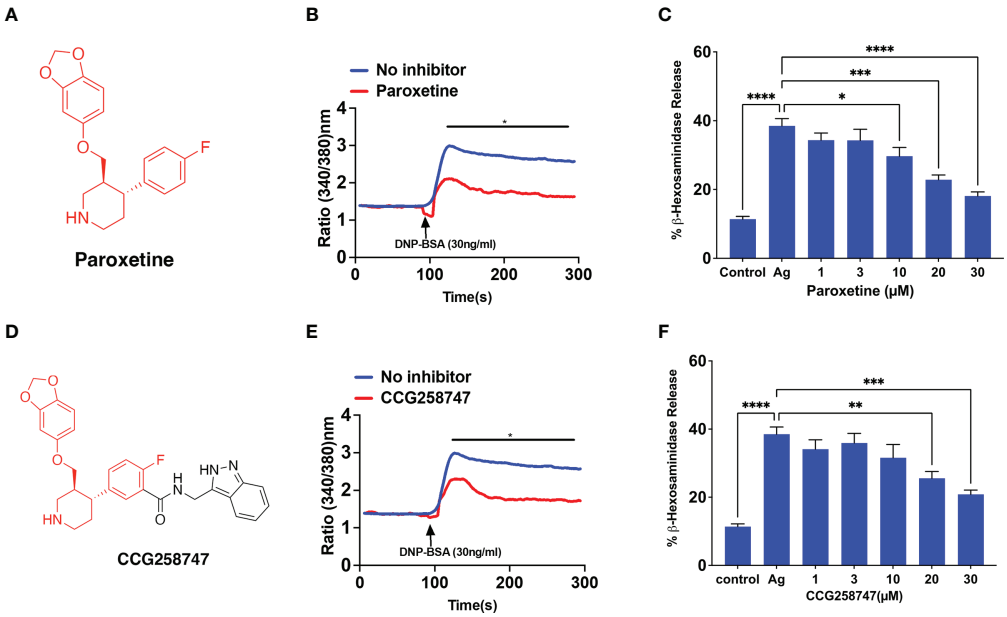

FIGURE 1
Paroxetine and CCG258747 inhibit FcεRI-mediated response in RBL-2H3 cells. **(A)** Structure of paroxetine. **(B)** Measurement of Calcium mobilization upon antigen (DNP-BSA; 30 ng/mL) stimulation with/without pre-incubation of IgE-primed RBL-cells with paroxetine (30 μM, 30 min). **(C)** IgE-primed RBL cells were pre-incubated with different doses of paroxetine (0-30 μM) and stimulated with antigen (Ag, 30 ng/mL) and β-hexosaminidase release was measured. **(D)** Structure of compound CCG258747. Measurement of antigen-induced **(E)** calcium mobilization and **(F)** β-hexosaminidase release in IgE-primed RBL-2H3 cells in the absence or presence of CCG258747. Error bars are standard error of mean (SEM) from at least three independent experiments and significant differences were set at *p ≤ 0.05, **p ≤ 0.01, ***p ≤ 0.001 and ****p ≤ 0.0001. Error bars are not displayed for (B) and (E) for clarity. For figure B and E, C and F, data were generated simultaneously from the same experiment with same controls.

IgE-mediated degranulation (Figure 2B). To determine if paroxetine and CCG258747 can inhibit IgE-mediated anaphylaxis *in vivo*, we sensitized mice with intradermal injections with vehicle (PBS, 30 μL, left hind paw) or DNP-specific IgE (20 ng, 30 μL, right hind paw). After 24 h, we injected paroxetine, CCG258747 (5 mg/kg, 100 μL) or vehicle (PBS, 100 μL) intravenously. After 30 min, mice were challenged with intravenous injection of 100 μg DNP-BSA in 200 μL PBS containing 1% Evans blue for 30 min and vascular permeability was assessed by measuring the optical density of dye leakage. Consistent with the *in vitro* data, we found that both paroxetine and CCG258747 treated mice displayed significantly reduced vascular permeability compared to untreated mice (Figures 2C, D). These findings confirm that paroxetine and CCG258747 inhibit IgE-mediated MC degranulation *in vitro* and reduce anaphylaxis *in vivo*.

Paroxetine and CCG258747 induce intracellular calcium mobilization and degranulation *via* MRGPRX2

Wolf et al. (25), recently screened a library of pharmacologically active cationic amphiphilic compounds for their ability to activate MRGPRX2 *in vitro* and found that antidepressants desipramine, clomipramine and paroxetine activates MRGPRX2. The authors showed that paroxetine induces calcium mobilization in HEK293 cells transfected with cDNA encoding MRGPRX2 and in a human MC line (LAD2 cells) naturally expressing the receptor with EC_{50} values of 34 μM and 18 μM, respectively. However, the minimum concentration of paroxetine that induces degranulation in LAD2 cells and primary human MCs was 75 μM. The difference between the reported EC_{50} values for calcium mobilization and degranulation is not clear. We found that 30 μM paroxetine caused robust calcium mobilization and maximal degranulation in RBL-2H3 cells stably expressing MRGPRX2 but not in untransfected cells (Figures 3A, B). The minimum concentration of paroxetine to induce degranulation was 10 μM. We found CCG258747 at 10 μM induced a robust calcium mobilization and substantial degranulation (Figures 3C, D). Interestingly, although the dose-response profiles of paroxetine and CCG258747-induced degranulation are similar, the magnitude of the response induced by CCG258747 was greater than paroxetine at all concentrations tested (Figures 3B, D). Recently, cryo-electron microscopy structures of agonist stabilized MRGPRX2/G protein complexes have been solved (30, 31). Interestingly, unlike other class A family of GPCRs, MRGPRX2 displays a shallow negatively charged

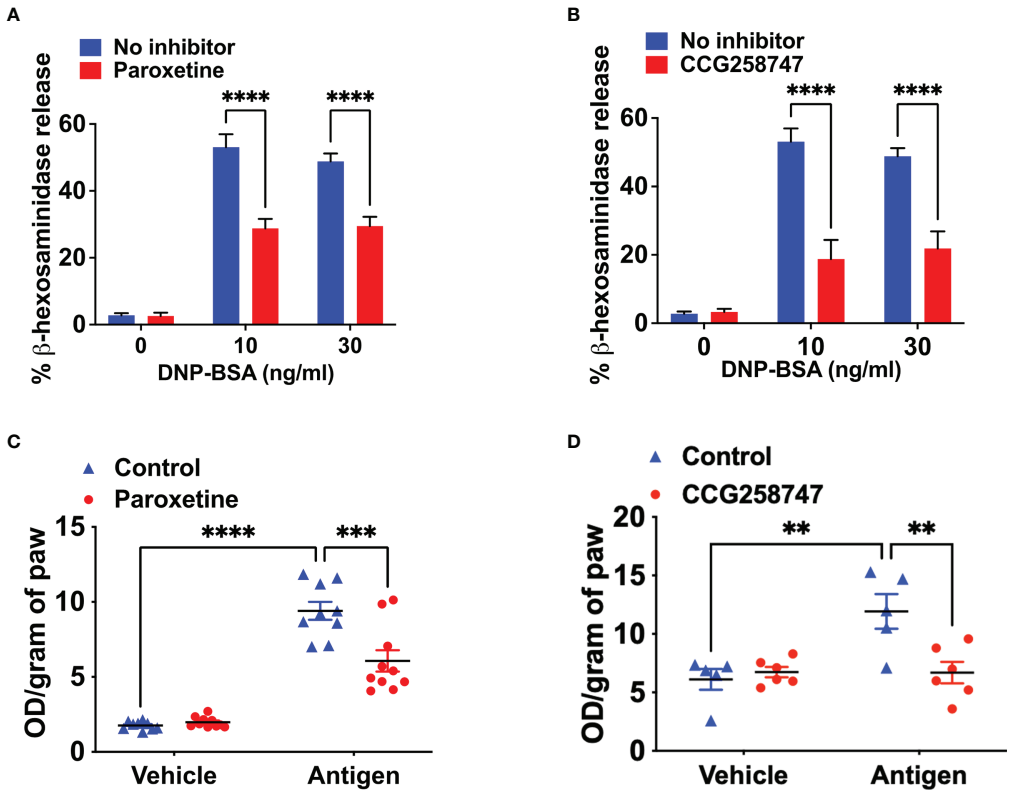

FIGURE 2
Paroxetine and CCG258747 inhibit IgE-mediated degranulation in primary LMCs *in vitro* and cutaneous anaphylaxis *in vivo*. Measurement of β-hexosaminidase release in IgE-primed LMCs pre-incubated with **(A)** paroxetine (30 μM) and **(B)** CCG258747 (30 μM) and challenged with antigen (30 ng/mL). C57BL/6 mice (n=8-10) were sensitized with IgE (20 ng, 30 μL, right hind paw) and vehicle (PBS, 30 μL, left hind paw) for 24 hrs and were intravenously injected with paroxetine or CCG258747 (5 mg/kg, 100 μL, 30 min) or respective vehicle (100 μL, 30 min) following antigen (20 μg, 200 μL in 1% Evans blue dye in PBS, 30 min) challenge or vehicle (PBS) intravenously. Evans blue dye extravasation was determined. Quantification of vascular permeability for **(C)** paroxetine **(D)** CCG258747. Error bars are standard error of mean (SEM) and significant differences were set at $^{**}p \leq 0.01$, $^{***}p \leq 0.001$ and $^{****}p \leq 0.0001$.

subpocket that facilitates agonist binding and may explain why the receptor is promiscuously activated by positively charged small molecules and peptides. In addition, the receptor contains a second subpocket that facilitates hydrophobic interactions (30). The fact that CCG258747 contains an additional hydrophobic residue (Figure 1), could explain why it has a higher efficacy than paroxetine.

Paroxetine and CCG258747 activate murine MCs *in vitro* and *in vivo via* MRGPRB2

Wolf et al., showed that paroxetine induces degranulation in PMCs but the role of MRGPRB2 on this response was not tested. Compound 48/80 (C48/80) is a classic MC degranulating agent that functions *via* MRGPRB2 (16). We first validated *Mrgprb2*$^{-/-}$ PMCs by demonstrating that while C48/80 induces robust degranulation in cells cultured from WT mice, this response was abolished in cells cultured from *Mrgprb2*$^{-/-}$ mice (Figures 4A, B). We then sought to determine if paroxetine and CCG258747 induce degranulation in mouse PMCs and if they did so *via* MRGPRB2. We found that unlike the situation for MRGPRX2, 10 μM paroxetine did not induce degranulation in PMCs but at 30 μM it induced a small but significant response that was not present in *Mrgprb2*$^{-/-}$ PMCs (Figure 4A). However, unlike paroxetine, 10 μM of CCG258747 induced a robust degranulation response and the compound at 30 μM caused a response that was ~5-fold higher than that induced by the same concentration of paroxetine (Figure 4B).

Although Wolf et al. (25), showed that intradermal injection of compounds similar to paroxetine (desipramine, clomipramine) induce scratching behavior in mice *via* MRGPRB2, the effect induced by paroxetine *in vivo* was independent of MRGPRB2. The reason for this difference is not clear. However, it is well documented that MC degranulation *in vivo* is associated with increased local vascular permeability (32). Thus, we tested whether the observed *in vitro* effect of paroxetine and

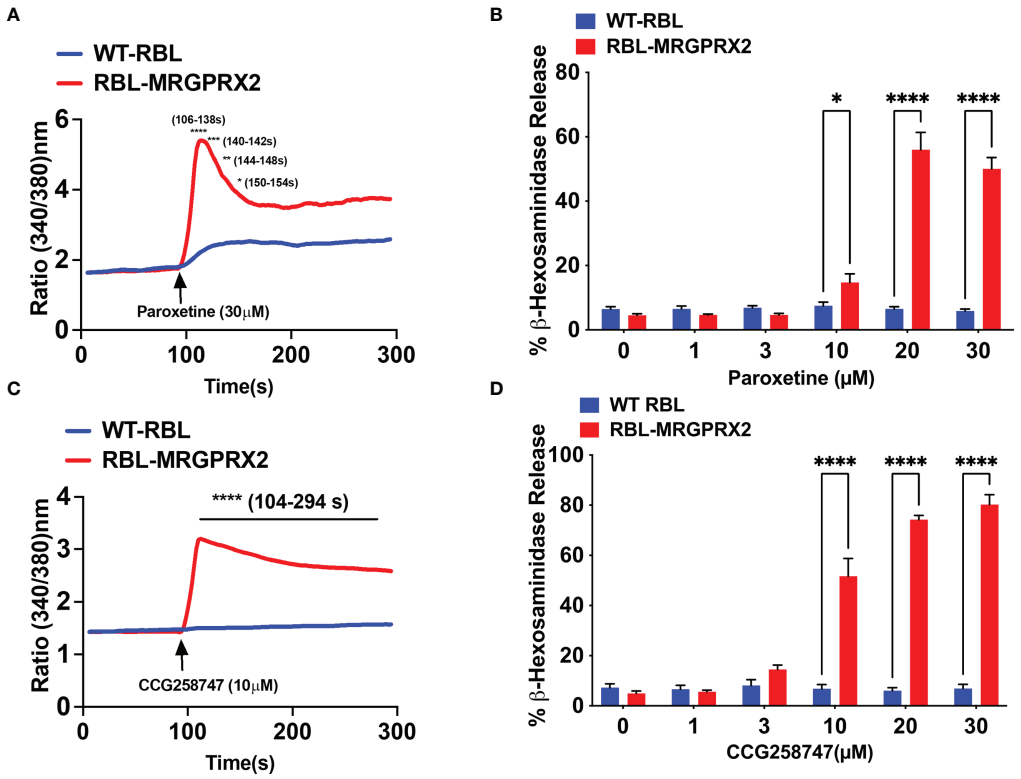

FIGURE 3
Paroxetine and CCG258747 induces intracellular calcium mobilization and degranulation *via* MRGPRX2. Untransfected RBL-2H3 (WT-RBL) and RBL-stably expressing MRGPRX2 (RBL-MRGPRX2) were exposed to paroxetine and **(A)** calcium mobilization (30 μM) and **(B)** β-hexosaminidase release (0 - 30 μM) were measured. Likewise, CCG258747-induced **(C)** calcium mobilization (10 μM) and **(D)** β-hexosaminidase release (0 - 30 μM) was measured. Error bars are standard error of mean (SEM) from three independent experiments and significant differences were set at *p ≤ 0.05, **p ≤ 0.01, ***p ≤ 0.001 and ****p ≤ 0.0001. Error bars are not displayed for A and C for clarity.

CCG258747 *via* MRGPRB2 can be translated *in vivo* by quantitating injection site vascular permeability. For this, 8-12 weeks of WT and *Mrgprb2*$^{-/-}$ mice were injected intradermally with paroxetine (30 μL, 100 μg/mL, right hind paw) or CCG258747 (20 μL, 100 μg/mL, right hind paw) and respective vehicle control (left hind paw) following 1% Evans blue dye intravenously for 30 min, and vascular permeability was assessed by measuring the optical density of dye leakage. Consistent with the *in vitro* data, we found that paroxetine-challenged paw displayed significantly enhanced vascular permeability compared to vehicle control in WT mice, but this effect was significantly reduced in *Mrgprb2*$^{-/-}$ mice (Figure 4C). Additionally, MRGPRB2 activation contributes to host defense against bacterial infection by releasing MC-mediators and recruiting neutrophils to the sites of infection (21). Evidence shows that paroxetine exerts antimicrobial activity against different bacterial strains (33). Thus, we tested whether paroxetine could recruit neutrophils at the injection site *via* MRGPRB2 activation to harness its immunomodulatory property. Complementing the reduced vascular permeability, paroxetine-treated mice also displayed significantly reduced neutrophil recruitment in *Mrgprb2*$^{-/-}$ compared to WT mice (Figure 4D). MRGPRB2 is expressed in connective tissue-type of murine MCs such as those found in the peritoneum and skin but at low levels in the lung or gut (17, 18). Thus, it was not surprising that paroxetine (5 mg/kg) when injected intraperitoneally did not induce systemic anaphylaxis as measured by temperature drop from baseline (Figure 4E). Similar to paroxetine, CCG258747 challenged *Mrgprb2*$^{-/-}$ mice also displayed reduced vascular permeability compared to WT (Figure 4F). These findings show that both paroxetine and CCG258747 activates MC *via* MRGPRB2 both *in vitro* and *in vivo*.

Paroxetine inhibits antigen/IgE-mediated degranulation in PMCs *in vitro* and anaphylaxis *in vivo* in the absence of MRGPRB2

Data presented thus far suggest that paroxetine and CCG258747 display dual roles in MCs; in the absence of MRGPRX2 and MRGPRB2 they inhibit IgE-mediated responses but in their presence, they couple to these receptors to induce

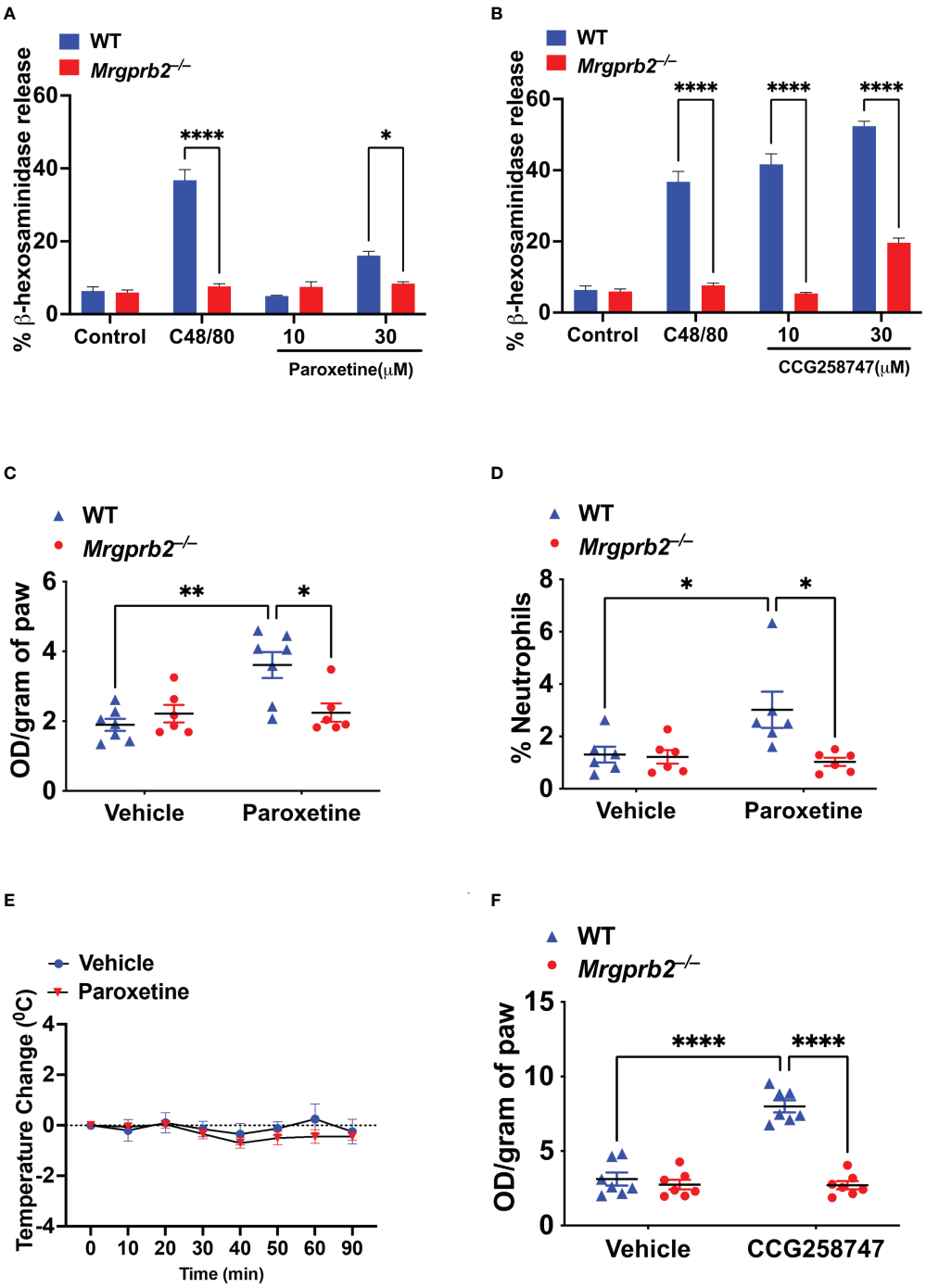

FIGURE 4
Paroxetine and CCG258747 activate murine MCs *in vitro* and *in vivo via* MRGPRB2. WT and *Mrgprb2*$^{-/-}$ PMCs were stimulated with **(A)** C48/80 (10 μg/mL) and paroxetine (10 and 30 μM), or **(B)** C48/80 (10 μg/mL) and CCG258747 (10 and 30 μM), and β-hexosaminidase release was measured. WT and *Mrgprb2*$^{-/-}$ (n = 6-7) mice were intradermally injected with paroxetine (0.1 mg/kg, 30 μL, 30 min), **(C)** Evans blue dye extravasation and **(D)** neutrophil recruitment was measured. **(E)** Paroxetine (5 mg/kg, 100 μL) or PBS control was injected intraperitoneal in WT (n=5) mice to assess systemic anaphylaxis *via* rectal temperature drop from baseline. **(F)** Evans blue dye extravasation with intradermal injection with CCG258747 (0.1 mg/kg, 20 μL, 30 min). Error bars are standard error of mean (SEM) and significant differences were set at *$p \leq 0.05$, **$p \leq 0.01$ and ****$p \leq 0.0001$.

degranulation. Thus, we wanted to further confirm whether paroxetine and CCG258747 inhibit antigen/IgE-mediated degranulation in *Mrgprb2*$^{-/-}$ PMCs. Indeed, we found that both paroxetine and CCG258747 caused significant inhibition of antigen/IgE-mediated degranulation in *Mrgprb2*$^{-/-}$ PMCs (Figures 5A, B). Additionally, unlike the situation in WT mice, where paroxetine induced increased vascular permeability (Figures 4C, D), in *Mrgprb2*$^{-/-}$ mice, paroxetine (30 µL of 100 µg/mL) caused significant inhibition of IgE-mediated anaphylaxis as measured by Evans blue extravasation (Figure 5C).

Discussion

Phosphorylation of many GPCRs by GRK2 and the subsequent desensitization provides an important mechanism to prevent detrimental effects of sustained signaling (2, 3). However, in pathologies associated with upregulated GRK2, such as cardiovascular, renal, metabolic, cancer, and neurodegenerative diseases, enhanced receptor desensitization is not always desirable (2, 3). This is the reason why paroxetine-mediated direct inhibition of GRK2 has been reported to be fruitful in mice studies for improving osteoarthritis, cardiac hypertrophy, myocardial infarction, and heart failure (4–8). Furthermore, Tian et al. (9), also showed that paroxetine improves cardiac function in patients which correlates to the reduction of GRK2 expression. Because of this success, efforts have been made to generate more potent and GRK2-specific analogs of paroxetine such as CCG258747 (11). In contrast to its function in GPCR desensitization, GRK2 promotes IgE/FcεRI mediated MC signaling, which is well-documented in the development and progression of several MC-mediated allergic diseases and hypersensitive reaction (14, 34–37). Utilizing both cell lines and primary MCs, we have shown that paroxetine and CCG258747 inhibit FcεRI-induced mediator release *in vitro* and anaphylaxis *in vivo*.

In several pre-clinical models and in patients with cardiovascular and metabolic diseases, GRK2 expression and activity is enhanced leading to the disease progression and severity due to enhanced desensitization (5, 38). Although not related to the desensitization function of GRK2, patients with allergic asthma (likely MC-mediated) exhibit GRK2 levels that are enhanced in the lungs compared to healthy controls. Additionally, T-cell-specific GRK2 promotes the pathogenesis of allergic asthma in a mouse model (12). We demonstrated that in mice, paroxetine and CCG258747 treatment reduce IgE-mediated MC degranulation *in vivo*. Thus, the prospect of using paroxetine based GRK2 inhibitors against allergic asthma is an attractive possibility. Furthermore, a randomized control trial also revealed that paroxetine has been successful for therapy against pruritus (39, 40), which is likely mediated *via* MC activation. Thus, in such precedent where paroxetine is clinically approved, paroxetine-based inhibitors may be attractive therapeutics against allergy.

Although CCG258747 is reported to be more potent and specific for GRK2 compared to paroxetine (11), we found that its inhibitory profile for IgE-mediated responses in RBL-2H3 were similar to paroxetine. However, in LMCs, the inhibition was slightly stronger for CCG258747 compared to paroxetine. The reason for this difference is not clear but could reflect differences between a cell line and primary MCs. Nevertheless, the possibility that paroxetine and CCG258747 inhibit IgE-mediated response independent of GRK2 cannot be ruled out. Both compounds are SSRI inhibitors, however, this is an unlikely mechanism because RNA-sequencing analysis revealed that primary LMCs do not express serotonin transporters

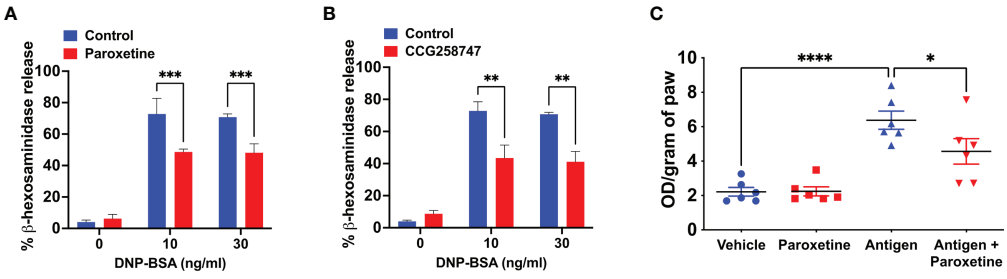

FIGURE 5
Paroxetine inhibits antigen/IgE-mediated MC degranulation *in vitro* and passive cutaneous anaphylaxis response *in vivo* in *Mrgprb2*$^{-/-}$ mice. IgE-primed *Mrgprb2*$^{-/-}$ PMCs were preincubated with **(A)** paroxetine (30 µM) and **(B)** CCG258747 (30 µM) and exposed to different concentrations of antigen (DNP-BSA, 0 - 30 ng/mL) and β-hexosaminidase release was measured. Passively sensitized *Mrgprb2*$^{-/-}$ mice were intradermally injected with paroxetine (0.1 mg/kg, 30 µL, 30 min, right hind paw) or vehicle (PBS, 30 µL, 30 min, left hind paw) followed by antigen (20 µg, 200 µL in 1% Evans blue dye in PBS, 30 min) or vehicle (200 µL in 1% Evans blue dye in PBS, 30 min) challenge intravenously. **(C)** Evans blue dye extravasation was determined. Error bars are standard error of mean (SEM) and significant differences were set at *p ≤ 0.05, **p ≤ 0.01, ***p ≤ 0.001 and ****p ≤ 0.0001.

(unpublished data). There has been a previous postulation that SSRIs suppress IgE-ATP positive feedback *via* purinergic receptors (41), which could be one of the possible mechanisms of action and will be the subject of future studies.

We made an interesting observation that paroxetine and CCG258747 cause MRGPRB2 activation when injected intradermally in mice. However, we did not observe any systemic reaction induced by paroxetine in mice. Furthermore, when injected intravenously, paroxetine did not induce cutaneous anaphylaxis, but instead inhibited FcεRI-induced response *in vivo*. Paroxetine induces only dermal reaction but not systemic, likely since MRGPRB2 is expressed abundantly in the skin. Nevertheless, the clinical use of paroxetine is oral, and it undergoes metabolism in the gut and liver and its metabolites may have different effects than the parent compound and hence the skin reaction may not be clinically relevant. This could explain why a widely used drug like paroxetine that activates MRGPRX2 does not have many reported allergic reactions (42). Whether paroxetine and CCG258747 induce inflammatory processes is currently unknown. However, very rare cases of dermatological adverse effects of paroxetine such as rash (2%–3%), photosensitivity (2%), and eczema (1%) have been reported (42). Thus, caution may have to be exercised when using these especially in patients who are pre-disposed to co-morbidities where MRGPRX2 is either upregulated (asthma, mastocytosis) or mutated (43–45).

Several reports suggest that SSRI inhibitors such as paroxetine have antimicrobial activity and can be a promising alternative for treating bacterial infection (33, 46, 47). In addition to direct antimicrobial activity, antimicrobial peptides can activate MCs to harness their immunomodulatory properties (26, 48–50). Recent evidence suggests that this immunomodulatory property is mediated *via* activation of MRGPRB2 and it plays a crucial role in host defense and clearing antibacterial infection (19, 20, 22, 26). A surprising observation of our study was that paroxetine evoked an acute inflammatory response by causing increased cutaneous vascular permeability and neutrophil recruitment *via* MRGPRB2. Folleto et al. (33), showed that paroxetine not only has antimicrobial activity but also synergizes with the antimicrobial activity of ciprofloxacin. However, the mechanism of antimicrobial activity of paroxetine is not known. It is possible that this antimicrobial activity of paroxetine is mediated *via* MRGPRX2/MRGPRB2 activation and in addition to its direct antimicrobial property, it can serve to enhance host defense.

In summary, we demonstrated that paroxetine and a related GRK2 inhibitor not only have an attractive clinical prospect in targeting allergic reactions, but also may serve to enhance host defense *via* MRGPRX2/MRGPRB2 activation. These interesting findings of dual regulation have attractive clinical utility, and detailed mechanistic studies in humans are needed to delineate these prospects.

Data availability statement

The raw data supporting the conclusions of this article will be made available by the authors, without undue reservation.

Ethics statement

The animal study was reviewed and approved by Institutional Animal Care and Use Committee at The University of Pennsylvania.

Author contributions

HA contributed to conception, supervision, and funding acquisition of the study. MT contributed to the conception and MT and AA performed the experiments and analyzed the data. MT wrote the first draft of the manuscript. JJGT provided the compound CCG258747 for the experiments. All authors contributed to the article and approved the submitted version.

Funding

This work was supported by National Institutes of Health grants R01-AI124182, R01-AI143185 and R01-AI149487 to HA, F31 AI154765-01A1 to MT, and R01-HL071818 to JJGT.

Acknowledgments

We thank the University of Pennsylvania's CRISPR/Cas9 Targeting Core and Transgenic and Chimeric mouse facility for generating the *Mrgprb2*$^{-/-}$ mice for our laboratory.

Conflict of interest

The authors declare that the research was conducted in the absence of any commercial or financial relationships that could be construed as a potential conflict of interest.

Publisher's note

References

1. Hauser AS, Attwood MM, Rask-Andersen M, Schiöth HB, Gloriam DE. Trends in GPCR drug discovery: New agents, targets and indications. *Nat Rev Drug Discovery* (2017) 16(12):829–42. doi: 10.1038/nrd.2017.178

2. Penela P, Ribas C, Sánchez-Madrid F, Mayor F. G Protein-coupled receptor kinase 2 (GRK2) as a multifunctional signaling hub. *Cell Mol Life Sci* (2019) 76 (22):4423–46. doi: 10.1007/s00018-019-03274-3

3. Murga C, Arcones AC, Cruces-Sande M, Briones AM, Salaices M, Mayor F. G Protein-coupled receptor kinase 2 (GRK2) as a potential therapeutic target in cardiovascular and metabolic diseases. *Front Pharmacol* (2019) 10:112. doi: 10.3389/fphar.2019.00112

4. Thal DM, Homan KT, Chen J, Wu EK, Hinkle PM, Huang ZM, et al. Paroxetine is a direct inhibitor of G protein-coupled receptor kinase 2 and increases myocardial contractility. *ACS Chem Biol* (2012) 7(11):1830–9. doi: 10.1021/cb3003013

5. Schumacher SM, Gao E, Zhu W, Chen X, Chuprun JK, Feldman AM, et al. Paroxetine-mediated GRK2 inhibition reverses cardiac dysfunction and remodeling after myocardial infarction. *Sci Transl Med* (2015) 7(277):277ra31. doi: 10.1126/scitranslmed.aaa0154

6. Carlson EL, Karuppagounder V, Pinamont WJ, Yoshioka NK, Ahmad A, Schott EM, et al. Paroxetine-mediated GRK2 inhibition is a disease-modifying treatment for osteoarthritis. *Sci Transl Med* (2021) 13(580):eaau8491. doi: 10.1126/scitranslmed.aau8491

7. Sun X, Zhou M, Wen G, Huang Y, Wu J, Peng L, et al. Paroxetine attenuates cardiac hypertrophy *Via* blocking GRK2 and ADRB1 interaction in hypertension. *J Am Heart Assoc* (2021) 10(1):e016364. doi: 10.1161/JAHA.120.016364

8. Kowalska M, Nowaczyk J, Fijałkowski Ł, Nowaczyk A. Paroxetine–overview of the molecular mechanisms of action. *Int J Mol Sci* (2021) 22(4):1662. doi: 10.3390/ijms22041662

9. Tian X, Wang Q, Guo R, Xu L, Chen QM, Hou Y. Effects of paroxetine-mediated inhibition of GRK2 expression on depression and cardiovascular function in patients with myocardial infarction. *Neuropsychiatr Dis Treat* (2016) 12:2333–41. doi: 10.2147/NDT.S109880

10. Bouley R, Waldschmidt HV, Cato MC, Cannavo A, Song J, Cheung JY, et al. Structural determinants influencing the potency and selectivity of indazole-paroxetine hybrid G protein–coupled receptor kinase 2 inhibitors. *Mol Pharmacol* (2017) 92(6):707–17. doi: 10.1124/mol.117.110130

11. Bouley RA, Weinberg ZY, Waldschmidt HV, Yen YC, Larsen SD, Puthenveedu MA, et al. A new paroxetine-based GRK2 inhibitor reduces internalization of the μ-opioid receptor. *Mol Pharmacol* (2020) 97(6):392–401. doi: 10.1124/mol.119.118661

12. Kammala AK, Yang C, Panettieri RA, Das R, Subramanian H. G Protein-coupled receptor kinase 2 (GRK2) regulates T cell response in a murine model of house dust mite-induced asthma. *Front Allergy* (2021) 2:14. doi: 10.3389/falgy.2021.656886

13. DeFord-Watts LM, Young JA, Pitcher LA, van Oers NSC. The membrane-proximal portion of CD3 epsilon associates with the serine/threonine kinase GRK2. *J Biol Chem* (2007) 282(22):16126–34. doi: 10.1074/jbc.M609418200

14. Galli SJ, Tsai M. IgE and mast cells in allergic disease. *Nat Med* (2012) 18 (5):693–704. doi: 10.1038/nm.2755

15. Subramanian H, Gupta K, Parameswaran N, Ali H. Regulation of Fc∈RI signaling in mast cells by G protein-coupled receptor kinase 2 and its RH domain. *J Biol Chem* (2014) 289(30):20917–27. doi: 10.1074/jbc.M113.523969

16. McNeil BD, Pundir P, Meeker S, Han L, Undem BJ, Kulka M, et al. Identification of a mast-cell-specific receptor crucial for pseudo-allergic drug reactions. *Nature.* (2015) 519(7542):237–41. doi: 10.1038/nature14022

17. Motakis E, Guhl S, Ishizu Y, Itoh M, Kawaji H, de Hoon M, et al. Redefinition of the human mast cell transcriptome by deep-CAGE sequencing. *Blood.* (2014) 123(17):e58. doi: 10.1182/blood-2013-02-483792

18. Plum T, Wang X, Rettel M, Krijgsveld J, Feyerabend TB, Rodewald HR. Human mast cell proteome reveals unique lineage, putative functions, and structural basis for cell ablation. *Immunity.* (2020) 52(2):404–16.e5. doi: 10.1016/j.immuni.2020.01.012

19. Subramanian H, Gupta K, Guo Q, Price R, Ali H. Mas-related gene X2 (MrgX2) is a novel G protein-coupled receptor for the antimicrobial peptide LL-37 in human mast cells. *J Biol Chem* (2011) 286(52):44739–49. doi: 10.1074/jbc.M111.277152

20. Arifuzzaman M, Mobley YR, Choi HW, Bist P, Salinas CA, Brown ZD, et al. MRGPR-mediated activation of local mast cells clears cutaneous bacterial infection and protects against reinfection. *Sci Adv* (2019) 5(1):eaav0216. doi: 10.1126/sciadv.aav0216

21. Pundir P, Liu R, Vasavda C, Serhan N, Limjunyawong N, Yee R, et al. A connective tissue mast-Cell-Specific receptor detects bacterial quorum-sensing molecules and mediates antibacterial immunity. *Cell Host Microbe* (2019) 26 (1):114–22.e8. doi: 10.1016/j.chom.2019.06.003

22. Roy S, Chompunud Na Ayudhya C, Thapaliya M, Deepak V, Ali H. Multifaceted MRGPRX2: New insight into the role of mast cells in health and disease. *J Allergy Clin Immunol* (2021) 148(2):293–308. doi: 10.1016/j.jaci.2021.03.049

23. Navinés-Ferrer A, Serrano-Candelas E, Lafuente A, Muñoz-Cano R, Martín M, Gastaminza G. MRGPRX2-mediated mast cell response to drugs used in perioperative procedures and anaesthesia. *Sci Rep* (2018) 8(1):11628. doi: 10.1038/s41598-018-29965-8

24. McNeil BD. MRGPRX2 and adverse drug reactions. *Front Immunol* (2021) 12:676354. doi: 10.3389/fimmu.2021.676354

25. Wolf K, Kühn H, Boehm F, Gebhardt L, Glaudo M, Agelopoulos K, et al. A group of cationic amphiphilic drugs activates MRGPRX2 and induces scratching behavior in mice. *J Allergy Clin Immunol* (2021) 148(2):506–22.e8. doi: 10.1016/j.jaci.2020.12.655

26. Amponnawarat A, Chompunud Na Ayudhya C, Ali H. Murepavadin, a small molecule host defense peptide mimetic, activates mast cells *via* MRGPRX2 and MRGPRB2. *Front Immunol* (2021) 12:689410. doi: 10.3389/fimmu.2021.689410

27. Roy S, Gupta K, Ganguly A, Ali H. β-Arrestin2 expressed in mast cells regulates ciprofloxacin-induced pseudoallergy and IgE-mediated anaphylaxis. *J Allergy Clin Immunol* (2019) 144(2):603–6. doi: 10.1016/j.jaci.2019.04.024

28. Zhong H, Shlykov SG, Molina JG, Sanborn BM, Jacobson MA, Tilley SL, et al. Activation of murine lung mast cells by the adenosine A3 receptor. *J Immunol* (2003) 171(1):338–45. doi: 10.4049/jimmunol.171.1.338

29. Ko KI, Merlet JJ, DerGarabedian BP, Zhen H, Horiuchi Y, Hedberg ML, et al. NF-kB perturbation reveals unique immunomodulatory functions in Prx1+ fibroblasts that promote development of atopic dermatitis. *Sci Transl Med* (2022) 14(630):eabj0324. doi: 10.1126/scitranslmed.abj0324

30. Cao C, Kang HJ, Singh I, Chen H, Zhang C, Ye W, et al. Structure, function and pharmacology of human itch GPCRs. *Nature.* (2021) 600(7887):170–5. doi: 10.1038/s41586-021-04126-6

31. Yang F, Guo L, Li Y, Wang G, Wang J, Zhang C, et al. Structure, function and pharmacology of human itch receptor complexes. *Nature* (2021) 600 (7887):164–9. doi: 10.1038/s41586-021-04077-y

32. Oschatz C, Maas C, Lecher B, Jansen T, Björkqvist J, Tradler T, et al. Mast cells increase vascular permeability by heparin-initiated bradykinin formation in vivo. *Immunity.* (2011) 34(2):258–68. doi: 10.1016/j.immuni.2011.02.008

33. Foletto VS, Serafin MB, Bottega A, da Rosa TF, Machado C de S, Coelho SS, et al. Repositioning of fluoxetine and paroxetine: study of potential antibacterial activity and its combination with ciprofloxacin. *Med Chem Res* (2020) 29(3):556–63. doi: 10.1007/s00044-020-02507-6

34. Brown JM, Wilson TM, Metcalfe DD. The mast cell and allergic diseases: Role in pathogenesis and implications for therapy. *Clin Exp Allergy* (2008) 38(1):4–18. doi: 10.1111/j.1365-2222.2007.02886.x

35. Fajt ML, Gelhaus SL, Freeman B, Uvalle CE, Trudeau JB, Holguin F, et al. Prostaglandin D_2 pathway upregulation: relation to asthma severity, control, and TH2 inflammation. *J Allergy Clin Immunol* (2013) 131(6):1504–12. doi: 10.1016/j.jaci.2013.01.035

36. Kawakami T, Ando T, Kimura M, Wilson BS, Kawakami Y. Mast cells in atopic dermatitis. *Curr Opin Immunol* (2009) 21(6):666–78. doi: 10.1016/j.coi.2009.09.006

37. Schuerwegh AJ, De Clerck LS, De Schutter L, Bridts CH, Verbruggen A, Stevens WJ. Flow cytometric detection of type 1 (IL-2, IFN-gamma) and type 2 (IL-4, IL-5) cytokines in T-helper and T-suppressor/cytotoxic cells in rheumatoid arthritis, allergic asthma and atopic dermatitis. *Cytokine* (1999) 11(10):783–8. doi: 10.1006/cyto.1998.0483

38. Penela P, Murga C, Ribas C, Tutor AS, Peregrín S, Mayor F. Mechanisms of regulation of G protein-coupled receptor kinases (GRKs) and cardiovascular disease. *Cardiovasc Res* (2006) 69(1):46–56. doi: 10.1016/j.cardiores.2005.09.011

39. Zylicz Z, Krajnik M, van Sorge AA, Costantini M. Paroxetine in the treatment of severe non-dermatological pruritus: a randomized, controlled trial. *J Pain Symptom Manage* (2003) 26(6):1105–12. doi: 10.1016/j.jpainsymman.2003.05.004

40. Kraut RY. Treatment of pruritus in a palliative care patient with low-dose paroxetine: a case report. *J Med Case Rep* (2017) 11:280. doi: 10.1186/s13256-017-1437-6

41. Haque T, Ryan JJ. Selective serotonin reuptake inhibitors suppress mast cell function. *J Immunol* (2018) 200(Suppl 1):105.8–8.

42. Food and Drug Administration. Paxil® (Paroxetine hydrochloride) Prescribing Information. (2012). Available at: https://www.accessdata.fda.gov/drugsatfda_docs/label/2012/020031s067%2C020710s031.pdf (Accessed August 10, 2022).

43. Pyatilova P, Ashry T, Luo Y, He J, Bonnekoh H, Jiao Q, et al. The number of MRGPRX2-expressing cells is increased in skin lesions of patients with indolent systemic mastocytosis, but is not linked to symptom severity. *Front Immunol* (2022) 13:930945. doi: 10.3389/fimmu.2022.930945

44. Deepak V, Komarow HD, Alblaihess AA, Carter MC, Metcalfe DD, Ali H. Expression of MRGPRX2 in skin mast cells of patients with maculopapular cutaneous mastocytosis. *J Allergy Clin Immunol Pract* (2021) 9(10):3841–43.e1. doi: 10.1016/j.jaip.2021.05.042

45. Manorak W, Idahosa C, Gupta K, Roy S, Panettieri R, Ali H. Upregulation of mas-related G protein coupled receptor X2 in asthmatic lung mast cells and its activation by the novel neuropeptide hemokinin-1. *Respir Res* (2018) 19(1):1. doi: 10.1186/s12931-017-0698-3

46. Munoz-Bellido JL, Munoz-Criado S, Garcìa-Rodrìguez JA. Antimicrobial activity of psychotropic drugs: Selective serotonin reuptake inhibitors. *Int J Antimicrob Agents* (2000) 14(3):177–80. doi: 10.1016/S0924-8579(99)00154-5

47. Mandal A, Sinha C, Jena AK, Ghosh S, Samanta A. An investigation on *in vitro* and *in vivo* antimicrobial properties of the antidepressant: amitriptyline hydrochloride. *Braz J Microbiol* (2010) 41:635–42. doi: 10.1590/S1517-83822010000300014

48. Röhrl J, Yang D, Oppenheim JJ, Hehlgans T. Human β-defensin 2 and 3 and their mouse orthologs induce chemotaxis through interaction with CCR2. *J Immunol* (2010) 184(12):6688–94. doi: 10.4049/jimmunol.0903984

49. Niyonsaba F, Iwabuchi K, Someya A, Hirata M, Matsuda H, Ogawa H, et al. A cathelicidin family of human antibacterial peptide LL-37 induces mast cell chemotaxis. *Immunology* (2002) 106(1):20–6. doi: 10.1046/j.1365-2567.2002.01398.x

50. Gupta K, Subramanian H, Ali H. Modulation of host defense peptide-mediated human mast cell activation by LPS. *Innate Immun* (2016) 22(1):21–30. doi: 10.1177/1753425915610643

frontiers | Frontiers in Immunology

TYPE Original Research
PUBLISHED 06 October 2022
DOI 10.3389/fimmu.2022.1033794

OPEN ACCESS

EDITED BY
Ulrich Blank,
Institut National de la Santé et de la Recherche Médicale (INSERM), France

REVIEWED BY
Margarita Martin,
University of Barcelona, Spain
Wolfgang Bäumer,
Freie Universität Berlin, Germany

*CORRESPONDENCE
Hydar Ali
alih@upenn.edu

†These authors have contributed equally to this work and share first authorship

SPECIALTY SECTION
This article was submitted to Molecular Innate Immunity, a section of the journal Frontiers in Immunology

RECEIVED 31 August 2022
ACCEPTED 16 September 2022
PUBLISHED 06 October 2022

CITATION
Bawazir M, Amponnawarat A, Hui Y, Oskeritzian CA and Ali H (2022) Inhibition of MRGPRX2 but not FcεRI or MrgprB2-mediated mast cell degranulation by a small molecule inverse receptor agonist. *Front. Immunol.* 13:1033794. doi: 10.3389/fimmu.2022.1033794

Inhibition of MRGPRX2 but not FcεRI or MrgprB2-mediated mast cell degranulation by a small molecule inverse receptor agonist

Maram Bawazir[1,2†], Aetas Amponnawarat[1,3†], Yvonne Hui[4], Carole A. Oskeritzian[4] and Hydar Ali[1*]

[1]Department of Basic and Translational Sciences, School of Dental Medicine, University of Pennsylvania, Philadelphia, PA, United States, [2]Department of Oral Diagnostic Sciences, Faculty of Dentistry, King Abdulaziz University, Jeddah, Saudi Arabia, [3]Department of Family and Community Dentistry, Faculty of Dentistry, Chiang Mai University, Chiang Mai, Thailand, [4]Department of Pathology, Microbiology and Immunology, University of South Carolina School of Medicine, Columbia, SC, United States

Mas-related G protein-coupled receptor-X2 (MRGPRX2) expressed on mast cells (MCs) contributes to hypersensitivity reactions to cationic US-Food and Drug Administration (FDA) approved drugs such as the neuromuscular blocking agent, rocuronium. In addition, activation of MRGPRX2 by the neuropeptide substance P (SP) and the pro-adrenomedullin peptide (PAMP-12) is associated with a variety of cutaneous conditions such as neurogenic inflammation, pain, atopic dermatitis, urticaria, and itch. Thus, small molecules aimed at blocking MRGPRX2 constitute potential options for modulating IgE-independent MC-mediated disorders. Two inverse MRGPRX2 agonists, named C9 and C9-6, have recently been identified, which inhibit basal G protein activation and agonist-induced calcium mobilization in transfected HEK293 cells. Substance P serves as a balanced agonist for MRGPRX2 whereby it activates both G protein-mediated degranulation and β-arrestin-mediated receptor internalization. The purpose of this study was to determine if C9 blocks MRGPRX2's G protein and β-arrestin-mediated signaling and to determine its specificity. We found that C9, but not its inactive analog C7, inhibited degranulation in RBL-2H3 cells stably expressing MRGPRX2 in response to SP, PAMP-12 and rocuronium with an IC_{50} value of ~300 nM. C9 also inhibited degranulation as measured by cell surface expression of CD63, CD107a and β-hexosaminidase release in LAD2 cells and human skin-derived MCs in response to SP but not the anaphylatoxin, C3a or FcεRI-aggregation. Furthermore, C9 inhibited β-arrestin recruitment and MRGPRX2 internalization in response to SP and PAMP-12. We found that a G protein-coupling defective missense MRGPRX2 variant (V282M) displays constitutive activity for β-arrestin recruitment, and that this response was significantly inhibited by C9.

Rocuronium, SP and PAMP-12 caused degranulation in mouse peritoneal MCs and these responses were abolished in the absence of MrgprB2 or cells treated with pertussis toxin but C9 had no effect. These findings suggest that C9 could provide an important framework for developing novel therapeutic approaches for the treatment of IgE-independent MC-mediated drug hypersensitivity and cutaneous disorders.

KEYWORDS

mast cell (MC), MRGPRX2, PAMP-12, substance P, rocuronium, antagonist, MRGPRX2 antagonist

Introduction

Mast cells (MCs) are tissue-resident immune cells that arise from hematopoietic lineage and are found close to peripheral nerve endings and blood vessels beneath the surface epithelium (1, 2). Although MCs are critical for host defense against microbial infection, they are best known for their roles in allergic disorders such as food allergy and asthma (1). These reactions are initiated following the cross-linking of high-affinity IgE receptors (FcεRI) by allergens resulting in the release of histamine from secretory granules followed by newly synthesized mediators (3). Hypersensitivity reactions to Food and Drug Administration (FDA)-approved drugs such as neuromuscular blocking agents (NMBAs), fluoroquinolones, vancomycin, and radiographic contrast agents occur as a result of MC activation (1, 4). Since most patients with hypersensitivity reactions to NMBAs have not been previously exposed to the drug (5), an IgE-independent activation of MCs likely contributes to these reactions but the receptors involved remained a mystery until recently. In addition to FcεRI, a subtype of MCs found predominantly in connective tissues express Mas-related G protein-coupled receptor X2 (MRGPRX2; mouse counterpart MrgprB2). The seminal observation by McNeil et al. (6), that all cationic drugs including NMBAs that induce hypersensitivity reactions activate human and mouse MCs *via* MRGPRX2 and MrgprB2, respectively solved the mystery as to how these drugs could induce IgE-independent adverse reactions.

A unique feature of MRGPRX2 is that in addition to FDA-approved cationic drugs, it can be triggered by a wide range of endogenous agonists such as the neuropeptides substance P (SP), cortistatin, neuromedin, pro-adrenomedullin peptide (PAMP-12), eosinophil-derived major basic proteins and the host defense peptides (1, 7–10). Furthermore, MRGPRX2 has recently been implicated in the pathogenesis of mastocytosis (11), neurogenic inflammation (12), chronic urticaria (13), chronic prurigo (8), rosacea (14, 15), atopic dermatitis (16), and allergic contact dermatitis/itch (17). Thus, given the new and emerging role of MRGPRX2 on the pathogenesis of a variety of cutaneous conditions, the development of high-affinity receptor inhibitors may provide a novel approach for the modulation of these IgE-independent MC-mediated disorders (18).

Current strategies to modulate MRGPRX2 function involve direct inhibition of the receptor and its downstream signaling (10, 18, 19). It is noteworthy that although human MRGPRX2 and mouse MrgprB2 are activated by the same group of cationic ligands, there are important differences in the concentrations required to activate these receptors. Thus, EC_{50} value of SP towards MRGPRX2 is ~360-fold lower than that for MrgprB2. By contrast, the EC_{50} value of rocuronium for MRGPRX2 is ~12-fold higher than that for MrgprB2 (6, 20). This difference is attributed to the low amino acid sequence identity (~53%) between MRGPRX2 and MrgprB2 (21). Surprisingly, however, many of the small molecule inhibitors that attenuate MRGPRX2-mediated responses in human MCs *in vitro* also block MrgprB2-mediated responses *in vivo*. For example, it is generally accepted that the cathelicidin LL-37, which is elevated in the skin of rosacea patients, contributes to the disease through the activation of MCs *via* MRGPRX2 (14, 22). Callahan et al. (15), recently showed that osthole, a natural plant coumarin, inhibits LL-37-induced degranulation of human skin MCs *in vitro* and prevents LL-37-induced rosacea in mice. The authors

Abbreviations: BAT, basophil activation test; FcεRI, high-affinity immunoglobulin E receptor; FITC, fluorescein isothiocyanate; IgER-CL, IgE receptor cross-linking; GPCR, G Protein-coupled receptor; MCs, mast cells; MFI, mean fluorescent intensity; MrgprB2, Mas-related G protein-coupled receptor B2; MRGPRX2, Mas-related G protein-coupled receptor X2; NMBAs, neuromuscular blocking agents; PAMP-12, pro-adrenomedullin peptide-12; PE, phycoerythrin; PTx, Pertussis toxin; PMCs, peritoneal mast cells; RBL-2H3, rat basophilic leukemia-2H3 cells; RBL-MRGPRX2, RBL-2H3 stably expressing MRGPRX2; rhSCF, recombinant human stem cell factor; MAT, mast cell activation test; MW, molecular weight; SCF, stem cell factor; SP, substance P; TANGO assay, transcriptional activation following arrestin translocation assay; WT, wild-type.

proposed that osthole allosterically modulates MRGPRX2, and perhaps MrgprB2, to prevent LL-37-induced rosacea in mice. However, Roy et al. (14), showed that while MCs are required for LL-37-induced rosacea in mice, MrgprB2 does not fully mediate this response. In addition to MrpgrB2, mouse connective tissue MCs express transcripts for MrgprB1, MrgprB8, and MrgprB13 (23, 24). It is therefore possible that in addition to MrgprB2, one or more of these receptors contribute to rosacea-like inflammation in mice and that osthole prevents this response by modulating multiple receptors in mouse MCs. Thus, to develop specific small molecule inhibitors to modulate MRGPRX2-mediated disorders, it is first critical to identify compounds that selectively inhibit MRGPRX2 but not MrgprB2 or other receptor-mediated signaling and mediator release *in vitro*.

In 2019, Ogasawara et al. (19), of Japan Tobacco Inc. screened an in-house library consisting of ~12,000 commercially available compounds for their ability to inhibit SP-induced Ca^{2+} mobilization in HEK293 cells stably expressing MRGPRX2. The authors identified two compounds designated as compound 1 (MW 223.6) and compound 2 (MW 223.6) that inhibit MRGPRX2-mediated calcium (Ca^{2+}) mobilization and MC degranulation with an IC_{50} value of ~2 μM. However, for therapeutic utility, it is desirable to develop compounds that specifically block MRGPRX2 at concentrations lower than those reported for compounds 1 and 2. Recently, Cao et al. (25), utilized compounds 1 and 2 as templates to search the ZINC database (http://zinc15.docking.org) and performed two rounds of analog modeling in the ultra-large make-on-demand library. This led to the identification of two compounds, named C9 (MW 275) and C9-6 (MW 258) that serve as inverse agonists to inhibit MRGPRX2-mediated G protein activation and Ca^{2+} mobilization in transfected HEK293 cells without blocking responses to a number of other GPCRs (25). However, the possibility that these compounds inhibit MC degranulation in response to SP, PAMP-12, and rocuronium has not been determined. Also, their effects on MrgprB2 and IgE-mediated responses have not been determined.

In addition to G proteins, many MRGPRX2 agonists also cause β-arrestin recruitment to promote receptor internalization (26, 27). Furthermore, many naturally occurring missense MRGPRX2 variants have been identified that may contribute to the receptor's role in either protecting from or promoting MC-mediated disorders (1, 28, 29). In the present study, we first sought to determine the effects of C9 on MRGPRX2-mediated G protein activation, Ca^{2+} mobilization, degranulation, β-arrestin recruitment, and receptor internalization. We then asked whether it could modulate the constitutive activity of a missense variant of MRGPRX2. Finally, we sought to evaluate the specificity of C9 for MRGPRX2 by testing its ability to inhibit MrgprB2 and FcεRI-mediated degranulation in MCs. The data presented herein suggest that C9 could provide an important framework for developing novel and specific high-affinity small molecules to modulate MRGPRX2-mediated drug hypersensitivity and inflammatory disorders.

Materials and methods

Reagents

Cell culture reagents were purchased from Invitrogen (Carlsbad, CA); PAMP-12 from MedChem Express (Monmouth, NJ); Substance P from AnaSpec (Fremont, CA): Rocuronium from the Cayman chemical (Hayward, CA). Recombinant mouse interleukin-3 (IL-3), mouse stem cell factor (SCF), and recombinant human SCF (rhSCF) were obtained from Peprotech (Rocky Hill, NJ). Compounds C9 (2-sulfanyl-3-[(1,3-thiazol-2-yl)methyl]-3,4-dihydroquinazolin-4-one, MW 275), C9-6 (3-[furan-2-yl)methyl]-2-sulfanyl-3,4-dihydroquinazolin-4-one, MW. 258), and C7 (3-[2-(pyridin-2-yl)ethyl]-2-sulfanyl-3,4-dihydroquinazolin-4-one, MW 283), were obtained from Enamine LLC (Monmouth, NJ). P-nitrophenyl-N-acetyl-b-D-glucosamine (PNAG) and dimethyl sulfoxide (DMSO) were obtained from Sigma-Aldrich (St. Louis, MO). Fura-2 acetoxymethyl ester from Abcam (Cambridge, MA). Bright-Glo Luciferase was from Promega (Madison, WI). Lipofectamine™ 2000 transfection reagent from Invitrogen (Carlsbad, CA). PE anti-human MRGPRX2 antibody (Clone K125H4, Catalog 359004), FITC anti-human FcεRIα (Clone AER-37, Catalog 334608), purified anti-human FcεRIα (Clone AER-37, Catalog 334602), APC anti-human CD63 (Clone H5C6, Catalog 353008), and FITC anti-human CD107a (Clone H4A3, Catalog 328606) antibodies were from BioLegend (San Diego, CA). PE IgG2b Isotype control (Clone eB149/10H5, Catalog 12-4031-81) and FITC IgG Isotype control (Clone eBio299Arm, Catalog 11-4888-81) antibodies were from Invitrogen (Carlsbad, CA). Pertussis toxin (PTx) was obtained from List Biological Laboratories (Campbell, CA).

Mice

Mice were housed in pathogen-free conditions and autoclaved hardwood bedding. Mice aged from 8 to 10 weeks old, and both genders were used in all experiments. C57BL/6 mice were obtained from the Jackson Laboratory (Bar Harbor, ME, USA), and mice $MrgprB2^{-/-}$ mice were generated using CRISPR/Cas9 technology by CRISPR core of the University of Pennsylvania as previously described (30). Approval for the use of mice was obtained from the Institutional Animal Care and Use Committee at the University of Pennsylvania.

Cell line culture

RBL-2H3 cells stably expressing human MRGPRX2 (RBL-MRGPRX2) were cultured in Dulbecco's modified Eagle's medium (DMEM) supplemented with 10% FBS, L-glutamine (2 mM), penicillin (100 IU/ml), streptomycin (100 mg/ml) and 1 mg/ml G418 (31). HTLA cells and cells stably expressing MRGPRX2-Tango (HTLA-MRGPRX2) were cultured similarly to RBL-2H3 cells in addition to the presence of hygromycin B (200 µg/ml), puromycin (5 mg/ml), and G418 (500 µg/ml) (32, 33). Laboratory of Allergic Diseases 2 (LAD2) cells were provided by Dr. A. Kirshenbaum and Dr. D. Metcalfe (National Institute of Allergy and Infectious Diseases, National Institutes of Health, Bethesda, MD, USA). Cells were maintained in a complete StemPro-34 medium supplemented with L-glutamine (2 mM), penicillin (100 IU/ml), streptomycin (100 µg/ml), and 100 ng/ml recombinant human stem cell factor (rhSCF). Weekly hemidepletions using media containing rhSCF were carried out as described (34).

Mouse peritoneal mast cell isolation and culture

Cells were isolated from peritoneal lavages of WT and MrgprB2$^{-/-}$ mice and were cultured for 4–8 weeks in complete Roswell Park Memorial Institute 1640 Medium (RPMI 1640) containing 10% FCS, penicillin (100 IU/ml), streptomycin (100 mg/ml), recombinant mouse IL-3 (10 ng/ml) and SCF (30 ng/ml). Cells were used within 4–8 weeks (27, 35). All cell cultures were kept at a 37°C incubator with 5% CO_2. Suspension cells were used later in the experiments as peritoneal MCs (PMCs) and purity of the cultured cells was determined by flow cytometry using anti-mouse c-kit and FcεRI antibodies (20).

Human skin-derived mast cell isolation and culture

Surgical skin samples were obtained through the Cooperative Human Tissue Network of the National Cancer Institute, as approved by the University of South Carolina's Internal Review Board. Human skin MCs were collected and cultured from three individual donors, as described previously (20, 36). Briefly, subcutaneous fat was removed by blunt dissection, and the remaining tissue was chopped into 1- to 2-mm pieces before being digested for 2 h at 37°C with type 2 collagenase (1.5 mg/ml), hyaluronidase (0.7 mg/ml), and type 1 DNase (0.3 mg/ml) in HBSS. The dispersed cells were collected and resuspended in HBSS containing 1% FCS and 10 mM HEPES and filtered through a No. 80 mesh sieve. Cells were then resuspended in HBSS and layered over 75% Percoll in an HBSS cushion and centrifuged at 800×g at 37°C for 20 min. The interface between the buffer and Percoll was used to collect the nucleated cells. Percoll gradient-enriched cells were resuspended in a serum-free X-VIVO 15 medium containing rhSCF (100 ng/ml) at a concentration of 1×10^6 cells/ml. MCs were used after 6–10 weeks of culture, toluidine blue staining was utilized to confirm the purity of MCs was approximately 100%.

Degranulation measured by β-hexosaminidase release assay

RBL-MRGPRX2 cells (5×10^4 cells/well), LAD2 cells (1×10^4 cells/well), primary human skin-derived MCs (5×10^3 cells/well), and PMCs (1×10^4 cells/well) were seeded into a 96-well plate in a total volume of 50 µl HEPES buffer containing 0.1% bovine serum albumin (BSA). Cells were preincubated in the absence or presence of MRGPRX2 antagonist for 5 min followed by the addition of SP, PAMP-12, or rocuronium for 30 min at 37°C. To determine the total β-hexosaminidase, cells were lysed in 50 µl of 0.1% Triton X-100. Aliquots (20 µl) of supernatants were incubated with 20 µl of 1 mM p-nitrophenyl-N-acetyl-b-D-glucosamine (PNAG) at 37°C for 1 h (RBL-MRGPRX2 cells), and 1.5 h (LAD2, primary human skin-derived MCs, and PMCs). Finally, 250 µl of stop solution was added (0.1 M Na_2CO_3/0.1 M $NaHCO_3$) to stop the reaction. The absorbance was measured with a microplate reader at a wavelength of 405 nm using a Versamax microplate spectrophotometer (Molecular Devices, San Jose, CA). Percentage of β-hexosaminidase degranulation was calculated by dividing the β-hexosaminidase release in the sample by total β-hexosaminidase release (37).

Degranulation measured by the surface expression of CD107a and CD63

MC degranulation was also assessed by flow cytometric measurement of cell surface CD107a (Lysosomal-Associated Membrane Protein 1, LAMP-1) and CD63 (LAMP-3) following agonist stimulation (38–40). LAD2 cells and human skin-derived MCs (1×10^5 cells) were pre-incubated with compounds C9, C7, or vehicle control for 5 min at 37°C then stimulated with SP (0.3 µM), anti-human FcεRIα (Clone AER-37; 0.3 µg/ml) (41) or C3a (3 nM) for 5 min at 37°C. The cells were then immediately fixed with fixation buffer (Biolegend, Catalog 420801) for 15 min at room temperature. After washing with FACS buffer (PBS containing 2% fetal calf serum [FCS] and 0.02% sodium azide), non-specific binding was blocked with 1% BSA in PBS for 30 min at 4°C. Cells were exposed to FITC-conjugated anti-CD107a and APC-conjugated anti-CD63 antibodies for 30 min at 4°C. Cell surface expression of CD107a and CD63 were analyzed by a BD LSR II flow

cytometer (San Jose, CA) and FlowJo software version 10.7.2 (Tree Star Inc., Ashland, OR).

Calcium mobilization assay

RBL-MRGPRX2 cells (2×10^6 cells) were loaded with Fura-2 acetoxymethyl ester (1 μM) in HEPES buffer containing 0.1% BSA for 30 min in the dark at 37°C, followed by 15 min period for de-esterification in dark at room temperature. Cells were washed and resuspended in HEPES-buffered saline and Ca^{2+} mobilization was measured for the designated time. Calcium mobilization was determined by measuring the fluorescence ratio between dual excitation wavelengths of 340 and 380 nm, and an emission wavelength of 510 nm using a Hitachi F-2700 Fluorescence Spectrophotometer (29).

Generation of HTLA cells transiently expressing MRGPRX2 and V282M missense

Transient transfection of HTLA cells to express MRGPRX2 or its missense V282M variant was performed as described previously (29, 35). Briefly, HTLA cells (2×10^6 cells) were plated in a 6-well plate in a complete medium and incubated overnight at 37°C. Cells were transiently transfected the next day with 2 μg of MRGPRX2 or its variant V282M in Tango plasmids using Lipofectamine™ 2000 DNA transfection reagent, according to the manufacturer protocol. Cells were then incubated in an antibiotic-free medium (DMEM supplemented with 10% FBS and L-glutamine) overnight at 37°C with 5% CO_2 and used within 16-24 h after transfection.

Transcriptional activation following arrestin translocation (TANGO) assay

HTLA cells stably expressing MRGPRX2 (5×10^4 cells/well) were plated into a 96-well plate with an antibiotic-free medium and incubated for 6 h to allow cells' adherence at 37°C with 5% CO_2. Following 6 h of incubation, the medium was aspirated, and cells were incubated with C9 (1 or 10 μM) in an antibiotic-free medium for 5 min, followed by stimulation with MRGPRX2 agonist for an additional 16 h at 37°C with a 5% CO_2 incubator. After 16 h, the medium was aspirated and replaced with 100 μl of Bright-Glo solution (Promega). The relative luminescence unit was measured in a Thermo Labsystems Luminoskan Ascent 392 Microplate Luminometer (42). For HTLA cells transiently transfected with MRGPRX2 or its missense variant, V282M tango plasmid, cells treated with C9 (10 μM), C7 (10 μM), or non-treated control and assay were performed similarly (32).

MRGPRX2 internalization

RBL-MRGPRX2 or HTLA-MRGPRX2 cells ($0.5x10^6$ cells), and LAD2 cells ($0.3x10^6$ cells) were stimulated with SP, PAMP-12, and rocuronium in the presence and absence of C9. Cells were washed and suspended in FACS buffer (PBS containing 2% fetal calf serum [FCS] and 0.02% sodium azide) and incubated with the PE-conjugated anti-MRGPRX2 antibody for 30 min at 4°C in the dark. Cells were washed in FACS buffer, fixed in 1.5% paraformaldehyde and acquired using a BD LSR II flow cytometer (San Jose, CA) and analyzed with the FlowJo software version 10.8.1 (Tree Star Inc., Ashland, OR).

Statistical analysis

GraphPad PRISM software version 9.0.1 (San Diego, CSA) was used to perform the statistical analysis. Results were expressed as mean ± standard error of the mean (SEM) values. SEM values were derived from three independent experiments. Statistical significance was measured by t-test for single comparisons and one-way analysis of variance (ANOVA) or two-way ANOVA for multiple comparisons. A P-value ≤ 0.05 was considered to be significant.

Results

Compounds C9 and C9-6 inhibit substance P, PAMP-12, and rocuronium-induced degranulation and Ca^{2+} mobilization in RBL-2H3 cells stably expressing MRGPRX2

ZINC-3573 has been identified as a potent MRGPRX2 agonist (33). Using calcium mobilization as an assay in HEK293 cells stably expressing MRGPRX2, Cao et al. (25), showed that C9 and C9-6 inhibit ZINC-3573-induced responses with Ki values of 43 nM and 58 nM, respectively. C9 also inhibited ZINC3573-induced degranulation in a human MC line (LAD2 cells) endogenously expressing MRGPRX2 but with an IC_{50} value of >1 μM (25). However, an inactive analog of C9, known as C7, had no inhibitory activity on ZINC3573-induced responses in HEK293 cells or LAD2 cells. We first sought to determine the effects of C9, C9-6, and C7 on degranulation in response to two endogenously generated MRGPRX2 agonists (SP and PAMP-12) that contribute to a variety of MC-dependent disorders and an FDA-approved drug that is associated with hypersensitivity (rocuronium). For this, we preincubated RBL-2H3 cells stably expressing MRGPRX2 (RBL-MRGPRX2) with C9, C9-6, or C7 (10 μM, 5 min) and tested their effects on β-hexosaminidase release in response to SP (0.3 μM), PAMP-12 (0.3 μM) and rocuronium (1 mg/ml). As shown in

Figure 1A, C9 and C9-6 abolished degranulation in response to these agonists but C7 had no effect. For subsequent studies, we used C9 and the inactive analog C7, where appropriate.

To determine the minimal concentration of C9 required to cause significant inhibition of degranulation, we preincubated RBL-MRGPRX2 cells with different concentrations of C9 (0.01 μM – 10 μM, 5 min) and assessed β-hexosaminidase release in response to SP, PAMP-12, and rocuronium. C9 inhibited degranulation in response to all agonists tested in a dose-dependent manner with an IC_{50} value of ~0.3 μM (Figures 1B–D). Because Ca^{2+} mobilization is required for MC degranulation, we tested the effect of C9 on SP and PAMP-12-induced Ca^{2+} response in RBL-MRGPRX2 cells. For this, Fura-2-loaded cells were preincubated with C9 (10 μM, 5 min) and exposed to SP or PAMP-12 (0.3 μM) and Ca^{2+} mobilization was measured continuously for the next 10 min. We found that C9 caused substantial inhibition of the Ca^{2+} response to both agonists at all time points tested (Figures 1E, F).

C9 inhibits MRGPRX2-mediated degranulation in LAD2 cells and human skin MCs without affecting C3a receptor and FcεRI-mediated responses

LAD2 cell is a human MC line that endogenously expresses MRGPRX2 and C3a receptor (C3aR) and has been used extensively to GPCR function in MCs (35, 43, 44). We, therefore, sought to determine if C9 inhibits degranulation in response to MRGPRX2 agonists. As shown in Figure 2A, preincubation of LAD2 cells with C9, but not C7 (1 μM, 5 min), resulted in a substantial reduction of SP, PAMP-12, and rocuronium-induced degranulation as measured by β-hexosaminidase release. CD107a and CD63 are granule-associated proteins that undergo externalization during the degranulation (45). We found that both SP and the anaphylatoxin C3a, caused increased cell surface expression of CD107a and CD63, as measured by flow cytometry (Figures 2B, C). Furthermore, preincubation of LAD2 cells with C9 (1 μM, 5 min), but not C7, abolished the SP response. By contrast, C9 or C7 had no effect on C3a-induced cell surface expression of CD107a and CD63. Quantitative results are shown in Figures 2D, E.

To determine the biological relevance of the findings in LAD2 cells, we performed selected experiments with primary human skin-derived MCs obtained from three healthy donors. When the purity of cultured MCs reached ~100%, flow cytometry was used to determine MRGPRX2 and FcεRI expression (Figures 3A–C). Consistent with MRGPRX2 expression, skin MCs from donors 1 and 3 responded to SP for degranulation, as assessed by β-hexosaminidase release and this response was significantly inhibited by C9 (1 μM) (Figures 3D–F). Although MCs from all three donors expressed cell surface FcεRI, those from donors 1 and 2 responded to FcεRIα-aggregation for β-hexosaminidase

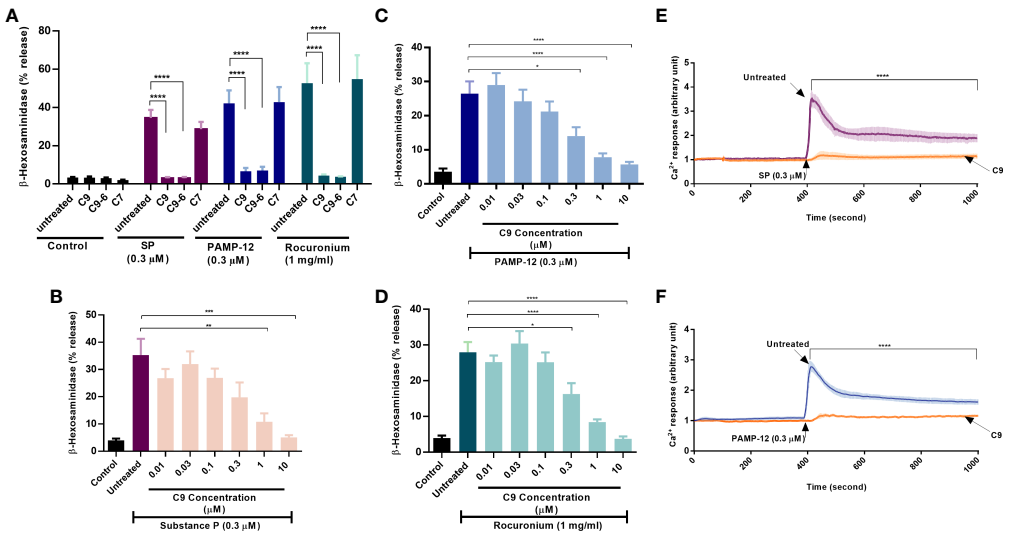

FIGURE 1
Compounds C9 and C9-6 inhibit substance P, PAMP-12, and rocuronium-induced degranulation and Ca^{2+} mobilization in RBL-2H3 cells stably expressing MRGPRX2. **(A)** RBL-MRGPRX2 cells were preincubated with C9, C9-6, or C7 (10 μM, 5 min) before exposure to indicated concentrations of agonists for 30 min, and the degranulation was determined by quantitating β-hexosaminidase release. **(B, C, D)** RBL-MRGPRX2 cells were preincubated with different concentrations of C9 (5 min) followed by agonist stimulation and β-hexosaminidase release was measured. **(E,F)** Cells were preincubated with C9 (DMSO for control) and Ca^{2+} mobilization was determined following stimulation with SP or PAMP-12 (0.3 μM, 10 min). Data are the mean ± SEM of at least three experiments. Statistical significance was determined using one-way ANOVA test at a value $^*P < 0.05$, $^{**}P < 0.01$, $^{***}P < 0.001$ and $^{****}P < 0.0001$.

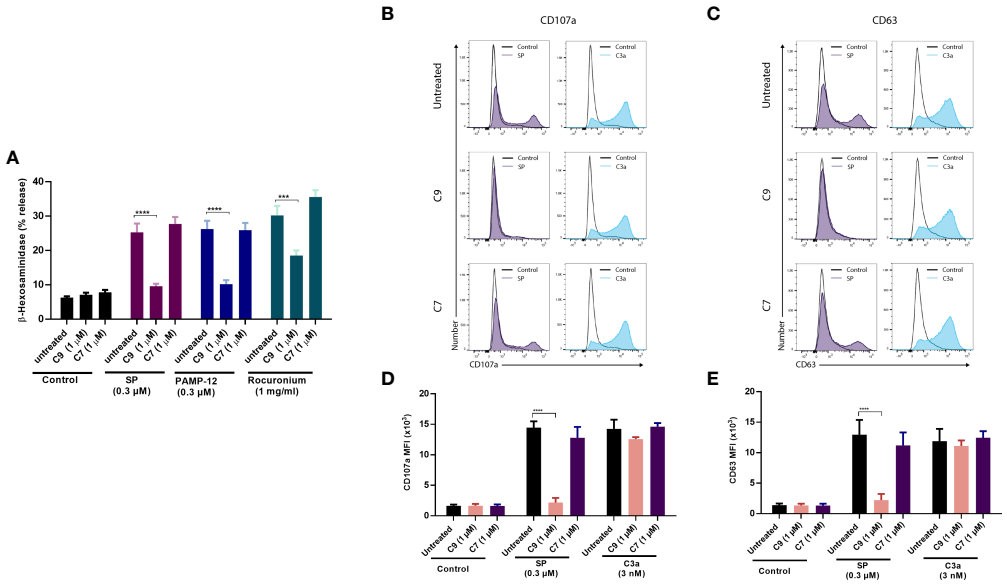

FIGURE 2
C9 inhibits MRGPRX2-mediated MC degranulation in LAD2 cells without affecting the C3aR response. **(A)** LAD2 cells were preincubated with C9 and inactive analog C7 (1 μM, for 5 min) then exposed to agonists at the indicated concentrations, and degranulation was assayed by measuring the release of β-hexosaminidase. **(B, C)** Cells were stimulated with SP (0.3 μM) or C3a (3 nM) for 5 min in the presence or absence of C9 or C7. Cell surface expression of CD107a and CD63 were determined by flow cytometry. Representative histograms of three independent experiments are shown. **(D, E)** The mean fluorescent intensity (MFI) levels of CD107a and CD63 are shown. Data are expressed as mean ± SEM. Statistical significance was determined by two-way ANOVA test at a value ***$P < 0.001$ and ****$P < 0.0001$.

release but this response was resistant to inhibition by C9 (Figures 3D–F). To further validate the specificity of C9, we tested its ability to inhibit cell surface CD107a and CD63 expression in response to SP and FcεRIα-aggregation. In agreement with the β-hexosaminidase release, SP (donor 1 and donor 3) and FcεRIα-aggregation (donor 1 and donor 2) induced significant upregulation of cell surface CD107a and CD63 (Figures 4A–C). C9 significantly blocked SP, but not FcεRIα-aggregation responses (Figures 4A–C). The quantification of flow cytometry data is shown in Figures 4D–F. Together, these findings demonstrate that C9 specifically inhibits MRGPRX2-mediated MC degranulation without affecting the responses to C3a or FcεRIα-aggregation.

Pre-incubation of RBL-MRGPRX2 cells with C9 is not required for its ability to inhibit MRGPRX2-mediated Ca^{2+} mobilization and degranulation

For experiments described above, cells were preincubated with C9 for 5 min before exposure to stimulants. We next sought to determine if C9 could reverse an ongoing MRGPRX2-mediated response using Ca^{2+} mobilization as an assay in RBL-MRGPRX2 cells. As shown in Figure 5A, when C9 was added 100 sec after stimulation with SP, it caused an immediate and significant reduction of the response for the entire duration of the experiment when compared to C7 control. Our next goal was to determine the effect of C9 on ongoing degranulation in response to SP. For this, we first assessed the time-course (1 to 30 min) of SP-induced β-hexosaminidase release. As shown in Figure 5B, SP caused half-maximal degranulation at 2.5 min after stimulation and the reaction reached a maximal value at 15 min after stimulation. Next, for one set of experiments, we stopped the reaction at 2.5 min after stimulation with SP. For the second set, we added C9 at 2.5 min after SP stimulation and allowed degranulation to proceed until 15 min. As shown in Figure 5C, there was no significant difference in SP-induced degranulation at 2.5 min without C9 when compared to the response at 15 min after the addition of C9 at 2.5 min. These findings clearly demonstrate that C9 is able to stop an ongoing Ca^{2+} mobilization and degranulation in response to SP.

C9 inhibits MRGPRX2-mediated β-arrestin recruitment and receptor internalization

Using transcriptional activation following arrestin translocation (TANGO) assay in HTLA cells stably expressing

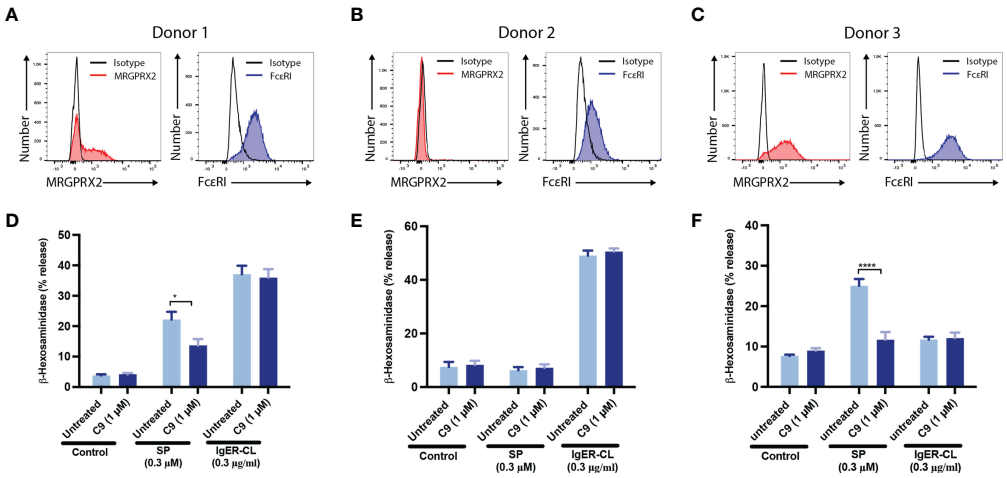

FIGURE 3
C9 inhibits MRGPRX2-mediated degranulation in human skin-derived MCs without affecting the FcεRI response. **(A-C)** Flow cytometry histograms demonstrating MRGPRX2 and FcεRI expression of cultured human skin-derived MCs from 3 healthy donors are shown. **(D-F)** Cells were preincubated with C9 (1 μM, 5 min) and exposed to SP (0.3 μM) or FcεRIα-aggregation antibody, IgER-CL (IgE receptor cross-linking) (0.3 μg/ml) and β-hexosaminidase release was determined. Data are expressed as mean ± SEM. Statistical significance was determined by two-way ANOVA test at a value $*P < 0.05$, and $****P < 0.0001$.

MRGPRX2 (HTLA-MRGPRX2), we previously showed that SP causes β-arrestin translocation and that this is associated with receptor internalization (27, 33). However, the possibility that PAMP-12 causes β-arrestin signaling has not been determined. Thus, we first tested the ability of all 3 agonists to cause β-arrestin translocation using the TANGO assay. Cells were exposed to either buffer (control) or agonists for 16 h and β-arrestin-mediated gene expression (indicative of β-arrestin recruitment) was measured. As per previous report, we found that SP induced substantial β-arrestin recruitment, and that PAMP-12 also induced a similar response (Figure 6A). Lansu et al. (33), reported that rocuronium at a concentration of 100 μM does not induce TANGO in HTLA-MRGPRX2 cells. However, we found that rocuronium at a concentration of 300 μM induces a significant β-arrestin signal, which was similar in magnitude to that induced by SP and PAMP-12 (Figure 6A). To determine if C9 inhibits β-arrestin recruitment, we preincubated HTLA-MRGPRX2 cells with different concentrations of the antagonist and quantitated using the TANGO assay. We found that C9 at a concentration of 1 μM caused significant inhibition of response to all three agonists (Figure 6A).

To determine the effect of C9 on receptor internalization, HTLA-MRGPRX2 cells, RBL-MRGPRX2 cells, and LAD2 cells were preincubated with C9, then exposed to SP, PAMP-12, and rocuronium, and receptor internalization was assessed by determining loss of cell surface receptor expression by flow cytometry. In all three cell types, SP and PAMP-12 caused MRGPRX2 internalization and C9 inhibited this response but the magnitude of inhibition was greater in RBL cells when compared to HTLA, or LAD2 cells (Figures 6B–D). Interestingly, although rocuronium induced substantial β-arrestin recruitment, this was not associated with MRGPRX2 internalization in HTLA, RBL, or LAD2 cells (Figures 6A–D).

Constitutive β-arrestin recruitment in response to a naturally occurring missense MRGPRX2 variant is inhibited by C9

We recently identified a naturally occurring MRGPRX2 missense variant (V282M) that displays a loss of function phenotype for G protein-mediated degranulation (29, 35). We found that transient transfection of HTLA cells resulted in a similar level of cell surface expression of the V282M variant when compared to the wild-type receptor (Figure 7A). Surprisingly, however, expression of V282M is associated with constitutive recruitment of β-arrestin in the absence of agonist stimulation. Interestingly, this response was significantly inhibited by C9 but not by its inactive analog, C7 (Figure 7B).

C9 does not inhibit MrgprB2-mediated degranulation in mouse peritoneal MCs

Although MRGPRX2 and MrgprB2 share the same agonists there are important differences in the concentrations of SP and rocuronium required to activate these receptors (6). Consistent with previous reports, we found that SP at 100 μM induced only a small and variable degranulation, as measured by β-

10.3389/fimmu.2022.1033794

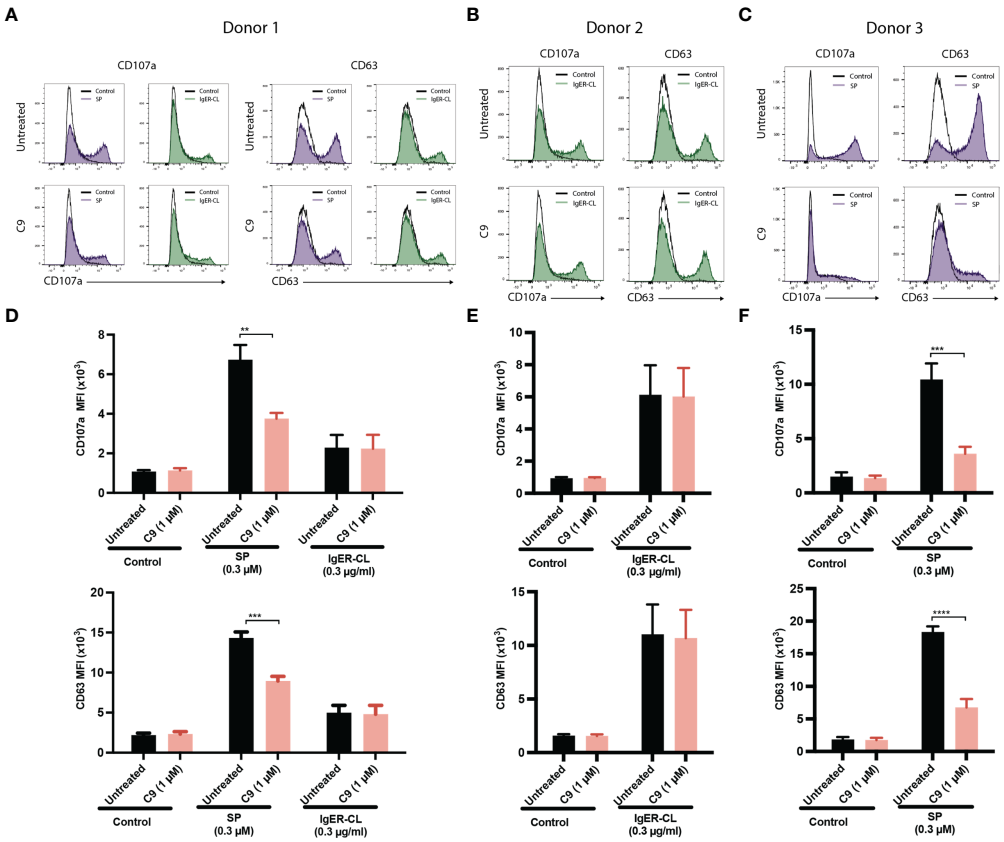

FIGURE 4
C9 inhibits the upregulation of cell surface expression of CD107a and CD63 in response to SP in human skin-derived MCs. **(A-C)** Cells from three donors were preincubated with buffer or C9 (1 μM, 5 min), stimulated with SP (0.3 μM) or FcεRIα-aggregation antibody, IgER-CL (0.3 μg/ml) for an additional 5 min and cell surface expression of CD107a and CD63 was determined by flow cytometry. Representative histograms of CD107a and CD63 expression are shown. **(D–F)** The mean fluorescent intensity (MFI) levels of CD107a and CD63 are shown. Data are expressed as mean ± SEM. Statistical significance was determined by two-way ANOVA test at a value $^{**}P < 0.01$, $^{***}P < 0.001$, and $^{****}P < 0.0001$.

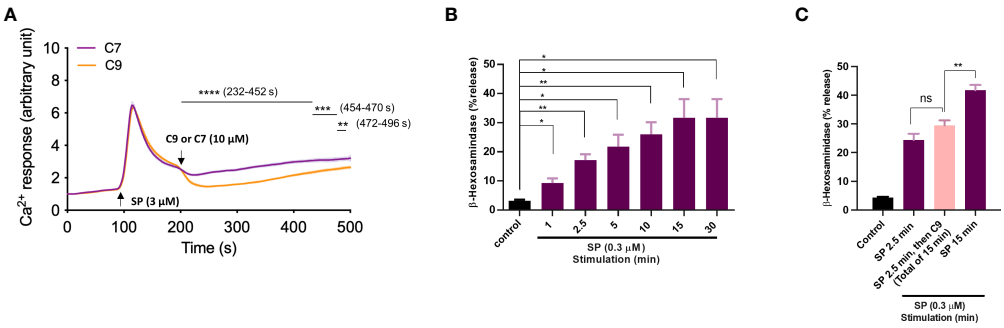

FIGURE 5
Pre-incubation of cells with C9 is not required for its ability to inhibit MRGPRX2-mediated Ca^{2+} mobilization and degranulation. **(A)** Ca^{2+} mobilization measurement of Fura-2 loaded RBL-MRGPRX2 cells following stimulation with SP (3 μM). As the response approached the plateau phase, the C9 or C7 (10 μM) was introduced and the response was measured for an additional 5 min. **(B)** RBL-MRGPRX2 cells were exposed to SP (0.3 μM) and the time-course of degranulation was assayed by measuring the release of β-hexosaminidase. **(C)** Cells were exposed to SP (0.3 μM) and degranulation was quantitated after 2.5 min (left, purple) or 15 min (right purple). Alternatively, cells were stimulated with SP for 2.5 min and then exposed to C9 (10 μM) for an extra 12.5 min (total of 15 min), and β-hexosaminidase release was determined (middle, pink). Data are expressed as mean ± SEM. Statistical significance was determined by unpaired *t*-test for single comparison and one-way ANOVA for multiple comparisons at a value $^{*}P < 0.05$, $^{**}P < 0.01$, $^{***}P < 0.001$, $^{****}P < 0.0001$, and ns denotes "not significant".

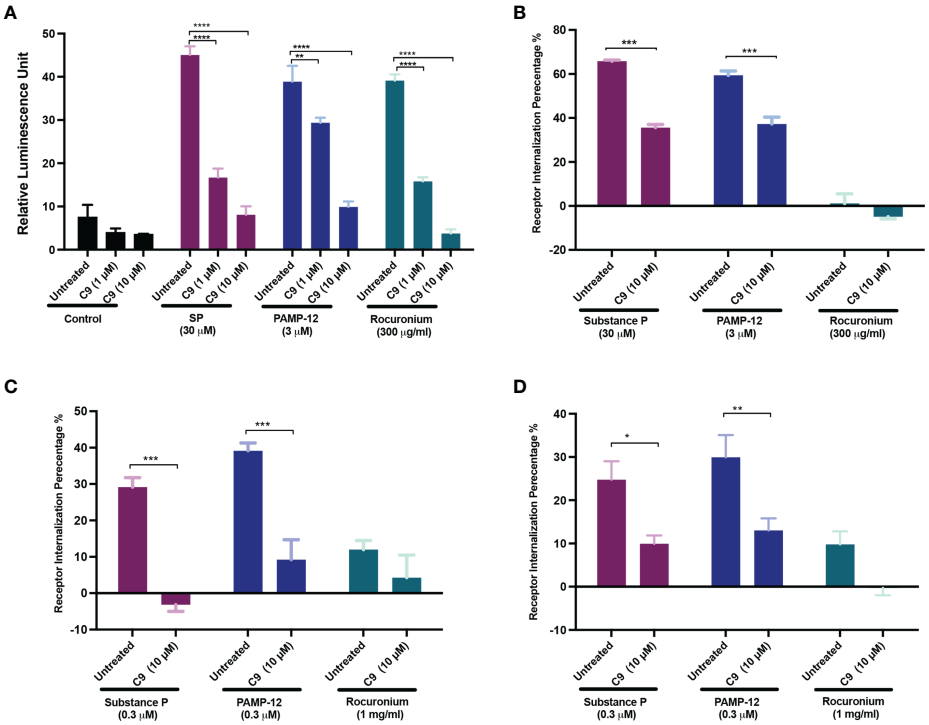

FIGURE 6
C9 inhibits MRGPRX2-mediated β-arrestin recruitment and receptor internalization. **(A)** HTLA-MRGPRX2 cells were preincubated with C9 (1 μM and 10 μM, 5 min) and then exposed to SP, PAMP-12, or rocuronium for 16h The medium was removed and substituted with the Bright-Glo solution (100 μl/well) in a 96-well plate. β-arrestin translocation-mediated gene expression was quantitated as a relative luminescence unit. **(B-D)** Quantitative analysis of receptor internalization in **(B)** HTLA-MRGPRX2, **(C)** RBL-MRGPRX2, and **(D)** LAD2 cells. Cells were preincubated with C9 (10 μM, 5 min), exposed to buffer or MRGPRX2 agonists (30 min) and cell surface receptor expression was determined by flow cytometry. The percentage of receptor internalization was calculated using a mean fluorescent intensity (MFI) in comparison to the untreated or vehicle controls. Data are expressed as mean ± SEM. Statistical significance was determined by two-way ANOVA test at a value $*P < 0.05$, $**P < 0.01$, $***P < 0.001$, and $****P < 0.0001$.

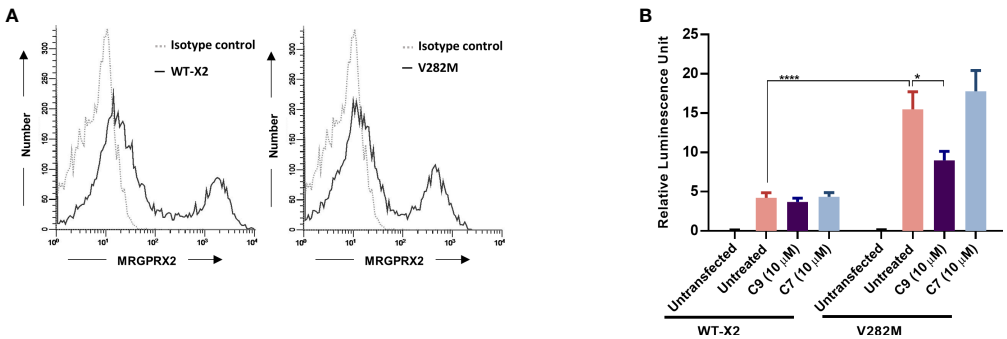

FIGURE 7
Constitutive β-arrestin recruitment in response to a naturally occurring missense MRGPRX2 variant is inhibited by C9. **(A)** HTLA cells transiently expressing MRGPRX2 (WT-X2) and its variant V282M were incubated with PE-conjugated anti-MRGPRX2 antibody or isotype controls and the cell surface receptor expression was determined by flow cytometry. **(B)** Cells were exposed to C9 (10 μM) or C7 (10 μM) without any agonist stimulation. After 16 h, the medium was removed and substituted with Bright-Glo solution (100 μl/well) in a 96-well plate. β-arrestin gene translocation-mediated gene expression was measured in a relative luminescence unit. Data are expressed as mean ± SEM. Statistical significance was determined by two-way ANOVA test at a value $*P < 0.05$ and $****P < 0.0001$.

hexosaminidase release, but rocuronium at 20 μg/ml caused a substantial response in mouse PMCs (Figure 8A) (20). We first validated that degranulation in response to SP, PAMP-12, and rocuronium is mediated *via* MrgprB2 by demonstrating that PMCs cultured from MrgprB2$^{-/-}$ mice do not respond to these agonists (Figure 8A). Although inhibition of Gαi proteins by pertussis toxin (PTx) leads to almost complete inhibition of MRGPRX2-mediated degranulation in human CD34^{+} cell-derived MCs (19), its effect on MrgprB2-mediated degranulation is unknown. We therefore preincubated PMCs from WT mice with pertussis toxin (PTx; 100 ng/ml for 16 h) and tested the ability of SP, PAMP-12, and rocuronium to induce degranulation. The result presented in Figure 8B shows that PTx-pretreatment almost completely blocked β-hexosaminidase release in response to all three agonists, suggesting that, similar to MRGPRX2, MrgprB2-mediated response is mediated by Gαi. Next, we tested the ability of C9 (10 μM) to inhibit MrgprB2-mediated degranulation in PMCs generated from WT mice. Because SP induces a small and variable response, we utilized PAMP-12 and rocuronium for this set of experiments. Interestingly, we found that C9 was unable to inhibit MrgprB2-mediated β-hexosaminidase release (Figure 8C). The results from these studies demonstrate that similar to MRGPRX2 in human MCs, PAMP-12 and rocuronium couple to MrgprB2 and Gαi proteins but C9 is highly specific to human receptor MRGPRX2.

Discussion

It is well documented that IgE-mediated MC activation participates in food allergy, anaphylaxis, and asthma. However, there has been an explosion in interest in the role of non-IgE-mediated MC activation, in particular MRGPRX2, on drug-induced hypersensitivity and a variety of cutaneous disorders. Cao et al. (25), recently identified C9, as a small molecule inverse agonist of MRGPRX2, which inhibits basal G protein activation and blocks ZINC-3573-induced calcium mobilization in transfected HEK293 cells. In the present study, we utilized transfected cell lines (RBL and HTLA), a human MC line endogenously expressing MRGRPX2 (LAD2), primary human skin-derived MCs, and mouse peritoneal MCs derived from WT and MrgprB2$^{-/-}$ mice to show that C9 specifically inhibits MRGPRX2-mediated degranulation without affecting responses to FcεRI or MrgprB2.

Cao et al. (25), showed that C9 inhibits ZINC-3573-induced Ca^{2+} mobilization in transfected HEK293 cells with a Ki value 43 nM. However, C9 at 1 μM inhibited ZINC-3573-induced degranulation in LAD2 cells by <50% and required >10 μM for almost complete inhibition of degranulation. The reason for this difference is not clear but could reflect the agonist and cell types used. Our studies focused on three MRGPRX2 agonists that are implicated in a variety of cutaneous conditions and drug-induced hypersensitivity. However, unlike the situation with ZINC-3573 (25), C9 inhibited degranulation in response to SP, PAMP-12 and rocuronium with an IC_{50} value of ~300 nM and 1 μM of the compound caused substantial inhibition of the response. Cryo-EM structure of MRGPRX2 with a number of agonists has recently been resolved (25, 46). MRGPRX2 has two binding pockets, one with the negative charge and the other with hydrophobic residues (25). The neuropeptide cortistatin utilizes both pockets for binding whereas the synthetic small molecule MRGPRX2 agonist ZINC-3573 binds only to one pocket. Whether this difference reflects the high concentration of C9 required to inhibit degranulation induced by ZINC-3573 in LAD2 cells remains to be determined (25).

Since the description of CD63 as a surface degranulation marker, a flow cytometry-based assay known as basophil activation test (BAT) was developed and has been reliably used for the diagnosis of IgE-mediated allergic responses (47). As LAD2 cells and human peripheral CD34^{+} cell-derived MCs express MRGPRX2, a flow cytometric assay, known as MC activation test (MAT) that quantitates cell surface expression of CD63 and CD107a has been developed, which could be used to test MRGPRX2 activation by sera of patients undergoing drug hypersensitivity reactions (45, 48). Navines-Ferrer et al. (49), recently utilized CD63 upregulation as a measure of MC degranulation by sera obtained from healthy controls and patients who had experienced an anaphylactoid reaction due to drug administration. It was demonstrated that sera from patients who had undergone anaphylactoid reactions induced an upregulation of CD63 expression on LAD2 cells and that this response was reduced in MRGPRX2-silenced cells. Based on these findings, it was concluded that MRGPRX2 is a candidate for mediating hypersensitivity reactions. In the present study, we utilized MAT to show that while SP and C3a caused MC degranulation, C9 at 1 μM selectively blocked SP-induced response. In primary human skin-derived MCs, both SP and FcεRI-aggregation caused increased expression of CD63 and CD107a but C9 blocked the response to SP, but not FcεRI-aggregation. These findings suggest that C9 could be utilized as a novel diagnostic tool to determine the role of MRGPRX2 not only in drug-induced hypersensitivity but also in other MC-mediated disorders.

Sugammadex is a modified γ-cyclodextrin that reverses neuromuscular blockade by encapsulating rocuronium and atracurium and removing it from the neuromuscular junction. Coincubation of atracurium with sugammadex, in molar excess, inhibits atracurium and rocuronium-induced MRGPRX2-mediated MC activation (50, 51). However, given that sugammadex does not stop atracurium-induced MC degranulation, once initiated, it is unlikely to be useful in patients with ongoing atracurium or rocuronium-mediated perioperative anaphylaxis (51–53). We have shown that preincubation of RBL-MRGPRX2 cells with C9 is not required for its ability to block SP-induced Ca^{2+} mobilization and degranulation. Thus, when cells were exposed to SP for Ca^{2+}

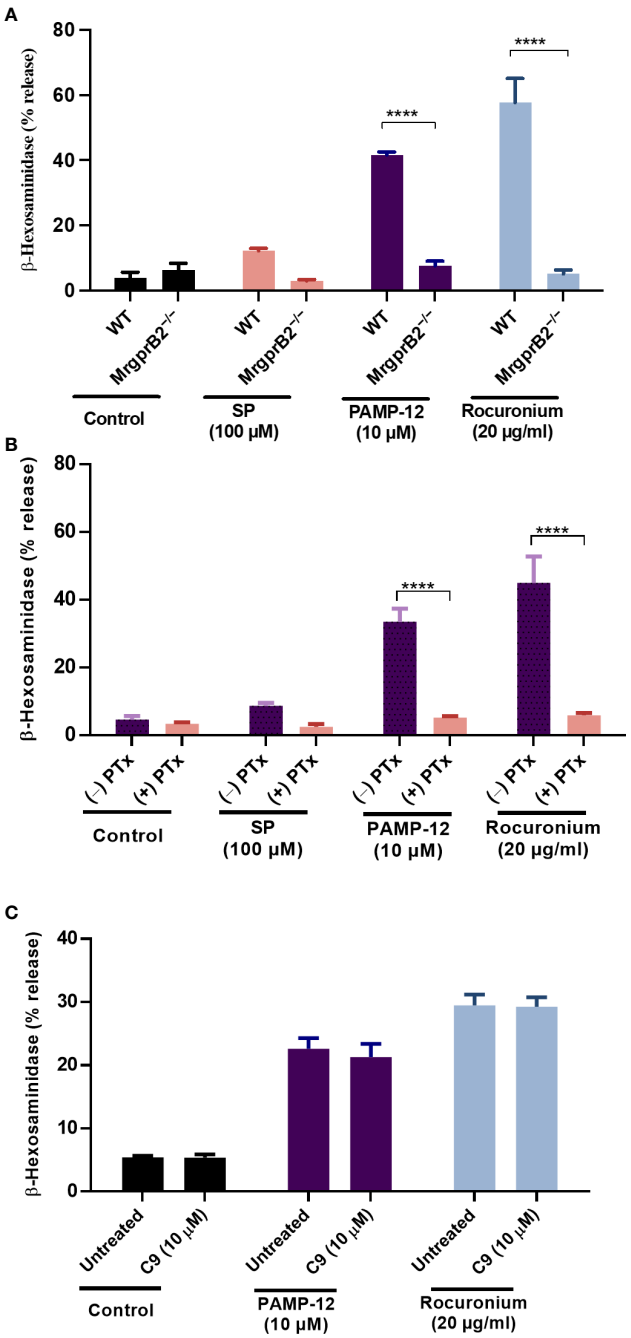

FIGURE 8
C9 does not inhibit MrgprB2-mediated degranulation in mouse peritoneal MCs. **(A)** Wild type (WT) and MrgprB2$^{-/-}$ peritoneal-derived MCs (PMCs) were exposed to SP (100 μM), PAMP-12 (10 μM), and rocuronium (20 μg/ml) for 30 min and β-hexosaminidase release was measured. **(B)** WT-PMCs were cultured in the absence or presence of PTx (100 ng/mL, 16 h), exposed to SP, PAMP-12, or rocuronium for 30 min, and β-hexosaminidase release was determined. **(C)** WT-PMCs were preincubated with C9 (10 μM, 5 min), stimulated with PAMP-12 or rocuronium and β-hexosaminidase release was measured. All data points are the mean ± SEM of at least three experiments performed in triplicate. Statistical significance was determined by two-way ANOVA test at a value ****$P < 0.0001$.

mobilization, the response was reversed almost immediately after C9 was added. Similarly, ongoing degranulation was also halted immediately after the addition of C9. These findings have clinical implications for the potential utilization of C9 or its derivatives for targeting MRGPRX2-mediated drug hypersensitivity and inflammatory disorders. Thus, it will be interesting to see if prophylactic administration of C9 or a similar drug before surgical procedures lowers overall perioperative patient

mortality. Given that SP and PAMP-12 are implicated in urticaria, atopic dermatitis, and allergic contact dermatitis, it should be possible to utilize C9 or small molecules based on this compound for topical application to treat these conditions.

In addition to G protein, SP also couples to β-arrestin-mediated signaling to promote receptor internalization (27). We found that PAMP-12 also induced β-arrestin recruitment and receptor internalization. Interestingly, C9 inhibited both SP and PAMP-induced β-arrestin recruitment in HTLA cells. C9 also blocked SP and PAMP-12-induced MRGPRX2 internalization but the magnitude of the inhibition was dependent on whether the experiment was performed in transfected RBL-2H3 cells, HTLA cells, or LAD2 cells which endogenously express MRGPRX2. Rocuronium caused robust β-arrestin recruitment, which was inhibited by C9. However, rocuronium induced minimal MRGPRX2 internalization in transfected RBL-2H3 and HTLA cells as well as LAD2 cells. This suggests that depending on the ligand used, β-arrestin recruitment could be dissociated from receptor internalization. Despite this difference, it is clear that C9 inhibits both G protein and β-arrestin-dependent signaling. From a mechanistic standpoint, Cao et al. (25), showed that C9 inhibits basal recruitment of Gαq by MRGPRX2, thus exhibiting inverse agonist activity. Our finding that C9 also causes significant inhibition of constitutive β-arrestin recruitment by the missense MRGPRX2 variant V282M, supports the notion that it serves as an inverse agonist. However, the original compounds (compound 1 and 2) from which C9 was derived inhibit SP binding to MRGPRX2 and block GTP-γS binding activities of a Gα protein (19). Based on these findings, it was proposed that they serve as competitive antagonists of MRPGRX2. Additional studies will be required to determine the exact mechanism *via* which compound 1, 2 and C9 inhibit MRGPRX2-mediated responses in MCs.

In summary, we have shown that C9 is a potent and selective inhibitor of MRGPRX2-mediated MC degranulation using three different assays; cell surface expression of CD63, CD107a and β-hexosaminidase release. MRGPRX2 is highly polymorphic and most of the missense mutants remain uncharacterized (1). We have shown that the V282M missense mutation, which displays a loss of function phenotype for G protein activation and MC degranulation, promotes constitutive activity for β-arrestin recruitment and that C9 inhibits this response. It is possible that certain individuals display a gain of function phenotype for degranulation contributing to MRGPRX2-mediated disorders. It should be feasible to generate MCs from the peripheral blood of these individuals and determine if C9 inhibits constitutive activity. Elevated expression of MRGPRX2 has been reported in skin MCs of patients with allergic contact dermatitis, chronic spontaneous urticaria, rosacea, and mastocytosis (11, 13, 14, 54). Beyond the skin, MRGPRX2-expressing MCs are increased in the gingiva of patients with chronic periodontitis, and lung MCs of individuals who died from asthma (55, 56). Thus, there is tremendous therapeutic potential for utilizing small molecule MRGPRX2 blockers to modulate a variety of MC-mediated disorders. Compound C9 could be the starting point for developing such therapeutics but bioavailability, stability, toxicity, and its possible off-target effects need to be determined. Furthermore, given that C9 does not modulate MrgprB2-mediated MC degranulation, preclinical studies will require humanized mice or transgenic mice that express MRGPRX2 in MCs.

Data availability statement

The raw data supporting the conclusions of this article will be made available by the authors, without undue reservation.

Author contributions

HA contributed to the conception and supervision. HA and CO contributed to funding acquisition of the study. MB and AA performed the experiments and analyzed the data. YH and CO provided human skin MCs for the study. MB, AA, and HA wrote the first draft of the manuscript. All authors contributed to the article and approved the submitted version.

Funding

This work was supported by grants R01-AI143185, R01-AI149487, and R01-AI124182 to HA; and R21-AR067996 and P20 GM-103641 to CO.

Acknowledgments

We thank the FACS core facility of the University of Pennsylvania School of Dental Medicine for flow cytometry acquisition and analysis.

Conflict of interest

The authors declare that the research was conducted in the absence of any commercial or financial relationships that could be construed as a potential conflict of interest.

Publisher's note

References

1. Roy S, Chompunud Na Ayudhya C, Thapaliya M, Deepak V, Ali H. Multifaceted MRGPRX2: New insight into the role of mast cells in health and disease. *J Allergy Clin Immunol* (2021) 148(2):293–308. doi: 10.1016/j.jaci.2021.03.049

2. Varricchi G, Pecoraro A, Loffredo S, Poto R, Rivellese F, Genovese A, et al. Heterogeneity of human mast cells with respect to MRGPRX2 receptor expression and function. *Front Cell Neurosci* (2019) 13:299. doi: 10.3389/fncel.2019.00299

3. Ali H. Regulation of human mast cell and basophil function by anaphylatoxins C3a and C5a. *Immunol Lett* (2010) 128(1):36–45. doi: 10.1016/j.imlet.2009.10.007

4. McNeil BD. MRGPRX2 and adverse drug reactions. *Front Immunol* (2021) 12:676354. doi: 10.3389/fimmu.2021.676354

5. Fisher MM, Munro I. Life-threatening anaphylactoid reactions to muscle relaxants. *Anesth Analg* (1983) 62(6):559–64. doi: 10.1213/00000539-198306000-00003

6. McNeil BD, Pundir P, Meeker S, Han L, Undem BJ, Kulka M, et al. Identification of a mast-cell-specific receptor crucial for pseudo-allergic drug reactions. *Nature* (2015) 519(7542):237–41. doi: 10.1038/nature14022

7. Tatemoto K, Nozaki Y, Tsuda R, Konno S, Tomura K, Furuno M, et al. Immunoglobulin e-independent activation of mast cell is mediated by mrg receptors. *Biochem Biophys Res Commun* (2006) 349(4):1322–8. doi: 10.1016/j.bbrc.2006.08.177

8. Kolkhir P, Pyatilova P, Ashry T, Jiao Q, Abad-Perez AT, Altrichter S, et al. Mast cells, cortistatin, and its receptor, MRGPRX2, are linked to the pathogenesis of chronic prurigo. *J Allergy Clin Immunol* (2022) 149(6):1998–2009 e5. doi: 10.1016/j.jaci.2022.02.021

9. Matsuo Y, Yanase Y, Irifuku R, Takahagi S, Mihara S, Ishii K, et al. Neuromedin U directly induces degranulation of skin mast cells, presumably *via* MRGPRX2. *Allergy* (2018) 73 (11):2256–60. doi: 10.1111/all.13555

10. Ogasawara H, Furuno M, Edamura K, Noguchi M. Peptides of major basic protein and eosinophil cationic protein activate human mast cells. *Biochem Biophys Rep* (2020) 21:100719. doi: 10.1016/j.bbrep.2019.100719

11. Deepak V, Komarow HD, Alblaihess AA, Carter MC, Metcalfe DD, Ali H. Expression of MRGPRX2 in skin mast cells of patients with maculopapular cutaneous mastocytosis. *J Allergy Clin Immunol Pract* (2021) 9 (10):3841–3.e1. doi: 10.1016/j.jaip.2021.05.042

12. Green DP, Limjunyawong N, Gour N, Pundir P, Dong X. A mast-Cell-Specific receptor mediates neurogenic inflammation and pain. *Neuron* (2019) 101 (3):412–20.e3. doi: 10.1016/j.neuron.2019.01.012

13. Fujisawa D, Kashiwakura J, Kita H, Kikukawa Y, Fujitani Y, Sasaki-Sakamoto T, et al. Expression of mas-related gene X2 on mast cells is upregulated in the skin of patients with severe chronic urticaria. *J Allergy Clin Immunol* (2014) 134(3):622–33.e9. doi: 10.1016/j.jaci.2014.05.004

14. Roy S, Alkanfari I, Chaki S, Ali H. Role of MrgprB2 in rosacea-like inflammation in mice: Modulation by beta-arrestin 2. *J Invest Dermatol* (2022) S0022–202X (22):00403–1. doi: 10.1016/j.jid.2022.05.005

15. Callahan BN, Kammala AK, Syed M, Yang C, Occhiuto CJ, Nellutla R, et al. Osthole, a natural plant derivative inhibits MRGPRX2 induced mast cell responses. *Front Immunol* (2020) 11:703. doi: 10.3389/fimmu.2020.00703

16. Serhan N, Basso L, Sibilano R, Petitfils C, Meixiong J, Bonnart C, et al. House dust mites activate nociceptor-mast cell clusters to drive type 2 skin inflammation. *Nat Immunol* (2019) 20(11):1435–43. doi: 10.1038/s41590-019-0493-z

17. Kim HS, Hashimoto T, Fischer K, Bernigaud C, Chosidow O, Yosipovitch G. Scabies itch: an update on neuroimmune interactions and novel targets. *J Eur Acad Dermatol Venereol* (2021) 35(9):1765–76. doi: 10.1111/jdv.17334

18. Ogasawara H, Noguchi M. Therapeutic potential of MRGPRX2 inhibitors on mast cells. *Cells* (2021) 10(11):2906. doi: 10.3390/cells10112906

19. Ogasawara H, Furuno M, Edamura K, Noguchi M. Novel MRGPRX2 antagonists inhibit IgE-independent activation of human umbilical cord blood-derived mast cells. *J Leukoc Biol* (2019) 106(5):1069–77. doi: 10.1002/JLB.2AB1018-405R

20. Chompunud Na Ayudhya C, Amponnawarat A, Roy S, Oskeritzian CA, Ali H. MRGPRX2 activation by rocuronium: Insights from studies with human skin mast cells and missense variants. *Cells* (2021) 10(1):156. doi: 10.3390/cells10010156

21. Subramanian H, Gupta K, Ali H. Roles of mas-related G protein-coupled receptor X2 on mast cell-mediated host defense, pseudoallergic drug reactions, and chronic inflammatory diseases. *J Allergy Clin Immunol* (2016) 138(3):700–10. doi: 10.1016/j.jaci.2016.04.051

22. Mascarenhas NL, Wang Z, Chang YL, Di Nardo A. TRPV4 mediates mast cell activation in cathelicidin-induced rosacea inflammation. *J Invest Dermatol* (2017) 137(4):972–5. doi: 10.1016/j.jid.2016.10.046

23. Dwyer DF, Barrett NA, Austen KF. Immunological genome project c. expression profiling of constitutive mast cells reveals a unique identity within the immune system. *Nat Immunol* (2016) 17(7):878–87. doi: 10.1038/ni.3445

24. Plum T, Wang X, Rettel M, Krijgsveld J, Feyerabend TB, Rodewald HR. Human mast cell proteome reveals unique lineage, putative functions, and structural basis for cell ablation. *Immunity* (2020) 52(2):404–16.e5. doi: 10.1016/j.immuni.2020.01.012

25. Cao C, Kang HJ, Singh I, Chen H, Zhang C, Ye W, et al. Structure, function and pharmacology of human itch GPCRs. *Nature* (2021) 600 (7887):170–5. doi: 10.1038/s41586-021-04126-6

26. Babina M, Wang Z, Roy S, Guhl S, Franke K, Artuc M, et al. MRGPRX2 is the codeine receptor of human skin mast cells: Desensitization through β-arrestin and lack of correlation with the FcεRI pathway. *J Invest Dermatol* (2021) 141 (5):1286–96.e4. doi: 10.1016/j.jid.2020.09.017

27. Chompunud Na Ayudhya C, Amponnawarat A, Ali H. Substance p serves as a balanced agonist for MRGPRX2 and a single tyrosine residue is required for β-arrestin recruitment and receptor internalization. *Int J Mol Sci* (2021) 22(10):5318. doi: 10.3390/ijms22105318

28. Alkanfari I, Gupta K, Jahan T, Ali H. Naturally occurring missense MRGPRX2 variants display loss of function phenotype for mast cell degranulation in response to substance P, Hemokinin-1, human beta-Defensin-3, and icatibant. *J Immunol* (2018) 201(2):343–9. doi: 10.4049/jimmunol.1701793

29. Chompunud Na Ayudhya C, Roy S, Alkanfari I, Ganguly A, Ali H. Identification of gain and loss of function missense variants in MRGPRX2's transmembrane and intracellular domains for mast cell activation by substance p. *Int J Mol Sci* (2019) 20(21):5247. doi: 10.3390/ijms20215247

30. Alkanfari I, Freeman KB, Roy S, Jahan T, Scott RW, Ali H. Small-molecule host-defense peptide mimetic antibacterial and antifungal agents activate human and mouse mast cells *via* mas-related GPCRs. *Cells* (2019) 8(4):311. doi: 10.3390/cells8040311

31. Subramanian H, Kashem SW, Collington SJ, Qu H, Lambris JD, Ali H. PMX-53 as a dual CD88 antagonist and an agonist for mas-related gene 2 (MrgX2) in human mast cells. *Mol Pharmacol* (2011) 79(6):1005–13. doi: 10.1124/mol.111.071472

32. Kroeze WK, Sassano MF, Huang XP, Lansu K, McCorvy JD, Giguere PM, et al. PRESTO-tango as an open-source resource for interrogation of the druggable human GPCRome. *Nat Struct Mol Biol* (2015) 22(5):362–9. doi: 10.1038/nsmb.3014

33. Lansu K, Karpiak J, Liu J, Huang XP, McCorvy JD, Kroeze WK, et al. In silico design of novel probes for the atypical opioid receptor MRGPRX2. *Nat Chem Biol* (2017) 13(5):529–36. doi: 10.1038/nchembio.2334

34. Kirshenbaum AS, Akin C, Wu Y, Rottem M, Goff JP, Beaven MA, et al. Characterization of novel stem cell factor responsive human mast cell lines LAD 1 and 2 established from a patient with mast cell sarcoma/leukemia; activation following aggregation of FcepsilonRI or FcgammaRI. *Leuk Res* (2003) 27(8):677–82. doi: 10.1016/S0145-2126(02)00343-0

35. Amponnawarat A, Chompunud Na Ayudhya C, Ali H. Murepavadin, a small molecule host defense peptide mimetic, activates mast cells *via* MRGPRX2 and MrgprB2. *Front Immunol* (2021) 12:689410. doi: 10.3389/fimmu.2021.689410

36. Kambe N, Kambe M, Kochan JP, Schwartz LB. Human skin-derived mast cells can proliferate while retaining their characteristic functional and protease phenotypes. *Blood* (2001) 97(7):2045–52. doi: 10.1182/blood.V97.7.2045

37. Ali H, Richardson RM, Tomhave ED, Didsbury JR, Snyderman R. Differences in phosphorylation of formylpeptide and C5a chemoattractant receptors correlate with differences in desensitization. *J Biol Chem* (1993) 268 (32):24247–54. doi: 10.1016/S0021-9258(20)80517-1

38. Roy S, Gupta K, Ganguly A, Ali H. β-Arrestin2 expressed in mast cells regulates ciprofloxacin-induced pseudoallergy and IgE-mediated anaphylaxis. *J Allergy Clin Immunol* (2019) 144(2):603–6. doi: 10.1016/j.jaci.2019.04.024

39. Chaki S, Alkanfari I, Roy S, Amponnawarat A, Hui Y, Oskeritzian CA, et al. Inhibition of orai channel function regulates mas-related G protein-coupled receptor-mediated responses in mast cells. *Front Immunol* (2021) 12:803335. doi: 10.3389/fimmu.2021.803335

40. Elst J, van der Poorten MM, Van Gasse AL, De Puysseleyr L, Hagendorens MM, Faber MA, et al. Mast cell activation tests by flow cytometry: A new diagnostic asset? *Clin Exp Allergy* (2021) 51(11):1482–500. doi: 10.1111/cea.13984

41. Babina M, Wang Z, Li Z, Franke K, Guhl S, Artuc M, et al. FcepsilonRI- and MRGPRX2-evoked acute degranulation responses are fully additive in human skin mast cells. *Allergy* (2022) 77(6):1906–9. doi: 10.1111/all.15270

42. Roy S, Ganguly A, Haque M, Ali H. Angiogenic host defense peptide AG-30/5C and bradykinin B(2) receptor antagonist icatibant are G protein biased agonists for MRGPRX2 in mast cells. *J Immunol* (2019) 202(4):1229–38. doi: 10.4049/jimmunol.1801227

43. Guo Q, Subramanian H, Gupta K, Ali H. Regulation of C3a receptor signaling in human mast cells by G protein coupled receptor kinases. *PloS One* (2011) 6(7):e22559. doi: 10.1371/journal.pone.0022559

44. Gupta K, Subramanian H, Klos A, Ali H. Phosphorylation of C3a receptor at multiple sites mediates desensitization, beta-arrestin-2 recruitment and inhibition of NF-kappaB activity in mast cells. *PloS One* (2012) 7(10):e46369. doi: 10.1371/journal.pone.0046369

45. Ebo DG, Heremans K, Beyens M, van der Poorten M-LM, Van Gasse AL, Mertens C, et al. Flow-based allergen testing: Can mast cells beat basophils? *Clin Chim Acta* (2022) 532:64–71. doi: 10.1016/j.cca.2022.05.014

46. Yang F, Guo L, Li Y, Wang G, Wang J, Zhang C, et al. Structure, function and pharmacology of human itch receptor complexes. *Nature* (2021) 600 (7887):164–9. doi: 10.1038/s41586-021-04077-y

47. Knol EF, Mul FP, Jansen H, Calafat J, Roos D. Monitoring human basophil activation *via* CD63 monoclonal antibody 435. *J Allergy Clin Immunol* (1991) 88(3 Pt 1):328–38. doi: 10.1016/0091-6749(91)90094-5

48. Ebo DG, Elst J, Moonen N, van der Poorten MM, Van Gasse AL, Garvey LH, et al. Mast cell activation test: A new asset in the investigation of the chlorhexidine cross-sensitization profile. *Clin Exp Allergy* (2022). doi: 10.1111/cea.14129

49. Navines-Ferrer A, Serrano-Candelas E, Lafuente A, Munoz-Cano R, Martin M, Gastaminza G. MRGPRX2-mediated mast cell response to drugs used in perioperative procedures and anaesthesia. *Sci Rep* (2018) 8(1):11628. doi: 10.1038/s41598-018-29965-8

50. Elst J, Maurer M, Sabato V, Faber MA, Bridts CH, Mertens C, et al. Novel insights on MRGPRX2-mediated hypersensitivity to neuromuscular blocking agents and fluoroquinolones. *Front Immunol* (2021) 12:668962. doi: 10.3389/fimmu.2021.668962

51. Fernandopulle NA, Zhang SS, Soeding PF, Mackay GA. MRGPRX2 activation in mast cells by neuromuscular blocking agents and other agonists: Modulation by sugammadex. *Clin Exp Allergy* (2020) 51 (7):976–7. doi: 10.1111/cea.13801

52. Garvey LH, Dewachter P, Hepner DL, Mertes PM, Voltolini S, Clarke R, et al. Management of suspected immediate perioperative allergic reactions: an international overview and consensus recommendations. *Br J Anaesth* (2019) 123 (1):e50–64. doi: 10.1016/j.bja.2019.04.044

53. Leysen J, Bridts CH, De Clerck LS, Ebo DG. Rocuronium-induced anaphylaxis is probably not mitigated by sugammadex: evidence from an *in vitro* experiment. *Anaesthesia* (2011) 66(6):526–7. doi: 10.1111/j.1365-2044.2011.06729.x

54. Meixiong J, Anderson M, Limjunyawong N, Sabbagh MF, Hu E, Mack MR, et al. Activation of mast-Cell-Expressed mas-related G-Protein-Coupled receptors drives non-histaminergic itch. *Immunity* (2019) 50(5):1163–71.e5. doi: 10.1016/j.immuni.2019.03.013

55. Manorak W, Idahosa C, Gupta K, Roy S, Panettieri RJr., Ali H. Upregulation of mas-related G protein coupled receptor X2 in asthmatic lung mast cells and its activation by the novel neuropeptide hemokinin-1. *Respir Res* (2018) 19(1):1. doi: 10.1186/s12931-017-0698-3

56. Gupta K, Idahosa C, Roy S, Lee D, Subramanian H, Dhingra A, et al. Differential regulation of mas-related G protein-coupled receptor X2-mediated mast cell degranulation by antimicrobial host defense peptides and porphyromonas gingivalis lipopolysaccharide. *Infect Immun* (2017) 85(10):e00246-17. doi: 10.1128/IAI.00246-17

frontiers | Frontiers in Immunology

TYPE Original Research
PUBLISHED 09 November 2022
DOI 10.3389/fimmu.2022.1000405

OPEN ACCESS

EDITED BY
Ulrich Blank,
Institut National de la Santé et de la Recherche Médicale (INSERM), France

REVIEWED BY
Wei-Yu Chen,
National Cheng Kung University, Taiwan
Hydar Ali,
University of Pennsylvania, United States

*CORRESPONDENCE
Ivan L. Dzhagalov
ivan.dzhagalov@nycu.edu.tw

SPECIALTY SECTION
This article was submitted to Molecular Innate Immunity, a section of the journal Frontiers in Immunology

RECEIVED 22 July 2022
ACCEPTED 17 October 2022
PUBLISHED 09 November 2022

CITATION
Herrera-Heredia SA, Hsu H-P, Kao C-Y, Tsai Y-H, Yamaguchi Y, Roers A, Hsu C-L and Dzhagalov IL (2022) Heparin is required for the formation of granules in connective tissue mast cells.
Front. Immunol. 13:1000405.
doi: 10.3389/fimmu.2022.1000405

Heparin is required for the formation of granules in connective tissue mast cells

Sandra Abril Herrera-Heredia[1], Hsuan-Po Hsu[1], Cheng-Yen Kao[1], Yu-Huan Tsai[1], Yu Yamaguchi[2], Axel Roers[3], Chia-Lin Hsu[1] and Ivan L. Dzhagalov[1*]

[1]Institute of Microbiology and Immunology, National Yang Ming Chiao Tung University, Taipei, Taiwan, [2]Sanford Burnham Prebys Medical Discovery Institute, La Jolla, CA, United States, [3]Institute for Immunology, Heidelberg University Hospital, Heidelberg, Germany

Mast cells are innate immune cells strategically positioned around blood vessels near body surfaces. Their primary weapons are bioactive amines, mast cell-specific proteases, and cytokines stored in preformed granules. Mast cells granules constituents are packaged efficiently with the help of the highly negatively charged Heparan sulfate-derivative, Heparin. Heparin is one of the most widely used drugs to treat coagulation disorders, yet, it is not found in the circulation at a steady state, casting doubt that the prevention of blood clotting is its physiological function. Early studies using *Ndst2*$^{-/-}$ mice have shown that Heparin is essential for mast cells granules formation. However, these mice could still produce less sulfated Heparan sulfate that could potentially replace Heparin. Here, we have created and validated a novel genetic model for Heparin deficiency, specifically in connective tissue mast cells, to address the physiological role of this molecule. Using this model, we have demonstrated that Heparin is required for mast cell granules formation; without it, mast cells are reduced in the peritoneal cavity and the skin. The absence of Heparin impaired the response to passive cutaneous anaphylaxis but, surprisingly, enhanced ear swelling in an irritant dermatitis model and reduced the lesion size and bacterial burden in a *Staphylococcus aureus* necrotizing dermatitis model. The altered function of Heparin-deficient mast cells in the latter two models was not mediated through enhanced Histamine or TNFα release. However, the *Mrgprb2* receptor was up-regulated in knock-out mast cells, potentially explaining the enhanced response of mutant mice to irritant and necrotizing dermatitis. Altogether our results expand our current understanding of the physiological role of Heparin and provide unique tools to further dissect its importance.

KEYWORDS

Heparin, mast cells, granules, *Mrgprb2*, irritant dermatitis, necrotizing dermatitis

Abbreviations: MC, mast cell; HS, Heparan sulfate; *Ndst2*, N-deacetylase/N-sulfotransferase 2; M-GFP, *Mcpt5*^{Cre} X *ROSA26*$^{LSL\text{-}GFP}$; M-Ext1, *Mcpt5*^{Cre} X *Ext1*$^{f/f}$; BMMC, bone marrow-derived mast cell; NETs, neutrophil extracellular traps; PCA, passive cutaneous anaphylaxis.

10.3389/fimmu.2022.1000405

Introduction

Mast cells (MCs) are tissue-resident innate immune cells that play essential roles in allergic reactions and toxin neutralization (1). In rodents, they can be divided into two subsets: connective tissue MCs and mucosal MCs (2). Connective tissue MCs are present in the skin, peritoneal cavity, and most connective tissues and produce the glycosaminoglycan Heparin and a specific set of MC proteases. Mucosal MCs are positioned at the mucosal surfaces of the intestine and the lungs, contain Chondroitin sulfate, and produce a distinct set of proteases. Upon activation, MCs can quickly release preformed mediators that can induce immediate and powerful effects at local and systemic levels that can kill humans and animals within minutes – a phenomenon called anaphylaxis, which is MCs most well-known function. The search for positive effects of MCs led to the discovery that MCs do not develop in c-kit mutant mice, which has resulted in many studies showing wide-ranging activities of MCs (3). However, many of these effects have been questioned because c-kit is essential for the development and function of other cell types as well (4). In recent years, the field of MC biology has been undergoing a re-evaluation of their functions using c-kit-independent models (5, 6).

MCs' primary weapons are their granules that contain many mediators (7). These include bioactive amines, of which Histamine is the most important; several mast cell-specific proteases such as Mcpt1, Mcpt4, Mcpt5, Mcpt6, and Cpa3; and cytokines such as TNFα, IL-4, VEGF, Fgf2. These MCs granules constituents are all positively charged and are packaged together with the help of Heparin – a highly negatively charged Heparan sulfate (HS) derivative (8). Heparin is produced only in MCs and is an important drug used to treat coagulation disorders (9). It activates Serpin C1 (Anti-Thrombin III) and limits blood clotting. However, no Heparin could be found in the blood of people or animals, and it appears that its physiological function is not related to coagulation.

The first glimpse into the physiological role of Heparin came from two studies that deleted the enzyme N-deacetylase/N-sulfotransferase 2 (*Ndst2*), which is essential for the sulfation of HS to produce Heparin (10, 11). The authors found that in the absence of Heparin, the granules of MCs were largely missing, and some of the mediators stored in the granules were greatly reduced. However, the two studies differed in some important aspects. Forsberg et al. found that the MCs were substantially reduced in the peritoneal cavity of *Ndst2*$^{-/-}$ mice, and they contained significantly less Histamine than controls (10). In contrast, Humphries et al. reported unchanged numbers of MCs and Histamine content (11). One limitation of both studies is that although Heparin could not be produced in the mutant animals, they could still make HS with a lesser degree of sulfation that could potentially substitute for Heparin in MCs.

The physiological importance of Heparin has also been studied in mice lacking Serglycin – a protein rich in Serine and Glycine that is the physical carrier of Heparin chains in MCs. Serglycin knock-out mice were found to have fewer granules, and many granule constituents such as MC-specific proteases, Histamine, and Serotonin were significantly reduced (12, 13). However, using the same animal model, Abrink et al. reported that the peritoneal MCs were almost absent in *Serglycin*$^{-/-}$ mice (12), while Ringvall et al. found a typical abundance of peritoneal MCs (13). These mice also had decreased clearance of *Klebsiella pneumoniae* infection (14) but a normal response to Lymphocytic choriomeningitis virus infection (15). However, Serglycin is expressed in many hematopoietic and non-hematopoietic cells, and the phenotype in the knock-out mice cannot be attributed solely to the lack of Heparin in MCs (16). Moreover, Serglycin can carry other glycosaminoglycans in addition to Heparin, such as Chondroitin sulfate. Thus, its deletion might impair functions that are not dependent on Heparin.

Altogether, although the studies of *Ndst2*$^{-/-}$ and *Serglycin*$^{-/-}$ mice have provided valuable insight into what does Heparin do in our body, the discrepancies between studies using the same animal model and the limitations of different genetically deficient mouse strains leave open the question: What is the physiological function of Heparin? Here, we addressed the role of Heparin by crossing *Mcpt5*^{Cre} mice with *Ext1*$^{f/f}$ and, thus, abolishing HS and Heparin synthesis, specifically in connective tissue MCs. Heparin-deficient MCs had significantly reduced granule content, including Histamine and TNFα, and their numbers in the peritoneal cavity and the skin were diminished considerably. Interestingly, although the reduced number of MCs and their granules resulted in weaker passive cutaneous anaphylaxis (PCA), the response of mutant mice to skin irritants and *S. aureus* necrotizing dermatitis was enhanced in part due to the up-regulation of the *Mrgprb2* receptor on MCs. Taken together, our studies provide important insights into the physiological functions of Heparin and the adaptations of MCs to its absence.

Material and methods

Mice

C57BL/6 mice were purchased from the National Laboratory Animal Center (Taipei, Taiwan). *ROSA26*$^{LSL-GFP}$ (B6.Cg-Gt (ROSA)26Sor$^{tm6(CAG-ZsGreen1)Hze}$/J, JAX stock# 007906) mice were purchased from The Jackson Laboratory (17). *Ext1*$^{f/f}$ (C57BL/6-Ext1^{tm1Yama}) (18) and *Mcpt5*^{Cre} (Tg(Cma1-cre) ARoer) mice have been previously described (19). All mice were housed in the animal facility of NYCU and used between 6 and 14 weeks of age. All animal experiments were approved by

the Institutional Animal Care and Use Committee (IACUC) of NYCU.

Cell isolation

Peritoneal cells were obtained by injecting 3 mL of cold phosphate-buffered saline (PBS) followed by a gentle massage of the peritoneal cavity. Cells were extracted using a syringe, washed, and resuspended in complete RPMI (cRPMI) medium containing 10% Fetal Bovine Serum, 1% Penicillin/Streptomycin, 1% L-Glutamine, and 0.1% 2-Mercaptoethanol (all from Gibco). For skin cell isolation, ears were cut, and dorsal and ventral sheets were separated and finely minced with scissors. The tissue pieces were collected and digested in cRPMI medium containing 1.0 mg/mL Collagenase P (Roche) and 0.1 mg/mL DNase I (Sigma) at 37°C for 40 min in constant agitation. The cells were filtered through 70 µm Nylon mesh (Small Parts) and washed with PBS. Cells were resuspended in 500 µL of 1X ACK (Ammonium-Chloride-Potassium) lysis buffer, incubated for 45 sec at room temperature (RT), washed, and resuspended in cRPMI. Small intestines were harvested, flushed with PBS, opened, and cut into 1 cm long pieces. Tissue pieces were transferred into a 50 mL conical tube and incubated in HBSS without Ca^{2+} and Mg^{2+} (Gibco) supplemented with 5 mM EDTA (Merck), 10 mM HEPES (Goldbio), and 5% Fetal Bovine Serum (Gibco) for 20 min at 37°C in constant agitation. Tissue pieces were washed with PBS and digested in cRPMI containing 1.0 mg/mL Collagenase P (Roche) and 0.1 mg/mL DNase I (Sigma) at 37°C for 40 min in constant agitation. Cells were passed through 100 and 70 µm cell strainers (Biologix) and washed twice, resuspended in 2 mL of 1X ACK buffer, incubated for 1 min at RT, washed and resuspended in cRPMI.

Flow cytometry

Single-cell suspensions were blocked with 100 µL supernatant from 2.4G2 hybridoma (a kind gift by Dr Fang Liao, Academia Sinica, Taipei, Taiwan) and stained with antibodies for 20 min on ice in 100 µL FACS buffer [PBS + 0.5% Bovine Serum Albumin (BSA, Bionovas) + 1 mM EDTA (Merck) + 0.1% NaN3 (Sigma)]. The following antibodies were used: anti-mouse CD45 PerCP/Cy5.5 (clone 30-F11), anti-mouse CD11b BV785 (clone M1/70), anti-mouse CD11b FITC (clone M1/70), anti-mouse TCRβ APC (clone H57-597), anti-mouse CD117 BV421 (clone 2B8), anti-mouse CD117 Pe/Cy7 (clone ACK2), anti-mouse CD5 Pe/Cy7 (clone 53-7.3), anti-mouse MHCII APC/Fire 750 (clone M5/114.15.2), anti-mouse FcεR1α PerCP/Cy5.5 (clone MAR-1), anti-mouse FcεR1α APC (clone MAR-1), anti-mouse B220 Biotin (clone RA3-6B2), anti-mouse B220 BV711 (clone RA3-6B2), anti-mouse Gr-1 APC/Cy7 (clone RB6-8C5), anti-mouse F4/80 BV421 (clone BM8), anti-mouse ICAM2 FITC (clone MIC2/4), anti-mouse Ly6c BV711 (clone HK1.4), anti-mouse Ly6c BV700 (clone HK1.4), anti-mouse Ly6c Biotin (clone HK1.4), anti-mouse CD3ε APC/Fire 750 (clone 145-2C11), anti-mouse CD3ε biotin (clone 145-2C11) (all from BioLegend). After staining, cells were washed with FACS buffer and, if required, incubated with Streptavidin PE or Streptavidin APC/Cy7 (BioLegend). The cells were washed and resuspended in FACS buffer containing Propidium Iodine (Sigma) or DAPI (ThermoFisher). To detect Heparin by Serpin C1 binding, cells were incubated with Zombie Aqua (BioLegend) for 30 min, washed, and stained with the required antibodies for surface markers. Later, cells were fixed with 2% paraformaldehyde (PFA, Electron Microscopy Sciences) for 15 min at RT and washed with FACS buffer. For permeabilization, cells were incubated in 500 µL of permeabilization buffer [PBS + 1% Triton X-100 (Sigma)], washed, incubated for 30 min with biotinylated Serpin C1, washed, and incubated with Streptavidin PE or Streptavidin APC (BioLegend) as required. Finally, cells were washed and resuspended in FACS buffer. The data were acquired on LSR Fortessa (BD Biosciences) flow cytometer running Diva 8 software and analyzed with FlowJo 10.7.1 (BD Biosciences).

Serpin C1 biotinylation

Serpin C1 protein (MyBioSource) was diluted in binding buffer [10 mM sodium phosphate (Bionovas) + 150 mM NaCl (Sigma), pH 7.4], and loaded into a pre-equilibrated HiTrap Heparin HP column (GE Healthcare). The flow-through was reloaded into the column twice to ensure complete binding, and then the column was washed with binding buffer. EZ-Link™ Sulfo-NHS-LC-biotin (Thermo Scientific) was prepared and applied in 50-fold molar excess of Serpin C1 per column volume and incubated for 1 hour at RT. The reaction was terminated by washing the column four times with termination buffer [Binding buffer + 100 mM glycine (Sigma), pH 7.4]. Then, the column was washed with binding buffer. The biotinylated Serpin C1 was eluted with elution buffer [10 mM sodium phosphate + 4 M NaCl, pH 7.4]. The whole procedure was performed on ÄKTA (GE Healthcare) protein purification system. Biotinylated Serpin C1 was dialyzed and concentrated in Dulbecco's Phosphate Buffered Saline (DPBS, Gibco) with a Vivaspin 6 MWCO 3 kDa spin column (Sartorius). Finally, Biotinylated Serpin C1 aliquots were prepared in DPBS containing 2.0% glycerol (MP Biomedicals) and 0.2% BSA (Bionovas) and preserved at –20°C until use.

Immunofluorescent microscopy

Shaved back skin was dissected and fixed for 2 hours in 4% PFA (Electron Microscopy Sciences)/10% sucrose (Sigma) at 4°C, followed by overnight incubation in 30% sucrose (Sigma) at

4°C. After fixation, the tissue was embedded in Tissue-Tek O.C.T compound (Sakura Fintek), frozen, and stored at -80°C until use. Skin sections were cut with a thickness of 10 µm at -20°C in a cryostat microtome (NX50, Thermo Scientific). The sections were fixed in acetone (Honeywell) for 10 minutes at -20°C, air-dried, and blocked with 5% donkey serum (Jackson ImmunoResearch) in PBS + 0.25% Triton X-100 (Sigma) for 2 hours at room temperature, followed by overnight incubation at 4°C in the dark with rabbit polyclonal anti-Histamine antibody (GeneTex) diluted in 2.4G2 supernatant. After incubation, sections were washed 3 times and incubated for 2 hours at room temperature in the dark with AF555 donkey anti-rabbit antibody (Invitrogen) diluted in 2.4G2 supernatant, washed, stained with DAPI (Thermo Fisher) for 5 minutes at RT, washed, and mounted in glycerol (Sigma) containing 0.1% n-propyl gallate (Sigma). Images were obtained with the Axio Observer 7 microscope (Zeiss) equipped with ApoTome.2 and Axiocam 702 monochrome camera (both from Zeiss). Image analysis was performed using the "Spot" function of Imaris 8.0.2 (Bitplane).

Avidin staining

Avidin was stained as previously described (20). Briefly, skin sections were fixed in acetone (Honeywell) for 10 min at -20°C and air-dried. Avidin conjugated with AF488 (Invitrogen) was diluted in immunohistochemistry buffer [0.1 M Tris (Bionovas) + 0.5% w/v BSA (Bionovas), pH 7.4] containing 2% Triton X-100 (Sigma) and 0.5% skim milk. Sections were incubated with Avidin-AF488 overnight at RT in the dark with constant agitation. Then the sections were washed with immunohistochemistry buffer and stained with DAPI (Thermo Fisher) for 5 min at RT washed and mounted in glycerol + 0.1% n-propyl gallate.

Cytospin and histological stainings

Ear and peritoneal cavity single-cell suspensions were enriched with CD117 conjugated magnetic beads (Miltenyi) and mounted with a cytospin (Cytospin 3, Shandon) onto Superfrost Plus slides (Thermo Scientific) under the following conditions: 500 rpm for 5 min. The slides were air-dried and stained with Giemsa (Merck) or Toluidine Blue O (Sigma) following standard procedures. Images were obtained with the Axio Observer 7 microscope equipped with Axiocam 702 monochrome camera (Zeiss).

Bone marrow-derived mast cells

Bones were dissected aseptically from 14-weeks-old mice, and the marrow was flushed in complete Iscove's modified Dulbecco (cIMDM) medium supplemented with 10% Fetal Bovine Serum, 1% Penicillin/Streptomycin, 1% L-Glutamine, and 0.1% 2-Mercaptoethanol (all from Gibco). The cells were cultured in cIMDM media for at least 4 weeks at 37°C in 5% CO_2 with 10 ng/mL of recombinant murine IL-3 (PreproTech) or until the purity of MCs (defined as $CD117^+$ and $Fc\varepsilon R1^+$) reached > 90%. Purity was assessed weekly by flow cytometry.

Ext1 copy number

Peritoneal cavity single-cell suspensions were enriched with CD117 conjugated magnetic beads (Miltenyi) and sorted on BD FACSMelody (BD Biosciences) cell sorter running BD FACSChorus (BD Biosciences) software version 1.3.3 after labeling with antibodies described in the flow cytometry section. Sorted cells were incubated with proteinase K (Arrowtec) at 60°C for 5 min to lyse the cells, followed by the extraction of the genomic DNA using the gSYNC extraction kit (Geneaid) following the manufacturer's instructions. *Ext1* and *Tfrc* genes were amplified together using TaqMan Copy Number Assay ID Mm00613274_cn labeled with FAM and TaqMan Copy Number Reference Assay (cat. # 4458366 labeled with VIC), respectively (both from ThermoFisher) in a PCR thermal cycler (StepOne Real-Time, Applied Biosystems) with the following conditions: 1 cycle of denaturation/enzyme activation at 95°C for 10 min, 40 cycles of denaturation at 95°C for 15 sec followed by annealing/extension at 60°C for 1 min. *Ext1* and *Tfrc* genes expression were analyzed on StepOne (Applied Biosystems) software version 2.3, and fold increase was calculated using the comparative CT (ΔΔCT) method on Microsoft Excel (Microsoft). *Ext1* expression in each sample was normalized using the *Tfrc* gene expression.

Mrgprb2 expression

Skin single-cell suspensions were stained as described in the flow cytometry section and sorted with FACSMelody cell sorter (BD Biosciences) running BD FACSChorus (BD Biosciences) software version 1.3.3. $CD45^+CD3^-CD11b^-Fc\varepsilon R1^+c\text{-}kit^+$ sorted cells were directly collected in TRI Reagent (Invitrogen) for RNA extraction. Cells were lysed and homogenized in TRI reagent (Invitrogen) by pipetting and incubated for 5 min at RT. 10% of 1-bromo-3-chloropropane (BCP, Sigma) was added, samples were mixed, incubated for 10 min at RT, and centrifuged. The aqueous phase was transferred to a new tube, and RNA was precipitated with isopropanol (Sigma). 1 µg/µL of glycogen (Gene M) was added as an RNA carrier, and samples were incubated overnight at -80°C. Pellets were washed twice with 75% ethanol (J.T. Baker), air-dried, and resuspended in nuclease-free water (Invitrogen). cDNA was synthesized from the isolated RNA using the High-Capacity RNA to cDNA kit

(Applied Biosystems) in a thermal cycler (C-1000 Touch, Biorad) with the following conditions: 1 cycle at 37°C for 60 min and 1 cycle at 95°C for 5 min. *Mrgprb2* and *Rpl19* mRNA were amplified together using TaqMan Gene Expression Assays: for *Mrgprb2* Assay ID: Mm01701139_m1 labeled with FAM and for *Rpl19* – Assay ID: Mm02601633_g1 labeled with VIC, primer-limited (both from ThermoFisher)] in a PCR thermal cycler (StepOne Real-Time, Applied Biosystems) with the following conditions: 1 Hold cycle at 50°C for 2 min, 1 Denaturation cycle at 95°C for 10 min and 40 cycles of denaturation at 95°C for 15 sec and annealing/extension 60°C for 1 min, respectively. *Mrgprb2* and *Rpl19* genes expression were analyzed on StepOne (Applied Biosystems) software version 2.3, and fold increase was calculated using the comparative CT (ΔΔCT) method on Microsoft Excel (Microsoft). The expression of *Mrgprb2* in each sample was normalized using the *Rpl19* gene expression.

Sterile peritonitis model

Mice were injected intraperitoneally with 1 mL of 4% Brewer modified Thioglycolate medium (Sigma). Four days post-injection, the peritoneal cells were obtained as described in the Cell Isolation paragraph and analyzed by flow cytometry.

Bacterial strains

Listeria monocytogenes expressing chicken Ovalbumin was purchased from Sungyee Biotechnology (Nanjing, China) (21). The bacteria were cultured overnight at 37°C in constant agitation in Brain Heart Infusion (BHI, BD Diagnostic Systems) broth containing 5 μg/mL of erythromycin (Sigma) and then diluted 1:20 in fresh BHI broth (BD Diagnostic Systems) until the culture reached the log phase. Frozen stocks were prepared in BHI broth containing 20% glycerol (MP Biomedicals) and stored at -80°C until use. *Staphylococcus aureus* strain JE2 (BEI Resources, NIH, USA) (22) was cultured in Tryptone Soy Broth (TSB, Neogen) overnight at 37°C under constant agitation and then diluted at 1:100 in fresh TSB (Neogen) until the culture reached the log phase. Stocks were prepared in TSB containing 20% glycerol (MP Biomedicals) and stored at -80°C until use. Prior to mice infection, stocks were thawed on ice, washed, and resuspended in sterile PBS.

Listeria monocytogenes infection model

Mice were injected intraperitoneally with 10^7 CFUs of *L. monocytogenes* in 100 μL of sterile PBS. On day 2 or 7 post-infection, mice were sacrificed, spleen and liver were harvested and placed in a 14 mL polypropylene round-bottom tube (Falcon) filled with cold, sterile PBS. Organs were homogenized with a high-speed homogenizer system (T25, IKA). To determine bacterial burden, serial dilutions of the homogenates were plated on BHI agar (BD Biosciences and Amresco) plates, incubated overnight at 37°C, and colonies were manually counted.

Staphylococcus aureus infection model

Two–three days before infection, mice were anesthetized with ketamine (Toronto Research Chemicals) and xylazine (Sigma), backs were shaved with a clipper (MB-021, Urbaner), and hair was removed with a hair removal cream (Nair). For infection, mice were injected intradermally with 10^7 CFUs of *S. aureus* in 30 μL of sterile PBS. Lesions were measured every two days starting on day 1 and up to day 9 as follows: Lesions borders were manually marked on tracing paper, and the total area was calculated using ImageJ after digital scanning of the tracers' sheets. To determine the bacterial burden, mice were sacrificed on day 3 and 10 post-infection, 2 – 3 mm of the skin surrounding the lesions was harvested, weighed, and placed in a 14 mL polypropylene round-bottom tube (Falcon) with cold, sterile PBS. Harvested skin was homogenized using a high-speed homogenizer system (T25, IKA). Serial dilutions of the homogenate were plated in Tryptic Soy Agar (BD Diagnostic Systems and Amresco) plates, incubated overnight at 37°C, and colonies were manually counted. The number of colonies was normalized to the weight of the tissue for each sample.

Irritant cutaneous dermatitis

Mice were treated with 50 μL of 0.5% of 1-Fluoro-2,4-dinitrobenzene (DNFB, Sigma) in acetone/olive oil (4:1) (25 μL each side of the ear). Ear thickness was measured with an analog micrometer (Mitutoyo 103-129).

Passive cutaneous anaphylaxis

Mice ears were injected intradermally with 100 ng of αOVA-IgE antibody (clone E-C1, Chondrex, Inc). The following day mice were injected intravenously with 100 μg of OVA (Sigma). Ear thickness was measured with an analog micrometer (Mitutoyo 103-129).

Statistical analysis

Data analyses were performed in Prism 9 (GraphPad). All data were analyzed with an unpaired Student t-test except for the

bacterial burden in Figure 4F and Figures 5C, D, which was analyzed with a non-parametric Mann-Whitney test, and presented as mean ± SEM. Statistical significance was defined as follows: *p < 0.05, **p <0.01; ***p <0.001 and ****p < 0.0001. Graphs were created with Prism 9 (GraphPad) and Adobe Illustrator 2022 (Adobe).

Results

Connective tissue but not mucosal MCs express *Mcpt5*^{Cre}

To ablate all Heparan sulfate and Heparin specifically in MCs, we decided to use *Mcpt5*^{Cre} mice (19). As a first step, we tested the specificity of this model by crossing *Mcpt5*^{Cre} to *ROSA26*$^{LSL-GFP}$ mice (17) and examining the degree of labeling of MCs with GFP. Among peritoneal lavage cells, the c-kit^{+}FcεR1^{+} MCs were ~1.5% of all cells, and they numbered ~8x10^{4} (Figure 1A). The presence of the two transgenes in *Mcpt5*^{Cre} X *ROSA26*$^{LSL-GFP}$ (M-GFP) mice did not significantly change MCs proportions and numbers, but more than 90% of peritoneal MCs expressed GFP (Figure 1B). In ear skin single-cell suspensions, c-kit^{+} CD45^{+} CD11b^{-} CD3^{-} MCs percentages and numbers were comparable to *ROSA26*$^{LSL-GFP}$ controls, and more than 95% of MCs from M-GFP mice were GFP^{+} (Figures 1C, D). Frozen sections from shaved back skin of M-GFP mice confirmed the presence of scarce GFP^{+} cells located in the dermis close to hair follicles, consistent with MCs location description (Figure 1E) (2).

To assess the labeling of mucosal MCs in M-GFP mice, we analyzed the expression of GFP in c-kit^{+} CD45^{+} MCs from the epithelial layer and lamina propria of the small intestine. Notably, mucosal MCs from M-GFP mice were GFP negative without any significant changes in percentages when compared with controls (Figures 1F–I). Thus, we conclude that *Mcpt5*^{Cre} is active specifically in connective tissue MCs but not mucosal MCs, making it a reliable model to selectively target connective tissue MCs.

Peritoneal MCs from Heparin deficient mice are reduced in numbers and lack granules

To eliminate Heparan sulfate and Heparin from connective tissue MCs, we crossed *Mcpt5*^{Cre} mice with *Ext1*$^{f/f}$ mice (18). *Ext1* encodes the glycosyltransferase Exostosin 1, which is essential for the synthesis of both HS and Heparin (23). First, we tested the deletion efficiency of *Ext1* in MCs of *Mcpt5*^{Cre} X *Ext1*$^{f/f}$ (M-Ext1) mice. *Ext1*$^{f/f}$ mice were used as controls throughout the study. We could not detect the *Ext1* gene in sorted peritoneal MCs from M-Ext1 mice. However, *Ext1* deletion was incomplete in BMMCs of the same mice (Figure 2A). Around 20% of BMMCs had an intact *Ext1* allele (Figure 2A). Hence, we conclude that *Ext1* is efficiently deleted only in primary connective tissue MCs but not in ex vivo differentiated BMMCs.

To ensure that Heparin is absent from M-Ext1 MCs, we permeabilized and stained peritoneal exudate cells with biotinylated Serpin C1, which specifically interacts with Heparin (24). While we could clearly detect Serpin C1 binding to control peritoneal MCs, M-Ext1 MCs did not stain with this reagent confirming that *Ext1* deletion results in the absence of Heparin (Figure 2B) and validating that M-Ext1 MCs lack Heparin.

Then, we investigated the changes in peritoneal MCs in the absence of Heparin. Peritoneal MCs from 6-weeks-old M-Ext1 mice were significantly decreased in numbers and percentages (Figure 2C). Furthermore, our flow cytometry data revealed that Heparin-deficient MCs were smaller and less granular than controls (Figure 2D) and had reduced c-kit expression (Figure 2E). Giemsa and Toluidine blue staining of c-kit-microbeads enriched peritoneal cells confirmed the great reduction in the granule content in MCs from M-Ext1 mice (Figure 2F). Nevertheless, the defects in the peritoneal cavity of M-Ext1 mice were restricted to MCs, as all other cell types appeared in normal proportions (Figure 2G).

To find out whether the observed changes in peritoneal MCs were permanent, we analyzed 14-week-old mice and found similar changes in numbers, percentages, granularity, c-kit expression, and Heparin content in M-Ext1 MCs (Supplementary Figures 1A–E). Thus, these data suggest that deletion of *Ext1* in peritoneal MCs results in reduced numbers of these cells, defects in their granular content, and lower c-kit expression.

Reduced numbers and granularity of skin MCs from older M-Ext1 mice

To find out if other connective tissue MCs in M-Ext1 mice have defects, we characterized skin MCs. Surprisingly, MCs from 6-weeks-old M-Ext1 mice showed no difference in numbers, percentages, size, granularity, and c-kit surface expression compared to control mice (Supplementary Figures 2A–C). Giemsa and Toluidine Blue staining showed MCs with large numbers of granules in their cytoplasm (Supplementary Figure 2D), despite the efficient deletion of *Ext1* evidenced by the absence of Serpin C1 binding to skin MCs from young M-Ext1 mice (Supplementary Figure 2E). In contrast, MCs from 14-weeks-old M-Ext1 mice were reduced in proportions and numbers (Figure 3A) and had decreased granularity and size (Figures 3B, D), although they did not express statistically significantly lower levels of c-kit on their surface (Figure 3C). Consistently, Heparin could not be detected with Serpin C1 staining inside the cells, suggesting efficient deletion of *Ext1* (Figure 3E). The percentages of CD11b^{+} myeloid cells and CD3^{+} T cells in the skin were not changed in M-Ext1 mice. Hence the defects in the skin are limited to the MC pool (Figure 3F and Supplementary Figure 2F).

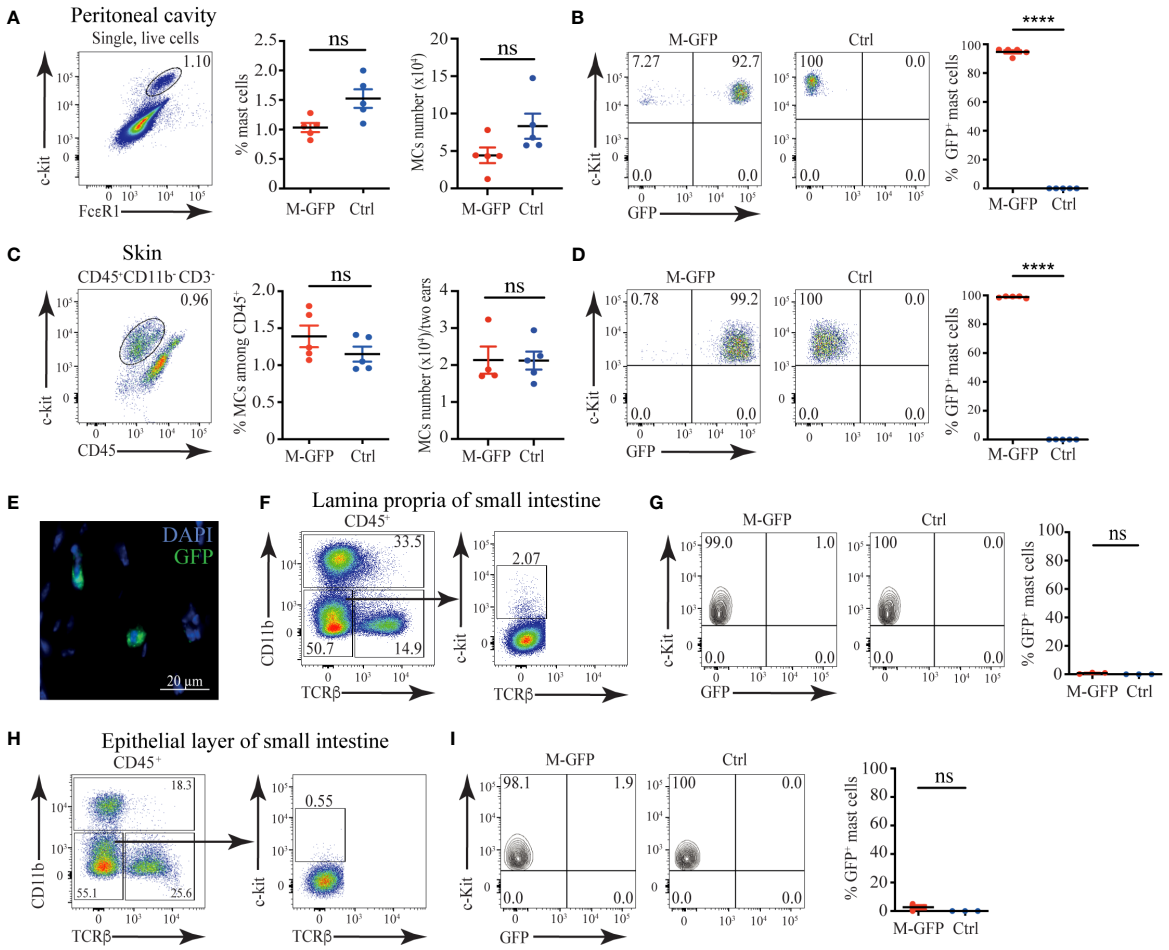

FIGURE 1
Connective tissue MCs are efficiently labeled in *Mcpt5*^{Cre} X *ROSA26*$^{LSL\text{-}GFP}$ (M-GFP) mice. **(A)** Representative gating strategy, percentages, and numbers of c-kit$^+$FcεR1$^+$ MCs among peritoneal exudate cells in M-GFP and control mice determined by flow cytometry. **(B)** Representative flow cytometry plots and percentages of GFP$^+$ peritoneal MCs in M-GFP and control mice. **(C)** Representative gating strategy, percentages, and numbers of skin MCs in M-GFP and control mice determined by flow cytometry. **(D)** Representative flow cytometry plots and percentages of GFP$^+$ skin MCs in M-GFP and control mice. **(E)** Representative immunofluorescent microscopy image of skin MCs in M-GFP mice. **(F)** Representative gating strategy and percentages of MCs among CD45$^+$ cells in lamina propria of the small intestine of M-GFP and control mice. **(G)** Representative flow cytometry plots and percentages of GFP$^+$ MCs in lamina propria of the small intestine of M-GFP and control mice. **(H)** Representative gating strategy and percentages of MCs among CD45$^+$ cells in the epithelial layer of the small intestine of M-GFP and control mice. **(I)** Representative flow cytometry plots and percentages of GFP$^+$ MCs in the epithelial layer of the small intestine of M-GFP and control mice. Results are represented as mean ± SEM. Each symbol in the graph represents an individual mouse. Flow cytometry plots in **(A–D)** are representative of 5 individual experiments, while the plots in **(F–H)**, and **(I)** are representative of 3 individual experiments. The image in **(E)** is representative of 3 different mice. Statistical significance was determined by unpaired Student's t-test. Values of $p < 0.05$ were considered statistically significant, ****$p < 0.0001$, ns, not significant.

Heparin plays no major role in recruiting inflammatory cells during sterile peritonitis and the pathogen clearance during bacterial peritonitis

To determine the importance of Heparin in physiological settings, we decided to use two mouse models of peritonitis, in which the roles of MCs have been characterized previously. Recruitment of inflammatory cells during sterile peritonitis has been shown to depend on MCs (25). To test the role of Heparin in the process, we injected 6 weeks-old M-Ext1 mice and controls intraperitoneally with 4% Thioglycolate and 4 days later analyzed the peritoneal exudate cells (PECs) by flow cytometry. The total numbers of PECs were indistinguishable between M-Ext1 and control mice (Figure 4A). MCs percentages, numbers, size, and granularity were still reduced in the Heparin-deficient mice compared with controls (Figures 4B, C). However, there were no statistically significant changes in the percentages and numbers of any other cell type (Figures 4D, E), suggesting that Heparin and MCs granules are dispensable for the recruitment of inflammatory

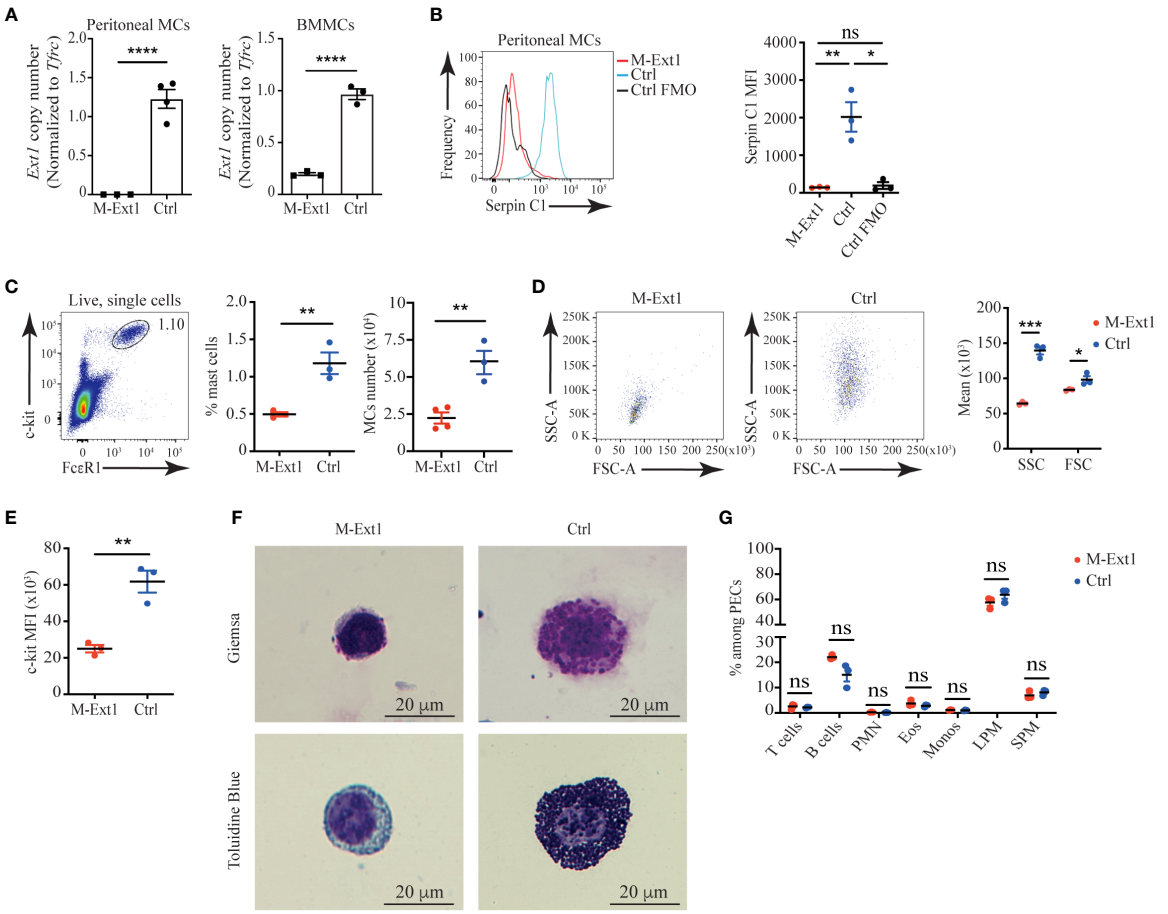

FIGURE 2
Peritoneal MCs in 6-weeks old Heparin deficient mice are reduced in numbers and lack granules. **(A)** *Ext1* gene copy number analyzed by qPCR from sorted peritoneal MCs and bone marrow-derived mast cells (BMMCs) from M-Ext1 and control mice. **(B)** Representative histograms and statistics of mean fluorescent intensity (MFI) of Serpin C1 binding to fixed and permeabilized peritoneal MCs. Staining of control cells with the omission of the biotinylated SerpinC1 was used as fluorescence minus one (FOM) control. **(C)** Representative gating strategy, percentages and numbers of peritoneal MCs in M-Ext1, and control mice. **(D)** Representative flow cytometry plots and geometric means of forward scatter (FSC) representing size and side scatter (SSC) representing granularity of peritoneal MCs in M-Ext1 and control mice. **(E)** Mean fluorescent intensity of c-kit expression in peritoneal MCs in M-Ext1 and control mice. **(F)** Representative Giemsa and Toluidine Blue staining of c-kit-magnetic beads enriched peritoneal cavity MCs from M-Ext1 and control mice. **(G)** Percentages of different cell populations isolated from the peritoneal cavity determined by flow cytometry; PMN – polymorphonuclear granulocytes, Eos – eosinophils, Monos – monocytes, LPM – large peritoneal macrophages, SPM – small peritoneal macrophages. Results are represented as mean ± SEM. Each symbol in the graphs is an individual mouse. Flow cytometry plots in **(B–E, G)** are representative of 3 individual experiments. Images in **(F)** are representative of 3 individual mice of each genotype. Statistical significance was determined by unpaired Student's t-test. Values of $p<0.05$ were considered statistically significant, *$p < 0.05$, **$p < 0.01$, ***$p < 0.001$, ****$p < 0.0001$, ns, not significant.

cells at d. 4 of Thioglycolate induced peritonitis. We observed a similar MCs phenotype in 14-weeks-old Heparin deficient mice (Supplementary Figures 3A–C) and did not find any differences in the proportions and numbers of any PECs populations (Supplementary Figures 3D, E). Therefore, we conclude Heparin is not required for inflammatory cell recruitment during sterile peritonitis.

To test the role of Heparin in bacterial peritonitis, we used intraperitoneal *L. monocytogenes* infection as MCs depletion enhances susceptibility to *L. monocytogenes* peritonitis (26). We infected 6 weeks-old M-Ext1 and control mice intraperitoneally with *L. monocytogenes* and determined the bacterial burden at days 2 and 7 post-infection. We found comparable bacterial burden and organ weight in Heparin-deficient and control mice (Figures 4F, G). Hence, we conclude that Heparin is not required for *L. monocytogenes* infection clearance in the peritoneal cavity. Thus, in both peritonitis models that we used, the absence of Heparin was dispensable for the recruitment of inflammatory cells and the clearance of the pathogen.

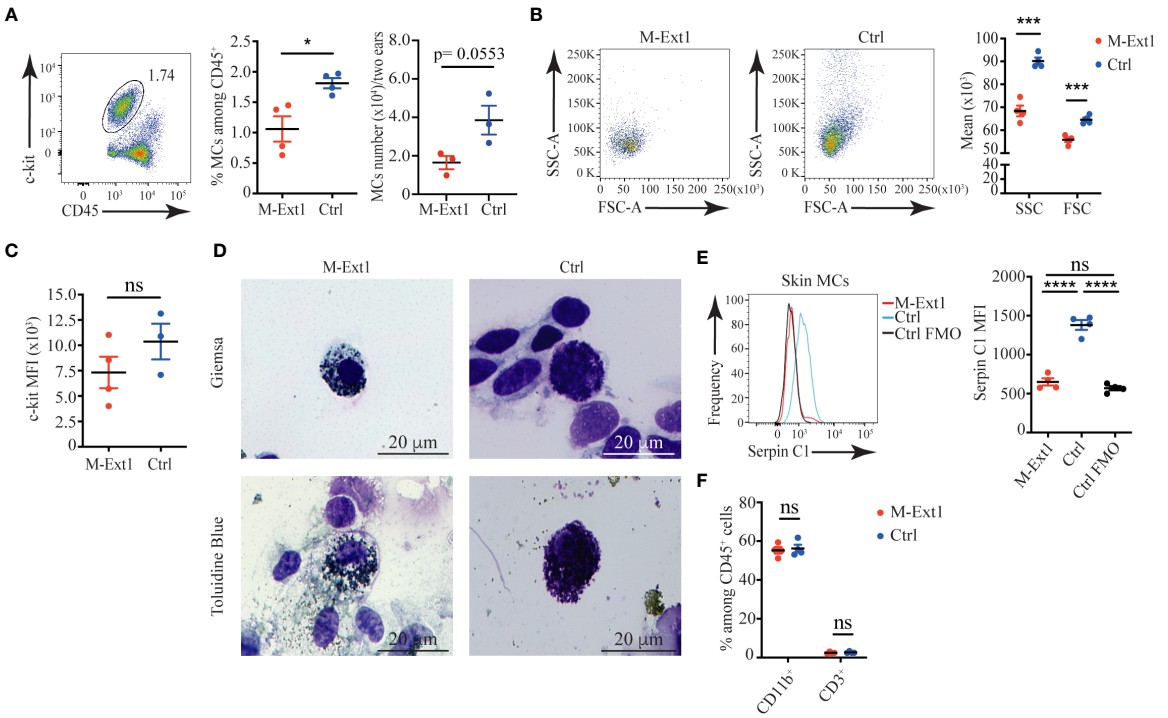

FIGURE 3
Reduced numbers and granularity in 14-weeks old M-Ext1 skin MCs. **(A)** Representative gating strategy, percentages, and numbers of skin MCs in M-Ext1 and control mice. **(B)** Representative dot plots and graphs of geometric means of size (FSC) and granularity (SSC) of skin MCs. **(C)** Mean fluorescent intensity of c-kit expression in skin MCs in M-Ext1 and control mice. **(D)** Representative Giemsa and Toluidine Blue staining of c-kit-magnetic beads enriched skin MCs from M-Ext1 and control mice. **(E)** Representative histograms and statistics of mean fluorescent intensity (MFI) of Serpin C1 binding to fixed and permeabilized skin MCs from M-Ext1 and control mice. **(F)** Percentages of $CD11b^+$ and $CD3^+$ cells in the skin from M-Ext1 and control mice. Results are represented as mean ± SEM. Each symbol in the graphs is an individual mouse. Flow cytometry plots in **(A–C, E)** are representative of 4 individual experiments. Images in **(D)** are representative of 3 individual mice of each genotype. Statistical significance was determined by unpaired Student's t-test. Values of $p<0.05$ were considered statistically significant, $^*p < 0.05$, $^{***}p < 0.001$, $^{****}p < 0.0001$, ns, not significant.

Heparin enhances the spread of skin infection

To test the importance of skin MC Heparin in combatting bacterial infection, we used necrotizing dermatitis caused by *S. aureus*. The absence of MCs promotes the spread of skin lesions in this model (27). We infected M-Ext1 and control mice intradermally with *S. aureus* strain JE2 and measured the lesion area every 2 days post-infection. Surprisingly, the skin lesions on M-Ext1 mice were smaller than control mice (Figures 5A, B). The difference was the greatest at early time points (day 1-3) and disappeared after day 5. Corresponding to the skin lesions, the bacterial burden in the tissue was significantly lower in M-Ext1 mice on day 3 (Figure 5C), while there was no difference on day 10 (Figure 5D). Thus, the absence of Heparin facilitates bacterial killing and limits the spread of necrotizing dermatitis caused by *S. aureus* at early time points.

Heparin deficiency augments skin inflammation upon irritant challenge

The smaller lesion size of *S. aureus* necrotizing dermatitis in M-Ext1 mice was unexpected and prompted us to further explore the importance of Heparin in skin MCs. First, we turned to an inflammatory model that depends exclusively on MCs – the irritant dermatitis. Application of the irritant DNFB to the skin on mouse ears without prior sensitization leads to ear swelling within hours, which is abolished in MC-deficient mice (5). Indeed, DNFB painting induced ear swelling that peaked at 3 h in control 14-weeks-old mice (Figure 6A). However, the ear swelling was much greater and occurred faster in M-Ext1 mice, suggesting that the absence of Heparin enhances inflammation. This phenomenon occurred only in older (14-weeks-old) but not in younger mice (6-weeks-old) M-Ext1 mice, in which the ear swelling was identical to controls (Supplementary Figure 4A). This result is consistent with the absence of skin MCs defects in younger mice. Another model

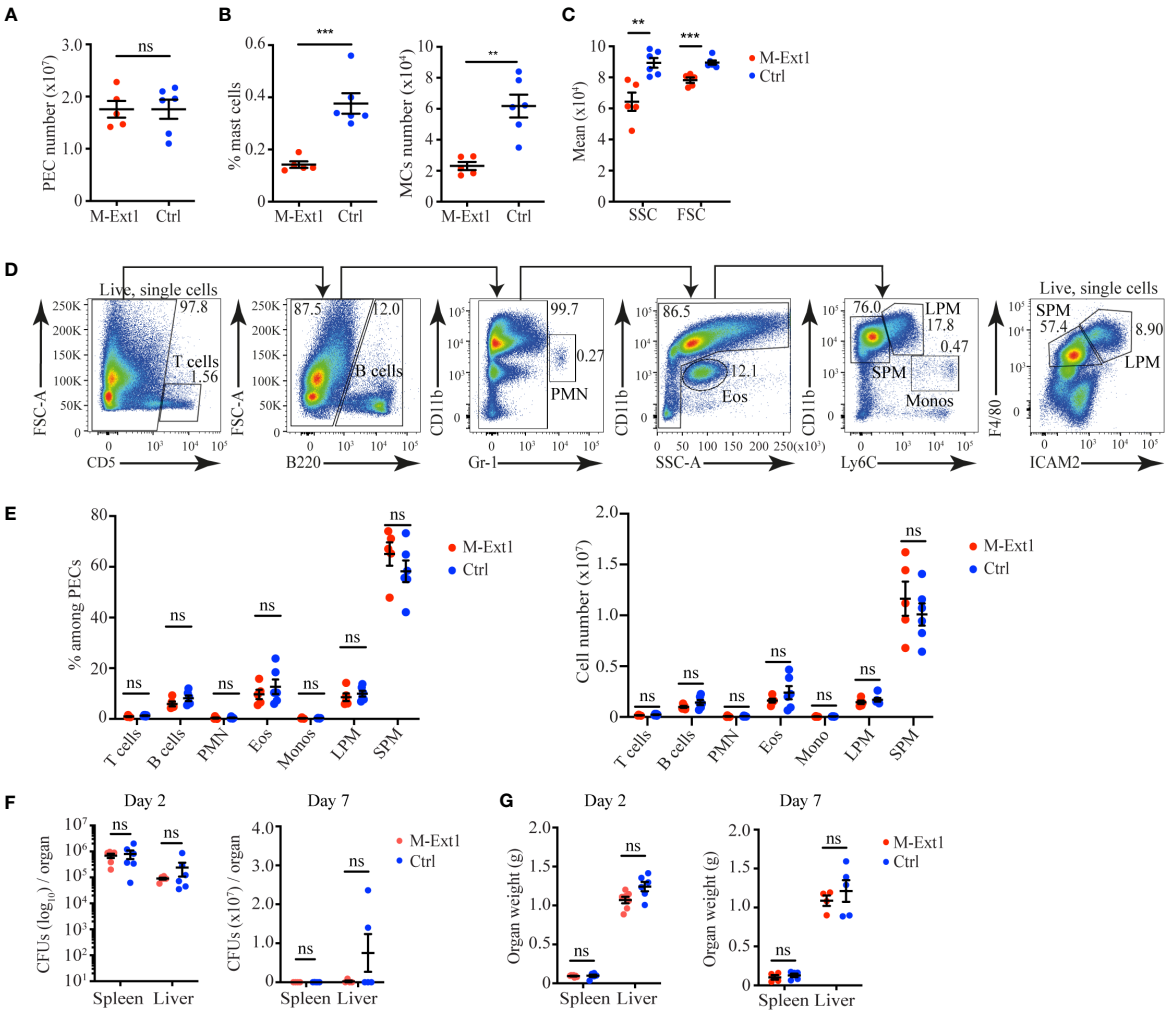

FIGURE 4
Unimpaired recruitment of inflammatory cells in M-Ext1 mice during sterile peritonitis and pathogen clearance during bacterial peritonitis in 6-weeks old mice. **(A)** The total number of peritoneal exudate cells isolated from the peritoneal cavity of M-Ext1 and control mice at day 4 post intraperitoneal injection with 4% Thioglycolate. **(B)** MCs percentages and numbers among peritoneal cells at day 4 after Thioglycolate injection in M-Ext1 and control mice. **(C)** Geometric means of size (FSC) and granularity (SSC) of peritoneal cavity MCs from M-Ext1 and control mice injected intraperitoneally with 4% Thioglycolate 4 days in advance. **(D)** Gating strategy for identifying different populations within the peritoneal exudate cells. **(E)** Percentages and numbers of different cell populations isolated from the peritoneal cavity of M-Ext1 and control mice injected intraperitoneally with 4% Thioglycolate 4 days in advance. **(F)** Bacterial burden in spleens and livers from M-Ext1 and control mice infected intraperitoneally with *L. monocytogenes* determined at day 2 and day 7 post-infection. **(G)** Weights of spleens and livers from *L. monocytogenes* infected M-Ext1 and control mice determined at day 2 and day 7 post-infection. Results are represented as mean ± SEM. Each symbol in the graphs is an individual mouse. Data in **(A–C, E)** are from 5-6 mice per group. Flow cytometry plots in **(D)** are representative of 6 individual experiments. Data in **(F, G)** are from 5-6 mice per group. Statistical significance was determined by unpaired Student's t-test, except for **(F)**, in which non-parametric Mann-Whitney test was used. Values of $p<0.05$ were considered statistically significant, $^{**}p<0.01$, $^{***}p<0.001$, ns, not significant.

that relies on skin MCs for inducing inflammation is PCA (28). Injection of a model antigen (chicken ovalbumin – Ova) caused ear swelling in mice pre-sensitized with anti-Ova IgE (Figure 6B). In contrast to the irritant dermatitis, the response to IgE crosslinking was significantly decreased at several time points in 14-weeks old Heparin-deficient mice. No difference from controls was observed in younger, 6 weeks old mice in PCA (Supplementary Figure 4B). Taken together, our results indicate that M-Ext1 mice have exaggerated skin response to irritants but not FcεR1 ligation.

Heparin-deficient skin MCs contain less Histamine and TNFα but have enhanced expression of *Mrgprb2*

We assessed several critical inflammatory mediators stored in mast cell granules to understand the mechanism behind the enhanced ear-swelling upon DNFB application in M-Ext1 mice. Histamine is one of the most important biogenic amines and regulates vascular permeability, smooth muscle contraction, and

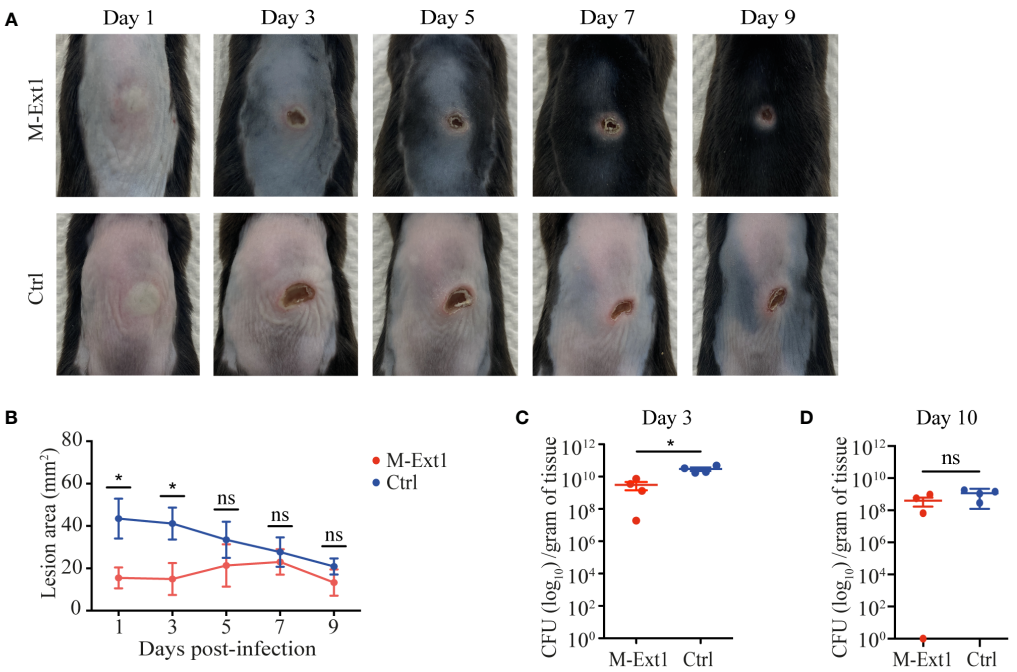

FIGURE 5
Heparin enhances the spread of skin infection. **(A)** Representative images of skin lesions from M-Ext1 and control mice at the indicated time points post i.d. infection with 10^7 *S. aureus* strain JE2. **(B)** Comparison of the areas of skin lesions in infected M-Ext1 and control mice at indicated times. **(C)** Bacterial burden in homogenized skin tissue surrounding the lesions determined at day 3 post-infection in infected M-Ext1 and control mice. **(D)** Bacterial burden in homogenized skin tissue surrounding the lesions at day 10 post-infection in M-Ext1 and control mice. Results are represented as mean ± SEM from 4 mice of each genotype. Each symbol in the graphs is an individual mouse. Images in **(A)** are representative of 4 individual mice. Statistical significance in **(B)** was determined by unpaired Student's t-test comparing M-Ext1 to control mice at each time point. Statistical significance in **(C, D)** was determined by two-tailed Mann-Whitney test. Values of $p<0.05$ were considered statistically significant, *$p < 0.05$, ns, not significant.

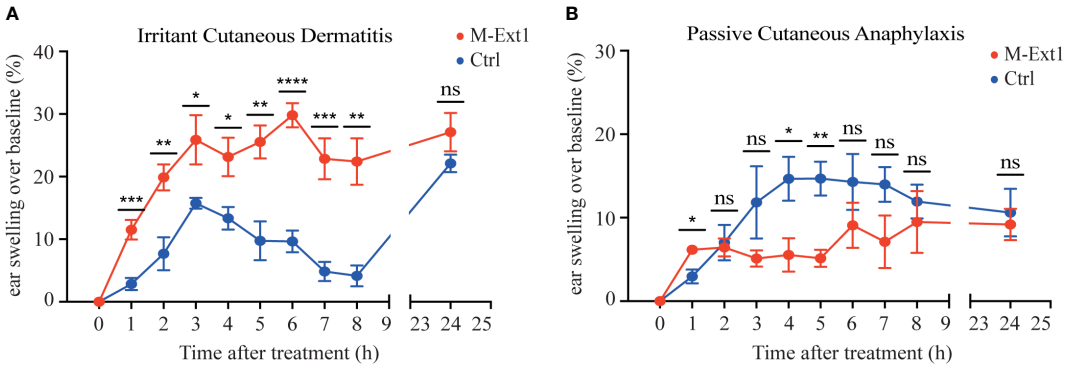

FIGURE 6
Heparin deficiency augments skin inflammation upon irritant challenge but not in PCA model in 14-weeks old mice. **(A)** The change of ear thickness over baseline between M-Ext1 and control mice at the indicated time points after 0.5% DNFB application. **(B)** The change of ear thickness over baseline between M-Ext1 and control mice after i.v. injection of chicken ovalbumin (Ova) following prior sensitization with mouse anti-Ova IgE of M-Ext1 and controls mice. Results are represented as mean ± SEM from 3-6 mice of each genotype. Each symbol in the graphs is an individual mouse. Statistical significance was determined by unpaired Student's t-test. In **(A, B)**, the comparison between M-Ext1 and control mice was done for each time point. Values of $p<0.05$ were considered statistically significant, *$p < 0.05$, **$p < 0.01$, ***$p < 0.001$, ****$p < 0.0001$, ns, not significant.

many other biological processes (29). We used immunofluorescent staining of skin sections from M-Ext1 and control mice to reveal the abundance of Histamine in skin mast cells. To identify the mast cells in mutant mice, we crossed them to *ROSA26*$^{LSL\text{-}GFP}$ so that connective tissue mast cells would express GFP. Each control mast cell contained numerous granules staining with anti-Histamine antibody (Figure 7A). However, Histamine was barely detectable in mast cells lacking Heparin, and very few Histamine-positive granules could be detected in the skin of these mice. Another essential inflammatory mediator stored in mast cell granules is the cytokine TNFα. It is critically important for mast cell-mediated neutrophil recruitment (30). TNFα was detectable in peritoneal and skin mast cells (Figures 7B, C), but it was expressed at significantly lower levels in Heparin-deficient mast cells compared to controls. Moreover, neutrophil recruitment 2 hours after DNFB application to the skin was reduced in M-Ext1 mice (Figure 7D), confirming the indispensable role of TNFα in neutrophil recruitment. Thus, both Histamine and TNFα were reduced in Heparin-deficient mast cells and cannot explain the increased ear swelling following skin irritants application and the smaller lesion size in *S. aureus* necrotizing dermatitis in M-Ext1 mice.

The differential responsiveness of M-Ext1 mice to irritant dermatitis caused by DNFB and IgE-mediated PCA prompted us to investigate the expression of *Mrgprb2*. *Mrgprb2* is a receptor for basic secretagogues such as several irritants, peptides, and toxins, including *S. aureus* δ-toxin, that can activate MCs independently of FcεR1 (31, 32). We sorted skin MCs from 14-week-old mice and evaluated the expression of *Mrgprb2* by qPCR. We found that *Mrgprb2* expression was significantly up-regulated in M-Ext1 MCs compared to controls (Figure 7E), potentially explaining the enhanced sensitivity of M-Ext1 MCs to irritants such as DNFB.

Discussion

Here, we show that Heparin deficiency has a profound effect on connective tissue MCs. The absence of Heparin resulted in reduced granule content and a lower number of MCs in the peritoneal cavity and the skin. MC Heparin was not required to recruit inflammatory cells during sterile peritonitis nor for pathogen clearance during bacterial peritonitis. However, necrotizing dermatitis lesions caused by *S. aureus* were smaller and had a lower bacterial burden in Heparin-deficient mice, and the mice exhibited exaggerated irritant dermatitis. We ruled out increased production and storage of Histamine and TNFα as reasons for the altered functions of the Heparin-deficient mast cells. However, these cells featured overexpression of the irritant receptor *Mrgprb2*, which could potentially explain the enhanced responsiveness of M-Ext1 mice to DNFB and *S. aureus* producing the *MrgprB2* ligand δ-toxin (32).

Just as described before in the *Ndst2*$^{-/-}$ strains (11, 10), the absence of Heparin in M-Ext1 mice diminished the number of MCs and their granularity, confirming the requirement for Heparin in packaging the granule mediators. An important difference between the two mouse strains is that *Ndst2*$^{-/-}$ mice lack only sulfation but not the HS backbone of Heparin. It is possible that the unsulfated HS chains on Serglycin maintain some of Heparin's functions. Nevertheless, the similarity in the phenotype between the two mouse strains argues that Heparin sulfation is essential for the packaging of MC granules.

Although first demonstrated more than 20 years ago, the requirement of Heparin for MC survival has not been completely explained. The leading theory is that the enzymatically active proteases need to be restrained by Heparin to prevent proteolytic damage. However, ~50% of MCs survive without any Heparin indicating adaptation of these cells most likely through down-regulation of protease expression as has been demonstrated for Mcpt4, Mcpt5, Mcpt6, and Cpa (10-12). An additional factor for the lower number of MCs could be the lower expression of c-kit, the essential growth factor for MCs that has also been reported by Abrink et al. (12). It was surprising that peritoneal MCs were reduced in both young and older mice, but skin MCs were found in normal numbers in young (6 weeks) but not in older (14 weeks) mice. The reason for this discrepancy might lie in the developmentally programmed increase in Heparin content (20) and the existence of a threshold above which Heparin-unbuffered proteases might become toxic. Alternatively, potential differences in the reliance on Heparin and the maintenance of MCs from different origins (early erythro-myeloid progenitors vs. late erythro-myeloid progenitors vs. adult hematopoietic stem cells) could also be at play (33).

Surprisingly, despite their reduced numbers of MCs and lack of granules, Heparin-deficient mice responded stronger to certain stimuli. In irritant dermatitis induced by DNFB, the ear swelling was greater in M-Ext1 mice than in controls. However, the enhanced response could not be attributed to higher production of Histamine or TNFα-mediated neutrophil recruitment, as both of these mediators were lower in Heparin-deficient mast cells. One possibility is that increased Tryptase release from these cells could account for the increased swelling as Tryptase facilitates edema formation (34). Moreover, *Ndst2*$^{-/-}$ mice seem to have higher mRNA levels of *Mcpt7*, which is a Tryptase (11). Unfortunately, the Tryptase activity in sorted primary mast cells was below the detection threshold.

Exaggerated MCs response has been previously observed in mice deficient for Langerhans cells, specialized antigen-presenting cells in the epidermis (27). In this study, skin MCs were found to express higher levels of the receptor *Mrgprb2*, which is responsible for FcεR1-independent MCs degranulation following a variety of stimuli, including antibiotics, DNCB, croton oil, house dust mite, Substance P, and so on (27, 31)

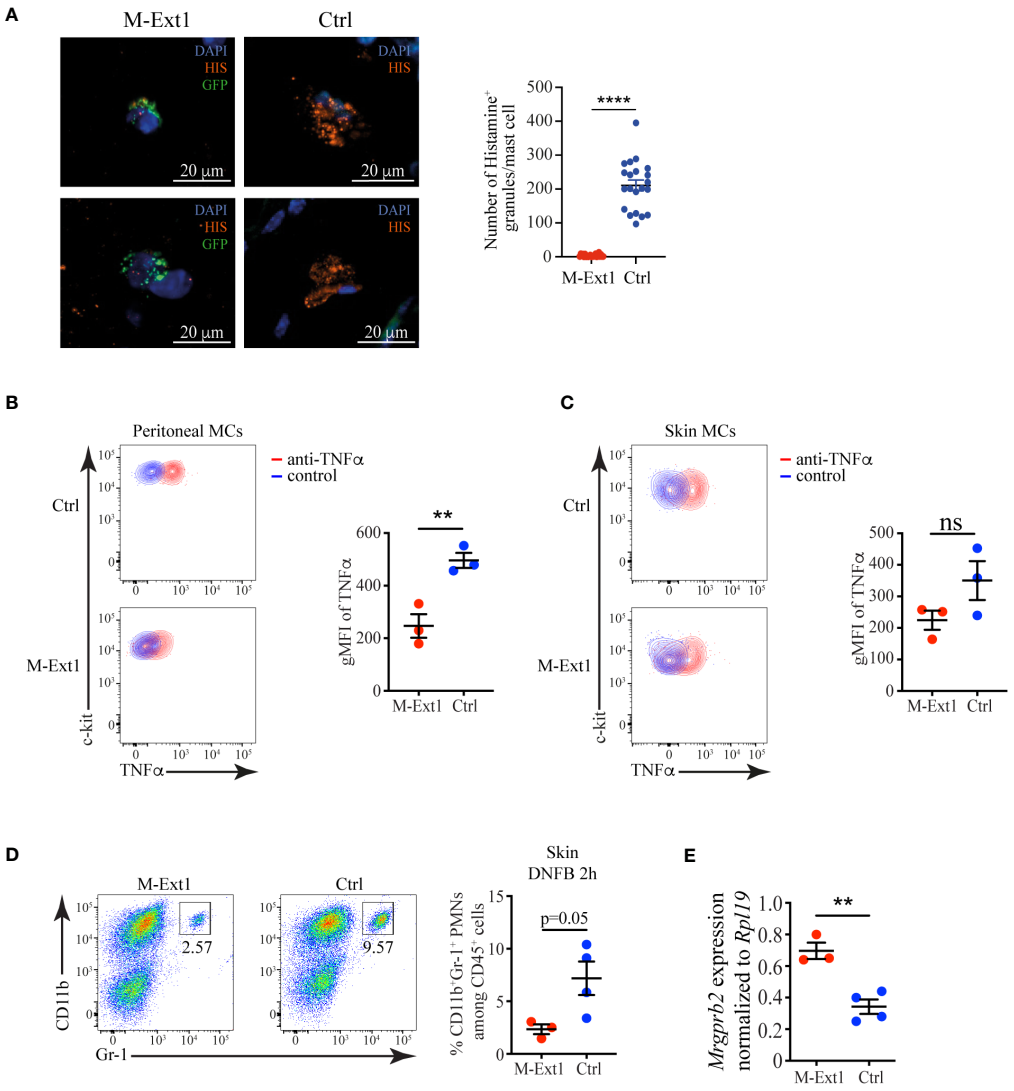

FIGURE 7
Reduced levels of Histamine and TNFα, but an enhanced expression of *Mrgprb2* in Heparin-deficient mast cells. **(A)** Immunofluorescent staining for Histamine of skin sections from M-Ext1 crossed to *ROSA26*$^{LSL\text{-}GFP}$ and control (*Ext1*$^{f/f}$) mice and quantification of the number of Histamine$^+$ granules in skin mast cells from both genotypes. Histamine$^+$ granules were counted in 3-4 fields of view from sections from three different mice per genotype. **(B)** Flow cytometry plots showing TNFα expression in peritoneal mast cells and comparison of the geometric mean fluorescent intensity (gMFI) between M-Ext1 and control peritoneal mast cells. **(C)** Flow cytometry plots showing TNFα expression in skin mast cells and comparison of the geometric mean fluorescent intensity (gMFI) between M-Ext1 and control skin mast cells. **(D)** Flow cytometry plots showing the abundance of CD11b$^+$Gr1$^+$ monocytes 2 h after DNFB application on the ears of M-Ext1 and control mice. The numbers inside the flow cytometry plots are the percentages of neutrophils among CD45$^+$ hematopoietic cells. **(E)** *Mrgprb2* mRNA expression determined by qPCR from sorted skin MCs from M-Ext1 and control mice. Results are represented as mean ± SEM from 3-4 mice of each genotype. Each symbol in the graphs is an individual mouse. Statistical significance was determined by unpaired Student's t-test. Values of p<0.05 were considered statistically significant, **p < 0.01, ****p < 0.0001, ns, not significant.

(35, 36). Thus, upregulation of *Mrgprb2* could account for the increased ear swelling in response to DNFB and the reduced lesion size in the *S. aureus* necrotizing dermatitis model in M-Ext1 mice. Zhang et al. showed that the absence of Langerhans cells caused a reduction in *MrgprD*-expressing skin neurons that normally suppress MC via glutamate release in the skin (27). Whether this is the case in M-Ext1 mice remains to be determined.

Another explanation for the enhanced killing of bacteria in M-Ext1 mice could lie in the ability of Heparin to dismantle neutrophil extracellular traps (NETs) (37). The highly negatively charged Heparin can interact with and neutralize the positive

charge of histones – major components of NETs (38). Thus, in the absence of Heparin in M-Ext1 mice, there will be greater NETs formation, a higher level of inflammation, and enhanced bacterial clearance. However, this phenomenon only appears influential in the first 3-5 days.

The enhanced ear swelling following DNFB application in M-Ext1 mice was in contrast to the decreased response of these mice in the PCA model. This outcome could result from the reduced number of MCs combined with a normal reaction to FcεR1 ligation. The activation of MCs by IgE crosslinking in Langerhans cells-deficient mice was also normal despite the heightened sensitivity to *MrgprB2* ligands (27). Moreover, PCA severity was slightly reduced but still present in *Ndst2*$^{-/-}$ mice (11). Thus, our findings feed into a model of at least two independent activation modules in MCs – FcεR1-induced and MrgprB2-induced.

Despite the reduction in peritoneal cavity MCs, we could not find a defect in the immune cell recruitment in sterile peritonitis or the pathogen clearance in bacterial peritonitis. These data are consistent with the normal recruitment of neutrophils after IgE injection in *Ndst2*$^{-/-}$ mice (10). The role of MCs in protection against bacterial infection in the peritoneum is controversial. Early studies found a critical protective role for MCs (39). However, more recent work has pointed to detrimental functions of these cells, for example, inhibition of macrophage phagocytosis (40). Additional stimuli and time points need to be tested to conclusively determine the role of Heparin in mast cells for inflammatory cell recruitment.

In summary, our results clarify some of the physiological functions of Heparin and will, undoubtedly, open new avenues of research into the roles of MCs and their granules in health and disease.

Data availability statement

The raw data supporting the conclusions of this article will be made available by the authors, without undue reservation.

Ethics statement

The animal study was reviewed and approved by The Institutional Animal Care and Use Committee of National Yang Ming Chiao Tung University.

Author contributions

SAH-H designed and performed all the experiments, interpreted data, and wrote the manuscript; H-PH biotinylated and tested Serpin C1 as a tool to detect Heparin; Y-HT provided guidance in bacterial infection models; C-YK provided *S. aureus* for necrotizing dermatitis model; YY provided the *Ext1*$^{f/f}$ mice; AR provided *Mcpt5*^{Cre} mice; C-LH conceptualized research and designed experiments; ID conceptualized research, designed experiments, interpreted data, and wrote the manuscript. All authors contributed to the article and approved the submitted version.

Funding

This work was supported by the Ministry of Science and Technology (MOST) grants 106-2320-B-010- 026-MY3, 107-2320-B-010-016-MY3, and 110-2320-B-A49A-521 – to ILD and grants from the Yen Tjing Ling Medical Foundation, CI-107-6, CI-108-5, and CI-111-6 to ID.

Acknowledgments

We would like to thank Dr. Fang Liao (Academia Sinica, Taiwan) for 24G2 hybridoma; Dr. Jie-Rong Huang (NYCU, Taiwan) for help with protein purification and biotinylation; Dr. Rebecca Gentek (Aix-Marseille University, France) for sharing the Avidin-AF488 staining protocol; Dr. Shih-Lien Wang (Tzu-Chi University, Taiwan) for help with *Listeria monocytogenes* experiments. The following reagent was provided by the Network on Antimicrobial Resistance in *Staphylococcus aureus* (NARSA) for distribution by BEI Resources, NIAID, NIH: *Staphylococcus aureus subsp. aureus*, Strain JE2, NR-46543.

Conflict of interest

The authors declare that the research was conducted in the absence of any commercial or financial relationships that could be construed as a potential conflict of interest.

Publisher's note

Supplementary material

The Supplementary Material for this article can be found online at: https://www.frontiersin.org/articles/10.3389/fimmu.2022.1000405/full#supplementary-material

References

1. Galli SJ GN, Tsai M. Mast cells in inflammation and disease: Recent progress and ongoing concerns. *Ann Rev Immunol* (2020) 38:49–77. doi: 10.1146/annurev-immunol-071719-094903

2. Dwyer DF, Barrett NA, Dwyer DF, Barrett NA, Austen KF, Kim EY, et al. Expression profiling of constitutive mast cells reveals a unique identity within the immune system. *Nat Immunol* (2016) 17:878–87. doi: 10.1038/ni.3445

3. Kitamura Y, Go S, Hatanaka K. Decrease of mast cells in W/Wv mice and their increase by bone marrow transplantation. *Blood* (1978) 52:447–52. doi: 10.1182/blood.V52.2.447.bloodjournal522447

4. Rodewald H-R, Feyerabend TB. Widespread immunological functions of mast cells: Fact or fiction? *Immunity* (2012) 37:13–24. doi: 10.1016/j.immuni.2012.07.007

5. Dudeck A, Dudeck J, Scholten J, Petzold A, Surianarayanan S, Köhler A, et al. Mast cells are key promoters of contact allergy that mediate the adjuvant effects of haptens. *Immunity* (2011) 34:973–84. doi: 10.1016/j.immuni.2011.03.028

6. Feyerabend TB, Weiser A, Tietz A, Stassen M, Harris N, Kopf M, et al. Cre-mediated cell ablation contests mast cell contribution in models of antibody- and T cell-mediated autoimmunity. *Immunity* (2011) 35:832–44. doi: 10.1016/j.immuni.2011.09.015

7. Wernersson S, Pejler G. Mast cell secretory granules: Armed for battle. *Nat Rev Immunol* (2014) 14:478–94. doi: 10.1038/nri3690

8. Mulloy B, Lever R, Page CP. Mast cell glycosaminoglycans. *Glycoconj J* (2017) 34:351–61. doi: 10.1007/s10719-016-9749-0

9. Mulloy B, Hogwood J, Gray E, Lever R, Page CP. Pharmacology of heparin and related drugs. *Pharmacol Rev* (2016) 68:76–141. doi: 10.1124/pr.115.011247

10. Forsberg E, Pejler G, Ringvall M, Lunderius C, Tomasini-Johansson B, Kusche-Gullberg M, et al. Abnormal mast cells in mice deficient in a heparin-synthesizing enzyme. *Nature* (1999) 400:773–6. doi: 10.1038/23488

11. Humphries DE, Wong GW, Friend DS, Gurish MF, Qiu WT, Huang C, et al. Heparin is essential for the storage of specific granule proteases in mast cells. *Nature* (1999) 400:769–72. doi: 10.1038/23481

12. Åbrink M, Grujic M, Pejler G. Serglycin is essential for maturation of mast cell secretory granule. *J Biol Chem* (2004) 279:40897–905. doi: 10.1074/jbc.M405856200

13. Ringvall M, Rönnberg E, Wernersson S, Duelli A, Henningsson F, Åbrink M, et al. Serotonin and histamine storage in mast cell secretory granules is dependent on serglycin proteoglycan. *J Allergy Clin Immunol* (2008) 121:1020–6. doi: 10.1016/j.jaci.2007.11.031

14. Niemann CU, Åbrink M, Pejler G, Fischer RL, Christensen EI, Knight SD, et al. Neutrophil elastase depends on serglycin proteoglycan for localization in granules. *Blood* (2007) 109:4478–86. doi: 10.1182/blood-2006-02-001719

15. Grujic M, Christensen JP, Sørensen MR, Åbrink M, Pejler G, Thomsen AR. Delayed contraction of the CD8+ T cell response toward lymphocytic choriomeningitis virus infection in mice lacking serglycin. *J Immunol* (2008) 181:1043–51. doi: 10.4049/jimmunol.181.2.1043

16. Kolset SO, Pejler G. Serglycin: A structural and functional chameleon with wide impact on immune cells. *J Immunol (Baltimore Md 1950)* (2011) 187:4927–33. doi: 10.4049/jimmunol.1100806

17. Madisen L, Zwingman TA, Sunkin SM, Oh SW, Zariwala HA, Gu H, et al. A robust and high-throughput cre reporting and characterization system for the whole mouse brain. *Nat Neurosci* (2009) 13:133–40. doi: 10.1038/nn.2467

18. Inatani M, Irie F, Plump AS, Tessier-Lavigne M, Yamaguchi Y. Mammalian brain morphogenesis and midline axon guidance require heparan sulfate. *Sci (New York NY)* (2003) 302:1044–6. doi: 10.1126/science.1090497

19. Scholten J, Hartmann K, Gerbaulet A, Krieg T, Müller W, Testa G, et al. Mast cell-specific Cre/loxP-mediated recombination *in vivo*. *Transgenic Res* (2007) 17:307–15. doi: 10.1007/s11248-007-9153-4

20. Gentek R, Ghigo C, Hoeffel G, Bulle MJ, Msallam R, Gautier G, et al. Hemogenic endothelial fate mapping reveals dual developmental origin of mast cells. *Immunity* (2018) 48:1160–71.e5. doi: 10.1016/j.immuni.2018.04.025

21. Foulds KE, Zenewicz LA, Shedlock DJ, Jiang J, Troy AE, Shen H. Cutting edge: CD4 and CD8 T cells are intrinsically different in their proliferative responses. *J Immunol* (2002) 168:1528–32. doi: 10.4049/jimmunol.168.4.1528

22. Paudel A, Panthee S, Hamamoto H, Grunert T, Sekimizu K. YjbH regulates virulence genes expression and oxidative stress resistance in staphylococcus aureus. *Virulence* (2021) 12:470–80. doi: 10.1080/21505594.2021.1875683

23. McCormick C, Leduc Y, Martindale D, Mattison K, Esford LE, Dyer AP, et al. The putative tumour suppressor EXT1 alters the expression of cell-surface heparan sulfate. *Nat Genet* (1998) 19:158–61. doi: 10.1038/514

24. Ersdal-Badju E, Lu A, Zuo Y, Picard V, Bock SC. Identification of the antithrombin III heparin binding site. *J Biol Chem* (1997) 272:19393–400. doi: 10.1074/jbc.272.31.19393

25. Qureshi R, Jakschik BA. The role of mast cells in thioglycollate-induced inflammation. *J Immunol* (1988) 141:2090–6.

26. Gekara NO, Weiss S. Mast cells initiate early anti-listeria host defences. *Cell Microbiol* (2008) 10:225–36. doi: 1011/j1462-5822-2007.01033.x

27. Zhang S, Edwards TN, Chaudhri VK, Wu J, Cohen JA, Hirai T, et al. Nonpeptidergic neurons suppress mast cells *via* glutamate to maintain skin homeostasis. *Cell* (2021) 184:2151–66.e16. doi: 10.1016/j.cell.2021.03.002

28. Zabel BA, Nakae S, Zúñiga L, Kim JY, Ohyama T, Alt C, et al. Mast cell-expressed orphan receptor CCRL2 binds chemerin and is required for optimal induction of IgE-mediated passive cutaneous anaphylaxis. *J Exp Med* (2008) 205:2207–20. doi: 10.1084/jem.20080300

29. Ohtsu H. Histamine synthesis and lessons learned from histidine decarboxylase deficient mice. *Adv Exp Med Biol* (2010) 709:21–31. doi: 10.1007/978-1-4419-8056-4_3

30. Dudeck J, Kotrba J, Immler R, Hoffmann A, Voss M, Alexaki VI, et al. Directional mast cell degranulation of tumor necrosis factor into blood vessels primes neutrophil extravasation. *Immunity* (2021) 54:468–483.e5. doi: 10.1016/j.immuni.2020.12.017

31. McNeil BD, Pundir P, Meeker S, Han L, Undem BJ, Kulka M, et al. Identification of a mast-cell-specific receptor crucial for pseudo-allergic drug reactions. *Nature.* (2015) 519:237–41. doi: 10.1038/nature14022

32. Azimi E, Reddy VB, Lerner EA. Brief communication: MRGPRX2, atopic dermatitis and red man syndrome. *Itch (Phila)* (2017) 2:e5. doi: 10.1097/itx.0000000000000005

33. Li Z, Liu S, Xu J, Zhang X, Han D, Liu J, et al. Adult connective tissue-resident mast cells originate from late erythro-myeloid progenitors. *Immunity.* (2018) 49:640–53.e5. doi: 10.1016/j.immuni.2018.09.023

34. Steinhoff M, Vergnolle N, Young SH, Tognetto M, Amadesi S, Ennes HS, et al. Agonists of proteinase-activated receptor 2 induce inflammation by a neurogenic mechanism. *Nat Med* (2000) 6:151–8. doi: 10.1038/72247

35. Meixiong J, Anderson M, Limjunyawong N, Sabbagh MF, Hu E, Mack MR, et al. Activation of mast-Cell-Expressed mas-related G-Protein-Coupled receptors drives non-histaminergic itch. *Immunity* (2019) 50:1163–1171.e5. doi: 10.1016/j.immuni.2019.03.013

36. Serhan N, Basso L, Sibilano R, Petitfils C, Meixiong J, Bonnart C, et al. House dust mites activate nociceptor-mast cell clusters to drive type 2 skin inflammation. *Nat Immunol* (2019) 20:1435–43. doi: 10.1038/s41590-019-0493-z

37. Hogwood J, Pitchford S, Mulloy B, Page C, Gray E. Heparin and non-anticoagulant heparin attenuate histone-induced inflammatory responses in whole blood. *PloS One* (2020) 15:e0233644. doi: 10.1371/journal.pone.0233644

38. Fuchs TA, Brill A, Duerschmied D, Schatzberg D, Monestier M, Myers DD, et al. Extracellular DNA traps promote thrombosis. *Proc Natl Acad Sci U S A* (2010) 107:15880–5. doi: 10.1073/pnas.1005743107

39. Echtenacher B, Männel DN, Hültner L. Critical protective role of mast cells in a model of acute septic peritonitis. *Nature* (1996) 381:75–7. doi: 10.1038/381075a0

40. Dahdah A, Gautier G, Attout T, Fiore F, Lebourdais E, Msallam R, et al. Mast cells aggravate sepsis by inhibiting peritoneal macrophage phagocytosis. *J Clin Invest* (2014) 124:4577–89. doi: 10.1172/JCI75212

frontiers | Frontiers in Immunology

TYPE Original Research
PUBLISHED 16 December 2022
DOI 10.3389/fimmu.2022.1055531

OPEN ACCESS

EDITED BY
Ulrich Blank,
Institut National de la Santé et de la Recherche Médicale (INSERM), France

REVIEWED BY
Ivan Dzhagalov,
National Yang Ming Chiao Tung University, Taiwan
Ana Clara Abadía-Molina,
University of Granada, Spain

*CORRESPONDENCE
Jinwook Shin
shin001@inha.ac.kr

†These authors have contributed equally to this work and share first authorship

SPECIALTY SECTION
This article was submitted to Molecular Innate Immunity, a section of the journal Frontiers in Immunology

RECEIVED 27 September 2022
ACCEPTED 01 December 2022
PUBLISHED 16 December 2022

CITATION
Kim M, Jang G, Kim KS and Shin J (2022) Detrimental effects of simulated microgravity on mast cell homeostasis and function.
Front. Immunol. 13:1055531.
doi: 10.3389/fimmu.2022.1055531

Detrimental effects of simulated microgravity on mast cell homeostasis and function

Minjin Kim[1,2†], Gyeongin Jang[1,2†], Kyu-Sung Kim[1,3] and Jinwook Shin[1,2*]

[1]Inha Research Institute for Aerospace Medicine, Inha University College of Medicine, Incheon, Republic of Korea, [2]Department of Microbiology, Inha University College of Medicine, Incheon, Republic of Korea, [3]Department of Otorhinolaryngology-Head and Neck Surgery, Inha University Hospital, Incheon, Republic of Korea

Exposure to microgravity causes significant alterations in astronauts' immune systems during spaceflight; however, it is unknown whether microgravity affects mast cell homeostasis and activation. Here we show that microgravity negatively regulates the survival and effector function of mast cells. Murine bone marrow-derived mast cells (BMMCs) were cultured with IL-3 in a rotary cell culture system (RCCS) that generates a simulated microgravity (SMG) environment. BMMCs exposed to SMG showed enhanced apoptosis along with the downregulation of Bcl-2, and reduced proliferation compared to Earth's gravity (1G) controls. The reduction in survival and proliferation caused by SMG exposure was recovered by stem cell factor. In addition, SMG impaired mast cell degranulation and cytokine secretion. BMMCs pre-exposed to SMG showed decreased release of β-hexosaminidase, interleukin-6 (IL-6), and tumor necrosis factor-α (TNF-α) upon stimulation with phorbol 12-myristate-13-acetate (PMA) plus calcium ionophore ionomycin, which correlated with decreased calcium influx. These findings provide new insights into microgravity-mediated alterations of mast cell phenotypes, contributing to the understanding of immune system dysfunction for further space medicine research.

KEYWORDS

mast cells, microgravity, growth, survival, function

Introduction

Spaceflight studies have demonstrated that a harsh space environment induces dysregulation of the human immune system in complex ways (1, 2). Astronauts suffer from latent virus reactivation and diverse allergic reactions during shuttle and International Space Station flights (3–5). Microgravity is a key environmental factor responsible for immune dysfunction in astronauts during and after space missions (6, 7).

Many ground-based instruments have been developed to simulate microgravity conditions, including rotating wall vessels (RWVs), clinostats, random positioning machines, and diamagnetic levitation (8). These tools allow us to investigate the effects of microgravity at the cell level cheaply but also to obtain results similar to those of space research (7, 9). Previous studies under SMG have reported various alterations in the growth, differentiation, signal transduction, function, and gene expression of hematopoietic stem cells (HSCs) and immune cells (10–19). However, the effects of microgravity on mast cells have not yet been documented.

Mast cells are tissue-resident immune cells of the hematopoietic lineage that participate in innate and adaptive immune responses against pathogens while also playing crucial roles in the pathogenesis of immediate hypersensitivity reactions and allergic diseases (20, 21). IL-3 and stem cell factor (SCF) are important for their maturation and survival (22). Activation of mast cells can be induced by the antigen crosslinking of immunoglobulin E (IgE) bound to FcεRI, SCF, compound 48/80, phorbol 12-myristate-13-acetate (PMA), and calcium ionophore (23). These immunological and chemical stimuli initiate multiple signaling events, including the phosphorylation of proximal protein tyrosine kinases and mitogen-activated protein kinases (MAPKs) as well as calcium immobilization, culminating in the immediate release of mediators stored in cytoplasmic granules such as histamine (24–26). In addition, the *de novo* synthesis of cytokines and chemokines in the activated cells contributes to late-phase allergic reactions including chronic inflammation (27, 28).

Herein, we explored whether microgravity affects mast cell homeostasis and function using murine bone marrow-derived mast cells (BMMCs) and a rotary cell culture system (RCCS) developed by the National Aeronautics and Space Administration (29) to generate an SMG culture environment. We showed that SMG negatively controls mast cell homeostasis by decreasing proliferation and increasing apoptosis. In addition, both degranulation and cytokine secretion were impaired in SMG-exposed cells after PMA plus calcium ionophore stimulation. Together, the proper gravitational force is a critical factor for the physiological and pathological roles of mast cells.

Materials and methods

BMMC culture

Bone marrow cells flushed from femurs and tibias of 6 to 8-week-old female C57BL/6 mice (DBL, South Korea) were cultured in IMDM–IL-3 medium for 4 to 5 weeks. IMDM–IL-3 is Iscove Modified Dulbecco Medium (IMDM; Welgene) supplemented with 10% fetal bovine serum (Hyclone), Penicillin-Streptomycin-Glutamine (Gibco), MEM Non-Essential Amino Acids (Gibco), 10 mM HEPES (pH 7.4), 1 mM sodium pyruvate, and 50 μM β-mercaptoethanol with 10% IL-3–conditioned medium generated from X63-IL-3 cells (kindly provided by Dr. X-P Zhong, Duke University Medical Center). BMMC purity was routinely monitored by flow cytometry using a BD FACS Calibur system (BD Biosciences) to detect FcεRI and c-Kit. BMMCs generated after culture for at least 4 weeks were used for further studies between 4 and 8 weeks during cell culture.

SMG environment

In order to create an SMG culture environment on the ground, a rotary cell culture system (RCCS, Synthecon) consisting of a High Aspect Ratio Vessel (HARV)-RWV, rotator base, and power supply was used according to the manufacturer's instruction. The HARV-RWV is a bioreactor with an oxygenator membrane that allows gas exchange. BMMC suspension (0.5×10^6 cells/ml) in IL-3–conditioned medium with or without 100 ng/ml SCF (Peprotech) was injected into HARV-RWVs, followed by the removal of bubbles generated to minimize turbulence using sterile syringes. The vessels were attached to the rotator base set in a 37°C–5% CO_2 incubator and rotated at 15 rpm for 24, 48, and 168 h (Figure 1A). The cells cultured in static dishes at the same time were used as a control.

Flow cytometry

BMMCs (0.5×10^6 cells/ml) were placed in HARV-RWVs of an RCCS for SMG or in static culture dishes for 1G and grown in a 37°C–5% CO_2 incubator for 48 h. Thereafter, the cells were stained directly with phycoerythrin (PE)-conjugated anti-mouse c-Kit antibody (BioLegend) or stained at 1h after sensitization with 1 μg/ml IgE (Sigma-Aldrich) followed by incubation with fluorescein isothiocyanate (FITC)-conjugated anti-mouse IgE (BioLegend), and then analyzed by flow cytometry. For apoptosis analysis, cells cultured under SMG and 1G for 48 and 168 h were stained with Annexin V (A5)-PE (BioLegend) for 15 min at RT in a buffer containing 10 mM HEPES (pH 7.4), 140 mM NaCl, and 2.5 mM $CaCl_2$. The proportions of A5-positive apoptotic cells were analyzed using a BD FACS Calibur system. To trace proliferation, cells were labeled with 5 μM CFSE (Invitrogen), a dye that split equally between the two daughter cells following each cell division, and exposed to SMG, SMG +1G, and 1G for 168 h. For SMG+1G, cells were cultured in HARV-RWV of RCCS, and after 24 h, the vessel was separated from RCCS, placed on the ground under 1G condition, and further incubated for 144 h. After the culture, the cells were stained with annexin V-PE. CFSE dilution in the A5-negative live population was analyzed. All the flow cytometry data were visualized using FlowJo V10 software (Tree Star).

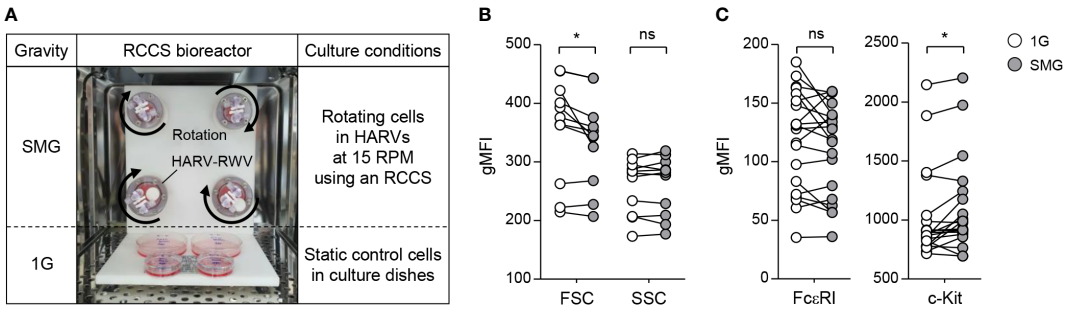

FIGURE 1
Effects of SMG on mast cell size, granularity, and surface expression of FcεRI and c-Kit. **(A)** BMMCs were cultured in HARV-RWVs of RCCS to simulate microgravity conditions or in static dishes under normal gravity (1G) controls. Round arrows indicate rotation. **(B)** Cell size and granularity were determined by geometric mean fluorescence intensity (gMFI) analyses of forward scatter (FSC) and side scatter (SSC) using flow cytometry after 48 h of SMG exposure, respectively (n = 11). **(C)** Scatter graphs represented surface expression of FcεRI and c-Kit on BMMCs after 48 h of SMG exposure. IgE-loaded cells were stained with PE-conjugated c-Kit and FITC-conjugated IgE antibodies (n = 20). Paired, two-tailed student's t-test was performed to detect the statistical significance (*$p < 0.05$). ns, not significant.

β-hexosaminidase and cytokine release

BMMCs (0.5×10^6 cells/ml) exposed to either SMG or 1G for 24 and 48 h were harvested, washed 3 times with pre-warmed Tyrode's solution (130 mM NaCl, 10 mM HEPES [pH 7.4], 1 mM $MgCl_2$, 5 mM KCl, 1.4 mM $CaCl_2$, 5.6 mM glucose and 1 mg/ml bovine serum albumin), and resuspended at 1×10^6 cells/ml. 100 µl cells were seeded in a 96-well plate and treated with 100 µl of either 100 ng/ml phorbol 12-myristate-13-acetate (PMA, Sigma-Aldrich) plus 500 ng/ml ionomycin (Sigma-Aldrich) (P+I) or DMSO (Mock). At 15 min after P+I stimulation, the cell supernatants were incubated with p-nitrophenyl-N-acetyl-b-D-glucosamide (Sigma-Aldrich) as a β-hexosaminidase substrate for 30 min. The enzymatic reactions were terminated by the addition of NaOH. Absorbance at 405 nm with a reference filter at 620 nm was read using a Synergy HTX plate reader (BioTek). The total cellular β-hexosaminidase activity was quantified using supernatant lysed with 0.1% Triton X-100. The percentage of released β-hexosaminidase was analyzed by calculating the stimulatory activity relative to the total activity. For cytokine release analysis, BMMCs were grown under either SMG or 1G for 48 h, followed by resuspension at 1×10^6 cells/ml and stimulation with P+I. The cell culture medium was collected at 6 h after stimulation and the amounts of IL-6 and TNF-α released were determined by ELISA assay using Mouse ELISA Max (BioLegend), according to the manufacturer's protocol.

Calcium flux

BMMCs exposed to either SMG or 1G for 48 h were loaded with FluoForte cell-permeable calcium binding dye using a FluoForte Ca^{2+} assay kit (Enzo Life Sciences, Farmingdale, NY, USA), according to the manufacturer's protocol. Cells were resuspended at 0.5×10^6 cells/ml in Hanks' Buffer with 20 mM HEPES (HHBS) containing dye efflux inhibitor and seeded in 96-well black plate, followed by the addition of 250 ng/ml ionomycin and DMSO control. Calcium responses were visualized by recording fluorescence signals (485 nm excitation and 528 nm emission) using a Synergy HTX plate reader (BioTek) for 420 sec.

Immunoblot assay

BMMC samples exposed to either SMG or 1G for 48 h were resuspended at 5×10^6 cells/ml, stimulated with P+I for 10 min, washed twice with ice-cold phosphate-buffered saline (PBS), and lysed with radio-immunoprecipitation assay buffer (RIPA) supplemented with protease and phosphatase inhibitor cocktails (Sigma-Aldrich). The lysates were quantified using a Bradford protein assay kit (Bio-Rad) and protein samples were separated by SDS-PAGE, transferred onto Nitrocellulose membrane (Bio-Rad), and probed with the following primary antibodies: Bcl-2 (sc-7382) and Bax (sc-7480) from Santa Cruz Biotechnology, and Bcl-xL (#2764), Bax (#7480), BAK (#12105), Vinculin (#13901), phospho (p)-Erk1/2 (#4370), Erk1/2 (#4695), p-Jnk (#4668), Jnk (#9252), p-p38 (#4511) and p38 (#8690) from Cell Signaling Technology. All these antibodies were used at a 1:1000 dilution. Band densities in immunoblots were quantified by densitometry analysis using Adobe Photoshop CS6 (Adobe Systems Software).

Statistical analysis

Data in graphs and immunoblot were presented as the mean ± standard error of the mean (SEM) and mean ± standard deviation (SD) of at least three independent experiments, respectively. Differences between data sets in graphs were

10.3389/fimmu.2022.1055531

evaluated by paired, two-tailed Student's t-test using GraphPad Prism 5 software (GraphPad Prism Software Inc, San Diego, CA, USA) and considered statistically significant at $p < 0.05$ (* $p < 0.05$, ** $p < 0.01$, and *** $p < 0.001$).

Results

Effects of SMG on mast cell apoptosis and proliferation

BMMCs were grown with IL-3 in RWVs of an RCCS bioreactor to create SMG and in static culture dishes for Earth's gravity (1G) control (Figure 1A). As shown in Figure 1B, SMG-exposed cells showed comparable side scatter but reduced forward scatter compared to the control cells after 48 h of culture, indicating a decrease in cell size without affecting granularity by SMG. In addition, SMG exposure had no effect on FcεRI expression but increased c-Kit expression on the cell surface (Figure 1C). Elevated apoptotic death and reduced proliferation of T lymphocytes have been reported under both real microgravity and SMG conditions (30–33). To determine whether microgravity affects mast cell apoptosis, the cells were stained with fluorochrome-conjugated Annexin V (A5). There was no obvious difference in the apoptotic ratios between these cells after 48 h of culture; however, it increased by 1.9-fold in SMG-exposed cells after 168 h compared to 1G control cells (Figure 2A), suggesting that mast cells are more sensitive to apoptosis under SMG. To further investigate the molecular mechanism by which SMG promotes apoptosis in mast cells, we analyzed the protein levels of pro-survival Bcl-2 and Bcl-xL and pro-apoptotic Bax and Bak using immunoblot analysis. The Bcl-2 levels in SMG-exposed cells were significantly lower than those of 1G control cells (Figure 2B). The expression ratios of Bcl-2, Bcl-xL, Bax, and Bak relative to 1G controls in SMG-exposed cells were calculated to be 0.25, 0.92, 0.61, and 1.34, respectively. The c-Kit ligand stem cell factor (SCF) functions as a growth and survival factor in mast cells (34). To investigate whether SCF affects SMG-induced apoptosis in mast cells, BMMCs were cultured in IL-3 or IL-3+SCF medium in HARV-RWVs for 168 h. SMG-exposed cells exhibited increased apoptosis with or without SCF but survived in SCF medium at rates comparable to 1G controls (Figure 2C), indicating that SCF rescues mast cells from SMG-induced apoptosis.

To investigate whether microgravity affects mast cell growth, we labeled BMMCs with CFSE dye used as an indicator of cell proliferation and cultured them under 1G, SMG+1G, and SMG conditions. As shown in Figure 3A, the levels of CFSE were higher as exposure time to SMG increased, indicating the decline of cell proliferation under SMG, which was restored by SCF treatment (Figure 3B). Together, these results demonstrate that SMG negatively regulates mast cell homeostasis by inducing apoptosis and suppressing proliferation.

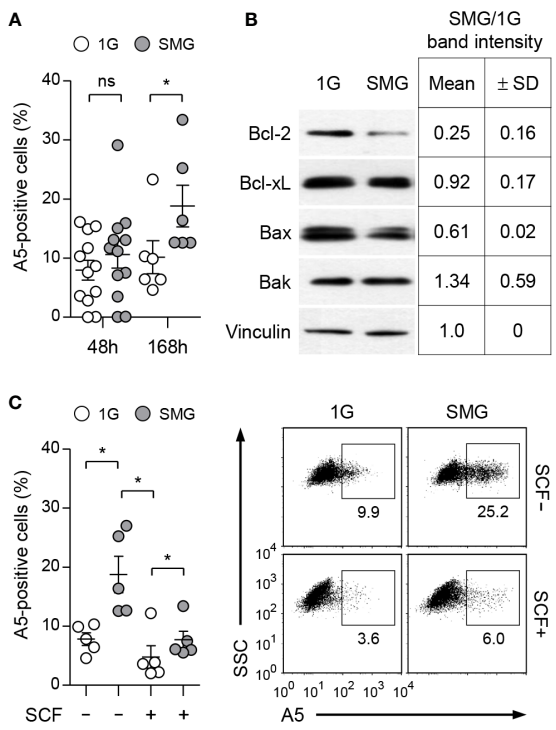

FIGURE 2
Effects of SMG on the apoptosis of mast cells. **(A)** BMMCs were cultured in IL-3 media at the indicated conditions. Apoptotic death was determined by analyzing Annexin V (A5)-positive stained cells using flow cytometry. Data shown are the mean ± SEM (n = 6 to 12). **(B)** Expression of Bcl-2 family proteins. Cells treated as in panel **(A)** for 48 h were lysed and analyzed by immunoblot with the indicated antibodies. Vinculin was used as the loading control. Band intensities were quantified by densitometry and the intensity ratios (SMG/1G) were shown as the mean ± SD (n = 3) from the samples of 3 independent experiments. **(C)** Cells were cultured with IL-3 ± 100 ng/ml SCF under SMG or 1G for 168 h and stained with PE-conjugated A5. Data shown are representative of 5 experiments (n = 5, mean ± SEM). *p < 0.05 by Student's t-test. ns, not significant.

Effects of SMG on mast cell effector functions

Activation of mast cells results in the degranulation of preformed mediators and the release of newly synthesized cytokines in a phasic manner (35). To investigate the effects of SMG on mast cell effector functions, we stimulated BMMCs that were cultured under SMG for 48 h with the diacylglycerol analog PMA plus calcium ionophore ionomycin (P+I). Co-treatment of diacylglycerol analog and calcium ionophore can mimic the FcεRI-mediated activation of mast cells (36, 37). Following activation, β-hexosaminidase released together with histamine from mast cell granules is widely used as an indicator of degranulation (38, 39). Cellular functional degranulation was assessed by measuring the enzymatic activity of β-hexosaminidase on its substrate. The P+I-induced release of β-

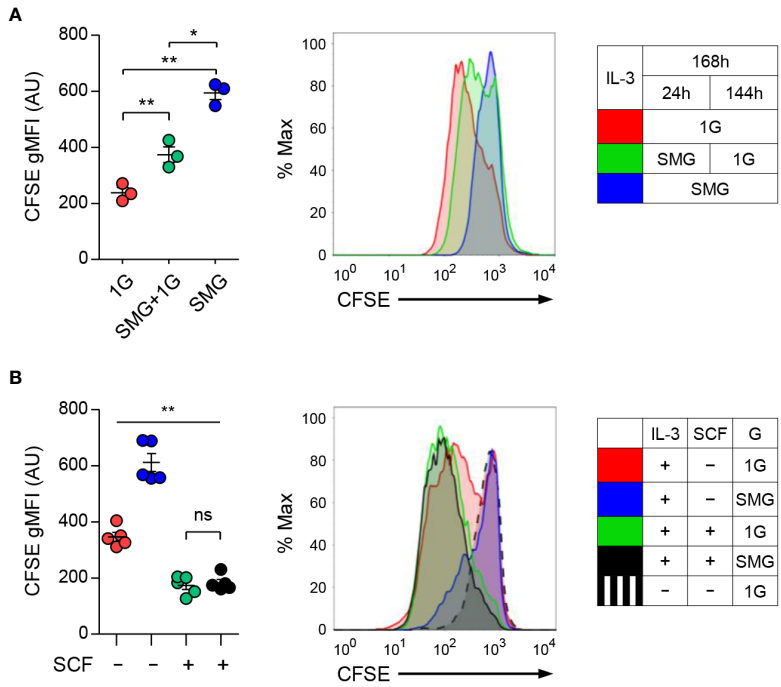

FIGURE 3
Effects of SMG on the proliferation of mast cells. **(A)** Carboxyfluorescein succinimidyl ester (CFSE)-labeled BMMCs were cultured with IL-3 under 1G, SMG+1G, and SMG conditions for 168 h. CFSE is a cell-permeable dye diluted during cell division. After the exclusion of A5-stained cells, CFSE dilutions were monitored using flow cytometry. Data are shown as the mean ± SEM (n = 3). **(B)** CFSE-labeled cells were cultured with IL-3 ± SCF under SMG or 1G for 168 h and cell proliferation was analyzed using flow cytometry. Data are shown as the mean ± SEM of 5 experiments. The gMFI of each graph represents the cell proliferation activity. CFSE-labeled cells cultured without IL-3 and SCF were used as a negative control for cell proliferation (black dashed line). The P-value comparisons between all groups in **(B)** were determined as $^{**}p < 0.01$ except ns, not significant. $^{*}p < 0.05$.

hexosaminidase was significantly diminished by SMG pre-exposure (Figure 4A), indicating the inhibition of P+I-induced degranulation by SMG. The activities in whole cell lysates were not obviously different between these cells (Figure 4B), indicating the minimal effect of SMG on β-hexosaminidase production. In addition, to evaluate the effect of SMG on the late-phase function of activated mast cells, the culture media were collected at 6 h after stimulation and were subjected to ELISA to measure secreted cytokines. Compared to 1G controls, the amounts of IL-6 and TNF-α secreted from SMG-pre-exposed cells were decreased by 20% and 36%, respectively (Figure 4C). Together, these results demonstrated that SMG inhibits both immediate and late-phase reactions in mast cell activation.

Effects of SMG on calcium flux and MAPK signals

To understand the mechanism of mast cell dysfunction under SMG, we examined calcium mobilization in mast cells. Calcium signal acts as a second messenger in mast cells and is essential for degranulation and the production and release of cytokines including IL-6 and TNF-α (40, 41). BMMCs exposed to either SMG or 1G were loaded with FluoForte calcium binding indicator followed by ionomycin treatment. As shown in Figure 5A, ionomycin-triggered calcium influx was significantly reduced by SMG exposure, which suggests that SMG impairs mast cell effector function by inhibiting the calcium signal. MAPKs also play critical roles in mast cell activation (36, 42). The phosphorylations of Erk1/2, Jnk, and p38 MAPKs were induced by P+I treatment, but no obvious differences were detected between the cells exposed to SMG and 1G (Figure 5B).

Discussion

During deep-space exploration, astronauts are exposed to harsh environmental factors such as microgravity, ionizing radiation, and extreme temperatures, all of which reportedly induce a series of changes in human physiology, including vision impairment, bone and muscle loss, and nervous and immune system dysregulation (43, 44). Among these, immune dysfunction has been particularly concerning because of its

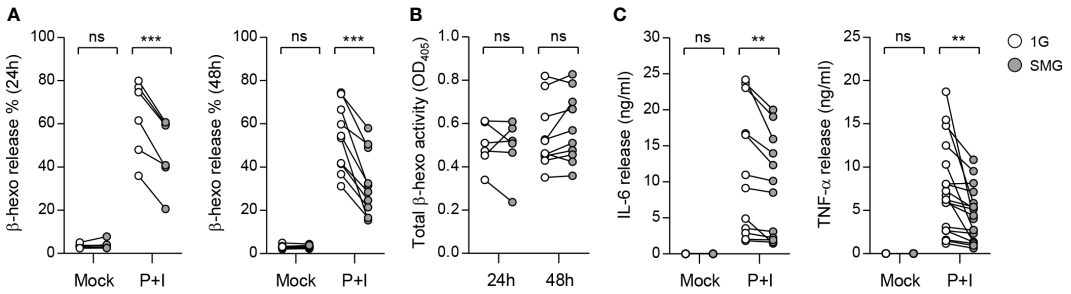

FIGURE 4
Effects of SMG on mast cell functions. BMMCs were exposed to SMG for 24 to 48 h, and then incubated in Tyrode's solution with either 50 ng/ml phorbol 12-myristate-13-acetate (PMA) plus 250 ng/ml ionomycin (P+I) or DMSO (Mock). **(A)** Degranulation was accessed by measuring β-hexosaminidase release at 15 min after stimulation. Pairwise scatter plots represented the percentages of released β-hexosaminidase (n = 6 at 24 h; n = 10 at 48 h). **(B)** Total β-hexosaminidase activity in **(A)** was measured using a cell supernatant dissolved in Triton X-100 and represented by a scatter graph. **(C)** Cells were exposed to SMG for 48 h and the amounts of IL-6 and TNF-α cytokines in the culture media were determined using ELISA at 6 h after stimulation (n = 12 in IL-6; n = 18 in TNF-α). **p < 0.01 and ***p < 0.001, Student's t-test. ns, not significant.

clinical impacts on astronauts during and after space missions. A growing body of studies has reported the impacts of spaceflight on both innate and adaptive immune cells. Examples include altered activation and gene expression profiles of T cells (45–47), decreased phagocytosis and oxidative burst capacity of monocytes and neutrophils (48, 49), and decreased cytotoxicity of natural killer cells (50). Recent case studies have documented the incidence of persistent skin rash, hypersensitivity, and rhinitis onboard the International Space Station (4, 5). Since the results of spaceflight research are complexly affected by various space environments, it is difficult to interpret the effects of specific factors. This present study provides the first evidence that microgravity is an environmental inhibitor for mast cell survival and function.

The balance and interaction between pro-survival and pro-apoptotic Bcl-2 family decide the cell life or death. SMG-induced apoptosis with a reduction in Bcl-2 has been reported in endothelial cells (51, 52), osteoblastic cells (53, 54), and carcinoma cells (55). Bcl-2 can bind to activated Bax, thereby preventing it from disrupting the mitochondrial outer membrane (56). We found that exposure to SMG enhanced apoptosis but reduced the proliferation of mast cells, when cultured in IL-3 medium (Figures 2A, 3A). Correlated with increased apoptosis, diminished expression of Bcl-2 was observed in these cells, where the ratios of

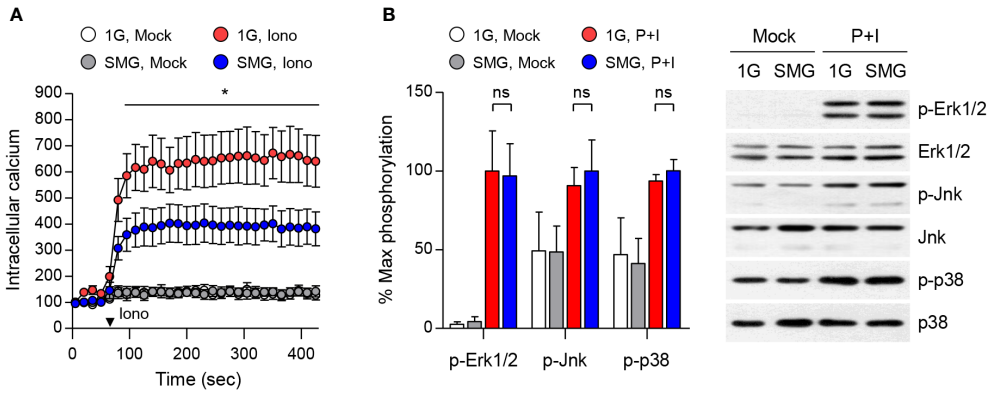

FIGURE 5
Effects of SMG on calcium influx and MAPK signaling. **(A)** After exposure to either 1G or SMG, BMMCs loaded with FluoForte calcium binding dye were treated with 250 ng/ml ionomycin (Iono) at the time marked by an inverted triangle. Intracellular calcium levels were visualized by fluorescence microplate reader for 420 sec. Data are shown as the mean ± SEM of 5 independent experiments. **(B)** BMMCs exposed to either 1G or SMG were stimulated with P+I for 10 min and the cell lysates were subject to immunoblot assay using the indicated antibodies. Band intensities of p-Erk1/2, p-Jnk, and p-p38 were normalized to their total protein expression and are shown as the mean ± SEM (n = 8 in p-Erk1/2; n = 3 in p-Jnk; n = 3 in p-p38). *p < 0.05 by Student's t-test. ns, not significant.

Bax/Bcl-2 protein levels increased to about 2.4 (Figure 2B), suggesting that microgravity controls mast cell apoptosis through the mitochondrial pathway. Interestingly, the upregulation of microRNAs targeting *bcl-2* messages under SMG has been reported. Following RWV culture, the upregulation of miR-503-5p induced endothelial cell apoptosis by decreasing Bcl-2 (52) and the increased level of miR-34a was detected in lymphoblastoid cells (57). Thus, the increase of unknown microRNAs may be associated with diminished Bcl-2 expression and enhanced apoptosis in SMG-exposed mast cells in the current study. Furthermore, we found that SCF supplement efficiently recovered the defects in survival and proliferation (Figures 2C, 3B). Given that Bcl-2 is a key regulator of apoptosis in mast cells (58–60), and its expression is upregulated by SCF (59, 61), this supports the notion that unbalancing the Bcl-2 family, mainly by blocking Bcl-2, contributes to SMG-induced apoptosis in mast cells. The recovery of proliferation by SCF indicates that SCF signaling is intact in mast cells under SMG. In contrast, SMG reportedly inhibits the proliferation of HSCs by decreasing the SCF-Kit-Ras/cAMP-CREB pathway (62). In addition, short-term exposure to SMG caused a more severe reduction in the Concanavalin A-induced proliferation of CD4T cells than CD8T cells (31). Together, these results suggest that the action of microgravity depends on cell types and cell contexts. The molecular mechanism by which SMG controls mast cell survival and proliferation remains to be characterized.

Ca^{2+} signaling plays a central role in various cell lineages, including lymphocytes. Studies on lymphocytes have documented that short-duration spaceflight reduced IL-6 production in human blood samples upon P+I stimulation (63), and SMG pre-exposure decreased IL-2 and IFN-γ production in T cells upon P+I stimulation (13, 31). We showed that SMG-pre-exposed BMMCs manifest a decline in degranulation as well as IL-6 and TNF-α secretion in response to P+I stimulation (Figure 4), which correlated with decreased Ca^{2+} responses to ionomycin (Figure 5A). Thus, it is possible that microgravity contributes to immune dysfunction through altered Ca^{2+} regulation. Intracellular Ca^{2+} mobilization is a critical process in granule exocytosis and cytokine production of mast cells (41); it also plays important roles in mast cell motility, chemotaxis, and the synthesis of arachidonic acid, which is the precursor for leukotrienes and prostaglandins. Thus, it is also possible that microgravity suppresses not only degranulation and cytokine production but also other Ca^{2+}-related functions in mast cells. A recent study showed that SMG suppressed macrophage development from HSCs by altering the Ras/Erk/NF-κB pathway (16). This study also showed that IFN-γ and lipopolysaccharide-induced TNF-α and IL-6 productions were reduced in macrophages differentiated under SMG. However, there were no obvious differences in P+I-induced Erk1/2, Jnk, and p38 phosphorylation in our study (Figure 5B), suggesting that microgravity desensitizes mast cells to P+I stimuli through MAPK-independent pathways.

In summary, microgravity is a negative regulator of mast cell homeostasis and function. SMG inhibits mast cell growth and survival through the downregulation of Bcl-2. In addition, it impaired the P+I-induced degranulation and cytokine secretion, which were associated with impaired Ca^{2+} influx. The effects of microgravity on mast cells require further studies to determine its physiological relevance. However, our findings provide new insights into microgravity-induced immune dysfunction and suggest the application of microgravity environments on Earth as a potential therapeutic strategy in mast cell-related diseases.

Data availability statement

The raw data supporting the conclusions of this article will be made available by the authors, without undue reservation.

Ethics statement

The animal study was reviewed and approved by the Institutional Animal Care and Use Committee of Inha University (INHA 161214-465).

Author contributions

K-SK and JS contributed conception and design of the study. MK and GJ performed the experiments. MK, GJ, JS analyzed the data. JS wrote the first draft of the manuscript. All authors contributed to manuscript revision, read and approved the submitted version.

Funding

This work was supported by the Basic Science Research Program through the National Research Foundation of Korea (NRF) funded by the Ministry of Education (2018R1A6A1A0302552322) and the NRF grant funded by the Korea government (MSIT) (2020R1A2C100845013).

Acknowledgments

We would like to thank all the members of the Inha Research Institute for Aerospace Medicine for their helpful discussions.

Conflict of interest

The authors declare that the research was conducted in the absence of any commercial or financial relationships that could be construed as a potential conflict of interest.

Publisher's note

References

1. Crucian BE, Chouker A, Simpson RJ, Mehta S, Marshall G, Smith SM, et al. Immune system dysregulation during spaceflight: Potential countermeasures for deep space exploration missions. *Front Immunol* (2018) 9:1437. doi: 10.3389/fimmu.2018.01437

2. Borchers AT, Keen CL, Gershwin ME. Microgravity and immune responsiveness: Implications for space travel. *Nutrition* (2002) 18(10):889–98. doi: 10.1016/s0899-9007(02)00913-9

3. Rooney BV, Crucian BE, Pierson DL, Laudenslager ML, Mehta SK. Herpes virus reactivation in astronauts during spaceflight and its application on earth. *Front Microbiol* (2019) 10:16. doi: 10.3389/fmicb.2019.00016

4. Crucian B, Johnston S, Mehta S, Stowe R, Uchakin P, Quiriarte H, et al. A case of persistent skin rash and rhinitis with immune system dysregulation onboard the international space station. *J Allergy Clin Immunol Pract* (2016) 4(4):759–62.e8. doi: 10.1016/j.jaip.2015.12.021

5. Crucian B, Babiak-Vazquez A, Johnston S, Pierson DL, Ott CM, Sams C. Incidence of clinical symptoms during long-duration orbital spaceflight. *Int J Gen Med* (2016) 9:383–91. doi: 10.2147/IJGM.S114188

6. Nguyen N, Kim G, Kim K-S. Effects of microgravity on human physiology. *KJAsEM* (2020) 30(1):25–9. doi: 10.46246/KJAsEM.30.1.25

7. Bradbury P, Wu H, Choi JU, Rowan AE, Zhang H, Poole K, et al. Modeling the impact of microgravity at the cellular level: Implications for human disease. *Front Cell Dev Biol* (2020) 8:96. doi: 10.3389/fcell.2020.00096

8. Herranz R, Anken R, Boonstra J, Braun M, Christianen PC, de Geest M, et al. Ground-based facilities for simulation of microgravity: Organism-specific recommendations for their use, and recommended terminology. *Astrobiology* (2013) 13(1):1–17. doi: 10.1089/ast.2012.0876

9. Nguyen HP, Tran PH, Kim KS, Yang SG. The effects of real and simulated microgravity on cellular mitochondrial function. *NPJ Microgravity* (2021) 7(1):44. doi: 10.1038/s41526-021-00171-7

10. Tackett N, Bradley JH, Moore EK, Baker SH, Minter SL, DiGiacinto B, et al. Prolonged exposure to simulated microgravity diminishes dendritic cell immunogenicity. *Sci Rep* (2019) 9(1):13825. doi: 10.1038/s41598-019-50311-z

11. Savary CA, Grazziuti ML, Przepiorka D, Tomasovic SP, McIntyre BW, Woodside DG, et al. Characteristics of human dendritic cells generated in a microgravity analog culture system. *In Vitro Cell Dev Biol Anim* (2001) 37 (4):216–22. doi: 10.1007/BF02577532

12. Ma C, Xiong Y, Han P, Zhang X, Cao Y, Wang B, et al. Simulated microgravity potentiates hematopoietic differentiation of human pluripotent stem cells and supports formation of 3D hematopoietic cluster. *Front Cell Dev Biol* (2021) 9:797060. doi: 10.3389/fcell.2021.797060

13. Bradley JH, Stein R, Randolph B, Molina E, Arnold JP, Gregg RK. T Cell resistance to activation by dendritic cells requires long-term culture in simulated microgravity. *Life Sci Space Res (Amst)* (2017) 15:55–61. doi: 10.1016/j.lssr.2017.08.002

14. Martinez EM, Yoshida MC, Candelario TL, Hughes-Fulford M. Spaceflight and simulated microgravity cause a significant reduction of key gene expression in early T-cell activation. *Am J Physiol Regul Integr Comp Physiol* (2015) 308(6):R480–8. doi: 10.1152/ajpregu.00449.2014

15. Spielmann G, Agha N, Kunz H, Simpson RJ, Crucian B, Mehta S, et al. B cell homeostasis is maintained during long-duration spaceflight. *J Appl Physiol (1985)* (2019) 126(2):469–76. doi: 10.1152/japplphysiol.00789.2018

16. Shi L, Tian H, Wang P, Li L, Zhang Z, Zhang J, et al. Spaceflight and simulated microgravity suppresses macrophage development *via* altered RAS/ERK/NfκB and metabolic pathways. *Cell Mol Immunol* (2021) 18(6):1489–502. doi: 10.1038/s41423-019-0346-6

17. Li Q, Mei Q, Huyan T, Xie L, Che S, Yang H, et al. Effects of simulated microgravity on primary human NK cells. *Astrobiology* (2013) 13(8):703–14. doi: 10.1089/ast.2013.0981

18. Ludtka C, Silberman J, Moore E, Allen JB. Macrophages in microgravity: the impact of space on immune cells. *NPJ Microgravity* (2021) 7(1):13. doi: 10.1038/s41526-021-00141-z

19. Prasad B, Grimm D, Strauch SM, Erzinger GS, Corydon TJ, Lebert M, et al. Influence of microgravity on apoptosis in cells, tissues, and other systems *in vivo* and *in vitro*. *Int J Mol Sci* (2020) 21(24):9373. doi: 10.3390/ijms21249373

20. Metcalfe DD, Baram D, Mekori YA. Mast cells. *Physiol Rev* (1997) 77 (4):1033–79. doi: 10.1152/physrev.1997.77.4.1033

21. Jimenez M, Cervantes-Garcia D, Cordova-Davalos LE, Perez-Rodriguez MJ, Gonzalez-Espinosa C, Salinas E. Responses of mast cells to pathogens: Beneficial and detrimental roles. *Front Immunol* (2021) 12:685865. doi: 10.3389/fimmu.2021.685865

22. Iemura A, Tsai M, Ando A, Wershil BK, Galli SJ. The c-kit ligand, stem cell factor, promotes mast cell survival by suppressing apoptosis. *Am J Pathol* (1994) 144(2):321–8.

23. Theoharides TC, Alysandratos KD, Angelidou A, Delivanis DA, Sismanopoulos N, Zhang B, et al. Mast cells and inflammation. *Biochim Biophys Acta* (2012) 1822(1):21–33. doi: 10.1016/j.bbadis.2010.12.014

24. Gilfillan AM, Tkaczyk C. Integrated signalling pathways for mast-cell activation. *Nat Rev Immunol* (2006) 6(3):218–30. doi: 10.1038/nri1782

25. Zhang C, Baumgartner RA, Yamada K, Beaven MA. Mitogen-activated protein (MAP) kinase regulates production of tumor necrosis factor-α and release of arachidonic acid in mast cells. indications of communication between p38 and p42 MAP kinases. *J Biol Chem* (1997) 272(20):13397–402. doi: 10.1074/jbc.272.20.13397

26. Rakhmanova V, Jin M, Shin J. Inhibition of mast cell function and proliferation by mTOR activator MHY1485. *Immune Netw* (2018) 18(3):e18. doi: 10.4110/in.2018.18.e18

27. Mukai K, Tsai M, Saito H, Galli SJ. Mast cells as sources of cytokines, chemokines, and growth factors. *Immunol Rev* (2018) 282(1):121–50. doi: 10.1111/imr.12634

28. Beghdadi W, Madjene LC, Benhamou M, Charles N, Gautier G, Launay P, et al. Mast cells as cellular sensors in inflammation and immunity. *Front Immunol* (2011) 2:37. doi: 10.3389/fimmu.2011.00037

29. Schwarz RP, Goodwin TJ, Wolf DA. Cell culture for three-dimensional modeling in rotating-wall vessels: An application of simulated microgravity. *J Tissue Cult Methods* (1992) 14(2):51–7. doi: 10.1007/BF01404744

30. Schatten H, Lewis ML, Chakrabarti A. Spaceflight and clinorotation cause cytoskeleton and mitochondria changes and increases in apoptosis in cultured cells. *Acta Astronaut* (2001) 49(3-10):399–418. doi: 10.1016/s0094-5765(01)00116-3

31. Luo H, Wang C, Feng M, Zhao Y. Microgravity inhibits resting T cell immunity in an exposure time-dependent manner. *Int J Med Sci* (2014) 11(1):87–96. doi: 10.7150/ijms.7651

32. Battista N, Meloni MA, Bari M, Mastrangelo N, Galleri G, Rapino C, et al. 5-lipoxygenase-dependent apoptosis of human lymphocytes in the international space station: Data from the ROALD experiment. *FASEB J* (2012) 26(5):1791–8. doi: 10.1096/fj.11-199406

33. Maccarrone M, Battista N, Meloni M, Bari M, Galleri G, Pippia P, et al. Creating conditions similar to those that occur during exposure of cells to microgravity induces apoptosis in human lymphocytes by 5-lipoxygenase-mediated mitochondrial uncoupling and cytochrome c release. *J Leukoc Biol* (2003) 73(4):472–81. doi: 10.1189/jlb.0602295

34. Okayama Y, Kawakami T. Development, migration, and survival of mast cells. *Immunol Res* (2006) 34(2):97–115. doi: 10.1385/IR:34:2:97

35. Krystel-Whittemore M, Dileepan KN, Wood JG. Mast cell: A multi-functional master cell. *Front Immunol* (2015) 6:620. doi: 10.3389/fimmu.2015.00620

36. Olenchock BA, Guo R, Silverman MA, Wu JN, Carpenter JH, Koretzky GA, et al. Impaired degranulation but enhanced cytokine production after FcεRI stimulation of diacylglycerol kinase ζ-deficient mast cells. *J Exp Med* (2006) 203 (6):1471–80. doi: 10.1084/jem.20052424

37. Wolfe PC, Chang EY, Rivera J, Fewtrell C. Differential effects of the protein kinase c activator phorbol 12-myristate 13-acetate on calcium responses and

secretion in adherent and suspended RBL-2H3 mucosal mast cells. *J Biol Chem* (1996) 271(12):6658–65. doi: 10.1074/jbc.271.12.6658

38. Fukuishi N, Murakami S, Ohno A, Yamanaka N, Matsui N, Fukutsuji K, et al. Does β-hexosaminidase function only as a degranulation indicator in mast cells? the primary role of β-hexosaminidase in mast cell granules. *J Immunol* (2014) 193(4):1886–94. doi: 10.4049/jimmunol.1302520

39. Shin J, Zhang P, Wang S, Wu J, Guan Z, Zhong XP. Negative control of mast cell degranulation and the anaphylactic response by the phosphatase lipin1. *Eur J Immunol* (2013) 43(1):240–8. doi: 10.1002/eji.201242571

40. Baba Y, Nishida K, Fujii Y, Hirano T, Hikida M, Kurosaki T. Essential function for the calcium sensor STIM1 in mast cell activation and anaphylactic responses. *Nat Immunol* (2008) 9(1):81–8. doi: 10.1038/ni1546

41. Holowka D, Calloway N, Cohen R, Gadi D, Lee J, Smith NL, et al. Roles for Ca^{2+} mobilization and its regulation in mast cell functions. *Front Immunol* (2012) 3:104. doi: 10.3389/fimmu.2012.00104

42. Kimata M, Inagaki N, Kato T, Miura T, Serizawa I, Nagai H. Roles of mitogen-activated protein kinase pathways for mediator release from human cultured mast cells. *Biochem Pharmacol* (2000) 60(4):589–94. doi: 10.1016/s0006-2952(00)00354-3

43. Afshinnekoo E, Scott RT, MacKay MJ, Pariset E, Cekanaviciute E, Barker R, et al. Fundamental biological features of spaceflight: Advancing the field to enable deep-space exploration. *Cell* (2020) 183(5):1162–84. doi: 10.1016/j.cell.2020.10.050

44. Setlow RB. The hazards of space travel. *EMBO Rep* (2003) 4(11):1013–6. doi: 10.1038/sj.embor.embor7400016

45. Crucian B, Stowe R, Mehta S, Uchakin P, Quiriarte H, Pierson D, et al. Immune system dysregulation occurs during short duration spaceflight on board the space shuttle. *J Clin Immunol* (2013) 33(2):456–65. doi: 10.1007/s10875-012-9824-7

46. Morukov B, Rykova M, Antropova E, Berendeeva T, Ponomaryov S, Larina I. T-Cell immunity and cytokine production in cosmonauts after long-duration space flights. *Acta Astronautica* (2011) 68:739–46. doi: 10.1016/j.actaastro.2010.08.036

47. Hughes-Fulford M, Chang TT, Martinez EM, Li CF. Spaceflight alters expression of microRNA during T-cell activation. *FASEB J* (2015) 29(12):4893–900. doi: 10.1096/fj.15-277392

48. Kaur I, Simons ER, Castro VA, Ott CM, Pierson DL. Changes in monocyte functions of astronauts. *Brain Behav Immun* (2005) 19(6):547–54. doi: 10.1016/j.bbi.2004.12.006

49. Kaur I, Simons ER, Castro VA, Mark Ott C, Pierson DL. Changes in neutrophil functions in astronauts. *Brain Behav Immun* (2004) 18(5):443–50. doi: 10.1016/j.bbi.2003.10.005

50. Bigley AB, Agha NH, Baker FL, Spielmann G, Kunz HE, Mylabathula PL, et al. NK cell function is impaired during long-duration spaceflight. *J Appl Physiol (1985)* (2019) 126(4):842–53. doi: 10.1152/japplphysiol.00761.2018

51. Zhao H, Shi Y, Qiu C, Zhao J, Gong Y, Nie C, et al. Effects of simulated microgravity on ultrastructure and apoptosis of choroidal vascular endothelial cells. *Front Physiol* (2020) 11:577325. doi: 10.3389/fphys.2020.577325

52. Tang NP, Hui TT, Ma J, Mei QB. Effects of mir-503-5p on apoptosis of human pulmonary microvascular endothelial cells in simulated microgravity. *J Cell Biochem* (2019) 120(1):727–37. doi: 10.1002/jcb.27430

53. Nakamura H, Kumei Y, Morita S, Shimokawa H, Ohya K, Shinomiya K. Antagonism between apoptotic (Bax/Bcl-2) and anti-apoptotic (IAP) signals in human osteoblastic cells under vector-averaged gravity condition. *Ann N Y Acad Sci* (2003) 1010:143–7. doi: 10.1196/annals.1299.023

54. Bucaro MA, Fertala J, Adams CS, Steinbeck M, Ayyaswamy P, Mukundakrishnan K, et al. Bone cell survival in microgravity: evidence that modeled microgravity increases osteoblast sensitivity to apoptogens. *Ann N Y Acad Sci* (2004) 1027:64–73. doi: 10.1196/annals.1324.007

55. Kossmehl P, Shakibaei M, Cogoli A, Infanger M, Curcio F, Schonberger J, et al. Weightlessness induced apoptosis in normal thyroid cells and papillary thyroid carcinoma cells *via* extrinsic and intrinsic pathways. *Endocrinology* (2003) 144(9):4172–9. doi: 10.1210/en.2002-0171

56. Czabotar PE, Lessene G, Strasser A, Adams JM. Control of apoptosis by the bcl-2 protein family: Implications for physiology and therapy. *Nat Rev Mol Cell Biol* (2014) 15(1):49–63. doi: 10.1038/nrm3722

57. Mangala LS, Zhang Y, He Z, Emami K, Ramesh GT, Story M, et al. Effects of simulated microgravity on expression profile of microRNA in human lymphoblastoid cells. *J Biol Chem* (2011) 286(37):32483–90. doi: 10.1074/jbc.M111.267765

58. Shin J, Pan H, Zhong XP. Regulation of mast cell survival and function by tuberous sclerosis complex 1. *Blood* (2012) 119(14):3306–14. doi: 10.1182/blood-2011-05-353342

59. Mekori YA, Gilfillan AM, Akin C, Hartmann K, Metcalfe DD. Human mast cell apoptosis is regulated through bcl-2 and bcl-xL. *J Clin Immunol* (2001) 21(3):171–4. doi: 10.1023/a:1011083031272

60. Peter B, Cerny-Reiterer S, Hadzijusufovic E, Schuch K, Stefanzl G, Eisenwort G, et al. The pan-Bcl-2 blocker obatoclax promotes the expression of puma, noxa, and bim mRNA and induces apoptosis in neoplastic mast cells. *J Leukoc Biol* (2014) 95(1):95–104. doi: 10.1189/jlb.1112609

61. Baghestanian M, Jordan JH, Kiener HP, Bevec D, Agis H, Fritsch G, et al. Activation of human mast cells through stem cell factor receptor (KIT) is associated with expression of bcl-2. *Int Arch Allergy Immunol* (2002) 129(3):228–36. doi: 10.1159/000066773

62. Wang P, Tian H, Zhang J, Qian J, Li L, Shi L, et al. Spaceflight/microgravity inhibits the proliferation of hematopoietic stem cells by decreasing kit-Ras/cAMP-CREB pathway networks as evidenced by RNA-seq assays. *FASEB J* (2019) 33(5):5903–13. doi: 10.1096/fj.201802413R

63. Crucian B, Stowe R, Quiriarte H, Pierson D, Sams C. Monocyte phenotype and cytokine production profiles are dysregulated by short-duration spaceflight. *Aviat Space Environ Med* (2011) 82(9):857–62. doi: 10.3357/asem.3047.2011

frontiers | Frontiers in Immunology

TYPE Original Research
PUBLISHED 21 March 2023
DOI 10.3389/fimmu.2023.1078958

OPEN ACCESS

EDITED BY
Ulrich Blank,
INSERM, France

REVIEWED BY
Markku Varjosalo,
Faculty of Agriculture and Forestry, University of Helsinki, Finland
Gunnar Nilsson,
Karolinska Institutet (KI), Sweden

*CORRESPONDENCE
Ana Olivera
ana.olivera@nih.gov

†These authors have contributed equally to this work and share first authorship

SPECIALTY SECTION
This article was submitted to Molecular Innate Immunity, a section of the journal Frontiers in Immunology

RECEIVED 24 October 2022
ACCEPTED 03 March 2023
PUBLISHED 21 March 2023

CITATION
Bandara G, Falduto GH, Luker A, Bai Y, Pfeiffer A, Lack J, Metcalfe DD and Olivera A (2023) CRISPR/Cas9-engineering of HMC-1.2 cells renders a human mast cell line with a single D816V-KIT mutation: An improved preclinical model for research on mastocytosis.
Front. Immunol. 14:1078958.
doi: 10.3389/fimmu.2023.1078958

CRISPR/Cas9-engineering of HMC-1.2 cells renders a human mast cell line with a single D816V-KIT mutation: An improved preclinical model for research on mastocytosis

Geethani Bandara[1†], Guido H. Falduto[1†], Andrea Luker[1], Yun Bai[1], Annika Pfeiffer[1], Justin Lack[2], Dean D. Metcalfe[1] and Ana Olivera[1*]

[1]Mast Cell Biology Section, Laboratory of Allergic Diseases, National Institute of Allergy and Infectious Diseases, National Institutes of Health, Bethesda, MD, United States, [2]National Institute of Allergy and Infectious Diseases (NIAID), Collaborative Bioinformatics Resource (NCBR), National Institute of Allergy and Infectious Diseases, National Institutes of Health, Bethesda, MD, United States

The HMC-1.2 human mast cell (huMC) line is often employed in the study of attributes of neoplastic huMCs as found in patients with mastocytosis and their sensitivity to interventional drugs *in vitro* and *in vivo*. HMC-1.2 cells express constitutively active KIT, an essential growth factor receptor for huMC survival and function, due to the presence of two oncogenic mutations (D816V and V560G). However, systemic mastocytosis is commonly associated with a single D816V-KIT mutation. The functional consequences of the coexisting KIT mutations in HMC-1.2 cells are unknown. We used CRISPR/Cas9-engineering to reverse the V560G mutation in HMC-1.2 cells, resulting in a subline (HMC-1.3) with a single mono-allelic D816V-KIT variant. Transcriptome analyses predicted reduced activity in pathways involved in survival, cell-to-cell adhesion, and neoplasia in HMC-1.3 compared to HMC-1.2 cells, with differences in expression of molecular components and cell surface markers. Consistently, subcutaneous inoculation of HMC-1.3 into mice produced significantly smaller tumors than HMC-1.2 cells, and in colony assays, HMC-1.3 formed less numerous and smaller colonies than HMC-1.2 cells. However, in liquid culture conditions, the growth of HMC-1.2 and HMC-1.3 cells was comparable. Phosphorylation levels of ERK1/2, AKT and STAT5, representing pathways associated with constitutive oncogenic KIT signaling, were also similar between HMC-1.2 and HMC-1.3 cells. Despite these similarities in liquid culture, survival of HMC-1.3 cells was diminished in response to various pharmacological inhibitors, including tyrosine kinase inhibitors used clinically for treatment of advanced systemic mastocytosis, and JAK2 and BCL2 inhibitors, making HMC-1.3 more susceptible to these drugs than HMC-1.2 cells. Our study thus reveals that the additional V560G-KIT oncogenic variant in HMC-1.2 cells

10.3389/fimmu.2023.1078958

modifies transcriptional programs induced by D816V-KIT, confers a survival advantage, alters sensitivity to interventional drugs, and increases the tumorigenicity, suggesting that engineered huMCs with a single D816V-KIT variant may represent an improved preclinical model for mastocytosis.

KEYWORDS

KIT variants, D816V-KIT, neoplastic human mast cells, mastocytosis, mast cell survival, HMC-1.2 cells

Introduction

KIT (CD117) is a transmembrane tyrosine kinase receptor critical for mast cell survival, proliferation, homing and responsiveness (1–3). Activation of KIT normally occurs by binding to its ligand stem cell factor (SCF), which induces KIT dimerization and activation of its kinase domain that then trans-phosphorylates multiple tyrosine residues in the receptor resulting in recruitment and activation of signaling cascades (4). Various gain-of-function polymorphisms in KIT can also cause KIT dimerization and tyrosine kinase activation in the absence of ligand (4–6). These activating KIT variants, mostly somatic, have been associated with human malignancies, including mast cell proliferative disorders such as mastocytosis (1, 4). In patients with mastocytosis, mast cells accumulate in the tissues, and increased levels of mast cell mediators are thought to contribute to the symptoms associated with this disease (such as recurrent episodes of flushing, shortness of breath, abdominal pain, etc.) (7).

Most oncogenic KIT variants identified in human neoplasms occur in mutational hot spots. In more than 80% of adult patients with systemic mastocytosis, KIT mutations are found in the kinase domain (KD) of KIT (exon 17), commonly in position 816 (D816V), while in childhood mastocytosis D816V has a lower incidence, and a number of mutations occur in the extracellular domain of KIT (exons 8 and 9). Mutations in the juxtamembrane (JM) domain of KIT such as V560G (exon 11) are rare in mastocytosis but frequent in gastrointestinal tumors (GIST) (1, 4, 8) (see Figure 1A). Variants in the KD may differ quantitatively and qualitatively from those in the JM domain, particularly regarding the oncogenic signaling pathways they induce, transforming potential (4) and sensitivity to inhibitors of KIT or signaling pathways, a feature of clinical significance for diagnosis and treatment of disease (8, 9).

Abbreviations: BIM (BCL2L11), BCL-2 interacting mediator of cell death; Cas9, CRISPR-associated protein 9; CRISPR, clustered regularly interspaced short palindromic repeats; ddPCR, droplet digital PCR; GIST, gastrointestinal tumors; gRNA, guide RNAs; hSCF, human stem cell factor; huMC, human mast cell; IPA, Ingenuity pathway analysis; JM, juxtamemembrane; KD, kinase domain; KIT, Stem cell factor receptor; MFI, Mean Fluorescence Intensity; MCL1, myeloid cell leukemia 1; PI, propidium iodide; SCF, stem cell factor; SM, systemic mastocytosis; ssODN, single-stranded oligodeoxynucleotide; WT, wildtype.

In recent years, novel tyrosine kinase inhibitors as well as other strategies have been tested to reduce KIT activity in hematological neoplasms, with some candidates approved and others in clinical trials. However, there is still an unmet medical need for approaches that may reduce mast cell burden/activity in these disorders (9–11). One widely used preclinical model for the evaluation of potential treatments is the human mast cell line HMC-1, isolated from a patient with mast cell leukemia (12, 13). Subsequently, two sublines within HMC-1 cultures were identified: HMC-1.1 cells, containing a heterozygous mutation in V560G-KIT; and HMC-1.2 cells, containing the V560G and D816V-KIT mutations (14) (Figure 1A). The use of HMC-1 mast cells as a pre-clinical model (15) has several advantages: (-i-) the expression of KIT variants frequently found in mastocytosis and other diseases; (-ii-) rapid growth in culture, which allows for high-throughput pharmacological studies; (-iii-) development of tumors in xenograft mouse models for *in vivo* drug testing; and (-iv-) commercial availability. However, a drawback of this model is that neither HMC-1.1 or HMC-1.2 cells carry only the D816V mutation. HMC-1.2 cells which do carry D816V-KIT also carry V560G-KIT and, thus, it is unknown to what extent the signaling pathways, cell responses or sensitivity to drugs are affected by the combined effects of the two KIT variants. Although the presence of more than one KIT mutation has been described in patients with childhood mastocytosis (16) and in instances of acute myeloid leukemia (17) and GIST refractory to treatment (18), most patients with systemic mastocytosis present with D816V-KIT alone (1, 16), emphasizing the need for a neoplastic mast cell model expressing KIT with the single D816V-KIT mutation.

With these considerations, we employed clustered regularly interspaced short palindromic repeats (CRISPR)/CRISPR-associated protein 9 (Cas9) engineering to correct the V560G mutation in HMC-1.2 cells and compared cell attributes between the resulting cell line and the parental line to investigate potential combinatorial effects of the KIT variants. The CRISPR/Cas9 approach successfully delivered a new subline (HMC-1.3) with the single mono-allelic D816V-KIT of the parental cell line but lacking V560G-KIT. As will be shown, we found that the removal of V560G in D816V-containing huMCs did not significantly affect cell growth or constitutive signaling under normal culture conditions compared to the parental HMC-1.2 but resulted in altered transcriptional programs and reduced tumor growth and metastasis in a xenograft model. The gene expression changes

10.3389/fimmu.2023.1078958

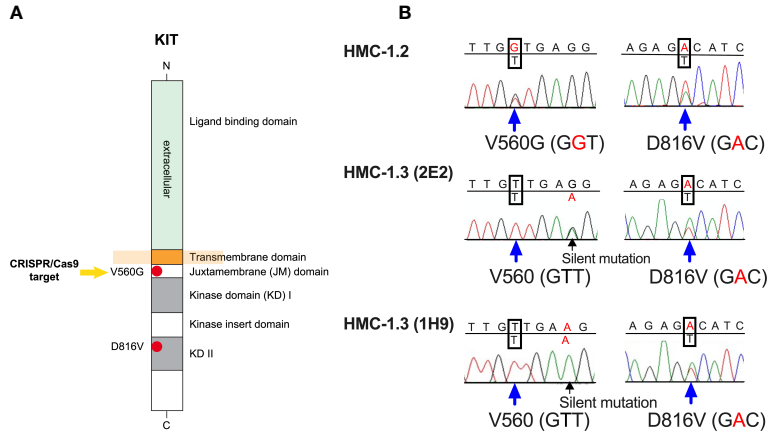

FIGURE 1
The huMC line HMC-1.3 generated by CRISPR/Cas9-mediated editing of HMC-1.2 cells has a single D816V-KIT mutation. **(A)** Schematic representation of the structure of KIT, highlighting the presence in HMC-1.2 cells of the oncogenic V560G variant in the juxtamembrane (JM) domain and of D816V-KIT in the kinase domain (KD). The arrow indicates the target mutation for CRISPR/Cas9 editing. **(B)** Representative Sanger sequencing chromatograms of KIT exons from HMC-1.2 or two separate clones (1H9 and 2E2) of HMC-1.3 cells, demonstrating heterozygous presence of D816V in both HMC-1.2 and in HMC-1.3, and a heterozygous V560G mutation in HMC-1.2 (GGT) that was reversed to the normal allele on this site (GTT) after the CRISPR/Cas9-mediated editing in HMC-1.3.

resulted in a higher propensity to cell death in HMC-1.3 cells that was modest under homeostatic conditions but enhanced in the presence of certain pharmacological inhibitors of KIT and signaling targets, such as inhibitors of JAK2, making them more sensitive to these drugs. These results suggest that the presence of V560G-KIT acts as a functional modifier in D816V-KIT mutated cells, enhancing transcriptional programs of survival and potentially other molecular functions. This data is consistent with the conclusion that the engineered HMC-1.3 cell line with a single D816V-KIT variant represents an additional and improved preclinical model for mastocytosis.

Materials and methods

Reagents

Antibodies against phospho-AKT(Ser473), ERK, phospho-ERK (Thr202/Tyr204), STAT5, and phospho-STAT5 were obtained from Cell Signaling Technology (Danvers, MA); anti-KIT from R&D Systems (Minneapolis, MN) and Santa Cruz Biotechnology (Santa Cruz, CA); anti-phospho-KIT(Tyr823) from Invitrogen (Carlsbad, CA); anti-AKT from BD Biosciences (San Diego, CA); and anti-β actin from Sigma Aldrich (St. Louis, MO); and anti-rabbit IgG 800CW and anti-mouse IgG 680 RD from Licor Biosciences (Lincoln, NE). Human TruStain FcX and APC-conjugated anti-human c-KIT (clone 104D2), unlabeled anti-human KIT antibody (clone 104D2) and Zombie Aqua fixable viability dye were obtained from Biolegend (San Diego, CA); KIT antibody for IHC from Dako-Agilent (Santa Clara, CA); human SCF from R & D Systems; avapritinib, imatinib, dasatinib, midostaurin, fedratinib, STAT5-IN-1, SH4-54, venetoclax, ripretinib (DCC-2618), ruxolitinib, tofacitinib, and C188-9 from SelleckChem (Houston, TX); LY294002 and U0126 from Tocris (Minneapolis, MN); Pierce BCA assay and CyQuant cell proliferation assay from Thermo Fisher Scientific (Waltham, MA); and ViaStain propidium iodide (PI) staining solution from Nexelom Biosciences (Lawrence, MA).

Cell cultures

HMC-1.1 and HMC-1.2 were kindly provided by Dr. Butterfield at the Mayo Clinic (12) under a Uniform Biological Material Transfer Agreement. HMC-1.3 were modified from the parental HMC-1.2 as explained below. All sublines were cultured in IMDM medium supplemented with FBS (10%), L-glutamine (2 mM), penicillin (100 units/ml), and streptomycin (100 µg/ml) and were refreshed from an earlier stock every 3 months.

Genome editing of the KIT-V560G variant in HMC-1.2 using CRISPR/Cas9

Genome editing of HMC-1.2 to revert the heterozygous single nucleotide G560 mutation in KIT (G, GGT) to WT (V, GTT) (Figure 1A) was done by Applied StemCell (Milpitas, CA). A proprietary CRISPR/Cas9 genome editing technology was employed following the steps illustrated in Supplementary Figure 1. Two guide RNAs (gRNAs) were designed using a proprietary gRNA design tool by Applied Stem Cell. Based on the proximity to the target site, off-target profile and predicted activity, the gRNA "Kitex11g2" (5′-AGTACAGTGGAAGGTTGGTG -3′) was selected. The single-stranded oligodeoxynucleotide donor (ssODN) was designed to be used as a repair template for generating the desired GGT>GTT point mutation flanked by 5' and 3' homology arms for the targeted region to the gRNA cut sites during the homology-directed repair process (ssODN sequence: 5'-TGTTCTCTCTCCAGAGTGCTCTAAT

GACTGAGACAATAATTATTAAAAGGTGATCTATTTTTCCC TTTCTCCCCACAGAAACCCATGTATGAAGTACAGTGGAAGG TTGTTGAAGAGATAAATGGAAACAATTATGTTTA CATAGACCCAACACAACTTCCTTATGATCACAAATGGGA GTTTCCCAGAAACAGGCTGA- 3'). In the design of the ssODN, a silent mutation (GAG to GAA, corresponding to aminoacidic position 561) was introduced to destroy a PAM site and prevent re-cutting in the modified genome after repair. Double-stranded gRNA was inserted between the two Bbs1 sites into a bicistronic vector (pBT-U6-Cas9–2A-GFP) for co-expression with the Cas9 protein (pBT-U6-Cas9–2A-GFP). The resulting plasmid was transfected by electroporation together with the ss-ODN into HMC-1.2 cells using 1500 V, 10 ms, and 3 ps in the Neon Transfection System (Thermo Fisher Scientific). Cells were cultured for 48 h, and then selected by puromycin (1 µg/ml) for two to three weeks. The resulting cell population was then further subjected to limiting dilution for cloning and genotype analysis. Fifty single clones were genotyped around the 560 and 816 regions, and 16 were confirmed with the predicted WT sequence in position 560 but containing the mono-allelic D816V variant like the parental line. Sanger sequencing of all KIT exons in five of the clones further confirmed that no other areas in KIT, except those intended, differed from the parental KIT sequence.

Western blots

Cell lysates for Western blots were prepared from $1x10^6$ cells in RIPA buffer as described (19). Protein content in each sample was determined by Pierce BCA assay for equal loading. To assess the effect of SCF on signaling, cells were serum-starved for 2 h. After rinsing twice and resuspending in HEPES buffer containing 0.04% BSA (20), cells were activated with human SCF (100 ng/mL) for the indicated times. Cell protein extracts (20 µg) were resolved by SDS-PAGE (4-12% acrylamide gradient gels) and transferred to nitrocellulose membranes. Membranes were blocked for 60 min with Odyssey blocking buffer (LI-COR Biosciences) and incubated overnight with the primary antibodies (1:1000 dilution). Blots were washed and after 60 min of incubation with the IR-dye (680RD or 800CW)-labeled secondary antibodies, immunoreactive proteins were visualized using an Odyssey CLx imager (LI-COR Biosciences).

Determination of cell surface and intracellular KIT by FACS

Cells ($1x10^6$) were serum-starved for 2 h and then immediately resuspended in cold Azide-containing FACS buffer and placed on ice for 15 min to minimize receptor turn-over. All cells were stained with Zombie Aqua Fixable Viability dye and Fc receptors blocked with Human TruStain FcX according to manufacturer's instructions. Cells were then divided among three tubes for surface, intracellular, and total KIT staining. To quantify intracellular KIT, the cell surface was first saturated with unlabeled anti-human KIT antibody, followed by fixation, permeabilization, and intracellular staining with the same clone of APC-conjugated anti-human KIT. To quantify surface KIT, intact cells were stained with APC-conjugated KIT antibody; these samples were similarly fixed and permeabilized to maintain consistent scatter profiles. To quantify total KIT, intact cells were first stained with APC-conjugated KIT and then fixed/permeabilized for intracellular staining with APC-conjugated KIT. This measured total mean fluorescence intensity (MFI) was statistically indistinguishable from the summative value of Surface MFI + Intracellular MFI using a student t-test, thus validating the staining protocol. Each staining step was performed by incubating the cells on ice for 20 min with 0.5 µg of antibody. Data acquisition was performed with a LSRFortessa™ Cell Analyzer (BD Biosciences) and analyzed using FlowJo (v10) software. The proportion of KIT on the cell surface was calculated as follows:

$$\%\ \text{Surface KIT} = \frac{Surface\ \ MFI}{(Surface\ \ MFI) + (Intracellular\ \ MFI)} \times 100$$

RNA isolation, RNA seq and transcriptome analysis

HMC-1.1, HMC-1.2 and the two individual clones of HMC-1.3 cells (1H9 and 2E2) were plated ($3x10^5$) in triplicates in 6 well plates. After 72 h, total RNA from 2×10^6 cells was extracted using RNeasy plus mini kit (Qiagen, Valencia, CA) and treated with DNase (Bio-Rad, Hercules, CA) to eliminate gDNA contamination. 600 ng of total RNA from each of the 12 samples (4 cell lines done in triplicates) was used as input for an mRNA capture with oligo-dT coated magnetic beads. The mRNA was fragmented, and then a random-primed cDNA synthesis was performed. The resulting double-strand cDNA were pooled and sequenced on NextSeq2000 using Illumina Stranded mRNA Prep Ligation Library Prep and paired-end sequencing. The samples had 67 to 99 million pass filter reads with more than 94% of bases above the quality score of Q30. Samples were processed from raw fastq through to raw expression values using the RNA-seek workflow (https://github.com/OpenOmics/RNA-seek). Within that workflow, raw reads were trimmed for adapters and low-quality bases using Cutadapt v2.10 (21) before alignment to the human reference genome (hg38) and the Gencode Release 39 annotation using STAR v2.5.3 in two-pass mode (22). PCR duplicates were marked using Picard MarkDuplicates v2.27.3 (https://broadinstitute.github.io/picard/). The average mapping rate of all samples was 97%, and unique alignment was above 89%. The mapping statistics were calculated using Picard software. Percent coding bases were between 57-59%. Percent UTR bases were 35-36%, and mRNA bases were between 93-94% for all the samples. The samples had 69-72% non-duplicate reads. From the alignment files, gene-level quantification was performed using RSEM v1.3.0 (23) and pairwise differential expression was performed using DESeq2 (24) implemented in iDEP v94 (25). Raw and normalized expression matrices were uploaded to the Gene Expression Omnibus (GEO) and are available under the accession ID# GSE216446 (https://www.ncbi.nlm.nih.gov/geo/query/acc.cgi?acc=GSE216446). Data were also analyzed with the use of QIAGEN IPA (QIAGEN Inc., https://digitalinsights.qiagen.com/IPA) (26).

qPCR and droplet digital PCR

Total RNA was extracted from 1-3 × 10^6 cells using RNeasy plus mini kit (Qiagen). To quantify various gene transcripts in the samples, one-step reverse transcription and real time-qPCR reactions were performed using iTaq Universal Probes One-Step Kit and the PrimePCR™ probe sets: MCL1 (qHsaCEP0039327) and BCL2L11 (BIM) (qHsaCEP0025251) (Bio Rad). GAPDH (qHsaCEP0041396) and ACTB (qHsaCEP0036280) were used as reference genes.

For ddPCR determinations of allelic frequency of D816V-KIT, genomic DNA was extracted from 1×10^6 cells using a QIAamp DNA blood mini kit (Qiagen). PCR amplifications were performed in nanoliter sized droplets generated using a manual droplet generator (Bio-Rad) after mixing the samples with a primer/probe set (PrimePCR ddPCR mutation assay kit, Bio-Rad) following the manufacturer's instructions. This set is designed to distinguish wild-type KIT from D816V-KIT. Droplets were analyzed on a QX200 Droplet Reader (Bio-Rad).

Determination of viable and dead cells in liquid cultures

HMC-1 cells (2.5×10^4 in in 100 µL) were plated in black clear-bottom 96 well plates (Fisher Scientific Pittsburgh, PA) in normal media in the presence or absence of the indicted inhibitors. After 72 h, or as indicated in the figures, 10 µL of ViaStain propidium iodine (PI) staining solution (Nexelom Biosciences, Lawrence, MA) was added to detect dead cells. Total and dead cells were counted using a Celigo Image Cytometer automated system (Nexelom Biosciences). The number of viable cells was calculated by subtracting the number of dead cells from the total numbers. In some experiments, cells were plated in serum-free media and the number of viable and dead cells determined over time as above.

In other experiments, the number of viable cells was determined using a fluorometric CyQuant assay. Cells were plated as above and after 48 or 72 h, an equal volume of 2X CyQuant®Direct detection reagent (Thermo Fisher Scientific) containing a fluorescent nucleic acid stain for viable cells was added to the wells to determine cell growth. After 1 h at 37°C, fluorescence was measured at 480/535 nm.

Cell growth in semi-solid media

For colony assays, 7.5x10^4 cells were mixed with complete media containing 0.5% Bacto agar (soft agar) and plated in 48 well plates. Alternatively, cells were similarly embedded into Matrigel (Corning Incorporated, Tewksbury, MA) diluted 1:1 in cell culture media following the manufacturer's protocol. After 6 days, colonies were counted using a Celigo Imager Cytometer.

Xenograft model of aggressive systemic mastocytosis

NSG mice (NOD.Cg-Prkdcscid Il2rgtm1Wjl/SzJ, J; stock number 005557) were obtained from The Jackson Laboratory and housed for the length of the experiments in a vivarium of the National Institute of Allergy and Infectious Diseases (NIAID), accredited by the American Association for the Accreditation of Laboratory Animal Care (AAALAC). The protocols with live mice were performed under an animal study proposal (LAD2E) approved by the NIAID Division of Intramural Research (DIR) Animal Care and Use Committee under the guidance of the Office of Animal Care and Use of the National Institutes of Health.

Eight-week-old male NSG mice were injected subcutaneously with 1 × 10^6 HMC-1.2 or HMC-1.3 cells into the right flank. The tumors were allowed to establish until they reached a volume of 50 mm^3 (usually 18-25 days after injection). From this point, considered Day 0, caliper (Mitutoyo, Japan) measurements were taken daily and the solid tumor volume was calculated as volume (mm^3) = (length × $width^2$)/2 (27). On Day 14, the mice were euthanized for tissue collection. Tumor, spleen, and liver were weighed and fixed in 10% neutral buffered formalin overnight, transferred to 70% ethanol and paraffin embedded. Slides were prepared for histopathology by Histoserv Inc. (Germantown, MD). Slides were deparaffinized and hydrated before antigen retrieval at pH 9. After blocking with hydrogen peroxide, slides were incubated with 1:200 dilution of anti-KIT (CD117) antibody at room temperature followed by incubation with an HRP-conjugated goat-anti-rabbit secondary antibody. Slides were developed using 3,3'-Diaminobenzidine and counterstained with eosin.

Statistical analysis

Statistical analyses were performed using GraphPad Prism software (version 9.3.1). Unpaired Student's t tests and 2-way ANOVA tests were used to determine statistical significance as specified in the legends to figures. A p value of less than 0.05 was considered significant. Each experiment was done in triplicates or quadruplicates and experiments were repeated at least 3 independent times. Data are shown as mean ± SD or SEM of n≥3 independent experiments as indicated in the figure legends.

Results

Correction of the V560G mutation in HMC-1.2 cells by CRISPR/Cas9 engineering generated a huMC line with a single D816V-KIT mutation

After gene editing with CRISPR/Cas9 (Supplementary Figure 1), we isolated 16 individual clones with a correct reversal of the mono-allelic mutation in position 560 from GGT (mutated allele) to GTT (normal allele) in the JM domain of KIT (Figure 1A). Five of these clones were randomly selected to confirm by Sanger's sequencing that the complete exon sequences of KIT matched that of the parental HMC-1.2 cells except for the intended base pair conversions (Figure 1B). The resulting mast cell clones, containing a single D816V-KIT mutation instead of the double D816V- plus V560G-KIT mutations in the parental cell line, were named HMC-

1.3. Two clones (2E2 and 1H9) were chosen for further studies, as they exhibited growth characteristics representative of the average growth rate of all five individual clones (Supplementary Figure 2).

The allelic frequency of D816V tested by ddPCR in the sublines was 0% for HMC-1.1 cells and ~50% for HMC-1.2 (50.0 ± 3.3; mean ± SD, n=6), HMC-1.3 (2E2) (51.1 ± 2.8; mean ± SD, n=4) and HMC-1.3 (1H9) (50.5 ± 0.4; mean ± SD, n=4), consistent with the expected mono-allelic presence of D816V in all the corresponding sublines.

HMC-1.3 cells show similar growth characteristics, cellular distribution of KIT and signaling as the parental HMC-1.2 cells

To assess whether the rapid growth characteristics of cultured HMC-1.2 cells could be partly influenced by the presence of V560G in addition to D816V in KIT, we compared the growth rate of the new subline (HMC-1.3) with the parental subline. The two individual HMC-1.3 clones (1H9 and 2E2) grew similarly in liquid cultures (Figure 2A and Supplementary Figure 2) and thus, for simplicity, the results from subsequent experiments are often shown as averages of both HMC-1.3 subclones. The growth of HMC-1.3 over the course of six days was indistinguishable from that of the parental HMC-1.2 but was greater than for HMC-1.1 cells (Figure 2A, middle panel). Unlike HMC-1.1, both HMC-1.2 and HMC-1.3 cells exhibited some ability to expand in the absence of serum (Figure 2A right panel), suggesting that although factors in the serum stimulate the growth of all these cell lines irrespective of their mutational status, the presence of D816V-KIT in these cells is sufficient to confer growth capacities in the absence of added factors.

We next examined the potential effects of the reversal of the V560G-KIT mutation on the expression, cellular distribution, and signaling of KIT. Constitutively active KIT is known to accumulate intracellularly due to rapid internalization of the receptor and/or defective transit to the plasma membrane (4, 28–31). FACS analyses indicated that all HMC-1 sublines had similarly increased frequencies of intracellular KIT (solid bar, 50-60%) compared to LAD2 cells, a mast cell line expressing normal KIT (Figure 2B). Thus, the KIT variants in HMC-1 cells did not significantly alter the cellular localization of KIT, but the cells with D816V-KIT tended to have a lower proportion of cell surface KIT than HMC-1.1 cells. Total KIT expression measured by FACS analysis was modestly reduced in HMC-1.2 compared to HMC-1.1 or HMC-1.3 cells (Figure 2B, right panel). However, this reduced expression was not always detected by Western blot and on average there were no statistically significant differences (Figure 2C).

As expected, KIT was constitutively phosphorylated in all HMC-1 sublines but more so in those with D816V-KIT (HMC-1.2 and HMC-1.3 cells) (Figure 2C). Similarly, constitutive phosphorylation of AKT, ERK1/2 and STAT5, which reflect, respectively, the activity of the prominent PI3K, MAPK and STAT5 pathways in oncogenic KIT signaling (4, 30, 32), was elevated in both cell lines with D816V compared to HMC-1.1 cells. These results agree with other studies that D816V-KIT is a more potent driver of KIT autophosphorylation and oncogenic signaling in the absence of ligand than cells with only V560G. As reported (33), total STAT5 expression was increased in HMC-1.2 compared to HMC-1.1 cells, but also when compared to HMC-1.3 (Figure 2C bottom panels and Figure 2D). The expression of STAT5 was thus the only noted difference in signaling proteins between HMC-1.2 and HMC-1.3 cells. However, the ratio of phospho-STAT5 to total STAT5 was similar in both cell lines with D816V (alone or in combination with V560G) (Figure 2C).

Cells with gain-of function in KIT are known to appear refractory to SCF (31). The fold change in KIT phosphorylation induced by SCF was more pronounced in HMC-1.1 than in D816V-containing cell lines, which show greater constitutive phosphorylation (Figures 2C, D). Nevertheless, at the times examined, the maximal phosphorylation levels induced by SCF in KIT, AKT, ERK, and STAT5 were comparable in all sublines (Figure 2D). Note that the quantifications were determined through actin normalization, and thus the apparent higher phosphorylation levels of STAT5 after SCF stimulation in HMC-1.2 are likely due to the elevated STAT5 protein content.

These results demonstrate that HMC-1 mast cells containing D816V KIT alone or in combination with V560G-KIT exhibit similar characteristics in terms of growth, receptor localization, KIT phosphorylation and downstream signal activation in the absence or presence of SCF under the experimental conditions of this study.

HMC-1.3 cells have distinct transcriptional patterns, altered cell surface markers, and predicted molecular and cellular functions compared to HMC-1.2

We next performed transcriptome profiling of the sublines to gain insight into potential differences in cellular activation or function. Transcriptome-wide sample clustering based on the first three principal components (Figure 3A) as well as k-means clustering (k=2) based on the top 6,000 most variable genes (Figure 3B), revealed that the transcriptome of the HMC-1.3 clones (1H9 and 2E2) was unexpectedly distinct from the parental HMC-1.2, and relatively more similar to the HMC-1.1 cells. These observations suggest that despite the similarities observed in the major signaling pathways studied (Figure 2), the combined mutations in the JM region (V560G) and KD (D816V) of KIT, have a broader impact on the transcriptome than any of the individual KIT mutations, regardless of the site. Some of the gene expression changes between HMC-1.2 and HMC-1.3 cells included up- or down-regulation in certain cell surface markers aberrantly expressed in malignant mast cells such as CD25, CD44, CD87, and CD2; interleukin receptors including those for IL-7, IL-33, IL-18, and IL-9; and other receptors and adhesion molecules such as CXCR4, CD164, ICAM4, OX40 (CD134), FAS, and SIGLEC8 and 14 (Table 1), many of them known to impact mast cell function.

To better understand the potential molecular and functional implications of these differences in the transcriptional profile, we

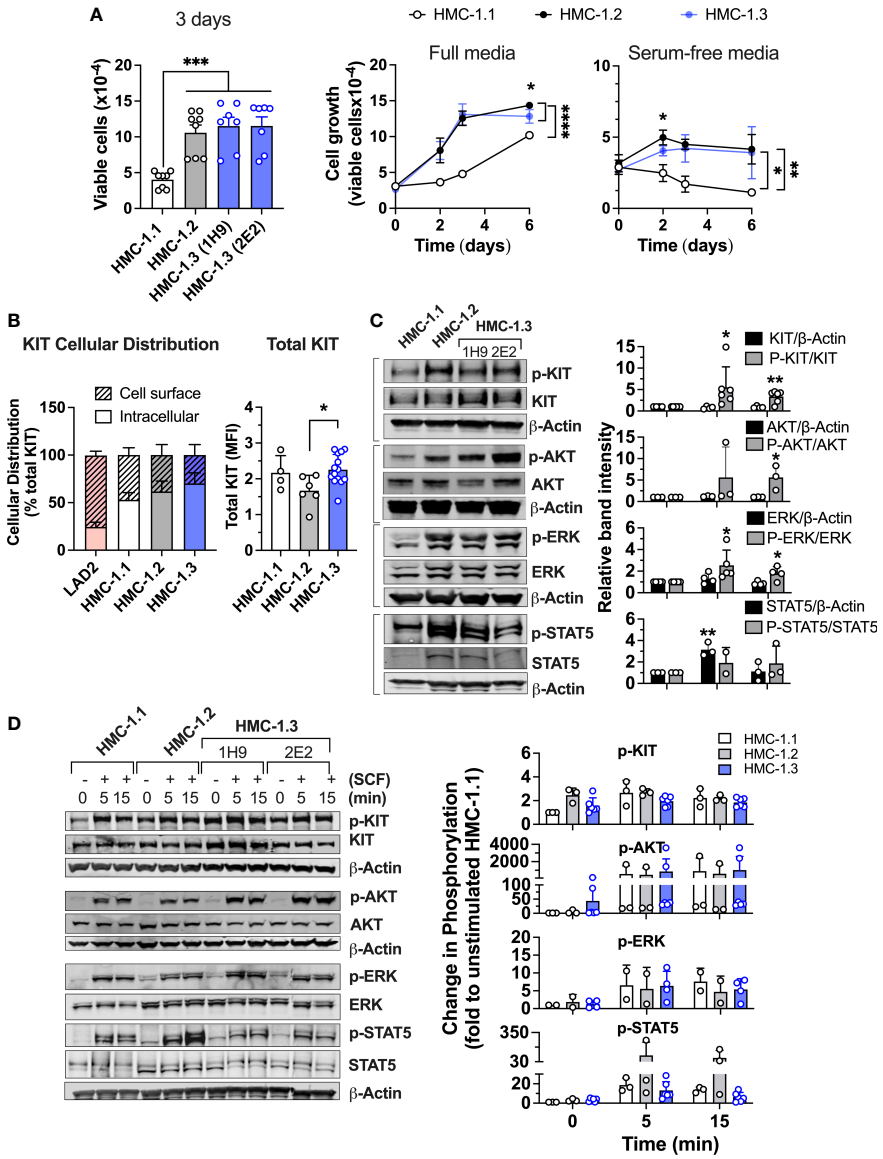

FIGURE 2
Comparison of cell growth, KIT expression and oncogenic KIT signaling in the various HMC-1 sublines. **(A)** Cell growth of HMC-1.1, HMC-1.2 and HMC-1.3 (1H9 and 2E2) in standard growing conditions after 72 h (bar graph; n ≥ 7 experiments; Mean ± SEM) and growth curves over time in full (middle panel) or serum-free media (right panel) (n ≥ 3 experiments; Mean ± SEM) showing HMC-1.3 as the average of both 1H9 and 2E2 subclones. *p<0.05; **p<0.01; ***p<0.001;****p<0.0001 using unpaired t-tests or when indicated with a bracket on the side of the curves, two-way ANOVA. Total cells were counted using a Celigo image cytometer and viable cells were calculated after subtraction of the number of dead cells determined by using PI staining. **(B)** Percent distribution (left) or total cellular expression (right) of KIT protein as determined by FACS analysis where data for HMC-1.3 is the average of both 1H9 and 2E2 subclones. Intracellular KIT was estimated from the difference between total and cell surface. *p<0.05 using an unpaired t-test. Shown is the Mean ± SD. **(C)** Western blot analysis showing constitutive phosphorylation of proteins in prominent oncogenic KIT signaling pathways in the indicated HMC-1 cell lines grown in normal culture conditions. Representative blots are on the left and quantifications of the average relative band intensities are on the bar graphs on the right (Mean ± SD; n ≥ 3 independent experiments). Relative band intensities in each sample were corrected by the relative intensity of β-actin or total protein expression (as indicated) and expressed as fold change compared to HMC-1.1. *p<0.05; **p<0.01 using unpaired t-tests. **(D)** Western blot analysis showing phosphorylation changes induced by 100 ng/mL SCF for the indicated times. Cells were serum starved for 2 h before the addition of SCF. Representative blots are on the left and quantifications of the average changes in relative band intensities are on the right (Mean ± SD of 2 to 3 independent experiments). Relative band intensities in each sample were normalized to the relative intensity of β-actin and expressed as fold change compared to HMC-1.1. Full scans of blots shown in **(C, D)** are shown in Supplementary Figures 8, 9, respectively.

analyzed differentially expressed genes between HMC-1.3 and the parental HMC-1.2 by Ingenuity Pathway Analysis (IPA). IPA (using genes with a fold change >1.5 or< -1.5, and with FDR<0.05) predicted that functional annotations related to "apoptosis" were increased (Z score=2.8) while those related to "cell viability/survival" were significantly reduced (Z scores< -2) in HMC-1.3 compared to HMC-1.2 cells, suggesting the possibility that the presence of the double mutation (D816V plus V560G-KIT) may confer survival advantages compared to the single mutation under certain conditions (Figure 3C).

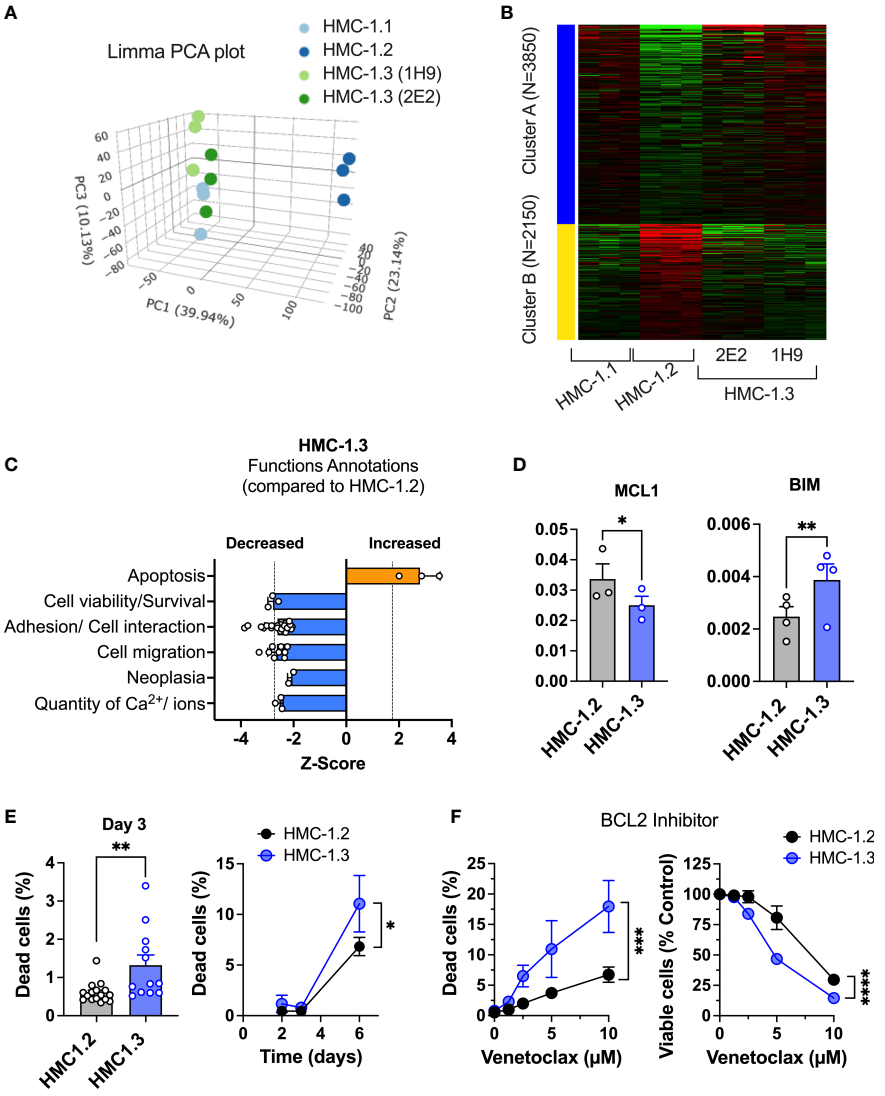

FIGURE 3
Repair of the G560V-KIT mutation in HMC-1.2 results in distinct transcriptional patterns and reduced pathways that promote survival. **(A)** Principal component analysis plot (Limma) of RNAseq analysis from HMC-1.1, HMC-1.2 and HMC-1.3 subclones illustrating total transcriptional differences between the sublines. **(B)** Heatmap of 6000 differentially expressed genes between the indicated HMC-1 sublines. **(C)** Z-Scores of Functions Annotations predicted to be significantly altered in HMC-1.3 compared to HMC-1.2 using QIAGEN IPA. Each bar represents the average z-scores (Mean ± SD) of similar Functions Annotations terms. These Functional Annotations were categorized by IPA in four top Molecular and Cellular Functions categories: Cellular Movement, Cell Death and Survival, Cell-to-Cell Signaling and Interaction, and Cell Signaling and Molecular transport. **(D)** Relative mRNA expression of the antiapoptotic gene MCL1 and the pro-apoptotic BIM (BCL2L11) in the HMC-1.2 and HMC-1.3 sublines, as indicated. The mRNA levels relative to GAPDH and ACTB (ΔCt) were determined by qPCR. Data are expressed as Mean ± SEM of 3 or 4 independent experiments. * p<0.05; ** p<0.01 using an unpaired t-test. **(E)** Percentage of dead cells in standard growing conditions for 72 h (n=13 experiments; Mean ± SEM) or at days 2, 3, and 6, as indicated (n=3 independent experiments, Mean ± SD). **(F)** Effect of BCL-2 inhibitor (venetoclax) on growth and cell death (n=3 independent experiments; Mean ± SD). Viable and dead cells were determined using PI staining and a Celigo Image Cytometer. Data on HMC-1.3 are the average of both 1H9 and 2E2 subclones. *p<0.05; **p<0.01; ***p<0.001; **** p<0.0001 unpaired t-tests or when indicated with a bracket on the side of the curves, two-way ANOVA.

Genes involved in pathways of apoptosis/survival and reported in association with mastocytosis, such as the BCL2 member myeloid cell leukemia 1 (MCL1) and the pro-apoptotic BCL-2 interacting mediator of cell death (BCL2L11, also known as BIM), were among other differentially expressed genes with fold change >1.2 or <-1.2, and with FDR<0.05, in the comparison of HMC-1.3 versus HMC-1.2 cells (Supplementary Figure 3A). MCL1 promotes survival of mast cells and other hematopoietic cells (34, 35) and its downregulation counteracts viability of neoplastic mast cells (36). BIM is suppressed by expression of D816V-KIT (37). We confirmed by qPCR that the relative expression levels of the antiapoptotic MCL1 were significantly reduced in HMC-1.3, while those of the pro-apoptotic BIM were significantly increased compared to the parental cell line (Figure 3D). Furthermore, IPA predicted the tumor suppressor protein P53 to be activated (with Z scores >3.1) in HMC-1.3 compared to HMC-1.2 as an upstream regulator. P53 is

10.3389/fimmu.2023.1078958

TABLE 1 Expression changes in cell surface markers, receptors, and molecular targets in HMC-1.3 compared to HMC-1.2 cells.

Gene name	FPKM (average of n=3)				Fold Change	*p* value	Fold Change	*p* value
	HMC-1.1	HMC-1.2	HMC-1.3 (2E2)	HMC-1.3 (1H9)	2E2 vs HMC-1.2		1H9 vs HMC-1.2	
CD13 (ANPEP)	121.3	119.0	126.3	129.9	1.02	4.4E-01	-1.08	1.2E-03
CD25 (IL2RA)	37.0	66.2	40.9	34.4	-1.73	3.8E-75	-2.15	3.2E-133
CD33 (SIGLEC3)	48.6	54.5	56.0	52.4	-1.01	8.0E-01	-1.08	6.4E-02
CD44	183.8	340.9	226.8	228.0	-1.53	3.0E-108	-1.70	1.2E-130
CD52	34.0	29.2	50.1	34.6	1.59	4.9E-08	1.12	2.0E-01
CD87 (PLAUR)	27.4	44.3	27.0	28.5	-1.72	2.4E-30	-1.66	6.2E-25
CD117 (KIT)	414.2	355.6	404.56	450.4	1.11	2.7E-09	1.21	8.0E-17
CD32 (FCGR2B)	6.8	15.2	3.70	8.1	-4.16	5.4E-75	-1.92	1.1E-22
CD32 (FCGR2A)	39.5	45.2	36.7	47.8	-1.27	3.7E-11	1.08	3.3E-02
CD59	65.9	50.3	73.5	61.6	1.45	9.6E-34	1.27	3.1E-14
CD63	578.2	552.2	624.7	623.6	1.10	5.1E-04	1.08	1.8E-03
CD66a (CEACAM1)	2.0	3.4	4.1	2.3	1.20	2.7E-02	-1.60	2.0E-07
CD69	2.3	10.1	3.3	2.1	-3.12	7.0E-61	-4.98	7.0E-61
CD71 (TFRC)	50.1	74.9	66.8	41.8	-1.14	3.2E-08	-1.87	6.9E-154
CD95 (FAS)	8.9	5.6	10.9	9.4	1.96	1.3E-28	1.63	5.8E-14
CD116 (CSF2RA)	10.5	10.4	7.4	15.0	-1.39	4.5E-07	1.40	5.9E-09
CD127 (IL7R)	2.7	5.0	3.4	2. 6	-1.51	1.2E-11	-2.10	2.4E-30
CD129 (IL9R)	21.8	9.2	21.4	23.3	2.68	4.9E-66	2.80	1.9E-72
IL1RL1 (ST2)	132.6	205.5	116.5	138.2	-1.90	2.5E-242	-1.60	5.4E-92
CD164	555.4	239.0	398.5	518.0	1.63	2.8E-156	2.05	6.1E-278
CD184 (CXCR4)	0.4	3.0	0.4	0.3	-7.09	4.0E-28	-9.42	1.3E-30
CD203c (ENPP3)	0.3	10.7	0.7	0.5	-17.90	1.9E-193	-23.61	1.8E-188
CD213a1 (IL13RA1)	9.1	9.2	11.7	9.3	1.22	1.9E-06	-1.06	1.8E-01
CD218a (IL18R1)	13.1	16.1	9.7	9.9	-1.69	1.7E-22	-1.70	3.8E-07
CD2	3.4	0.1	0.9	3.3	6.00	5.2E-07	23.38	1.6E-30
CD9	194.3	170.2	235.7	205.2	1.36	2.3E-36	1.16	8.5E-09
CD15 (FUT4)	3.8	4.8	4.2	3.8	-1.17	9.3E-04	-1.32	8.5E-08
CD19	4.2	4.7	2.5	5.3	-2.04	2.9E-07	1.02	8.7E-01
CD48	152.0	92.1	144.8	172.7	1.53	9.8E-48	1.79	2.2E-67
CD50 (ICAM3)	53.7	62.5	53.9	59.7	-1.17	1.4E-06	-1.09	1.0E-02
CD54 (ICAM1)	14.0	14.8	15.4	16.8	1.04	2.9E-01	1.12	4.6E-03
CD58	16.59	14.6	17.7	16.6	1.18	1.3E-02	1.11	1.4E-01
CD134 (TNFRSF4)	1.9	4.5	2.9	2.2	-1.65	1.4E-04	-2.26	1.8E-08
ICAM4	41.9	21.1	37.3	42.1	1.72	1.2E-27	1.90	3.5E-36
ICAM5	8.1	9.0	9.5	9.0	1.00	9.7E-01	-1.02	7.7E-01
SIGLEC14	57.2	37.5	76.6	64.0	2.01	2.1E-107	1.64	2.1E-48

(Continued)

TABLE 1 Continued

Gene name	FPKM (average of n=3)				Fold Change	*p* value	Fold Change	*p* value
	HMC-1.1	HMC-1.2	HMC-1.3 (2E2)	HMC-1.3 (1H9)	2E2 vs HMC-1.2		1H9 vs HMC-1.2	
SIGLEC6	283.6	224.7	268.0	309.7	1.14	2.8E-11	1.32	1.2E-29
SIGLEC8	48.0	6.0	21.2	45.1	3.30	6.3E-145	6.70	0.0E+00

Genes in this table were selected based on described cell surface proteins expressed in mastocytosis-like cell lines and/or malignant mast cells in patients with mastocytosis (15). Highlighted in grey are genes whose expression is significantly changed by >1.5 fold in the two HMC-1.3 clones compared to the parental HMC-1.2. Fold changes in red indicate upregulation in HMC-1.3, and in blue, downregulation compared to HMC-1.2.

known to regulate the function of MCL-1 and BIM (38) and alter life/death decisions in mast cells (39–41). The data thus suggest a transcriptional environment in HMC-1.3 less supportive of survival than in HMC-1.2.

In general agreement with this profile, HMC-1.3 consistently showed higher percentages of dead cells in normal culture conditions (Figure 3E). However, these percentages were very low (<2%) and hence did not significantly affect the total number of viable cells. Percentages of dead cells were slightly but consistently increased in HMC-1.3 to ~10% after 6 days in normal media (Figure 3E) or after two days in serum-free media (Supplementary Figure 3B), coinciding with a slight but significant reduction in the number of viable cells (Supplementary Figure 3C and middle and right panels of Figure 2A) at those time points. To demonstrate whether the reduced survival in the HMC-1.3 cell line may be consequential under stress conditions, we treated the cells with an inhibitor of BCL2, a treatment approved for leukemia that has been shown to promote apoptosis in HMC-1 cells and proposed as a potential therapy for advanced mastocytosis (42). The BCL2 inhibitor venetoclax caused a concentration dependent increase in cell death (Figure 3F, left) parallel to a drastic reduction in the number of viable cells (Figure 3F, right), and these changes were significantly more pronounced in HMC-1.3 than in HMC-1.2, consistent with the higher propensity of these cells to cell death predicted by IPA.

In addition to cell survival/cell death, functional annotations and molecular functions related to cell-to-cell adhesion, migration and neoplasia were predicted by IPA to be reduced (Z scores<-2) in HMC-1.3 compared to the parental cell line (Figure 3C). This was accompanied by changes in the gene expression of adhesion molecules including CD44 (Table 1) and other molecules known to be chemoattractant molecules and receptors for mast cells such as CXCR4 (Table 1) and CCL2 (or MCP-1) (Supplementary Figures 3D–F) and with reported functions in mastocytosis (43–48). Some of these are also depicted in Supplementary Figure 3D with predicted upstream regulators by IPA and effects on migration/binding of leukocytes, blood, and tumor cells.

Overall, these results indicate that despite the similarities in KIT levels, intracellular distribution, and constitutive signaling of typical oncogenic KIT pathways between cells with D816V alone or with V560G, the additional presence of V560G causes distinct transcriptional changes including cell surface markers and genes associated with protection against cell death and enhancement of neoplastic/metastatic potential.

HMC-1.3 cells show reduced transformation potential in a xenograft model and reduced colony formation in soft agar

Given the IPA prediction of reduced activity in pathways related to neoplasia, migration, and apoptosis/survival in HMC-1.3 compared to HMC-1.2 cells (Figure 3C), we used a xenograft model to examine potential differences *in vivo*, under a more physiological environment than the culture conditions. NSG mice were injected with $1x10^6$ HMC-1.2 or -1.3 cells subcutaneously in the flank and allowed to establish an estimated tumor volume of 50 mm^3 within 18-25 days (Figure 4A). Subsequent daily measurements revealed HMC-1.2 cells exhibited accelerated growth, resulting in large, well-formed, and dense tumors, while the injected HMC-1.3 cells were surprisingly slow-growing and resulted in tumors that were significantly smaller in volume and weight and with a soft appearance (Figures 4B, C). Histologically, the tumors appeared as a monomorphic mass of KIT positive cells. Other than size, no apparent differences in vascularization/hemorrhage or cellular necrosis were observed between tumors formed by HMC-1.2 and HMC-1.3 cells (Figure 4D). We then examined the growth of these cells in colony-forming assays using semi-solid media which provide extracellular scaffolds and thus may be more suitable microenvironment to determine tumorigenicity than the liquid cultures. While both cell lines formed colonies in both soft agar and Matrigel, the colonies formed by HMC-1.3 cells were reduced in number and apparent size compared to those produced by HMC-1.2 cells (Supplementary Figure 4), observations consistent with the differences in tumor size *in vivo* (Figures 4B–D). These results support a reduced tumorigenicity in HMC-1.3 compared to the parental cells, as also suggested by transcriptome analysis (Figure 3C).

To evaluate the metastatic capability into peripheral organs, spleen and liver were also collected during endpoint analysis. These organs collected from HMC-1.2 mice had increased weight compared to those from HMC-1.3 mice, suggesting augmented cellular infiltration (Figure 4E). Histological analysis of livers revealed the presence of well-formed tumor foci in mice injected with HMC-1.2 cells (Figure 4F), as previously reported (49). In contrast, only one out of six mice injected with HMC-1.3 exhibited three small groups of KIT-positive cells that could represent emerging, but not mature, foci (Figure 4F). The spleens of mice injected with HMC-1.2 cells were grossly enlarged compared to

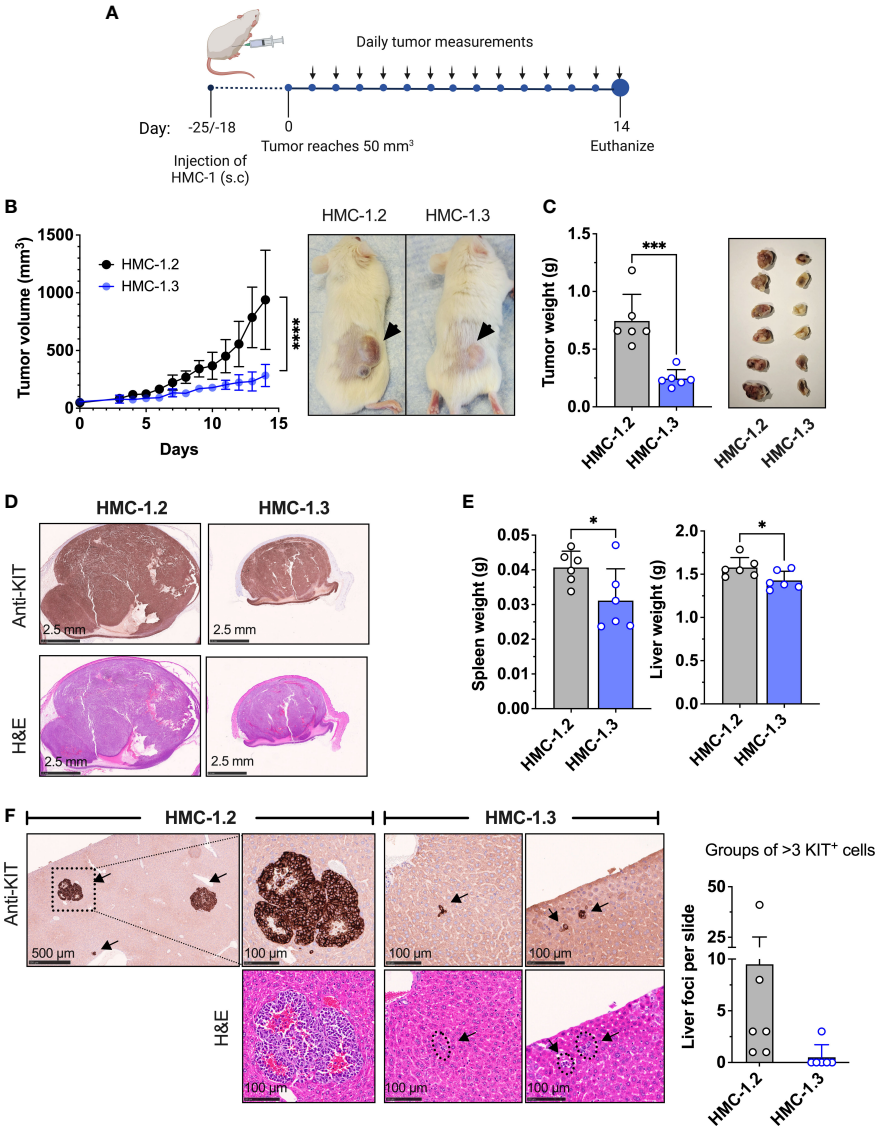

FIGURE 4
Repair of the V560G-KIT mutation in HMC-1.2 results in diminished tumor growth and metastasis. **(A)** Illustration of the xenograft protocol. Mice (6 per group) were injected with 1 × 10^6 HMC-1.2 or HMC 1.3 cells (shown is the 1H9 subclone; similar results were obtained using the other subclone 2E2) into the right flank subcutaneously. Once the tumor volume reached 50 mm^3 (usually 18-25 days after injection), measurements were performed daily using a caliper. On day 14, mice were euthanized for tissue collection. This illustration was created using Biorender (biorender.com) (agreement number BT24ABIPLB). **(B)** Tumor volume measurements on live mice over time. ****p<0.0001 between curves using a two-way ANOVA test. Representative images of the appearance of tumors at endpoint in mice injected with either HMC-1.2 or HMC-1.3 cells. **(C)** Weight of tumors excised on day 14 from mice injected with either HMC-1.2 or HMC-1.3 cells. The images on the right are all fixed tumors collected in this experiment. **(D)** Histology slides of excised tumors from mice injected with HMC-1.2 and HMC-1.3 stained with anti-KIT or H&E, as indicated. **(E)** Average of spleen and liver weights on day 14. **(F)** Representative images of well-formed foci in livers from mice injected with HMC-1.2 cells or groups of >3 KIT positive cells in livers of mice injected with HMC-1.3 cells (indicated by arrows). KIT immunostaining and H&E staining are shown as indicated. The graph represents the numbers of groups of > 3 cells or foci containing KIT-positive cells in the histological slides (each dot represents one mouse). Data represent Mean ± SD. *p<0.05; ***p<0.001 using unpaired t-tests.

those of mice injected with HMC-1.3 cells, mostly evident in the white pulp area (Supplementary Figure 5A). However, spleens from neither group developed tumor foci, instead presenting with scattered intense KIT positive staining consistent with the appearance of transformed huMCs, especially in spleens of mice injected with HMC-1.2 cells (Supplementary Figures 5A, B).

Overall, these results are consistent with the conclusion that the presence of the two KIT mutations in D816V and V560G confers additional tumorigenicity and metastatic potential.

HMC-1.3 cells show greater sensitivity to commonly used KIT inhibitors and JAK2 inhibitors than HMC-1.2 cells

Neoplastic mast cell lines are widely employed for the evaluation of new therapeutic targets and testing or validation of new drugs. Since HMC-1.3 cells showed reduced transformation potential (Figures 4B–F) and were more susceptible to death-inducing drugs than HMC-1.2 cells (Figure 3F), we investigated

the impact of the dual or single KIT mutations on the efficacy of drugs that inhibit neoplastic mast cell growth.

Tyrosine kinase inhibitors are used as a major pharmacological strategy to target KIT activity in KIT-driven diseases but vary in efficacy depending on the type of KIT mutations. Imatinib mesylate (STI571, Gleevec or Glivec) and derivatives effectively inhibit KIT with mutations in the JM domain but are unsuccessful in inhibiting the active conformation resulting from the D816V-KIT mutation. Indeed, the cell lines HMC-1.3 and HMC-1.2 expressing D816V-KIT were resistant to imatinib while HMC-1.1 cells showed significantly reduced cell growth (Figure 5A) and increased cell death (Figure 5B). In contrast, treatment with other tyrosine kinase inhibitors including dasatinib, midostaurin, the recently developed switch-pocket KIT inhibitor ripretinib and the PDGF receptor inhibitor avapritinib, effectively reduced the growth of sublines with D816V (HMC-1.2 and HMC-1.3) (Figure 5A) as well as cells with V560G-KIT (HMC-1.1) (Supplementary Figures 6A, B). This was expected given that these inhibitors effectively block normal and mutated KIT activity, including D816V-KIT. However, HMC-1.3 cells were generally more sensitive than the parental cell line to these inhibitors, particularly dasatinib, avapritinib and ripretinib (Figure 5A), which caused a significant increase in cell death in HMC-1.3 (ranging from 15 to 24%) compared to HMC-1.2 (ranging from 5 to 10%) (Figure 5B). Thus, although the KIT inhibitors show the expected relative efficacy on both cell lines harboring D816V compared to HMC-1.1, the presence of D816V plus V560G-KIT confers a survival advantage, as cells with a single D816V mutation in KIT are more susceptible than the parental cells.

We also examined the effects of JAK/STAT inhibitors and inhibitors of oncogenic KIT pathways that could hinder

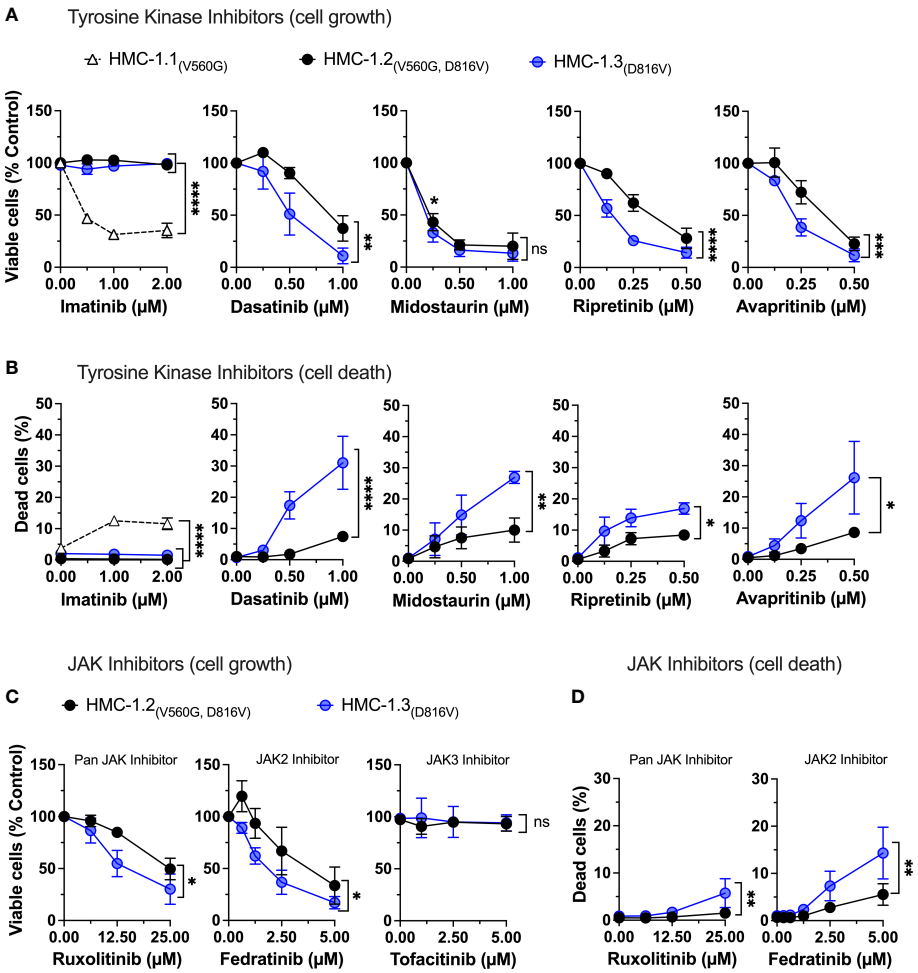

FIGURE 5
Repair of the G560V-KIT mutation in HMC-1.2 results in higher sensitivity to common tyrosine kinase inhibitors and JAK2 inhibitors. Effects of the indicated tyrosine kinase inhibitors on cell growth **(A)** and cell death **(B)** in HMC-1.2 and HMC-1.3 cells. Graph represents the percentage of viable or dead cells after 72 h in the presence of the indicated concentrations of inhibitors compared to the corresponding cells treated with vehicle (0 μM). Effects of the JAK inhibitors on cell growth **(C)** and cell death **(D)** in HMC-1.2 and HMC-1.3 cells. Graph represents the percentage of viable or dead cells after 72 h in the presence of the indicated concentrations of inhibitors compared to cells treated with vehicle (0 μM). Total cells were counted using a Celigo Image Cytometer and viable cells calculated after subtraction of dead cells which were positive for PI staining. In **(A-D)**, data represent Mean ± SD of 3 independent experiments. ns not significant; *p<0.05; **p<0.01; ***p<0.001; ****p<0.0001 using two-way ANOVA are indicated as brackets between the curves. Note that there were no differences between the curves of inhibition by midostaurin, but at 0.25 μM the percentage inhibition was significantly greater in HMC-1.3 (* p<0.05) using multiple comparison 2-way ANOVA). Data on HMC-1.3 are the average of both 1H9 and 2E2 subclones.

neoplastic mast cell growth. In agreement with the known connection of KIT with JAK2 activation, the specific JAK2 inhibitor fedratinib but not a JAK3 inhibitor, and to a lesser extent the pan-JAK inhibitor ruxolitinib, reduced growth in both cell lines. Growth inhibition was more prominent in cells with only D816V-KIT (Figure 5C), in association with greater cell death in this subline (Figure 5D), similar to cells with only V560G (Supplementary Figures 6C, D).

Downstream of JAK, inhibition of STAT3 by C188-9 or inhibition of both STAT3 and STAT5 by a non-selective inhibitor that targets both (SH454), effectively reduced HMC-1.2 and HMC-1.3 growth to a similar extent (Supplementary Figure 7A). This was accompanied by a prominent increase in number of dead cells in both cell lines, particularly with the STAT3 inhibitor (30%) (Supplementary Figure 7B). Similarly, inhibition of other oncogenic KIT pathways, such as the MAPK/ERK (by U0126) and PI3K/AKT (by LY294002) pathways reduced the number of viable cells similarly in HMC-1.2 and HMC-1.3 (Supplementary Figure 7C) in agreement with the similar phosphorylation status of proteins in these pathways (Figures 2C, D). The percentage of dead cells trended to be higher in HMC-1.3 in the presence of these inhibitors but generally below 10% and thus had little impact on the overall growth (Supplementary Figures 7C, D).

Overall, the engineered HMC-1.3 huMC line containing a single mutation in D816V-KIT is more sensitive than the parental cell line to various KIT and signaling target inhibitors, an effect that appears to be partly the result of increased susceptibility to cell death mechanisms. These findings may have implications for the predictability of the model on drug screening.

Discussion

A limited number of huMC lines have been established to date, especially those with oncogenic KIT variants that drive human malignancies (i.e, HMC-1 and ROSA^{KITD186V}) (12, 15, 50–53). HMC-1 cells containing common KIT variants, isolated from a patient with mast cell leukemia (12), remain one of the most frequent preclinical models to test the efficacy of drugs targeting oncogenic KIT activity and to predict signaling pathways and behavior of neoplastic mast cells (15). In HMC-1.2 cells, KIT genes are composed of a normal and a mutant allele that contains two point mutations, one in the JM region (V560G) and one in the KD (D816V) (13). Heterozygous KIT mutations are representative of the situation in patients with somatic KIT variants but the presence of these two separate KIT point mutations in one KIT allele is rare. Given the complex structural and functional inter-relationship between these regions of KIT (4, 54, 55), it is unclear whether the presence of the two intramolecular mutations may be redundant or result in altered responses. Here we demonstrate, by using CRISPR/Cas9-mediated correction of V560G-KIT in HMC-1.2, that the additional V560G mutation modifies transcriptional programs, molecular components, pharmacological responses, and oncogenic potential in D816V containing cells, features that are important when evaluating potential drug efficacy in D816V-KIT-driven diseases. Thus, the neoplastic huMCs line with a single mono-allelic D816V-KIT described herein (HMC-1.3) provides an improved model of neoplastic huMCs compared to HMC-1.2 and potentially other cell models based on homozygous D816V-KIT, particularly for pharmacological and *in vivo* studies. Furthermore, the results presented herein may help explain the aggressive nature of the HMC-1.2 cell line in contrast to the usually indolent nature of systemic mastocytosis, and resistance to drugs in cells carrying dual alterations in both the JM region and KD isolated from lesions in patients with refractory GIST (18).

The first evidence that the presence of double V560G-KIT and D816V-KIT mutations can have compounding effects came from transcriptome-wide analysis showing that the double KIT mutations have broader effects on the overall transcriptional profile than each mutation independently. Despite the gene expression differences, under our experimental conditions the growth rate in liquid culture, cellular distribution of KIT, and constitutive activation of the KIT oncogenic pathways known to be important for cell growth [such as PI3K, MAPK and STAT5 pathways (1, 4)] were relatively similar between HMC-1.3 and the parental HMC-1.2 cells, but distinct from HMC-1.1 cells. In agreement, inhibition of the PI3K and MAPK pathways or STAT inhibition reduced the growth of HMC-1.2 and HMC-1.3 cells in a similar manner. However, reduced growth and survival between HMC-1.3 and the parental HMC-1.2 cells were unveiled when survival signals such as those derived from KIT activity, BCL2 and JAK2 were blocked by small-molecule inhibitors or when the cells were inoculated *in vivo* in a xenograft model that likely represents a more physiological environment with additional complexities compared to liquid cultures. These may include closer interactions with other cells, extracellular components, and presence of gradients of nutrients, oxygen, metabolites, growth factors, etc., that in total, may help reveal cell behaviors that are masked in the *in vitro* liquid conditions. In support, cell growth assays in semi-solid media, which provide a three-dimensional microenvironment, also reproduced the reduced tumorigenicity of the HMC-1.3 cells observed *in vivo* as they formed fewer and smaller colonies.

The enhanced percentage of dead cells in HMC-1.3 cells in response to the indicated inhibitors also agrees with a transcriptional environment predicted to be less supportive for survival and more conducive to apoptosis than in HMC-1.2, including a predicted increase in P53 activity which is important for the regulation of normal and neoplastic mast cell homeostasis (39–41). Further, these findings are supported by a reduced mRNA expression in HMC-1.3 of the pro-survival MCL-1 protein and increased expression of the pro-apoptotic BIM, both proteins with essential roles in the regulation of mast cell survival/death (34, 36, 37, 56). The differences in gene expression, growth of ectopic tumors or semi-solid media and sensitivity to death by pharmacological agents between HMC-1.2 and HMC-1.3 imply that the combination of the two KIT variants may contribute to other quantitative, qualitative and/or temporal differences in signaling. The higher susceptibility of HMC-1.3 cells to inhibition of JAK2, upstream of the STAT pathways offer JAK2 as one of the potential contributing signaling factors. However, the specific mechanisms and signals for the observed effects may be driven by multiple factors. For instance, potential conformational changes in

KIT due to the dual mutations may favor particular KIT dimers among the stochastic combinations of mutated and non-mutated KIT molecules, cause quantitative, qualitative and/or dynamic/temporal changes in certain signaling complexes, or aberrant localization of signals in specific subcellular compartments. Clarification of these aspects would require further investigation.

Notably, our results closely resemble those in another report where point mutations were introduced in the JM Y568 and Y570 of KIT, tyrosines representing docking sites for multiple signaling proteins (54). These mutations, like those described herein, caused an unexpected increase in the transforming capacity of D816V-KIT mutants *in vivo* and modified transcriptional programs *in vitro* but were not accompanied by changes in the PI3K or MAPK signaling pathways or growth in culture (54). Although the KIT constructs in the study using Y568F/Y570F/D816V mutants are distinct to KIT genes with V560G/D816V double mutations, the possibility exists that structural changes imposed by the presence of V560G impedes tyrosine phosphorylation in the JM tyrosine residues or causes equivalent structural alterations, resulting in similar scenarios. Regardless, one conclusion that can be drawn from our results and those from Chaix et al. (54) is that such mutations in the JM region prevent a negative regulatory mechanism on D816V-KIT activity, enhancing its oncogenic potential. Previous reports using *in silico* modeling of KIT showed that a single mutation in the KD such as D816V already causes long range changes in the JM domain that weakens its binding to the KD and prevents its inhibitory role on KIT activity (4, 55), which is consistent with the constitutive KIT signaling observed in cells with D816V (5, 13, 14, 30, 31, 53). However, our study and the other report (54) suggest that the structural changes imposed by the D816V-KIT mutation do not prevent the full inhibitory potential of the JM region which is unveiled when additional KIT mutations such as V560G or Y568F/Y570F are present. This added partial inhibition by the JM domain V560G mutation may also explain in part why single mutations in D816V are considered of low oncogenic potential if not accompanied by other genetic mutations (57–59).

HMC-1.3 cells, as HMC-1.2, injected subcutaneously grew into tumors in a xenotransplantation mouse model, which is a useful feature of both sublines when exploring the efficacy of small molecule inhibitors *in vivo*. However, HMC-1.3 cells not only produced smaller tumors than those produced by HMC-1.2, they also were less metastatic as assessed by the absence of well-formed neoplastic foci in livers of mice injected with HMC-1.3 cells and reduced size of livers and spleens in these mice, indicating globally reduced cell infiltrates. In agreemint with this observation, among the multiple differentially expressed genes between the two cell lines, those related to pathways of cell adhesion, migration, and neoplasia were predicted to be downregulated in HMC-1.3. Thus, it is possible that, in addition to potential differences in the survival or growth of these cells *in vivo*, some of these gene modifications that affect cell migration and their implantation in other niches may contribute to the phenotypical differences in this model. For instance, the mRNA levels of the receptors CD44 and CXCR4, significantly downregulated in HMC-1.3 compared to HMC-1.2 (Table 1), are important for homing of stem cells, huMCs and/or huMC progenitors (46–48, 60) and have been associated with hematological malignancies, including systemic mastocytosis (47, 61, 62). Furthermore, similar to the situation in HMC-1.3, downregulation of CD44 expression in neoplastic huMCs reduced mortality in a xenograft model and metastatic cell growth in lungs (47). Another attractive candidate is the chemokine and proangiogenic factor CCL2 (MCP-1), whose mRNA expression was also downregulated in HMC-1.3 compared to HMC-1.2 cells (Supplementary Figures 3D–F). CCL2, produced by mast cells in addition to many other cell types and a chemoattractant for mast cells and mast cell progenitors (43, 45, 63, 64) was reported to be elevated in the serum of patients with aggressive mastocytosis, and the levels correlated with poor prognosis (44). Knockdown of CCL2 in neoplastic MCs resulted in reduced tumor growth *in vivo* compared with CCL2-expressing cells and reduced microvessel density in the tumors (44). Thus, although a cause-effect for the reduced expression of these and other genes and the observed phenotype is not established in our study, the reduced tumor growth and metastatic potential of HMC-1.3 align with reports of these proteins as markers of disease severity in mastocytosis.

It is important to note that despite the differences between HMC-1.2 and HMC-1.3, both cell lines containing D816V differ from huMCs cells containing V560G (HMC-1.1 cells) in the general pharmacological profile to inhibitors, growth and constitutive signaling. Thus, both HMC-1.2 and HMC-1.3 were resistant to imatinib, confirming the open conformation of KIT in these sublines, while HMC-1.1 cell growth was compromised by this inhibitor as expected (1, 65, 66). Other tyrosine kinase inhibitors known to target the open conformation of D816V (18, 67–69) were effective in inhibiting the growth of both HMC-1.2 and HMC-1.3 cells albeit at different degrees as they generally caused more cell death in HMC-1.3. In addition, both cell lines with D816V grew faster in culture than HMC-1.1 cells even in the absence of serum where HMC-1.1 cells did not strive, confirming the growth factor-independency of cell lines expressing D816V. Nevertheless, the data also underline that despite the demonstrated usefulness of HMC-1.2 cells as a model of huMCs with D816V-KIT for testing drug efficacy, the combination of the two oncogenic KIT variants has complex effects on cell behavior and survival, thus reducing the predictability of the model. Our findings also support the notion, as other studies have suggested (16, 54, 70), that other double-hit KIT variants, when present in some patient populations with KIT-driven diseases, may not be functionally redundant even if they are gain-of-function and may have unforeseen consequences in pharmacological efficacy studies and molecular cell outcomes.

In summary, in this study we have shown that an intramolecular V560G-KIT mutation, in addition to D816V-KIT, promotes transcriptional programs that lead to increased survival in response to pharmacological inhibitors of KIT and other inhibitors of potential cytoreductive interest and produce smaller tumors with less metastatic capacity, suggesting that in cells with a single D816V-KIT mutation, the JM domain still bears a negative modulatory function. Thus, HMC-1.3 cells modified by CRISPR/Cas9 from the parental HMC-1.2 cell line may represent, in conjunction with the ROSA$^{KIT\ D816V}$ cell line created by lentiviral transduction of D816V-KIT (53), more representative mast cell models for systemic mastocytosis.

Data availability statement

The datasets presented in this study can be found in online repositories. The names of the repository/repositoriesand accession number(s) can be found below: https://www.ncbi.nlm.nih.gov/geo/query/acc.cgi?acc=GSE216446.

Ethics statement

The animal study was reviewed and approved by the NIAID Division of Intramural Research (DIR) Animal Care and Use Committee under the guidance of the Office of Animal Care and Use of the National Institutes of Health, protocol # LAD2E.

Author contributions

GB and GF designed and conducted experiments, analyzed data, and contributed to the writing of the manuscript. AL, YB, and AP performed experiments and analyzed data. JL processed and analyzed RNASeq data sets. AO supervised the study, designed, and performed experiments, prepared figures, and wrote the manuscript. DM supervised the study and allocated resources. All authors contributed to the article and approved the submitted version.

Funding

This work was supported by the Division of Intramural Research of the National Institutes of Health (NIH), National Institute of Allergy and Infectious Diseases (NIAID).

Acknowledgments

We thank all MCBS members for their valuable intellectual contributions. We also thank the NCI sequencing facility for performing the RNASeq and the NIAID Collaborative Bioinformatics Resource (NCBR) for the analysis of the RNASeq datasets. Illustrations were created with BioRender.com.

Conflict of interest

The authors declare that the research was conducted in the absence of any commercial or financial relationships that could be construed as a potential conflict of interest.

Publisher's note

Supplementary material

The Supplementary Material for this article can be found online at: https://www.frontiersin.org/articles/10.3389/fimmu.2023.1078958/full#supplementary-material

References

1. Cruse G, Metcalfe DD, Olivera A. Functional deregulation of KIT: link to mast cell proliferative diseases and other neoplasms. *Immunol Allergy Clin North Am* (2014) 34(2):219–37. doi: 10.1016/j.iac.2014.01.002

2. Galli SJ, Tsai M, Wershil BK, Tam SY, Costa JJ. Regulation of mouse and human mast cell development, survival and function by stem cell factor, the ligand for the c-kit receptor. *Int Arch Allergy Immunol* (1995) 107(1-3):51–3. doi: 10.1159/000236928

3. Jensen BM, Akin C, Gilfillan AM. Pharmacological targeting of the KIT growth factor receptor: a therapeutic consideration for mast cell disorders. *Br J Pharmacol* (2008) 154(8):1572–82. doi: 10.1038/bjp.2008.204

4. Lennartsson J, Ronnstrand L. Stem cell factor receptor/c-kit: from basic science to clinical implications. *Physiol Rev* (2012) 92(4):1619–49. doi: 10.1152/physrev.00046.2011

5. Lennartsson J, Jelacic T, Linnekin D, Shivakrupa R. Normal and oncogenic forms of the receptor tyrosine kinase kit. *Stem Cells* (2005) 23(1):16–43. doi: 10.1634/stemcells.2004-0117

6. Kitayama H, Kanakura Y, Furitsu T, Tsujimura T, Oritani K, Ikeda H, et al. Constitutively activating mutations of c-kit receptor tyrosine kinase confer factor-independent growth and tumorigenicity of factor-dependent hematopoietic cell lines. *Blood* (1995) 85(3):790–8. doi: 10.1182/blood.V85.3.790.bloodjournal853790

7. Metcalfe DD, Mekori YA. Pathogenesis and pathology of mastocytosis. *Annu Rev Pathol* (2017) 12:487–514. doi: 10.1146/annurev-pathol-052016-100312

8. Arock M, Sotlar K, Akin C, Broesby-Olsen S, Hoermann G, Escribano L, et al. KIT mutation analysis in mast cell neoplasms: Recommendations of the European competence network on mastocytosis. *Leukemia* (2015) 29(6):1223–32. doi: 10.1038/leu.2015.24

9. Ustun C, DeRemer DL, Akin C. Tyrosine kinase inhibitors in the treatment of systemic mastocytosis. *Leuk Res* (2011) 35(9):1143–52. doi: 10.1016/j.leukres.2011.05.006

10. Dhillon S. Avapritinib: First approval. *Drugs* (2020) 80(4):433–39. doi: 10.1007/s40265-020-01275-2

11. Falduto GH, Pfeiffer A, Luker A, Metcalfe DD, Olivera A. Emerging mechanisms contributing to mast cell-mediated pathophysiology with therapeutic implications. *Pharmacol Ther* (2021) 220:107718. doi: 10.1016/j.pharmthera.2020.107718

12. Butterfield JH, Weiler D, Dewald G, Gleich GJ. Establishment of an immature mast cell line from a patient with mast cell leukemia. *Leuk Res* (1988) 12(4):345–55. doi: 10.1016/0145-2126(88)90050-1

13. Furitsu T, Tsujimura T, Tono T, Ikeda H, Kitayama H, Koshimizu U, et al. Identification of mutations in the coding sequence of the proto-oncogene c-kit in a human mast cell leukemia cell line causing ligand-independent activation of c-kit product. *J Clin Invest* (1993) 92(4):1736–44. doi: 10.1172/JCI116761

14. Sundstrom M, Vliagoftis H, Karlberg P, Butterfield JH, Nilsson K, Metcalfe DD, et al. Functional and phenotypic studies of two variants of a human mast cell line with a distinct set of mutations in the c-kit proto-oncogene. *Immunology* (2003) 108(1):89–97. doi: 10.1046/j.1365-2567.2003.01559.x

15. Arock M, Wedeh G, Hoermann G, Bibi S, Akin C, Peter B, et al. Pre-clinical human models and emerging therapeutics for advanced systemic mastocytosis. *Haematologica* (2018) 103(11):1760–71. doi: 10.3324/haematol.2018.195867

16. Bodemer C, Hermine O, Palmerini F, Yang Y, Grandpeix-Guyodo C, Leventhal PS, et al. Pediatric mastocytosis is a clonal disease associated with D816V and other activating c-KIT mutations. *J Invest Dermatol* (2010) 130(3):804–15. doi: 10.1038/jid.2009.281

17. Paschka P, Marcucci G, Ruppert AS, Mrozek K, Chen H, Kittles RA, et al. Adverse prognostic significance of KIT mutations in adult acute myeloid leukemia with inv(16) and t(8;21): A cancer and leukemia group b study. *J Clin Oncol* (2006) 24 (24):3904–11. doi: 10.1200/JCO.2006.06.9500

18. Evans EK, Gardino AK, Kim JL, Hodous BL, Shutes A, Davis A, et al. A precision therapy against cancers driven by KIT/PDGFRA mutations. *Sci Transl Med* (2017) 9 (414):eaao1690. doi: 10.1126/scitranslmed.aao1690

19. Kim DK, Beaven MA, Metcalfe DD, Olivera A. Interaction of DJ-1 with Lyn is essential for IgE-mediated stimulation of human mast cells. *J Allergy Clin Immunol* (2018) 142(1):195–206.e8. doi: 10.1016/j.jaci.2017.08.030

20. Tkaczyk C, Metcalfe DD, Gilfillan AM. Determination of protein phosphorylation in fc epsilon RI-activated human mast cells by immunoblot analysis requires protein extraction under denaturing conditions. *J Immunol Methods* (2002) 268(2):239–43. doi: 10.1016/s0022-1759(02)00210-7

21. Martin M. Cutadapt removes adapter sequences from high-throughput sequencing reads. *EMBnet J* (2011) 17:10–2. doi: 10.14806/ej.17.1.200

22. Dobin A, Davis CA, Schlesinger F, Drenkow J, Zaleski C, Jha S, et al. STAR: ultrafast universal RNA-seq aligner. *Bioinformatics* (2013) 29(1):15–21. doi: 10.1093/bioinformatics/bts635

23. Li B, Dewey CN. RSEM: Accurate transcript quantification from RNA-seq data with or without a reference genome. *BMC Bioinf* (2011) 12:323. doi: 10.1186/1471-2105-12-323

24. Love MI, Huber W, Anders S. Moderated estimation of fold change and dispersion for RNA-seq data with DESeq2. *Genome Biol* (2014) 15(12):550. doi: 10.1186/s13059-014-0550-8

25. Ge SX, Son EW, Yao R. iDEP: an integrated web application for differential expression and pathway analysis of RNA-seq data. *BMC Bioinf* (2018) 19(1):534. doi: 10.1186/s12859-018-2486-6

26. Kramer A, Green J, Pollard JJr., Tugendreich S. Causal analysis approaches in ingenuity pathway analysis. *Bioinformatics* (2014) 30(4):523–30. doi: 10.1093/bioinformatics/btt703

27. Tomayko MM, Reynolds CP. Determination of subcutaneous tumor size in athymic (nude) mice. *Cancer Chemother Pharmacol* (1989) 24(3):148–54. doi: 10.1007/BF00300234

28. Bougherara H, Subra F, Crepin R, Tauc P, Auclair C, Poul MA. The aberrant localization of oncogenic kit tyrosine kinase receptor mutants is reversed on specific inhibitory treatment. *Mol Cancer Res MCR* (2009) 7(9):1525–33. doi: 10.1158/1541-7786.MCR-09-0138

29. Obata Y, Hara Y, Shiina I, Murata T, Tasaki Y, Suzuki K, et al. N822K- or V560G-mutated KIT activation preferentially occurs in lipid rafts of the golgi apparatus in leukemia cells. *Cell Commun Signal* (2019) 17(1):114. doi: 10.1186/s12964-019-0426-3

30. Obata Y, Toyoshima S, Wakamatsu E, Suzuki S, Ogawa S, Esumi H, et al. Oncogenic kit signals on endolysosomes and endoplasmic reticulum are essential for neoplastic mast cell proliferation. *Nat Commun* (2014) 5:5715. doi: 10.1038/ncomms6715

31. Shi X, Sousa LP, Mandel-Bausch EM, Tome F, Reshetnyak AV, Hadari Y, et al. Distinct cellular properties of oncogenic KIT receptor tyrosine kinase mutants enable alternative courses of cancer cell inhibition. *Proc Natl Acad Sci U S A* (2016) 113(33): E4784–93. doi: 10.1073/pnas.1610179113

32. Harir N, Boudot C, Friedbichler K, Sonneck K, Kondo R, Martin-Lanneree S, et al. Oncogenic kit controls neoplastic mast cell growth through a Stat5/PI3-kinase signaling cascade. *Blood* (2008) 112(6):2463–73. doi: 10.1182/blood-2007-09-115477

33. Tobio A, Bandara G, Morris DA, Kim DK, O'Connell MP, Komarow HD, et al. Oncogenic D816V-KIT signaling in mast cells causes persistent IL-6 production. *Haematologica* (2020) 105(1):124–35. doi: 10.3324/haematol.2018.212126

34. Hazzan T, Eberle J, Worm M, Babina M. Apoptotic resistance of human skin mast cells is mediated by mcl-1. *Cell Death Discovery* (2017) 3:17048. doi: 10.1038/cddiscovery.2017.48

35. Thomas LW, Lam C, Edwards SW. Mcl-1; the molecular regulation of protein function. *FEBS Lett* (2010) 584(14):2981–9. doi: 10.1016/j.febslet.2010.05.061

36. Aichberger KJ, Mayerhofer M, Gleixner KV, Krauth MT, Gruze A, Pickl WF, et al. Identification of MCL1 as a novel target in neoplastic mast cells in systemic mastocytosis: Inhibition of mast cell survival by MCL1 antisense oligonucleotides and synergism with PKC412. *Blood* (2007) 109(7):3031–41. doi: 10.1182/blood-2006-07-032714

37. Aichberger KJ, Gleixner KV, Mirkina I, Cerny-Reiterer S, Peter B, Ferenc V, et al. Identification of pro-apoptotic bim as a tumor suppressor in neoplastic mast cells: role of KIT D816V and effects of various targeted drugs. *Blood* (2009) 114(26):5342–51. doi: 10.1182/blood-2008-08-175190

38. Aubrey BJ, Kelly GL, Janic A, Herold MJ, Strasser A. How does p53 induce apoptosis and how does this relate to p53-mediated tumour suppression? *Cell Death Differ* (2018) 25(1):104–13. doi: 10.1038/cdd.2017.169

39. Bandara G, Munoz-Cano R, Tobio A, Yin Y, Komarow HD, Desai A, et al. Targeting sphingosine kinase isoforms effectively reduces growth and survival of neoplastic mast cells with D816V-KIT. *Front Immunol* (2018) 9:631. doi: 10.3389/fimmu.2018.00631

40. Falduto GH, Pfeiffer A, Zhang Q, Yin Y, Metcalfe DD, Olivera A. A critical function for the transcription factors GLI1 and GLI2 in the proliferation and survival of human mast cells. *Front Immunol* (2022) 13:841045. doi: 10.3389/fimmu.2022.841045

41. Ryan JJ, Kashyap M, Bailey D, Kennedy S, Speiran K, Brenzovich J, et al. Mast cell homeostasis: A fundamental aspect of allergic disease. *Crit Rev Immunol* (2007) 27 (1):15–32. doi: 10.1615/critrevimmunol.v27.i1.20

42. Peter B, Cerny-Reiterer S, Hadzijusufovic E, Schuch K, Stefanzl G, Eisenwort G, et al. The pan-Bcl-2 blocker obatoclax promotes the expression of puma, noxa, and bim mRNA and induces apoptosis in neoplastic mast cells. *J Leukoc Biol* (2014) 95(1):95–104. doi: 10.1189/jlb.1112609

43. Collington SJ, Hallgren J, Pease JE, Jones TG, Rollins BJ, Westwick J, et al. The role of the CCL2/CCR2 axis in mouse mast cell migration *in vitro* and in vivo. *J Immunol* (2010) 184(11):6114–23. doi: 10.4049/jimmunol.0904177

44. Greiner G, Witzeneder N, Berger A, Schmetterer K, Eisenwort G, Schiefer AI, et al. CCL2 is a KIT D816V-dependent modulator of the bone marrow microenvironment in systemic mastocytosis. *Blood* (2017) 129(3):371–82. doi: 10.1182/blood-2016-09-739003

45. Gschwandtner M, Derler R, Midwood KS. More than just attractive: How CCL2 influences myeloid cell behavior beyond chemotaxis. *Front Immunol* (2019) 10:2759. doi: 10.3389/fimmu.2019.02759

46. Juremalm M, Hjertson M, Olsson N, Harvima I, Nilsson K, Nilsson G. The chemokine receptor CXCR4 is expressed within the mast cell lineage and its ligand stromal cell-derived factor-1alpha acts as a mast cell chemotaxin. *Eur J Immunol* (2000) 30(12):3614–22. doi: 10.1002/1521-4141(200012)30:12<3614::AID-IMMU3614>3.0.CO;2-B

47. Mueller N, Wicklein D, Eisenwort G, Jawhar M, Berger D, Stefanzl G, et al. CD44 is a RAS/STAT5-regulated invasion receptor that triggers disease expansion in advanced mastocytosis. *Blood* (2018) 132(18):1936–50. doi: 10.1182/blood-2018-02-833582

48. Nakamura T, Maeda S, Horiguchi K, Maehara T, Aritake K, Choi BI, et al. PGD2 deficiency exacerbates food antigen-induced mast cell hyperplasia. *Nat Commun* (2015) 6:7514. doi: 10.1038/ncomms8514

49. Snider DB, Arthur GK, Falduto GH, Olivera A, Ehrhardt-Humbert LC, Smith E, et al. Targeting KIT by frameshifting mRNA transcripts as a therapeutic strategy for aggressive mast cell neoplasms. *Mol Ther* (2022) 30(1):295–310. doi: 10.1016/j.ymthe.2021.08.009

50. Kirshenbaum AS, Akin C, Wu Y, Rottem M, Goff JP, Beaven MA, et al. Characterization of novel stem cell factor responsive human mast cell lines LAD 1 and 2 established from a patient with mast cell sarcoma/leukemia; activation following aggregation of FcepsilonRI or FcgammaRI. *Leuk Res* (2003) 27(8):677–82. doi: 10.1016/s0145-2126(02)00343-0

51. Kirshenbaum AS, Yin Y, Sundstrom JB, Bandara G, Metcalfe DD. Description and characterization of a novel human mast cell line for scientific study. *Int J Mol Sci* (2019) 20(22):5520. doi: 10.3390/ijms20225520

52. Laidlaw TM, Steinke JW, Tinana AM, Feng C, Xing W, Lam BK, et al. Characterization of a novel human mast cell line that responds to stem cell factor and expresses functional FcepsilonRI. *J Allergy Clin Immunol* (2011) 127(3):815–22.e1-5. doi: 10.1016/j.jaci.2010.12.1101

53. Saleh R, Wedeh G, Herrmann H, Bibi S, Cerny-Reiterer S, Sadovnik I, et al. A new human mast cell line expressing a functional IgE receptor converts to tumorigenic growth by KIT D816V transfection. *Blood* (2014) 124(1):111–20. doi: 10.1182/blood-2013-10-534685

54. Chaix A, Arcangeli ML, Lopez S, Voisset E, Yang Y, Vita M, et al. KIT-D816V oncogenic activity is controlled by the juxtamembrane docking site Y568-Y570. *Oncogene* (2014) 33(7):872–81. doi: 10.1038/onc.2013.12

55. Raghav PK, Singh AK, Gangenahalli G. A change in structural integrity of c-kit mutant D816V causes constitutive signaling. *Mutat Res* (2018) 808:28–38. doi: 10.1016/j.mrfmmm.2018.02.001

56. Reinhart R, Rohner L, Wicki S, Fux M, Kaufmann T. BH3 mimetics efficiently induce apoptosis in mouse basophils and mast cells. *Cell Death Differ* (2018) 25(1):204–16. doi: 10.1038/cdd.2017.154

57. Mayerhofer M, Gleixner KV, Hoelbl A, Florian S, Hoermann G, Aichberger KJ, et al. Unique effects of KIT D816V in BaF3 cells: Induction of cluster formation, histamine synthesis, and early mast cell differentiation antigens. *J Immunol* (2008) 180 (8):5466–76. doi: 10.4049/jimmunol.180.8.5466

58. Yang Y, Letard S, Borge L, Chaix A, Hanssens K, Lopez S, et al. Pediatric mastocytosis-associated KIT extracellular domain mutations exhibit different functional and signaling properties compared with KIT-phosphotransferase domain mutations. *Blood* (2010) 116(7):1114–23. doi: 10.1182/blood-2009-06-226027

59. Zappulla JP, Dubreuil P, Desbois S, Letard S, Hamouda NB, Daeron M, et al. Mastocytosis in mice expressing human kit receptor with the activating Asp816Val mutation. *J Exp Med* (2005) 202(12):1635–41. doi: 10.1084/jem.20050807

60. Ochi H, Hirani WM, Yuan Q, Friend DS, Austen KF, Boyce JA. T Helper cell type 2 cytokine-mediated comitogenic responses and CCR3 expression during differentiation of human mast cells in vitro. *J Exp Med* (1999) 190(2):267–80. doi: 10.1084/jem.190.2.267

61. Cancilla D, Rettig MP, DiPersio JF. Targeting CXCR4 in AML and ALL. *Front Oncol* (2020) 10:1672. doi: 10.3389/fonc.2020.01672

62. Kiran MY, Apaydin Arikan E, Sanli Y, Yegen G, Kuyumcu S. CXCR4 expression demonstrated by 68Ga-pentixafor PET/CT imaging in a case of systemic mastocytosis mimicking lymphoma. *Clin Nucl Med* (2021) 46(12):e563–e64. doi: 10.1097/RLU.0000000000003817

63. Tam IYS, Ng CW, Lau HYA, Tam SY. Degradation of monocyte chemoattractant protein-1 by tryptase Co-released in immunoglobulin e-dependent activation of primary human cultured mast cells. *Int Arch Allergy Immunol* (2018) 177 (3):199–206. doi: 10.1159/000490533

64. Tam IYS, Ng CW, Tam SY, Lau HYA. Novel six-week protocol for generating functional human connective tissue-type (MCTC) mast cells from buffy coats. *Inflammation Res* (2017) 66(1):25–37. doi: 10.1007/s00011-016-0989-z

65. Frost MJ, Ferrao PT, Hughes TP, Ashman LK. Juxtamembrane mutant V560GKit is more sensitive to imatinib (STI571) compared with wild-type c-kit whereas the kinase domain mutant D816VKit is resistant. *Mol Cancer Ther* (2002) 1 (12):1115–24.

66. Ma Y, Zeng S, Metcalfe DD, Akin C, Dimitrijevic S, Butterfield JH, et al. The c-KIT mutation causing human mastocytosis is resistant to STI571 and other KIT kinase inhibitors; kinases with enzymatic site mutations show different inhibitor sensitivity profiles than wild-type kinases and those with regulatory-type mutations. *Blood* (2002) 99(5):1741–4. doi: 10.1182/blood.v99.5.1741

67. Jawhar M, Schwaab J, Naumann N, Horny HP, Sotlar K, Haferlach T, et al. Response and progression on midostaurin in advanced systemic mastocytosis: KIT D816V and other molecular markers. *Blood* (2017) 130(2):137–45. doi: 10.1182/blood-2017-01-764423

68. Smith BD, Kaufman MD, Lu WP, Gupta A, Leary CB, Wise SC, et al. Ripretinib (DCC-2618) is a switch control kinase inhibitor of a broad spectrum of oncogenic and drug-resistant KIT and PDGFRA variants. *Cancer Cell* (2019) 35(5):738–51.e9. doi: 10.1016/j.ccell.2019.04.006

69. Valent P, Akin C, Hartmann K, Nilsson G, Reiter A, Hermine O, et al. Advances in the classification and treatment of mastocytosis: Current status and outlook toward the future. *Cancer Res* (2017) 77(6):1261–70. doi: 10.1158/0008-5472.CAN-16-2234

70. Zhang JQ, Bosbach B, Loo JK, Vitiello GA, Zeng S, Seifert AM, et al. The V654A second-site KIT mutation increases tumor oncogenesis and STAT activation in a mouse model of gastrointestinal stromal tumor. *Oncogene* (2020) 39(49):7153–65. doi: 10.1038/s41388-020-01489-4

frontiers | Frontiers in Immunology

TYPE Brief Research Report
PUBLISHED 29 March 2023
DOI 10.3389/fimmu.2023.1155777

OPEN ACCESS

EDITED BY
Ulrich Blank,
Institut National de la Santé et de la Recherche Médicale (INSERM), France

REVIEWED BY
Michael Huber,
RWTH Aachen University, Germany
John Joseph Ryan,
Virginia Commonwealth University, United States

*CORRESPONDENCE
Hydar Ali
alih@upenn.edu

SPECIALTY SECTION
This article was submitted to Molecular Innate Immunity, a section of the journal Frontiers in Immunology

RECEIVED 31 January 2023
ACCEPTED 15 March 2023
PUBLISHED 29 March 2023

CITATION
Thapaliya M and Ali H (2023) GRK2 differentially regulates FcεRI and MRGPRB2-mediated responses in mast cells.
Front. Immunol. 14:1155777.
doi: 10.3389/fimmu.2023.1155777

GRK2 differentially regulates FcεRI and MRGPRB2-mediated responses in mast cells

Monica Thapaliya and Hydar Ali*

Department of Basic and Translational Sciences, University of Pennsylvania School of Dental Medicine, Philadelphia, PA, United States

In addition to high-affinity IgE receptor (FcεRI), a subtype of mouse mast cells (MCs) expresses a G protein-coupled receptor known as Mas-related G protein-coupled receptor (GPCR)-B2 (MRGPRB2; human ortholog MRGPRX2). GPCR kinase 2 (GRK2) is a Serine/Threonine kinase that phosphorylates GPCRs to promote their desensitization and internalization. We previously showed that silencing GRK2 expression in mouse bone marrow-derived MCs (BMMCs) blocks IgE-mediated degranulation. Compound 48/80 (C48/80), substance P (SP) and LL-37 cause degranulation in human and mouse MCs *via* MRGPRX2 and MRGPRB2, respectively. We also reported that C48/80 and SP cause desensitization and internalization of MRGPRX2, but LL-37 does not. Here, we generated mice with MC-specific deletion of *Grk2* (*Cpa3Cre*$^{+}$/*Grk2*$^{fl/fl}$) to determine its role on IgE-mediated responses and to assess whether it differentially regulates degranulation in response to LL-37, C48/80 and SP. Absence of GRK2 substantially inhibited IgE-mediated tyrosine phosphorylation of STAT5, calcium mobilization, and degranulation in mouse primary lung-derived MCs (PLMCs). By contrast, peritoneal MCs (PMCs) from *Cpa3Cre*$^{+}$/*Grk2*$^{fl/fl}$ mice demonstrated significant enhancement of degranulation in response to C48/80 and SP, but not LL-37. Deletion of *Grk2* in MCs attenuated IgE-mediated passive cutaneous anaphylaxis (PCA) and itch but not passive systemic anaphylaxis (PSA). Surprisingly, PSA was significantly reduced in *Mrgprb2*$^{-/-}$ mice. These findings suggest that GRK2 contributes to PCA and itch but not PSA. By contrast, GRK2 desensitizes MRGPRX2/B2-mediated responses to C48/80 and SP but not LL-37. However, IgE-mediated PSA likely involves the activation of MRGPRB2 by LL-37 or a similar agonist, whose function is resistant to modulation by GRK2.

KEYWORDS

MRGPRX2/MRGPRB2, GRK2, itch, anaphylaxis, mast cells, FcεRI, STAT5

Abbreviations: MC, mast cell; PMCs, peritoneal mast cell; PLMC, primary lung-derived mast cell; GRK2, G Protein-coupled receptor kinase 2; FcεRI, High-affinity IgE receptor; LAMP-1, lysosomal-associated membrane protein 1; MRGPRX2/B2, Mas related G Protein-Coupled receptor X2/B2; STAT5, Signal Transducer and Activator of Transcription 5; C48/80, compound 48/80; SP, substance P; PCA, passive cutaneous anaphylaxis; PSA, passive systemic anaphylaxis.

Introduction

Mast cells (MCs) are tissue-resident immune cells that are responsible for allergic disorders such as anaphylaxis, atopic dermatitis and asthma (1, 2). Cross-linking of high-affinity IgE receptor (FcεRI) by allergens on MCs results in the release of prestored inflammatory mediators followed by newly synthesized mediators that are primary drivers of these allergic disorders (2). G protein-coupled receptor (GPCR) kinases (GRKs) are Serine/Threonine (Ser/Thr) protein kinases that are best known for their roles in GPCR desensitization (3, 4). We have recently shown that silencing GRK2 expression in mouse bone marrow-derived MCs (BMMCs) results in significant inhibition of IgE-mediated degranulation (5). By contrast, overexpression of GRK2 in rat basophilic leukemia (RBL-2H3) cells results in enhanced IgE-mediated degranulation and cytokine generation without affecting the expression levels of any of the FcεRI subunits (α,β,γ) or IgE-mediated phosphorylation of Fcγ (5). One objective of the present study was to generate mice with MC-specific deletion of *Grk2* to determine if its absence attenuates IgE-mediated passive cutaneous anaphylaxis (PCA), itch and passive systemic anaphylaxis (PSA) *in vivo*.

In addition to FcεRI, a MC subtype predominantly found in the human skin expresses a novel G protein-coupled receptor (GPCR) called Mas-related GPCR-X2, (MRGPRX2, mouse counterpart MRGPRB2) (6, 7). Serhan et al. (8) recently showed that house dust mice antigen causes the release of the neuropeptide substance P (SP) from sensory neurons. This SP then activates cutaneous MCs *via* MRGPRB2, which contributes to the development of atopic dermatitis-like lesion in mouse skin. However, McNeil et al (7), showed that MRGPRB2 does not contribute to IgE-mediated cutaneous anaphylaxis. By contrast, using a pharmacological approach, Oskeritzian et al. (9), showed that release of Sphingosine-1-phosphate from MCs in response to FcεRI transactivates its cognate GPCR in MCs and contributes to PSA. However, the possibility that MRGPRB2 contributes to IgE-mediated PSA and if GRK2 regulates this response has not been determined.

It is generally accepted that agonist-induced phosphorylation of GPCRs by GRKs and the subsequent recruitment of the adapter protein, β-arrestin promotes their desensitization and internalization (3, 10). However, our lab was the first to demonstrate that although the antimicrobial peptide LL-37 activates human MCs *via* MRGPRX2, the receptor is resistant to LL-37-induced phosphorylation, desensitization, and internalization (11). In addition, shRNA-mediated knockdown of GRK2 had no effect on LL-37-induced MC degranulation (11). Subsequent studies from our lab led to the characterization of MRGPRX2 agonists into two groups, termed G protein-biased and balanced agonists. G protein-biased agonists such as LL-37, icatibant and murepavadin activate G proteins and are resistant to desensitization and internalization (11–13). By contrast, balanced agonists such as C48/80 and SP not only activate G proteins but also promote MRGPRX2 desensitization and internalization (14, 15). Here, we also sought to determine if GRK2 modulates degranulation in response to selected G protein-biased and balanced agonists in mouse peritoneal MCs that endogenously expresses MRGPRB2 *in vitro* and to assess if the receptor contributes to IgE-mediated PSA *in vivo*.

Materials and methods

Reagents

DNP-specific mouse IgE (SPE-7) and all cell culture reagents were purchased from Invitrogen (Carlsbad, CA). Recombinant mouse interleukin-3 (IL-3) and mouse stem cell factor (SCF) used in the study were obtained from Peprotech (Rocky Hill, NJ). DNP-BSA, p-nitrophenyl-N-acetyl-β-D-glucosamine (PNAG), Ionomycin, Phorbol 12-myristate 13-acetate (PMA), Evans blue dye and protease inhibitor were obtained from Sigma-Aldrich (St. Louis, MO). KIT antibody conjugated with Phycoerythrin (PE), FcεRI antibody conjugated with Fluorescein isothiocyanate (FITC) and Allophycocyanin (APC) were purchased from eBiosciences (San Diego, CA). Anti-mouse LAMP-1 antibody conjugated with Alexa Fluor 647 and anti-mouse CD31 antibody conjugated with Alexa Fluor 488-conjugated were purchased from BioLegend (San Diego, CA). Halt Phosphatase Inhibitor Cocktail was purchased from Pierce Endogen. Antibodies against HRP-labeled goat anti-rabbit IgG, GRK2, β-actin, P-STAT5 (Tyr 694) and STAT5 were purchased from Cell Signaling Technology (Danvers, MA). SuperSignal® Pico plus Chemiluminescent Substrate was from Thermo Scientific (Rockford, IL). Fura-2 AM and Texas Red-conjugated Avidin was purchased from Molecular Probes (Eugene, OR). LL-37, Substance P (SP) and Compound 48/80 (C48/80) were obtained from AnaSpec (Fremont, CA).

Mice

Pathogen-free cages with autoclaved hardwood beddings were used to house all mice used in the study. *Cpa3Cre* mice were kindly provided by Dr. Stephen Galli (Stanford University, Stanford, CA) (16) and *Grk2*$^{fl/fl}$ mice were kind gift from Dr. Hariharan Subramanian (Michigan State University). Mice with MC-specific deletion of *Grk2* (*Cpa3Cre*$^{+}$/*Grk2*$^{fl/fl}$) were generated by Cre-Lox breeding scheme by crossing *Cpa3Cre* mice with *Grk2*$^{fl/fl}$ mice. Absence of *Grk2* in mice were validated at genomic level based on Cre and Flox specific PCR using *Cpa3Cre*$^{-}$/*Grk2*$^{fl/fl}$ mice as respective controls with the primer sets: *Cpa3Cre* Fwd: ACT GTT CAT CCC CAG GAA CC; *Cpa3Cre* Rev: CAG GTT CTT GCG AAC CTC AT; *Grk2*-Flox Fwd: TGA GGC TCA GGG ATA CCT GTC AT; *Grk2*-Flox Rev: CAG GCA TTC CTG CTG GAC TAG. The wild type (WT, C57BL/6), mice used in this study with were obtained from the Jackson Laboratory (Bar Harbor, ME, USA). CRISPR-Cas9 core facility of the University of Pennsylvania generated *Mrgprb2* deficient mice (*Mrgprb2*$^{-/-}$) in the C57BL/6 background. This study was approved by Institutional Animal Care and Use Committee at The University of Pennsylvania and constituted of 8-12 weeks mice.

Cells

Primary lung-derived MCs (PLMCs)

PLMCs were obtained from *Cpa3Cre*$^{+}$/*Grk2*$^{fl/fl}$ and *Cpa3Cre*$^{-}$/*Grk2*$^{fl/fl}$ fresh lung tissue from mice *via ex-vivo* differentiation as described (17). Briefly, lungs were excised and collected in a 15 mL falcon tube with complete media (Gibco Roswell Park Memorial Institute (RPMI) 1640 media with GlutaMAX and 25mM HEPES supplemented with 10% FBS, 5% Non-Essential Amino Acid (NEAA), penicillin (100 IU/mL) and streptomycin (100 µg/mL). They were then washed with PBS once and chopped into fine pieces with scissors. Chopped lungs were then cultured in complete media with β-mercaptoethanol (45.6 µM) supplemented with murine IL-3 (10 ng/mL), and murine SCF (10 ng/mL). After 7-10 days fat like droplets left behind in the culture were strained. The cells were then cultured continuously removing adherent cells 1-2 times/week for a duration of 4-6 weeks. The purity of the MCs were determined by flow cytometry (BD LSR II flow cytometer, BD Biosciences) using anti-KIT-PE and anti-FcεRI-FITC antibodies.

Peritoneal MCs (PMCs)

PMCs from *Cpa3Cre*$^{+}$/*Grk2*$^{fl/fl}$ and *Cpa3Cre*$^{-}$/*Grk2*$^{fl/fl}$ mice were isolated and purified as described (12). Briefly, cells were lavaged from peritoneal cavity using Hank's Balanced Salt Solution (HBSS) supplemented with 3% fetal bovine serum (FBS) and 1mM HEPES in 10ml volume. The cells were then cultured in complete medium same as PLMCs supplemented with murine IL-3 (10 ng/mL), and murine SCF (30 ng/mL). After 48 hours non-adherent cells were removed. Suspension cells were further cultured in fresh medium for 4-8 weeks supplementing IL-3 and SCF once every week. After 4 weeks of culture, alcian/safranin staining was used to confirm that > 90% of cells were PMCs as described (18). The purity of MCs were determined with same flow cytometric procedure as PLMCs.

Mast cell staining

Cultured PMCs (5×10^4) were stained with alcian/safranin as described (18). Images were captured using Nikon E600 microscope at 10X ND image were analyzed using NIS Elements Software. Dermal sheets of ears from *Cpa3Cre*$^{+}$/*Grk2*$^{fl/fl}$ and *Cpa3Cre*$^{-}$/*Grk2*$^{fl/fl}$ mice were stained using Texas Red-Avidin (MCs)and Alexa Fluor 488-conjugated CD31 antibody (endothelial cells) as described previously (18). Briefly, the dermal sheets were fixed in 3.7% paraformaldehyde overnight, blocked with 0.3% triton and 1% BSA in PBS for 30 min, incubated overnight with Texas Red-Avidin and Alexa Fluor 488-conjugated CD31 antibody, washed for 1 hour and mounted with antifade mounting solution. Nikon A1R laser scanning confocal microscope was used to capture the images with a 40X water objective (NA=1.2). Nikon NIS Elements software was used for image analysis.

FcεRI and KIT expression

Cell surface receptor expression in PLMCs and PMCs from *Cpa3Cre*$^{+}$/*Grk2*$^{fl/fl}$ and *Cpa3Cre*$^{-}$/*Grk2*$^{fl/fl}$ were analyzed *via* flow cytometry. Briefly, cells (0.4×10^6) were washed with buffer PBS containing 2% FBS and 0.02% sodium azide and stained with anti-KIT-PE and anti-FcεRI-APC (PMCs)/anti-FcεRI-FITC (PLMCs) for 30 min on ice. Cells were washed and fixed in 1.5% paraformaldehyde solution. BD LSR II flow cytometer (BD Biosciences) was used to acquire flow cytometry data and analyzed by WinList software.

Western blotting

To confirm the absence of GRK2, protein lysate was prepared from PLMCs and PMCs from *Cpa3Cre*$^{+}$/*Grk2*$^{fl/fl}$ and *Cpa3Cre*$^{-}$/*Grk2*$^{fl/fl}$ using RIPA cell lysis buffer with protease inhibitor. Protein then was separated in SDS-PAGE (10%), immunoblotted onto PVDF membranes, blocked, and probed with anti-GRK2 antibody (1:1000). SuperSignal® West Femto Chemiluminescent Substrate was used for membrane development following incubation by HRP-conjugated secondary antibody. The membrane was further subjected to stripping and re-probing with β-actin similarly. IgE-primed PLMCs were stimulated with antigen (DNP-BSA) for different time point and lysed and probed with anti-p-STAT5 antibody. The blot was further stripped and probed with total STAT5 and β-actin antibody.

Calcium mobilization

IgE primed PLMCs (0.5×10^6) with DNP-specific mouse IgE antibody (1 µg/mL, 16 h) were first washed in HEPES-buffered saline containing 0.1% BSA. Next, the cells were loaded with 1 µM Fura-2 acetoxymethyl ester for 30 min at 37°C. They were further allowed to undergo de-esterification in the buffer for an additional 15 min incubation at room temperature. Cells were stimulated with 10 ng/ml of DNP-BSA at 100 sec. Calcium mobilization data was collected using a Varioskan™ LUX Multimode Microplate Readers (Thermo Scientific). The dual excitation wavelength used were 340 and 380 nm with an emission wavelength of 510 nm.

Degranulation

IgE-primed PLMCs (4×10^4/well) with anti-DNP specific IgE antibody (1 µg/mL, 16 h) were incubated with different concentrations of antigen (DNP-BSA, 0 -100 ng/mL) at 37°C for 30 min in a round bottom 96 well plate. To measure total β-hexosaminidase release, unstimulated cells were subjected to lysis in 50 µL of 0.1% Triton X-100. Aliquots (20 µL) of supernatant or cell lysates were transferred into fresh wells and 20 µL of 1 mM p-nitrophenyl-N-acetyl-β-D-glucosamine was added. The reaction was further incubated for 1 h at 37°C and was stopped by adding 250 µL of a 0.1M Na_2CO_3/0.1M $NaHCO_3$ buffer. The absorbance was measured at 405 nm. For experiments with PMCs, cells (1×10^4/well) were stimulated with C48/80 (10 µg/mL), SP (50 µM) and LL-37 (10 µM) for 30 min at 37°C. For PMA/ionomycin stimulation, PLMCs were exposed to PMA (50 nM for 5 min) and subsequently stimulated with ionomycin (0 – 2 µg/mL) for additional 30 min and β-hexosaminidase release was determined. Percentage degranulation was calculated by diving sample β-hexosaminidase release with total β-hexosaminidase release. For accessing degranulation *via* cell surface lysosomal-associated membrane protein1 (LAMP-1) expression, IgE-primed cells (0.5×10^6) were stimulated with DNP-BSA (10 ng/mL) for 10 min,

washed and incubated with anti-LAMP-1 Alexa Fluor 647 antibody for 1 hour on ice. Flow cytometric assay was used to determine cell surface expression of LAMP-1 as described (18).

Passive cutaneous anaphylaxis

For experiments with IgE-mediated anaphylaxis, mice were intradermally injected with DNP-specific IgE (20 ng, 30 µL) into the right or PBS in the left ear/paw (control). After 24 h, mice were challenged with an intravenous injection of 100 µg DNP-BSA in 200 µL PBS containing 1% Evans blue in PBS. For experiment to assess C48/80-induced vascular permeability, mice were intradermally injected with C48/80 (100 ng, 10 µL, right hind paw) or PBS (10 µL, left hind paw) following an intravenous injection of 100 µL of 1% Evans blue in PBS. After 30 min both experimental tissues were collected and weighed. They were then dissolved in 600 µL formamide and incubated at 55°C for 24 h. For paw tissues, dry weight was recorded after drying at 55°C for 24 h before formamide incubation. Next, supernatant was collected and measuring the absorbance at 650 nm dye extravasation was determined.

Passive systemic anaphylaxis

PSA mediated *via* IgE was performed as previously described (9). Briefly, mice were passively sensitized with 20 µg of anti-DNP-BSA in 200 µl of PBS intraperitoneally. After 24 hours, mice were challenged with 200 µg of DNP-BSA in 200 µl of PBS intraperitoneally. Every 10 min for 60 min and every 30 min after that until 120 min core body temperature was measured with a rectal thermometer (physitemp) and recorded. After 120 min mice were euthanized. Temperature drop from the baseline was calculated by subtracting each temperature with the baseline temperature without challenge. Mice injected with PBS vehicle showed no significant changes in body temperature (± 1°C).

Ovalbumin-induced itch

To test the behavioral response of itch, mice were sensitized intraperitoneally with 50 µg of ovalbumin (Ova) in 100 µL volume on Day 0, 20 µg on Day 11 and challenged with 50 µg of Ova or vehicle (PBS) on day 19 intradermally into the cheek in 10 µL volume, and bouts of scratching for a period of 30 min was quantified as described (19). For behavior experiments prior to the injection, mice were subjected to acclimatization period in the test chamber for 10 min on the day of the experiment. Ova or PBS was injected into the cheek, and scratching behavior was recorded for 30 min. Continuous scratching movement at the injection site utilizing hind paw was defined and recorded as a bout of scratching. The number of scratching bouts during the 30 min observation period was quantified by counting in slow motion frame by frame using Elmedia video player.

Statistical analysis

To maintain and ensure reproducibility and scientific rigor, 6-10 mice per experiment were used for all *in vivo* experiments. No sex dependent response has been reported yet and thus equal number of males and females were used. Results are represented as mean ± standard error of the mean (SEM) values. Different batches of cells culture (at least 3) were used in all *in vitro* experiments repeated 3-4 times ran in triplicates. For calcium mobilization, SEM has been omitted from figure for clarity. Statistical significance was determined by two-way ANOVA with multiple comparison and were set at $^{*}P \leq 0.05$, $^{**}P \leq 0.01$, $^{***}P \leq 0.001$ and $^{****}P \leq 0.0001$ analyzed by GraphPad Prism version 9. The statistical comparison that resulted in non-significant p-values were omitted from the graph for more clarity.

Results

To investigate the role of GRK2 on FcεRI and MRGPRB2-mediated responses, we generated mice with MC-specific deletion of *Grk2* by crossing *Cpa3Cre* mice with $Grk2^{fl/fl}$ mice. Zhong et al. (17), showed that incubation of finely chopped mouse upper airway fragments with SCF and IL-3 results in the generation of primary lung-derived MCs (PLMCs), which express functional FcεRI. We therefore generated mouse PLMCs from $Cpa3Cre^{-}/Grk2^{fl/fl}$ and $Cpa3Cre^{+}/Grk2^{fl/fl}$ mice. Using Western blotting, we confirmed that GRK2 is absent in PLMCs generated from $Cpa3Cre^{+}/Grk2^{fl/fl}$ mice (Figure 1A). Flow cytometry experiment with FcεRI and KIT antibodies demonstrated that absence of GRK2 has no effect on the differentiation of PLMCs (Figure 1B). However, the absence of GRK2 resulted in significant inhibition of IgE-mediated calcium mobilization (Figure 1C) and degranulation as assessed by cell surface expression of Lysosomal-associated membrane protein 1 (LAMP-1) (Figure 1D) and β-hexosaminidase release (Figure 1E). By contrast, degranulation induced by phorbol 12-myristate 13-acetate/Ca^{2+} ionophore was unaffected suggesting that the inhibitory effect of GRK2 on IgE-mediated degranulation results from the modification of a signaling component upstream of calcium mobilization (Figure 1F).

Signal Transducers and Activators of Transcription (STATs) are ubiquitously expressed cytoplasmic proteins and are well documented to play an important role in the development, survival, and proliferation of MCs (20, 21). It was recently demonstrated that tyrosine phosphorylation of STAT5 contributes to IgE-mediated signaling in MCs (22, 23). Given that absence of GRK2 and STAT5 (24) display similar IgE-mediated *in vitro* MC response, we hypothesized that GRK2 could contribute to FcεRI signaling by promoting tyrosine phosphorylation of STAT5. As per previous report (22), we found that activation of control cells with antigen/IgE resulted in robust but transient tyrosine phosphorylation of STAT5. However, the absence of GRK2 resulted in significant inhibition of STAT5 phosphorylation (Figures 1G, H).

Immunofluorescent staining of dermal MCs in mouse ear with Texas Red Avidin (MCs) and Alexa Fluor 488-conjugated CD31 (endothelial cells) revealed that GRK2 has no effect on the number and distribution of MCs adjoining blood vessels (Figure 2A). We next sought to determine the effects of *Grk2*-deletion on IgE-mediated passive cutaneous anaphylaxis (PCA) and itch *in vivo*. For PCA, $Cpa3Cre^{-}/Grk2^{fl/fl}$ and $Cpa3Cre^{+}/Grk2^{fl/fl}$ mice were sensitized with intradermal injection of DNP-specific IgE (right ear/paw) or PBS vehicle (left ear/paw), and after 24 h, mice were

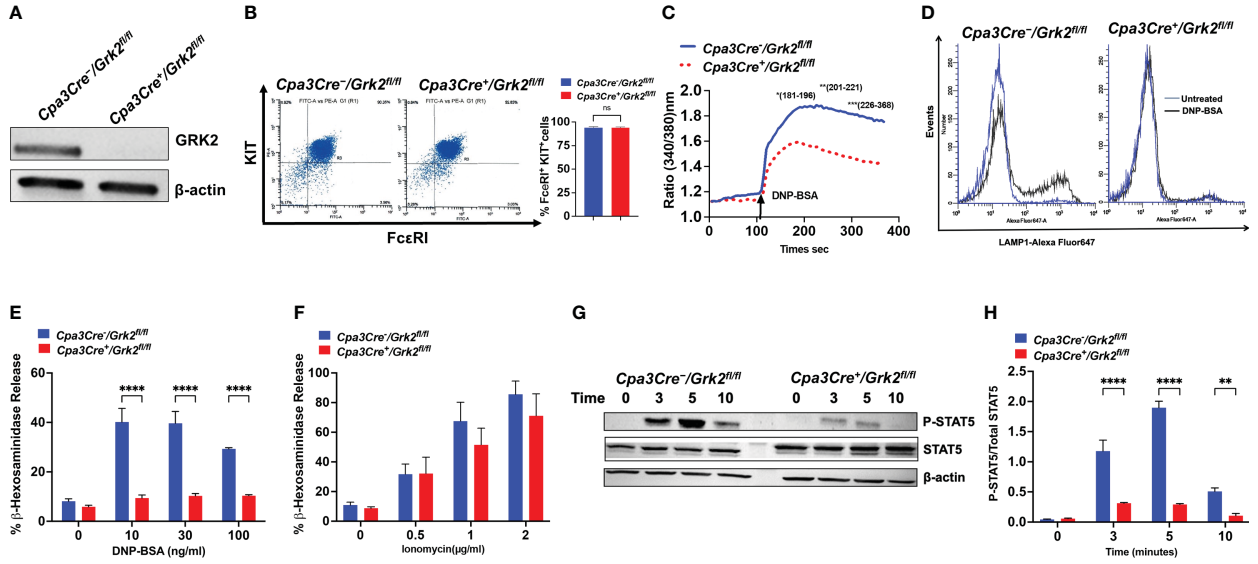

FIGURE 1
Grk2-deletion inhibits FcεRI-induced primary lung-derived MCs (PLMCs) activation. In PLMCs generated from *Cpa3Cre*$^{-}$/*Grk2*$^{fl/fl}$ and *Cpa3Cre*$^{+}$/*Grk2*$^{fl/fl}$ mice, **(A)** Western blotting for GRK2 protein expression with β-actin as loading control, **(B)** cell surface expression of FcεRI and KIT receptors as determined by flow cytometry; DNP-BSA-induced **(C)** calcium mobilization (10 ng/ml), **(D)** lysosomal-associated membrane protein1 (LAMP-1) expression (10 ng/ml) and **(E)** β-hexosaminidase release (0 -100 ng/ml) in cells primed with DNP-specific IgE (1 μg/mL, 16 h); **(F)** PMA (50 nM)-Ionomycin (0-2 μg/ml)-induced β-hexosaminidase release; **(G)** Immunoblots for P-STAT5 and STAT5 expression and **(H)** quantification of intensities (P-STAT5/STAT5) upon DNP-BSA (30 ng/ml; 0, 3, 5,10 min) challenge. Each experiment was performed 3-4 times at least in 3 different batches of cells. Error bars are standard error of mean (SEM) and significant differences were set at **p ≤ 0.01 and ****p ≤ 0.0001.

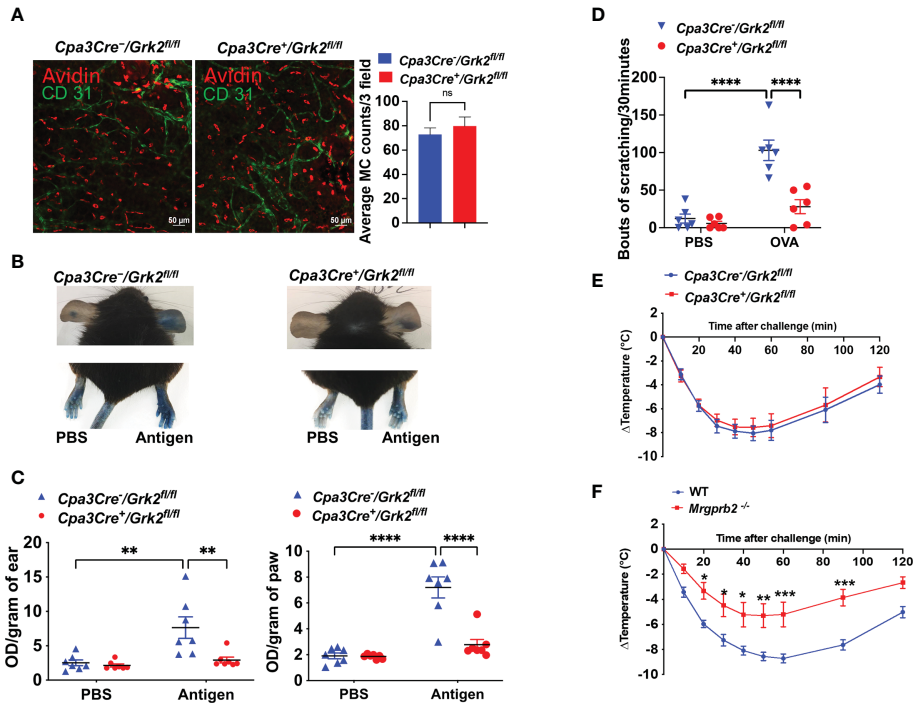

FIGURE 2
Grk2-deletion inhibits IgE-mediated anaphylaxis and itch but not passive systemic anaphylaxis (PSA). In *Cpa3Cre*$^{-}$/*Grk2*$^{fl/fl}$ and *Cpa3Cre*$^{+}$/*Grk2*$^{fl/fl}$ mice, **(A)** Confocal images of ear stained with Texas Red-conjugate Avidin (Mast Cells) and Alexa Fluor488-conjugated anti-CD31 antibody (Endothelial cells); Measurement of vascular permeability in passively sensitized mice (n=6-7) with DNP-specific IgE (20 ng, right ear/hind paw) or PBS (left ear/hind paw) intravenously challenged with DNP-BSA (20 μg in Evans blue). **(B, C)** Representative images and quantification of Evans blue extravasation; **(D)** Bouts of scratching (30 min) in ovalbumin-sensitized (Day 0: 50 μg; Day 11: 20 μg) and challenged (Day 19: 50 μg, cheek) mice. Measurement of core body temperature drop in passively sensitized **(E)** *Cpa3Cre*$^{-}$/*Grk2*$^{fl/fl}$ and *Cpa3Cre*$^{+}$/*Grk2*$^{fl/fl}$ (n=8) and **(F)** Wild-type and *Mrgprb2*$^{-/-}$ mice (n=7-9) with DNP-specific IgE (20 μg, intraperitoneal, 24 hours) and challenged with DNP-BSA (200 μg). Error bars are standard error of mean (SEM) and significant differences were set at *p ≤ 0.05, **p ≤ 0.01, ***p ≤ 0.001 and ****p ≤ 0.0001.

challenged with an intravenous injection of DNP-BSA in 1% Evans blue, and local vascular permeability was measured. As shown in Figures 2B, C, *Cpa3Cre*$^{+}$/*Grk2*$^{fl/fl}$ mice displayed significantly reduced vascular permeability compared to control mice in both experimental tissue locations (ear and paw). For itch studies, mice were sensitized intraperitoneally with ovalbumin (Ova) on Day 0 and 11 and challenged with Ova on day 19 intradermally into the cheek, and bouts of scratching for a period of 30 minutes was quantified (19). As shown in Figure 2D, *Cpa3Cre*$^{+}$/*Grk2*$^{fl/fl}$ mice displayed significantly reduced number of scratching compared to control mice. We further tested the effect of *Grk2*-deletion on IgE-mediated systemic anaphylactic response utilizing the PSA model. For this, *Cpa3Cre*$^{-}$/*Grk2*$^{fl/fl}$ and *Cpa3Cre*$^{+}$/*Grk2*$^{fl/fl}$ mice were sensitized with intraperitoneal injection of DNP-specific IgE and after 24 h challenged with an intraperitoneal injection of DNP-BSA. Core body temperature was measured with a rectal thermometer every 10 min for 60 min and every 30 min after that until 120 min and temperature drop from the baseline was assessed. To our surprise, we found that unlike PCA and itch, *Grk2*-deletion had no effect on PSA (Figure 2E).

Until recently, IgE-mediated MC activation were thought to contribute to atopic dermatitis and allergic contact dermatitis, but it is now realized that MRGPRB2 plays an important role in these responses through its activation by agonists generated from nerve endings (substance P) and keratinocytes (proadrenomedullin N-terminal peptides), respectively (8, 19). Although MRGPRB2 was originally thought to be expressed mostly in skin MCs, transcripts for this receptor are also found in fat, nasopharyngeal, peritoneal and colon MCs (25, 26). We, therefore, hypothesized that MRGPRB2 could contribute to IgE-mediated systemic anaphylaxis. Indeed, we found that IgE-mediated PSA was significantly reduced in *Mrgprb2*$^{-/-}$ mice compared to control mice (Figure 2F). This raises the interesting possibility that IgE-mediated MC activation leads to the secretion of endogenous agonists that activate MRGPRB2, thus suggesting a plausible mechanism for the role of this receptor in PSA. However, the ligand involved is not known.

MRGPRX2 agonists are categorized into G-protein biased or balanced based on downstream activation (13–15). The role of GRK2 in such regulation is not known. Thus, we selected G protein-biased (LL-37) and balanced agonists (C48/80 and SP) to assess if GRK2 differentially regulates degranulation response induced by these agonists. Unlike PLMCs, cells cultured from the mouse peritoneum (PMCs) expresses functional MRGPRB2 (27). We, therefore, performed *in vitro* studies with PMCs cultured from peritoneal lavage cells of *Grk2*-deleted mice (*Cpa3Cre*$^{+}$/*Grk2*$^{fl/fl}$) and their control littermates (*Cpa3Cre*$^{-}$/*Grk2*$^{fl/fl}$). We found that the absence of GRK2 (Figure 3A) had no effect in alcian/safranin staining property (Figure 3B) or cell surface expression of FcεRI and KIT (Figure 3C). Furthermore, absence of GRK2 had no effect on LL-37-induced degranulation in mouse PMCs (Figure 3D), which is consistent with our previous report that silencing the expression of GRK2 in a human MC line endogenously expressing MRGPRX2 has no effect on LL-37-induced degranulation (11).

In contrast to LL-37, SP- and C48/80-induced degranulation was significantly enhanced in the absence of GRK2 (Figures 3E, F). This enhanced response to SP and C48/80 is unlikely due to increased MRGPRB2 expression as degranulation in response to LL-37 remained unaffected in the absence of GRK2. Based on our previous findings that SP and C48/80 cause MRGPRX2

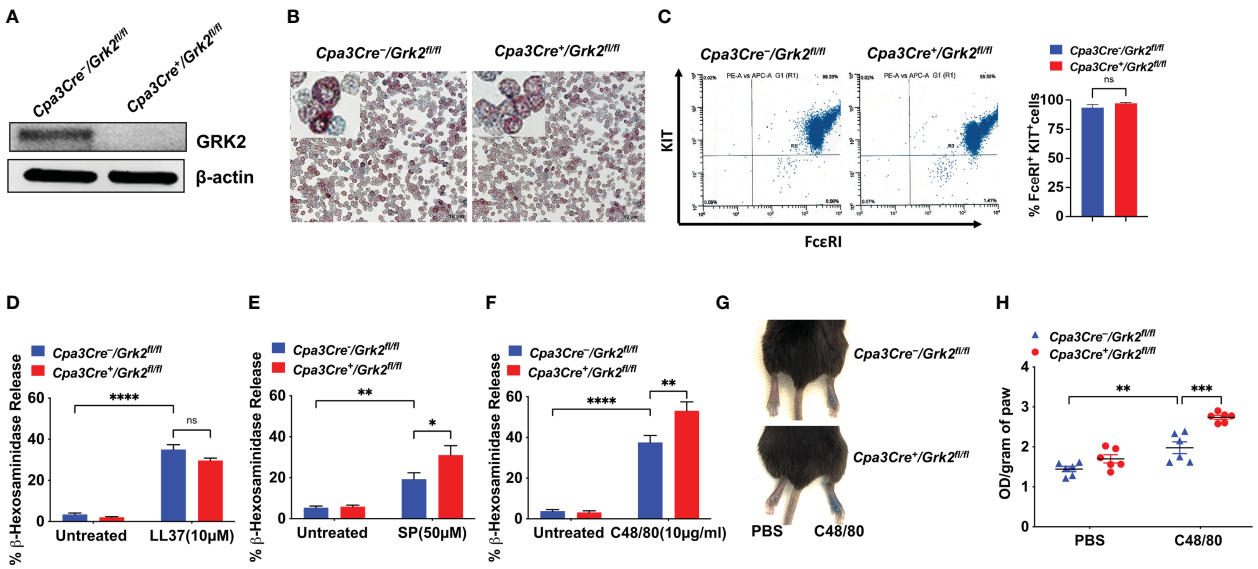

FIGURE 3
Grk2-deletion has no effect on LL-37-induced degranulation but enhances the response to Substance P (SP) and Compound 48/80 (C48/80). In peritoneal MC (PMCs) from *Cpa3Cre*$^{-}$/*Grk2*$^{fl/fl}$ and *Cpa3Cre*$^{+}$/*Grk2*$^{fl/fl}$ mice, **(A)** Western blotting for GRK2 protein expression with β-actin as loading control, **(B)** alcian/safranin staining, **(C)** cell surface expression of FcεRI and KIT receptors as determined by flow cytometry; β-hexosaminidase release induced by **(D)** LL-37 (10 μM), **(E)** SP (50 μM) **(F)** C48/80 (10 μg/ml); Each experiment was performed 3-4 times at least in 3 different batches of cells. **(G, H)** Evans blue extravasation after intradermal-injection with C48/80 (100 ng) in *Cpa3Cre*$^{-}$/*Grk2*$^{fl/fl}$ and *Cpa3Cre*$^{+}$/*Grk2*$^{fl/fl}$ mice (n=6). Error bars are standard error of mean (SEM) and significant differences were set at *p ≤ 0.05, **p ≤ 0.01, ***p ≤ 0.001 and ****p ≤ 0.0001.

desensitization and receptor internalization (12, 14, 15), it is likely that GRK2 phosphorylates Ser/Thr on MRGPRB2 and the enhanced response in the absence of GRK2 reflects a lack of receptor phosphorylation and desensitization. To determine the *in vivo* consequence of *Grk2* deletion, we intradermally injected C48/80 (right) or PBS vehicle (left) in the hind paw of *Cpa3Cre*$^{-}$/*Grk2*$^{fl/fl}$ and *Cpa3Cre*$^{+}$/*Grk2*$^{fl/fl}$ mice following the intravenous injection of Evans blue dye. Consistent with C48/80-induced degranulation in mouse PMCs, there was a significant enhancement of vascular permeability, as measured by dye extravasation, in *Cpa3Cre*$^{+}$/*Grk2*$^{fl/fl}$ mice when compared to control mice (Figures 3G, H). These findings clearly demonstrate that the ability of GRK2 to modulate MRGPRB2-mediated MC degranulation depends on the agonist used for activation.

Discussion

GRK2 is a Ser/Thr kinase that phosphorylates agonist-stimulated GPCRs to promote their desensitization and internalization (3, 10). However, we recently showed that GRK2 contributes to FcεRI (a non-GPCR)-mediated MC responses (5, 28), but the mechanism and *in vivo* relevance is unknown. We have previously shown that C48/80 and SP serve as balanced agonists for MRGPRX2 and promote desensitization and receptor internalization (14, 15). By contrast, LL-37 serves as a G protein-biased agonist for MRGPRX2 and that silencing GRK2 expression in a human MC line (LAD2 cells) has no effect on degranulation in response to this agonist (11, 29). However, the consequence of *Grk2*-deletion on MRGPRB2-mediated degranulation in response to C48/80, SP and LL-37 is not known. In this study, we demonstrated that while GRK2 promotes IgE-mediated calcium mobilization and degranulation in PLMCs *in vitro via* the tyrosine phosphorylation of STAT5, it promotes local cutaneous anaphylaxis but not systemic anaphylaxis. Interestingly, we found a previously unknown role for MRGPRB2 in IgE-mediated systemic anaphylaxis. We also demonstrated that GRK2 does not regulate MRGPRB2-mediated degranulation in response to LL-37.

Pullen et al. (22), reported a novel observation that Fyn-dependent tyrosine phosphorylation of STAT5 is required for IgE-mediated MC function and that these responses are independent of canonical Syk and ERK activation. Additionally, STAT5-deficient mice demonstrated reduced MC degranulation *in vivo*, a similar phenotype that we observed in *Grk2*-deleted mice. STAT5 regulation in IgE-mediated signaling is poorly understood. Thus, this novel role of GRK2 in IgE-mediated STAT5 activation is intriguing. GRK2 is a Ser/Thr kinase, thus direct tyrosine phosphorylation of STAT5 by GRK2 is unlikely. STAT5 co-localizes with FcεRI, and its activity is controlled by Fyn kinase and the negative regulators, Gab2 and SH2 domain-containing phosphatase-1 (SHP-1) (22). Thus, it is possible that GRK2 either acts as an adaptor protein that directly associates with the receptor to facilitate the recruitment of STAT5 to promote Fyn activation or it serves to block the inhibitory activity of Gab2 and SHP-1. These possibilities will be subject of our future investigations.

Although aggregation of FcεRI on MCs provides a well-established mechanism for atopic and hypersensitivity reactions, recent evidence suggests that MRGPRB2 activation by SP contributes to atopic dermatitis (8), which was previously thought to be modulated *via* IgE-mediated pathway (1). In the present study, we have shown that absence of GRK2 enhances SP-induced MRGPRB2-mediated MC degranulation. This raises the interesting possibility that unlike IgE-mediated PCA and itch, GRK2 provides an inhibitory signal for atopic dermatitis through MRGPRX2/B2 desensitization.

Although experimental PCA and PSA in mice are initiated through IgE sensitization and activation of MCs, there appears to be differences in requirement for GPCRs. Thus, while MRGPRB2 does not participate in PCA (7), sphingosine-1-phosphate released from activated MCs activates its cognate GPCR and contributes to PSA (9). The present study provides the first demonstration that MRGPRB2 contributes to IgE-mediated PSA and that GRK2 does not regulate this response. These findings suggests that IgE-mediated MC activation in PSA results in the release of G protein-biased MRGPRB2 agonists, which in turn activate MCs resulting in hypothermia. LL-37 is a G protein-biased agonist for MRGPRX2 (11, 29), which is released from activated MCs and epithelial cells (30–32). We recently showed that LL-37-induced degranulation in mouse PMCs is substantially reduced in the absence of MRGPRB2 (33) and the present study demonstrated that absence of GRK2 has no effect on LL-37-induced degranulation. The possibility that LL-37 or other endogenously derived MRGPRB2 agonist that contribute to IgE-mediated PSA remains to be determined.

In summary, we have shown that GRK2 contributes to IgE-mediated PCA and itch likely *via* the formation of a signaling complex with FcεRI, Fyn, STAT5, Gab2 and SHP-1. Thus, disrupting the interaction of GRK2 with these signaling proteins may provide a new approach to modulate these responses. An intriguing finding of this study is that MRGPRB2 is required for IgE-mediated systemic anaphylaxis and that this response is not modulated by GRK2. Humanized mice have been used to study the role of human MCs in PCA and PSA (34). Furthermore, specific MRGPRX2 antagonists that do not inhibit FcεRI or MRGPRB2-mediated MC degranulation have been developed (35). These reagents could be utilized in the future to determine the role of MRGPRX2 in systemic anaphylaxis, including food allergy.

Data availability statement

The raw data supporting the conclusions of this article will be made available by the authors, without undue reservation.

Ethics statement

The animal study was reviewed and approved by Institutional Animal Care and Use Committee at The University of Pennsylvania.

Author contributions

HA contributed to conception, supervision, and funding acquisition of the study. MT contributed to the conception, performed the experiments and analyzed the data and wrote the first draft of the manuscript. All authors contributed to manuscript revision, read, and approved the final manuscript. All authors contributed to the article and approved the submitted version.

Funding

This work was supported by National Institutes of Health grants R01-AI124182, R01-AI143185 and R01-AI149487 to HA, F31 AI154765-01A1 to MT.

Acknowledgments

We thank the FACS core facility of the University of Pennsylvania School of Dental Medicine for flow cytometry acquisition and analysis. We also thank the University of Pennsylvania's CRISPR/Cas9 Targeting Core and Transgenic and Chimeric mouse facility for generating the *Mrgprb2*$^{-/-}$ mice for our laboratory. We thank Dr. Aetas Amponnawarat for his help in formatting figures and proofreading the manuscript.

Conflict of interest

The authors declare that the research was conducted in the absence of any commercial or financial relationships that could be construed as a potential conflict of interest.

Publisher's note

References

1. Kawakami T, Ando T, Kimura M, Wilson BS, Kawakami Y. Mast cells in atopic dermatitis. *Curr Opin Immunol* (2009) 21(6):666–78. doi: 10.1016/j.coi.2009.09.006

2. Galli SJ, Tsai M. IgE and mast cells in allergic disease. *Nat Med* (2012) 18(5):693–704. doi: 10.1038/nm.2755

3. Benovic JL. Historical perspective of the G protein-coupled receptor kinase family. *Cells* (2021) 10(3):555. doi: 10.3390/cells10030555

4. Guo Q, Subramanian H, Gupta K, Ali H. Regulation of C3a receptor signaling in human mast cells by G protein coupled receptor kinases. *PloS One* (2011) 6(7):e22559. doi: 10.1371/journal.pone.0022559

5. Subramanian H, Gupta K, Parameswaran N, Ali H. Regulation of FcεRI signaling in mast cells by G protein-coupled receptor kinase 2 and its RH domain. *J Biol Chem* (2014) 289(30):20917–27. doi: 10.1074/jbc.M113.523969

6. Motakis E, Guhl S, Ishizu Y, Itoh M, Kawaji H, de Hoon M, et al. Redefinition of the human mast cell transcriptome by deep-CAGE sequencing. *Blood* (2014) 123(17): e58–67. doi: 10.1182/blood-2013-02-483792

7. McNeil BD, Pundir P, Meeker S, Han L, Undem BJ, Kulka M, et al. Identification of a mast-cell-specific receptor crucial for pseudo-allergic drug reactions. *Nature* (2015) 519(7542):237–41. doi: 10.1038/nature14022

8. Serhan N, Basso L, Sibilano R, Petitfils C, Meixiong J, Bonnart C, et al. House dust mites activate nociceptor-mast cell clusters to drive type 2 skin inflammation. *Nat Immunol* (2019) 20(11):1435–43. doi: 10.1038/s41590-019-0493-z

9. Oskeritzian CA, Price MM, Hait NC, Kapitonov D, Falanga YT, Morales JK, et al. Essential roles of sphingosine-1-phosphate receptor 2 in human mast cell activation, anaphylaxis, and pulmonary edema. *J Exp Med* (2010) 207(3):465–74. doi: 10.1084/jem.20091513

10. Pitcher JA, Freedman NJ, Lefkowitz RJ. G Protein-coupled receptor kinases. *Annu Rev Biochem* (1998) 67:653–92. doi: 10.1146/annurev.biochem.67.1.653

11. Subramanian H, Gupta K, Guo Q, Price R, Ali H. Mas-related gene X2 (MrgX2) is a novel G protein-coupled receptor for the antimicrobial peptide LL-37 in human mast cells: resistance to receptor phosphorylation, desensitization, and internalization. *J Biol Chem* (2011) 286(52):44739–49. doi: 10.1074/jbc.M111.277152

12. Amponnawarat A, Chompunud Na Ayudhya C, Ali H. Murepavadin, a small molecule host defense peptide mimetic, activates mast cells *via* MRGPRX2 and MrgprB2. *Front Immunol* (2021) 12:689410. doi: 10.3389/fimmu.2021.689410

13. Roy S, Ganguly A, Haque M, Ali H. Angiogenic host defense peptide AG-30/5C and bradykinin B2 receptor antagonist icatibant are G protein biased agonists for MRGPRX2 in mast cells. *J Immunol* (2019) 202(4):1229–38. doi: 10.4049/jimmunol.1801227

14. Chompunud Na Ayudhya C, Amponnawarat A, Ali H. Substance p serves as a balanced agonist for MRGPRX2 and a single tyrosine residue is required for beta-arrestin recruitment and receptor internalization. *Int J Mol Sci* (2021) 22(10):5318. doi: 10.3390/ijms22105318

15. Babina M, Wang Z, Roy S, Guhl S, Franke K, Artuc M, et al. MRGPRX2 is the codeine receptor of human skin mast cells: Desensitization through beta-arrestin and lack of correlation with the FcepsilonRI pathway. *J Invest Dermatol* (2021) 141 (5):1286–96 e4. doi: 10.1016/j.jid.2020.09.017

16. Lilla JN, Chen CC, Mukai K, BenBarak MJ, Franco CB, Kalesnikoff J, et al. Reduced mast cell and basophil numbers and function in Cpa3-cre; mcl-1fl/fl mice. *Blood* (2011) 118(26):6930–8. doi: 10.1182/blood-2011-03-343962

17. Zhong H, Shlykov SG, Molina JG, Sanborn BM, Jacobson MA, Tilley SL, et al. Activation of murine lung mast cells by the adenosine A3 receptor. *J Immunol* (2003) 171(1):338–45. doi: 10.4049/jimmunol.171.1.338

18. Roy S, Gupta K, Ganguly A, Ali H. Beta-Arrestin2 expressed in mast cells regulates ciprofloxacin-induced pseudoallergy and IgE-mediated anaphylaxis. *J Allergy Clin Immunol* (2019) 144(2):603–6. doi: 10.1016/j.jaci.2019.04.024

19. Meixiong J, Anderson M, Limjunyawong N, Sabbagh MF, Hu E, Mack MR, et al. Activation of mast-Cell-Expressed mas-related G-Protein-Coupled receptors drives non-histaminergic itch. *Immunity* (2019) 50(5):1163–71 e5. doi: 10.1016/j.immuni.2019.03.013

20. Shelburne CP, McCoy ME, Piekorz R, Sexl V, Roh KH, Jacobs-Helber SM, et al. Stat5 expression is critical for mast cell development and survival. *Blood* (2003) 102 (4):1290–7. doi: 10.1182/blood-2002-11-3490

21. Shelburne CP, McCoy ME, Piekorz R, Sexl VV, Gillespie SR, Bailey DP, et al. Stat5: an essential regulator of mast cell biology. *Mol Immunol* (2002) 38(16-18):1187–91. doi: 10.1016/S0161-5890(02)00061-5

22. Pullen NA, Barnstein BO, Falanga YT, Wang Z, Suzuki R, Tamang TD, et al. Novel mechanism for Fc{epsilon}RI-mediated signal transducer and activator of transcription 5 (STAT5) tyrosine phosphorylation and the selective influence of STAT5B over mast cell cytokine production. *J Biol Chem* (2012) 287(3):2045–54. doi: 10.1074/jbc.M111.311142

23. Barnstein BO, Li G, Wang Z, Kennedy S, Chalfant C, Nakajima H, et al. Stat5 expression is required for IgE-mediated mast cell function. *J Immunol* (2006) 177 (5):3421–6. doi: 10.4049/jimmunol.177.5.3421

24. Kiwanuka KN, Motunrayo Kolawole E, McLeod JJA, Baker B, Paez PA, Zellner MP, et al. Stat5B is required for IgE-mediated mast cell function *in vitro* and in vivo. *Cell Immunol* (2021) 364:104344. doi: 10.1016/j.cellimm.2021.104344

25. Dwyer DF, Barrett NA, Austen KF. Immunological genome project c. expression profiling of constitutive mast cells reveals a unique identity within the immune system. *Nat Immunol* (2016) 17(7):878–87. doi: 10.1038/ni.3445

26. Pundir P, Liu R, Vasavda C, Serhan N, Limjunyawong N, Yee R, et al. A connective tissue mast-Cell-Specific receptor detects bacterial quorum-sensing

molecules and mediates antibacterial immunity. *Cell Host Microbe* (2019) 26(1):114–22 e8. doi: 10.1016/j.chom.2019.06.003

27. Chompunud Na Ayudhya C, Amponnawarat A, Roy S, Oskeritzian CA, Ali H. MRGPRX2 activation by rocuronium: Insights from studies with human skin mast cells and missense variants. *Cells* (2021) 10(1):156. doi: 10.3390/cells10010156

28. Thapaliya M, Amponnawarat A, Tesmer JJG, Ali H. GRK2 inhibitors, paroxetine and CCG258747, attenuate IgE-mediated anaphylaxis but activate mast cells *via* MRGPRX2 and MRGPRB2. *Front Immunol* (2022) 13:1032497. doi: 10.3389/fimmu.2022.1032497

29. Chen E, Chuang LS, Giri M, Villaverde N, Hsu NY, Sabic K, et al. Inflamed ulcerative colitis regions associated with MRGPRX2-mediated mast cell degranulation and cell activation modules, defining a new therapeutic target. *Gastroenterology* (2021) 160(5):1709–24. doi: 10.1053/j.gastro.2020.12.076

30. Di Nardo A, Vitiello A, Gallo RL. Cutting edge: mast cell antimicrobial activity is mediated by expression of cathelicidin antimicrobial peptide. *J Immunol* (2003) 170 (5):2274–8. doi: 10.4049/jimmunol.170.5.2274

31. Agerberth B, Grunewald J, Castanos-Velez E, Olsson B, Jornvall H, Wigzell H, et al. Antibacterial components in bronchoalveolar lavage fluid from healthy individuals and sarcoidosis patients. *Am J Respir Crit Care Med* (1999) 160(1):283–90. doi: 10.1164/ajrccm.160.1.9807041

32. Zuyderduyn S, Ninaber DK, Schrumpf JA, van Sterkenburg MA, Verhoosel RM, Prins FA, et al. IL-4 and IL-13 exposure during mucociliary differentiation of bronchial epithelial cells increases antimicrobial activity and expression of antimicrobial peptides. *Respir Res* (2011) 12:59. doi: 10.1186/1465-9921-12-59

33. Roy S, Alkanfari I, Chaki S, Ali H. Role of MrgprB2 in rosacea-like inflammation in mice: Modulation by beta-arrestin 2. *J Invest Dermatol* (2022) 142(11):2988–97 e3. doi: 10.1016/j.jid.2022.05.005

34. Bryce PJ, Falahati R, Kenney LL, Leung J, Bebbington C, Tomasevic N, et al. Humanized mouse model of mast cell-mediated passive cutaneous anaphylaxis and passive systemic anaphylaxis. *J Allergy Clin Immunol* (2016) 138(3):769–79. doi: 10.1016/j.jaci.2016.01.049

35. Bawazir M, Amponnawarat A, Hui Y, Oskeritzian CA, Ali H. Inhibition of MRGPRX2 but not FcepsilonRI or MrgprB2-mediated mast cell degranulation by a small molecule inverse receptor agonist. *Front Immunol* (2022) 13:1033794. doi: 10.3389/fimmu.2022.1033794

frontiers | Frontiers in Immunology

TYPE Original Research
PUBLISHED 30 March 2023
DOI 10.3389/fimmu.2023.1154416

OPEN ACCESS

EDITED BY
Ulrich Blank,
Institut National de la Santé et de la Recherche Médicale (INSERM), France

REVIEWED BY
Julie Gosse,
University of Maine, United States
Joakim Dahlin,
Karolinska Institutet (KI), Sweden

*CORRESPONDENCE
Sandro Capellmann
scapellmann@ukaachen.de
Michael Huber
mhuber@ukaachen.de

SPECIALTY SECTION
This article was submitted to Molecular Innate Immunity, a section of the journal Frontiers in Immunology

RECEIVED 30 January 2023
ACCEPTED 20 March 2023
PUBLISHED 30 March 2023

CITATION
Capellmann S, Sonntag R, Schüler H, Meurer SK, Gan L, Kauffmann M, Horn K, Königs-Werner H, Weiskirchen R, Liedtke C and Huber M (2023) Transformation of primary murine peritoneal mast cells by constitutive KIT activation is accompanied by loss of *Cdkn2a/Arf* expression. *Front. Immunol.* 14:1154416. doi: 10.3389/fimmu.2023.1154416

Transformation of primary murine peritoneal mast cells by constitutive KIT activation is accompanied by loss of *Cdkn2a/Arf* expression

Sandro Capellmann[1*], Roland Sonntag[2], Herdit Schüler[3], Steffen K. Meurer[4], Lin Gan[5], Marlies Kauffmann[1], Katharina Horn[1], Hiltrud Königs-Werner[6], Ralf Weiskirchen[4], Christian Liedtke[2] and Michael Huber[1*]

[1]Institute of Biochemistry and Molecular Immunology, Medical Faculty, Rheinisch-Westfälische Technische Hochschule (RWTH) Aachen University, Aachen, Germany, [2]Department of Internal Medicine III, University Hospital, Rheinisch-Westfälische Technische Hochschule (RWTH) Aachen University, Aachen, Germany, [3]Institute of Human Genetics, Medical Faculty, Rheinisch-Westfälische Technische Hochschule (RWTH) Aachen University, Aachen, Germany, [4]Institute of Molecular Pathobiochemistry, Experimental Gene Therapy and Clinical Chemistry (IFMPEGKC), Medical Faculty, Rheinisch-Westfälische Technische Hochschule (RWTH) Aachen University, Aachen, Germany, [5]Genomics Facility, Interdisciplinary Center for Clinical Research (IZKF), Medical Faculty, Rheinisch-Westfälische Technische Hochschule (RWTH) Aachen University, Aachen, Germany, [6]Electron Microscopy Facility, Institute of Pathology, Medical Faculty, Rheinisch-Westfälische Technische Hochschule (RWTH) Aachen University, Aachen, Germany

Mast cells (MCs) are immune cells of the myeloid lineage distributed in tissues throughout the body. Phenotypically, they are a heterogeneous group characterized by different protease repertoires stored in secretory granules and differential presence of receptors. To adequately address aspects of MC biology either primary MCs isolated from human or mouse tissue or different human MC lines, like HMC-1.1 and -1.2, or rodent MC lines like L138.8A or RBL-2H3 are frequently used. Nevertheless, cellular systems to study MC functions are very limited. We have generated a murine connective tissue-like MC line, termed PMC-306, derived from primary peritoneal MCs (PMCs), which spontaneously transformed. We analyzed PMC-306 cells regarding MC surface receptor expression, effector functions and respective signaling pathways, and found that the cells reacted very similar to primary wildtype (WT) PMCs. In this regard, stimulation with MAS-related G-protein-coupled receptor member B2 (MRGPRB2) ligands induced respective signaling and effector functions. Furthermore, PMC-306 cells revealed significantly accelerated cell cycle progression, which however was still dependent on interleukine 3 (IL-3) and stem cell factor (SCF). Phenotypically, PMC-306 cells adopted an immature connective tissue-like MCs appearance. The observation of cellular transformation was accompanied by the loss of *Cdkn2a* and *Arf* expression, which are both described as critical cell cycle regulators. The loss of *Cdkn2a* and *Arf* expression could be mimicked in primary bone marrow-derived mast cells (BMMCs) by sustained SCF supplementation strongly arguing for an involvement of KIT activation in the regulation of *Cdkn2a/Arf* expression. Hence, this new cell line might be a useful tool to study further aspects of PMC function and to address tumorigenic processes associated with MC leukemia.

KEYWORDS

KIT, cell cycle, transformation, Mrgprb2, protease, cyclin-dependent kinase inhibitor

Introduction

Mast cells (MCs) are tissue-resident immune cells of myeloid origin and well-known effectors of type I hypersensitivity (1–3). Besides, MCs can contribute to cancer progression by supporting angiogenesis, extracellular matrix degradation, and epithelial-to-mesenchymal transition (4, 5). The immune response to viral and bacterial infections is fundamentally triggered by MCs as they are strategically located at interfaces between host and environment (3, 6). Therefore, they belong to the first line of defence against intruders and fulfil the task to alert other immune cells to migrate to infected tissues (7, 8). Finally, MCs also contribute to tissue repair and homeostasis in the resolution phase of inflammation by secreting anti-inflammatory IL-10 and helping to remodel the extracellular matrix (9–11).

Understanding fundamental MC functions is often impeded by adequate cellular model systems. One reason is that a prototypical MC does not exist. The term mast cell comprises a heterogeneous cell population that can be classified into multiple subgroups depending on the receptor repertoire, composition of secretory granules and tissue residency (12). Thus, finding *in vitro* models that represent all aspects of different MC subtypes is not possible. Different tissue sources used for isolation and differences concerning *in vitro* differentiation and/or culturing of MCs using various cytokine and growth factor combinations influences analyses of general MC features. Due to the difficulties to isolate mature tissue-derived MCs from human or murine sources, many studies dealing with MCs have been conducted using human MC lines like HMC-1.1, -1.2, LUVA and LAD2 (13–15) or rodent MC lines like RBL-2H3 or L138.8A (16, 17). However, results obtained with these cell lines have to be interpreted with caution. Immortalized leukemic cell lines, like the HMC-1 lines usually contain oncogenic mutations, e.g. in the *KIT* gene (18), which influences studies on MC biology. Furthermore, the HMC-1 cell lines do not express a functional FcεR1 on the cell surface impeding studies on IgE receptor signaling. Likewise, the RBL-2H3 cell line, for instance, shows substantial genomic rearrangements whose consequences are scarcely characterized but certainly affect signaling pathways and cellular physiology in multiple ways (19, 20).

In mouse and rats, MCs are – in a simplified way – divided into two groups based on their histochemical staining properties reflecting different granule mediator content. Connective tissue MCs (CTMCs) typically contain tryptase, chymases, carboxypeptidase A3 (CPA3) and heparin proteoglycans, whereas granules of mucosal MCs (MMCs) lack tryptase and instead of heparin predominantly contain chondroitin sulfate (21). *In vitro*, murine mucosal-like MCs can be obtained from multipotent bone marrow-derived precursor cells, which require a long-lasting differentiation process in the presence of IL-3 and (optionally) stem cell factor (SCF). The resulting MCs are referred to as bone marrow-derived MCs (BMMCs). However, *in vitro* differentiated cultures of murine BMMC frequently result in an incompletely differentiated population of MCs, which morphologically and histochemically do not fully correspond to finally differentiated MCs observed in mouse tissues (22). Connective tissue-like MCs can be isolated from peritoneum – hence they are referred to as murine peritoneum-derived MCs (PMCs) – and subsequently enriched and expanded in culture in the presence of IL-3 and SCF (23). Challenging about PMCs is, however, that peritoneal lavages often yield only strictly limited amounts of enriched PMCs that cannot be cultured over a longer time period. As a consequence, to extensively characterize PMC biology, plenty of mice need to be sacrificed to yield validated scientific data, which is not in agreement with the 3R principles of animal welfare (24).

To obtain a comprehensive picture of general MC characteristics and functions, a combined approach analyzing cell lines, primary cells and *in vivo* models is required. In the present study, we describe the generation of a PMC-derived spontaneously transformed murine MC line termed PMC-306 that we propose as a new additional tool to study MC biology. We analyzed the MC characteristics in terms of morphology, cell surface marker expression, pro-inflammatory effector responses to different stimuli and protease expression in relation to wildtype (WT) PMCs. We could reveal that the PMC line retained its MC features. PMC-306 cells express functional high-affinity IgE and MRGPRB2 receptors and can therefore be used for respective signaling studies. In addition, we investigated proliferation, survival and the cell cycle pattern of PMC-306, which showed dependence on the cytokines SCF and IL-3. The chromosomal analysis did not reveal major chromosomal abnormalities apart from a heterozygous deletion of regions qC4-qC7 on chromosome 4. This region, amongst others, encodes the cyclin-dependent kinase inhibitor 2A (*Cdkn2a*, also known as INK4A or p16) and *Arf* (also known as p19), both of which function as central cell cycle inhibitors regulating the p53 and Rb pathways (25, 26). Intriguingly, despite the observed heterozygosity of the change on DNA level, mRNA expression of *Cdkn2a* and *Arf* was not detectable in PMC-306 cells. We demonstrated that these aberrations lead to an enhanced cell cycle activity, a strongly increased proliferative capacity and suspect that they might be involved in the mechanism of PMC transformation. We could further induce loss of *Cdkn2a* and *Arf* expression by sustained SCF supplementation of BMMC cultures pointing to a role of constitutive KIT activation in the regulation of *Cdkn2a*/*Arf* expression. Our initial characterization of PMC-306 provides the basis for using this cell line in prospective studies as a new tool to address differential MC functions.

Material and methods

Animals and cell culture

Murine peritoneal MCs (PMCs) and bone marrow-derived MCs (BMMCs) were isolated and cultured as described previously (23). Primary WT PMCs were cultured in conventional cell culture medium [RPMI1640 (Invitrogen, #21875-0991) containing 15% FCS (Capricorn, #FBS-12A), 10 mM HEPES (pH 7.4), 50 units/ml Penicillin and 50 mg/ml Streptomycin, 100 µM β-mercaptoethanol, 30 ng/ml IL-3 from X63-Ag8-653 conditioned medium (27) and approximately, depending on its biological activity, 20 ng/ml SCF from CHO culture supernatant (23)]. For cultivation of PMC-306 cells, the amounts of FCS and SCF were reduced from 15% to 10% and from

20 ng/ml to 5 ng/ml, respectively. Primary BMMCs were cultivated like PMCs, however, SCF was only supplemented to analyze the influence of KIT activation. PMC-306 cells were frozen at -150°C in 90% FCS and 10% DMSO in aliquots of 10 x 10^6 cells per ml. WT PMCs were freshly isolated and were cultured for a maximum of 8 weeks. All mice used in this study were on a mixed C57BL/6 x 129/Sv background. Experiments were performed in accordance with German legislation governing animal studies and following the principles of laboratory animal care. Mice were held in the Institute of Laboratory Animal Science, Medical Faculty of RWTH Aachen University. The institute holds a license for husbandry and breeding of laboratory animals from the veterinary office of the Städteregion Aachen (administrative district). The institute follows a quality management system, which is certified according to DIN EN ISO 9001:2015. All protocols are reviewed by a Governmental Animal Care and Use Committee at the Landesamt für Umwelt-, Natur- und Verbraucherschutz, Recklinghausen (LANUV). No human samples were used and no experiments were conducted involving living animals. Mice were sacrificed by cervical dislocation to isolate cells either from peritoneum to enrich PMCs or from femurs to obtain bone marrow-derived cells, which were differentiated to BMMCs.

β-Hexosaminidase assay

Measuring FcεRI-dependent degranulation, MCs were preloaded with 0.15 µg/ml IgE (clone Spe-7, Sigma, #A2831) overnight (37°C, 5% CO_2). This step was skipped when cells were stimulated *via* MRGPRB2. Cells were washed in sterile PBS, resuspended at a density of 1.2 x 10^6 (PMC-306 line) or 0.6 x 10^6 (WT PMCs) per ml in Tyrode's buffer (130 mM NaCl, 5 mM KCl, 1.4 mM $CaCl_2$, 1 mM $MgCl_2$, 5.6 mM glucose, and 0.1% BSA in 10 mM HEPES, pH 7.4) and allowed to adapt to 37°C 15 min. For stimulation, different concentrations of antigen (Ag; DNP-HSA, Sigma, #A6661), Mastoparan (Sigma, #M5280) or Compound 48/80 (C48/80) (Sigma, #C2313) were applied for 30 minutes. The amount of released β-hexosaminidase was determined by an enzymatic assay as described in (28). Degranulation was calculated as

$$\%\ Degranulation = \frac{amount\ of\ released\ \beta - hexosaminidase}{(amount\ of\ released\ \beta - hexosaminidase + amount\ of\ intracellular\ \beta - hexosaminidase)}$$

Cytokine ELISA

To determine IL-6 and TNF secretion, WT PMCs and PMC-306 were stimulated as indicated in the respective experiments. If cells were stimulated with Ag, MCs were pre-loaded with IgE. Cell number was adjusted to 1.2 x 10^6/ml in stimulation medium [RPMI 1640 + 0.1% BSA (Serva, #11930.04)], cells were allowed to adapt to 37°C and stimulated for 3 hours. Supernatants were collected after centrifugation. 96-well ELISA plates (Corning, #9018) were coated with capturing anti-IL-6 (1:250, BD Biosciences, #554400) or anti-TNF (1:200, R&D Systems, #AF410-NA) antibodies diluted in PBS overnight at 4°C. ELISA plates were washed three times with PBS +0.1% Tween and subsequently blocked with PBS + 2% BSA (IL-6 ELISA) or PBS + 1% BSA + 5% sucrose (TNF ELISA) for 90 min before loading the supernatants (50 µl for IL-6 ELISA, 100 µl for TNF ELISA). Additionally to loading of supernatants, IL-6 (BD Pharmingen, #554582) and TNF (R&D Systems, #410-MT-010) standards in 1:2 dilutions were added and plates were incubated overnight at 4°C. Thereupon, plates were washed three times again followed by incubation with biotinylated anti-IL-6 (1:500, BD Biosciences, #554402) and anti-TNF antibodies (1:250, R&D Systems, #BAF-410) diluted in PBS+1% BSA for 45 minutes and 2 hours, respectively, at room temperature (RT). After 3 washing steps, Streptavidin alkaline phosphatase (SAP, 1:1000, BD Pharmingen, #554065) was added for 30 minutes at RT. After 3 more washing steps, the substrate p-Nitro-phenyl-phosphate (1 pill per 5 ml in sodium carbonate buffer (2 mM $MgCl_2$ in 50 mM sodium carbonate, pH 9.8), Sigma, #S0942-200TAB) was added and OD_{450} was recorded using a plate reader (BioTek Eon).

Flow cytometry, viability assay, LAMP-1 assay and cell cycle analysis

Flow cytometry was performed to analyze MC surface marker expression. Roughly 0.5 x 10^6 cells were washed in FACS buffer (PBS + 3% FCS + 0.1% sodium azide) and stained with either FITC-coupled anti-FcεR1 (1:100, clone MAR-1, BioLegend, #134306) and PE-coupled anti-CD117 (1:100, clone 2B8, BioLegend, #105808) or FITC-coupled anti-ST2 (1:100, clone DJ8, MD Bioproducts, #101001F) and PE-coupled anti-CD13 (1:100, clone R3-242, BD Pharmingen, #558745), respectively, for 20 minutes at 4°C in the dark. Thereupon, cells were washed again in FACS buffer, resuspended in 200 µl FACS buffer and analyzed using a FACSCanto II (BD Biosciences).

To determine viability of WT PMCs and PMC-306 cells, cells were seeded at a density of 0.3 x 10^6 (PMC-306) or 0.5 x 10^6 (WT PMCs) cells/ml and incubated under different cytokine deprivation conditions for 72 hours. Thereupon, cells were washed in FACS buffer and stained with Annexin V (1:100, BioLegend, #640912) diluted in culture medium for 20 minutes at 4°C in the dark. Immediately before analysis by flow cytometry using the FACSCanto II, propidium iodide (Sigma, #P4864) at a concentration of 1 µg/ml was added.

For LAMP-1 assay, MCs were preloaded with IgE (Spe7) overnight. Cells were washed and cell number was adjusted to 1 x 10^6 cells per ml in RPMI 1640 + 0.1% BSA. Stimulation was performed for indicated time points with Ag (DNP-HSA). The reaction was stopped by centrifugation at 4°C followed by staining of cell surface LAMP-1 (CD107a) using FITC-coupled anti-LAMP-1 antibody (clone 1D4B, BioLegend, #121605) for 20 minutes at 4°C in the dark. Cells were washed in FACS buffer and LAMP-1 cell surface expression was determined by flow cytometry using a FACSCanto II.

For analysis of cell cycle parameters, background values of pooled (from n=3 per PMC cell type), unstained cells were subtracted from values of three independent stained samples.

Cultured cells were pelleted by centrifugation (1400 rpm, 4°C, 10 min), subsequently stained with fluorophore-labelled antibodies against the surface markers CD117-PE-Cy7 (1:100, # 561681, BD Biosciences) and FcεR1-FITC (1:100, #11-5895-81, Invitrogen Thermo Fisher Scientific) in FACS-blocking buffer (mixture of 0.66% human/rabbit/mouse serum, Sigma-Aldrich, and 1% Bovine Serum Albumin, Sigma-Aldrich) for 40 minutes at 4°C. Cell fixation and permeabilization was performed using the eBioscience Foxp3/Transcription Factor Staining Buffer Set (Invitrogen Thermo Fisher Scientific) according to the manufacturer's protocol. Intracellular co-staining of cells was performed using a mix of fluorophore-labelled antibodies against pH2Ax-PerCP-Cy5.5 (1:100, #564718, S139, BD Biosciences) together with pH3-AL647 (1:100, #3458, S10, Cell Signaling Technology) or MKi67-AL700 (1:100, #56-5698-82, Invitrogen Thermo Fisher Scientific) diluted in FACS-blocking buffer (mixture of 0.66% human/rabbit/mouse serum, Sigma-Aldrich, and 1% Bovine Serum Albumin, Sigma-Aldrich in PBS) for 30 minutes at 4°C. The cellular DNA content was determined by DAPI staining (BD Pharmingen, 1:1000 in 1x PBS). Compensation of each fluorochrome was automatically performed using OneComp ebeads (#01-111-42, Invitrogen Thermo Fisher Scientific) according to manufacturer's recommendations. Measurements were performed using a BD LSRFortessa (BD Biosciences).

Acquired flow cytometry data were analyzed with FlowJo software v10 (Tree Star).

RT-qPCR

Total RNA was isolated from 4 x 10^6 cells using NucleoSpin RNA Plus Kit (Macherey Nagel, #740955.50) according to manufacturer's instructions. 1 µg of RNA was reverse transcribed using random oligonucleotides (Roche, #11034731.001) and Omniscript Reverse Transcription (RT) Kit (Qiagen, #205113) according to manufacturer's instructions. Quantification of transcript expression was performed using Sybr green reaction mix SensiFAST (Bioline, #BIO-86005) and 10 pmol of specific primers. PCR reaction was performed on a Rotorgene Q (Qiagen). Transcript expression was normalized to the housekeeping gene *Hprt* and relative expression was calculated according to the delta-C_T method (29). Following primers were used: *Hprt*-fwd: GCTGGTGAAAAGGACCTCC, *Hprt*-rev: CACAGGACTAGAACACCTGC, *Cdkn2a*-fwd: CTTTCGGT CGTACCCCGATT, *Cdkn2a*-rev: AGAAGGTAGTGGGG TCCTCG, *Arf*-fwd: TGGTGAAGTTCGTGCGATCC, *Arf*-rev: TACGTGAACGTTGCCCATCA, *Rbl1*-fwd: AACTGAA CCTGGACGAGGGA, *Rbl1*-rev: GAGCATGCCAGCCAGTGT AT, *Dennd4c*-fwd: GGGAGAGACTCTGTCGCCTA, *Dennd4c*-rev: AACGTCTCCACTGCTGCTAC; *Mllt3*-fwd: ATGGC TAGCTCGTGTGCC, *Mllt3*-rev: GAACACCATCCAGTCGT GGG, *Plaa*-fwd: CAGACAGTCCTAACAGGGGC, *Plaa*-rev: TCCTCCAGTGGCAATCAGTC, *Cpa3*-fwd: AATTGCTCC TGTCCACTTTGA, *Cpa3*-rev: TCACTAACTCGGAAATCC ACAGT, *Gzmb*-fwd: ATGGCCCCAATGGGCAAATA, *Gzmb*-rev: CCGAAAGGAAGCACGTTTGG, *Mcpt2*-fwd: TTCACCAC TAAGAACGGTTCG, *Mcpt2*-rev: CTCCAAGGATGAC ACTGATTTCA, *Mcpt4*-fwd: GTGGGCAGTCCCAGAAAGAA, *Mcpt4*-rev: GCATCTCCGCGTCCATAAGA, *Tpsab1 (Mcpt7)*-fwd: GCCAATGACACCTACTGGATG, *Tpsab1 (Mcpt7)*-rev: GAGCT GTACTCTGACCTTGTTG, *Cma1*-fwd: ACGGACAGAGGTTC TGAGGA, *Cma1*-rev: GAGCTCCAAGGGTGACAGTG, *Mrgprb2*-fwd: CCTCAGCCTGGAAAACGAAC, *Mrgprb2*-rev: CCATCCCAACCAGGGAAATGA, *Ccnd1*-fwd: TCAAGACGG AGGAGACCTGT, *Ccnd1*-rev: GGAAGCGGTCCAGG TAGTTC.

Stimulation of MCs, western blotting and antibodies

For Ag-dependent MC stimulation, cells were preloaded with IgE (0.15 µg/ml) overnight. For FcεRI-independent stimulation, cells were not preloaded with IgE. Cells were washed with sterile PBS and concentration was adjusted to 1 x 10^6 cells per ml in RPMI1640 + 0.1% BSA. 1 x 10^6 cells were stimulated as indicated. Stimulation was stopped by snap-freezing in liquid nitrogen and subsequent lysis in phosphorylation solubilization buffer (PSB) (50 mM HEPES, 100 mM sodium fluoride, 10 mM sodium pyrophosphate, 2 mM sodium orthovanadate, 2 mM EDTA, 2 mM sodium molybdate, 0.5% NP-40, 0.5% sodium deoxycholate and 0.03% sodium dodecylsulfate (SDS)) for 30 minutes at 4°C. Cell lysates were centrifuged (10 min, 13,0000 x g) and subjected to SDS-PAGE and Western blot analysis as described previously (30). The following antibodies were used for detection of p-PLCγ1 (Y783, Cell Signaling Technology (CST), #2821), PLCγ1 (CST, #2822), p-PKB (S473, CST, #9271), PKB (CST, #9272), p-ERK1/2 (T202/Y204, CST, #4370), ERK2 (Santa Cruz, #sc-1647), ERK1/2 (CST, #4696), p-p38 (T180/Y182, CST, #9216), p38 (Santa Cruz, #sc-81621), p-IκBα (S32, CST, #2859), IκBα (CST, #4812), p-KIT (Y719, CST, #3391), KIT (CST, #3074), GAPDH (Santa Cruz, #166574), HSP 90 (CST, #4877), actin (Santa Cruz, #sc-8432), granzyme B (CST, #4275) and tryptase (Santa Cruz, #sc-32889). Secondary antibodies coupled to horseradish peroxidase were purchased from Dako Cytomation [goat anti-rabbit HRP (#P0448), rabbit anti-mouse HRP (#P0161)].

Proliferation and XTT assay

Cells were seeded at a density of 0.3 x 10^6 cells per ml (PMC-306) or 0.5 x 10^6 cells per ml (WT PMCs) in medium containing different amounts of cytokines and growth factors or different amounts of Imatinib (Selleckchem, #S1026) using DMSO (Applichem, #A3072) as control. After 24 hours of incubation in a humidified atmosphere (37°C, 5% CO_2), cells were resuspended and 50 µl of cell suspension were diluted in 10 ml PBS. Cell count and viability was determined using Casy cell counter (Innovatis). Cell count was monitored over a period of 72 hours.

Metabolic activity was determined using XTT Cell proliferation kit II (Roche, #11465015001). Cells were seeded at a density of 0.3 x

10^6 (PMC-306) or 0.5 x 10^6 (WT PMCs) cell per ml in wells of a 96-well microplate and a final volume of 100 µl. Metabolic activity was measured after an incubation time of 72 hours under humidified culture conditions (37°C, 5% CO_2) by adding 50 µl of XTT reagent to each well and measuring spectrophotometrical absorbance of the resulting formazan product at a wavelength of 475 nm and a reference wavelength of 650 nm. For analysis, the measured absorbances at 475 nm and 650 nm were blanked to medium controls and for total absorbance the blanked absorbance at 475 nm was subtracted from blanked absorbance at 650 nm (blanked A_{475} – blanked A_{650}). These calculated values are provided in the Figures.

Electron microscopy

5 x 10^6 primary WT PMCs or transformed PMC-306 were centrifuged and resuspended in 500 µl regular growth medium. For fixation, 3% glutaraldehyde dissolved in PBS was added for four hours. The subsequent steps for sample preparations and image acquisition were conducted by the Department of Electron Microscopy at the Institute of Pathology at the University Hospital Aachen. Briefly, the cells were embedded in 5% low-melting agarose (Sigma, #2070-OP), washed in phosphate buffer, post-fixed in 1% OsO4 (Roth, #8371.1) in 25 mM sucrose buffer and dehydrated by ascending ethanol series (30, 50, 70, 90 and 100%) for 10 min each. Last step was repeated 3 times. Dehydrated specimens were incubated in propylene oxide (Serva, #33715.01) for 30 min, in a mixture of Epon resin (Serva, #21045.01) and propylene oxide (1:1) for 1h and finally in pure Epon for 1h. Samples were embedded in pure Epon and polymerized at 37°C for 12 hours and at 80°C for 48 hours. Ultrathin sections (70-100 nm) were stained with 0.5% uranyl acetate and 1% lead citrate (both EMS, #22400, #17600) to enhance contrast. Samples were viewed at an acceleration voltage of 60 kV using a Zeiss Leo 906 (Carl Zeiss) transmission electron microscope.

May-Grünwald-Giemsa staining

1 x 10^6 primary PMCs were centrifuged (1,200 rpm, 5 min, 21°C) and resuspended in 100 µL PBS. 50 µL of the cell suspension was spotted onto an ethanol cleaned glass slide (microscope slides, 76 x 26 mm, pre-cleaned, R. Langenbrink, Emmendingen, Germany) and distributed equally. The glass slide was thoroughly air dried. For the cell line PMC-306 1.5 x 10^6 cells were centrifuged (800 rpm, 5 min, 21° C) and resuspended in 120 µL PBS. 40 µL of the cell suspension was spotted onto an ethanol cleaned glass slide and distributed equally. The glass slide was thoroughly air dried. The cells were fixed by dipping 10 times in pre-cooled ice-cold acetone (VWR, #20066.296) in a glass tray. Thereafter, the glass slide was thoroughly air dried. The staining of MCs with the MGG stain was performed automated according to standard procedures. Microscopic analysis was done by using a slide scanner device ("Fritz" slide scanner, PreciPoint, Germany) equipped with a 40 x objective and the software MicroPoint (V.2021-01). Higher resolution was obtained by digital zoom. To view or transfer data, the software ViewPoint (V1.0.0.9628) and ConvertPoint (V1.0.0.299) were used.

Cytogenetic analysis

Structural and numerical chromosome alterations were investigated by conventional karyotyping of the PMC-306 cell line using GTG banding at a 400 to 550 band level (31). Standard procedure to obtain metaphase spreads were performed (32). Cell division was blocked at metaphase followed by hypotonic treatment and methanol/acetic acid fixation (3:1). The banding techniques included use of a trypsin pre-treatment, which was done according to standard protocols (33). Microscopic evaluation was performed using Axioplan fluorescence microscope (Carl Zeiss) and IKARUS digital imaging systems (MetaSystems). 18 to 24 GTG banded metaphases were analyzed.

Next generation sequencing

5 x 10^6 cells were harvested directly from the respective cell cultures of primary WT PMCs and PMC-306 and washed in PBS. Cell pellets were resuspended in RNAlater buffer (Qiagen, #1017980) and stored at -80°C. The quantity of RNA was analyzed with the Quantus Fluorometer (Promega, Madison, USA). RNA quality control was done using the 4200 TapeStation System (Agilent Technologies, Inc., Santa Clara, USA). An RNA Integrity Number (RIN) of at least 7.3 verified the high quality of all included RNA samples. Sequencing libraries were generated from 1000 ng of total RNA using TruSeq Stranded Total RNA Library Preparation Kit (Illumina, San Diego, USA, #20020596). The libraries were run on an Illumina NextSeq500 High Output 150 cycles Kit v2.5 (Illumina, San Diego, USA, #20024906). FASTQ files were generated using bcl2fastq (Illumina) with standard parameters. Samples were then processed using the nf-core/RNA-seq pipeline version 3.5 (34) implemented in Nextflow 21.10.6 (35) using Docker 20.10.12 (36) with the minimal command. In brief, lane-level reads were trimmed using Trim Galore 0.6.7 (37) and aligned to the mouse genome (GRCm39) using STAR 2.7.9a (38). Gene-level and transcript-level quantification was done by Salmon v1.5.2 (39).

Statistical analysis

All data shown were generated from at least three independent experiments. Statistical analysis and graphing of data was performed using GraphPad Prism 9 (GraphPad Software, San Diego, CA 92108). All statistical test procedures were done as described in the respective figure legends. *P*-values were considered statistically significant according to the GP style in GraphPad Prism (ns: $p>0.05$, * $p<0.05$, ** $p<0.01$, *** $p<0.001$, **** $p<0.0001$). The respective number of independent biological replicates per experiment is indicated in the figure legends.

Results

The murine peritoneal MC line PMC-306 spontaneously developed from murine WT peritoneum-derived MCs. Primary PMCs were isolated and enriched from mice with a mixed C57BL/6;129Sv genetic background as described previously (23). After a culture period of 3 weeks, purity of the parental PMC culture was verified. The homogenous cell population showed ≥ 90% double positivity for FcεRI and KIT/CD117 (Supplementary Figure 1A). While usually after a maximum of 8 weeks in culture, PMC proliferation and viability decreases, PMC-306 cells showed accelerated proliferation with increasing passages. Besides, PMC-306 could easy be cryopreserved for storage and thawed to be re-cultivated again. These observations led us to characterize the phenotype of the PMC-306 cell line.

PMC-306 cells are smaller and less granulated than primary WT PMCs

One hallmark of MCs are their secretory granules containing, amongst others, biogenic amines and proteases, which can be released upon stimulation in the process of degranulation (40). Electron microscopy analysis revealed drastically reduced granularity of PMC-306 cells compared to primary PMCs, which showed a cytoplasm densely packed with electron dense and seemingly empty granular structures (Figure 1A). Similarly, primary PMCs exhibited an increased cytoplasm-to-nucleus relation and were larger compared to PMC-306 as shown by MGG staining (Figure 1B). In FACS analysis, reduced granularity and smaller size of PMC-306 was confirmed. The population of primary WT PMCs shifted towards higher SSC intensities and showed more heterogeneity compared to PMC-306 (Figure 1C). Primary WT PMCs express the typical MC markers FceRI, KIT, ST2 and CD13 on the cell surface, which we could show by FACS analysis (Figure 1E, left panel). Though differences appeared in morphological characteristics, PMC-306 stained positive for the four typical MC markers, as well, confirming that PMC-306 cells still had MC characteristics (Figures 1D, E, right panel).

PMC-306 show increased but still cytokine-dependent proliferation

Established human MC leukemia cell lines like HMC-1.1 and HMC-1.2 are known for their high proliferative capacity and cytokine-independent growth due to mutations in the receptor-tyrosine kinase KIT (13, 41). Therefore, we sought to determine the cytokine dependence and proliferative capacity of PMC-306. We first compared the proliferation rate of PMC-306 to primary PMCs over 3 days in SCF- and IL-3-containing culture medium. PMC-306 had a doubling time of about 24 hours while primary PMCs proliferated marginally within an investigated time frame of 72 h (Figure 2A). Due to the slow proliferation of primary PMCs, we analyzed the impact of IL-3 and SCF withdrawal on the proliferation only for PMC-306 cells. Both cytokines were reduced independently, while one factor was kept constant. Reduction of IL-3 to 1% and complete withdrawal of IL-3 significantly, but moderately reduced proliferation after 72 hours, while at earlier time points proliferation remained unaffected (Figure 2B). Instead, reducing the amount of SCF had a substantial impact on proliferation of PMC-306. Reduction by 90% substantially attenuated proliferation already at 48 hours after withdrawal. Further reduction of SCF completely abrogated proliferation of PMC-306 (Figure 2C). Additionally, we measured the viability of primary WT PMCs and PMC-306 after 72 hours of incubation under different deprivation conditions. Reducing the amount of IL-3 had no impact on viability of primary PMCs but significantly attenuated the viability of PMC-306 (Figure 2D; Supplementary Figure 2). Reduction of the SCF concentration significantly reduced viability of primary PMCs. However, 10% remaining SCF reduced viability of PMC-306 without affecting viability of WT PMCs. Under harsher SCF deprivation conditions, viability of PMC-306 cells decreased stronger indicating increased SCF dependence of PMC-306 cells over WT PMCs (Figure 2D; Supplementary Figures 2A, B). Interestingly, when metabolic activity under IL-3-deprivating conditions was measured, primary PMCs maintained higher metabolic rates compared to a faster decline in metabolic activity of PMC-306 cells (Figure 2F). SCF withdrawal reduced metabolic activity similarly in both cell types (Figure 2F). In line with increased KIT expression and stronger dependence on SCF for survival, PMC-306 cells were more sensitive to KIT inhibition by Imatinib. 1 μM of Imatinib was sufficient to significantly reduce metabolic activity in PMC-306 cells while primary PMCs appeared more resistant showing sustained metabolic activity at the same inhibitor concentration (Figure 2G). Conclusively, the PMC-306 cell line is slightly dependent on IL-3, and even more – compared to primary WT PMCs – on SCF for proliferation and survival.

Ag-dependent MC effector functions of PMC-306 are comparable to primary WT PMCs

Leukemic MCs proliferate fast, while the reaction to stimulatory signals associated with degranulation and cytokine production is often attenuated due to their immature phenotype or loss of receptor expression (e.g. the FcεRI α- and β-subunits in case of HMC-1.1 and -1.2 cells) (42–44). Therefore, we were interested in determining the capacity of degranulation and pro-inflammatory cytokine production of PMC-306 cells in response to different stimuli. The FcεRI is known to respond to increasing concentrations of Ag with a bell-shaped dose response curve (45). The activity of released β-hexosaminidase from cytoplasmic granules can be used as readout for degranulation. Alternatively, to the latter bulk measurement, externalization of the granular transmembrane marker LAMP1 can be measured by FACS analysis to quantify the extent and kinetics of granule fusion with the plasma membrane on a single cell basis. PMC-306 and primary PMCs both showed similar bell-shaped dose-response behaviour with

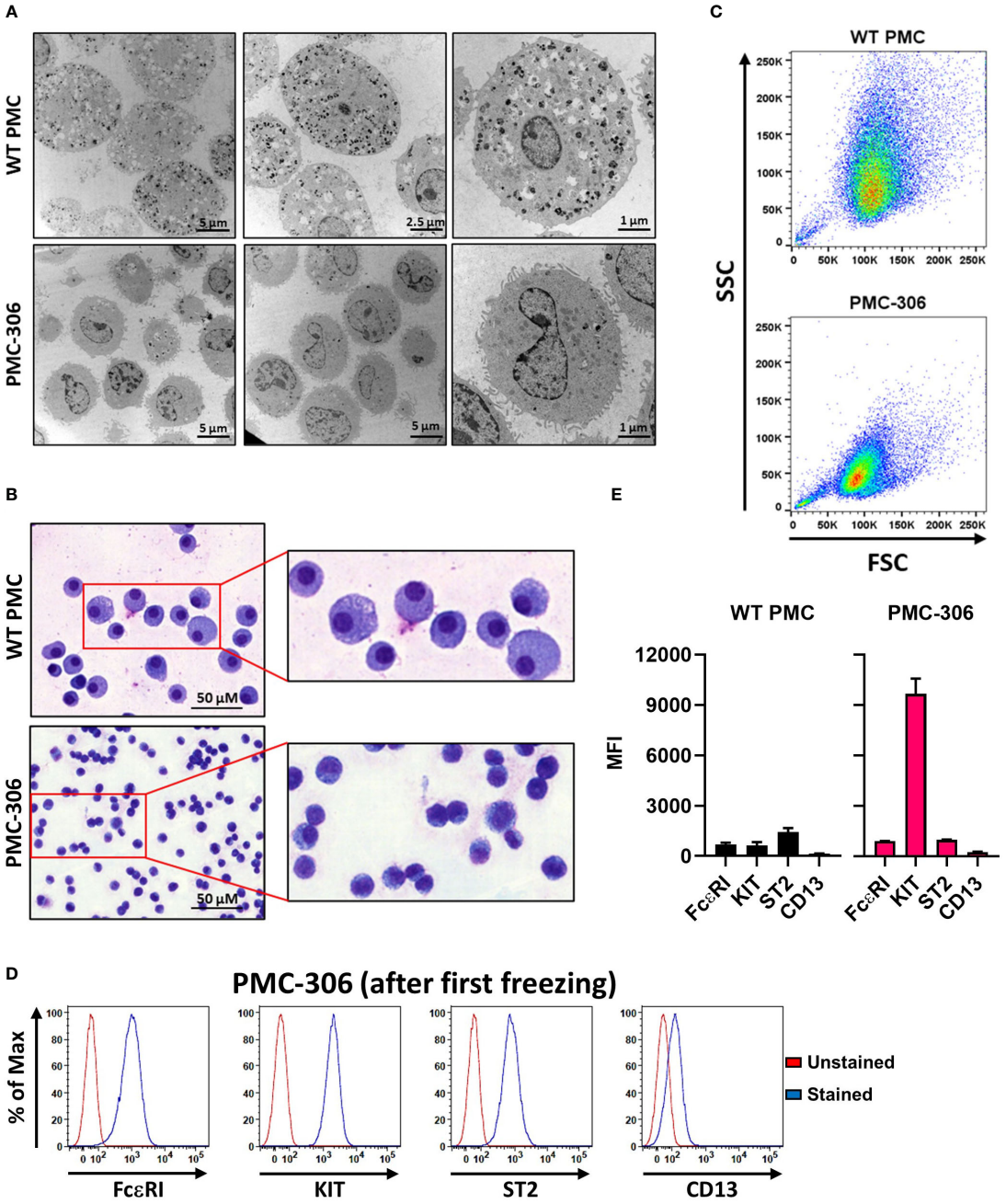

FIGURE 1
Phenotypic characterization of PMC-306 cells reveals morphological differences to primary WT PMCs. **(A)** Representative electron micrographs of glutaraldehyde-fixed and agarose embedded primary WT PMCs and PMC-306 cells. **(B)** Representative microscopy images of fixed MGG-stained primary WT PMCs and PMC-306 cells. **(C)** Representative FACS analysis of size and granularity of primary WT PMCs in comparison to PMC-306. Forward/side scatter intensities of 30,000 cells were recorded with the same settings to show differences between the two cell types (n=3). **(D)** Representative FACS histograms showing surface localisation of FcεRI, KIT, ST2 and CD13 in PMC-306 cells after freeze-thaw in relation to an unstained control. (n=3) **(E)** FACS analysis of the MC surface markers FcεRI, KIT (CD117), ST2 and CD13. Geometric mean fluorescence intensities (MFI) are plotted for each surface marker (n=4). Data are shown as mean + SD.

increasing Ag concentrations, reaching a maximum release of β-hexosaminidase at 20 ng/ml (Figure 3A). Additionally, we determined the kinetics of degranulation measured as time-dependent LAMP1 externalization. Again, the kinetics of LAMP1 externalization was qualitatively similar between primary PMCs and PMC-306 cells reaching maximal LAMP1 MFIs after 5 minutes of stimulation (Figure 3B). Another receptor triggering MC degranulation independent of IgE is the GPCR MRGPRB2, which is exclusively expressed in connective tissue-like MCs and can be stimulated by cationic peptides (46–48). Thus, to prove expression of MRGPRB2 in PMC-306, we stimulated primary PMCs and the PMC-306 line with either C48/80 or Mastoparan – compounds that are known to potently activate MRGPRB2 – and measured β-hexosaminidase release. Primary PMCs and PMC-306 both

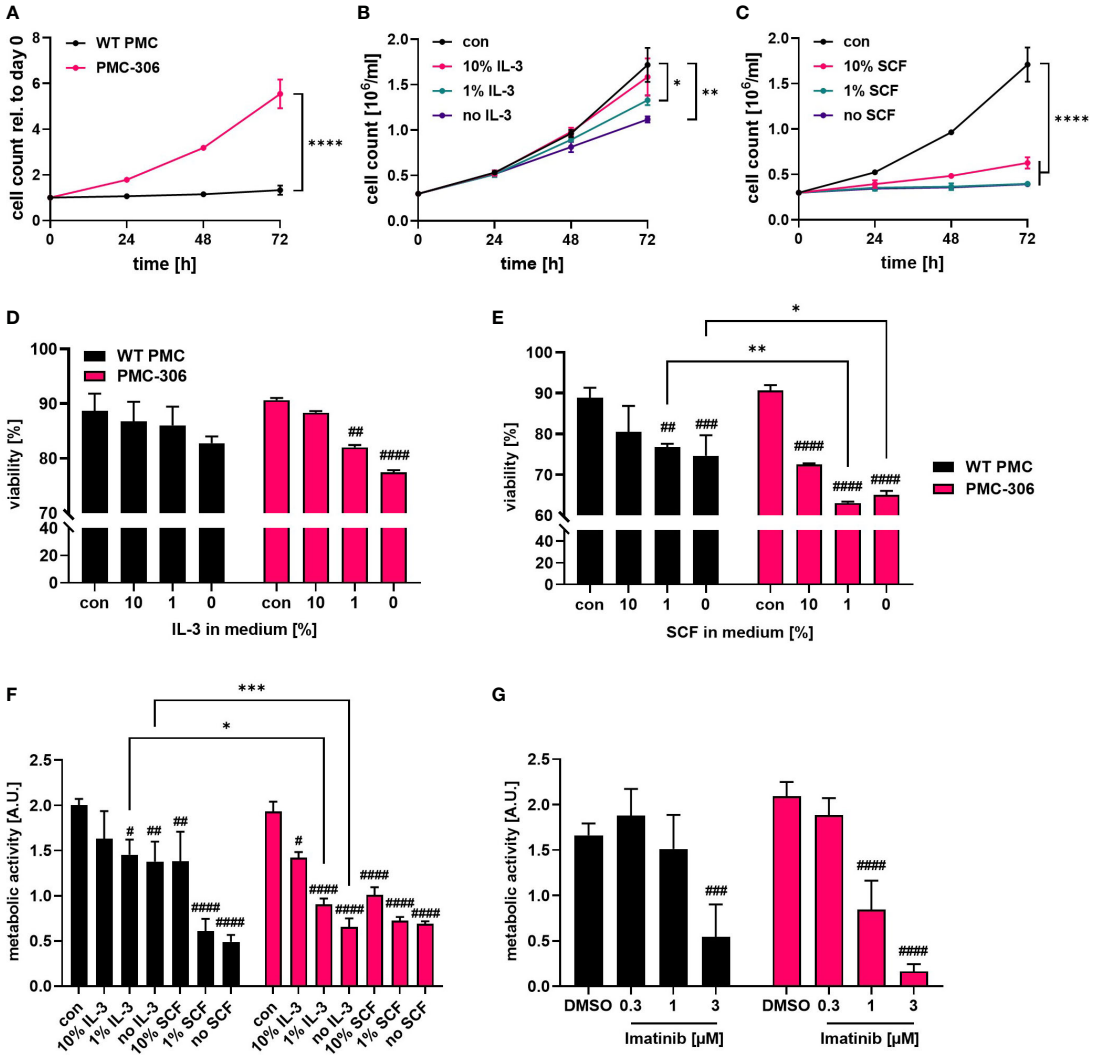

FIGURE 2
PMC-306 show faster proliferation compared to primary PMCs, which is dependent on IL-3 and SCF. **(A)** Cell number of primary WT PMCs and PMC-306 cells was measured every 24 hours for up to 72 hours using a CASY Cell counter (n=3). Both cell types were cultivated under the same conditions (20 ng/ml SCF and 15% FCS) to allow direct comparison. Proliferation of PMC-306 cells grown under reduced IL-3 (n=3) **(B)** or SCF (n=3) **(C)** concentrations was determined every 24 hours up to 72 hours using a CASY Cell counter. Viability of primary PMCs and PMC-306 cells was determined by FACS analysis using Annexin V and propidium iodide staining after 72 hours incubation in medium containing reduced IL-3 (n=3) **(D)** or SCF (n=3) **(E)**. **(F)** The metabolic activity of primary PMCs and PMC-306 after 72 hours cultivation under IL-3 or SCF deprivation was determined by XTT assays (n=3). **(G)** The metabolic activity of Imatinib-treated primary PMCs and PMC-306 cells was determined after 72 hours by XTT assays (n=3). Both cell types, primary PMCs and PMC-306 cells were cultivated under the same medium conditions with the control condition reflecting normal PMC medium containing 20 ng/ml SCF and 15% FCS so that % reduction in SCF refers to the same initial control concentration. Data are shown as mean + SD. **(A)** Two-tailed, unpaired Student's T test of data at 72 hours. **(B, C)** One-way ANOVA followed by Tukey multiple comparisons test of data at 72 hours. **(D-G)** Ordinary two-way ANOVA followed by Sídák multiple comparisons test. $p>0.05$ ns, $^{\#}$and $^{*}p<0.05$, $^{\#\#}$and $^{**}p<0.01$, $^{\#\#\#}$and $^{***}p<0.001$, $^{\#\#\#\#}$and $^{****}p<0.0001$. * indicates significant differences between groups, while # indicates significant differences relative to control conditions within one group.

degranulated in response to both stimuli in a dose-dependent manner confirming the connective tissue nature of PMC-306 (Figures 3C, D). While degranulation of MCs happens within minutes, secretion of pro-inflammatory cytokines takes several hours of stimulation. We determined secretion of IL-6 and TNF from primary PMCs and PMC-306 in response to FcεRI stimulation. As described above, the response to Ag stimulation followed a bell-shaped dose-response curve in both cell types (Figure 3E). Primary WT PMCs and PMC-306 secreted highest amounts of IL-6 and TNF upon stimulation with 2 and 20 ng/ml Ag and the pro-inflammatory cytokine response decreased with lower and higher Ag concentrations. This phenocopies the dose response behaviour previously seen for the b-hexosaminidase release in response to increasing Ag concentrations for both cell types. We further observed no pro-inflammatory cytokine secretion in response to TLR4 (LPS), TLR2/6 (FSL-1), KIT (SCF) and MRGPRB2 (C48/80) stimulation at the given stimuli concentrations for both cell types (Figure 3F). Besides, PMC-306 did not react to IL-33 activating the ST2/IL1RAP (IL-1 receptor accessory protein) receptor complex, while primary PMCs secreted

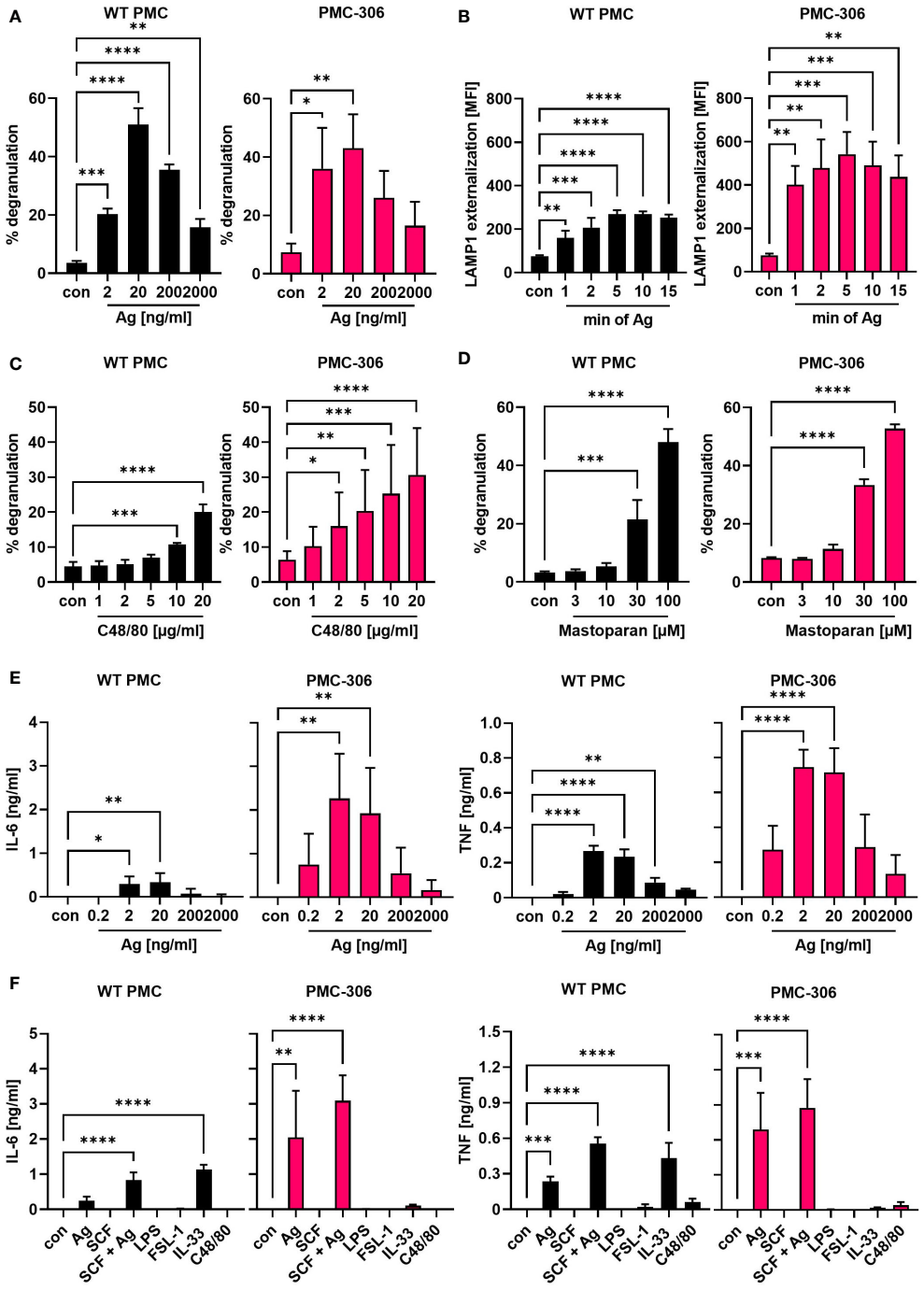

FIGURE 3
The qualitative degranulation and proinflammatory cytokine responses of PMC-306 and primary PMCs are similar. **(A)** Degranulation of primary WT PMCs (left panel) and PMC-306 cells (right panel) in response to increasing Ag concentrations was determined by β-hexosaminidase release assay (n=3). **(B)** The time-dependent externalization of LAMP1 was determined by quantifying the LAMP1 on the cell surface in FACS analysis as MFI upon stimulation with 20 ng/ml Ag in primary PMCs (left panel) and PMC-306 cells (right panel) (n=3). The degranulation responses of primary PMCs (left panel) and PMC-306 cells (right panel) to increasing concentrations of the MRGPRB2 agonists C48/80 **(C)** and Mastoparan **(D)** were determined by β-hexosaminidase release assays (n=3). The secretion of IL-6 [**(E) left**] and TNF [**(E) right**] in response to indicated Ag concentrations was determined by ELISA (n=3). The pro-inflammatory cytokine production of primary WT PMCs and PMC-306 to Ag (20 ng/ml) in comparison to other stimuli (SCF: 100 ng/ml, SCF+Ag: 100 ng/ml and 20 ng/ml, LPS: 1µg/ml, FSL-1: 1 µg/ml, IL-33: 10 ng/ml, C48/80: 10 µg/ml) was determined by IL-6 [**(F) left**] and TNF [**(F) right**] ELISAs (n=3). Data are shown as mean +SD. One-way ANOVA followed by Dunnett multiple comparisons test. Stars indicate significance within one group relative to control. $p>0.05$ ns, *$p<0.05$, **$p<0.01$, ***$p<0.001$, ****$p<0.0001$.

pro-inflammatory cytokines upon IL-33 stimulation. (Figure 3F). Briefly, we could show that the PMC-306 line expresses a functional FcεRI and MRGPRB2 receptor, maintained the ability to degranulate in response to Ag and MRGPRB2 activation but could neither be activated by TLR ligands nor by IL-33 stimulation.

Signaling pathway activation downstream of typical MC receptors is functional in PMC-306 cells

In comparison to BMMCs, PMCs have a greater active protease repertoire stored within the cytoplasmic granules. This complicates signaling studies and makes protein interaction studies using immunoprecipitation nearly impossible as the lysis of cells in classical lysis buffers containing a mixture of protease inhibitors is not sufficient to prevent protease-dependent protein degradation (12, 40, 49). We therefore aimed to test whether the PMC-306 is suitable for signaling studies upon lysis in normal lysis buffer containing typical protease inhibitors. Further, we wanted to confirm that differential activation of the PMC-306 line leads to comparable activation of signaling pathways as in primary PMCs to verify its suitability for MC signaling studies. Stimulation of PMC-306 with Ag rapidly increased phosphorylation of PLCγ1 at tyrosine 783, which is critical for the initiation of the Ca^{2+} response and PKC activation. Activation of the mitogen-activated protein kinases (MAPK) ERK1/2 and p38, as well as phosphorylation of protein kinase B (PKB) occurred within one minute of stimulation, while strongest phosphorylation/activation and degradation of NFκB inhibitor α (IκBα) – a readout for NFκB pathway activation – started at 5 minutes after Ag stimulation (Figure 4A). This indicates that pathways necessary for cytokine production, like the MAPK and NFκB pathways, are functional and strongly responsive to Ag stimulation, which is in line with the described cytokine measurements (Figures 3E, F). Although we could not observe cytokine secretion in response to SCF stimulation, activation of KIT (auto-phosphorylation at Y719) could be detected in response to SCF. However, phosphorylation of KIT, PKB, and MAPK were transient and rapidly decreased after one minute of stimulation (Figure 4B) correlating with the lack of detectable cytokine production, which would require a sustained signal strong enough to induce transcriptional changes in gene expression. Likewise, we could see transient activation of the NFκB and ERK pathways in response to IL-33 though the cytokine production was strongly attenuated compared to WT PMCs (Figure 3F). Interestingly, Y719 of KIT was phosphorylated upon IL-33 stimulation, which corroborates previous findings that revealed a role for KIT in contributing to ST2 signaling in MCs (Figure 4C) (50). Additionally, while most cell lines have substantially elevated basal levels of phosphorylated signaling proteins emerging in Western blot analysis, we did not observe obvious activation/phosphorylation of investigated proteins in PMC-306 cells under unstimulated conditions. Surprisingly, we could not detect considerable cytokine production in response to C48/80 at a concentration of 10 µg/ml, which in previous experiments elicited substantial β-hexosaminidase release (Figure 3C) and was also used in preceding studies to stimulate MRGPRB2 (46). Yet, we noticed a strong induction of cytokine release in response to 3-fold lower C48/80 concentrations (Supplementary Figure 3A). Accordingly, we used 3 µg/ml C48/80 to analyze activation of MRGPRB2 signaling in the PMC-306 cell line. As shown in Figure 4D, a transient activation of the PKB, ERK and NFκB signaling pathways could be detected after five minutes of stimulation. Notably, the concentrations stimulating cytokine production did not or did only hardly induce degranulation. Besides, stimulation with higher concentrations of C48/80 and Mastoparan previously reported to induce degranulation led to a significant reduction in protein concentration in the cell pellet after lysis, which did not occur with Ag (Supplementary Figure 3B), indicating loss of cellular content upon C48/80 stimulation. Moreover, we were not able to measure an externalization of LAMP1 in response to C48/80 at 10 µg/ml neither in PMC-306 cells (data not shown) nor in primary PMCs (Supplementary Figure 3C) pointing to a substantially different mechanism of degranulation compared to Ag, which potentially involves cellular disintegration.

Reduced protease expression of PMC-306 suggests an immature phenotype

Our data so far demonstrated that the PMC-306 line still has MC-like properties in terms of morphology and cellular reactivity. Nonetheless, we also noted differences in proliferation and the fact that in contrast to primary WT PMCs, PMC-306 cells have become immortal. Hence, we were interested in transcriptomic differences between PMC-306 and primary WT PMCs that we aimed to uncover by next generation sequencing. For validation of NGS data, we first concentrated on variations in MC granular proteins as the electron micrographs revealed differences in number of granules between WT PMCs and PMC-306. We determined the relative β-hexosaminidase content of equal cell numbers of primary PMCs and PMC-306 and found significantly less β-hexosaminidase activity in cell lysates of PMC-306 (Figure 5A). On mRNA level, we found that expression of the proteases *Cpa3*, *Cma1* and *Gzmb* was reduced compared to WT PMCs but still detectable in PMC-306 (Figures 5B–D). However, we could not detect expression of *Mcpt2*, *Mcpt4* and *Tpsab1* in PMC-306 cells (Figures 5E–G). On protein level, we verified expression of granzyme B and tryptase in primary WT PMCs and could confirm a total lack of tryptase expression in PMC-306 cells. Strikingly, despite residual mRNA expression of *Gzmb* in PMC-306, there was hardly any granzyme B protein present (Figure 5H). This pattern of protease expression in PMC-306 is reminiscent of immature MC precursors, that lack expression of proteases up-regulated in late stages of MC differentiation like *Mcpt2* and *Tpsab1* (51, 52). In addition, we wanted to verify expression of the CTMC-specific receptor MRGPRB2, since we could show similar responsivity between PMC-306 and WT PMCs (Figures 3C, D). Though, PMC-306 cells exhibited significantly reduced mRNA expression of *Mrgprb2* (Figure 5I). However, our data suggests that this does not affect the respective degranulation response (compare Figure 3C).

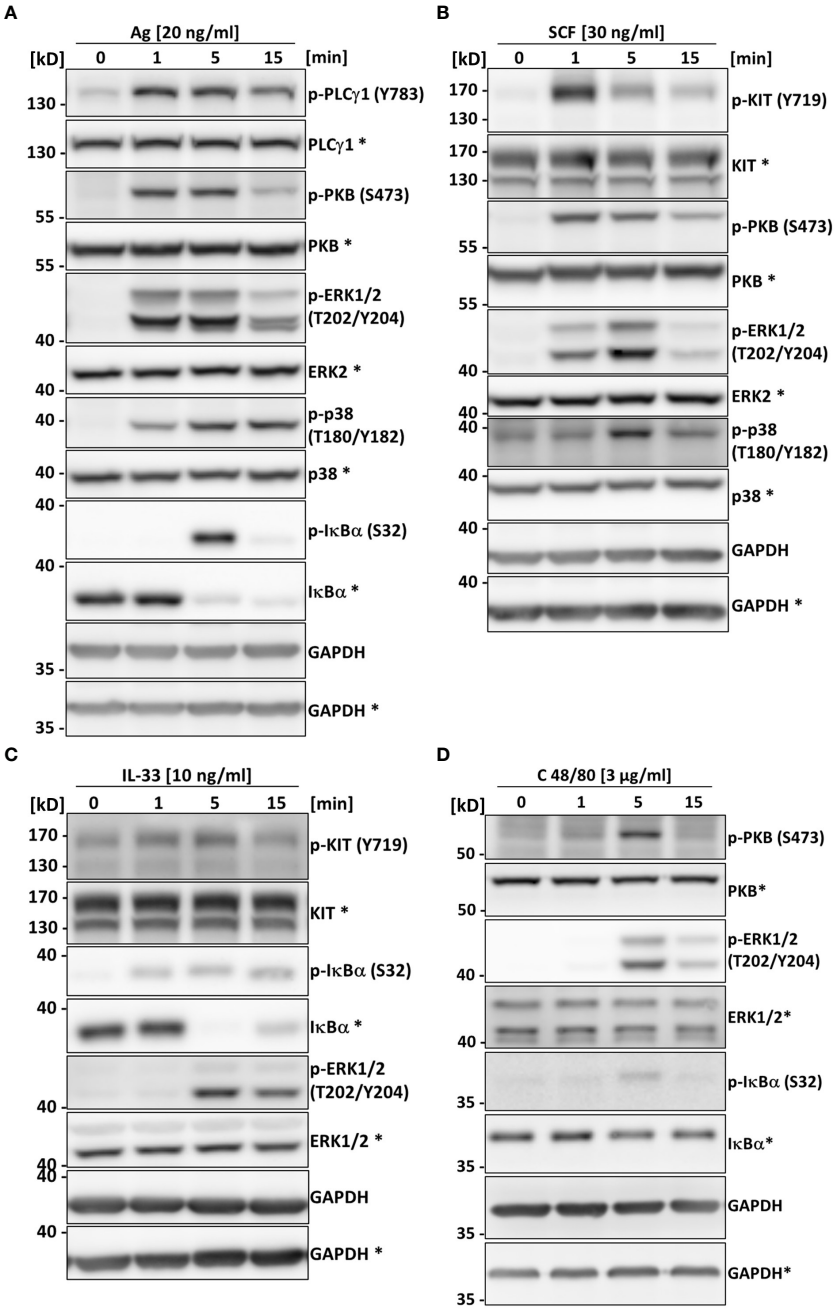

FIGURE 4
The PMC-306 cell line can be used to analyze signaling in response to Ag, SCF, IL-33 and C48/80. The activation of PLCγ1, PKB, the MAPKs ERK and p38, KIT and the NFκB pathway in response to Ag (20 ng/ml) **(A)** (n=3), SCF (30 ng/ml) **(B)** (n=3), IL-33 (10 ng/ml) **(C)** (n=3) or C48/80 (3 µg/ml) **(D)** (n=3) after 1, 5 and 15 minutes of stimulation was studied by Western blot analysis. Activation of the pathways was analyzed by phospho-specific antibodies (p-PLCγ1 (Y783), p-KIT (Y719), p-PKB (S473), p-ERK1/2 (T202/Y204), p-p38 (T180/Y182), p-IκBα (S32) for key signaling proteins. For loading controls, antibodies recognizing the respective total proteins were used. Asterisks indicate detection on the same membrane. GAPDH served as control for equal loading of both gels. Representative experiments are depicted for each stimulation condition.

As stated in the methods section, we used different culture conditions for primary PMCs and PMC-306 as well as PMC-303 cells. While primary PMCs were cultivated in medium containing 15% FCS and 20 ng/ml SCF, these amounts were both reduced to 10% and 5 ng/ml, respectively, for both cell lines. Our intention was to slow down the enormous proliferation, which – we were afraid – could favour the accumulation of additional mutations rendering the cells genetically more unstable. In initial experiments we carefully titrated the amounts of SCF and FCS needed to assure proper viability and proliferation of PMC-306 cells avoiding the use of SCF and FCS concentrations that are far beyond the cellular requirements and hence decided for the above-mentioned culture conditions. As we immediately compared mRNA expression of MC proteases between primary PMCs and PMC-306 cells, we aimed at verifying whether this is due to different culture conditions or an actual phenotype of PMC-306 cells. Therefore, we cultivated PMC-

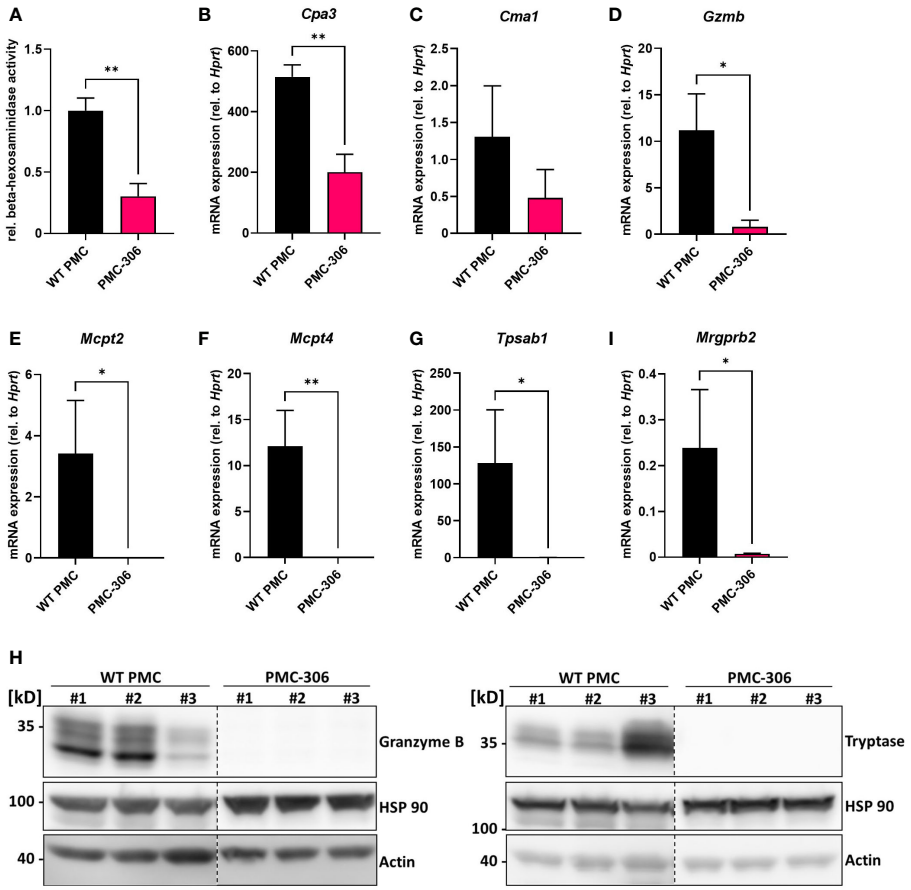

FIGURE 5
The repertoire of protease expression is reduced in PMC-306 cells revealing an immature MC phenotype. **(A)** The β-hexosaminidase content in primary PMCs and PMC-306 cells was determined by measuring the relative β-hexosaminidase activity in equal numbers of primary PMCs and PMC-306 cells (n=3). **(B–G)** The protease expression of *Cpa3*, *Cma1*, *Gzmb*, *Mcpt2*, *Mcpt4* and *Tpsab1* (*Mcpt7*) and the expression of *Mrgprb2* **(H)** were quantified by RT-qPCR in samples from fully differentiated primary PMCs and PMC-306 cells. Data are expressed as mRNA expression relative to *Hprt* determined according to the deltaC$_t$ method (n=3). **(H)** Representative Western blots of three lysates from three independent primary WT PMCs and independently taken samples from PMC-306 cells comparing the expression of granzyme B and tryptase on protein level. HSP 90 and actin served as loading controls. Data are shown as mean +SD. Unpaired, two-tailed Student's *t*-test with Welsh's correction. *p<0.05, **p<0.01.

306 cells in medium containing reduced FCS and SCF as well as in medium containing normal amounts of both FCS and SCF mimicking primary PMC conditions. As depicted in Supplementary Figures 4A–H, neither *Cdkn2a*/*Arf* expression nor expression of *Cma1*, *Cpa3*, *Gzmb*, *Mcpt2*, *Mcpt4* and *Tpsab1* was influenced by higher SCF/FCS concentrations. Besides, mRNA expression of Mrgprb2 was unaltered irrespective of the medium used for cultivation of PMC-306 cells (Supplementary Figure 4I). Moreover, we tested whether the different cultivation conditions changed the size or granularity or affected expression of MC surface markers of PMC-306 cells. Of note, size and granularity as well as the amount of surface-localized FcεRI, ST2 and CD13 did not change upon cultivation in medium containing higher amounts of FCS and SCF (Supplementary Figures 4J, K). However, KIT expression at the cell surface of PMC-306 cells was significantly reduced under primary PMC-like culture conditions (Supplementary Figures 4J, K), which can most likely be attributed to the increased internalization of KIT in response to higher SCF concentrations. In summary, the differences in cultivation conditions between primary PMCs and PMC-306 cells had only marginal effects on the characterized phenotype of the cell line.

PMC-306 cells are characterized by a loss of *Cdkn2a* and *Arf* tumour suppressor gene expression

Next, we addressed the question, which genomic or transcriptional alterations are responsible for the transformation and increased proliferation of the PMC-306 line. We first analyzed the karyotype of PMC-306 cells, which revealed a typical male murine diploid (19XY) telocentric set of chromosomes (Figure 6A). However, a prominent structural aberration of chromosome 4 characterized by a heterozygous interstitial deletion (Del(4)(C4-C7) was detected (Figure 6A, marked by a red arrow). This structural aberration was consistent in all analyzed cells (Supplementary Figure 4A) as depicted in Figure 6B showing

10.3389/fimmu.2023.1154416

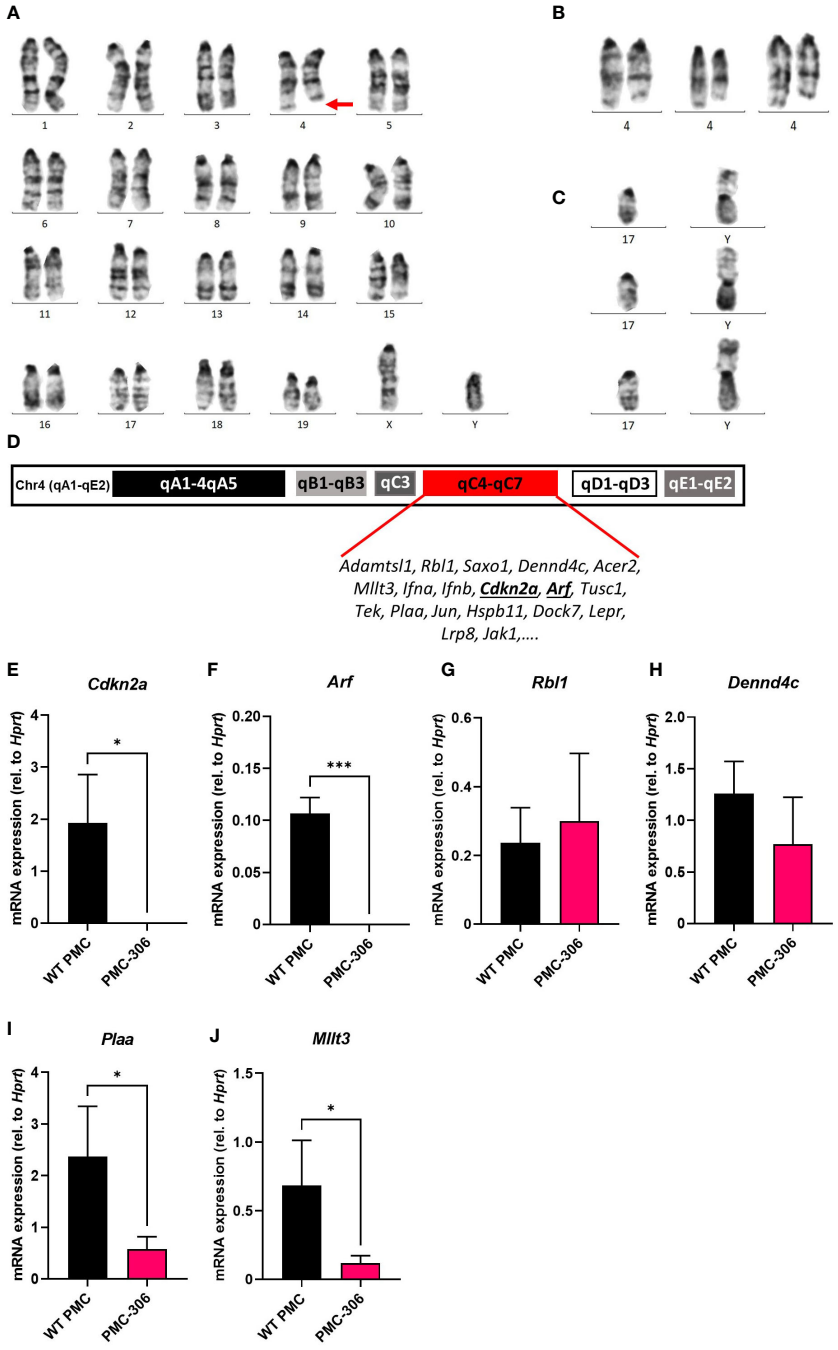

FIGURE 6
Cytogenetic and gene expression analysis identified loss of *Cdkn2a*/*Arf* expression as potential cause for immortalization of PMC-306. Mitotic chromosomes of PMC-306 were cytogenetically analyzed. **(A)** Representative image of a conventional G-banded karyotype with structural aberration. Red arrow indicates interstitial deletion of chromosome 4 [Del(4)(C4-C7)]. **(B)** Further examples of partial karyotypes showing structurally aberrant chromosomes 4 with the same interstitial deletion. **(C)** Three representative partial karyotypes representing the Y-autosome translocation [T(Y;17)] – confirmed by fluorescence *in situ* hybridization with a Y-specific whole mouse chromosome painting-probe (confirmatory FISH analysis not shown)). **(D)** Architecture of murine chromosome 4 with highlighted region qC4-qC7 and exemplary genes encoded within this region. **(E–J)** RT-qPCR analysis of *Cdkn2a*, *Arf*, *Rbl1*, *Dennd4c*, *Plaa* and *Mllt3* mRNA expression in primary WT PMCs and PMC-306 cells (n=3). Data are expressed as mean +SD. Unpaired, two-tailed Student's t test with Welsh's correction. *$p<0.05$, ***$p<0.001$.

three further examples of partial karyotypes of the heterozygously deleted chromosome 4 region (Del(4)(C4-C7). The second most prominent chromosomal aberration represented a Y-autosome translocation [T(Y;17)] (Figure 6C) appearing in roughly one third of analyzed karyotypes (Supplementary Figure 4A), which has not been described so far so that its significance for the transformation process is presently unclear.

Interestingly, within the heterozygously deleted region of chromosome 4 the INK4/ARF locus is encoded (Figure 6D) (53). p16/INK4A and p19/ARF are responsible for regulation of the RB

and p53 pathways, respectively, thus controlling two essential cell cycle regulators (25, 54). As PMC-306 cells showed a faster proliferation than WT PMCs, we suspected that expression of genes within the INK4/ARF locus might be reduced in PMC-306 cells. We could confirm that mRNA expression of *Cdkn2a* encoding INK4A and *Arf* was not only reduced – as one would expect as a result of a heterozygous deletion – but completely absent in PMC-306 cells (Figures 6E, F). Remarkably, other genes located in the same chromosomal region exhibited a different behaviour. Expression of *Rbl1* and *Dennd4c* was unaffected suggesting that one allele is sufficient to compensate for the deletion of the second (Figures 6G, H), while expression of *Plaa* and *Mllt3* was reduced compared to primary PMCs as one could expect if one allele is lost (Figures 6I, J). Curiously, an independently mutated PMC line, PMC-303, not showing the interstitial deletion on chromosome 4 (Supplementary Figure 4B) also completely lost *Cdkn2a* and *Arf* expression (Supplementary Figures 5C, D), while other genes within the same chromosomal region were not (*Rbl1*, *Mllt3*, *Plaa*) or only slightly (*Dennd4c*) affected (Supplementary Figures 5E–H). In addition, PMC-303 cells showed a trisomy 8 due to a homologous Robertsonian translocation of chromosome 8 (Rb(8.8)) in 24 of 35 analyzed metaphasic spreads (Supplementary Figure 5B), which we did not observe in PMC-306 cells. As we could not identify a prominent chromosomal aberration present in all metaphasic spreads of PMC-303 cells, which might indicate a certain genomic instability, we did not primarily focus on characterizing this cell line. However, we found that similar to PMC-306 cells, also PMC-303 cells remained positive for FcεRI, KIT, ST2 and CD13 in flow cytometry analysis after freeze-thawing the cells (Supplementary Figure 6A). As previously explained for the cultivation of the PMC-306 cell line, we likewise reduced the SCF and FCS concentration in the culture medium of PMC-303 cells, as well. Evaluation of electron microscopy micrographs similarly revealed reduced granularity of PMC-303 cells. This was accompanied by a reduced total β-hexosaminidase content determined by an enzymatic assay measuring β-hexosaminidase activity in cell lysates obtained from equal numbers of primary PMCs and PMC-303 cells (Supplementary Figures 6B, C). Also, in line with what we described for the PMC-306 cell line, PMC-303 cells degranulated in response to C48/80 stimulation suggesting functionality of MRGPRB2 receptor (Supplementary Figure 6D). In addition, PMC-303 cells degranulated to a comparable extent to Ag concentrations between 2 and 200 ng/ml indicating that they are highly sensitive especially to low Ag concentrations and analogously to primary WT PMCs and PMC-306 cells we could measure LAMP1 externalization by flow cytometry upon FcεRI activation starting after 2 minutes after Ag stimulation for up to 15 minutes (Supplementary Figures 6D–F). Finally, the pattern of pro-inflammatory cytokine response of PMC-303 cells towards different stimuli emerged as well similar to PMC-306 cells. While we observed strong IL-6 and TNF production in response to Ag and the co-stimulation of SCF + Ag, there was no detectable cytokine secretion upon triggering of the TLRs TLR4 and TLR2/6 and only a slight but insignificant production of IL-6 and TNF upon IL-33 and C48/80 stimulation (Supplementary Figures 6G, H). Overall, we could establish that PMC-303 cells phenotypically and with respect to MC characteristics as well as the status of *Cdkn2a/Arf* expression emerged to be highly comparable to PMC-306 cells.

The PMC-306 cell line has a de-regulated cell cycle

It is well known that uncontrolled proliferation and loss of cell cycle regulation is one of the hallmarks of cancer (25, 54–57). As we have shown above, PMC-306 cells have a strongly accelerated proliferation, which likely is a consequence of the observed loss of *Cdkn2a* and *Arf* expression. Hence, we supposed that in PMC-306 the cell cycle is de-regulated to enable fast proliferation. To prove this, we performed RNAseq with both PMC lines PMC-303 and -306 as well as primary WT PMCs as control. The NGS data have been deposited in NCBI's Gene Expression Omnibus and are accessible through the GEO Series accession number GSE227065 (https://www.ncbi.nlm.nih.gov/geo/query/acc.cgi?acc=GSE227065). RNA expression was analyzed from cells directly taken from conventional culture medium without additional treatment. We searched the mRNA expression data for global transcriptomic changes between primary PMCs and the PMC-306 line and focussed on genes that were at least 5-fold regulated. GO enrichment analysis unveiled that the top 15 GO terms were all related to cell cycle, mitosis and cell division (Supplementary Figure 7A). This result led us to investigate the cell cycle by comparing the obtained long-term cultures of spontaneously transformed PMC-306 line with primary WT PMCs using flow cytometry. The gating strategy and unstained controls for background determination for each cell type are shown in Supplementary Figures 7B–D. We first examined cell cycle activity in non-transformed primary WT PMCs and the PMC-306 cell line using the established general cell cycle marker MKI67. As expected, PMC-306 cells revealed substantially (*i.e.* approximately twofold) higher cell cycle activity when compared to primary WT PMCs in terms of MKI67 positive cells (~60-63% vs. 31%) and it´s expression strength as determined by mean fluorescence intensity (Figures 7A, B). In good agreement, we further detected significantly enhanced mitotic activities in the PMC-306 cells in relation to primary WT PMCs after analyzing phospho-Histone H3 (pH3). PMC-306 cells displayed a higher amount of pH3 positive cells (2%) compared to primary PMCs (1%, Figure 7C). Additionally, we determined the DNA content by DAPI-staining. As expected, MKI67 was found to be expressed in the cell cycle phases Gap1 (G_1, 2n), DNA-synthesis (S-phase, 2-4n) to Gap2 (G_2, 4n) and mitosis (M-phase, 4n) in primary WT PMCs and PMC-306 cells (Supplementary Figure 7E, left panel). Furthermore, mitotic active pH3-positive cells were specifically found at a DNA content of 4n in primary PMCs and PMC-306 cells (Supplementary Figure 7E, right panel). Importantly, PMC-306, but not primary PMCs, additionally exhibited an MKI67 and pH3 positive cell fraction with a DNA content above 4n, indicating chromosomal abnormalities such as aneuploidy after the transformation step (Supplementary Figure 7E). Finally, we investigated the DNA integrity by staining of phospho-histone 2Ax (pH2Ax), a well-described marker for DNA-double strand breaks. We found low levels of pH2Ax in WT PMCs (~1%) and slightly

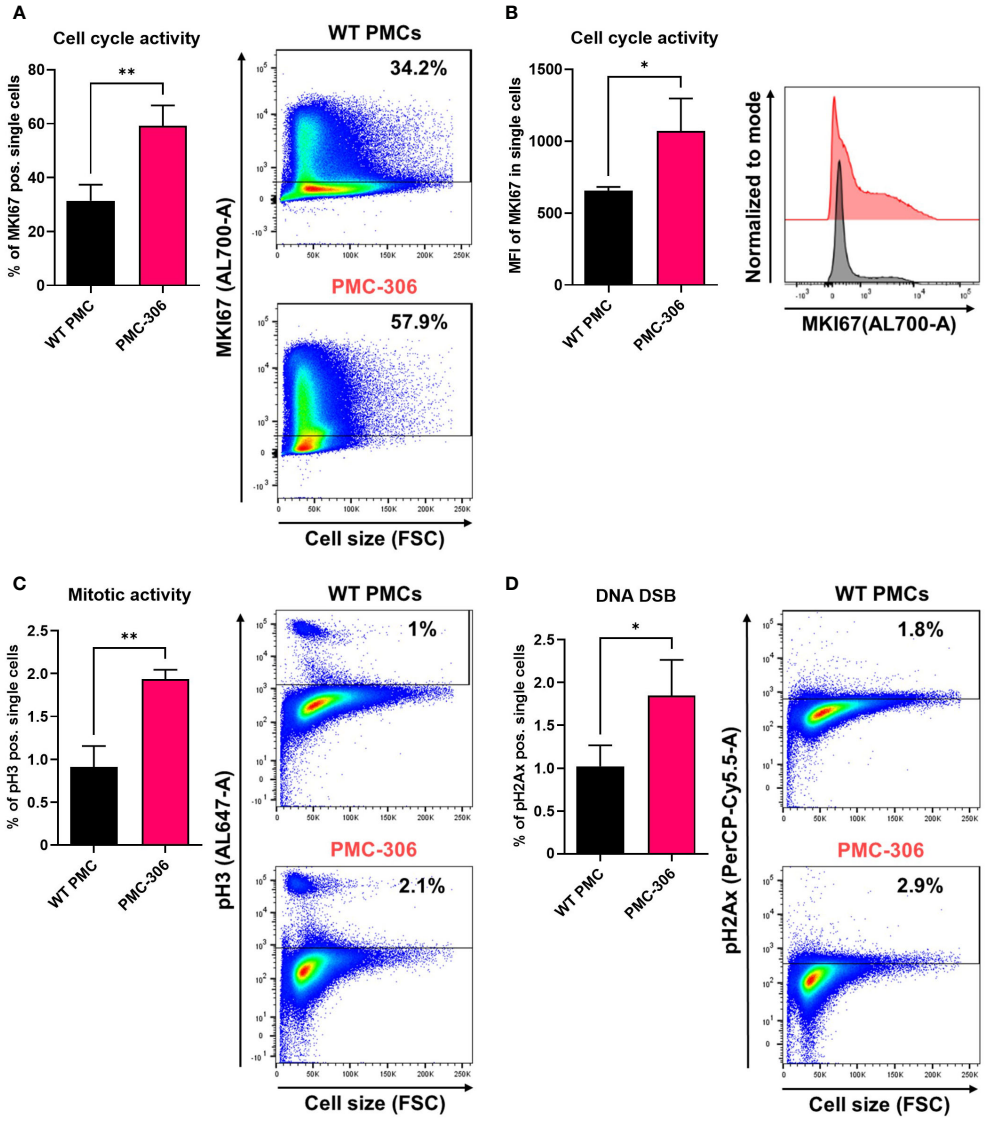

FIGURE 7
PMC-306 cells are characterized by enhanced cell cycle activity and sporadic DNA damage. The cell cycle of primary WT PMCs was compared to PMC-306 cells. **(A)** Cells were stained with an antibody directed against MKI67 (AL700-A). Left: Quantification of MKI67+ cells (% of single cells, n=3). Right: Representative FACS-plots of MKI67+ cells (% of single cells, n=3). **(B)** Quantification of the mean fluorescence intensity (MFI, n=3) of MKI67 in single cells (left) and a representative histogram showing MKI67 intensities in primary PMCs and PMC-306 cells. **(C)** Cells were stained with an antibody directed against phosphorylated histone H3 (pH3, AL647-A). Left: Quantification of pH3 cells (% of single cells, n=3). Right: Representative FACS-plots of pH3+ cells (% of single cells). **(D)** Cells were stained with an antibody directed against phosphorylated Histone H2Ax (pH2Ax, PerCP-Cy5.5-A). Left: Quantification of pH2ax cells (% of single cells, n=3). Right: Representative FACS-plots of pH2Ax+ cells (% of single cells). Data are expressed as mean +SD. Unpaired, two-tailed Student's t test with Welsh's correction. *$p<0.05$, **$p<0.01$.

increased levels in PMC-306 (~2%, Figure 7D). Together, the cell cycle of PMC-306 cells is characterized by a higher mitotic activity, increased DNA damage and aneuploidy.

Constitutive KIT activation regulates *Cdkn2a* and *Arf* expression in BMMCs

Finally, we aimed at identifying the mechanism for loss of *Cdkn2a/Arf* expression in primary PMCs and suspected KIT activation as a crucial pro-survival and potentially transformation-promoting mechanism due to the occurrence of frequent KIT mutations in leukemic MC lines (41, 58). Therefore, instead of using PMCs, we analyzed the behaviour of BMMCs, which in contrast to PMCs do not necessarily need SCF for proper differentiation into MCs, and cultivated them from the beginning of the differentiation phase in the absence or presence (mimicking PMC culture conditions) of SCF. We noticed remarkable phenotypic changes of BMMC cultures induced by SCF supplementation. After the differentiation phase of 4 weeks, BMMCs cultivated in the presence of SCF were larger (increased FSC) and more granular (increased SSC) compared to BMMCs from the same mouse only supplemented with IL-3 (Figure 8A left two panels, Figure 8B left and middle, Figure 8C left and middle).

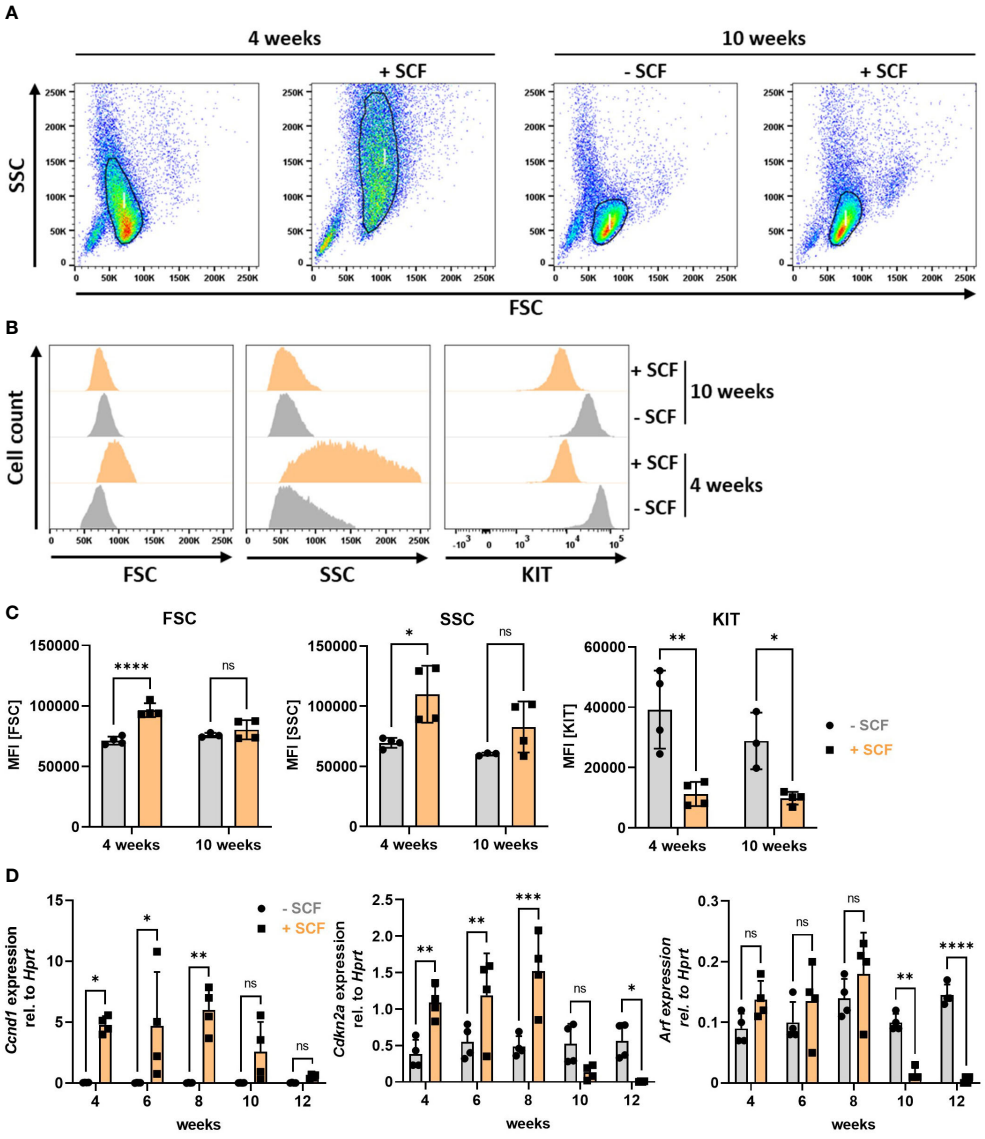

FIGURE 8
Constitutive KIT activation induces morphological changes and loss of *Cdkn2a/Arf* expression in BMMCs. **(A)** Representative FACS-plots showing BMMC populations cultivated with or without SCF for 4 (left) or 10 (right) weeks (n=4). **(B)** Representative histograms showing frequency distributions of forward scatter (left), side scatter (middle) and KIT expression (right) of BMMCs cultivated for 4 or 10 weeks with or without SCF (n=4). **(C)** Quantified data (MFI) of parameters analyzed in **(B)** [n=4 for all data except for BMMCs -SCF at 10 weeks (n=3)]. **(D)** RT-qPCR analysis of *Ccnd1*, *Cdkn2a* and *Arf* mRNA expression in BMMCs supplemented or not with SCF over a period of 12 weeks (n=4). Symbols indicate biological replicates. **(C)** and **(D)** Ordinary two-way ANOVA followed by Sídák multiple comparisons test. $p>0.05$ ns, *$p<0.05$, ** $p<0.01$, *** $p<0.001$, **** $p<0.0001$.

Intriguingly, these morphological differences disappeared after 10 weeks, when size and granularity of SCF-supplemented BMMCs decreased to levels of BMMCs cultivated without SCF (Figure 8A right panels, Figures 8B, C). As a control for SCF treatment we stained for KIT at the cell surface. KIT is known to be internalized upon SCF binding (59). Consequently, less KIT remains on the cellular surface under chronic KIT-stimulating conditions. We could confirm this observation by FACS analysis, as BMMCs supplemented with SCF expressed significantly less KIT at the plasma membrane (Figure 8B right panel, Figure 8C right panel). It is further known that KIT can increase proliferation by inducing transcription of cyclins *via* the PI3K-AKT pathway (60). Indeed, we observed increased proliferation of SCF-treated BMMCs and strong upregulation of the G_1/S cyclin *Ccnd1* until 8 weeks. After 10 weeks, however, *Ccnd1* expression decreased constantly to levels similar to BMMCs grown in the absence of SCF (Figure 8D, left). Notably, we found a strikingly similar expression pattern for the negative cell cycle regulator *Cdkn2a*, whose expression was increased by SCF supplementation over the first 8 weeks and then dropped to levels below the expression of control BMMCs (Figure 8D, middle). Accordingly, expression of *Arf*, though not significantly increased in the beginning, drastically decreased after 10 weeks in the presence of SCF, as well (Figure 8D, right). Loss of *Cdkn2a* and *Arf* expression thus timely and reproducibly correlates with cell

shrinkage and perfectly mimics the phenotype of PMC-306 cells. Finally, we tested whether BMMCs after 12 weeks of culturing in SCF-containing medium could be cryopreserved. Indeed, we could confirm that specifically SCF-supplemented BMMCs survived freeze-thawing (data not shown). Hence, this observation suggests that constitutive KIT activation might be the driver for cell cycle deregulation and especially prolonged (>10 weeks) SCF supplementation seems to promote decreased *Cdkn2a/Arf* expression

Discussion

Advancing research of the characteristics and activation mechanisms of MCs either requires the isolation of MCs from donor tissue, *ex vivo* differentiation of human CD34-positive precursor cells or the use of adequate cell lines. Problematically, suitable cell lines with MC-like properties are restricted to few examples with several limitations including loss of FcεRI expression in HMC-1.1, -1.2 and LUVA cells or long doubling times in case of LAD2 cells (14, 15, 42). Thus, MC research is encumbered by MC lines sharing as much features as possible with tissue-resident MCs *in vivo*. Here we present a novel murine MC line, which overcomes these limitations. We showed that the PMC-306 cell line stably expresses a functional FcεRI, has a short doubling time, maintained MC characteristics over multiple passages and is easy to freeze and thaw. These features suggest that PMC-306 cells can be used as a new tool to address questions related to MC research.

We extensively characterized PMC-306 cells and compared their appearance, activation and growth behaviour to non-transformed primary WT PMCs. PMC-306 cells share all characteristics of MCs as they stained positive for the MC surface markers FcεRI, KIT (CD117), CD13 and T1/ST2. We could further demonstrate a strictly IL-3- and SCF-dependent growth and Imatinib sensitivity of PMC-306 excluding KIT activating or Imatinib-resistant mutations, which are often detected in MC leukemia and complicate studies on general MC properties. HMC-1.1 and -1.2 cells bearing KIT mutations have a high basal activity of pro-survival signaling pathways including PI3K/PKB, STAT5 and RAS/RAF/MEK/ERK (58). This complicates studies on signaling pathways activated by other receptors due to enhanced background signals. Importantly, PMC-306 cells, despite cultivated in SCF-containing medium, did not show these high background phospho-signals making them an interesting tool to study MC signaling.

The PMC-306 cell line is derived from primary WT PMCs, which have connective tissue-like MC characteristics. We confirmed this by verifying expression and functionality of the connective tissue MC-specific receptor MRGPRB2. This MC-specific receptor has recently gained attention as its discovery has led to many new insights into the role of MCs in adverse drug reactions, communication with nerve cells and the development of a new tool for skin MC ablation (46, 47, 61). However, studies on the MC activating mechanisms in terms of signal transduction of MRGPRB2 are scarce. We showed that PMC-306 cells are an appropriate model to study – apart from FcεRI-dependent MC activation – also MRGPRB2-dependent effects. PMC-306 cells substantially reacted to MRGPRB2 activating ligands in terms of degranulation and cytokine production. Strikingly, the results showed that the degranulation seems to involve a completely different mechanism from that of Ag-triggered degranulation as we could not detect externalization of the granular marker LAMP1 and cells significantly lost a bigger part of their protein content within the first minutes of stimulation. A study from Gaudenzio et al. (62) already proposed that MC activation *via* the MRGPRB2 receptor is faster, does not involve compound exocytosis of granules and that the cytokine secretion profile is substantially different in comparison to Ag-dependent degranulation. Nevertheless, they did not deeply look into a mechanistic level how this is regulated by the cell. We further determined the pro-inflammatory cytokine production potential of PMC-306 cells in response to different stimuli. Interestingly, both primary WT and PMC-306 cells potently responded to Ag and IL-33, while TLR agonists like LPS and FSL-1 did not elicit a response. This is in agreement with a proteomic study revealing that primary human connective tissue type MCs lack crucial innate immune receptors including TLR-2, -3, -4, -7, -8 and -11, which is conserved between mouse and human (47). Looking at the overall picture of MC effector functions, there was great similarity between primary WT PMCs and the PMC-306 line.

One hallmark of MCs is their numerous densely packed secretory granules within the cytoplasm storing preformed pro-inflammatory mediators. PMC-306 cells appeared less granulated, showed reduced total β-hexosaminidase content and lacked expression of *Tpsab1*, *Mcpt2*, *Mcpt4* and *Cma1*. However, proteases that appear early in MC differentiation like *Cpa3* and *Gzmb* (52) were still present on mRNA level, which might indicate that the culture of PMC-306 consists of an incompletely differentiated transformed connective tissue MC type. However, GZMB protein expression was entirely absent. This could be a consequence of the drastically increased cell cycle progression, which does not permit the cell to build up complex granular structures resulting in post-transcriptional attenuation of mRNA translation not essential for proliferation. Mechanistically, the lavage of the murine peritoneal cavity may lead to isolation of MCs of different differentiation stages including fully mature and immature MC types. Of note, malignant transformation of myeloid cells often occurs at early differentiation stages, where the proliferative potential is high (52, 63, 64). These circumstances might have contributed to the transformation of the PMC-306 cell line and would well fit to the observed phenotype.

We cultivated primary PMCs and both cell lines, PMC-303 and PMC-306, under different culture conditions. While we strictly followed the established protocol for cultivation of primary PMCs (23), we re-evaluated the culture conditions of the PMC cell lines after noticing cellular transformation. The reason for this was, that we observed an enormous proliferation of both cell lines under primary PMC cultivation conditions, which we thought could have

negative consequences for genomic stability after long-term cultivation of the cells due to the accumulation of additional mutations. Indeed, it has been shown that extremely proliferating tumour cells and inflammation-induced proliferation favour the accumulation of genetic mutations (65, 66) and we could observe by staining pH2Ax that the frequency of DNA double strand breaks was slightly enhanced in PMC-306 cells in relation to primary PMCs despite the reduced SCF/FCS growth conditions. Importantly, before establishing the PMC cell lines as a new MC tool, we reduced SCF and FCS concentrations to levels, which did not negatively affect viability of both cell lines. We could also show that reduced SCF and FCS concentrations in culture medium did not affect the experimental outcome with respect to the analysis of protease expression and granularity of the cells. The only parameter that was influenced by increased SCF concentrations was the cell surface localization of KIT, which reportedly internalizes upon SCF binding (59), while expression of other MC surface markers was not changed. Crucially, cell cycle activity and proliferation were still substantially elevated in PMC-306 cells compared to primary PMCs despite reduced SCF and FCS concentrations in the culture medium.

Spontaneous transformation of cells *in vitro* can either occur due to activating mutations in pro-survival pathways and/or genetic loss of tumour suppressor proteins (55). Transformation of cells is often associated with loss of cell type-specific characteristics. We could exclude an activating mutation in the prominent MC growth factor receptor KIT as we could show that SCF supplementation is still required for PMC-306 cell proliferation and PMC-306 cells are still sensitive to KIT inhibition by Imatinib excluding KIT mutations leading to Imatinib resistance. However, we found complete loss of expression of the two central cell cycle regulators *Cdkn2a* and *Arf* both located on the heterozygously deleted region of chromosome 4. While p16/INK4A inhibits CDK4 and CDK6, thereby preventing entry into S phase by activation of RB (67), p19/ARF inhibits the ubiquitin ligase MDM2, which leads to p53 stabilization and, amongst others, initiation of apoptosis (68, 69). Thus, absence of both of these proteins fuels the cell cycle, circumvents cell cycle control and accelerates cell proliferation as quantified for PMC-306 cells by MKI67 and pH3 staining. The rapid proliferation rate is likely accompanied by a reduced time to build up more complex intracellular structures like MC granules, which is in line with the reduced granular content of PMC-306. Importantly, we detected loss of *Cdkn2a* and *Arf* expression also in the independently transformed PMC-303 line, which we did not characterize as extensively as the PMC-306 cell line in this report. However, PMC-303 cells did not show any abnormalities on chromosome 4 suggesting a different mechanism of gene silencing potentially involving epigenetic mechanisms. Interestingly, the PMC-303 cell line had a trisomy 8, which frequently occurs in murine embryonic stem cells and is associated with increased proliferation, genome instability but does not seem to affect cellular differentiation (70, 71). Nevertheless, similar to PMC-306 cells, the PMC-303 cell line retained its MC-like characteristic effector functions and morphology despite transformation. Crucially, as we observed inactivation of the *Cdkn2a/Arf* locus in two independent MC lines, it is tempting to speculate that the presence of this tumour suppressor locus might be a central player in preventing MC transformation. Still, our evidence does not allow to draw a direct causal connection between lost *Cdkn2a/Arf* expression and cellular transformation as we cannot for certain declare that this mutation is the first to be acquired during transformation. However, it could potentially also be interesting to investigate the role of *Cdkn2a/Arf* in the context of clonal MC diseases like mastocytosis or MC leukemia.So far, a *CDKN2A* mutation was only described in a case report of a patient suffering from MC leukemia with persistent myelodysplastic syndrome (72) without further characterization. As *Cdkn2a/Arf* inactivation appeared to be a recurrent phenomenon in MCs, we suspected that the culture conditions, notably the presence of SCF, might contribute to the regulation of *Cdkn2a/Arf* mRNA expression. In this regard, it is known that activation of the epidermal growth factor receptor (EGFR) correlates with *Cdkn2a* loss in glioblastoma formation (73). Likewise, tyrosine kinase inhibitor resistance of Philadelphia chromosome-positive leukemia correlates with deletion of the *CDKN2* gene (74), and cooperativity between PTEN loss and loss of *Cdkn2a* and *Arf* in histiocytic sarcoma has been reported (75). This wealth of data suggests that activation of RTKs and downstream PI3K-PKB signaling, which induces cyclin expression and accelerates proliferation (60), is necessary for *Cdkn2a/Arf* inactivation. Indeed, we could show that constitutive KIT activation by SCF downregulated *Cdkn2a* and *Arf* expression in BMMCs. SCF-supplemented BMMCs tried to counterbalance the enormous upregulation of *Ccnd1* by KIT activation through upregulation of *Cdkn2a* up to the first 8 weeks, while prolonged SCF-treatment inactivated the negative regulatory cell cycle regulators. It is reported that mitogenic stimuli, like SCF-mediated KIT activation, upregulate *Cdkn2a/Arf* expression to enable better control of cell cycle progression (76–79), which likely accounts for the increased *Cdkn2a* levels within weeks 4-8. A model could be envisaged in which prolonged cultivation in SCF-containing medium might potentially have favoured the selection of cells with a epigenetically silenced or genetically deleted *Cdkn2a/Arf* locus, which ultimately may have overgrown the cells with intact cell cycle regulation. After the loss of *Cdkn2a/Arf* expression, high cyclin expression obviously became unnecessary because normal cyclin levels were sufficient to fuel the cell cycle in the absence of negative regulatory proteins. This may explain the decrease in *Ccnd1* expression at the same time expression of *Cdkn2a/Arf* was lost in SCF-treated BMMCs. In essence, KIT is an abundant RTK present on all types of differentiated MCs and a potent activator of the PI3K-PKB pathway, thus possessing all requirements to induce the above-described cell cycle regulatory changes, which might have ultimately enabled unrestricted proliferation.

In summary, we herein characterized a new murine FcεRI- and MRGPRB2-positive connective tissue type-like MC line displaying similar characteristics to primary PMCs including several advantages. Importantly, the low number of chromosomal abnormalities reflects the WT MC-like behaviour, which is a great

advantage in comparison to RBL-2H3 cells that have been shown to contain a mean chromosome number of 67 (19). Technically, increased proliferation and reduced protease expression of PMC-306 overcomes the problems of cell number limitations and protein degradation in cell lysates using conventional cell lysis conditions (49) related to experiments with primary PMCs. Ultimately, alternatives to isolation of cells from and experiments with laboratory animals are needed to reduce the number of animals sacrificed for research. Thus, establishing new cell lines supports the 3R guidelines (24) and will help to achieve the future aim of ending the use of animals in research in the USA and the European Union (67). This new MC model will therefore sustain future studies on mechanisms and pharmacologic intervention of MC activation.

Data availability statement

The NGS data have been deposited in NCBI's Gene Expression Omnibus and are accessible through the GEO Series accession number GSE227065 (https://www.ncbi.nlm.nih.gov/geo/query/acc.cgi?acc=GSE227065).

Ethics statement

The animal study was approved by the Governmental Animal Care and Use Committee at the State Agency for Nature, Environment and Consumer Protection, Recklinghausen (LANUV).

Author contributions

SC, RS, HS, SM, LG, MK, KH and HK-W performed experiments and analyzed the data. SC and MH conceptualized the study. SC wrote the first draft of the manuscript. SC, RW, CL and MH contributed to review and editing. RW, CL and MH contributed to funding acquisition. All authors contributed to the article and approved the submitted version.

Funding

This work was supported by grants from the Deutsche Forschungsgemeinschaft (DFG). HU794/12-1 and HU794/14-1 to MH, LI1045/6-1 to CL, WE2554/15-1 to RW and ME3431/2-1 to SM.

Acknowledgments

We thank Thomas Wilhelm (RWTH Aachen University) for proofreading and fruitful discussions. Moreover, we are grateful to Bernhard Lüscher (RWTH Aachen University) for sharing his expertise in mechanisms of cellular transformation. The content of this manuscript previously appeared online as a preprint at bioRxiv (https://doi.org/10.1101/2023.01.24.525344) (68).

Conflict of interest

The authors declare that the research was conducted in the absence of any commercial or financial relationships that could be construed as a potential conflict of interest.

Publisher's note

Supplementary material

The Supplementary Material for this article can be found online at: https://www.frontiersin.org/articles/10.3389/fimmu.2023.1154416/full#supplementary-material

SUPPLEMENTARY FIGURE 1
MC surface marker expression of PMC-306 before and after immortalization. **(A)** Representative FACS analysis of PMC-306 cells before transformation after 3 weeks under regular PMC culture conditions. FSC/SSC dot plot shows a typical WT PMC population of 93.6% FcεRI and KIT double-positive cells (n=3).

SUPPLEMENTARY FIGURE 2
Analysis of primary WT PMC and PMC-306 viability under cytokine deprivation conditions. Representative FACS dot plots showing Annexin V and propidium iodide positivity in primary PMCs and PMC-306 cells under IL-3 (n=3) **(A)** or SCF (n=3) **(B)** deprivation for 72 hours. The percentage of single positive, double positive, and double negative cells is provided in the associated gates.

SUPPLEMENTARY FIGURE 3
Analysis of MRGPRB2 activation shows unconventional degranulation and impact on cellular integrity. **(A)** ELISA measurement of secreted IL-6 (left) or TNF (right) from PMC-306 cells stimulated with increasing concentrations of C48/80 (n=4). **(B)** BCA assay to determine the protein concentration in cell lysates of PMC-306 cells stimulated with either Ag [20 ng/ml], C48/80 [10 µg/ml] or Mastoparan [30 µM] for the indicated time points (n=3). **(C)** Representative flow cytometry dot plots and histograms of primary WT PMCs stimulated with either Ag [20 ng/ml] or C48/80 [10 µg/ml] for indicated time points and stained with anti-LAMP1 to determine granule externalization (n=3). Data are shown as mean +SD. **(A)** Ordinary one-way ANOVA followed by Dunnett multiple comparisons test. **(B)** Two-way ANOVA followed by Sídák multiple comparisons test. $p>0.05$ ns, $*p<0.05$, $**p<0.01$, $***p<0.001$, $****p<0.0001$. Stars indicate the significance level relative to the respective controls.

SUPPLEMENTARY FIGURE 4
Different culture conditions do not affect the general PMC-306 phenotype. **(A–I)** PMC-306 cells were cultivated either under reduced conditions with 10% FCS and 5 ng/ml SCF or primary PMC conditions (full, 15% FCS and 20 ng/ml SCF) to analyze potential effects on different culture conditions on gene expression. Primary WT PMCs cultivated under normal PMC conditions served as reference. mRNA expression of *Cdkn2a* **(A)**, *Arf* **(B)**, *Cma1* **(C)**, *Cpa3* **(D)**, *Gzmb* **(E)**, *Mcpt2* **(F)**, *Mcpt4* **(G)**, *Tpsab1* **(H)** and *Mrgprb2* **(I)** were analyzed by qPCR. Expression of the respective genes of interest was quantified by the delta C_T method using *Hprt* as a housekeeping gene (n=3). **(J)** Representative FACS dot plots and normalized histograms showing expression of FcεRI, KIT, ST2 and CD13 in PMC-306 cells

cultivated either under reduced (blue) or full medium (red) conditions. The upper two panels show frequency distributions relative to an unstained control (grey) while the lower panel shows frequency distribution comparing reduced and full medium conditions. **(K)** Quantification of the FACS surface marker analysis depicted in **(J)** with MFIs showing staining intensities for the respective surface markers as well as FSC and SSC parameters (n=3). **(A–I)** One-way ANOVA followed by Dunnett multiple comparisons test. **(K)** Unpaired, two-tailed Student's *t*-test with Welsh's correction. Data are expressed as mean +SD. $p>0.05$ ns, $*p<0.05$, $**p<0.01$, $***p<0.001$, $****p<0.0001$.

SUPPLEMENTARY FIGURE 5

Cytogenetic and gene expression analysis of the independently transformed PMC cell line PMC-303. **(A)** Table of all discovered cytogenetic aberrations of mitotic chromosomes of the PMC-306 cell line with associated frequencies. **(B)** Representative G-banded karyotype of the PMC-303 cell line with trisomy 8 due to a homologous Robertsonian translocation of chromosome 8 (Rb (8.8)). **(D–H)** RT-qPCR analysis of genes encoded within in the region of chromosome 4, which is deleted in the PMC-306 cell line (Chr4 qC4-qC7). Gene expression of *Cdkn2a*, *Arf*, *Rbl1*, *Mllt3*, *Dennd4c* and *Plaa* were measured in PMC-303 cells in comparison to primary WT PMCs (n=3). Data are expressed as mean +SD. Unpaired, two-tailed Student's *t*-test with Welsh's correction. $*p<0.05$.

SUPPLEMENTARY FIGURE 6

Characterization of the PMC-303 cell line. **(A)** Representative FACS histograms showing surface localization of FcεRI, KIT, ST2 and CD13 in PMC-303 cells after freeze-thaw relative to an unstained control (n=3). **(B)** Representative electron micrographs showing the ultrastructure of PMC-303 cells. **(C)** Quantification of the relative β-hexosaminidase activity in lysates of primary PMCs and PMC-303 cells determined by an enzymatic assay to quantify the amount of cellular β-hexosaminidase expressed in primary PMCs and PMC-306 cells (n=3). **(D)** Determination of the degranulation of PMC-303 cells in response to indicated concentrations of C48/80 assessed by β-hexosaminidase release assay (n=3). **(E)** Determination of the degranulation of PMC-303 cells in response to indicated concentrations of Mastoparan assessed by β-hexosaminidase release assay (n=3). **(F)** FACS analysis of PMC-303 cells stimulated with Ag [20 ng/ml] for indicated time points to determine externalization of LAMP1 externalization. Bar graphs shown MFIs for LAMP1 for each time point (n=3). **(G)** The pro-inflammatory cytokine production of PMC-303 cells to Ag (20 ng/ml) in comparison to other stimuli (SCF: 100 ng/ml, SCF+Ag: 100 ng/ml and 20 ng/ml, LPS: 1µg/ml, FSL-1: 1 µg/ml, IL-33: 10 ng/ml, C48/80: 10 µg/ml) was determined by IL-6 ELISA (n=3). **(H)** Same experiment as in **(G)**, but secreted amounts of TNF were determined by ELISA (n=3). Data are expressed as mean +SD. **(C)** Unpaired, two-tailed Student's *t*-test with Welsh's correction. **(D–H)** One-way ANOVA followed by Dunnett multiple comparisons test. Stars indicate significance within one group relative to control. $p>0.05$ ns, $*p<0.05$, $**p<0.01$, $***p<0.001$, $****p<0.0001$.

SUPPLEMENTARY FIGURE 7

GO Term analysis of the NGS data set, gating strategy and background determination for flow cytometry (FACS) and analysis of aneuploidy. **(A)** For the GO term enrichment analysis all genes regulated at least 5-fold between primary WT PMCs and PMC-306 cells were included. The top 15 GO terms with the lowest *p* values are depicted. GO term analysis was performed using the gene ontology knowledgebase server (http://geneontology.org/) **(B–D)** Gating strategy and background determination for the transformed PMC-306 line (red) and primary WT PMCs (black). **(B)** Left panels: Forward *versus* side scatter (FSC *vs.* SSC) gating for identification of cells of interest. FSC indicates cell size, SSC indicates cell granularity. Right panels: FSC-A *vs.* FCS-H gating for identification of single cells. **(C, D)** Unstained controls, which were not incubated with antibodies to assess background for staining against phospho-histone 3 (AL647-A, pH3) and phospho-histone H2Ax (pH2Ax, PerCP-Cy5.5-A) **(C)**, MKI67 (AL700-A) and DAPI (DNA content, BV421-A) **(D)**. **(E)** Representative histograms of primary WT PMCs and PMC-306 cells stained with an antibody directed against MKI67 (AL700-A) and phospho-histone H3 (pH3, AL647-A). Cellular DNA content was determined by DAPI staining (BV421-A) for assignment to the distinct cell cycle phases as follows: SubG1:< 2n DNA content; G1: 2n; S: 2-4n; G2/M: 4n; Aneuploidy: > 4n. Representative overlay of FACS-histograms of DNA content in all single cells (black) *versus* MKI67+ (yellow, left) or pH3+ (red, right) single cells (normalized to mode). Black arrows indicate MKI67+ and pH3+ cells with a DNA content above 4n (aneuploidy) (n=3).

References

1. Galli SJ, Gaudenzio N, Tsai M. Mast cells in inflammation and disease: Recent progress and ongoing concerns. *Annu Rev Immunol* (2020) 38:49–77. doi: 10.1146/annurev-immunol-071719-094903

2. Galli SJ, Tsai M. Mast cells in allergy and infection: versatile effector and regulatory cells in innate and adaptive immunity. *Eur J Immunol* (2010) 40(7):1843–51. doi: 10.1002/eji.201040559

3. Metz M, Maurer M. Mast cells–key effector cells in immune responses. *Trends Immunol* (2007) 28(5):234–41. doi: 10.1016/j.it.2007.03.003

4. Johnson C, Huynh V, Hargrove L, Kennedy L, Graf-Eaton A, Owens J, et al. Inhibition of mast cell-derived histamine decreases human cholangiocarcinoma growth and differentiation *via* c-Kit/Stem cell factor-dependent signaling. *Am J Pathol* (2016) 186(1):123–33. doi: 10.1016/j.ajpath.2015.09.016

5. Kondo K, Muramatsu M, Okamoto Y, Jin D, Takai S, Tanigawa N, et al. Expression of chymase-positive cells in gastric cancer and its correlation with the angiogenesis. *J Surg Oncol* (2006) 93(1):33–6. doi: 10.1002/jso.20394

6. Malaviya R, Ikeda T, Ross E, Abraham SN. Mast cell modulation of neutrophil influx and bacterial clearance at sites of infection through TNF-alpha. *Nature* (1996) 381(6577):77–80. doi: 10.1038/381077a0

7. Zimmermann C, Troeltzsch D, Giménez-Rivera VA, Galli SJ, Metz M, Maurer M, et al. Mast cells are critical for controlling the bacterial burden and the healing of infected wounds. *Proc Natl Acad Sci USA* (2019) 116(41):20500–4. doi: 10.1073/pnas.1908816116

8. Rathore APS, St John AL. Protective and pathogenic roles for mast cells during viral infections. *Curr Opin Immunol* (2020) 66:74–81. doi: 10.1016/j.coi.2020.05.003

9. Ramirez-GarciaLuna JL, Chan D, Samberg R, Abou-Rjeili M, Wong TH, Li A, et al. Defective bone repair in mast cell-deficient Cpa3Cre/+ mice. *PloS One* (2017) 12 (3):e0174396. doi: 10.1371/journal.pone.0174396

10. Grimbaldeston MA, Nakae S, Kalesnikoff J, Tsai M, Galli SJ. Mast cell-derived interleukin 10 limits skin pathology in contact dermatitis and chronic irradiation with ultraviolet b. *Nat Immunol* (2007) 8(10):1095–104. doi: 10.1038/ni1503

11. Maurer M, Theoharides T, Granstein RD, Bischoff SC, Bienenstock J, Henz B, et al. What is the physiological function of mast cells? *Exp Dermatol* (2003) 12(6):886–910. doi: 10.1111/j.0906-6705.2003.0109a.x

12. Huber M, Cato ACB, Ainooson GK, Freichel M, Tsvilovskyy V, Jessberger R, et al. Regulation of the pleiotropic effects of tissue-resident mast cells. *J Allergy Clin Immunol* (2019) 144(4S):S31–45. doi: 10.1016/j.jaci.2019.02.004

13. Butterfield JH, Weiler D, Dewald G, Gleich GJ. Establishment of an immature mast cell line from a patient with mast cell leukemia. *Leuk Res* (1988) 12(4):345–55. doi: 10.1016/0145-2126(88)90050-1

14. Laidlaw TM, Steinke JW, Tiñana AM, Feng C, Xing W, Lam BK, et al. Characterization of a novel human mast cell line that responds to stem cell factor and expresses functional FcεRI. *J Allergy Clin Immunol* (2011) 127(3):815. doi: 10.1016/j.jaci.2010.12.1101

15. Kirshenbaum AS, Akin C, Wu Y, Rottem M, Goff JP, Beaven MA, et al. Characterization of novel stem cell factor responsive human mast cell lines LAD 1 and 2 established from a patient with mast cell sarcoma/leukemia; activation following aggregation of FcepsilonRI or FcgammaRI. *Leuk Res* (2003) 27(8):677–82. doi: 10.1016/S0145-2126(02)00343-0

16. Eccleston E, Leonard BJ, Lowe JS, Welford HJ. Basophilic leukaemia in the albino rat and a demonstration of the basopoietin. *Nat New Biol* (1973) 244(133):73–6. doi: 10.1038/newbio244073b0

17. Rupp B, Löhning M, Werenskiold AK. Reversible expression of tryptases in continuous L138.8A mast cells. *Eur J Immunol* (2000) 30(10):2954–61. doi: 10.1002/1521-4141(200010)30:10<2954::AID-IMMU2954>3.0.CO;2-S

18. Haenisch B, Herms S, Molderings GJ. The transcriptome of the human mast cell leukemia cells HMC-1.2: an approach to identify specific changes in the gene expression profile in KitD816V systemic mastocytosis. *Immunol Res* (2013) 56 (1):155–62. doi: 10.1007/s12026-013-8391-1

19. Barsumian EL, Isersky C, Petrino MG, Siraganian RP. IgE-induced histamine release from rat basophilic leukemia cell lines: Isolation of releasing and nonreleasing clones. *Eur J Immunol* (1981) 11(4):317–23. doi: 10.1002/eji.1830110410

20. Passante E, Frankish N. The RBL-2H3 cell line: Its provenance and suitability as a model for the mast cell. *Inflamm Res* (2009) 58(11):737–45. doi: 10.1007/s00011-009-0074-y

21. Xing W, Austen KF, Gurish MF, Jones TG. Protease phenotype of constitutive connective tissue and of induced mucosal mast cells in mice is regulated by the tissue. *Proc Natl Acad Sci USA* (2011) 108(34):14210–5. doi: 10.1073/pnas.1111048108

22. Bischoff SC. Role of mast cells in allergic and non-allergic immune responses: comparison of human and murine data. *Nat Rev Immunol* (2007) 7(2):93–104. doi: 10.1038/nri2018

23. Meurer SK, Neß M, Weiskirchen S, Kim P, Tag CG, Kauffmann M, et al. Isolation of mature (Peritoneum-derived) mast cells and immature (Bone marrow-derived) mast cell precursors from mice. *PloS One* (2016) 11(6):e0158104–e0158104. doi: 10.1371/journal.pone.0158104

24. Justin M, Jež M, Košir A, Miceska S, Rožman P, Jazbec K. Application of the 3R principles: Vertebrae as an additional source of murine bone-marrow cells. *Lab Anim* (2021) 55(1):43–52. doi: 10.1177/0023677220922573

25. Kamijo T, Zindy F, Roussel MF, Quelle DE, Downing JR, Ashmun RA, et al. Tumor suppression at the mouse INK4a locus mediated by the alternative reading frame product p19ARF. *Cell* (1997) 91(5):649–59. doi: 10.1016/S0092-8674(00)80452-3

26. Sharpless NE. INK4a/ARF: a multifunctional tumor suppressor locus. *Mutat Res* (2005) 576(1–2):22–38. doi: 10.1016/j.mrfmmm.2004.08.021

27. Karasuyama H, Melchers F. Establishment of mouse cell lines which constitutively secrete large quantities of interleukin 2, 3, 4 or 5, using modified cDNA expression vectors. *Eur J Immunol* (1988) 18(1):97–104. doi: 10.1002/eji.1830180115

28. Nishizumi H, Yamamoto T. Impaired tyrosine phosphorylation and Ca2+ mobilization, but not degranulation, in Lyn-deficient bone marrow-derived mast cells. *J Immunol* (1997) 158(5):2350–5. doi: 10.4049/jimmunol.158.5.2350

29. Pfaffl MW. A new mathematical model for relative quantification in real-time RT-PCR. *Nucleic Acids Res* (2001) 29(9):e45–5. doi: 10.1093/nar/29.9.e45

30. Liu L, Damen JE, Cutler RL, Krystal G. Multiple cytokines stimulate the binding of a common 145-kilodalton protein to shc at the Grb2 recognition site of shc. *Mol Cell Biol* (1994) 14(10):6926–35. doi: 10.1128/mcb.14.10.6926-6935.1994

31. Shaffer LG, Tommerup N. *ISCN 2005: an international system for human cytogenetic nomenclature (2005): recommendations of the international standing committee on human cytogenetic nomenclature*. Karger Medical and Scientific Publishers (2005). Available at: https://www.ncbi.nlm.nih.gov/nlmcatalog?cmd=PureSearch&term=101256672%5Bnlmid%5D.

32. Islam MQ, Levan G. A new fixation procedure for improved quality G-bands in routine cytogenetic work. *Hereditas* (1987) 107(1):127–30. doi: 10.1111/j.1601-5223.1987.tb00277.x

33. Korf BR, Schuh BE, Salwen MJ, Warburton D, Miller OJ. The role of trypsin in the pre-treatment of chromosomes for giemsa banding. *Hum Genet* (1976) 31(1):27–33. doi: 10.1007/BF00270396

34. Ewels PA, Peltzer A, Fillinger S, Patel H, Alneberg J, Wilm A, et al. The nf-core framework for community-curated bioinformatics pipelines. *Nat Biotechnol* (2020) 38:276–8. United States. doi: 10.1038/s41587-020-0439-x

35. Di Tommaso P, Chatzou M, Floden EW, Barja PP, Palumbo E, Notredame C. Nextflow enables reproducible computational workflows. *Nat Biotechnol* (2017) 35:316–9. United States. doi: 10.1038/nbt.3820

36. Merkel D. Docker: Lightweight Linux containers for consistent development and deployment. *Linux J* (2014) 2014:2.

37. Krueger F, James F, Ewels P, Afyounian E, Schuster-Boeckler B. (2021) *FelixKrueger/TrimGalore: v0.6.7 - DOI via Zenodo (0.6.7)*. Zenodo. doi: 10.5281/zenodo.5127899

38. Dobin A, Davis CA, Schlesinger F, Drenkow J, Zaleski C, Jha S, et al. STAR: ultrafast universal RNA-seq aligner. *Bioinformatics* (2013) 29(1):15–21. doi: 10.1093/bioinformatics/bts635

39. Patro R, Duggal G, Love MI, Irizarry RA, Kingsford C. Salmon provides fast and bias-aware quantification of transcript expression. *Nat Methods* (2017) 14(4):417–9. doi: 10.1038/nmeth.4197

40. Wernersson S, Pejler G. Mast cell secretory granules: Armed for battle. *Nat Rev Immunol* (2014) 14(7):478–94. doi: 10.1038/nri3690

41. Furitsu T, Tsujimura T, Tono T, Ikeda H, Kitayama H, Koshimizu U, et al. Identification of mutations in the coding sequence of the proto-oncogene c-kit in a human mast cell leukemia cell line causing ligand-independent activation of c-kit product. *J Clin Invest* (1993) 92(4):1736–44. doi: 10.1172/JCI116761

42. Nilsson G, Blom T, Kusche-Gullberg M, Kjellén L, Butterfield JH, Sundström C, et al. Phenotypic characterization of the human mast-cell line HMC-1. *Scand J Immunol* (1994) 39(5):489–98. doi: 10.1111/j.1365-3083.1994.tb03404.x

43. Valent P, Akin C, Hartmann K, Nilsson G, Reiter A, Hermine O, et al. Advances in the classification and treatment of mastocytosis: Current status and outlook toward the future. *Cancer Res* (2017) 77(6):1261–70. doi: 10.1158/0008-5472.CAN-16-2234

44. Metcalfe DD. Mast cells and mastocytosis. *Blood* (2008) 112(4):946–56. doi: 10.1182/blood-2007-11-078097

45. Huber M. Activation/Inhibition of mast cells by supra-optimal antigen concentrations. *Cell Commun Signal* (2013) 11(1):7. doi: 10.1186/1478-811X-11-7

46. McNeil BD, Pundir P, Meeker S, Han L, Undem BJ, Kulka M, et al. Identification of a mast-cell-specific receptor crucial for pseudo-allergic drug reactions. *Nature* (2015) 519(7542):237–41. doi: 10.1038/nature14022

47. Plum T, Wang X, Rettel M, Krijgsveld J, Feyerabend TB, Rodewald H-R. Human mast cell proteome reveals unique lineage, putative functions, and structural basis for cell ablation. *Immunity* (2020) 52(2):404–416.e5. doi: 10.1016/j.immuni.2020.01.012

48. Pundir P, Liu R, Vasavda C, Serhan N, Limjunyawong N, Yee R, et al. A connective tissue mast-Cell-Specific receptor detects bacterial quorum-sensing molecules and mediates antibacterial immunity. *Cell Host Microbe* (2019) 26(1):114–122.e8. doi: 10.1016/j.chom.2019.06.003

49. Malbec O, Roget K, Schiffer C, Iannascoli B, Dumas AR, Arock M, et al. Peritoneal cell-derived mast cells: an *in vitro* model of mature serosal-type mouse mast cells. *J Immunol* (2007) 178(10):6465–75. doi: 10.4049/jimmunol.178.10.6465

50. Drube S, Heink S, Walter S, Löhn T, Grusser M, Gerbaulet A, et al. The receptor tyrosine kinase c-kit controls IL-33 receptor signaling in mast cells. *Blood* (2010) 115 (19):3899–906. doi: 10.1182/blood-2009-10-247411

51. Eklund KK, Ghildyal N, Austen KF, Friend DS, Schiller V, Stevens RL. Mouse bone marrow-derived mast cells (mBMMC) obtained *in vitro* from mice that are mast cell-deficient *in vivo* express the same panel of granule proteases as mBMMC and serosal mast cells from their normal littermates. *J Exp Med* (1994) 180(1):67–73. doi: 10.1084/jem.180.1.67

52. Lunderius C, Xiang Z, Nilsson G, Hellman L. Murine mast cell lines as indicators of early events in mast cell and basophil development. *Eur J Immunol* (2000) 30(12):3396–402. doi: 10.1002/1521-4141(2000012)30:12<3396::AID-IMMU3396>3.0.CO;2-O

53. Wu Y, Renard C-A, Apiou F, Huerre M, Tiollais P, Dutrillaux B, et al. Recurrent allelic deletions at mouse chromosomes 4 and 14 in myc-induced liver tumors. *Oncogene* (2002) 21(10):1518–26. doi: 10.1038/sj.onc.1205208

54. Sherr CJ. The INK4a/ARF network in tumour suppression. *Nat Rev Mol Cell Biol* (2001) 2(10):731–7. doi: 10.1038/35096061

55. Hanahan D, Weinberg RA, Francisco S. The hallmarks of cancer. *Cell* (2000) 100:57–70. doi: 10.1016/S0092-8674(00)81683-9

56. Matthews HK, Bertoli C, de Bruin RAM. Cell cycle control in cancer. *Nat Rev Mol Cell Biol* (2022) 23(1):74–88. doi: 10.1038/s41580-021-00404-3

57. Sherr CJ, McCormick F. The RB and p53 pathways in cancer. *Cancer Cell* (2002) 2(2):103–12. doi: 10.1016/S1535-6108(02)00102-2

58. Sundström M, Vliagoftis H, Karlberg P, Butterfield JH, Nilsson K, Metcalfe DD, et al. Functional and phenotypic studies of two variants of a human mast cell line with a distinct set of mutations in the c-kit proto-oncogene. *Immunology* (2003) 108(1):89–97. doi: 10.1046/j.1365-2567.2003.01559.x

59. Shimizu Y, Ashman LK, Du Z, Schwartz LB. Internalization of kit together with stem cell factor on human fetal liver-derived mast cells: New protein and RNA synthesis are required for reappearance of kit. *J Immunol* (1996) 156(9):3443–9. doi: 10.4049/jimmunol.156.9.3443

60. Reyes-Sebastian J, Montiel-Cervantes LA, Reyes-Maldonado E, Dominguez-Lopez ML, Ortiz-Butron R, Castillo-Alvarez A, et al. Cell proliferation and inhibition of apoptosis are related to c-kit activation in leukaemic lymphoblasts. *Hematology* (2018) 23(8):486–95. doi: 10.1080/10245332.2018.1444564

61. Green DP, Limjunyawong N, Gour N, Pundir P, Dong X. A mast-Cell-Specific receptor mediates neurogenic inflammation and pain. *Neuron* (2019) 101(3):412–420.e3. doi: 10.1016/j.neuron.2019.01.012

62. Gaudenzio N, Sibilano R, Marichal T, Starkl P, Reber LL, Cenac N, et al. Different activation signals induce distinct mast cell degranulation strategies. *J Clin Invest* (2016) 126(10):3981–98. doi: 10.1172/JCI85538

63. Haase D, Feuring-Buske M, Könemann S, Fonatsch C, Troff C, Verbeek W, et al. Evidence for malignant transformation in acute myeloid leukemia at the level of early hematopoietic stem cells by cytogenetic analysis of CD34+ subpopulations. *Blood* (1995) 86(8):2906–12. doi: 10.1182/blood.V86.8.2906.2906

64. Ball PE, Conroy MC, Heusser CH, Davis JM, Conscience JF. Spontaneous, *in vitro*, malignant transformation of a basophil/mast cell line. *Differentiation* (1983) 24 (1):74–8. doi: 10.1111/j.1432-0436.1983.tb01305.x

65. Kiraly O, Gong G, Olipitz W, Muthupalani S, Engelward BP. Inflammation-induced cell proliferation potentiates DNA damage-induced mutations *in vivo*. *PloS Genet* (2015) 11(2):e1004901. doi: 10.1371/journal.pgen.1004901

66. Grzywa TM, Koppolu AA, Paskal W, Klicka K, Rydzanicz M, Wejman J, et al. Higher mutation burden in high proliferation compartments of heterogeneous melanoma tumors. *Int J Mol Sci* (2021) 22(8):3886. doi: 10.3390/ijms22083886

67. Serrano M, Hannon GJ, Beach D. A new regulatory motif in cell-cycle control causing specific inhibition of cyclin D/CDK4. *Nature* (1993) 366(6456):704–7. doi: 10.1038/366704a0

68. Weber JD, Taylor LJ, Roussel MF, Sherr CJ, Bar-Sagi D. Nucleolar arf sequesters Mdm2 and activates p53. *Nat Cell Biol* (1999) 1(1):20–6. doi: 10.1038/8991

69. Honda R, Yasuda H. Association of p19(ARF) with Mdm2 inhibits ubiquitin ligase activity of Mdm2 for tumor suppressor p53. *EMBO J* (1999) 18(1):22–7. doi: 10.1093/emboj/18.1.22

70. Gaztelumendi N, Nogués C. Chromosome instability in mouse embryonic stem cells. *Sci Rep* (2014) 4(1):5324. doi: 10.1038/srep05324

71. Kim YM, Lee J-Y, Xia L, Mulvihill JJ, Li S. Trisomy 8: A common finding in mouse embryonic stem (ES) cell lines. *Mol Cytogenet* (2013) 6(1):3. doi: 10.1186/1755-8166-6-3

72. Yang J, Gabali A. Mast cell leukemia and hemophagocytosis in a patient with myelodysplastic syndrome. *Blood* (2019) 133(20):2243. doi: 10.1182/blood.2018886564

73. Acquaviva J, Jun HJ, Lessard J, Ruiz R, Zhu H, Donovan M, et al. Chronic activation of wild-type epidermal growth factor receptor and loss of Cdkn2a cause mouse glioblastoma formation. *Cancer Res* (2011) 71(23):7198–206. doi: 10.1158/0008-5472.CAN-11-1514

74. Xu N, Li Y, Li X, Zhou X, Cao R, Li H, et al. Correlation between deletion of the CDKN2 gene and tyrosine kinase inhibitor resistance in adult Philadelphia chromosome-positive acute lymphoblastic leukemia. *J Hematol Oncol* (2016) 9:40. doi: 10.1186/s13045-016-0270-5

75. Carrasco DR, Fenton T, Sukhdeo K, Protopopova M, Enos M, You MJ, et al. The PTEN and INK4A/ARF tumor suppressors maintain myelolymphoid homeostasis and cooperate to constrain histiocytic sarcoma development in humans. *Cancer Cell* (2006) 9(5):379–90. doi: 10.1016/j.ccr.2006.03.028

76. de Stanchina E, McCurrach ME, Zindy F, Shieh SY, Ferbeyre G, Samuelson AV, et al. E1A signaling to p53 involves the p19(ARF) tumor suppressor. *Genes Dev* (1998) 12(15):2434–42. doi: 10.1101/gad.12.15.2434

77. Zindy F, Eischen CM, Randle DH, Kamijo T, Cleveland JL, Sherr CJ, et al. Myc signaling *via* the ARF tumor suppressor regulates p53-dependent apoptosis and immortalization. *Genes Dev* (1998) 12(15):2424–33. doi: 10.1101/gad.12.15.2424

78. Palmero I, Pantoja C, Serrano M. p19ARF links the tumour suppressor p53 to ras. *Nature* (1998) 395:125–6. doi: 10.1038/25870

79. DeGregori J, Leone G, Miron A, Jakoi L, Nevins JR. Distinct roles for E2F proteins in cell growth control and apoptosis. *Proc Natl Acad Sci USA* (1997) 94 (14):7245–50. doi: 10.1073/pnas.94.14.7245

frontiers | Frontiers in Immunology

TYPE Original Research
PUBLISHED 30 March 2023
DOI 10.3389/fimmu.2023.1151754

OPEN ACCESS

EDITED BY
Ulrich Blank,
Institut National de la Santé et de la Recherche Médicale (INSERM), France

REVIEWED BY
Margarita Martin,
University of Barcelona, Spain
Nadine Varin-Blank,
Institut National de la Santé et de la Recherche Médicale (INSERM), France

*CORRESPONDENCE
Elin Rönnberg
elin.ronnberg.hockerlind@ki.se
Gunnar Nilsson
gunnar.p.nilsson@ki.se

SPECIALTY SECTION
This article was submitted to Molecular Innate Immunity, a section of the journal Frontiers in Immunology

RECEIVED 26 January 2023
ACCEPTED 15 March 2023
PUBLISHED 30 March 2023

CITATION
Rönnberg E, Ravindran A, Mazzurana L, Gong Y, Säfholm J, Lorent J, Dethlefsen O, Orre A-C, Al-Ameri M, Adner M, Dahlén S-E, Dahlin JS, Mjösberg J and Nilsson G (2023) Analysis of human lung mast cells by single cell RNA sequencing. *Front. Immunol.* 14:1151754. doi: 10.3389/fimmu.2023.1151754

Analysis of human lung mast cells by single cell RNA sequencing

Elin Rönnberg[1*], Avinash Ravindran[1,2], Luca Mazzurana[2], Yitao Gong[1], Jesper Säfholm[3], Julie Lorent[4], Olga Dethlefsen[4], Ann-Charlotte Orre[5], Mamdoh Al-Ameri[5], Mikael Adner[3], Sven-Erik Dahlén[3], Joakim S. Dahlin[1], Jenny Mjösberg[2] and Gunnar Nilsson[1,6*]

[1]Division of Immunology and Allergy, Department of Medicine Solna, Karolinska Institutet, and Karolinska University Hospital, Stockholm, Sweden, [2]Center for Infectious Medicine, Department of Medicine Huddinge, Karolinska Institutet, Stockholm, Sweden, [3]Unit for Experimental Asthma and Allergy Research Centre for Allergy Research, The Institute of Environmental Medicine, Karolinska Institutet, Stockholm, Sweden, [4]National Bioinformatics Infrastructure Sweden, Science for Life Laboratory, Stockholm University, Stockholm, Sweden, [5]Thoracic Surgery, Department of Molecular Medicine and Surgery, Karolinska Institutet, Karolinska University Hospital, Stockholm, Sweden, [6]Department of Medical Sciences, Uppsala University, Uppsala, Sweden

Mast cells are tissue-resident cells playing major roles in homeostasis and disease conditions. Lung mast cells are particularly important in airway inflammatory diseases such as asthma. Human mast cells are classically divided into the subsets MC_T and MC_{TC}, where MC_T express the mast cell protease tryptase and MC_{TC} in addition express chymase, carboxypeptidase A3 (CPA3) and cathepsin G. Apart from the disctintion of the MC_T and MC_{TC} subsets, little is known about the heterogeniety of human lung mast cells and a deep analysis of their heterogeniety has previously not been performed. We therefore performed single cell RNA sequencing on sorted human lung mast cells using SmartSeq2. The mast cells showed high expression of classical mast cell markers. The expression of several individual genes varied considerably among the cells, however, no subpopulations were detected by unbiased clustering. Variable genes included the protease-encoding transcripts *CMA1* (chymase) and *CTSG* (cathepsin G). Human lung mast cells are predominantly of the MC_T subset and consistent with this, the expression of *CMA1* was only detectable in a small proportion of the cells, and correlated moderately to *CTSG*. However, in contrast to established data for the protein, *CPA3* mRNA was high in all cells and the correlation of *CPA3* to *CMA1* was weak.

KEYWORDS

mast cells (MC), single cell RNA sequencing, lung, heterogeniety, chymase (CMA1), cathepsin G (CTSG), carboxypeptidase A3 (CPA3)

Introduction

Mast cells play important roles in the lung both in homeostasis and in disease and they are particularly recognized for their role in asthma (1). Mast cells are found in all different compartments of the human lung; *i.e.*, in the epithelium, in smooth muscle bundles, around pulmonary vessels, and in the parenchyma (2). Upon activation, mast cells release their preformed granule content, including histamine, proteases, proteoglycans and some cytokines/chemokine. In addition mast cells also start *de novo* synthesis of lipid mediators and cytokines/chemokines (3). Together, these mediators have multiple effects on the lung causing smooth muscle constriction, mucus production, and edema (1).

Human mast cells are classically divided into the MC_T and MC_{TC} subsets depending on the expression of specific proteases. The MC_T subset expresses tryptase and MC_{TC} in addition expresses chymase, CPA3 and cathepsin G (4). This distinction has been made with immunohistochemical methods and little is known about the mRNA expression of the proteases at the single cell level. Moreover, the heterogeneity of human lung mast cells appears to be much more diverse, beyond protease expression, including the expression of receptors, enzymes and other markers in different compartments of the lung (5). Recently, using flow cytometry, we demonstrated that human lung mast cell heterogeneity has a continuous nature, rather than distinct populations, both in regard to various cell surface markers but also the classical heterogeneity markers chymase and CPA3 (6). Similarly, a recent scRNAseq study of human mast cells from nasal polyps in patients with chronic rhinosinusitis with nasal polyososis (CRSwNP) also found the heterogeneity of the mast cells to be of a continuous transient nature from MC_T to MC_{TC}, but the study also found a separate cluster of proliferative mast cells (7).

Several scRNAseq studies using droplet based techniques have been performed on lung tissue in different human diseases, including asthma (8), COPD (9, 10), COVID-19 (11) and lung cancer (12, 13), and a mast cell cluster has been detected in these studies. The mast cell cluster was shown to be enriched in asthma (8) and in one COPD study (9), but the same was not seen in a separate COPD study (10). However, these studies have not been focused on mast cells, and the heterogeneity of the mast cells have therefore not been examined.

In this study, we set out to investigate the heterogeneity of sorted human lung mast cells by scRNAseq using SmartSeq2, a method that provides deeper sequencing than the previous studies that have used droplet-based techniques.

Materials and methods

Ethical approval

The local ethics committee approved the collection of lung tissue from patients undergoing lobectomy, and all patients provided informed consent (Regionala Etikprövningsnämnden Stockholm, 2010/181-31/2).

Cell preparation

Lung tissue was obtained from patients undergoing lobectomy due to lung cancer (age 57–76 year old, three females, one male). All patients were ex smokers and none of them had preoperative chemo- or radiotherapy. Macroscopically healthy tissue distal to the tumour was used. Single-cell suspensions were obtained by digesting the tissue as previously described (14). Briefly, human lung tissue was cut into small pieces and enzymatically digested for 45 min with DNase I and collagenase. Thereafter, the tissue was mechanically disrupted by shearing with a syringe, debris was removed by 30% Percoll centrifugation and red blood cells lysed with an ACK buffer.

Flow cytometry analysis and cell sorting

For single cell sorting of mast cells the following antibodies were used: V500-CD45 (BD Biosciences, clone HI30), FITC- CD3 (Biolegend, clone SK7), FITC- CD19 (BD Biosciences, clone 4G7), FITC- CD14 (Dako, clone TUK4), FITC- CD1a (Biolegend, clone HI149), FITC- CD123 (Biolegend, clone 6H6), FITC- BDCA2 (Miltenyi Biotech, clone AC144), FITC- TCR α/β (Biolegend, clone IP26), FITC- TCR γ/δ (Biolegend, clone B1), FITC- CD94 (Biolegend, clone DX22), FITC- CD34 (Biolegend, clone 581), PECy5.5-CD117 (Beckman Coulter, clone 104D2D1), and Invitrogen Live/Dead™ Fixable Green Dead Cell Stain kit. FlowJo software was used for flow cytometry data analysis. The mast cells were gated as Live cells, Lineage negative (CD3, CD14, CD19, CD1a, CD123, BDCA2, TCRα/β, TCR γ/δ, CD94, CD34), CD45 positive and CD117 high.

Single cell RNA sequencing

The isolated human lung mast cells were single cell sorted into 384 well plate containing lysis buffer using a BD FACS Fusion. In total, 332 single mast cells were sorted from 4 lung tissues (83 mast cells per tissue).The quality of cDNA was assessed by agilent high sensitivity DNA assay as previously described (15). Single cell RNA sequencing (scRNA seq) libraries were prepared and sequenced using Smart-seq2 protocol (16) by the SciLifeLab Eukaryotic Single-cell Genomics Facility, Stockholm.

Data processing and analyses

Data processing and analyses was performed by the National Bioinformatics Infrastructure Sweden (NBIS) and the computations were performed on resources provided by SNIC through Uppsala Multidisciplinary Center for Advanced Computational Science (UPPMAX). Reads were aligned to the reference genome GRCh38 (primary assembly) using star/2.5.3a with default settings (17). Counts per gene (an arbitrary unit of the number or reads that were detected per gene) were calculated for each

10.3389/fimmu.2023.1151754

transcript using featureCounts from subread/1.5.2 using parameters -t exon -g gene_id (18).

The following analysis were performed using R version 3.6.3 (R Core Team 2020). Poor quality cells were excluded. Cells were considered of poor quality if they were outliers (defined using median absolute deviations (MADs)) in at least one of 6 criteria listed (1): cells with percentage of uniquely mapped reads with more than 3 MADs below the median (global median from all plates) (2) cells with percentage of uniquely mapped reads mapping to protein coding regions with more than 3 MADs below the median (global median from all plates) (3) cells with proportions of reads mapped to spike-in transcripts that are more than 3 MADs above the median (global median from all plates) (4) cells with proportions of mitochondrial reads that are more than 3 MADs above the median (global median from all plates) (5) cells with log-library sizes that are more than 3 MADs below the median log-library size of each plate (6) cells which log-transformed number of expressed genes that are more than 3 MADs below the median of each plate.

Genes with no expression (0 count across all mast cells) were removed as well as mitochondrial genes and rRNA genes. Counts were normalized using the logNormCounts function of the scater R/Bioconductor package version 1.14.6 where counts are divided by a cell-specific size factor (19).

Most analyzes were done separately on each plate so no batch correction was performed. The distribution of gene expression of selected marker genes (selected proteases, cell surface receptors and lipid metabolism genes) and the top 20 expressed genes was visualized using violin plots. For each plate, per-gene variance was modeled using spike-ins, highly variable genes across cells were selected using the scran Bioconductor package version 1.14.6 (20). Several dimensionality reduction methods were computed on highly variables genes on the single cell data for each plate separately. Principal Component Analysis (PCA) on the centered normalized log counts (the first 3 principal components were plotted). Uniform Manifold Approximation and Projection (UMAP) on the normalized log counts. t-Distributed Stochastic Neighbor Embedding (tSNE) on the normalized log counts with a perplexity parameter of 100.

The 2-by-2 correlations between CMA1, CPA3 and CTSG was assessed using scatter plots and Spearman's rank correlation coefficients.

Results

scRNA sequencing of human lung mast cells

Human lung mast cell heterogeneity has been thoroughly examined using immunohistochemistry and flow cytometry (5, 6). However, an unbiased high throughput investigation into human lung mast cell heterogeneity has not been performed. We therefore set out to perform scRNAseq on sorted human lung mast cells. The mast cells were gated as Live Lin^- $CD45^+$ $CD117^{high}$ (Figure 1) and scRNAseq was performed using the Smart-seq2 protocol. Among the genes with the highest counts (Figures 2A, B, Supplementary Figure S1) were many known mast cell genes such as the receptor for stem cell factor *KIT*, that is needed for mast cell maturation and survival, the mast cell proteases tryptase (*TPSAB1*) and carboxypeptidase A3 (*CPA3*), the proteoglycan serglycin (*SRGN*) that is needed for the packing of biogenic amines (histamine, serotonin, dopamine) and proteases in the secretory granules (21–23), and histidine decarboxylase (*HDC*) that is the rate limiting enzyme in the biosynthesis of histamine. However, we also noted four cells that had low to undetectable level of several mast cell signature genes, including TPSAB1, TPSB2, CPA3, HDC and IL1RL1, indicating that these could be contaminating non-mast cells (data not shown).

Many of the highest expressed genes were also involved in basic functions of cells and therefore highly expressed in most cells such as β2 microglobulin (*B2M*), β-actin (*ACTB*), vimentin (*VIM*), lamin (*LMNA*), glutamine synthase (*GLUL*). *MALAT1* is a long non-coding RNA that is frequently high in poly-A captured RNA sequencing data (24, 25). There are also several genes involved in transcription and translation, such as transcription factors *NFKBIA* and *FOSB*, regulator of transcription and splicing *DDX5*, and regulator of translation initiation *EIF1*, regulator of the transcription complex and chaperone *HSP90AA1*. Annexin A1 (*ANX1*) is a protein that binds phospholipids and inhibits phospholipase A2. Synthesis and secretion of annexin A1 is enhanced by glucocorticoids (26, 27) and mast cell activation is inhibited by annexin A1 (28). Another highly expressed gene was CD44, a ubiquitously expressed adhesion molecule with several ligands, including hyaluronic acid, that previously has been shown to be expressed by human mast cells (29, 30).

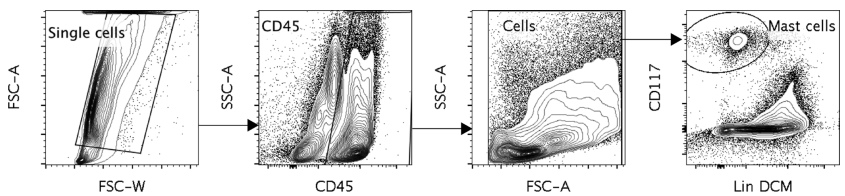

FIGURE 1
A representative figure of the gating of the human lung mast cells. Cells were gated as Single cells, $CD45^{+}$ cells selected in the FSC, SSC pattern, $CD117^{high}$, dead cell marker (DCM) ^{Low} and Lineage (Lin) ^{Low}. The Lineage markers consisted of CD3, CD14, CD19, CD1a, CD123, BDCA2, TCRα/β, TCR γ/δ, CD94 and CD34.

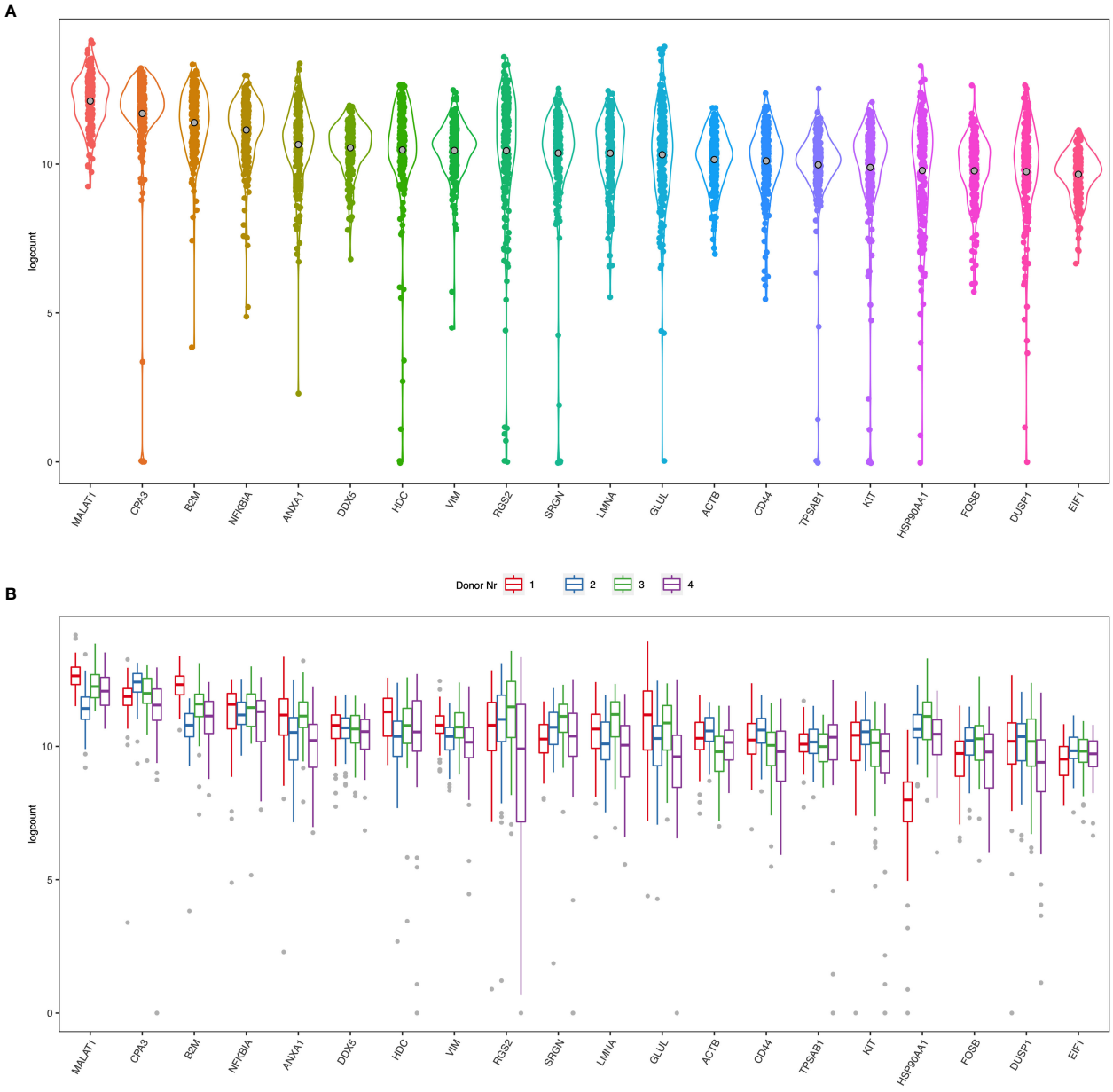

FIGURE 2
(A) Violin plots of the top 20 ranked genes in the dataset from all four donors **(B)** Boxplots of the top 20 ranked genes separated by each donor.

Heterogenous expression of mast cell genes

Next, we specifically examined the heterogeneity of expression of selected mast-cell related genes. The cell surface receptors *KIT* and the IL-33 receptor ST2 (*IL1RL1*) were as expected high in most cells, while the two of the subunits of the FcεRI receptor (*FCER1A* and *MS4A2*) and CD203c (*ENPP3*) had a more diverse expression pattern (Figure 3). Of the enzymes involved in lipid metabolism, arachidonate 5-lipoxygenase (*ALOX5*, also known as 5-LOX) was highly detectable in most cells (Figure 3). 5-LOX converts arachidonic acid to leukotriene A4 (LTA4), that is further metabolized to LTB_4 by LTA4 hydrolase (LTA4H) or to LTC_4 by leukotriene C4 synthase (LTC4S). In the human lung mast cells *LTA4H* was only detectable in a small proportion of the cells, while *LTC4S* was detectable in a higher proportion of the cells and had a variable expression pattern (Figure 3). Both cyclooxygenases that converts arachidonic acid to prostaglandin endoperoxide H2 (a precursor for the prostaglandins D_2, E_2 and F_2), prostaglandin-endoperoxide synthase 1 (*PTGS1*- also known as cyclooxygenase 1 (COX-1)) and *PTGS2* (also known as COX-2) were variably expressed (Figure 3). Of the proteases, the tryptases (*TPSAB1* and *TPSB2*) and CPA3 were high in most cells whereas chymase (*CMA1*) and Cathepsin G (*CTSG*) had a variable expression pattern (Figure 3).

10.3389/fimmu.2023.1151754

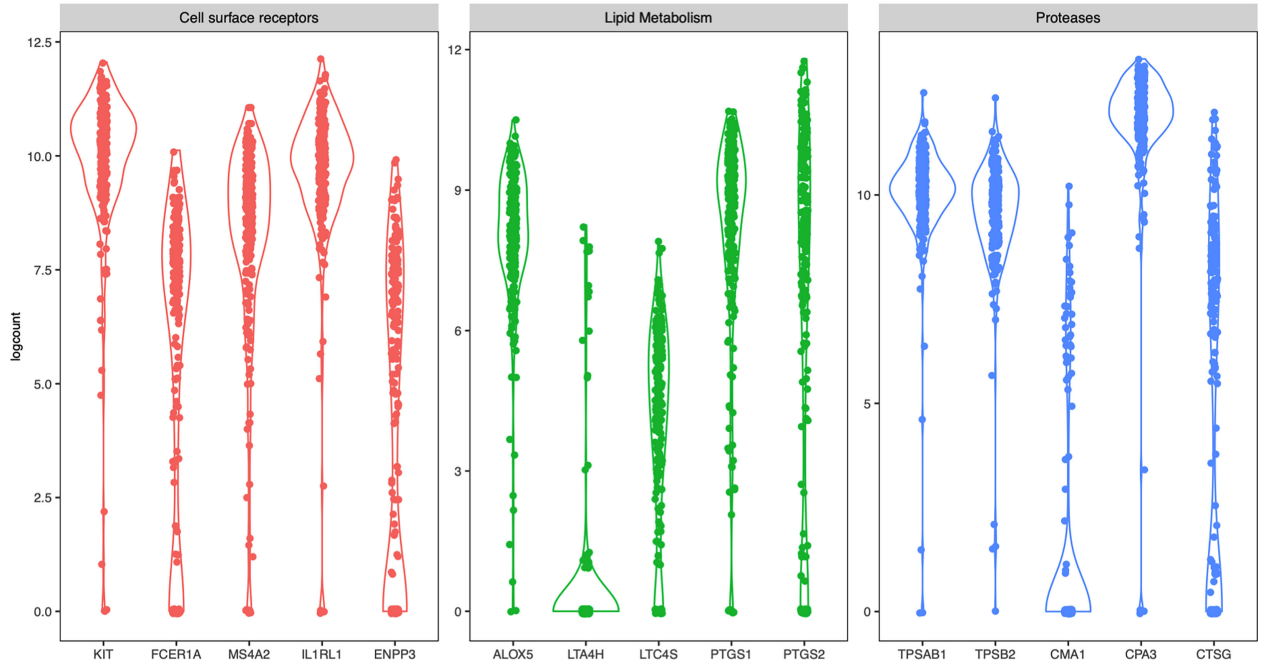

FIGURE 3
Violin plots of selected mast cells signature genes from all four donors.

No distinct mast cell subsets were detected

To examine possible subsets of human lung mast cells we used three different methods to cluster the cells based on the scRNAseq data: PCA, UMAP and tSNE plots. None of these three methods provided any obvious sub-clusters (one representative donor in Figure 4 and the additional three donor in Supplementary Figure S2). We noted that there were a few cells that positioned apart from the main cell cluster in two donors, these cells were mainly the suspected non- mast cells that had low to undectectable levels of the mast cell signature genes (Supplementary Figures S2A, C). To specifically examine the classical mast cell subsets MC_T and MC_{TC}, we examined the correlation in expression between the proteases that are present in the MC_{TC} subset, that is chymase, CPA3 and cathepsin G. To the contrary of the protein (6), the *CPA3* mRNA was highly detectable in all cells, and the correlation to *CMA1* and *CTSG* was weak (Figure 5). In contrast, the chymase, *CMA1* expression was only detected in a small fraction of the cells that also had relatively high *CTSG* expression, but on the other hand there where cells with high *CTSG* that did not have detectable *CMA1* expression. Thus, *CMA1* correlated moderately with that of *CTSG* with a Spearman's rank correlation coefficient of 0.5 (Figure 5). *CTSG* and *CMA1* did not show correlation (moderate or high, r_s>0.4) to any other genes in the dataset (Supplementary Tables S1, S2).

Discussion

We have investigated the heterogeneity of human lung mast cells using SmartSeq2, a method that provides deep sequencing of single cells. Among the genes with the highest counts were several mast cell genes, including *KIT*, tryptase (*TPSAB1*), carboxypeptidase A3 (*CPA3*), serglycin (*SRGN*), histidine decarboxylase (*HDC*), verifying the identity of the cells as mast cells.

The expression of two subunits of the FcεRI receptor was shown to be variable (Figure 3), they did not however correlate to each other (data not shown). Variable surface expression of FcεRI has previously been reported on human lung mast cells as well as for human skin mast cells (6, 31). The expression of the FcεRI protein on mast cells has also been shown to vary between different lung compartments, i.e. central airways, small airways, parenchyma, and pulmonary vessels, with particularly low expression on the parenchymal mast cells (5). The low parenchymal expression of FcεRI in healthy subjects is, however, increased in patients with atopic uncontrolled asthma (32). The underlying mechanism for the varying FcεRI expression is not completely known. The FcεRI mRNA expression has been shown to be regulated by IL-4 (33) and IL-33 (34, 35), and the receptor is stabilized on the cell-surface by the presence of IgE (36), but other mechanisms might also be involved in the regulation.

The main prostanoid released from human mast cells upon activation is PGD_2 (37–39), which have potent biological effects in the lung, such as broncoconstriction (40), vasodilation (41), and activation and recruitment of group 2 innate lymphoid cells (42). The first step in the biosynthesis of PGD_2, is catalyzed by two enzymes COX-1 (*PTGS1*) and COX-2 (*PTGS2*). In our study both genes encoding for COX-1 and -2, *PTGS1* and *PTGS2*, were variably expressed (Figure 3). However, the expression of the two genes did not correlate to each other (data not shown). Additionally, in nasal polyps, *PTGS2* is enriched in the MC_{TC} cluster (7), which we could not observe in HLMC. In human mast cells, PGD_2 biosynthesis

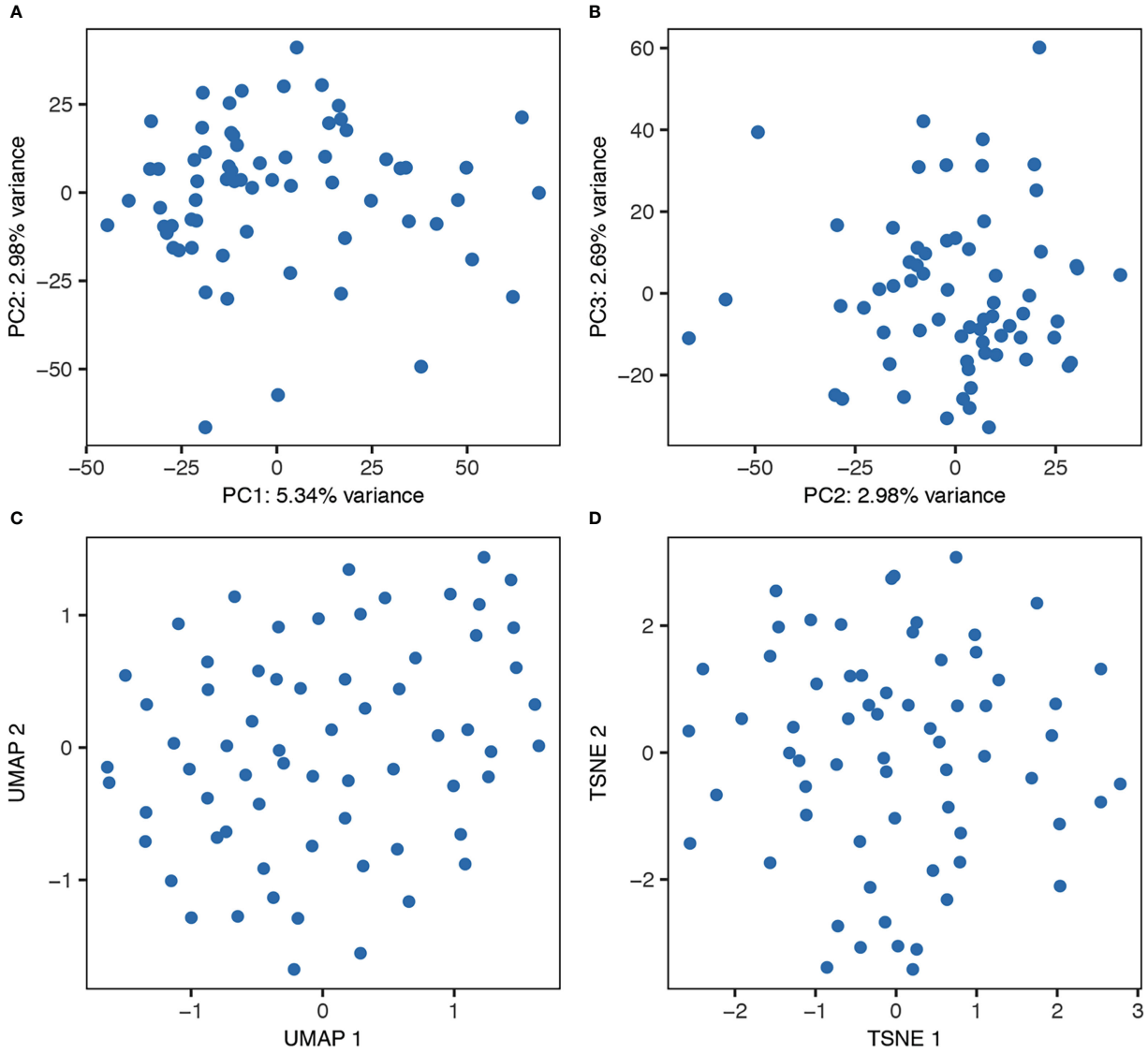

FIGURE 4
Unbiased clustering of the cells from one representative donor using PCA **(A, B)**, UMAP **(C)**, and tSNE **(D)**.

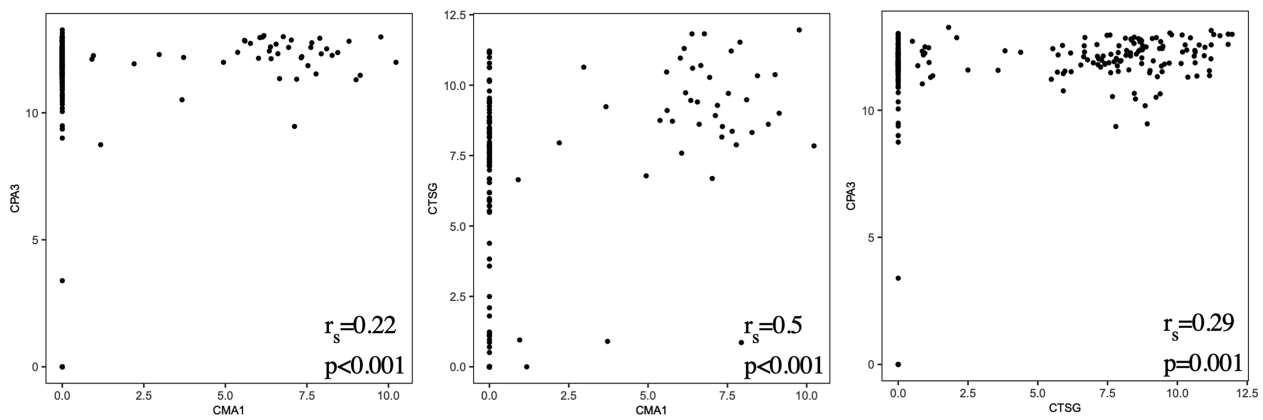

FIGURE 5
Scatter plots of *CPA3/CMA1/CTSG* expression from all four donors and Spearman's rank correlation coefficients (r_s).

have been shown to be entirely dependent on COX-1 (37, 43), so, why *PTGS2* (COX-2) is transcribed in these cells and under what conditions it is enzymatically active remains to be elucidated.

Human mast cells have been shown to be heterogeneous when it comes to the presence of proteases and thus divided into MC_T and MC_{TC} depending on their expression of chymase (*CMA1*). The MC_{TC} subset has in addition also been shown to contain CPA3 and cathepsin G (44, 45). Human lung mast cells are predominantly of the MC_T subtype, and consistent with this *CMA1* was only detectable in a small proportion of the cells (Figures 3, 5). We found high expression of *CPA3* mRNA in all lung mast cells and the correlation of this expression to *CMA1* was weak (Figures 3, 5). In contrast, CPA3 and chymase proteins strongly correlate in human lung mast cells as judged by flow cytometry (6). This discrepancy of CPA3 mRNA and protein has also been shown in human lung mast cells using RNAscope and immunohistochemistry (46). When the gene for the equivalent to chymase in mice (based on sequence alignment), mouse mast cells protease- 5 (mMCP-5), is deleted the granule storage of CPA3 is lost, despite the *CPA3* mRNA expression being unaffected (47). Similarly, if the *CPA3* gene is deleted, the granule storage of the mMCP-5 protein is lost (48). However, when CPA3 is mutated to render it inactive without deletion of the CPA3 protein, the storage of mMCP-5 is unaffective (49). Thus, in mice mMCP-5 and CPA3 protein are interdependent on each other for their granule storage in mast cells. One can speculate that the same situation could be true for human CPA3, that chymase needs to be present for the CPA3 protease to be stored in the granules. Supporting this hypothesis is the finding that when comparing lung and skin mast cells, skin mast cells have higher expression of chymase and store more CPA3 protein in spite of expressing lower level of *CPA3* mRNA. This theory does however raise the question; why do the cells express high levels of the mRNA if the protein is not stored? Is there a high CPA3 turnover or perhaps a continuous release of CPA3 in the MC_T subtype? Further studies are needed to answer these questions.

The mast cells in this study comes from lobectomies performed on cancer patients. The tissue used was macroscopically healthy distal to the tumour, nevertheless it is of course possible that the disease has affected the included mast cells. In this context it is worth noting that CPA3 counts were high (Figure 3) and CPA3 expression has been shown to correlate to decreased lung function in patients with severe chronic obstructive pulmonary disease (COPD) and idiopathic lung fibrosis (IPF) (50).

The aim of the present study was to investigate human lung mast cell heterogeneity in more depth using SmartSeq2 single-cell RNA sequencing. However, we could not detect any obvious transcriptional different subpopulations of the human lung mast cells (Figure 4). There could be several explanations for this. The human lung mast cells could be homogenous in nature but it could also be that the number of mast cells analyzed are too low to distinguish small subsets. The facts that the mRNA of one of the proteases present in the MC_{TC} subtype, *CPA3*, does not correlate to the protein, and that no other genes then *CTSG* show a correlation (r_s>0.4) to *CMA1*, likely contribute to the inability to distinguish the classical mast cell subsets based on unbiased clustering. Furthermore, our study covered mainly mast cells in the parenchyma and it might be that mast cells in different compartments of the lung show greater heterogeneity. Thus, additional analyses including higher number of single mast cells from different lung compartments will be instrumental to decipher further the heterogeneity of human lung mast cells.

Data availability statement

The data presented in the study are deposited in the Gene Expression Omnibus (GEO) repository, accession number GSE227712.

Ethics statement

The studies involving human participants were reviewed and approved by Regionala Etikprövningsnämden i Stockholm. The patients/participants provided their written informed consent to participate in this study.

Author contributions

GN, JM, AR, ER, and JD, conceived and designed the studies. AR, and LM, performed the experiments. JL, OD, YG, ER, and JD analyzed the data. JS, A-CO, MA-A, MA and S-ED provided samples. ER, AR and GN wrote the manuscript draft. All authors contributed to the article and approved the submitted version.

Funding

This study was supported by grants from the Swedish Research Council (2018-02070, 2020-01693, and 2022-00558); the Heart-Lung Foundation; The Swedish Cancer Society; the Ollie and Elof Ericssons Foundation, the Ellen, Walter and Lennart Hesselman Foundation; the Tore Nilsson Foundation; the Lars Hierta Memorial Foundation; the Konsul Th C Bergh Foundation; the Tornspiran Foundation; the O. E. and Edla Johanssons Foundation; the Swedish Society for Medical Research; The Magnus Bergvall Foundation; The Åke Wiberg Foundation; The Centre for Allergy Research Highlights Asthma Markers of Phenotype (ChAMP) consortium funded by the Swedish Foundation for Strategic Research; the AstraZeneca & Science for Life Laboratory Joint Research Collaboration; the Vårdal Foundation and the Karolinska Institutet. The authors declare that this study received funding from AstraZeneca. The funder was not involved in the study design, collection, analysis, interpretation of data, the writing of this article, or the decision to submit it for publication.

Acknowledgments

We would like to acknowledge support from National Bioinformatics Infrastructure Sweden (NBIS), Science for Life

Laboratory, the National Genomics Infrastructure (NGI), Swedish National Infrastructure for Computing (SNIC) and Uppsala Multidisciplinary Center for Advanced Computational Science (UPPMAX) for providing assistance in bioinformatics, massively parallel sequencing analysis and computational infrastructure.

Conflict of interest

S-ED reports personal fees from AstraZeneca, Cayman Chemicals, GSK, Novartis, Regeneron, Sanofi, and Teva, for consultancies outside the submitted work.

The remaining authors declare that the research was conducted in the absence of any commercial or financial relationships that could be construed as a potential conflict of interest.

Publisher's note

Supplementary material

The Supplementary Material for this article can be found online at: https://www.frontiersin.org/articles/10.3389/fimmu.2023.1151754/full#supplementary-material

References

1. Bradding P, Arthur G. Mast cells in asthma–state of the art. *Clin Exp Allergy* (2016) 46(2):194–263. doi: 10.1111/cea.12675

2. Erjefalt JS. Mast cells in human airways: The culprit? *Eur Respir Rev* (2014) 23 (133):299–307. doi: 10.1183/09059180.00005014

3. Dahlin JS, Maurer M, Metcalfe DD, Pejler G, Sagi-Eisenberg R, Nilsson G. The ingenious mast cell: Contemporary insights into mast cell behavior and function. *Allergy* (2021) 77(1):83–99. doi: 10.1111/all.14881

4. Irani AA, Schechter NM, Craig SS, DeBlois G, Schwartz LB. Two types of human mast cells that have distinct neutral protease compositions. *Proc Natl Acad Sci U.S.A.* (1986) 83(12):4464–8. doi: 10.1073/pnas.83.12.4464

5. Andersson CK, Mori M, Bjermer L, Lofdahl CG, Erjefalt JS. Novel site-specific mast cell subpopulations in the human lung. *Thorax* (2009) 64(4):297–305. doi: 10.1136/thx.2008.101683

6. Ronnberg E, Boey DZH, Ravindran A, Safholm J, Orre AC, Al-Ameri M, et al. Immunoprofiling reveals novel mast cell receptors and the continuous nature of human lung mast cell heterogeneity. *Front Immunol* (2021) 12:804812. doi: 10.3389/fimmu.2021.804812

7. Dwyer DF, Ordovas-Montanes J, Allon SJ, Buchheit KM, Vukovic M, Derakhshan T, et al. Human airway mast cells proliferate and acquire distinct inflammation-driven phenotypes during type 2 inflammation. *Sci Immunol* (2021) 6 (56):eabb7221. doi: 10.1126/sciimmunol.abb7221

8. Vieira Braga FA, Kar G, Berg M, Carpaij OA, Polanski K, Simon LM, et al. A cellular census of human lungs identifies novel cell states in health and in asthma. *Nat Med* (2019) 25(7):1153–63. doi: 10.1038/s41591-019-0468-5

9. Sauler M, McDonough JE, Adams TS, Kothapalli N, Barnthaler T, Werder RB, et al. Characterization of the copd alveolar niche using single-cell rna sequencing. *Nat Commun* (2022) 13(1):494. doi: 10.1038/s41467-022-28062-9

10. Li X, Noell G, Tabib T, Gregory AD, Trejo Bittar HE, Vats R, et al. Single cell rna sequencing identifies Igfbp5 and qki as ciliated epithelial cell genes associated with severe copd. *Respir Res* (2021) 22(1):100. doi: 10.1186/s12931-021-01675-2

11. Delorey TM, Ziegler CGK, Heimberg G, Normand R, Yang YM, Segerstolpe A, et al. Covid-19 tissue atlases reveal sars-Cov-2 pathology and cellular targets. *Nature* (2021) 595(7865):107. doi: 10.1038/s41586-021-03570-8

12. Wu F, Fan J, He Y, Xiong A, Yu J, Li Y, et al. Single-cell profiling of tumor heterogeneity and the microenvironment in advanced non-small cell lung cancer. *Nat Commun* (2021) 12(1):2540. doi: 10.1038/s41467-021-22801-0

13. Lu T, Yang X, Shi Y, Zhao M, Bi G, Liang J, et al. Single-cell transcriptome atlas of lung adenocarcinoma featured with ground glass nodules. *Cell Discovery* (2020) 6:69. doi: 10.1038/s41421-020-00200-x

14. Ravindran A, Ronnberg E, Dahlin JS, Mazzurana L, Safholm J, Orre AC, et al. An optimized protocol for the isolation and functional analysis of human lung mast cells. *Front Immunol* (2018) 9:2193. doi: 10.3389/fimmu.2018.02193

15. Bjorklund AK, Forkel M, Picelli S, Konya V, Theorell J, Friberg D, et al. The heterogeneity of human Cd127(+) innate lymphoid cells revealed by single-cell rna sequencing. *Nat Immunol* (2016) 17(4):451–60. doi: 10.1038/ni.3368

16. Picelli S, Faridani OR, Bjorklund AK, Winberg G, Sagasser S, Sandberg R. Full-length rna-seq from single cells using smart-Seq2. *Nat Protoc* (2014) 9(1):171–81. doi: 10.1038/nprot.2014.006

17. Dobin A, Davis CA, Schlesinger F, Drenkow J, Zaleski C, Jha S, et al. Star: Ultrafast universal rna-seq aligner. *Bioinformatics* (2013) 29(1):15–21. doi: 10.1093/bioinformatics/bts635

18. Liao Y, Smyth GK, Shi W. The subread aligner: Fast, accurate and scalable read mapping by seed-and-Vote. *Nucleic Acids Res* (2013) 41(10):e108. doi: 10.1093/nar/gkt214

19. McCarthy DJ, Campbell KR, Lun AT, Wills QF. Scater: Pre-processing, quality control, normalization and visualization of single-cell rna-seq data in r. *Bioinformatics* (2017) 33(8):1179–86. doi: 10.1093/bioinformatics/btw777

20. Lun AT, McCarthy DJ, Marioni JC. A step-by-Step workflow for low-level analysis of single-cell rna-seq data with bioconductor. *F1000Res* (2016) 5:2122. doi: 10.12688/f1000research.9501.2

21. Ronnberg E, Calounova G, Pejler G. Mast cells express tyrosine hydroxylase and store dopamine in a serglycin-dependent manner. *Biol Chem* (2012) 393(1-2):107–12. doi: 10.1515/BC-2011-220

22. Ringvall M, Ronnberg E, Wernersson S, Duelli A, Henningsson F, Abrink M, et al. Serotonin and histamine storage in mast cell secretory granules is dependent on serglycin proteoglycan. *J Allergy Clin Immunol* (2008) 121(4):1020–6. doi: 10.1016/j.jaci.2007.11.031

23. Abrink M, Grujic M, Pejler G. Serglycin is essential for maturation of mast cell secretory granule. *J Biol Chem* (2004) 279(39):40897–905. doi: 10.1074/jbc.M405856200

24. Aissa AF, Islam A, Ariss MM, Go CC, Rader AE, Conrardy RD, et al. Single-cell transcriptional changes associated with drug tolerance and response to combination therapies in cancer. *Nat Commun* (2021) 12(1):1628. doi: 10.1038/s41467-021-21884-z

25. Zhang B, Arun G, Mao YS, Lazar Z, Hung G, Bhattacharjee G, et al. The lncrna Malat1 is dispensable for mouse development but its transcription plays a cis-regulatory role in the adult. *Cell Rep* (2012) 2(1):111–23. doi: 10.1016/j.celrep.2012.06.003

26. Hannon R, Croxtall JD, Getting SJ, Roviezzo F, Yona S, Paul-Clark MJ, et al. Aberrant inflammation and resistance to glucocorticoids in annexin 1-/- mouse. *FASEB J* (2003) 17(2):253–5. doi: 10.1096/fj.02-0239fje

27. Peers SH, Smillie F, Elderfield AJ, Flower RJ. Glucocorticoid-and non-glucocorticoid induction of lipocortins (Annexins) 1 and 2 in rat peritoneal leucocytes in vivo. *Br J Pharmacol* (1993) 108(1):66–72. doi: 10.1111/j.1476-5381.1993.tb13441.x

28. Sinniah A, Yazid S, Bena S, Oliani SM, Perretti M, Flower RJ. Endogenous annexin-A1 negatively regulates mast cell-mediated allergic reactions. *Front Pharmacol* (2019) 10:1313. doi: 10.3389/fphar.2019.01313

29. Valent P, Majdic O, Maurer D, Bodger M, Muhm M, Bettelheim P. Further characterization of surface membrane structures expressed on human basophils and mast cells. *Int Arch Allergy Appl Immunol* (1990) 91(2):198–203. doi: 10.1159/000235115

30. Girodet PO, Ozier A, Trian T, Begueret H, Ousova O, Vernejoux JM, et al. Mast cell adhesion to bronchial smooth muscle in asthma specifically depends on Cd51 and Cd44 variant 6. *Allergy* (2010) 65(8):1004–12. doi: 10.1111/j.1398-9995.2009.02308.x

31. Babina M, Guhl S, Artuc M, Trivedi NN, Zuberbier T. Phenotypic variability in human skin mast cells. *Exp Dermatol* (2016) 25(6):434–9. doi: 10.1111/exd.12924

32. Andersson CK, Bergqvist A, Mori M, Mauad T, Bjermer L, Erjefalt JS. Mast cell-associated alveolar inflammation in patients with atopic uncontrolled asthma. *J Allergy Clin Immunol* (2011) 127(4):905–12 e1-7. doi: 10.1016/j.jaci.2011.01.022

33. Toru H, Ra C, Nonoyama S, Suzuki K, Yata J, Nakahata T. Induction of the high-affinity ige receptor (Fc epsilon ri) on human mast cells by il-4. *Int Immunol* (1996) 8 (9):1367–73. doi: 10.1093/intimm/8.9.1367

34. Ronnberg E, Ghaib A, Ceriol C, Enoksson M, Arock M, Safholm J, et al. Divergent effects of acute and prolonged interleukin 33 exposure on mast cell ige-mediated functions. *Front Immunol* (2019) 10:1361. doi: 10.3389/fimmu.2019.01361

35. Babina M, Wang Z, Franke K, Guhl S, Artuc M, Zuberbier T. Yin-yang of il-33 in human skin mast cells: Reduced degranulation, but augmented histamine synthesis through P38 activation. *J Invest Dermatol* (2019) 139(7):1516–25.e3. doi: 10.1016/j.jid.2019.01.013

36. Kraft S, Kinet JP. New developments in fcepsilonri regulation, function and inhibition. *Nat Rev Immunol* (2007) 7(5):365–78. doi: 10.1038/nri2072

37. Johnsson AK, Choi JH, Ronnberg E, Fuchs D, Kolmert J, Hamberg M, et al. Selective inhibition of prostaglandin D2 biosynthesis in human mast cells to overcome need for multiple receptor antagonists: Biochemical consequences. *Clin Exp Allergy* (2021) 51(4):594–603. doi: 10.1111/cea.13831

38. Lewis RA, Soter NA, Diamond PT, Austen KF, Oates JA, Roberts LJ2nd. Prostaglandin D2 generation after activation of rat and human mast cells with anti-ige. *J Immunol* (1982) 129(4):1627–31. doi: 10.4049/jimmunol.129.4.1627

39. Peters SP, MacGlashan DWJr., Schulman ES, Schleimer RP, Hayes EC, Rokach J, et al. Arachidonic acid metabolism in purified human lung mast cells. *J Immunol* (1984) 132(4):1972–9. doi: 10.4049/jimmunol.132.4.1972

40. Hardy CC, Robinson C, Tattersfield AE, Holgate ST. The bronchoconstrictor effect of inhaled prostaglandin D2 in normal and asthmatic men. *N Engl J Med* (1984) 311(4):209–13. doi: 10.1056/NEJM198407263110401

41. Alving K, Matran R, Lundberg JM. The possible role of prostaglandin D2 in the long-lasting airways vasodilatation induced by allergen in the sensitized pig. *Acta Physiol Scand* (1991) 143(1):93–103. doi: 10.1111/j.1748-1716.1991.tb09204.x

42. Xue L, Salimi M, Panse I, Mjosberg JM, McKenzie AN, Spits H, et al. Prostaglandin D2 activates group 2 innate lymphoid cells through chemoattractant receptor-homologous molecule expressed on Th2 cells. *J Allergy Clin Immunol* (2014) 133(4):1184–94. doi: 10.1016/j.jaci.2013.10.056

43. Baothman BK, Smith J, Kay LJ, Suvarna SK, Peachell PT. Prostaglandin D2 generation from human lung mast cells is catalysed exclusively by cyclooxygenase-1. *Eur J Pharmacol* (2018) 819:225–32. doi: 10.1016/j.ejphar.2017.12.005

44. Schechter NM, Irani AM, Sprows JL, Abernethy J, Wintroub B, Schwartz LB. Identification of a cathepsin G-like proteinase in the mctc type of human mast cell. *J Immunol* (1990) 145(8):2652–61. doi: 10.4049/jimmunol.145.8.2652

45. Irani AM, Goldstein SM, Wintroub BU, Bradford T, Schwartz LB. Human mast cell carboxypeptidase. *Selective Localization to Mctc Cells J Immunol* (1991) 147 (1):247–53.

46. Siddhuraj P, Clausson CM, Sanden C, Alyamani M, Kadivar M, Marsal J, et al. Lung mast cells have a high constitutive expression of carboxypeptidase A3 mrna that is independent from granule-stored Cpa3. *Cells* (2021) 10(2):309. doi: 10.3390/cells10020309

47. Stevens RL, McNeil HP, Wensing LA, Shin K, Wong GW, Hansbro PM, et al. Experimental arthritis is dependent on mouse mast cell protease-5. *J Biol Chem* (2017) 292(13):5392–404. doi: 10.1074/jbc.M116.773416

48. Feyerabend TB, Hausser H, Tietz A, Blum C, Hellman L, Straus AH, et al. Loss of histochemical identity in mast cells lacking carboxypeptidase a. *Mol Cell Biol* (2005) 25(14):6199–210. doi: 10.1128/MCB.25.14.6199-6210.2005

49. Schneider LA, Schlenner SM, Feyerabend TB, Wunderlin M, Rodewald HR. Molecular mechanism of mast cell mediated innate defense against endothelin and snake venom sarafotoxin. *J Exp Med* (2007) 204(11):2629–39. doi: 10.1084/jem.20071262

50. Siddhuraj P, Jonsson J, Alyamani M, Prabhala P, Magnusson M, Lindstedt S, et al. Dynamically upregulated mast cell Cpa3 patterns in chronic obstructive pulmonary disease and idiopathic pulmonary fibrosis. *Front Immunol* (2022) 13:924244. doi: 10.3389/fimmu.2022.924244

frontiers | Frontiers in Immunology

TYPE Original Research
PUBLISHED 09 May 2023
DOI 10.3389/fimmu.2023.1155740

OPEN ACCESS

EDITED BY
Carlo Pucillo,
University of Udine, Italy

REVIEWED BY
Violetta Borelli,
University of Trieste, Italy
Marco De Zuani,
Wellcome Sanger Institute (WT),
United Kingdom

*CORRESPONDENCE
Marianna Kulka
Marianna.Kulka@nrc-cnrc.gc.ca

RECEIVED 31 January 2023
ACCEPTED 17 April 2023
PUBLISHED 09 May 2023

CITATION
Raj S, Hlushak S, Arizmendi N, Kovalenko A and Kulka M (2023) Substance P analogs devoid of key residues fail to activate human mast cells *via* MRGPRX2. *Front. Immunol.* 14:1155740. doi: 10.3389/fimmu.2023.1155740

Substance P analogs devoid of key residues fail to activate human mast cells *via* MRGPRX2

Shammy Raj[1], Stepan Hlushak[2], Narcy Arizmendi[1], Andriy Kovalenko[1] and Marianna Kulka[1,3]*

[1]Nanotechnology Research Centre, National Research Council Canada, Edmonton, AB, Canada, [2]Department of Mechanical Engineering, University of Alberta, Edmonton, AB, Canada, [3]Department of Medical Microbiology and Immunology, Katz Group Centre, University of Alberta, Edmonton, AB, Canada

Mast cells play an important role in disease pathogenesis by secreting immunomodulatory molecules. Mast cells are primarily activated by the crosslinking of their high affinity IgE receptors (FcεRI) by antigen bound immunoglobulin (Ig)E antibody complexes. However, mast cells can also be activated by the mas related G protein-coupled receptor X2 (MRGPRX2), in response to a range of cationic secretagogues, such as substance P (SP), which is associated with pseudo-allergic reactions. We have previously reported that the *in vitro* activation of mouse mast cells by basic secretagogues is mediated by the mouse orthologue of the human MRGPRX2, MRGPRB2. To further elucidate the mechanism of MRGPRX2 activation, we studied the time-dependent internalization of MRGPRX2 by human mast cells (LAD2) upon stimulation with the neuropeptide SP. In addition, we performed computational studies to identify the intermolecular forces that facilitate ligand-MRGPRX2 interaction using SP. The computational predictions were tested experimentally by activating LAD2 with SP analogs, which were missing key amino acid residues. Our data suggest that mast cell activation by SP causes internalization of MRGPRX2 within 1 min of stimulation. Hydrogen bonds (h-bonds) and salt bridges govern the biding of SP to MRGPRX2. Arg1 and Lys3 in SP are key residues that are involved in both h-bonding and salt bridge formations with Glu164 and Asp184 of MRGPRX2, respectively. In accordance, SP analogs devoid of key residues (SP1 and SP2) failed to activate MRGPRX2 degranulation. However, both SP1 and SP2 caused a comparable release of chemokine CCL2. Further, SP analogs SP1, SP2 and SP4 did not activate tumor necrosis factor (TNF) production. We further show that SP1 and SP2 limit the activity of SP on mast cells. The results provide important mechanistic insight into the events that result in mast cell activation through MRGPRX2 and highlight the important physiochemical characteristics of a peptide ligand that facilitates ligand-MRGPRX2 interactions. The results are important in understanding activation through MRGPRX2, and the intermolecular forces that govern ligand-MRGPRX2 interaction. The elucidation of important physiochemical properties within a ligand that are needed for receptor interaction will aid in designing novel therapeutics and antagonists for MRGPRX2.

KEYWORDS

MRGPRX2, mast cells, substance P, amino acid residues, ligand-receptor interactions

Introduction

Mast cells (MCs) are sentinel and tissue-resident immune cells that rapidly release a diverse set of immune mediators upon activation (1–3). MCs are important immunomodulatory cells, which are involved in both the homeostatic process as well as in the pathogenic events in several diseases including atopic dermatitis (4), asthma (5), and arthritis (6) among others. Although MCs are classically activated by the antigen bound immunoglobulin (Ig)E and high affinity IgE receptor (FcεRI) complex, MCs are also activated by G protein-coupled receptors (GPCR). Of particular interest is the activation of MCs through the mas related G protein-coupled receptor X2 (MRGPRX2). Since its recent identification as the receptor responsible for pseudoallergic reactions (7), MRGPRX2's role in atopic dermatitis, psoriasis (8), asthma (9), and drug allergies (10) has been explored. Predominantly expressed by connective tissue MCs (MC_{TC}, mast cell that store both tryptase and chymase in their granules) (11), MRGPRX2 is an important biomarker of MCs that is activated by basic secretogogues such as substance P (SP), a neuropeptide involved in allergic inflammation (1, 12).

Since MRGPRX2 is very promiscuous and binds several different protein ligands and small molecules like proadrenomedullin N-terminal peptide, PAMP-12, albumin fragments, and SP, among others (13), it is unclear precisely where these ligands bind the MRGPRX2, and how they interact at a molecular level. Recent break through cryogenic electron microscopic (cryoEM) analyses have described the structure of MRGPRX2 receptor in complex with its ligands like compound 48/80, cortistatin-14, PAMP-12, and SP, and highlight the two distinct sub pockets within the ligand-binding domain of the receptor (14, 15). A highly electronegative sub pocket comprised of Asp184 and Glu164, and a hydrophobic pocket consisting of Trp243 and Phe170, characterize the binding pocket of the receptor. It was shown that mutations at these positions either inhibited or significantly reduced the activity of MRGPRX2 against its agonist compound 48/80 (14). In parallel, the complementary structures of MRGPRX2 ligands have also been examined. It has been shown that the presence of basic and hydrophobic residues within a peptide ligand (PAMP-12 and cortistatin-14), and in a specific peptide sequence, is required for MRGPRX2 activation (16, 17). Although these studies show the importance of amino acid composition on ligand interactions with MRGPRX2, the interaction of SP with MRGPRX2 and its association with specific functional outcomes, such as degranulation and cytokine release is still poorly understood.

In the present article we have examined the activation of MRGPRX2 on human MCs by SP and its analogs. SP is a neuropeptide that regulates several inflammatory diseases such as arthritis, inflammatory bowel disease, and asthma. Our results show that SP triggers a concentration dependent activation of the human mast cell line, LAD2. MRGPRX2 activation causes MRGPRX2 internalization, whereby more than 38% of the receptors are internalized after 1 min of activation. We further conducted molecular dynamic (MD) simulations to identify the important intermolecular forces and the important amino acid residues within SP and MRGPRX2 that facilitate binding. Arg1 and Lys3 in SP were deemed important for SP interaction with MRGPRX2, and the hydrogen bonds (h-bonds) and salt bridges governed the interactions. The computational findings were experimentally validated using SP analogs, wherein, the peptide sequences devoid of Lys3 failed to activate LAD2 cells, while mutations at other sites in SP had no effect on peptide activity in activating mast cells. Furthermore, we show that modulation in the amino acid residues within SP can help in designing potential antagonists of SP, which hold immense potential in therapeutics.

Materials and methods

Cell culture

The LAD2 cell line (a gift from Arnold Kirshenbaum and Dean Metcalfe from the National Institutes of Health, NIAID) was cultured in StemPro-34 SFM media (Life Technologies, Burlington, ON, Canada) supplemented with 2mM L-glutamine, 100 U/ml penicillin, 50 mg/ml streptomycin, and 100 ng/ml recombinant human SCF (Peprotech, Rocky Hill, NJ, USA). Cells were maintained at 1×10^5 cells/ml at 37°C and 5% CO_2 and periodically tested for the expression of CD117 (eBioscience, Invitrogen Carlsbad, CA, USA), and FcεRI (eBioscience, Invitrogen Carlsbad, CA, USA) by flow cytometry using a CytoFlex flow cytometer (Beckman Coulter, Brea, CA, USA).

Degranulation analysis

Degranulation was determined by measuring the release of the granule-associated β-hexosaminidase (β-hex). Briefly, LAD2 cells were washed with 0.4% BSA-HEPES buffer (10 mM HEPES, 137 mM NaCl, 2.7 mM KCl, 5.6 mM glucose, 5.6 mM Na_2HPO_4, 1.8 mM $CaCl_2$, and 1.3 mM $MgSO_4$ at a pH of 7.4) and 5×10^4 cells were added to each well of a 96 well plate, activated with different concentrations (0.1 to 10 µM) of SP and SP analogs (SP1, SP2, SP3, SP4 or SP5, RS synthesis, Louisville, KY, USA) for 30 min at 37°C and 5% CO_2; SP (5 µM, Sigma-Aldrich Canada, Oakville, ON, Canada) was included as positive control. For SP analog analysis, sets of cells were preincubated with SP analogs for 30 min, 1h, and 3h at 37°C, 5% CO_2, followed by 30 min SP treatment. For IgE-dependent activation assays, LAD2 cells were suspended in StemPro-34 SFM media at a cell density of 5×10^4, and sensitized with 0.5 µg/mL biotinylated IgE overnight at 37°C and 5% CO_2, and challenged with 0.1 µg/mL streptavidin for 30 min at 37°C and 5% CO_2. Untreated LAD2 cells were included as negative controls. After activation, LAD2 cells were centrifuged at $200 \times g$ for 5 min, and cell-free supernatants were collected in a different 96 well plate; cell fractions were resuspended and lysed with 0.1% Triton X-100. β-hex release was measured by the hydrolysis of p-nitrophenyl-N-acetyl-β-D-glucosamine (Sigma-Aldrich Canada, Oakville, ON, Canada) in 0.1 M sodium citrate Buffer (pH 4.5), and analyzed using a Biotek Synergy H1 microplate reader (Agilent Technologies, Inc. Santa Clara, CA,

USA). Results are reported as the percentage of intracellular β–hex released into the 0.4% BSA-HEPES buffer after correction for spontaneous release.

Histamine release

Histamine release was measured using *o*-phthalaldehyde as an indicator. Briefly, 1×10^5 LAD2 cells were pelleted at 200 × *g* for 5 min, washed with HEPES buffer, and resuspended in 100 µL HEPES buffer in presence of the indicated concentrations of SP analogs, and incubated for 30 min at 37°C and 5% CO_2. SP, and untreated cells were included as positive and negative controls respectively. Cells were pelleted at 200 × *g* for 5 min, and 60 µL of supernatant were transferred into a black 96 wells microplate (Greiner, Swedesboro, NJ, USA), 12 µL of 1M NaOH were added to the wells, followed by 2 µL of *o*-phthaldialdehyde dissolved in methanol (Sigma-Aldrich Canada, Oakville, ON, Canada) and incubated for 4 min at RT. The reaction was stopped by the addition of 6 µL of 3M HCl. Fluorescence intensity was measured using a 360 nm excitation, and 450 nm emission filters in a BioTek Synergy H1 microplate reader (Agilent Technologies, Inc. Santa Clara, CA, USA). Histamine released was measured by the interpolation from a histamine dihydrochloride (Sigma-Aldrich Canada, Oakville, ON, Canada) standard (8- 500 ng/mL in HEPES buffer) curve. Lower limit of detection for this assay is approximately 5-7 ng/ml (18). For SP analog studies, cells were preincubated with the indicated SP analogs for as indicated, and then were activated by SP for 30 min for the analysis of histamine.

Chemokine and cytokine (CCL2 and TNF) release

LAD2 cells (2×10^6/mL) were incubated for 24 h with 0.1, 1, and 10 µM concentrations of SP and SP analogs, at 37°C and 5% CO_2, and cytokine levels of TNF and CCL2 released in the cell-free supernatants were quantified using commercial enzyme-linked immunosorbent assay (ELISA) according to the manufacturer's (ThermoFisher Scientific, Waltham, MA, USA) instructions. SP-activated cells (5 µM), and untreated cells were included as positive and negative controls respectively. For SP analog studies, cells were preincubated as indicated, and then were activated by SP for 30 min and 24 h for the analysis of CCl2 and TNF.

Analysis of MRGPRX2 expression by flow cytometry

For the analysis of MRGPRX2 expression, LAD2 cell suspensions were seeded at a density of 2×10^5 cells/mL, and incubated with 5 µM of SP for 1 to 60 min at 37°C and 5% CO_2. Cells were washed twice with 0.1% BSA-PBS buffer at 200 × *g* for 5 min, resuspended in 0.1% BSA-PBS buffer, and incubated for 1 h in the dark at 4°C with anti-human MrgprX2-PE (Biolegend, San Diego, CA, USA); or anti-human FcεRIα-APC (eBioscience, Invitrogen Carlsbad, CA, USA); washed twice with 0.1% BSA-PBS buffer at 200 × *g* for 5 min, and fixed with 5% formalin neutral buffered solution (Sigma-Aldrich, Oakville, ON, CAN), for 15 min at RT followed by the addition of 3% BSA-PBS buffer, mixed and centrifuged at 200 × *g* for 10 min at 4°C, cells were then resuspended in 0.1% BSA-PBS buffer, and analyzed on a CytoFlex flow cytometer (Beckman Coulter, Brea, CA, USA). Mouse IgG2b, k isotype control-PE, and Armenian hamster IgG isotype control-APC (eBioscience, Invitrogen Carlsbad, CA, USA) were included as negative controls. Expression of MRGPRX2, and FcεRIα were analyzed using FlowJo v.10.8 software (BD Life Sciences, Ashland, OR, USA) and compared to control values. Results are reported as histograms and mean fluorescent intensity (MFI ± SEM).

SP and MRGPRX2 structure generation

The initial conformation of MRGPRX2 used in our molecular dynamics simulations was taken from K. Lansu et al, 2017 (19). The truncated structural model of MRGPRX2 in complex with dextromethorphan or ZINC-9232 was used in our study. SP was docked into the MRGPRX2 by the SMINA fork of AutoDock Vina software (20, 21). Nine different complexes were obtained and examined. MRGPRX2 was inserted into Dioleoylphosphatidylcholine (DOPC) membrane for further simulations. The starting conformation of the DOPC membrane was prepared with CHARRM-GUI (http://www.charmm-gui.org) (22). The prebuilt membrane was then equilibrated in TIP3P (computational water model) water with NPT (constant-temperature, constant-pressure ensemble) molecular dynamics (MD) simulation for several nanoseconds using GROMACS simulation package supplied with recently reported OPLS-aa parameters for lipids (23, 24). MRGPRX2 was inserted into the DOPC membranes using a inflation methodology (25).

Molecular docking calculations

Preferred binding modes of the SP to the aforementioned structure of MRGPRX2 was determined by molecular docking with SMINA version of the AutoDock Vina software. AutoDock Tools was used to prepare the input files (PDBQT) for SP and MRGPRX2. MRGPRX2 was kept rigid while the ligands were flexible. The dimensions of the grid box in the docking software setup were set to 100 × 100 × 100 points with a spacing of 0.374 Å. The center of the box was set to the same as that used for small molecules docked in MRGPX2 by K. Lansu et al, 2017. For enhanced accuracy and reproducibility of the predictions, the docking was performed with 1024 exhaustiveness parameter. The scoring function of the AutoDock Vina described was used to obtain the docking modes of SP.

Molecular dynamic simulations

The MD simulations of the SP-MRGPRX2 complexes were performed using GROMACS 2018 software (23). The OPLS-aa

force field was selected for the peptide-protein complexes (26, 27). Amino acids were parametrized using the GROMACS pdb2gmx program. The starting structure for each SP-MRGPRX2 complex was solvated in a periodic box of size 70.4 × 70.1 × 171.5 Å. The box was elongated along the z-axis to allow space for pulling SP out of the receptor. The water molecules inserted into the lipid bilayer were manually deleted. The TIP3P water model was applied to water molecules (28). Periodic boundary conditions were applied in all three directions with the explicit solvent model. Chloride ions were included to neutralize the system. The final number of atoms in the simulations including the peptide and water was about 70,000. The Maxwell distribution was employed to determine the initial velocities at 310 K. Equilibration consisted of short NVT (constant-temperature, constant-volume ensemble) and NPT simulations for 0.1 and 1 nanoseconds (ns), respectively. The V-rescale thermostat was used to keep the temperature constant by coupling to a reference temperature of 310 K during the NVT simulations (29). Nose-Hoover thermostat with semi-isotropic Parrinello-Rahman pressure coupling to a pressure of 1 bar was used during the NPT simulations (30). Coupling times of 0.5 and 2.0 picosecond (ps) were used for the thermostat and barostat, respectively. The isothermal compressibilities were set to 4.5×10^{-5} bar^{-1} in both x-y and z-directions of the semi-isotropic barostat.

Electrostatic interactions were determined using the Particle Mesh Ewald (PME) method (31). A cutoff of 12 Å was applied for van der Waals interactions. 5000 steps of energy minimization were carried out with the steepest descent algorithm before the equilibration. The two stages of equilibration (NVT and NPT) were performed without any restraints on the coordinates of the peptide and protein. Next, 30 ns NPT simulations were performed for all structures. Every 2 ps, the atomic coordinates were saved for subsequent analysis. Additionally, the stability of the docked SP-MRGPRX2 complexes were checked in separate MD simulations. Two stages of equilibration (NVT and NPT) were performed with a spring-like positional restraints (force constant of 5000 kJ mol^{-1} nm^{-2}) applied on the coordinates of the backbone C-atoms of SP and MRGPRX2 during the NVT equilibration. The final NPT simulations were performed for 1 ns without any constraints. Root mean square distance (RMSD) between the initial and the final SP configurations were compared to assess the stability of the binding poses predicted by the docking calculations.

Free energy calculations

Binding free energies of the docked SP-MRGPRX2 complexes were estimated with umbrella sampling methodology (31). Special MD simulations were performed in which the peptide was gradually pulled away from the complex to a distance of approximately 5 nm during a time of 1 ns (force constant of 2000 kJ mol^{-1} nm^{-2}). Next, 1000 different configurations of the system at different distances between SP and MRGPRX2 were extracted from the trajectory, and a set of 200 configurations was selected as initial configurations for umbrella sampling simulations. Umbrella sampling free energy calculations consisted of performing around 200 simulations at constrained (fixed) distances between the ligand and the receptor. The harmonic constraint force was applied to the center of mass of the ligand with constant of 2000 kJ mol^{-1} nm^{-2}. First, the 200 systems were equilibrated in NPT ensemble for 1 ns. Next, the actual production simulations were performed for 2.5 ns during which the force acting on the ligand was sampled. The sampled forces were then used in the weighted histogram analysis using *wham* software supplied in the GROMACS package to produce the free energy profiles (32). For every studied complex, the distance histograms between the protein and the ligand were manually checked to ensure proper overlap of the histograms and resulting accuracy of the results. The differences in the minimal and the maximal values of the profiles are then used as estimates of the binding free energies of the complexes. It should be noted that the actual sampling of the forces that are used for the free energy calculations is performed in fully equilibrated separate umbrella sampling runs, which might be regarded as a limiting case of infinitely slow pulling (33).

Statistical analysis

All cell activation experiments were performed in duplicate and represent at least three independent biological replicates ($n \geq 3$). Values are expressed as mean ± SEM. All statistical analyses were performed using GraphPad Prism statistical software (GraphPad, Sand Diego, CA, USA). Statistical differences in the mean values among treatment groups were determined by using a one-way analysis of variance (ANOVA) test with *post hoc* analysis with Tukey's multiple comparison tests. In all cases, a value for $P < 0.05$ was considered statistically significant.

Results

SP trigged mast cell activation is accompanied by MRGPRX2 internalization

SP has been shown to induce mast cell activation and degranulation through MRGPRX2 (34). LAD2 cells were activated with increasing concentrations of SP and degranulation was quantified by measuring β-hex release. Untreated cells and IgE sensitized cells did not degranulate and displayed only background levels of β-hex release of approximately 7-9% of total β-hex stored in the granules. FcεRI activated LAD2 (activated with biotinylated IgE and streptavidin) showed approximately 29% degranulation. As expected, SP caused a concentration-dependent release of β-hex (Figure 1A) and stimulation with 5 μM SP resulted in 55% release of β-hex. MCs contain several different classes of granules which contain different mediators (2, 3). Depending upon the stimulus, MCs release different sets of granules in a process known as piecemeal degranulation. Histamine is stored in distinct granules and is sometimes released independently of β-hex (3).

10.3389/fimmu.2023.1155740

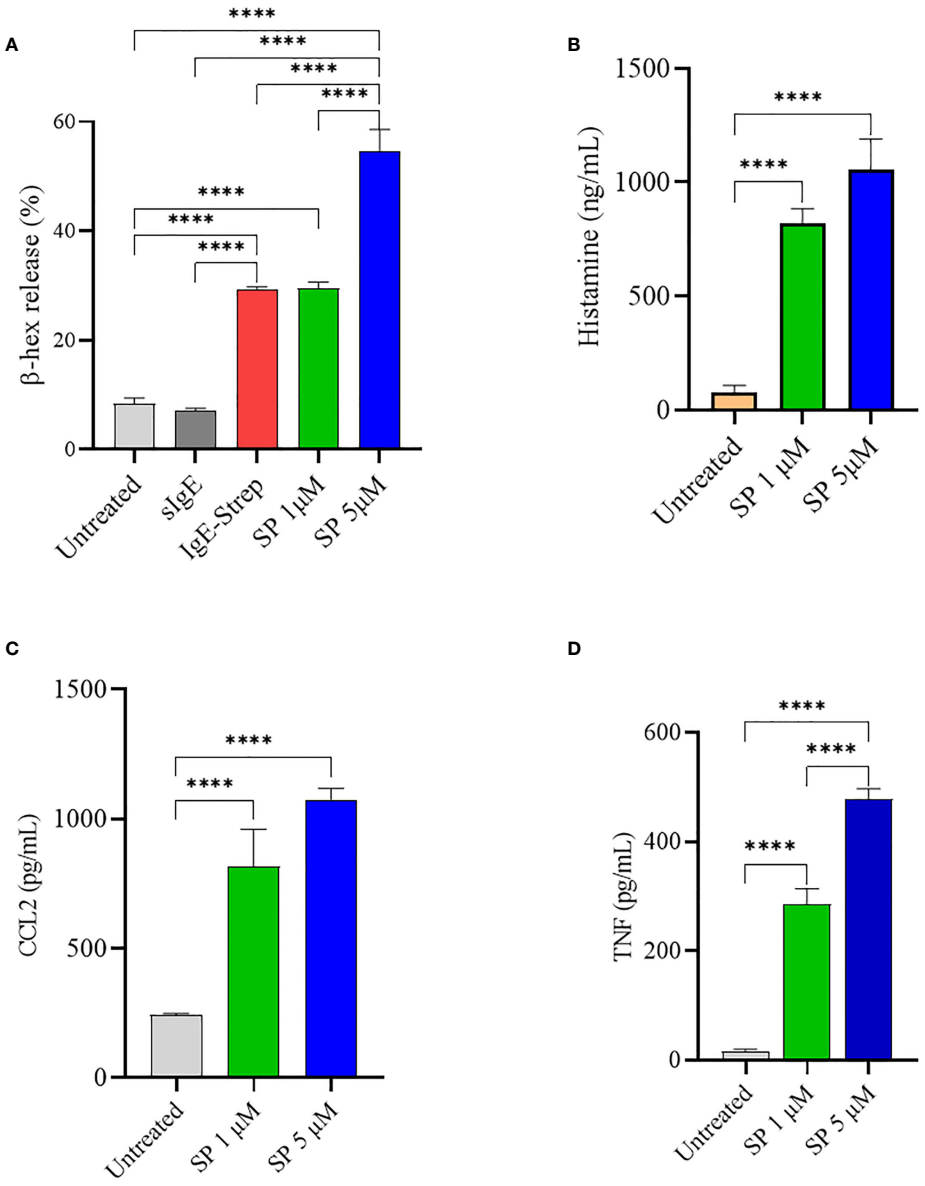

FIGURE 1
SP stimulates LAD2 degranulation and release of proinflammatory mediators. LAD2 cells were activated with SP for 30 min (1 μM and 5 μM). For comparison, LAD2 were sensitized with IgE (0.5 μg/mL) overnight and challenged with streptavidin (0.1 μg/mL) for 30 min. β-hex release **(A)** and histamine release **(B)** were measured as described in Methods. CCL2 **(C)** and TNF **(D)** production after SP activation for 24 h was measured by ELISA. Data is presented as mean ± SEM (n = 4, ****p < 0.0001).

We therefore evaluated histamine released upon SP triggered LAD2 degranulation (Figure 1B). SP (1 and 5 μM) activated significant histamine release compared to the untreated control. SP also activated the production of CCL2 and TNF by LAD2 (Figures 1C, D, respectively).

Like most GPCR, MRGPRX2 is internalized upon activation and initiates signaling through the β-arrestin pathway (12). To better understand how SP triggered MRGPRX2 internalization, we analyzed surface MRGPRX2 expression following SP activation using flow cytometry. When activated with SP, surface expression of MRGPX2 decreased rapidly (within 1 min), reaching minimal levels by 10-30 min (Figures 2A, B). In contrast, the treatment of LAD 2 with 5 μM SP showed no major changes in FcεRI expression with time (Figures 2C, D). The results indicate that the effect of SP is specific to MRGPRX2

SP-MRGPRX2 interaction is governed by h-bonds and salt bridges

To better understand mast cell activation through MRGPRX2, it is important to understand the intermolecular forces governing the interactions. Therefore, we examined the conformational and energetic relationships between SP and MRGPRX2. The probable poses of SP in the binding pocket of MRGPRX2 were determined

10.3389/fimmu.2023.1155740

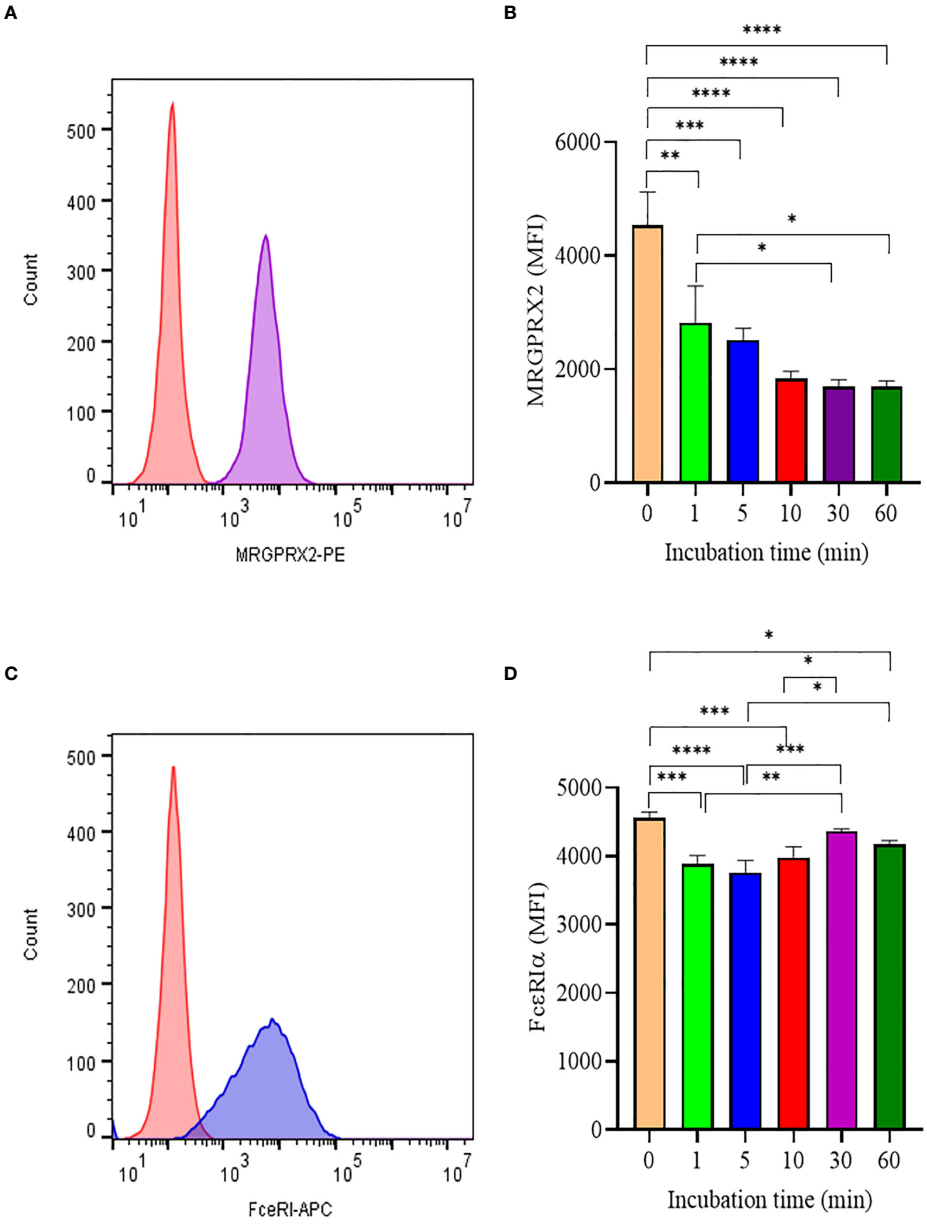

FIGURE 2
Analyis of MRGPRX2 and FcεRIα surface expression by flow cytometry. **(A)** LAD2 cells were treated with 5 µM SP and MRGPRX2 expression was assessed after 60 min (MRGPRX2 is purple curve; isotype control is red curve). **(B)** MRGPRX2 expression after 1, 5, 10, 30 and 60 min activation with SP as measured by mean fluorescence intensity (MFI). **(C)** Expression of FcεRIα after activation with SP as in **(B)** (FcεRIα is the blue curve; isotype control is the red histogram). **(D)** FcεRIα expression after 1, 5, 10, 30 and 60 min activation with SP as measured by MFI. Data is presented as mean ± SEM (n = 3, *p < 0.01, **<p 0.05, ***p < 0.001, ****p < 0.0001).

(Supplementary Figure 1) and were refined with MD simulations and free energy integrations.

Stability and structural analysis

Table 1 lists the binding affinity and the RMSD (before and after simulation) of the various poses of SP in the binding pocket of MRGPRX2 after 1ns MD simulation. Though all of the SP poses in the SP-MRGPRX2 complexes were stable (binding affinity of -9.5 - -9.1 for Complexes 1 – 9, Table 1), the SP-MRGPRX2 Complex 1 was found to be most stable in terms of most negative binding affinity (-9.5 kcal/mol) and showed lowest deviation from the initial position of the corresponding SP conformation (RMSD = 0.143 nm). To further substantiate the stability of the complexes, the distance between the center of masses of the corresponding SP pose and the MRGPRX2 before and after the short MD simulations for each SP-MRGPRX2 complex was determined (Table 1). Closer position of the ligand to the receptor suggests stronger interaction and hence a larger binding affinity. As seen in Table 1, the SP pose in Complex 1, which had the most negative binding affinity, was the closest to MRGPRX2 after equilibrium. The distance between the two centers of masses in

TABLE 1 Binding parameters determined computationally for various SP-MRGPRX2 complexes in the column order of i) SP-MRGPRX2 complexes, ii) values of the binding affinities of the docked SP-MRGPRX2 complexes predicted by SMINA using AutoDock Vina scoring functions, iii) root mean square deviation (RMSD) between the initial and the final states of the ligand after 1 ns of MD simulations, iv – vi) distances, D between the centers of mass of the ligand and the receptor of the SP-MRGPRX2 complexes at the initial (Init. D) and the final (Equil. D) states of the MD simulations, and vii) free energy differences (F.E. Diff) between the docked and undocked (water-solvated) states of the peptide as predicted by the umbrella sampling simulations for the SP-MRGPRX2 complexes.

A.D. Vina	Bind. Affinity, kcal/mol	RMSD, nm	Init. D., nm	Equil. D., nm	Δ, nm	F.E. Diff., kcal/mol
Complex 1	-9.5	0.143	1.376	1.391	0.015	59.5
Complex 2	-9.4	0.235	1.726	1.864	0.138	43.3
Complex 3	-9.3	0.146	1.691	1.724	0.033	42.4
Complex 4	-9.3	0.22	1.756	1.861	0.105	37.1
Complex 5	-9.2	0.22	1.742	1.867	0.125	34.6
Complex 6	-9.2	0.163	1.52	1.563	0.043	59.2
Complex 7	-9.2	0.295	1.799	1.894	0.095	56.2
Complex 8	-9.2	0.164	1.758	1.803	0.045	48.5
Complex 9	-9.1	0.197	1.508	1.525	0.017	91.4

RMSD= root mean square deviation.

Complex 1 was found to be 1.39 nm after simulation, causing a change of 0.015 nm from the initial SP position. Interestingly, the position of SP in Complex 9 was found to be stable as well. The center of mass of SP in Complex 9 changed only by 0.017 nm after equilibrium. These results suggest that SP poses in Complex 1 and Complex 9 are stable with a high negative binding affinity and stable position in the SP-MRGPRX2 complex.

Next, the relative binding free energy of the various SP poses were determined by mechanically pulling the corresponding SP pose from the SP-MRGPRX2 complexes. Binding free energy for every complex was estimated as the difference between the maximal and the minimal free energy values. Separate umbrella sampling calculation was performed for every SP-MRGPRX2 complex after 30 ns of NPT MD simulation. The resulting free energy profiles of the umbrella sampling are presented in Supplementary Figure 2, and the corresponding binding free energies are presented in Table 1. In accordance with the previous results, Complex 9 showed the highest binding free energy of 91.4 kcal/mol, and was followed by Complex 1 (59.5 kcal/mol). These results suggest that SP poses in Complex 1 and Complex 9 are closest to the MRGPRX2 receptor, were tightly bound, and were positioned deep in the binding pocket of the receptor. Deeper positioning of the complex in the binding pocket of the receptor allows for more interactions between the ligand and the receptor and, consequently, for higher binding free energies.

H-bonds and salt bridges between the peptide and the protein in each complex

Careful analysis of possible h-bonding and other intermolecular forces such as salt bridges are required for more insights in to SP-MRGPRX2 interactions. We examined the total number and the total active time of the h-bonds formed in each of the simulated SP-MRGPRX2 complexes. The h-bonds subprogram of GROMACS package was run on the 30 ns simulation trajectory of the membrane-inserted SP-MRGPRX2 complex. The total number of h-bonds for each complex active for 10 and 50% of simulation time are listed in Table 2. As expected, SP in Complex 1 formed the highest numbers of highly active h-bonds. Nineteen h-bonds in the SP-MRGPRX2 Complex 1 were active for more than 10% of simulation time, while 9 h-bonds were active for more than 50% of the simulation time. Complex 1 was followed successively by Complex 2 with 16 h-bonds active for more than 10% of simulation time and 8 h-bonds active for than 50% of simulation time. Complex 9 formed 14 h-bonds that were active for more than 10% of simulation time and 8 h-bonds that were active for more than 50% of simulation time.

Furthermore, we examined the trajectories of the MD simulations for possible salt bridges between SP and MRGPRX2 in the given SP-MRGPRX2 complexes. The salt bridges were automatically determined by an extension supplied with the Visual Molecular Dynamics (VMD) software package (35), which also measures the distance between the charged residues forming the salt bridge for every frame of the MD simulation trajectory. The detected salt bridge and the average distances between the charged amino acid residues for every complex are presented in Table 2. As can be seen from the table, the studied complexes formed only 1-2 salt bridges between SP and MRGPRX2 during the simulation time. The average distance between the participating residues were larger than 4 nm except Complex 9, wherein the average distance between Lys3 of SP and Glu164 of MRGPRX2 that formed salt bridge was 2.74 nm. These results indicate that the salt bridges (electrostatic interactions) were largely inactive, and the resulting interaction was rather weak (36). Complex 9 was the only SP-MRGPRX2 complex which formed stable salt bridge with the average distance between the residues less than 4 nm (36). Thus, in addition to a robust number of h-bonds, stable salt bridges modulate the strong interaction of the SP with MRGPRX2 receptor in Complex 9. We further identified the important amino acid residues in SP and

TABLE 2 Intermolecular forces governing the interaction of SP and MRGPRX2 receptor, in the column order of i) SP-MRGPRX2 complexes, ii) numbers of active h-bonds for more than 10% (N(THB)>10%) of simulation time, and iii) the number of highly active h-bonds for more than 50% (N (THB)>50%) of the total simulation time, iv-v) salt bridges (attractive force between two oppositely charges molecules) formed between the SP and MRGPRX2 detected by the VMD software package, and the corresponding average distances between the residues participating in the salt bridges for every studied complex.

A.D. Vina	N (T_{HB}>10%)	N (T_{HB}>50%)	Salt Bridges	Average Distance, nm
Complex 1	19	9	GLU164-ARG1	4.501
Complex 2	16	8	ASP174-ARG1	4.526
Complex 3	9	1		
Complex 4	19	2		
Complex 5	7	4	ASP174-LYS3 ASP247-ARG1	5.67 9.474
Complex 6	9	4		
Complex 7	14	3	ASP174-LYS3	8.179
Complex 8	16	2	GLU29-LYS3 ASP174-ARG1	5.411 4.258
Complex 9	14	7	GLU164-LYS3 ASP184-ARG1	2.74 4.565

MRGPRX2 in Complex 9 that participated in the formation of h-bonds (Table 3). Interestingly, the corresponding residues within SP and MRGPRX2, which formed salt bridges in Complex 9, also participated in h-bond interactions. Table 3, row 10 and 11 show that SP Lys3 and MRGPRX2 Glu164 formed active h-bonds for 67% and 31% of the simulation time respectively. Similarly, SP Arg1 and MRGPRX2 Asp184 formed active h-bonds. Gln5 and Gln6 of SP showed h-bond interactions with Phe170 and Asn85 of MRGPRX2 respectively. Thus, due to the stable salt bridge and the high number of h-bonds, the configuration of the peptide in Complex 9 seems to be the most probable among the ones studied in this contribution.

Ligand binding/unbinding reaction pathway

A steered MD simulation was performed by slowly pulling the SP out of the receptor for 5 nm during a time period of 1 ns. The

TABLE 3 H-bonds between SP and MRGPRX2 in Complex 9 together with the percent of time they were active during the simulation obtained with gmx hbonds software.

	Donor	Hydrogen	Acceptor	% of Time Active
1	ND2@ASN85	HD21@ASN85	OE1@GLN6	88%
2	OH@TYR89	HH@TYR89	O@GLN6	31%
3	OG@SER257	HG@SER267	O@GLN5	10%
4	N@ARG1	H1@ARG1	OD1@ASP184	88.40%
5	N@ARG1	H1@ARG1	OD2@ASP184	12.60%
6	N@ARG1	H1@ARG1	OG1@THR187	87.50%
7	NE@ARG1	HE@ARG1	O@LEU163	29.60%
8	NH1@ARG1	HH11@ARG1	OD1@ASP184	10.80%
9	NH1@ARG1	HH11@ARG1	OD2@ASP184	89.50%
10	NZ@LYS3	HZ1@LYS3	OE1@GLU164	67.40%
11	NZ@LYS3	HZ1@LYS3	OE2@GLU164	31.30%
12	NZ@LYS3	HZ1@LYS3	O@CYS168	26.60%
13	NE2@GLN5	HE21@GLN5	O@PHE170	66.90%
14	NE2@GLN6	HE21@GLN6	OG@SER257	57.40%

analysis of the pulling process provides a rough model of the binding/unbinding of the peptide to/from the receptor. We examined the changes in the number of h-bonds and salt bridges between the SP and MRGPRX2 receptor during the binding/unbinding process. Supplementary Figure 3 presents the number of h-bonds between SP and MRGPRX2 dependent on the distances between the centers of mass of SP and MRGPRX2 sampled during the pulling simulations. It could be seen that, while for the majority of the complexes the number of h-bonds gradually decays to zero shortly after the distance of 4 nm, Complex 1 and 9 depict a nonzero number of h-bonds even at a distance of 5 nm. This observation clearly suggests that some flexible part of the protein extends and follows the peptide during the unbinding (pulling) process.

A similar phenomenon is observed with respect to the salt bridges as well (Figure 3). Figures 3A, B show the stable salt bridges formed at a distance of 3.2 and 5 nm between centers of masses of SP and MRGPRX2 in Complex 9. Complex 9 is characterized by two salt bridges between residues Glu164 and Asp184 of MRGPRX2 and Lys3 and Arg1 of SP, respectively. The lifetime of the first and highly stable Glu164-Lys3 salt bridge extends from the initial configuration to a distance of about 3.7 nm. Salt bridge Asp184-Arg1 in Complex 9 appears to be initially inactive (residue distance more than 0.4 nm) but is activated for a significant range (~2 nm) of distances with values between approximately 4.25 and 5.25 nm.

SP analogs devoid of key residues fail to activate LAD2 cells

To confirm the results of MD simulation, and in accordance with other published data, a series of SP analogs (Supplementary Table 1) were tested for their activity against LAD2 cells. Figure 4A shows the degranulation induced by SP analogs. The results show that replacing Lys3 and Gly5 from SP (SP1 and SP2) greatly reduces the activity of the peptides. The degranulation of LAD2 upon stimulation by 0.1, 1, and 10 μM of SP1 and SP2 remained at basal level in comparison to 5 μM SP (62% degranulation). Further, since hydrophobic residues play an important role in ligand-MRGPRX2 interactions (17), Phe8 was replaced with 4-Benzoyl-Phe8 (SP4), as well; Phe7 and Phe8 were simultaneously replaced with 4-Chloro-Phe7 and 4-Choloro-Phe8 (SP5), respectively. Results showed that altering the hydrophobicity of amino acids did not alter the activation potential of the peptides. The degranulation of LAD2 upon stimulation by 0.1, 1, and 10 μM of SP4 were found to be 10, 36, and 55%, respectively, against 62% degranulation by 5 μM SP. Similarly, the degranulation of LAD2 upon stimulation by 0.1, 1, and 10 μM of SP5 were found to be 12, 42, and 63%, respectively. SP analog where Gly9 was replaced with Pro9 (SP3), showed no change in activity when compared to SP.

We also measured the production of CCL2 by LAD2 that were activated with the SP analogs (Figure 4B). All of the SP analogs elicited a concentration-dependent activation of CCL2 production. However, in contrast to β-hex release, the amount of CCL2 produced by cells activated with 10 μM of the peptides was either comparable or higher than that released by SP (5 μM). CCL2 released by 10 μM SP1 - 5 were 792, 1352, 1924, 1050, and 1813 pg/mL, respectively, in comparison to 1074 pg/mL CCL2 released by cells activated with 5 μM SP. This is in contrast to the negligible β-hex release by SP1 and SP2 when compared to SP. Furthermore, and surprisingly, only SP3 and SP5 (10 μM) triggered the release of TNF from the activated cells (Figure 4C). These results suggest that the level of degranulation (β-hex) and cytokine release is not directly comparable when cells are activated through MRGPRX2 by these peptides.

To confirm that the activity of SP analogs is mediated through MRGPRX2, we studied the effect of SP analogs (SP1, SP2 and SP4) on the surface expression of MRGPRX2 on LAD2 cells. Our results (Figure 5) show that SP derived peptides, like SP, caused an immediate and rapid decrease in the MRGPRX2 expression on the surface of LAD2. The results confirm that the activity of SP analogs is mediated through MRGPRX2. Further, since SP1 and SP2 activated less β-hex release than SP, it is possible that these peptides bound MRGPRX2 less efficiently and therefore could be used as competitive inhibitors of SP. To study this, LAD2 cells were preincubated with 10 μM of SP1 and SP2 for 30, 60 and 180 min and then were activated with 5 μM SP for 30 min (Figure 6). β-hex was measured as a gauge of degranulation. Results show that pretreatment of LAD2 with SP2 reduced the β-hex released by

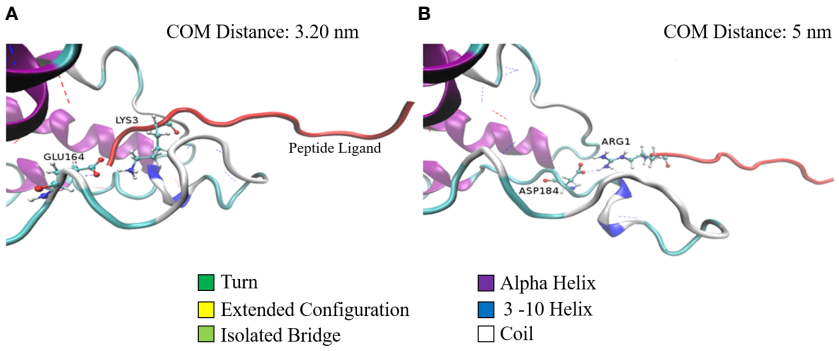

FIGURE 3
Two configurations of Complex 9 captured during the pulling simulation. Configurations of Complex 9 correspond to the center of mass distance of 3.2 nm **(A)** and 5.0 nm (**B**). MRGPRX2 (colored according to its secondary structure) and SP (red colored) are represented by cartoons (special VMD drawing method). Salt-bridge residues are represented by ball and stick models. Dashed lines denote h-bonds between the proteins.

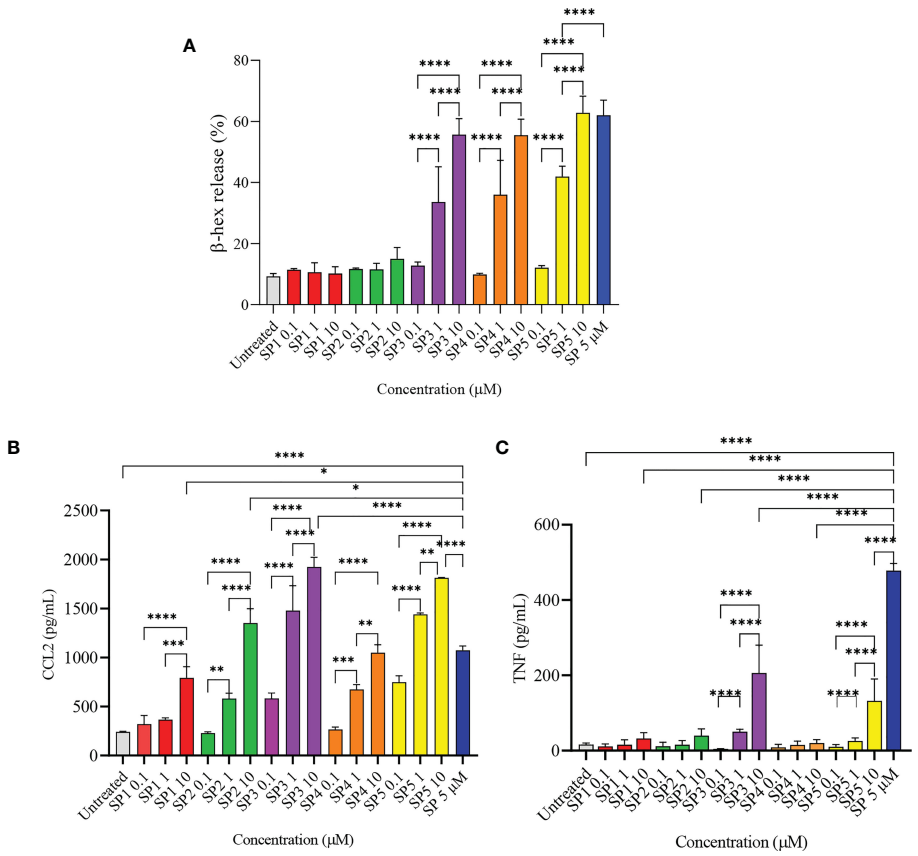

FIGURE 4
Release of immune mediators by LAD2 cells stimulated with SP analogs. **(A)** LAD2 cells were activated with SP analogs (SP1, to SP5) for 30 min, and β-hex release was measured. **(B)** CCL2, and **(C)** TNF release were analyzed after activation of LAD2 with SP analogs or SP (5 μM) for 24 h Untreated cells were included as negative controls. Data is presented as mean ± SEM (n = 5 for β-hex release, n = 3 for CCL2 release, and n = 4 for TNF release, *p<0.01, ** <p0.05, ***p<0.001, ****p<0.0001).

SP, and the effect was more pronounced at a longer incubation time (180 min). One hundred eighty min of pre-incubation with SP2 reduced the β-hex released by SP by 33% (Figure 6F). Since the SP analogs were more effective at 180 min, we also measured the histamine released by SP upon pre-incubation with SP1 and SP2 (Figures 6G, H). Both SP1 and SP2 reduced the histamine released by SP. Where SP1 reduced the histamine released by 40%, SP2 reduced the histamine released by 42%. These results suggest that SP1 and SP2 could be used as a therapeutic to suppress the inflammation caused by SP.

To further support the result, we also studied effect of SP analog preincubation on the release of CCL2 (Figure 7) and TNF (Figure 8) from the SP activated LAD2 cells. We included SP4 in our study as well, as it did not trigger TNF release by itself (Figure 4C). The effect was studied for the release of both preformed (30 min SP activation, Figures 7A, C, E and 8A, C, E) and *de novo* synthesized cytokines (24 h SP activation, Figures 7B, D, F and 8B, D, F) (37). The results of CCL2 release are in accordance with Figure 4B. Preincubation of LAD2 with peptides SP1, SP2 and SP4, triggered the release of CCL2, and successive stimulation with SP added to the total amount of CCL2 for both 30 min and 24 h time periods (Figure 7). In contrast, though the preincubation of LAD2 with SP1, SP2 and SP4 had no effect on the release of preformed TNF (Figures 8A, C, E), the preincubation of cells with the peptides significantly reduced the *de novo* synthesis of TNF upon SP activation (Figures 8B, D, F). The *de novo* synthesis of TNF by SP activated LAD2 preincubated with SP1, SP2 and SP4 was reduced by 46, 42 and 40% respectively, with respect to that released by SP alone. The results suggest that manipulation of important amino acid residues in a known ligand of MRGPRX2 receptor could help in developing peptide inhibitors for the receptor which hold immense potential in MRGPRX2 based therapeutics.

Discussion

The contribution of SP to inflammatory diseases such as atopic dermatitis, asthma, and arthritis has been extensively studied (38). It was presumed that SP activated mast cells exclusively *via* neurokinin-1receptor (NK-1R) but we have shown that the effect of SP can also be mediated through the MRGPRX2 receptor (7). Since each ligand of MRGPRX2 can induce the release of different mediators (39), we studied the important immune modulating molecules that are released from MCs upon SP activation. Our results show that SP activation causes a significant release of histamine, MCP-1/CCL2 and TNF. The results are important as

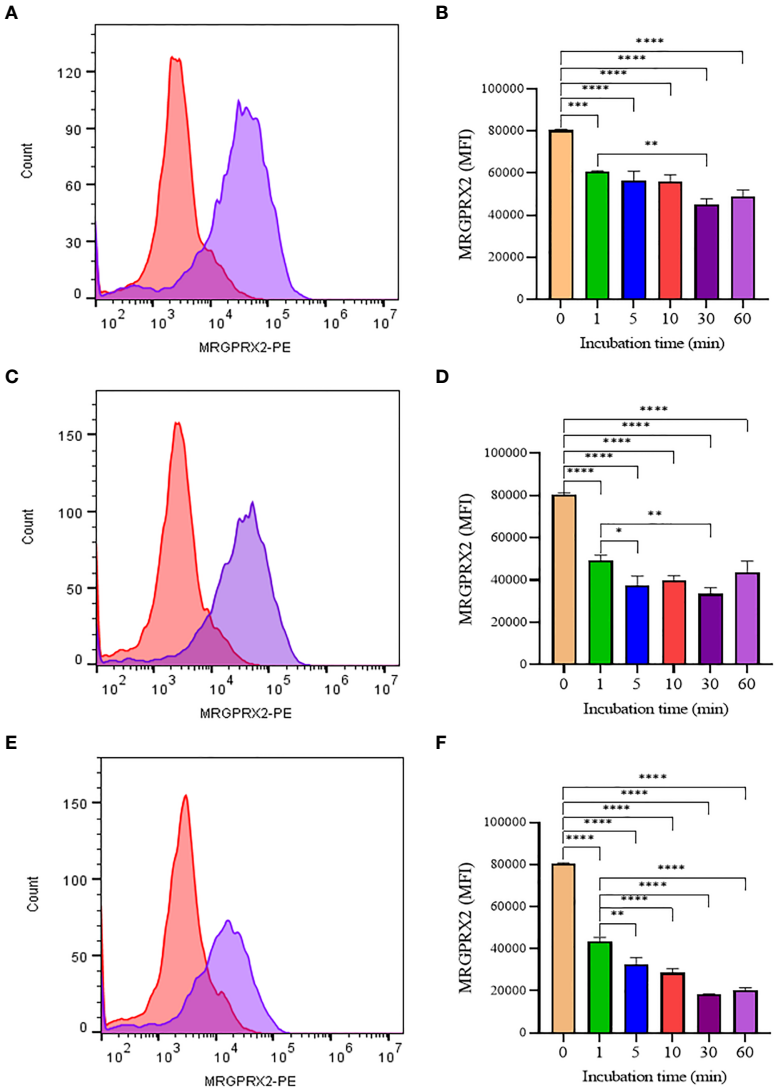

FIGURE 5
Flow cytometry analysis of SP analogs on MRGPRX2 expression in LAD2 cells. Histograms showing MRGPRX2 internalization effect after 60 **min** SP analogs treatment (A, SP1; C, SP2; E, SP4). LAD2 cells were treated overtime (1 to 60 min) with SP analogs (B, SP1; D, SP2; F, SP4), and MRGPRX2 expression was compared to untreated cells. Data is presented as mean ± SEM (n = 3, *<0.05, **<0.01, ***<0.001, ****<0.0001).

they identify the SP-specific mast cell released mediator that could play an important role in the pathogenesis of inflammatory diseases. The results are in accordance with earlier reported findings, where the activation of LAD2 by SP caused a release of histamine, MCP-1/CCL2 and TNF (40). In the study, the mediators released by SP were compared with those triggered by PAMP-12, and it was reported that PAMP-12 mediated LAD2 activation showed higher release of tryptase. However, the concentrations of SP and PAMP-12 peptides were compared in μg/mL instead of molar concentrations. Since SP and PAMP-12 have different molecular weights, a weight equivalence will result is overall different molar concentrations, and the yielded results could be attributed to the concentration differences. Furthermore, since there was no complete inhibition of one or more mediator, the relative difference in amount of mediator results could also be due to difference in activity of the respective peptide agonists (40).

Receptor internalization is an important event in the downstream signaling pathways, and is initiated when ligands bind MRGPRX2 (12). It has been suggested that ligands with different affinities may also alter the kinetics of internalization, resulting in different signaling and eventually mediators produced (41). Activation with 5 μM SP caused more than 38% of MRGPRX2 to internalize within 1 min of stimulation. The response was time-dependent, but stabilized after 10 min. It has been shown that MRGPRX2 internalization is mediated by the recruitment of β-arrestins. In a study with HEK cells stably expressing β-arrestin2-tobaco etch virus fusion gene and MRGPRX2 receptor, SP induced a concentration dependent recruitment of β-arrestin, and subsequent time-dependent internalization of MRGPRX2 (12). Interestingly, it has been reported that when cells were treated overnight with SP, a subsequent stimulation by SP failed to trigger mast cell activation suggesting that the receptor had been desensitized (12). Furthermore, internalization is mediated *via* parallel

10.3389/fimmu.2023.1155740

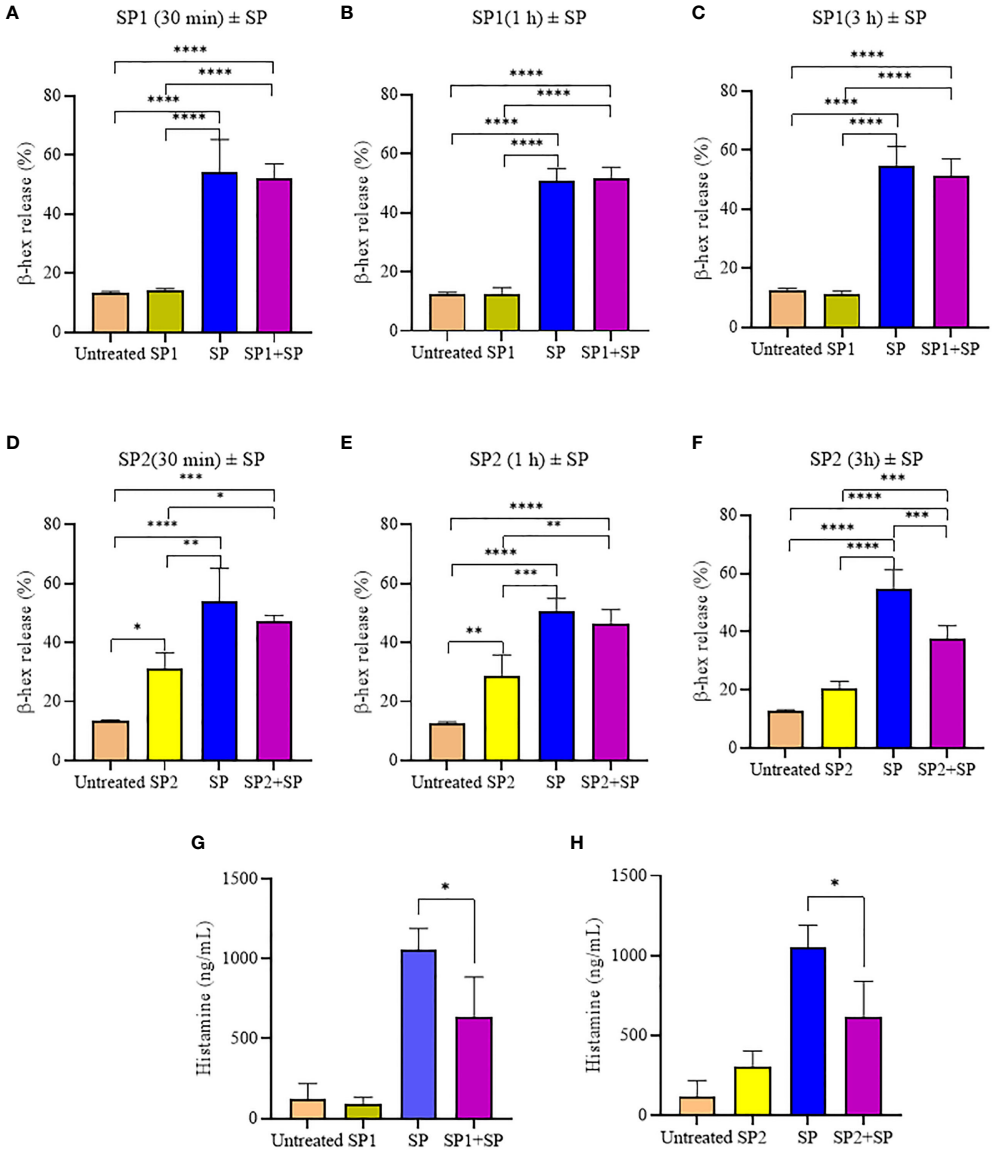

FIGURE 6
Inhibitory effect of SP analogs on the degranulation of LAD2 cells by the 30 **min** activation by SP. **(A-C)** Time dependent effect of SP1 preincubation on the β-hex release from the SP activated LAD2 cells. **(D-F)** Time dependent effect of SP2 preincubation on the β-hex release from the SP activated LAD2 cells. **(G-H)** Effect of 180 min SP1 and SP2 preincubation on the histamine release from the SP activated LAD2 cells. Untreated and SP treated β-hex and histamine values are included as controls in all tested conditions. Data is presented as mean ± SEM (n = 4, *p<0.01, **p<0.05, ***p<0.001, ****<0.0001).

endocytosis and micropinocytosis pathways, and upon activation with SP, MRGPRX2 internalizes and is compartmentalized into macropinosomes without degradation (42). These data suggest that it may be possible to desensitize MRGPRX2 using a peptide that induces internalization but does not activate degranulation.

We next used computational simulations to identify the important intermolecular forces that govern the SP-MRGPRX2 interaction, and to simultaneously identify the amino acid residues that are crucial for interaction. H-bonding was the dominant force between SP and MRGPX2 in their interaction. Arg1 and Lys3 were important basic residues within SP that acted as a donor in the h-bond formation, respectively with Asp186 and Glu164 of MRGPRX2 and which were active for 89 and 67% of the simulated time. Apart from these h-bond interactions, the basic residues Arg1 and Lys3 also formed salt bridges with the respective Asp186 and Glu164 and a distance of 4.6 and 2.7 nm between their centers of masses. These interactions were stable and mediated the interaction and successive activation of the MRGPRX2 receptor. To further gain insight into the initial events in interactions, we conversely performed MD simulation on the SP-MRGPRX2 complex by pulling SP from the SP-MRGPRX2 complex, and found that stable h-bondings and salt bridges extended up to a distance of 5 nm (Supplementary Figure 3). The extended lifetimes of the h-bonds and the salt bridges between SP and MRGPRX2 suggests some deformation in the structure of the receptor during the pulling (unbinding) process. A flexible segment of the receptor containing Glu164 and Asp184 residues, which take part in the formation of the

10.3389/fimmu.2023.1155740

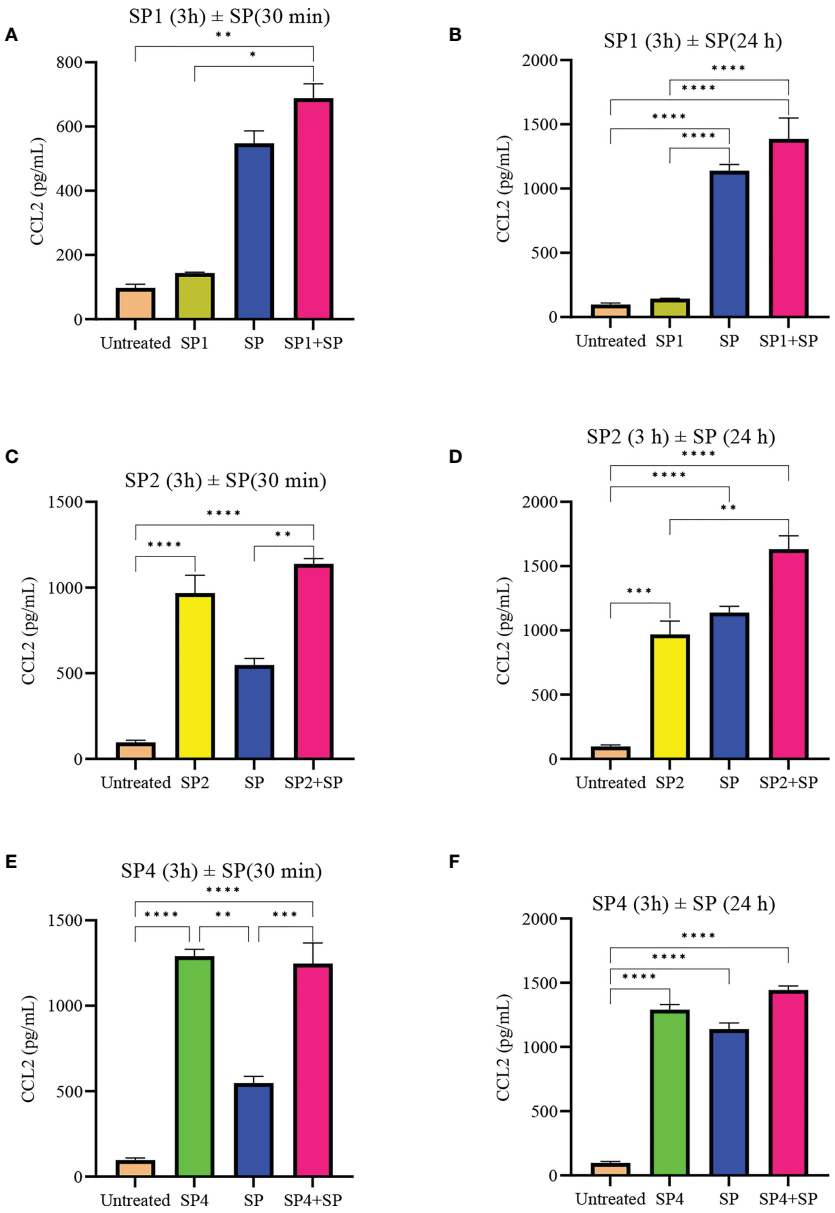

FIGURE 7
Inhibitory effect of SP analogs on the release of preformed and *de novo* synthesized CCL2 from SP activated LAD2 cells. LAD2 cells were preincubated with SP analogs for 3h and then were activated with SP for the mentioned amount of time. Data showing CCL2 release by the SP analog alone refers to the release of CCL2 due to the preincubation of LAD2 cells with SP analogs, and was measured after the 3h SP analog incubation. **(A)** Release of preformed CCL2 from the SP activated (30 min) LAD2 cells preincubated with SP1. **(C)** Release of preformed CCL2 from the SP activated LAD2 cells preincubated with SP2. **(E)** Release of preformed CCL2 from the SP activated LAD2 cells preincubated with SP4. **(B)** Release of *de novo* synthesized CCL2 from the SP activated LAD2 cells preincubated with SP1. **(D)** Release of *de novo* synthesized CCL2 from the SP activated LAD2 cells preincubated with SP2. **(F)** Release of *de novo* synthesized CCL2 from the SP activated LAD2 cells preincubated with SP4. Untreated and SP treated values are included as controls in all tested conditions. Data is represented as mean ± SEM (n = 3, *p<0.01, **p<0.05, ***p<0.001, ****<0.0001).

salt bridges, appears to be pulled with the ligand during the process, and as a result, the residues forming salt-bridge, which also participates in h-bond formations with SP, extend into the direction of the pulling force to participate in the interactions. This deformation could be observed in the trajectory of the pulling simulation, and is demonstrated in Figures 3A, B, on two snapshots characterized by the center of mass distances of 3.2 and 5 nm. The segment of the receptor of approximately 20 residues (from 164 to 184) extends into the direction of the retreating ligand while being pulled by the salt bridge and h-bonds. The strong interactions with the extending part of the receptor together with a number of h-bonds formed with this part during the unbinding process, conversely, is also suggestive of the binding reaction, which might occur in the exactly reverse order. Examination of the tentative "unbinding" reaction path of SP-MRGPRX2 complex predicted by the pulling simulations suggests that the reverse binding reaction pathway might involve initial salt-bridge and h-bonding interactions with the MRGPRX2 segment containing Glu164 and Asp184, and later gradual "absorption" of

10.3389/fimmu.2023.1155740

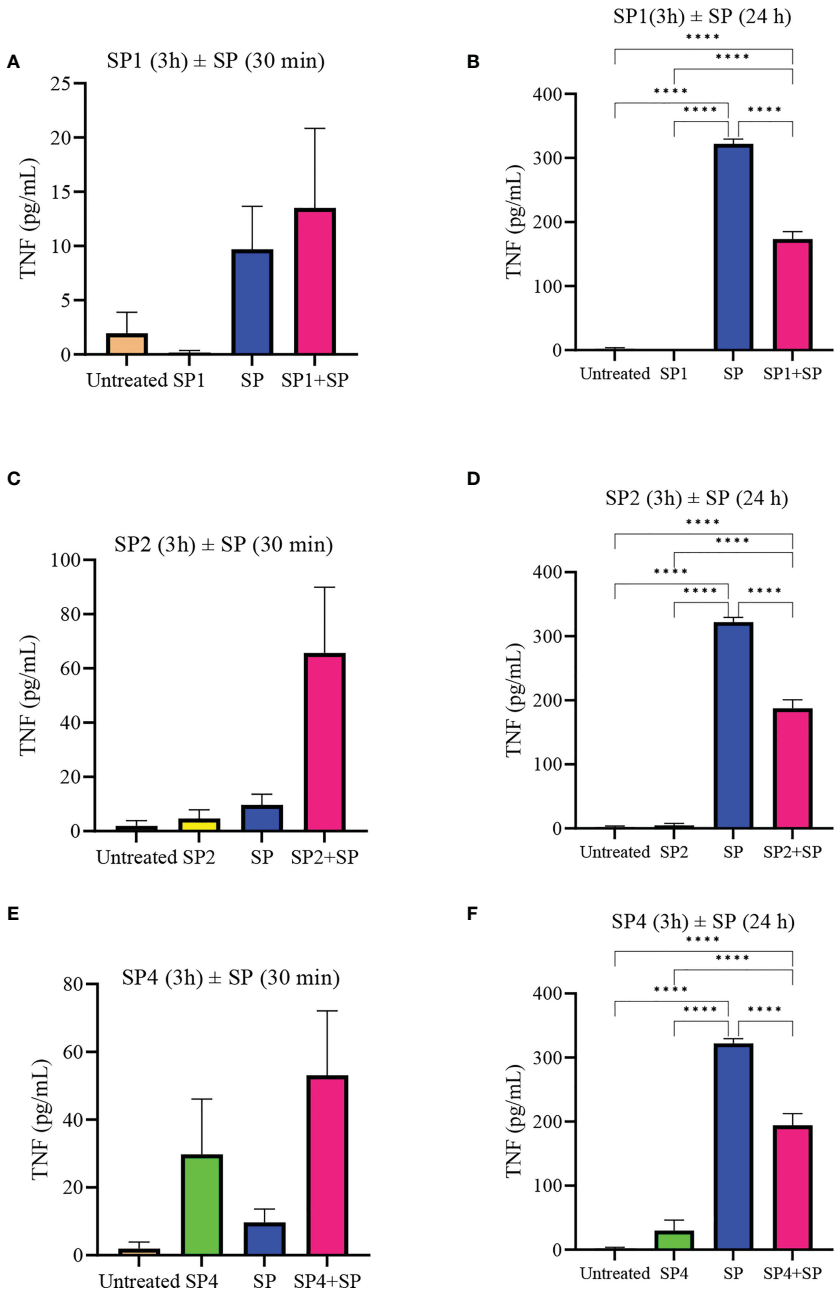

FIGURE 8
Inhibitory effect of SP analogs on the release of preformed and *de novo* synthesized TNF from SP stimulated LAD2 cells. LAD2 cells were preincubated with SP analogs for 3h and then were activated with SP for the mentioned amount of time. Data showing TNF release by the SP analog alone refers to the release of TNF due to the preincubation of LAD2 cells with SP analogs, and was measured after the 3h SP analog incubation. **(A)** Release of preformed TNF from the SP activated LAD2 cells preincubated with SP1. **(C)** Release of preformed TNF from the SP activated LAD2 cells preincubated with SP2. **(E)** Release of preformed TNF from the SP activated LAD2 cells preincubated with SP4. **(B)** Release of *de novo* synthesized TNF from the SP activated LAD2 cells preincubated with SP1. **(D)** Release of *de novo* synthesized TNF from the SP activated LAD2 cells preincubated with SP2. **(F)** Release of *de novo* synthesized TNF from the SP activated LAD2 cells preincubated with SP4. Untreated and SP treated values are included as controls in all tested conditions. Data is represented as mean ± SEM (n = 3, ****<0.0001).

the ligand into the binding pocket of the receptor through the increasing number of h-bonds and the salt bridges formed in the pocket.

A generalized motif of peptide ligands has been suggested (16, 17), and a common feature is a well-ordered positioning of basic and hydrophobic residues. The common feature of amino acids has been found to be the likes of hydrophobic residues separated by a group of basic and uncharged residues (17). SP with amino acid sequence Arg-*Pro-Lys-Pro-Gln-Gln-Phe*-Phe-Gly-Leu-Met, clearly bears the motif (italicized residues) and Lys3 forms a part of it. Our results support the hypothesis and further extend on the mechanism of interaction of such motifs which will be governed by h-bonds and salt bridges. Apart from peptide ligands, researchers have also presented the cryogenic electron microscopic structure of MRGPRX2 receptor (14, 15). The

ligand binding pocket of MRGPRX2 contains two sub pockets, an electronegative sub pocket consisting of Asp184 and Glu164, and a hydrophobic pocket where Trp243 and Phe170 plays crucial role, and it has been shown that mutations at these sites either inhibit or significantly reduce MGPRX2 activation. With respect to agonists, it has been shown that a peptide agonist having basic characteristics are most likely able to activate MRGPRX2 due to its binding to the electronegative sub pocket, irrespective of their overall conformation (15). These studies support our findings where we show that SP basic residues (Arg1 and Lys3) forms stable interactions with the Asp184 and Glu164 due to h-bond and salt bridges.

To test our computational predictions, we used SP analogs with amino acid substitutions in relevant and non-relevant sites to determine whether they could still activate MRGPRX2 on LAD2. SP derived peptides (SP1, 2 and 4), like SP, caused a rapid decrease in the MRGPRX2 expression on LAD2, suggesting MRGPRX2 mediated mode of cell activation. Further, we studied cell degranulation to examine the potency of peptides in MRGPRX2 mediated LAD2 activation. The results were in accordance with computation findings where removal of Lys3 (SP1 and SP2) limited the activity of analogs, while modifications at the hydrophobic residues (though the overall hydrophobicity was not lost) showed no significant effect on degranulation (SP3-5). In contrast to degranulation (β-hex), the ability of these analogues to activate transcription-dependent mediator production was unexpected. Even though SP1 and SP2 failed to cause β-hex release, there was a considerable amount of MCP-1/CCL2 released by these peptides. Surprisingly, all SP analogs were unable to produce the same amount of TNF as SP, except SP3 and SP5, though at higher concentration (10 μM). These results suggest that subtle changes in ligand structure could alter the binding of ligand to MRGPRX2 and therefore, could induce different signaling cascades, thereby leading to differential mediator production. Thus, it is important to measure both degranulation and *de novo* synthesized mediator production by MC when analyzing MRGPRX2 activation. Finally, we studied the effectiveness of SP1 and SP2 in acting as competitive agonists/antagonists for SP activation of LAD2. SP2 efficiently reduced the amount of β-hex and histamine released from SP-activated LAD2 cells in time dependent manner. Furthermore, peptides SP1, SP2 and SP4 also reduced the level of *de novo* synthesized TNF release upon activation by SP, though no effect was observed for CCL2 release or the release of preformed TNF. These are crucial findings, which suggest that the modulation of the crucial amino acids in a known peptide ligand of MRGPRX2 could help in designing therapeutics for the MRGPRX2 mediated inflammatory disease. Several recent studies have focused on identifying ways to inhibit or block the activation of mast cells through this receptor. In this regard, peptide QWF has been identified which have shown to inhibit MRGPRX2 activation through SP and compound 48/80 (43). Other molecules, which have been identified as an antagonist to MRGPRX2 are Osthole (against SP and compound 48/80), Quercetin (against SP and compound 48/80), Shikonin (against compound 48/80), Saikosaponin A (against compound 48/80), Resveratrol (against compound 48/80), and Roxithromycin (against compound 48/80) (44–50).

Conclusion

In conclusion, we have shown that SP-MRGPRX2 interaction is mediated by h-bonds and salt bridges. Arg1 and Lys3 in SP were deemed important for SP interaction with MRGPRX2, and that the mutations at key residues within SP changes the activity of the peptide against MCs. SP activated mast cells undergo rapid MRGPRX2 sensitization. Finally, we show that change in the physiochemical properties in a ligand could greatly vary the types and levels of mediators released from activated MCs, which has great significance in the study of disease pathogenesis. Finally, we show that the modulation of the amino acid residue of a known ligand could help in designing MRGPRX2 antagonists.

Data availability statement

The original contributions presented in the study are included in the article/Supplementary Material. Further inquiries can be directed to the corresponding author.

Author contributions

SH performed the molecular modeling analysis. NA performed the substance P activation studies. SR compiled and analyzed the data and wrote the manuscript. AK provided editorial feedback. MK designed the study, obtained necessary funding, obtained biosafety approvals and assisted in writing the final draft of the manuscript. All authors approved submission of the final version of the manuscript.

Funding

The project was funded by National Research Council, Canada.

Acknowledgments

Authors thank Dipankar Roy for his help in analyzing the computational data.

Conflict of interest

The authors declare that the research was conducted in the absence of any commercial or financial relationships that could be construed as a potential conflict of interest.

Publisher's note

claim that may be made by its manufacturer, is not guaranteed or endorsed by the publisher.

Supplementary material

The Supplementary Material for this article can be found online at: https://www.frontiersin.org/articles/10.3389/fimmu.2023.1155740/full#supplementary-material

SUPPLEMENTARY FIGURE 1
SP-MRGPRX2 Complex 1 **(A)** and Complex 9 **(B)**, as predicted by the SMINA fork of the Autodock Vina docking software. The protein receptor molecules are represented by cartoons with different colors depending on the secondary structure of the residues (white: coil, cyan: turn, magenta: alpha-helix). Ligand molecules are presented as a red cartoon

SUPPLEMENTARY FIGURE 2
Free energy profiles of the peptides as a function of the center of mass distances between the receptor and the peptide obtained with umbrella sampling simulations for the studied complexes

SUPPLEMENTARY FIGURE 3
(A, B) presents the numbers of h-bonds for every complex depending on the center of mass distance between SP and MRGPRX2 sampled during the pulling simulation of 1 ns; **(C)** presents the distance between the charged residues of the salt bridges formed between SP and MRGPRX2 in Complex 1 (black and red symbols) and 9 (yellow and orange symbols) during 1 ns pulling simulations. Thin horizontal black line denotes the threshold of 0.4 nm below which the salt bridges are assumed to be active.

SUPPLEMENTARY TABLE 1
Amino acid sequences of SP analogs.

References

1. Raj S, Unsworth LD. Targeting active sites of inflammation using inherent properties of tissue-resident mast cells. *Acta Biomater* (2023) 159:21–37. doi: 10.1016/j.actbio.2023.01.024

2. Wernersson S, Pejler G. Mast cell secretory granules: armed for battle. *Nat Rev Immunol* (2014) 14:478. doi: 10.1038/nri3690

3. Moon TC, Dean Befus A, Kulka M. Mast cell mediators: their differential release and the secretory pathways involved. *Front Immunol* (2014) 5:569. doi: 10.3389/fimmu.2014.00569

4. Mashiko S, Bouguermouh S, Rubio M, Baba N, Bissonnette R, Sarfati M. Human mast cells are major IL-22 producers in patients with psoriasis and atopic dermatitis. *J Allergy Clin Immunol* (2015) 136:351–9. doi: 10.1016/j.jaci.2015.01.033

5. Balzar S, Fajt ML, Comhair SAA, Erzurum SC, Bleecker E, Busse WW, et al. Mast cell phenotype, location, and activation in severe asthma: data from the severe asthma research program. *Am J Respir Crit Care Med* (2011) 183:299–309. doi: 10.1164/rccm.201002-0295OC

6. Rivellese F, Mauro D, Nerviani A, Pagani S, Fossati-Jimack L, Messemaker T, et al. Mast cells in early rheumatoid arthritis associate with disease severity and support b cell autoantibody production. *Ann Rheum Dis* (2018) 77:1773–81. doi: 10.1136/annrheumdis-2018-213418

7. McNeil BD, Pundir P, Meeker S, Han L, Undem BJ, Kulka M, et al. Identification of a mast-cell-specific receptor crucial for pseudo-allergic drug reactions. *Nature* (2015) 519:237–41. doi: 10.1038/nature14022

8. Nattkemper LA, Tey HL, Valdes-Rodriguez R, Lee H, Mollanazar NK, Albornoz C, et al. The genetics of chronic itch: gene expression in the skin of patients with atopic dermatitis and psoriasis with severe itch. *J Invest Dermatol* (2018) 138:1311–7. doi: 10.1016/j.jid.2017.12.029

9. Manorak W, Idahosa C, Gupta K, Roy S, Panettieri R, Ali H. Upregulation of mas-related G protein coupled receptor X2 in asthmatic lung mast cells and its activation by the novel neuropeptide hemokinin-1. *Respir Res* (2018) 19:1–5. doi: 10.1186/s12931-017-0698-3

10. Navinés-Ferrer A, Serrano-Candelas E, Lafuente A, Muñoz-Cano R, Martín M, Gastaminza G. MRGPRX2-mediated mast cell response to drugs used in perioperative procedures and anaesthesia. *Sci Rep* (2018) 8:11628. doi: 10.1038/s41598-018-29965-8

11. Varricchi G, Pecoraro A, Loffredo S, Poto R, Rivellese F, Genovese A, et al. Heterogeneity of human mast cells with respect to MRGPRX2 receptor expression and function. *Front Cell Neurosci* (2019) 13:299. doi: 10.3389/fncel.2019.00299

12. Chompunud Na Ayudhya C, Amponnawarat A, Ali H. Substance p serves as a balanced agonist for MRGPRX2 and a single tyrosine residue is required for β-arrestin recruitment and receptor internalization. *Int J Mol Sci* (2021) 22:5318. doi: 10.3390/ijms22105318

13. Lu L, Kulka M, Unsworth LD. Peptide-mediated mast cell activation: ligand similarities for receptor recognition and protease-induced regulation. *J Leukoc Biol* (2017) 102:237–51. doi: 10.1189/jlb.3RU1216-539R

14. Yang F, Guo L, Li Y, Wang G, Wang J, Zhang C, et al. Structure, function and pharmacology of human itch receptor complexes. *Nature* (2021) 600:164–9. doi: 10.1038/s41586-021-04077-y

15. Cao C, Kang HJ, Singh I, Chen H, Zhang C, Ye W, et al. Structure, function and pharmacology of human itch GPCRs. *Nature* (2021) 600:170–5. doi: 10.1038/s41586-021-04126-6

16. Nothacker H-P, Wang Z, Zeng H, Mahata SK, O'Connor DT, Civelli O. Proadrenomedullin n-terminal peptide and cortistatin activation of MrgX2 receptor is based on a common structural motif. *Eur J Pharmacol* (2005) 519:191–3. doi: 10.1016/j.ejphar.2005.07.001

17. Lu L, Raj S, Arizmendi N, Ding J, Eitzen G, Kwan P, et al. Identification of short peptide sequences that activate human mast cells *via* mas-related g-protein coupled receptor member x2. *Acta Biomater* (2021) 136:159–69. doi: 10.1016/j.actbio.2021.09.011

18. Shore PA. A method for the fluorometric assay of histamine in tissues. *J Pharmacol Exp Ther* (1959) 127:182–6.

19. Lansu K, Karpiak J, Liu J, Huang XP, McCorvy JD, Kroeze WK, et al. In silico design of novel probes for the atypical opioid receptor MRGPRX2. *Nat Chem Biol* (2017) 13:529–36. doi: 10.1038/nchembio.2334

20. Koes DR, Baumgartner MP, Camacho CJ. Lessons learned in empirical scoring with smina from the CSAR 2011 benchmarking exercise. *J Chem Inf Model* (2013) 53:1893–904. doi: 10.1021/ci300604z

21. Trott O, Olson AJ. AutoDock vina: improving the speed and accuracy of docking with a new scoring function, efficient optimization, and multithreading. *J Comput Chem* (2010) 31:455–61. doi: 10.1002/jcc.21334

22. Lee J, Cheng X, Swails JM, Yeom MS, Eastman PK, Lemkul JA, et al. CHARMM-GUI input generator for NAMDOpenMM, and CHARMM/OpenMM simulations using the CHARMM36 additive force field. *J Chem Theory Comput* (2016) 12:405–13. doi: 10.1021/acs.jctc.5b00935

23. Abraham MJ, Murtola T, Schulz R, Páll S, Smith JC, Hess B, et al. GROMACS: high performance molecular simulations through multi-level parallelism from laptops to supercomputers. *SoftwareX* (2015) 1:19–25. doi: 10.1016/j.softx.2015.06.001

24. Maciejewski A, Pasenkiewicz-Gierula M, Cramariuc O, Vattulainen I, Rog T. Refined OPLS all-atom force field for saturated phosphatidylcholine bilayers at full hydration. *J Phys Chem B* (2014) 118:4571–81. doi: 10.1021/jp5016627

25. Kandt C, Ash WL, Tieleman DP. Setting up and running molecular dynamics simulations of membrane proteins. *Methods* (2007) 41:475–88. doi: 10.1016/j.ymeth.2006.08.006

26. Jorgensen WL, Tirado-Rives J. The OPLS [optimized potentials for liquid simulations] potential functions for proteins, energy minimizations for crystals of cyclic peptides and crambin. *J Am Chem Soc* (1988) 110:1657–66. doi: 10.1021/ja00214a001

27. Jorgensen WL, Maxwell DS, Tirado-Rives J. Development and testing of the OPLS all-atom force field on conformational energetics and properties of organic liquids. *J Am Chem Soc* (1996) 118:11225–36. doi: 10.1021/ja9621760

28. Jorgensen WL, Chandrasekhar J, Madura JD, Impey RW, Klein ML. Comparison of simple potential functions for simulating liquid water. *J Chem Phys* (1983) 79:926–35. doi: 10.1063/1.445869

29. Bussi G, Donadio D, Parrinello M. Canonical sampling through velocity rescaling. *J Chem Phys* (2007) 126:014101. doi: 10.1063/1.2408420

30. Nosé S. A molecular dynamics method for simulations in the canonical ensemble. *Mol Phys* (1984) 52:255–68. doi: 10.1080/00268978400101201

31. Essmann U, Perera L, Berkowitz ML, Darden T, Lee H, Pedersen LG. A smooth particle mesh ewald method. *J Chem Phys* (1995) 103:8577–93. doi: 10.1063/1.470117

32. Hub JS, de Groot BL, van der Spoel D. g_wham a free weighted histogram analysis implementation including robust error and autocorrelation estimates. *J Chem Theory Comput* (2010) 6:3713–20. doi: 10.1021/ct100494z

33. Chipot C, Pohorille A. Free energy calculations. *Springer* (2007) 86:159–84. doi: 10.1007/978-3-540-38448-9

34. Azimi E, Reddy VB, Pereira PJS, Talbot S, Woolf CJ, Lerner EA. Substance p activates mas-related G protein–coupled receptors to induce itch. *J Allergy Clin Immunol* (2017) 140:447–53. doi: 10.1016/j.jaci.2016.12.980

35. Humphrey W, Dalke A, Schulten K. VMD: visual molecular dynamics. *J Mol Graph* (1996) 14:33–8. doi: 10.1016/0263-7855(96)00018-5

36. Kumar S, Nussinov R. Close-range electrostatic interactions in proteins. *ChemBioChem* (2002) 3:604–17. doi: 10.1002/1439-7633(20020703)3:7<604::AID-CBIC604>3.0.CO;2-X

37. Zhang B, Weng Z, Sismanopoulos N, Asadi S, Therianou A, Alysandratos K-D, et al. Mitochondria distinguish granule-stored from *de novo* synthesized tumor necrosis factor secretion in human mast cells. *Int Arch Allergy Immunol* (2012) 159:23–32. doi: 10.1159/000335178

38. O'Connor TM, O'Connell J, O'Brien DI, Goode T, Bredin CP, Shanahan F. The role of substance p in inflammatory disease. *J Cell Physiol* (2004) 201:167–80. doi: 10.1002/jcp.20061

39. Meixiong J, Anderson M, Limjunyawong N, Sabbagh MF, Hu E, Mack MR, et al. Activation of mast-cell-expressed mas-related G-protein-coupled receptors drives non-histaminergic itch. *Immunity* (2019) 50:1163–71. doi: 10.1016/j.immuni.2019.03.013

40. Che D, Zheng Y, Hou Y, Du X, Jia T, Zhao Q, et al. Action of substance(9-20) on different excitation sites of MRGPRX2 induces differences in mast cell activation. *Int Immunopharmacol* (2021) 101:108342. doi: 10.1016/j.intimp.2021.108342

41. Subramanian H, Gupta K, Guo Q, Price R, Ali H. Mas-related gene X2 (MrgX2) is a novel G protein-coupled receptor for the antimicrobial peptide LL-37 in human mast cells: resistance to receptor phosphorylation, desensitization, and internalization. *J Biol Chem* (2011) 286:44739–49. doi: 10.1074/jbc.M111.277152

42. Lazki-Hagenbach P, Kleeblatt E, Ali H, Sagi-Eisenberg R. Spatiotemporal patterns of substance p-bound MRGPRX2 reveal a novel connection between macropinosome resolution and secretory granule regeneration in mast cells. *Front Immunol* (2022) 13. doi: 10.3389/fimmu.2022.892239

43. Azimi E, Reddy VB, Shade K-TC, Anthony RM, Talbot S, Pereira PJS, et al. Dual action of neurokinin-1 antagonists on mas-related GPCRs. *JCI Insight* (2016) 1. doi: 10.1172/jci.insight.89362

44. Ogasawara H, Furuno M, Edamura K, Noguchi M. Novel MRGPRX2 antagonists inhibit IgE-independent activation of human umbilical cord blood-derived mast cells. *J Leukoc Biol* (2019) 106:1069–77. doi: 10.1002/JLB.2AB1018-405R

45. Callahan BN, Kammala AK, Syed M, Yang C, Occhiuto CJ, Nellutla R, et al. Osthole, a natural plant derivative inhibits MRGPRX2 induced mast cell responses. *Front Immunol* (2020) 11:703. doi: 10.3389/fimmu.2020.00703

46. Ding Y, Che D, Li C, Cao J, Wang J, Ma P, et al. Quercetin inhibits Mrgprx2-induced pseudo-allergic reaction *via* PLCγ-IP3R related Ca2+ fluctuations. *Int Immunopharmacol* (2019) 66:185–97. doi: 10.1016/j.intimp.2018.11.025

47. Wang J, Zhang Y, Li C, Ding Y, Hu S, An H. Inhibitory function of shikonin on MRGPRX2-mediated pseudo-allergic reactions induced by the secretagogue. *Phytomedicine* (2020) 68:153149. doi: 10.1016/j.phymed.2019.153149

48. Wang N, Che D, Zhang T, Liu R, Cao J, Wang J, et al. Saikosaponin a inhibits compound 48/80-induced pseudo-allergy *via* the Mrgprx2 pathway *in vitro* and *in vivo*. *Biochem Pharmacol* (2018) 148:147–54. doi: 10.1016/j.bcp.2017.12.017

49. Wang J, Zhang Y, Hu S, Ge S, Jia M, Wang N. Resveratrol inhibits MRGPRX2-mediated mast cell activation *via* Nrf2 pathway. *Int Immunopharmacol* (2021) 93:107426. doi: 10.1016/j.intimp.2021.107426

50. Zhang Y, Wang J, Ge S, Zeng Y, Wang N, Wu Y. Roxithromycin inhibits compound 48/80-induced pseudo-allergy *via* the MrgprX2 pathway both *in vitro* and *in vivo*. *Cell Immunol* (2020) 358:104239. doi: 10.1016/j.cellimm.2020.104239

frontiers | Frontiers in Immunology

TYPE Original Research
PUBLISHED 10 May 2023
DOI 10.3389/fimmu.2023.1154108

OPEN ACCESS

EDITED BY
Ulrich Blank,
Institut National de la Santé et de la Recherche Médicale (INSERM), Paris, France

REVIEWED BY
Guido Falduto,
University of Pittsburgh, United States
Ivan Dzhagalov,
National Yang Ming Chiao Tung University, Taiwan

*CORRESPONDENCE
Margarita Martín
martin_andorra@ub.edu

RECEIVED 30 January 2023
ACCEPTED 03 April 2023
PUBLISHED 10 May 2023

CITATION
Guo Y, Ollé L, Proaño-Pérez E, Aparicio C, Guerrero M, Muñoz-Cano R and Martín M (2023) MRGPRX2 signaling involves the Lysyl-tRNA synthetase and MITF pathway. *Front. Immunol.* 14:1154108. doi: 10.3389/fimmu.2023.1154108

MRGPRX2 signaling involves the Lysyl-tRNA synthetase and MITF pathway

Yanru Guo[1,2], Laia Ollé[1,2], Elizabeth Proaño-Pérez[1,2,3], Cristina Aparicio[1], Mario Guerrero[1], Rosa Muñoz-Cano[2,4,5] and Margarita Martín[1,2,5]*

[1]Biochemistry and Molecular Biology Unit, Biomedicine Department, Faculty of Medicine and Health Sciences, University of Barcelona, Barcelona, Spain, [2]Clinical and Experimental Respiratory Immunoallergy (IRCE), Institut d'Investigacions Biomediques August Pi i Sunyer (IDIBAPS), Barcelona, Spain, [3]Faculty of Health Sciences, Technical University of Ambato, Ambato, Ecuador, [4]Allergy Department, Hospital Clinic, University of Barcelona, Barcelona, Spain, [5]Redes de Investigación Cooperativa Orientadas a Resultados en Salud (RICORS), Instituto de Salud Carlos III, Madrid, Spain

MRGPRX2, a G-protein-coupled-seven transmembrane domain receptor, is mainly expressed in mast cells and neurons and is involved in skin immunity and pain. It is implicated in the pathophysiology of non-IgE-mediated immediate hypersensitivity and has been related to adverse drug reactions. Moreover, a role has been proposed in asthma, atopic dermatitis, contact dermatitis, and chronic spontaneous urticaria. Although it has a prominent role in disease, its signaling transduction is poorly understood. This study shows that MRGPRX2 activation with substance P increased Lysyl t-RNA synthetase (LysRS) translocation to the nucleus. LysRS is a moonlighting protein with a dual role in protein translation and IgE signaling in mast cells. Upon allergen- IgE-FcεRI crosslinking, LysRS is translocated to the nucleus and activates microphthalmia-associated transcription factor (MITF) activity. In this study, we found that MRGPRX2 triggering led to MITF phosphorylation and increased MITF activity. Therefore, overexpression of LysRS increased MITF activity after MRGPRX2 activation. MITF silencing reduced MRGPRX2-dependent calcium influx and mast cell degranulation. Furthermore, a MITF pathway inhibitor, ML329, impaired MITF expression, calcium influx, and mast cell degranulation. Moreover, drugs such as atracurium, vancomycin, and morphine, reported to induce MRGPRX2-dependent degranulation, increased MITF activity. Altogether, our data show that MRGPRX2 signaling enhances MITF activity, and its abrogation by silencing or inhibition resulted in defective MRGPRX2 degranulation. We conclude that MRGPRX2 signaling involves the LysRS and MITF pathway. Thus, MITF and MITF-dependent targets may be considered therapeutic approaches to treat pathologies where MRGPRX2 is implicated.

KEYWORDS

MRGPRX2, LysRS, MITF, mast cell degranulation, adverse drug reactions

Introduction

Mast-related G-protein-coupled receptor member X2 (MRGPRX2) is mainly expressed on mast cells (MC) (abundantly in skin MC) and neurons. MRGPRX2 is physiologically involved in host defense, tissue homeostasis and repair, nociception, inflammatory pain, and itch (1, 2). Endogenous and exogenous ligands have been described to bind MRGPRX2. Endogenous ligands such as substance P, human β-defensins, or vasointestinal peptide, directly involved in pain and itch, are directly related to its physiological functions (3). These effects can become chronic inflammation in a pathological state (4–6). Regarding exogenous ligands, several have been identified, such as mastoparan (bee wasp venom component), cationic peptidergic drugs, neuromuscular blocking agents (NMBAs) (e.g., atracurium, cisatracurium, and rocuronium), opiates, and antibiotics such as fluoroquinolones and vancomycin. Most of these exogenous ligands are the molecular basis of MRGPRX2-dependent adverse drug reactions (7, 8). Several molecules, such as natural compounds, cytokines, peptides, and DNA aptamers, have been described to prevent MRGPRX2-mediated pseudo-allergic responses and inflammation (9–11).

Yet, MRGPRX2 signaling is still poorly understood. To better understand how to modulate MRGPRX2 actions to dodge pathological states, some progress in unrevealing MRGPRX2 signaling has been made; however, more effort is needed. Proteins G, Gαi, and/or Gαq are involved in the early signals (12, 13), and calcium mobilization is rapid and transient (14). Further downstream events include MAP kinases (ERK1/2), p38, and PI3K (15). Furthermore, GTPase activation (Cdc42) upstream of the unconventional class I myosin 1f (MYO1F) regulates actin cytoskeleton dynamics and granule release (16). Lately, β arrestins 1 and 2 (involved in GPCR desensitization) have been proposed to interfere with MRGPRX2-dependent degranulation (17).

Microphthalmia associated-transcription factor (MITF) is a basic-helix-loop-helix-leucine zipper (bHLH-ZIP) family member. MITF involves many biological processes, including cell differentiation, survival, senescence, metabolism, and DNA damage repair (18). The principal cell types affected in MITF-deficient mice are MCs, osteoclasts, and melanocytes (19). Moreover, MC and basophil cell fates are determined by the antagonistic regulation of C/EBPα and MITF (20). Additionally, MITF is downstream of KIT and FcεRI pathways (21–23). Nevertheless, most information about MITF stems from its essential role in melanocyte biology and melanoma as an oncogene (24–26). Post-translational modifications are primarily subject to the transcriptional activity of MITF. MITF is phosphorylated by ERK1/2 at Ser73 and by p90 ribosomal S6 kinase (p90RSK) at Ser409 (27–29). MITF phosphorylation at Ser73 has been associated with increased activity and double phosphorylation at Ser73 and Ser409 has been related to proteasome degradation (29). MITF activity can be repressed by HINT1 (histidine triad nucleotide-binding protein 1) (30).

Lysyl-tRNA synthetase (LysRS), a paradigm of a multifunctional protein in MCs, is involved in protein translation (canonical function) and upon FcεRI triggering in MITF activation (non-canonical role) (23). After IgE crosslinking, MAP kinase activation phosphorylates cytosolic LysRS (Ser 207). Phosphorylation in LysRS alters its binding to the multi-tRNA synthetase complex (MSC)-p38 in the cytosol and allows translocation to the nucleus, synthesizing diadenosine tetraphosphate (Ap4A). The Ap4A accumulated in the nuclei of IgE-activated MCs binds to HINT1, a MITF repressor, and liberates MITF, activating MITF-dependent gene expression. MITF regulates numerous genes encoding essential proteins involved in MC proinflammatory events, such as histidine decarboxylase (Hdc) (31), which catalyzes histamine synthesis; granzyme B (GrB), which participates in the cytotoxic action of MCs (32) or PGD2 synthase increasing PGD2 levels (33).

Our group recently characterized the mutation LysRS P542R in a patient with severe anaphylaxis to Hymenoptera. A substitution of proline by arginine disrupts the protein's functional motion, promoting an open state similar to the phosphorylated wild-type form. Altogether, this results in a constitutive increase in MITF activity (34).

MRGPRX2 has been related to several pathologies, from immediate-type hypersensitivity reactions (adverse drug reactions, Hymenoptera venoms reactions) to prolonged type- 2 inflammation (such as chronic asthma or chronic spontaneous urticaria) (1, 2, 4). Therefore, it is essential to understand the molecular groundwork of MRGPRX2 and the associated intracellular signaling components to manage the treatment of MRGPRX2-associated diseases. The current study explores the MRGPRX2-LysR-MITF pathway in mast cell exocytosis.

Materials and methods

Antibodies and reagents

Anti-MITF (clone D5G7V) and phospho-p44/42 MAPK antibodies were from Cell Signaling Technology (Danvers, MA, USA). Anti-phospho-MITF (Ser73/180) and mouse anti-αTubulin antibodies were from Sigma-Aldrich (St. Louis, MO, USA). Rabbit anti-Lamin β1 antibody was purchased from Abcam (Cambridge, UK). PE anti-human FcεRI antibody was obtained from Thermo Fisher Scientific (Waltham, MA, USA). Anti-LysRS (D-4) and PE anti-human CD117 were obtained from Santa Cruz Biotechnology, Inc (Santa Cruz, CA, USA). PE anti-human MRGPRX2 was from Bio Legend (San Diego, CA, USA). APC anti-human CD63 and FITC Annexin V were from ImmunoTools GmbH (Friesoythe, Germany). Biotinylated human IgE was from Abbiotec (San Diego, CA, USA), and streptavidin was from Sigma (St. Louis, MO, USA). Substance P was from AnaSpec (Fremont, CA). ML329 was obtained from Axon Med Chem (Groningen, The Netherlands). Morphine was obtained from B. Braun Medical S.A (Spain), the muscle relaxant atracurium was from Pfizer Inc (NY, USA), meglumine amidotrizoate was from Juste Laboratories (Spain), and the vancomycin antibiotic was from Normon (Spain).

Cell culture

The LAD2 human mast cell line was a kind gift from Drs. A. Kirshenbaum and D.D. Metcalfe (National Institutes of Health, Bethesda, MD), culturing in StemPro-34 media, supplemented with StemPro-34 nutrient (Thermo Fisher Scientific; Waltham, MA, USA) and 2mM L-glutamine (Lonza), 100 U/mL penicillin (Lonza) and 100 µg/mL streptomycin (Lonza), and 100 ng/mL SCF (ImmunoTools GmbH, Friesoythe, Germany) (35). Primary human mast cells (huMCs) derived from $CD34^+$ -positive peripheral blood cells were obtained from healthy donors, CD117 MicroBeads Kit (Mitenyi Biotec, Germany) for $CD34^+$ progenitor cell isolation. Cells were cultured for 0-2 weeks with 100 ng/ml SCF, IL-6, and IL-3 (ImmunoTools GmbH, Friesoythe, Germany) and 2-6 weeks with 100 ng/ml IL-6 and SCF. After six weeks, $CD34^+$ -derived human MCs were assessed by surface expression of FcεRI and CD117. The expression of anti-human PE-MRGPRX2 was also checked for experiments. The HEK 293LTV cell line (Cell Biolabs Inc, San Diego, CA, USA) was used for lentivirus production.

Western blotting

$7{\cdot}10^6$ cells were activated with substance P (MedChemExpress, NJ, USA) at different times. Cellular fractioning was performed as described elsewhere (36). The protein concentration was determined using the Protein Assay Dye Bio-Rad Kit (Bio-Rad Laboratories, Inc. USA) according to the manufacturer's recommendations. Electrophoresis was performed using NuPage TM 4-12% Bis-Tris Gel, 1.5 mm 15 w (Invitrogen, USA), and electrotransferred to polyvinylidene difluoride (PVDF) membranes (Millipore, Bedford, MA, USA). In all blots, proteins, after specific antibody incubation, were visualized by enhanced chemiluminescence (Western Bright TM ECL, Advansta, USA).

Lentiviral transduction

Lentiviral particles were generated in HEK293LTV. The non-target (NT) sequence was as follows: 5'CCGGCAACAAGATGAAGAGCACCAACTCGAGTTGGTGCTCTTCATCTTGTTGTTTTT 3', MITF shRNA 2 sequence: 5'CCGGCGGGAAACTTGATTGATCTTTCTCGAGAAAGATCAATCAAGTTTCCCGTTTTTG 3'. MITF shRNA 3 sequence: 5' CCGGGGGAGCTCACAGCGTGTATTTCTCGAGAAATACACGCTGTGAGCTCCCTTTTTG 3'.

According to the manufacturer's instructions, lentiviral particles to silence MITF gene expression were generated using Mission ® shRNA technology (Sigma, St. Louis, MO, USA). LAD2 cells were transduced with polybrene 8 µg/ml (Santa Cruz) and selected with puromycin 1µg/ml. Cells were maintained with puromycin until the day of the experiment, when it was removed prior to cell activation.

FACS staining

FcεRI and MRGPRX2 expression were detected by direct staining with the indicated Abs for 30 minutes at 4°C. KIT expression was detected using PE- anti-human CD117. Cells were analyzed using a FACSCalibur flow cytometer (FACScan; BD Biosciences). Dead cells were excluded based on their Forward (FSC) and side scattering (SSC) profiles.

Degranulation assays

Degranulation was analyzed based on CD63 expression on the cell membrane assessed by flow cytometry or via levels of β-hexosaminidase activity in the supernatant, as described in previous studies (8). Briefly, for CD63 determination: $1{\cdot}10^5$ cells/point were incubated with Tyrode's buffer or SP at 37°C for 30 min. Cells were incubated with blocking buffer (0.1% NaN_3, 2% FBS, 20% rabbit serum, PBS) for 30 min on ice, and APC anti-human CD63 staining was performed for 30 min on ice. After washing, samples were incubated with propidium iodide (PI), acquired with a FACSCalibur flow cytometer, and analyzed with FlowJo software. PI-positive cells were excluded from the analysis. For β-hexosaminidase assays (37), cells were seeded at $3{\cdot}10^4$ cells/well in 96 well plates in Tyrode's buffer and then activated with SP or left untreated for 30 min. An equal number of viable cells were used in each case. Supernatants were collected and incubated with P-nitrophenyl-N-acetyl-β-D-glucopyranoside (Sigma Aldrich) for 1h at 37°C. Triton (1%) was used to obtain total cell lysates of β-hexosaminidase. Absorbance was read at 405nm. β-hexosaminidase enzyme activity was expressed as the release percentage: β-hexosaminidase release = [cell degranulation/(cell degranulation + total lysate)] x100.

PGD2 ELISA

PGD2 release was determined from the supernatants of cells ($2.5{\cdot}10^4$ cells/well) activated with substance P (2µM) overnight using a specific competitive Enzyme Immunoassay for PGD2 (Cusabio Technology LLC, Houston, TX, USA) according to the manufacturer's instructions.

Apoptosis assay

Apoptosis was measured using FITC Annexin V (BD Pharmingen, San Jose, CA, USA) according to the manufacturer's suggested protocol and analyzed by flow cytometry. Caspase activity was assayed using the Caspases-Glo® 3/7 Assay (Promega, San Luis Obispo, CA, USA) according to the manufacturer's instructions.

Calcium release assay

Cells were incubated with 2 μM Fluo-4, AM cell permeant (Thermo Fisher Scientific; Waltham, MA, USA), at 37°C for 30 minutes, then washed, and resuspended in Tyrode's buffer. An equal number of viable cells were used in each case. After defining basal conditions, SP (or ionomycin) was immediately added to the cells (Sigma-Aldrich, St. Louis, MO, USA), and fluorescence was determined every 10 sec using a TECAN SPARK microplate reader.

Luciferase assay

Firefly luciferase under the control of the TRPM1 promoter and control vector PGL3-Luciferase was a gift from David Fisher (Harvard Medical School) (38). $2.5{\cdot}10^4$ cells were transfected with the Firefly and Renilla reporters at a ratio of 7:1, respectively. This reporter gene was transfected to the cells with a Renilla luciferase reporter gene, and the results were normalized to the empty vector-transfected conditions. Transfections were performed with lipofectamine. We used SP at a higher concentration for this assay to see significant gene reporter activation. Luciferase activity was detected using the Dual-Luciferase® Reporter Assay System (Promega, Madison, WI) following the manufacturer's instructions. Firefly Luciferase data were normalized according to Renilla luciferase data.

GFP and LysRS WT-GFP transfection in LAD2 cells

LAD2 cells were transfected with human LysRS (KARS WT) pcDNA 3.1+C-eGFP vector and GFP empty vector (obtained from GenScript Biotech, The Netherlands)) as previously reported (34).

Statistical analysis

Statistical analyses were performed using PRISM 9 (GraphPad Software, La Jolla, CA, USA). All results are expressed as mean ± standard error of the mean (SEM). After determining the normal distribution of the samples and variance analysis, a t-test was used to determine significant differences (p-value) between two experimental groups, and two-way ANOVA was used to determine significant differences (p-value) between several experimental groups. "*"P<0.05, "**" P<0.01, "***"P<0.001, "****"P<0.0001.

Results

MRGPRX2 activation increases the translocation of LysRS to the nucleus

MRGPRX2 signaling transduction increases ERK1/2 activity (15). On the other hand, Lysyl-tRNA synthetase (LysRS) is phosphorylated at Ser 207 and translocated into the nucleus downstream of IgE/FcεRI signaling activation (23, 39). We wanted to explore whether MRGPRX2 signaling involves LysRS and its translocation to the nucleus. Ligands, such as SP, have shown MRGPRX2-dependent MC activity (40, 41). Thus, MCs (LAD2) were activated with substance P, cellular fractionation was carried out, and the LysRS location was explored. Our results show a rapid and transient phosphorylation of ERK1/2 and an increase in LysRS translocation to the nucleus of activated cells (Figure 1).

MRGPRX2 activation increases MITF phosphorylation

Downstream of IgE signaling, the translocation of LysRS into the nucleus switches its catalytic activity in the production of diadenosine oligophosphate Ap4A, which binds to HINT, dissociating the MITF-HINT repressor complex and liberating MITF (23, 42). We next analyzed MITF activity in the context of MRGPRX2 activation. Since phosphorylation of MITF at Ser 73 has been associated with transcriptional activity (29), we examined whether MRGPRX2 increased MITF phosphorylation. As shown in Figure 2, MRGPRX2-dependent activation enhanced MITF phosphorylation in the cytoplasm and nucleus (note the pMITF/MITF ratio). Interestingly, MITF expression was mainly detectable in the nucleus before stimulation. However, after MRGPRX2 triggering, MITF levels increased in the cytosol. After 15 minutes, MITF returned close to the steady state. This is consistent with data regarding MITF posttranscriptional regulation in melanocytes where phosphorylation of MITF regulates its nuclear export, and via this export-import cycle, MITF activity can be tuned (43).

MRGPRX2 signaling increases MITF activity

Next, we assessed whether LysRS translocation to the nucleus and MITF phosphorylation after MRGPRX2 signaling resulted in increased MITF activity. We used a reporter gene assay, Melastatin 1 (TRPM1) promoter-controlled firefly luciferase, for that purpose. MITF is the main transcriptional regulator of TRPM1 (44). Thus, luciferase expression correlates with MITF activity (45). Results show that MITF activity increased after MRGPRX2 stimulation (Figure 3A). Moreover, when cells overexpressed LysRS WT-GFP (Figure 3B), a notorious increase in MITF activity was detected after substance P stimulation (Figure 3C). In that context, we also analyzed whether this increase in activity was concomitant to an increase in a MITF-dependent target such as PGD2 (33). Results show that PGD2 significantly increased in LysRS WT-GFP transfected cells after MRGPRX2 activation (Figure 3D).

MITF silencing decreases MRGPRX2-dependent mast cell degranulation

We next explored the role of MITF in MRGPRX2-dependent degranulation. Cells were silenced using lentivirus technology with two specific sequences to that end. The two sequences satisfactorily

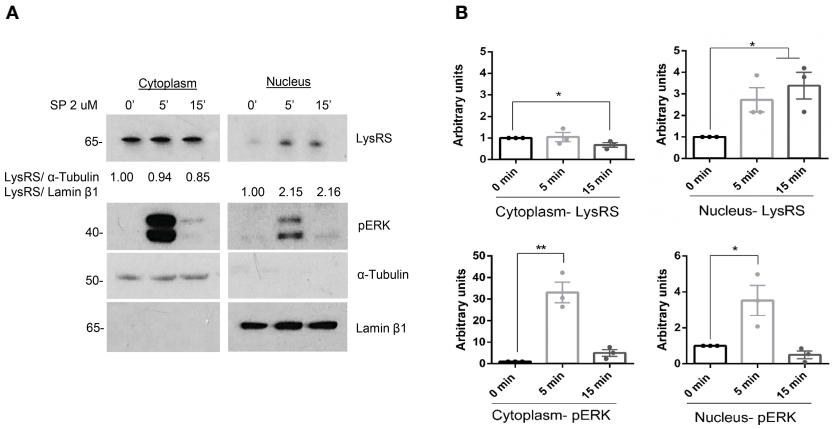

FIGURE 1
LysRS translocates to the nucleus after MRGPRX2 activation in mast cells (LAD2). **(A)** Cells were activated with 2 μM substance P (SP) at various times. Cytoplasmic and nuclear fractions were isolated, and western blots for LysRS and pERK were performed. α-tubulin and Lamin β1 markers for cytoplasm and nuclei, respectively, were used to assess cellular fraction purification and as loading controls. **(B)** The unpaired t-test was used for statistical analysis (*p < 0.05*, **p < 0.01). Experiments are the mean ± SEM (n=3).

knocked down the levels of MITF (Figure 4A). Degranulation measured by β-hexosaminidase release (Figure 4B) and CD63 expression by FACS (Figure 4C and Supplementary Figure 1A) showed a significant reduction after SP stimulation. In addition, calcium influx significantly diminished after MITF silencing in MRGPRX2 activation (Figure 4D). None or little difference was observed when ionomycin was used as a primary stimulus. MRGPRX2 expression levels after MITF silencing were consistent, and all cells were positive (Supplementary Figure 2A). The mean of fluorescence intensity was lower, however, total MRGPRX2 levels analyzed by blotting showed no reduction in MITF silencing samples compared to Non-target (NT) control (Supplementary Figure 3). MITF is involved in cell survival in different cellular models (46, 47), thus downregulation of this transcription factor may induce apoptosis. Next, we assessed apoptosis in MITF-knockdown cells. MITF silencing significantly increased cellular apoptosis (Supplementary Figure 4A). The increase in apoptosis was higher in cells with lower MITF levels. An equal number of live cells were used in all assays, exclusion of dead cells was performed when possible and MRGPRX2-dependent degranulation and calcium influx were still significantly decreased, in MITF-silenced cells.

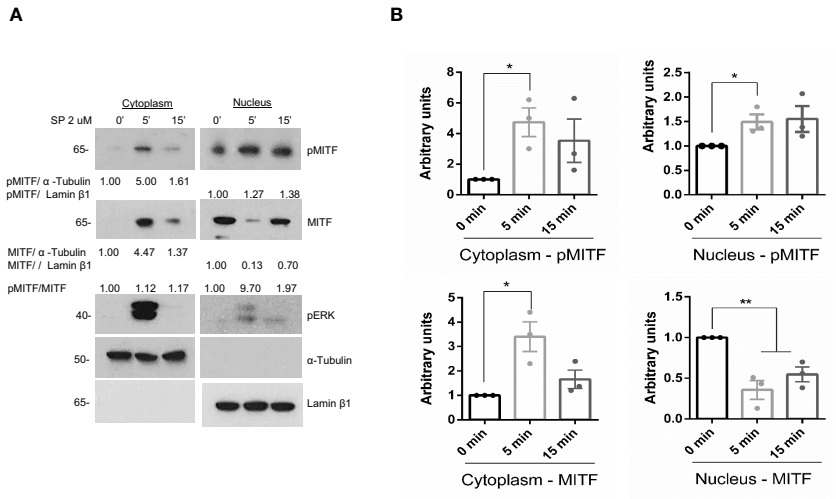

FIGURE 2
MITF is phosphorylated after MRGPRX2 activation in mast cells (LAD2). **(A)** Cells were activated with 2 μM substance P (SP) at various times. Cytoplasmic and nuclear fractions were isolated, western blots for pMITF (Ser 73/180), and MITF were performed, α-tubulin and Lamin β1 markers for cytoplasm and nuclei, respectively, were used to assess cellular fraction purification and as loading controls. **(B)** The unpaired t-test was used for statistical analysis (*p < 0.05, **p < 0.01). Experiments are the mean ± SEM (n=3).

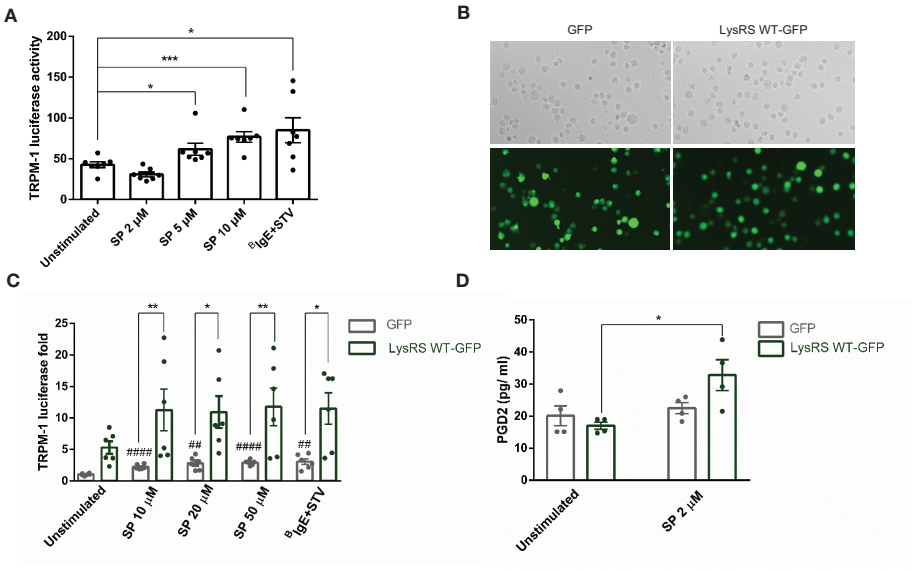

FIGURE 3
MRGPRX2 activation increases MITF activity via LysRS in mast cells (LAD2). **(A)** Cells were activated with 2 µM substance P (SP) at various concentrations for 6 hours in LAD2 cells transfected with TRPM1-luciferase gene reporter, as described in the materials and methods section. Biotinylated-IgE (0.1 µg/ml) was incubated overnight, and then, streptavidin (16 µg/mL) was added for 6 hours and used as a positive control. The unpaired t-test was used for statistical analysis (*p < 0.05, ***p < 0.001). **(B)** LAD2 cells were transfected with GFP and LysRS WT-GFP plasmids **(C)** and then activated at various SP concentrations, and biotinylated-IgE+ streptavidin was used as indicated above. The unpaired t-test used for statistical analysis (##p < 0.01, #### p<0.0001, SP *vs.* unstimulated GFP transfected LAD2 cells). The two-way ANOVA test was used for statistical analysis (*p < 0.05, **p < 0.01, GFP LAD2 *vs.* LysRS WT-GFP LAD2). **(D)** PGD2 after SP activation was measured in GFP and LysRS WT-GFP LAD2 cells. A two-way ANOVA test was used for statistical analysis (*p<0.05, GFP *vs.* LysRS WT-GFP). Experiments are the mean ± SEM (n=3).

ML329 inhibits MITF expression and impairs MRGPRX2-dependent mast cell degranulation

ML329 has been described to inhibit the MITF pathway (38, 48) therefore we used this inhibitor to reinforce data about MITF involvement in MRGPRX2 signaling. Cells treated with different concentrations of ML329 showed a decrease in MITF expression (Figure 5A). MITF reduction was always more consistent after day 5 thus the following experiments were performed on that day. Cells treated with ML329 showed decreased degranulation measured by CD63 expression (Figure 5B and Supplementary Figure 1B). Calcium influx was also impaired after MRGPRX2 activation, although the ionomycin response was not significantly affected (Figure 5C). MRGPRX2 expression after ML329 was similar in all cases (Supplementary Figure 2B). Like MITF silencing, ML329 also induced significant cellular apoptosis at a higher concentration (Supplementary Figure 4B). Altogether, decreased MITF levels correlated with reduced MRGPRX2-dependent degranulation and calcium influx.

$CD34^+$ -derived human MCs were also used to analyze the effect of MITF reduction on degranulation. Human MCs fully differentiated from CD34 cells were treated with ML329 for five days. Cells were activated with SP, and CD63 staining was used to measure degranulation (Figure 6). The analysis was performed in the live cell population (propidium iodide negative). Our results show that ML329 treatment led to a significant reduction in MRGPRX2-dependent mast cell degranulation.

Drug activation of MRGPRX2 induces MITF activity

One of the fascinating biological aspects that makes this receptor a current hot research topic is its ability to interact with several drugs and be involved in adverse drug reactions.

Our group showed that vancomycin, atracurium, and morphine induce MRGPRX2-dependent degranulation (8). Meglumine amidotrizoate was also described to interact with MRGPRX2 (49). Next, we analyzed whether these drugs were able to increase MITF activity by using Melastatin 1 (TRPM1) promoter-controlled firefly luciferase. Our results show that all were able to increase MITF activity (Figure 7). These data indicate that MITF activity is induced by several drugs reported to mediate their actions through MRGPRX2 signaling thus MITF is a MRGPRX2-dependent downstream signal for endogenous (SP) and exogenous ligands (atracurium, vancomycin…).

Discussion

Despite the increasing number of studies on MRGPRX2 in recent years, the dissection of its signaling pathway in MCs is poorly understood. Several studies focus on identifying new receptor ligands and how to block ligand recognition or involvement in pathology. To advance in the knowledge of MRGPRX2, one significant limitation is the lack of the crystal structure which prevents a complete characterization of ligand binding sites and a

10.3389/fimmu.2023.1154108

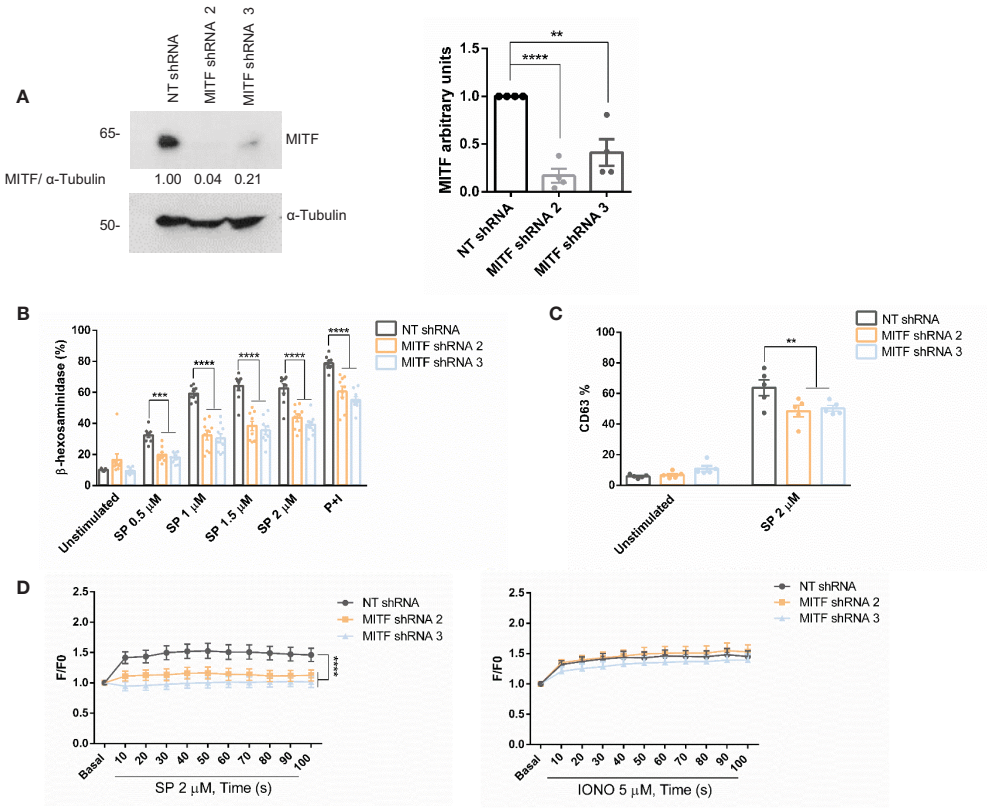

FIGURE 4
MITF silencing reduces degranulation and $Ca2^{+}$ influx. **(A)** LAD2 cells were transduced with control NT (non-target) shRNA or MITF shRNA 2 or MITF shRNA 3, and the efficiency of MITF silencing was assessed by western blot. α-Tubulin was used as a loading control. The unpaired t-test was used for statistical analysis (**p < 0.01*, ****p < 0.0001). Experiments are the mean ± SEM (n=4). **(B)** β-hexosaminidase was performed with different concentrations of SP and P+I (PMA+ionomycin, 10 ng/mL+0.5 µM) as a positive control in NT and MITF-silenced cells, n=4. **(C)** Degranulation was determined by flow cytometry using CD63 staining in unstimulated and SP (2uM) in the alive population (propidium iodide negative staining) in NT and MITF-silenced cells. **(D)** NT and MITF-silenced LAD2 cells were preincubated with Fluo4 and activated with SP (2µM) or ionomycin. A two-way ANOVA test was used for statistical analysis (**p<0.01, ***p<0.001, ****p<0.0001). Experiments are the mean ± SEM (n=3).

proper design of agonists/antagonists. Nevertheless, molecular modeling experiments have identified crucial amino acids for endogenous binding ligands, such as substance P, and exogenous ligands such as cationic agonists or opioids (12, 50, 51). MRGPRX2-triggered degranulation depends on Gαi, Gαq, Ca^{++} channels, ERK, and PI3K (14, 15). Cytoskeleton dynamics and granule exocytosis need Cdc42 GTPase activation and the participation of unconventional class I myosins, MYO1F (16), and β1 and β2 arrestins regulate the kinetics and the extent of MRGPRX2 cellular activity (17). The present study adds more insights into MRGPRX2 signals and demonstrates the involvement of the LysRS-MITF pathway.

LysRS is a moonlighting protein that belongs to the aminoacyl-tRNA synthetases (aaRS), which catalyze the aminoacylation reaction linking amino acids to their cognate tRNAs. They are highly conserved cytoplasmic and mitochondrial enzymes, one for each amino acid, and are responsible for the fidelity of gene code reading. During evolution, some aaRS acquired newly evolved domains that are not crucial for tRNA aminoacylation but are responsible for non-canonical functions (52). In this respect, LysRS, the aaRS that attaches lysine to its corresponding tRNA, is also involved in IgE-dependent signals upstream of the microphthalmia-associated transcription factor (MITF) in MCs (23). Upon IgE crosslinking, LysRS is phosphorylated (Ser 207) and translocated to the nucleus, where it catalyzes the synthesis of Ap4A as non-canonical activity. Ap4A binds to HINT, releasing MITF from the MITF-HINT1 inhibitory complex and causing an increase in the transcription of its target genes (23). MITF is a crucial hub in MC biology and function, according to the *Mitf*-mutant mouse phenotype, characterized by a reduced number and abnormal MCs (53–55).

In this study, we found that MRGPRX2 increases ERK1/2 phosphorylation rapidly and transiently. Our results agree with data showing that ERK1/2 is efficiently phosphorylated after MRGPRX2 in skin MCs and is more transiently induced than FcεRI signals (15). Nevertheless, this rapid signal allowed increased LysRS recruitment in the nucleus of MRGPRX2-activated cells. LysRS in the nucleus performs its non-canonical function, releasing MITF from the inactive HINT1-MITF complex (23). Moreover, MRGPRX2 signaling increased MITF phosphorylation (Ser 73).

10.3389/fimmu.2023.1154108

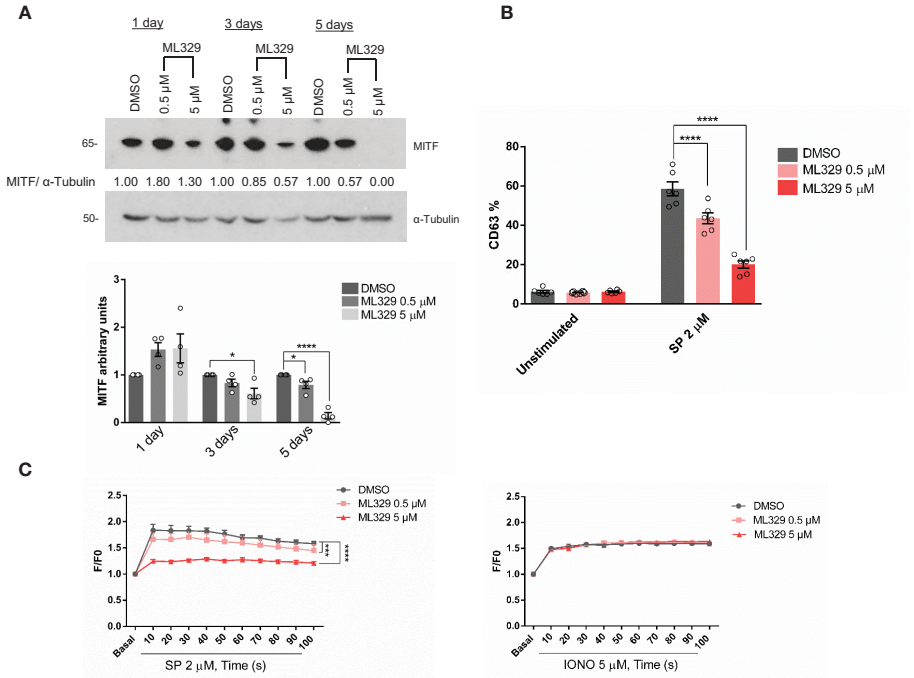

FIGURE 5
The MITF inhibitor ML329, reduces degranulation and $Ca2^{+}$ influx. **(A)** LAD2 cells were treated with either DMSO or ML329 at different concentrations on various days, and the efficiency of MITF silencing was assessed by western blot. α-Tubulin was used as a loading control. The unpaired t-test was used for statistical analysis after 5 days (*p < 0.05, ****p<0.0001). Experiments are the mean ± SEM (n=4). **(B)** Degranulation was determined by flow cytometry using CD63 staining in unstimulated and ML329 -treated cells (after 5 days) in the live population (propidium iodide negative staining). **(C)** DMSO and ML329 -treated cells (after 5 days) were preincubated with Fluo4 and activated with SP (2µM) or ionomycin. A two-way ANOVA test was used for statistical analysis (***p<0.001, ****p<0.0001). Experiments are the mean ± SEM (n=3).

The transcriptional activity of MITF is primarily regulated post-translationally. Most studies relating to MITF regulation have been performed in melanocytes showing that mainly ERK1/2 phosphorylates MITF at Ser73, p90 ribosomal S6 kinase (p90RSK) at Ser409, glycogen synthase kinase-3β (GSK3β) at Ser298, and p38 MAPK at Ser307 (27–29). MITF phosphorylation usually augments its activity. MAPK-mediated phosphorylation of MITF at Serine 73 combines the two coactivators, E1A binding protein p300 and cAMP-response element binding protein (p300/CBP), enhancing MITF transcriptional activity (56). However, dual phosphorylation at Ser73 and Ser409 endorses its ubiquitination and proteasome degradation (29). MITF A is the longest and most abundant isoform in mast cells (57). Ser 73 in MITF-M, the specific isoform in melanocytes, corresponds to Ser 180 in MITF-A.

Donor 1		
CD34⁺ derived mast cells		
Receptors	%	MFI
Iso/ KIT	4.89/ 96.10	3.63 / 40.90
Iso/ FcεRI	4.35/ 52.30	3.98 / 10.60
Iso/ MRGPRX2	5.85/ 73.00	3.69 / 12.70

Donor 2		
CD34⁺ derived mast cells		
Receptors	%	MFI
Iso/ KIT	5.03 / 94.70	3.02 / 43.00
Iso/ FcεRI	4.28 / 92.00	2.24 / 22.00
Iso/ MRGPRX2	4.43 / 99.80	3.71 / 95.70

Donor 3		
CD34⁺ derived mast cells		
Receptors	%	MFI
Iso/ KIT	5.88 / 63.10	3.65 / 25.10
Iso/ FcεRI	5.72 / 47.50	3.63 / 6.69
Iso/ MRGPRX2	5.61 / 25.70	3.75 / 5.30

Iso, Isotype ; MFI, mean fluorescence intensity

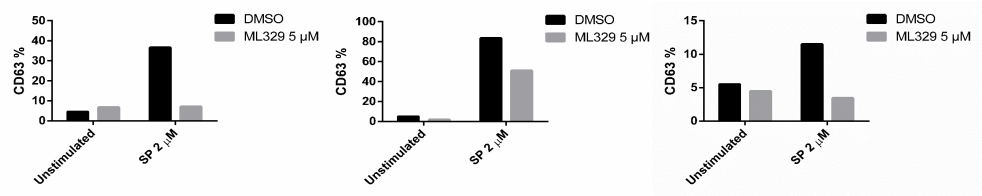

FIGURE 6
MITF inhibitor ML329 reduces $CD34^{+}$ derived hMCS degranulation. $CD34^{+}$ derived hMCs from three different healthy donors were assessed. KIT, FcεRI, and MRGPRX2 were checked by flow cytometry. Degranulation was determined by flow cytometry using CD63 staining in unstimulated and ML329-treated cells (after 5 days) in the live population (propidium iodide negative staining).

10.3389/fimmu.2023.1154108

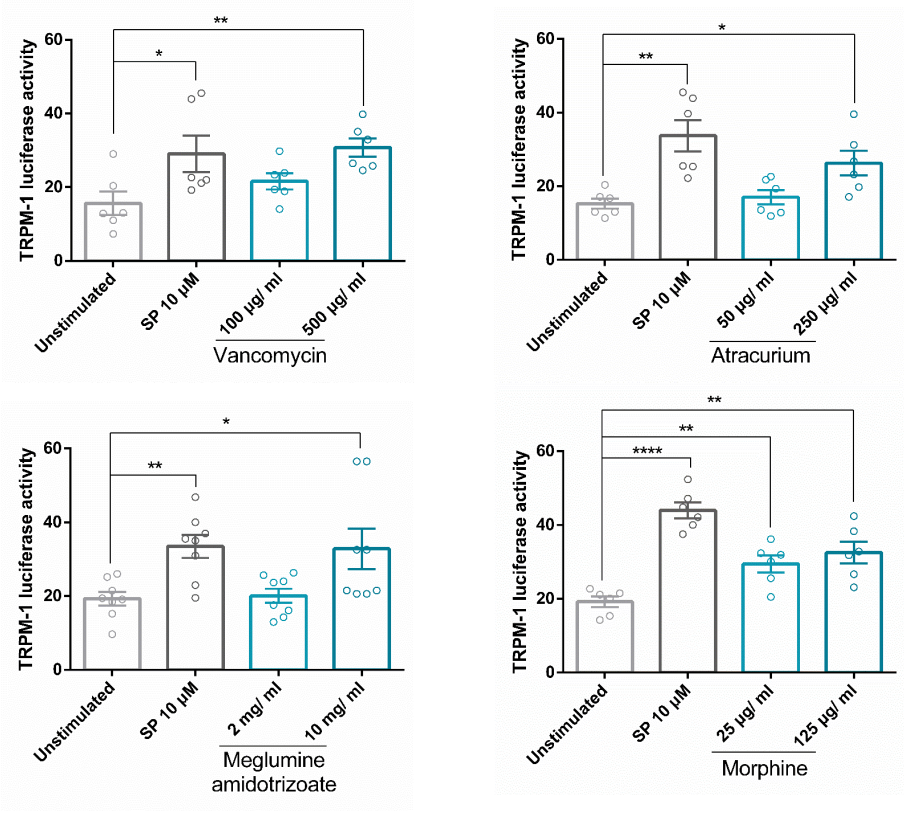

FIGURE 7
Drug activation of MRGPRX2 induces MITF activity. Cells were activated with SP or drugs (vancomycin, atracurium, morphine, and meglumine amidotrizoate) reported to induce MRGPRX2-dependent MC degranulation at various concentrations for 6 hours in LAD2 cells transfected with TRPM1-luciferase gene reporter. Experiments are the mean ± SEM (n=3 for vancomycin and atracurium, n=4 for meglumine amidotrixoate and morphine). The unpaired t-test was used for statistical analysis (*p < 0.05, **p < 0.01, ****p < 0.0001).

In our study, MRGPRX2 activation with SP increased MITF activity measured by the TRPM1-reporter gene. Overexpression of LysRS greatly enhanced MITF activity after SP stimulation. PGD2 production depends on MITF activity (33), thus, we observed that the augmented MITF activity was associated with an increase in PGD2. Altogether, MRGPRX2 ligation with substance P led to LysRS translocation to the nucleus, raising MITF activity. In parallel, MRGPRX2 signaling induced MITF phosphorylation, contributing to the increase in MITF activity.

MITF phosphorylation has been described as a mechanism of nuclear export-import of MITF to regulate the activity of this transcription factor in melanocytes (43). Interestingly, we found increased MITF in the cytosol after MRGPRX2 activation. Thus, it would be plausible that similar regulation events could occur in MCs. Nevertheless, this subject deserves further study.

MRGPRX2 ligation to exogenous ligands that can result in adverse drug reactions such as to atracurium, vancomycin, morphine, and meglumine amidotrizoate increases MITF activity, suggesting that endogenous and exogenous ligands use the LysRS-MITF pathway.

Selective silencing with MITF was effective after day 5, and previous experiments showed that the half-life of MITF was longer than expected for a transcription factor. Cycloheximide experiments from our group confirmed a complete reduction of protein levels after 96h drug treatment (data not shown). Similarly, using ML329, we see a significant decrease in protein levels at day 5. Our study indicates that MITF downregulation by shRNA silencing or ML329 treatment results in decreased MRGPRX2-dependent degranulation measured by β-hexosaminidase and CD63 plasma membrane expression. MITF function has been related to the biogenesis of lysosomes (58), and bone marrow-derived MCs from *Mitf* -/- mice display hypogranularity that can be restored with MITF addition (59). We examined whether our MITF-silenced cells had reduced granular content compared to control cells. Unfortunately, we could not find any apparent differences in our staining with Lysotracker in MITF-silenced cells compared to non-target controls (data not shown). Interestingly, downregulated MITF levels significantly decreased Ca2+ influx after substance P activation. MRGPRX2-dependent $Ca2^+$ is regulated by store-operated $Ca2^+$ entry (SOCE) *via* the calcium sensor, stromal interaction molecule 1 (STIM1) (60). STIM1 is an endoplasmic reticulum (ER) $Ca2^+$ sensor that, upon activation and decreased ER $Ca2^+$ levels, oligomerizes and activates Orai channels (Orai1/2/3), resulting in $Ca2^+$ influx (61). Indeed, STIM1 is crucial in promoting

the $Ca2^+$ influx needed for IgE-dependent mast cell activation and anaphylaxis (62). Recently, MITF has been reported to regulate STIM1 and SOCE expression in melanocytes (63). Chromatin immunoprecipitation (ChIP) and luciferase assays with truncated STIM1 promoters validated the MITF-STIM1 interaction. Functional assays confirmed that MITF regulates STIM1 expression and activity in primary human melanocytes (63). Further experiments are needed to see MITF-dependent STIM1 regulation in MCs.

A pool of MITF resides in mitochondria and regulates proteins independently of its function as a transcription factor of nuclear genes. MITF interacts with one of the three subunits of the pyruvate dehydrogenase (PDH) complex, an enzyme that catalyzes the conversion of pyruvate to acetyl CoA (64). Moreover, mitochondrial MITF regulates PDH activity, which is crucial to maintain glucose homeostasis and essential as a source of mitochondrial ATP to maintain energetic expenses for MC degranulation and cytokine secretion. MITF activation related to the phosphorylation of Serine 73 mediated by ERK1/2 activity accounts for increased mast cell activity (65).

MITF downstream of the KIT receptor governs mast cell differentiation and proliferation (66). KIT receptor signaling regulates MITF through miR-539 and miR381 downregulation (22). At the same time, MITF fosters KIT expression (67), showing a reciprocal regulation. The reduced and abnormal MC in *Mitf*-mutated mice is partly due to the low levels of KIT receptor and, hence, the low response to its ligand, SCF (68). In that context, our group reported that the adaptor protein 3BP2 participates in the KIT-MITF axis, delivering survival signals in MCs. Thus, silencing of 3BP2 reduced KIT and MITF protein levels and induced MC apoptosis. MITF overexpression rescued KIT protein levels in 3BP2 knockdown cells (69).

Since a reduction in MITF may affect cell viability, apoptosis was monitored. Indeed, MITF downregulation is also involved in the termination of MC-mediated response, apoptosis induction, and removal of exhausted cells (70, 71). Conversely, increased MITF levels and activity have been linked to increased mast cell activity and proliferation. MITF is required for the transformed phenotype of mastocytosis (72). Indeed, MITF downregulation leads to apoptosis of HMC-1 carrying the gain of function mutation KIT D816V (73). Moreover, MITF is highly expressed in bone marrow biopsies from patients with systemic mastocytosis and activating KIT mutations (22). Recently, we identified that a mutation in LysRS (P542R) in a patient with severe anaphylaxis to wasp venom favors the recruitment of this molecule to the nucleus resulting in a constitutive increase in MITF activity (34). This increased MITF activity accounts for an increase in histamine and PGD2 secretion. It is known that transcription factors GATA2 and MITF regulate Hdc gene expression, which is necessary for IgE/mast cell-mediated anaphylaxis (31).

Altogether, the LysRS-MITF pathway should be considered in MRGPRX2 signaling, and it is shared with FcεRI. Patients with alterations in this pathway may increase their range of susceptibility to a broad spectrum of substances that can trigger both receptors.

Increased knowledge of MRGPRX2 signaling may provide new approaches for upregulating responses, which may help treat antibiotic-resistant cutaneous infections, or downregulate MRGPRX2 to ameliorate allergic and inflammatory diseases *via* this receptor.

Data availability statement

The original contributions presented in the study are included in the article/Supplementary Material. Further inquiries can be directed to the corresponding author.

Ethics statement

The studies involving human participants were reviewed and approved by University of Barcelona. Written informed consent for participation was not required for this study in accordance with the national legislation and the institutional requirements.

Author contributions

YG performed and designed the experiments and wrote and reviewed the manuscript. LO, EP-P, and CA performed the experiments and reviewed the manuscript. MG provided technical support and reviewed the manuscript. RM-C conceived the experiments and reviewed the manuscript. MM conceived the experiments, provided secure funding, and wrote and reviewed the manuscript. All authors contributed to the article and approved the submitted version.

Funding

Grant PID2021-122898OB-100 funded by MCIN/AEI/10.13039/501100011033 and, as appropriate, by "ERDF A way of making Europe," by the "European Union" or by the "European Union NextGeneration EU/PRTR" and Thematic Networks and Co-operative Research Centres: RICORS RD21/0002/0058.

Acknowledgments

We are indebted to the service of advanced optical microscopy of the CCIT (University of Barcelona) and to the Cytomics core facility of the Institut d'Investigacions Biomèdiques August Pi i Sunyer (IDIBAPS) for technical support.

Conflict of interest

The authors declare that the research was conducted in the absence of any commercial or financial relationships that could be construed as a potential conflict of interest.

Publisher's note

All claims expressed in this article are solely those of the authors and do not necessarily represent those of their affiliated organizations, or those of the publisher, the editors and the reviewers. Any product that may be evaluated in this article, or claim that may be made by its manufacturer, is not guaranteed or endorsed by the publisher.

Supplementary material

The Supplementary Material for this article can be found online at: https://www.frontiersin.org/articles/10.3389/fimmu.2023.1154108/full#supplementary-material

References

1. Roy S, Chompunud Na Ayudhya C, Thapaliya M, Deepak V, Ali H. Multifaceted MRGPRX2: new insight into the role of mast cells in health and disease. *J Allergy Clin Immunol* (2021) 148:293–308. doi: 10.1016/j.jaci.2021.03.049

2. Quan PL, Sabaté-Brescó M, Guo Y, Martín M, Gastaminza G. The multifaceted mas-related G protein-coupled receptor member X2 in allergic diseases and beyond. *Int J Mol Sci* (2021) 22:4421. doi: 10.3390/ijms22094421

3. Subramanian H, Gupta K, Ali H. Roles of mas-related G protein–coupled receptor X2 on mast cell–mediated host defense, pseudoallergic drug reactions, and chronic inflammatory diseases. *J Allergy Clin Immunol* (2016) 138:700–10. doi: 10.1016/j.jaci.2016.04.051

4. Thapaliya M, Chompunud Na Ayudhya C, Amponnawarat A, Roy S, Ali H. Mast cell-specific MRGPRX2: a key modulator of neuro-immune interaction in allergic diseases. *Curr Allergy Asthma Rep* (2021) 21:3. doi: 10.1007/S11882-020-00979-5

5. Kolkhir P, Pyatilova P, Ashry T, Jiao Q, Abad-Perez AT, Altrichter S, et al. Mast cells, cortistatin, and its receptor, MRGPRX2, are linked to the pathogenesis of chronic prurigo. *J Allergy Clin Immunol* (2022) 149:1998–2009.e5. doi: 10.1016/J.JACI.2022.02.021

6. Shtessel M, Limjunyawong N, Oliver ET, Chichester K, Gao L, Dong X, et al. MRGPRX2 activation causes increased skin reactivity in patients with chronic spontaneous urticaria. *J Invest Dermatol* (2021) 141:678–681.e2. doi: 10.1016/J.JID.2020.06.030

7. McNeil BD, Pundir P, Meeker S, Han L, Undem BJ, Kulka M, et al. Identification of a mast-cell-specific receptor crucial for pseudo-allergic drug reactions. *Nature* (2015) 519:237–41. doi: 10.1038/nature14022

8. Navinés-Ferrer A, Serrano-Candelas E, Lafuente A, Muñoz-Cano R, Martín M, Gastaminza G. MRGPRX2-mediated mast cell response to drugs used in perioperative procedures and anaesthesia. *Sci Rep* (2018) 8:11628. doi: 10.1038/s41598-018-29965-8

9. Kumar M, Duraisamy K, Annapureddy RR, Chan CB, Chow BKC. Novel small molecule MRGPRX2 antagonists inhibit a murine model of allergic reaction. *J Allergy Clin Immunol* (2022) 151:1110–1122. doi: 10.1016/J.JACI.2022.12.805

10. Bawazir M, Amponnawarat A, Hui Y, Oskeritzian CA, Ali H. Inhibition of MRGPRX2 but not FcεRI or MrgprB2-mediated mast cell degranulation by a small molecule inverse receptor agonist. *Front Immunol* (2022) 13:1033794. doi: 10.3389/FIMMU.2022.1033794

11. Che D, Zheng Y, Hou Y, Li T, Du X, Geng S. Dehydroandrographolide targets CD300f and negatively regulated MRGPRX2-induced pseudo-allergic reaction. *Phytother Res* (2022) 36:2173–85. doi: 10.1002/PTR.7445

12. Cao C, Kang HJ, Singh I, Chen H, Zhang C, Ye W, et al. Structure, function and pharmacology of human itch GPCRs. *Nature* (2021) 600:170–5. doi: 10.1038/s41586-021-04126-6

13. Yang F, Guo L, Li Y, Wang G, Wang J, Zhang C, et al. Structure, function and pharmacology of human itch receptor complexes. *Nature* (2021) 600:164–9. doi: 10.1038/s41586-021-04077-y

14. Gaudenzio N, Sibilano R, Marichal T, Starkl P, Reber LL, Cenac N, et al. Different activation signals induce distinct mast cell degranulation strategies. *J Clin Invest* (2016) 126:3981–98. doi: 10.1172/JCI85538

15. Wang Z, Franke K, Bal G, Li Z, Zuberbier T, Babina M. MRGPRX2-mediated degranulation of human skin mast cells requires the operation of gαi, gαq, ca++ channels, ERK1/2 and PI3K-interconnection between early and late signaling. *Cells* (2022) 11:953. doi: 10.3390/CELLS11060953

16. Navinés-Ferrer A, Ainsua-Enrich E, Serrano-Candelas E, Proaño-Pérez E, Muñoz-Cano R, Gastaminza G, et al. MYO1F regulates IgE and MRGPRX2-dependent mast cell exocytosis. *J Immunol* (2021) 206:2277–89. doi: 10.4049/jimmunol.2001211

17. Wang Z, Li Z, Bal G, Franke K, Zuberbier T, Babina M. β-arrestin-1 and β-arrestin-2 restrain MRGPRX2-triggered degranulation and ERK1/2 activation in human skin mast cells. *Front Allergy* (2022) 3:930233. doi: 10.3389/FALGY.2022.930233

18. Goding CR, Arnheiter H. MITF–the first 25 years. *Genes Dev* (2019) 33:983–1007. doi: 10.1101/gad.324657.119

19. Moore KJ. Insight into the microphthalmia gene. *Trends Genet* (1995) 11:442–8. doi: 10.1016/S0168-9525(00)89143-X

20. Qi X, Hong J, Chaves L, Zhuang Y, Chen Y, Wang D, et al. Antagonistic regulation by the transcription factors C/EBPα and MITF specifies basophil and mast cell fates. *Immunity* (2013) 39:97–110. doi: 10.1016/j.immuni.2013.06.012

21. Kitamura Y, Morii E, Jippo T, Ito A. Effect of MITF on mast cell differentiation. *Mol Immunol* (2002) 38:1173–6. doi: 10.1016/S0161-5890(02)00058-5

22. Lee Y-N, Brandal S, Noel P, Wentzel E, Mendell JT, McDevitt MA, et al. KIT signaling regulates MITF expression through miRNAs in normal and malignant mast cell proliferation. *Blood* (2011) 117:3629–40. doi: 10.1182/blood-2010-07-293548

23. Lee Y-NN, Nechushtan H, Figov N, Razin E. The function of lysyl-tRNA synthetase and Ap4A as signaling regulators of MITF activity in FcεRI-activated mast cells. *Immunity* (2004) 20:145–51. doi: 10.1016/S1074-7613(04)00020-2

24. Cronin JC, Wunderlich J, Loftus SK, Prickett TD, Wei X, Ridd K, et al. Frequent mutations in the MITF pathway in melanoma. *Pigment Cell Melanoma Res* (2009) 22:435–44. doi: 10.1111/j.1755-148X.2009.00578.x

25. Kawakami A, Fisher DE. The master role of microphthalmia-associated transcription factor in melanocyte and melanoma biology. *Lab Investig* (2017) 97:649–56. doi: 10.1038/labinvest.2017.9

26. King R, Weilbaecher KN, McGill G, Cooley E, Mihm M, Fisher DE. Microphthalmia transcription factor. a sensitive and specific melanocyte marker for MelanomaDiagnosis. *Am J Pathol* (1999) 155:731–8. doi: 10.1016/S0002-9440(10)65172-3

27. Hartman ML, Czyz M. MITF in melanoma: mechanisms behind its expression and activity. *Cell Mol Life Sci* (2015) 72:1249–60. doi: 10.1007/s00018-014-1791-0

28. Levy C, Khaled M, Fisher DE. MITF: master regulator of melanocyte development and melanoma oncogene. *Trends Mol Med* (2006) 12:406–14. doi: 10.1016/j.molmed.2006.07.008

29. Wu M, Hemesath TJ, Takemoto CM, Horstmann MA, Wells AG, Price ER, et al. C-kit triggers dual phosphorylations, which couple activation and degradation of the essential melanocyte factor mi. *Genes Dev* (2000) 14:301–12. doi: 10.1101/gad.14.3.301

30. Genovese G, Ghosh P, Li H, Rettino A, Sioletic S, Cittadini A, et al. The tumor suppressor HINT1 regulates MITF and β-catenin transcriptional activity in melanoma cells. *Cell Cycle* (2012) 11:2206–15. doi: 10.4161/cc.20765

31. Li Y, Liu B, Harmacek L, Long Z, Liang J, Lukin K, et al. The transcription factors GATA2 and microphthalmia-associated transcription factor regulate hdc gene expression in mast cells and are required for IgE/mast cell–mediated anaphylaxis. *J Allergy Clin Immunol* (2018) 142:1173–84. doi: 10.1016/j.jaci.2017.10.043

32. Ito A, Morii E, Maeyama K, Jippo T, Kim D-K, Lee Y-M, et al. Systematic method to obtain novel genes that are regulated bymi transcription factor: impaired expression of granzyme b and tryptophan hydroxylase in mi/mi cultured mast cells. *Blood* (1998) 91:3210–21. doi: 10.1182/blood.V91.9.3210

33. Morii E, Oboki K. MITF is necessary for generation of prostaglandin d 2 in mouse mast cells. *J Biol Chem* (2004) 279:48923–9. doi: 10.1074/jbc.M407026200

34. Ribó P, Guo Y, Aranda J, Ainsua-Enrich E, Navinés-Ferrer A, Guerrero M, et al. Mutation in KARS: a novel mechanism for severe anaphylaxis. *J Allergy Clin Immunol* (2020) 147:1855–1864. doi: 10.1016/j.jaci.2020.12.637

35. Kirshenbaum AS, Akin C, Wu Y, Rottem M, Goff JP, Beaven MA, et al. Characterization of novel stem cell factor responsive human mast cell lines LAD 1 and 2 established from a patient with mast cell sarcoma/leukemia; activation following aggregation of FcεRI or FcγRI. *Leuk Res* (2003) 27:677–82. doi: 10.1016/S0145-2126(02)00343-0

36. Suzuki K, Bose P, Leong-Quong RY, Fujita DJ, Riabowol K. REAP: a two minute cell fractionation method. *BMC Res Notes* (2010) 3:294. doi: 10.1186/1756-0500-3-294

37. Ainsua-Enrich E, Álvarez-Errico D, Gilfillan AM, Picado C, Sayós J, Rivera J, et al. The adaptor 3BP2 is required for early and late events in FcεRI signaling in human mast cells. *J Immunol* (2012) 189:2727–34. doi: 10.4049/jimmunol.1200380

38. Faloon PW, Bennion M, Weiner WS, Smith RA, Wurst J, Weiwer M, et al. A small molecule inhibitor of the MITF molecular pathway. *Probe Reports from the NIH Molecular Libraries Program* (2010).

39. Yannay-Cohen N, Carmi-Levy I, Kay G, Yang CM, Han JM, Kemeny DM, et al. LysRS serves as a key signaling molecule in the immune response by regulating gene expression. *Mol Cell* (2009) 34:603–11. doi: 10.1016/j.molcel.2009.05.019

40. Tatemoto K, Nozaki Y, Tsuda R, Konno S, Tomura K, Furuno M, et al. Immunoglobulin e-independent activation of mast cell is mediated by mrg receptors. *Biochem Biophys Res Commun* (2006) 349:1322–8. doi: 10.1016/j.bbrc.2006.08.177

41. Fujisawa D, Kashiwakura JI, Kita H, Kikukawa Y, Fujitani Y, Sasaki-Sakamoto T, et al. Expression of mas-related gene X2 on mast cells is upregulated in the skin of patients with severe chronic urticaria. *J Allergy Clin Immunol* (2014) 134:622–633.e9. doi: 10.1016/j.jaci.2014.05.004

42. Yu J, Liu Z, Liang Y, Luo F, Zhang J, Tian C, et al. Second messenger Ap4A polymerizes target protein HINT1 to transduce signals in FcεRI-activated mast cells. *Nat Commun* (2019) 10:4664. doi: 10.1038/s41467-019-12710-8

43. Ngeow KC, Friedrichsen HJ, Li L, Zeng Z, Andrews S, Volpon L, et al. BRAF/MAPK and GSK3 signaling converges to control MITF nuclear export. *Proc Natl Acad Sci* (2018) 115:E8668–77. doi: 10.1073/pnas.1810498115

44. Miller AJ, Du J, Rowan S, Hershey CL, Widlund HR, Fisher DE. Transcriptional regulation of the melanoma prognostic marker melastatin (TRPM1) by MITF in melanocytes and melanoma. *Cancer Res* (2004) 64:509–16. doi: 10.1158/0008-5472.CAN-03-2440

45. Lu S, Slominski A, Yang S-E, Sheehan C, Ross J, Carlson JA. The correlation of TRPM1 (Melastatin) mRNA expression with microphthalmia-associated transcription factor (MITF) and other melanogenesis-related proteins in normal and pathological skin, hair follicles and melanocytic nevi. *J Cutan Pathol* (2010) 37:26–40. doi: 10.1111/j.1600-0560.2010.01504.x

46. McGill GG, Horstmann M, Widlund HR, Du J, Motyckova G, Nishimura EK, et al. Bcl2 regulation by the melanocyte master regulator mitf modulates lineage survival and melanoma cell viability. *Cell* (2002) 109:707–18. doi: 10.1016/S0092-8674(02)00762-6

47. Proaño-Pérez E, Serrano-Candelas E, García-Valverde A, Rosell J, Gómez-Peregrina D, Navinés-Ferrer A, Guerrero M, Serrano C, Martin M. The microphthalmia-associated transcription factor is involved in gastrointestinal stromal tumor growth. *Cancer Gene Ther* (2023) 30(2), 245–255. doi: 10.1038/s41417-022-00539-1

48. Sundaramurthi H, García-Mulero S, Tonelotto V, Slater K, Marcone S, Piulats JM, et al. Uveal melanoma cell line proliferation is inhibited by ricolinostat, a histone deacetylase inhibitor. *Cancers (Basel)* (2022) 14:782. doi: 10.3390/cancers14030782

49. Mencarelli A, Gunawan M, Su K, Yong M, Bist P, Sheng Tan WW, et al. A humanized mouse model to study mast cells mediated cutaneous adverse drug reactions. *J Leukoc Biol* (2020) 107:797–807. doi: 10.1002/JLB.3MA1219-210RR

50. Reddy VBB, Graham TAA, Azimi E. A single amino acid in MRGPRX2 necessary for binding and activation by pruritogens. *J Allergy Clin Immunol* (2017) 140:1726–8. doi: 10.1016/J.JACI.2017.05.046

51. Lansu K, Karpiak J, Liu J, Huang XPP, McCorvy JDD, Kroeze WKK, et al. In silico design of novel probes for the atypical opioid receptor MRGPRX2. *Nat Chem Biol* (2017) 13:529–36. doi: 10.1038/NCHEMBIO.2334

52. Guo M, Yang XL, Schimmel P. New functions of aminoacyl-tRNA synthetases beyond translation. *Nat Rev Mol Cell Biol* (2010) 11:668–74. doi: 10.1038/NRM2956

53. Stevens J, Loutit JF. Mast cells in spotted mutant mice (W ph mi). *Proc R Soc London - Biol Sci* (1982) 215:405–9. doi: 10.1098/rspb.1982.0050

54. Stechschulte DJ, Sharma R, Dileepan KN, Simpson KM, Aggarwal N, Clancy J, et al. Effect of the mi allele on mast cells, basophils, natural killer cells, and osteoclasts in C57Bl/6J mice. *J Cell Physiol* (1987) 132:565–70. doi: 10.1002/JCP.1041320321

55. Kitamura Y, Morii E, Jippo T, Ito A. Regulation of mast cell phenotype by MITF. *Int Arch Allergy Immunol* (2002) 127:106–9. doi: 10.1159/000048178

56. Hemesath TJ, Price ER, Takemoto C, Badalian T, Fisher DE. MAP kinase links the transcription factor microphthalmia to c-kit signalling in melanocytes. *Nature* (1998) 391:298–301. doi: 10.1038/34681

57. Lee S-HH, Lee J-HH, Lee Y-MM, Kim D-KK. Involvement of MITF-a, an alternative isoform of mi transcription factor, on the expression of tryptase gene in human mast cells. *Exp Mol Med* (2010) 42:366. doi: 10.3858/emm.2010.42.5.038

58. Ploper D, Taelman VF, Robert L, Perez BS, Titz B, Chen HW, et al. MITF drives endolysosomal biogenesis and potentiates wnt signaling in melanoma cells. *Proc Natl Acad Sci USA* (2015) 112:E420–9. doi: 10.1073/pnas.1424576112

59. Shahlaee AH, Brandal S, Lee Y-N, Jie C, Takemoto CM. Distinct and shared transcriptomes are regulated by microphthalmia-associated transcription factor isoforms in mast cells. *J Immunol* (2007) 178:378–88. doi: 10.4049/jimmunol.178.1.378

60. Occhiuto CJ, Kammala AK, Yang C, Nellutla R, Garcia M, Gomez G, et al. Store-operated calcium entry *via* STIM1 contributes to MRGPRX2 induced mast cell functions. *Front Immunol* (2020) 10:3143/FULL. doi: 10.3389/FIMMU.2019.03143/FULL

61. Smyth JT, Hwang SY, Tomita T, DeHaven WI, Mercer JC, Putney JW. Activation and regulation of store-operated calcium entry. *J Cell Mol Med* (2010) 14:2337–49. doi: 10.1111/J.1582-4934.2010.01168.X

62. Baba Y, Nishida K, Fujii Y, Hirano T, Hikida M, Kurosaki T. Essential function for the calcium sensor STIM1 in mast cell activation and anaphylactic responses. *Nat Immunol* (2008) 9:81–8. doi: 10.1038/NI1546

63. Tanwar J, Sharma A, Saurav S, Shyamveer, Jatana N, Motiani RK. MITF is a novel transcriptional regulator of the calcium sensor STIM1: significance in physiological melanogenesis. *J Biol Chem* (2022) 298:102681. doi: 10.1016/J.JBC.2022.102681

64. Sharkia I, Hadad Erlich T, Landolina N, Assayag M, Motzik A, Rachmin I, et al. Pyruvate dehydrogenase has a major role in mast cell function, and its activity is regulated by mitochondrial microphthalmia transcription factor. *J Allergy Clin Immunol* (2017) 140:204–214.e8. doi: 10.1016/j.jaci.2016.09.047

65. Paruchuru LB, Govindaraj S, Razin E. The critical role played by mitochondrial MITF serine 73 phosphorylation in immunologically activated mast cells. *Cells* (2022) 11:589. doi: 10.3390/cells11030589

66. Oppezzo A, Rosselli F. The underestimated role of the microphthalmia-associated transcription factor (MiTF) in normal and pathological haematopoiesis. *Cell Biosci* (2021) 11:18. doi: 10.1186/s13578-021-00529-0

67. Tsujimura T, Morii E, Nozaki M, Hashimoto K, Moriyama Y, Takebayashi K, et al. Involvement of transcription factor encoded by the mi locus in the expression of c-kit receptor tyrosine kinase in cultured mast cells of mice. *Blood* (1996) 88:1225–33. doi: 10.1182/BLOOD.V88.4.1225.BLOODJOURNAL8841225

68. Ebi Y, Kanakura Y, Jippo-Kanemoto T, Tsujimura T, Furitsu T, Ikeda H, et al. Low c-kit expression of cultured mast cells of mi/mi genotype may be involved in their defective responses to fibroblasts that express the ligand for c-kit. *Blood* (1992) 80:1454–62. doi: 10.1182/blood.V80.6.1454.1454

69. Ainsua-Enrich E, Serrano-Candelas E, Álvarez-Errico D, Picado C, Sayós J, Rivera J, et al. The adaptor 3BP2 is required for KIT receptor expression and human mast cell survival. *J Immunol* (2015) 194:4309–18. doi: 10.4049/jimmunol.1402887

70. Martelli F, Ghinassi B, Lorenzini R, Vannucchi AM, Rana RA, Nishikawa M, et al. Thrombopoietin inhibits murine mast cell differentiation. *Stem Cells* (2008) 26:912–9. doi: 10.1634/STEMCELLS.2007-0777

71. Tsujimura T, Hashimoto K, Morii E, Tunio GM, Tsujino K, Kondo T, et al. Involvement of transcription factor encoded by the mouse mi locus (MITF) in apoptosis of cultured mast cells induced by removal of interleukin-3. *Am J Pathol* (1997) 151:1043–51.

72. Lee Y-N, Noel P, Shahlaee A, Carter M, Kapur R, Wayne A, et al. Kit signaling regulates mitf expression in mastocytosis. *Blood* (2006) 108:3601–1. doi: 10.1182/blood.V108.11.3601.3601

73. Proaño-Pérez E, Ollé L, Guo Y, Aparicio C, Guerrero M, Muñoz-Cano R, et al. MITF downregulation induces death in human mast cell leukemia cells and impairs IgE-dependent degranulation. *Int J Mol Sci* (2023) 24:3515. doi: 10.3390/ijms24043515

frontiers | Frontiers in Immunology

TYPE Review
PUBLISHED 05 October 2023
DOI 10.3389/fimmu.2023.1216580

OPEN ACCESS

EDITED BY
Ronald Sluyter,
University of Wollongong, Australia

REVIEWED BY
Li-Na Wang,
Shanghai University of Traditional Chinese Medicine, China
Stephen Fuller,
The University of Sydney, Australia

*CORRESPONDENCE
Edward S. Schulman
es29@drexel.edu

RECEIVED 04 May 2023
ACCEPTED 04 September 2023
PUBLISHED 05 October 2023

CITATION
Schulman ES, Nishi H and Pelleg A (2023) Degranulation of human mast cells: modulation by P2 receptors' agonists. *Front. Immunol.* 14:1216580. doi: 10.3389/fimmu.2023.1216580

Degranulation of human mast cells: modulation by P2 receptors' agonists

Edward S. Schulman [1*], Haruhisa Nishi [2] and Amir Pelleg [3]

[1]Division of Pulmonary, Critical Care and Allergy, Drexel University College of Medicine, Philadelphia, PA, United States, [2]Department of Pharmacology, Jikei University School of Medicine, Tokyo, Japan, [3]Danmir Therapeutics, LLC, Haverford, PA, United States

Since the late 1970s, there has been an alarming increase in the incidence of asthma and its morbidity and mortality. Acute obstruction and inflammation of allergic asthmatic airways are frequently caused by inhalation of exogenous substances such as allergens cross-linking IgE receptors expressed on the surface of the human lung mast cells (HLMC). The degree of constriction of human airways produced by identical amounts of inhaled allergens may vary from day to day and even hour to hour. Endogenous factors in the human mast cell (HMC)'s microenvironment during allergen exposure may markedly modulate the degranulation response. An increase in allergic responsiveness may significantly enhance bronchoconstriction and breathlessness. This review focuses on the role that the ubiquitous endogenous purine nucleotide, extracellular adenosine 5'-triphosphate (ATP), which is a component of the damage-associated molecular patterns, plays in mast cells' physiology. ATP activates P2 purinergic cell-surface receptors (P2R) to trigger signaling cascades resulting in heightened inflammatory responses. ATP is the most potent enhancer of IgE-mediated HLMC degranulation described to date. Current knowledge of ATP as it relates to targeted receptor(s) on HMC along with most recent studies exploring HMC post-receptor activation pathways are discussed. In addition, the reviewed studies may explain why brief, minimal exposures to allergens (e.g., dust, cat, mouse, and grass) can unpredictably lead to intense clinical reactions. Furthermore, potential therapeutic approaches targeting ATP-related enhancement of allergic reactions are presented.

KEYWORDS

human lung mast cells, LAD2 cell line, P2 purinergic receptors, allergic degranulation, FcεRI, PI3K(δ), P2Y11R

Abbreviations: eATP, extracellular adenosine 5'-triphosphate; ATP; 2-MeSATP, 2-methylthio-ATP; ATPγS, adenosine 5'-(3-thio)triphosphate; HMC, human mast cell; HLMC, human lung mast cell; PDK-1, phosphoinositide-dependent kinase-1; PI3K(δ), phosphoinositide 3-kinase type δ; P2XR, purinergic receptor P2X ligand-gated ion channel; P2YR, metabotropic purinergic P2Y receptor; P2Y11R, metabotropic purinergic P2Y11 receptor; CD39, ectonucleoside triphosphate diphosphorylase-1; CD73, ecto-5'-nucleotidase; WAS, weak allergic stimulation.

Introduction

Within minutes of allergic activation of IgE receptors expressed by HMC, the cells release histamine and a spectrum of other pro-inflammatory mediators to induce airway bronchoconstriction and contribute to acute and chronic lung inflammation (1–3). Preformed cytoplasmic granular mediators are released over seconds (e.g., histamine and TNF alpha), select chemicals are newly formed over minutes (e.g., leukotrienes and other lipids), and other mediators including cytokines over hours (e.g., Interleukin (IL) -5, IL-13, IL-8, and GM-CSF) (1, 4). Depending on the strength of the stimulation, the localized inflammatory milieu, and the organs involved, mast cell (MC) activation can result in multiple responses including edema, hives, bronchoconstriction, or systemic anaphylaxis, which can not only decrease the quality of life but may also be life-threatening. Many publications have described studies of "human mast cells." Most of these studies have used neoplastic MC (5–7) or cells cultured *in vitro* derived from differing precursor cells (e.g., cord blood, peripheral blood, and fetal liver), using culture media that include various combinations of cytokines (8–19). Relatively few studies used freshly isolated and purified human lung mast cells (HLMC) as a model of the organ-specific responses of the human lung (20). Also, there is increasing appreciation that MC are heterogeneous, and their biology can differ markedly not only between species (e.g., mouse vs. human) but also between MC isolated from different human organ sources (e.g., skin vs. lung), within the same organ (e.g., gut), and freshly isolated organ-derived MC vs. *in vitro*-derived MC (8, 21–26).

Progress in understanding HLMC biology has been extremely slow because of difficulties in procuring freshly resected human specimens, time-consuming and technical challenges associated with the isolation and purification of these cells, and their limited survival *in vitro* (i.e., 2-4 days). Our seminal report on the methods of isolation and purification of HLMC (27) facilitated many subsequent studies on their biology including ultrastructure (28–32), heterogeneity (33–35), mediators' release biochemistry (36, 37), secretagogues (38–45), mediators (46–55), and pharmacological modulation of mediators' release (40–42, 45, 56).

The text below focuses on the progress made in recent years in our understanding of the critical interaction of the extracellular purine nucleotide adenosine 5′-triphosphate (ATP), with IgE-mediated activation of the HLMC (57, 58) and intracellular signal transduction pathway associated with IgE receptor activation in LAD2 cell line (6, 59, 60). Our own interest in this regard mostly relates to allergic asthma, but other important aspects of ATP's role in pulmonary pathophysiology have been investigated including cystic fibrosis, pulmonary embolism, cough, bronchoconstriction, pulmonary fibrosis, lung cancer, mechanical ventilation-induced lung injury, and pulmonary hypertension (61–68).

Intracellular ATP

Intracellular ATP plays a critical role in cellular metabolism and energetics (69). ATP is found at a concentration of 5–10 mM in every cell, except for platelets, in which its concentration is far higher. The concentration of ATP in chromaffin cells' secretory granules approaches 100 mM; platelets' ATP level is up to 500 mM. However, the concentration of extracellular ATP is only approximately 10 nM (70)(see below).

Extracellular ATP

Release of ATP from cells

In 1929, Drury and Szent-Gyorgyi described the effects of a simple extract of heart muscle and other tissues on the cardiovascular system. The active ingredient in this extract was identified as adenylic acid (71). Subsequent studies have shown that adenosine and ATP were the most active vasodilators and bradycardic ingredients of these extracts (72–74). ATP is released from cells by various mechanisms under physiologic and pathophysiologic conditions in response to different stimuli or micro-environmental conditions. These include exocytosis, large membrane pores, and specific trans-cell membrane ionic channels (75, 76). There are several sources of extracellular ATP (23, 77). Large amounts of ATP are found in platelets and ATP is released during platelet activation. Upon platelet aggregation, the serum concentration of ATP and adenosine diphosphate (ADP) reaches 50 uM but is much higher at the cell surface (78–80). ATP is also stored in red blood cells (RBC) from which it is released under conditions of imbalance between O_2 supply and O_2 demand (81–84). In addition, several biologic substances as well as increased blood flow can induce the release of ATP from vascular endothelial cells (77, 85–88) and smooth muscle cells (89, 90). Other ATPs release stimuli and cellular sources including mechanical deformation of cells, ischemic cells, immune cells, and necrotic/apoptotic cells (23, 91–94). Pannexin channel and connexin hemichannel play a critical role in this release (95). ATP is also released from neural elements as a co-transmitter and from exercising skeletal muscles (96). In the heart, ATP is released into the extracellular fluid under various conditions. Specifically, ATP release is evoked by sympathetic nerve stimulation and by catecholamines (97–101). In addition, ATP is released in the heart during acute myocardial ischemia (102) and from cardiac myocytes in response to hypoxia (103, 104).

Importantly, during inflammation, ATP is released from inflammatory cells. For example, elevated extracellular levels of ATP have been found in the lungs of COPD patients (105, 106). Similarly, pulmonary levels of ATP were increased in a mouse model of smoke-induced acute lung inflammation and emphysema (107–109).

Degradation of extracellular ATP

Extracellular ATP is rapidly and sequentially degraded by ectonucleotidases including ectonucleoside triphosphate diphosphorylase-1 (CD39), and ecto-5'-nucleotidase (CD73). CD39 hydrolyzes extracellular ATP and ADP to AMP. CD73 catalyzes the hydrolysis of AMP, releasing inorganic phosphate and adenosine, which exerts its own effects by activating P1 purinergic receptors (A1, A2a, A2b, and A3) (110–113).

CD73 is widely expressed in a variety of tissues, including the colon, kidney, brain, liver, heart, lung, spleen, and bone marrow (114). CD39 is expressed by multiple cell types including epithelial,

endothelial, and immune cells. It is highly expressed in different human tumor types (115). Adenosine is rapidly eliminated from the extracellular space by ectoadenosine deaminase and actively transported into cells (109). Therefore, the levels of CD39 and CD73 and their enzymatic activities play a critical role in controlling the duration and magnitude of autocrine and paracrine effects of ATP and adenosine. Multiple studies have shown that the level of these enzymes is altered during pathophysiologic conditions. For example, increased expression of CD39 and CD73 by pulmonary epithelial and endothelial cells was observed during high inspiratory pressure level-induced lung injury (116). Also, upregulation of CD39/CD73 expression has been observed in patients with small-cell lung cancer and patients with a broad spectrum of solid cancers (117).

ATP: A paracrine and autocrine agent

Extracellular ATP acts as a paracrine and autocrine agent (23, 91, 118), the actions of which are mediated by cell surface purinergic receptors (P2R) (109). The latter are divided into two families: P2Y: seven trans-cell membrane domain G-protein coupled receptors (metabotropic), and P2X: trans-cell membrane cationic channels (ionotropic). Eight P2YR and seven homotrimeric P2X receptors (P2X1-7) have been cloned heretofore (Figure 1). Multiple heteromeric assemblies comprising P2X subunits have been described including P2X2/P2X3, P2X4/P2X6, P2X2/P2X6, and P2X1/P2X5, but not all have been detected in native tissues (119).

In contrast to P2XR, which is principally activated by ATP, P2YR shows striking differential sensitivity for varying nucleotides. Single cells commonly express more than one P2YR, for which a given nucleotide has an affinity. Pharmacologically, P2YR are subdivided into adenine-nucleotides sensitive group responding mainly to adenosine diphosphate (P2Y1R, P2Y12R, and P2Y13R: ADP), adenosine triphosphate (P2Y11R: ATP), uridine triphosphate (P2Y4R: UTP), uridine diphosphate (P2Y6R: UDP), UDP and sugar derivatives sensitive receptor (P2Y14R: UDP-glucose and UDP-galactose), and receptors manifesting mixed agonist affinity (P2Y2R: ATP=UTP) (120) (Table 1). ATP is also an antagonist or partial agonist at the P2Y1 receptor (121). Furthermore, whereas ATP activates human P2Y11 receptors, ADP is a canine P2Y11 receptor agonist (122). P2Y1, -2, -4, -6, and -11 receptors belong to the P2Y1-like subfamily and couple to $G_{q/11}$, G_o, $G_{12/13}$, and G_s protein, whereas P2Y12, -13, and -14 receptors are categorized as P2Y12-like and couple to $G_{i/o}$ protein. ATP is the only agonist that can activate both P2XR and P2YR (23, 123) (Table 1).

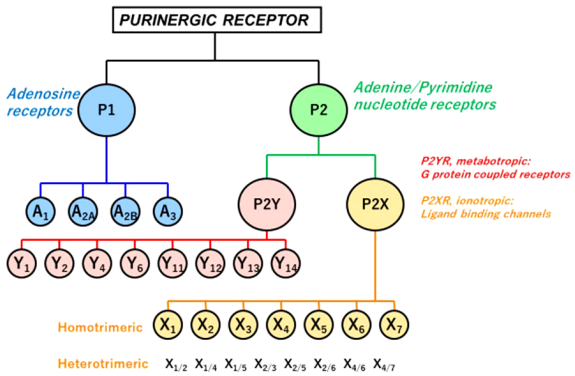

FIGURE 1
P1 and P2 Purinergic Receptors. Extracellular signals triggered by ATP, its hydrolytic products ADP and adenosine, and other nucleotides and nucleotide sugars (UTP, UDP, and UDP-glucose) regulate physiological and pathophysiological processes. Two families of purinoceptors are shown. P1R consists of four subtypes of adenosine-activated receptors. P2R is divided into P2XR ionotropic ligand-gated ion channel receptors, principally activated by ATP, P2YR, and G-protein-coupled (metabotropic) receptors. Also shown are multiple heteromeric assemblies comprising P2X subunits, but not all have been detected in native tissues (119).

Inhalation of aerosolized ATP triggered bronchoconstriction in healthy and more so in asthmatic human subjects; in the latter, ATP was 50-fold more potent than methacholine and 87-fold more potent than histamine in producing a 15% decrease in FEV1 (124). In 2002, based on multiple studies in both canine and human models (124–126), a mechanistic role of ATP in pulmonary disorders was proposed for the first time in a seminal review, and termed "*Adenosine 5′-triphosphate axis in obstructive airway diseases*" (127, 128).

ATP enhances IgE-mediated HLMC degranulation

Early experiments in HLMC suggested that ATP plays an important modulatory role in degranulation as measured by the percentage of total cellular histamine released within minutes following IgE-mediated challenge (58). In these experiments, freshly purified HLMC (10-50 x 10^3/tube) were incubated with or without purine nucleotides for 15 min prior to a 20 min challenge with anti-IgE (3 ug/ml), calcium ionophore A23187 (0.1 ug/ml), or buffer control. Cells were exposed to ATP, UTP, the stable ATP analogs α, β methylene-ATP (α, β-MeATP), (β, γ methylene-ATP (β, γ-MeATP), and 2-methylthio-ATP (2-MeSATP), as well as adenosine, the product of ATP's degradation.

Neither the nucleotides (10^{-7}-10^{-3} M) nor adenosine (10^{-6}–10^{-3} M) directly triggered degranulation, contrary to results obtained using murine mast cell models (129–133). In HLMC, adenosine exhibited a bimodal effect on anti-IgE-induced histamine release, enhancing it at 10^{-6} to 10^{-4} M ($P > 0.05$, NS) and inhibiting it at 10^{-3} M ($P < 0.05$) (58), in congruence with prior reports on HLMC (41, 134, 135). ATP (10^{-4} M) enhanced anti-IgE–induced histamine release (10.9 ± 2.7% to 19.2 ± 2.9%, n = 20, $P < 0.01$). Importantly, ATP's effects were most striking in cells manifesting low (< 3%) IgE-mediated net histamine release termed a weak allergic stimulation (WAS). When WAS-dependent histamine release was "low", i.e., 1.8 ± 0.4%; range: 0.5–2.9%; n=6), ATP (10^{-4} M) enhanced histamine release to 13.5 ± 2.7% (750% enhancement). In contrast, ATP had no effects on the ionophore A23187-induced histamine release (n = 10). All adenine nucleotides enhanced IgE-mediated HLMC histamine release, but ATP was the most potent followed by 2-MeSATP, α, β-MeATP, and β, γ-MeATP. This potency order strongly suggests that the action of ATP is mediated by a P2YR subtype (136). Further evidence against the involvement of a P2XR, especially P2X7R, was the failure of the selective P2XR

TABLE 1 P2Y Receptor Family.

RECEPTOR	PREFERRED AGONIST	G-PROTEIN COUPLING	COMMENTS
P2Y1	ADP>>ATP	G_q	ATP can be an agonist, depending on receptor reserve (antagonist or partial agonist).
P2Y2	ATP=UTP	G_q (+ G_i)	No agonist activity of ADP
P2Y4	UTP	G_q (+ G_i)	ATP is a partial agonist in humans and a full agonist in rat
P2Y6	UDP	G_q	Uracil nucleotides play a role as intercellular messengers independent of adenine nucleotides.
P2Y11	ATP	G_q + G_s	No murine P2Y11 gene
P2Y12	ADP	G_i	
P2Y13	ADP	G_i	
0P2Y14	UDP-Glucose UDP-Galactose	G_i	

antagonist pyridoxalphosphate-6-azophenyl-2′,4′-disulfonic acid (PPADS) (137) to affect ATP's enhancement.

The P2YR- agonist UTP also significantly enhanced anti-IgE–induced histamine release, which is most consistent with a P2YR and not P2XR mediation. However, UTP was less potent than ATP. Control anti-IgE–induced histamine release of 14.9 ± 3.9% was enhanced by ATP (10^{-4} M) to 23.0 ± 4.7% ($p < 0.05$), compared with 19.2 ± 5.0% ($p < 0.05$) in the presence of an equimolar concentration of UTP. This result did not support sole mediation by P2Y2R, of which UTP is the preferred agonist over ATP (138).

HLMCs fail to exhibit functional ecto-ATPase activities

Over the course of 15-minute incubations with ATP, HLMC's media did not contain breakdown products of ATP, indicating that the histamine-release enhancement by ATP was not mediated by ADP, AMP, or adenosine. It should be noted that under identical experimental conditions, products of ATP's degradation were found in media containing whole fragments of the human lung (58).

Expression of P2Rs in HLMC

Further support for a P2YR mediating the effects of ATP on IgE-mediated degranulation enhancement from HLMC was the constitutive expression of P2Y1R and P2Y2R and weak expression of P2Y4 demonstrated by reverse transcription–polymerase chain reaction (RT-PCR) of freshly purified HLMC (58). A receptor, previously known as P2Y7, was weakly manifested in the RT-PCR assay in one of five individual fresh isolations of HLMC. P2Y7 was later identified as the receptor for leukotriene B4 (B-LTR) (139). Feng et al. reported the expression of P2Y1, P2Y2, P2Y11, P2Y12, and P2Y13 by RT-PCR in cord blood-derived human MC and highlighted the potential roles of different P2YR in complementary or opposing functions in cell activation (140). Wareham et al. reported P2X7 expression by RT-PCR in HLMC that were cultured in a cytokine mix pre-experimentation. In addition, using a whole-cell patch-clamp technique, they described a P2X7-like non-desensitizing current in response to high concentrations of ATP (1–5 mM). P2X1 and P2X4 transcripts were also found in their HLMC preparations (141).

Stimulation of the P2YRs can result in the activation of two different pathways: one that involves pertussis toxin (PTX)-sensitive G protein(s) and adenylyl cyclase (G_i-coupled; P2Y12, P2Y13, and P2Y14), and the other that involves PTX-insensitive G protein and phospholipase C (G_q-coupled; P2Y1, P2Y2, P2Y4, P2Y6, and $G_{q/s}$-coupled; P2Y11) (142). Because PTX failed to modify the enhancing effect of ATP on IgE-mediated histamine release, it seems likely that the latter pathway mediates the effect of ATP (58). However, the exact post-P2YR mechanism(s) by which this pathway(s) operates to enhance IgE-mediated degranulation in HLMC remains to be elucidated.

ATP enhances IgE-mediated LAD2 HMC degranulation

Though P2YRs are expressed by HMC of different sources (58, 140, 143), until recently, only one receptor (i.e., P2Y14R) in LAD2 cells was proposed to be linked to allergen/IgE-induced degranulation (60). To further elucidate the specific receptor(s) and, importantly, post-receptor pathways accountable for nucleotide-P2YR mediated effects on IgE-mediated degranulation, sufficient cell numbers were needed beyond what the HLMC model could provide. The LAD2 human-derived MC line was developed at the NIH from a patient with systemic mastocytosis (5, 6, 10). As recently reported, LAD2 cells express five P2YRs (P2Y1, P2Y6, P2Y11, P2Y12, and P2Y14) along with three P1Rs (A2aR, A2bR, and A3R), and two P2XRs (P2X1 and P2X7) (59). LAD2 cells express CD39 but not CD73, suggesting extracellular nucleotides could be degraded to AMP but not to adenosine (59).

In non-sensitized LAD2 cells challenged with P1R and P2R agonists [adenosine, ATP, ADP, UTP, UDP, 2-methylthio-ATP (2-MeSATP)], and the P2Y11R non-hydrolysable agonist [adenosine 5'-(3-thio) triphosphate (ATPγS)] at physiological concentrations (1–

100 μM), none of the agonists alone triggered degranulation as measured by histamine or beta-hexosaminidase release. High concentrations (1mM) of BzATP, a P2X7R agonist, triggered degranulation in non-sensitized LAD2 cells. Sensitized LAD2 cells were then challenged in the absence and presence of P2YR agonists, using a predetermined low concentration of antigen to produce a weak allergic stimulation (WAS) and a low level of degranulation (<10% release). As noted above for HLMC, ATP's enhancement was most pronounced under WAS conditions; only the P2Y11R non-hydrolyzable agonist, ATPγS (144–147), mimicked the effects of ATP and produced a net 7-fold increase in release ($n = 4$; $p < 0.01$). The failure of UTP and ADP to enhance the release of histamine excluded the involvement of their respective receptors, P2Y1R, P2Y2, P2Y4R, P2Y12R, and P2Y13R. P2Y11R protein expression by LAD2 cells was confirmed by Western blot. The effects of ATPγS were dose-dependently inhibited by NF157, a P2Y11R antagonist (148, 149). Further evidence for P2Y11 as the receptor mediating the degranulation-enhancing effect of ATP in LAD2 cells is its known coupling to both $G_{q/11}$ and G_s proteins that are known to be linked to induction and suppression of MC degranulation, respectively.

None of the P2YR agonists tested in LAD2 cells, including high concentrations of ATPγS (1000 μM) enhanced the WAS-induced intracellular Ca^{2+} mobilization, which is an essential component of activated FcεRI-induced degranulation. The effects of ATPγS on the phosphorylation of key kinases related to intracellular PI3K(δ)'s activation cascades showed that both PI3K(δ) and Akt were phosphorylated by ATPγS and are further upregulated by WAS, especially in the case of Akt. However, PDK-1, which is known to be a link between PI3K(δ) and Akt, was not phosphorylated. These data indicated that the P2YR-mediated enhancement effect on IgE-mediated degranulation in an HMC is via the PI3K/protein kinase B pathway (Figure 2). In further experiments, a shRNA directed against PI3K(δ) and a PI3K(δ) inhibitor, compound 15e (150, 151), suppressed ATPγS's effect on WAS-induced degranulation enhancement, the latter in a concentration-dependent manner. In additional experiments, an antagonist of the P2Y11R and NF157 significantly inhibited the enhancing effects of ATPγS (100 μM) on WAS-induced degranulation and experiments using siRNA knockdown of the P2Y11R, which itself abolished the enhancing effects (59).

Discussion

Historical perspective

Over the past four decades, adenosine, but not adenine nucleotides, has received considerable attention for a potential role in human allergies and asthma (41, 57, 130, 134, 135, 152–156). In 1996, Pelleg and Hurt showed for the first time that extracellular ATP stimulates vagal sensory nerve terminals in the canine lungs by activating P2XR (125). Subsequent studies have indicated that this action of ATP leads to bronchoconstriction and cough and is probably also pro-inflammatory due to the localized release of neuropeptides via the axon reflex (62, 157, 158). The suggestion that this latter pathway could be mechanistically involved in asthma (159) prompted us to investigate the potential effects of extracellular ATP on HLMC. Our early findings indicated that ATP potentiates IgE-mediated degranulation from HLMC (58). Subsequent studies have shown a similar phenomenon in LAD2 cells, which was not mediated by adenosine, which is the product of ATP's degradation by ecto-enzymes. Since then, additional studies have investigated the role of extracellular and intra-MC ATP in MC's role in allergic inflammation (160).

Mechanisms of actions of ATP

Mediation by P2R

ATP is unimodal, only enhancing degranulation, whereas adenosine is bimodal; at high concentrations, it inhibits degranulation and at low concentrations, it potentiates degranulation. At equimolar concentrations, ATP is more potent than adenosine in enhancing HMC degranulation (57–59). ATP's enhancing effects on IgE-mediated degranulation in freshly isolated HLMC, without exposure to varied cytokine mixtures over days to weeks in cultures, is substantial and reproducible. The specific P2R subtype (s) mediating this degranulation-enhancing effect in HLMC remain unknown, but several lines of evidence strongly suggest the involvement of P2YR and not P2XR. It is also possible that two or more P2YRs are activated in concert during different physiologic conditions. Along these lines, Feng et al. reported the expression of multiple P2YRs in human cord blood-derived MC, including P2Y1R, P2Y2R, P2Y11R, P2Y12R, and P2Y13R, that could play complementary and opposing functions during mast cell activation (140). Regrettably, the difficulties involved in procuring specimens of human lungs and isolating and purifying HLMC stymied efforts to fully elucidate the relevant mechanisms of ATP's enhancement of the immune reaction-dependent MC degranulation.

More recently, insights into pathways involving P2YR expressed by HMC were obtained by quantifying the effects of

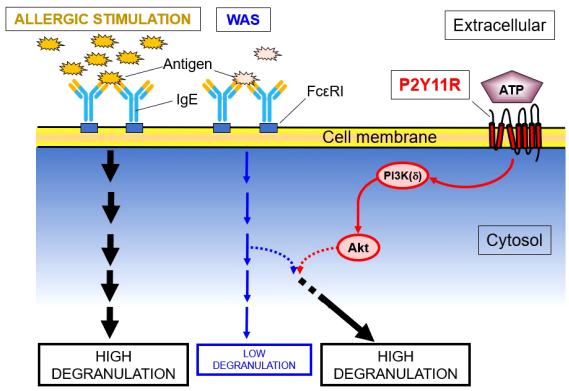

FIGURE 2
P2YR11 Modifies a WAS in LAD2 Human MC. This schematic shows that P2Y11R, an endogenous purine (ATP) receptor, modulates the enzymatic cascade between PI3K(δ) and Akt, leading to the enhancement of a weak allergic stimulus (WAS). PDK-1, though a known link between PI3K and Akt, is not phosphorylated and is not involved in the degranulation enhancement.

ATP on LAD2 cells, which are proliferating neoplastic HMC lines. However, LAD2 cells are more analogous to MCTC-type HMC which predominate in skin and other organs and represent a distinct minority population in the human lung where MCT predominates (25, 161–163). That notwithstanding, LAD2 cells do show similarity to HLMC: ATP does not trigger degranulation of these cells by itself as it does in murine MCs (130, 132, 141, 164), and ATP-induced enhancement of IgE-mediated degranulation is observed in both HLMC and LAD2 cells.

There is no evidence for P2X7R expression in freshly isolated HLMC which contrasts with the positive RT-PCR for P2X7R and functional activity under whole-cell patch clamp conditions reported in cultured HLMC by Wareham et al. (141). The latter also reported that HLMC express P2X1R and P2X4R and suggested that the differential findings related to P2X7R could be the result of different cell isolation techniques and/or differences in HLMC receptor expression at the time of fresh isolation vs. the pre-experimentation culture of the cells in cytokine-containing mixtures. However, we have performed long-term HLMC culture (2 weeks to 4 months) in a medium containing a combination of Stem Cell Factor and IL-4 (56) and still failed to identify the expression of P2X7R using RT-PCR. By contrast, RT-PCR assays showed that the HMC-1 mast cell leukemia line (58) and the LAD2 cell line do robustly express P2X7R, and in the latter's case, when challenged with BzATP triethylammonium salt, the prototypic P2X7R agonist will lead to degranulation. This agonist failed to trigger degranulation in HLMC (58).

Matsuoka et al. (165) and Yoshida et al. (166) clearly demonstrated that P2X4R activation potentiated Mas-related G protein-coupled receptor X2 (MrgprB2)-mediated pseudo-allergic responses in murine MC. MrgprB2 is the mouse ortholog of human MRGPRX2. However, few reports have demonstrated potentiating effects on P2X4R-stimulated allergic responses in HMC. Bonvini et al. reported that a Transient receptor potential cation channel, subfamily V, member 4 (TRPV4) agonist will cause ATP release from, but not contraction of, isolated airway smooth muscle. Smooth muscle contraction required co-incubation with HLMC. TRPV4-mediated ATP release by the airway smooth muscle-stimulated HLMC to release cysteinyl leukotrienes via a P2X4R-dependent mechanism which subsequently induced smooth muscle contractions in an IgE-independent fashion (167). In any case, these reports suggest that P2X4R, but not P2X7, expressed on MC may also be associated with pathological effects.

Additional evidence for a P2YR subtype(s) and not a P2XR subtype mediating the effects of ATP on HLMC goes beyond transcriptional data. Specifically, the pattern of pharmacologic responsiveness to stable analogs of ATP (i.e., ATP > 2-MeSATP > α, β -MeATP > β, γ-MeATP) is consistent with mediation by P2YR and not P2XR (23, 91, 118, 136). Second, we examined the putative P2XR-selective antagonist PPADS (137) on ATP's effects on enhancing IgE-mediated HLMC degranulation. The failure of this agent to influence ATP-induced enhancement of degranulation along with the previously stated failure of BzATP triethylammonium salt to stimulate HLMC release further argues against the involvement of P2XR.

ATP-induced enhancement of IgE-mediated degranulation in LAD2 cells shows responses linked to P2Y11R activation. This conclusion was based on (i) the robust expression of P2Y11R, (ii) the lack of enhancing effect of ADP and UTP, which excluded P2Y1R, P2Y2R, P2Y4R, P2Y12R, and P2Y13R, (iii) strong enhancing effects of ATPγS, which acts as an agonist at the P2Y11R (145, 168, 169), (iv) the marked inhibition of ATPγS' effects by NF157, which is a selective P2Y11R antagonist (148, 149), and (v) the fact that P2Y11R is coupled to both $G_{q/11}$ and G_s proteins (118), the former mediating enhancement of allergen-induced degranulation.

Gao et al. (60) reported that P2Y11R is the most robustly expressed among P2YRs in LAD2 cells, and P2Y11R agonists, including ATPγS, do not directly trigger degranulation. Gao et al. also investigated the role of P2YR in ATP's enhancement of allergic degranulation in LAD2 cells. They failed to find an effect of ATPγS. However, their test dose was at 10 μM, whereas ours was 100 μM. In addition, those investigators studied the effects on maximal but not minimal antigen-induced degranulation; they also proposed that multiple P2Rs including UDP-glucose-sensitive P2Y14R may play a role in this action of ATP.

Intracellular signal transduction pathways

P2Y11R activation in LAD2 cells leads to activation of intracellular pathways involving PI3K/Akt (Figure 2). As previously reported, the PI3K/Akt pathway can operate without the induction of intracellular Ca^{2+} mobilization (170, 171). It is well known that IgE receptor (FcεRI) activation itself, leading to degranulation, is associated with intracellular Ca^{2+} mobilization (172). Intracellular Ca^{2+}-independent steps in MC degranulation have previously been reported (173–176). This suggests that the potentiating effect of extracellular ATP on anti-IgE–induced degranulation is due to a complex interaction between the two relevant signal-transduction pathways, rather than merely an increase in Ca^{2+} influx induced by ATP.

That PI3Kδ plays a critical role in ATP enhancement is shown by a dose-dependent inhibition of the ATPγS' enhancing effects by compound 15e, a PI3K inhibitor (150, 151), and marked diminution of enhancing effects in PI3Kδ knockdown LAD2 cells (59). PDK-1 is a key element of the PI3K/Akt pathway (177–179), but the lack of PDK-1 phosphorylation does not support its involvement in ATPγS' enhancement of WAS in LAD2 cells.

Modulation by ecto-enzymes

The enhancement of WAS by ATPγS in LAD2 cells was unrelated to its rate of breakdown by ectonucleotidases. However, expressions of multiple purinergic receptors, and/or up- or down-regulation of ectonucleotidases *in vivo* may affect cell responses to extracellular nucleotides. Experiments showed that LAD2 cells' exposures to ATPγS did not affect extracellular concentrations of ATP for at least 60 minutes. However, under experimental conditions, ATP could be released from LAD2 cells.

We have previously reported that the half-life of extracellular ATP/ADP (1 mM) was 14.88 min in another human cell line expressing ectonucleotidases CD39, CD73, and alkaline phosphatase (180). Studies have emphasized the role of ectonucleotidases in the

magnitude of ATP's effects in pulmonary and other organ disorders (68, 181). Tsai and Takeda (160) have recently shown in mice that E-NPP3, an activation marker induced in IgE-mediated reactions, hydrolyzes extracellular ATP on basophil and MC surfaces to prevent ATP-dependent excess activation. In the absence of E-NPP3, basophils and MC become overactivated and the mice experience severe chronic allergic inflammation (160). This work suggests a potential therapeutic role for ATP hydrolysis strategies to control MC-mediated allergic responses. It increasingly appears that a complex of physiological factors interacts to either maintain or degrade extracellular ATP *in vivo*, depending on localized physiological conditions such as pH.

Concluding remarks

Extracellular ATP is a potent modulator of immune reaction-induced HLMC degranulation and thereby release of inflammatory mediators. Since extracellular ATP is rapidly degraded to ADP and adenosine by ecto-enzymes, and adenosine exerts its own effects on inflammatory cells, the variable levels of these enzymes under physiologic and pathophysiologic conditions are critical modulators of the effects of extracellular ATP and adenosine in this setting.

Although the exact mechanism of ATP's effect on HLMC degranulation has not been delineated heretofore, the voluminous relevant data strongly suggest that extracellular ATP plays an important mechanistic role in HLMC allergic reactions. Thus, because of the exponential research work in this arena over the past two decades since the original hypothesis of the "*ATP axis in the Lungs*" was put forward (127), we are now on the cusp of developing novel therapeutic approaches for allergic disorders in general and asthma in particular. This view is supported by the recent developments in a parallel field of ATP-chronic cough, in which pre-clinical studies and clinical trials with P2X3R antagonists are being evaluated as novel anti-tussive agents (182).

The effects of ATP are most pronounced with a concurrent WAS. It is plausible that the cellular ATP environment may change over short periods (e.g., exercise, irritants, etc.), while antigen exposure may not vary and/or remain weak (e.g., dust, cat, mouse, and grass), yet a full-blown asthmatic exacerbation or urticarial episode may ensue. The identity of the receptor(s) mediating the effects of ATP on HMC and the ectoenzymes that hydrolyze ATP in different tissues must be further explored so that novel therapeutic approaches can be tested in the clinical setting.

Author contributions

The potential role of purine nucleotides in the function of human lung MCs under physiologic and pathophysiologic conditions was originally conceived by AP and ES. The HLMC experiments were supervised by ES. HN conducted all LAD2 experiments. ES wrote the first draft of the manuscript, and it was edited by HN and AP. All authors have read the final draft of the manuscript and approved its submission for publication.

Funding

This work was supported by the Margaret Wolf Research Endowment (ESS), the LIXIL Jyukankyo Foundation, and The Jikei University Research Fund (HN).

Acknowledgments

We thank Prof. Arnold Kirshenbaum (NIH) for supplying the LAD2 cells.

Conflict of interest

AP is the CEO and CSO of Danmir Therapeutics, LLC, a biopharmaceutical company that focuses on P2 receptors' signal transductions.

The remaining authors declare that the research was conducted in the absence of any commercial or financial relationships that could be construed as a potential conflict of interest.

Publisher's note

References

1. Schulman ES, Samarasinghe A, Sporn P. Mast Cells and Eosinophils. In: Grippi M A-OD, Dela Cruz CS, Kotloff R, Kotton CN, Pack A, editors. *Fishman's Pulmonary Diseases and Disorders*, *6th ed*. New York: McGraw-Hill Medical (2022). p. 28–50.

2. Blank U, Huang H, Kawakami T. The high affinity IgE receptor: a signaling update. *Curr Opin Immunol* (2021) 72:51–8. doi: 10.1016/j.coi.2021.03.015

3. Levi-Schaffer F, Gibbs BF, Hallgren J, Pucillo C, Redegeld F, Siebenhaar F, et al. Selected recent advances in understanding the role of human mast cells in health and disease. *J Allergy Clin Immunol* (2022) 149(6):1833–44. doi: 10.1016/j.jaci.2022.01.030

4. Schulman ES. The role of mast cells in inflammatory responses in the lung. *Crit Rev Immunol* (1993) 13(1):35–70.

5. Kirshenbaum AS, Akin C, Wu Y, Rottem M, Goff JP, Beaven MA, et al. Characterization of novel stem cell factor responsive human mast cell lines LAD 1 and 2 established from a patient with mast cell sarcoma/leukemia; activation following aggregation of FcepsilonRI or FcgammaRI. *Leuk Res* (2003) 27(8):677–82. doi: 10.1016/S0145-2126(02)00343-0

6. Kirshenbaum AS, Petrik A, Walsh R, Kirby TL, Vepa S, Wangsa D, et al. A ten-year retrospective analysis of the distribution, use and phenotypic characteristics of the

LAD2 human mast cell line. *Int Arch Allergy Immunol* (2014) 164(4):265–70. doi: 10.1159/000365729

7. Kirshenbaum AS, Yin Y, Sundstrom JB, Bandara G, Metcalfe DD. Description and characterization of a novel human mast cell line for scientific study. *Int J Mol Sci* (2019) 20(22). doi: 10.3390/ijms20225520

8. Valent P, Akin C, Hartmann K, Nilsson G, Reiter A, Hermine O, et al. Mast cells as a unique hematopoietic lineage and cell system: From Paul Ehrlich's visions to precision medicine concepts. *Theranostics* (2020) 10(23):10743–68. doi: 10.7150/thno.46719

9. Bandara G, Metcalfe DD, Kirshenbaum AS. Growth of human mast cells from bone marrow and peripheral blood-derived CD34(+) pluripotent hematopoietic cells. *Methods Mol Biol* (2015) 1220:155–62. doi: 10.1007/978-1-4939-1568-2_10

10. Kirshenbaum AS, Metcalfe DD. Growth of human mast cells from bone marrow and peripheral blood-derived CD34+ pluripotent progenitor cells. *Methods Mol Biol* (2006) 315:105–12. doi: 10.1385/1-59259-967-2:105

11. Shimizu Y, Sakai K, Miura T, Narita T, Tsukagoshi H, Satoh Y, et al. Characterization of 'adult-type' mast cells derived from human bone marrow CD34(+) cells cultured in the presence of stem cell factor and interleukin-6. Interleukin-4 is not required for constitutive expression of CD54, Fc epsilon RI alpha and chymase, and CD13 expression is reduced during differentiation. *Clin Exp Allergy* (2002) 32(6):872–80. doi: 10.1046/j.1365-2222.2002.01373.x

12. Kambe M, Kambe N, Oskeritzian CA, Schechter N, Schwartz LB. IL-6 attenuates apoptosis, while neither IL-6 nor IL-10 affect the numbers or protease phenotype of fetal liver-derived human mast cells. *Clin Exp Allergy* (2001) 31(7):1077–85. doi: 10.1046/j.1365-2222.2001.01126.x

13. Oskeritzian CA, Zhao W, Pozez AL, Cohen NM, Grimes M, Schwartz LB. Neutralizing endogenous IL-6 renders mast cells of the MCT type from lung, but not the MCTC type from skin and lung, susceptible to human recombinant IL-4-induced apoptosis. *J Immunol* (2004) 172(1):593–600. doi: 10.4049/jimmunol.172.1.593

14. Igarashi Y, Kurosawa M, Ishikawa O, Miyachi Y, Saito H, Ebisawa M, et al. Characteristics of histamine release from cultured human mast cells. *Clin Exp Allergy* (1996) 26(5):597–602. doi: 10.1111/j.1365-2222.1996.tb00582.x

15. Inomata N, Tomita H, Ikezawa Z, Saito H. Differential gene expression profile between cord blood progenitor-derived and adult progenitor-derived human mast cells. *Immunol Lett* (2005) 98(2):265–71. doi: 10.1016/j.imlet.2004.12.001

16. Okayama Y, Okumura S, Sagara H, Yuki K, Sasaki T, Watanabe N, et al. FcepsilonRI-mediated thymic stromal lymphopoietin production by interleukin-4-primed human mast cells. *Eur Respir J* (2009) 34(2):425–35. doi: 10.1183/09031936.00121008

17. Saito H, Ebisawa M, Sakaguchi N, Onda T, Iikura Y, Yanagida M, et al. Characterization of cord-blood-derived human mast cells cultured in the presence of Steel factor and interleukin-6. *Int Arch Allergy Immunol* (1995) 107(1-3):63–5. doi: 10.1159/000236932

18. Saito H, Kato A, Matsumoto K, Okayama Y. Culture of human mast cells from peripheral blood progenitors. *Nat Protoc* (2006) 1(4):2178–83. doi: 10.1038/nprot.2006.344

19. Yanagida M, Fukamachi H, Takei M, Hagiwara T, Uzumaki H, Tokiwa T, et al. Interferon-gamma promotes the survival and Fc epsilon RI-mediated histamine release in cultured human mast cells. *Immunology* (1996) 89(4):547–52. doi: 10.1046/j.1365-2567.1996.d01-768.x

20. Ravindran A, Rönnberg E, Dahlin JS, Mazzurana L, Säfholm J, Orre AC, et al. An optimized protocol for the isolation and functional analysis of human lung mast cells. *Front Immunol* (2018) 9:2193. doi: 10.3389/fimmu.2018.02193

21. Andersen HB, Holm M, Hetland TE, Dahl C, Junker S, Schiøtz PO, et al. Comparison of short term in *vitro* cultured human mast cells from different progenitors - Peripheral blood-derived progenitors generate highly mature and functional mast cells. *J Immunol Methods* (2008) 336(2):166–74. doi: 10.1016/j.jim.2008.04.016

22. Derakhshan T, Bhowmick R, Ritchey JW, Gappa-Fahlenkamp H. Development of human mast cells from hematopoietic stem cells within a 3D collagen matrix: effect of stem cell media on mast cell generation. *Stem Cells Int* (2018) 2018:2136193. doi: 10.1155/2018/2136193

23. Bodin P, Burnstock G. Purinergic signalling: ATP release. *Neurochem Res* (2001) 26(8-9):959–69. doi: 10.1023/A:1012388618693

24. Falduto GH, Pfeiffer A, Luker A, Metcalfe DD, Olivera A. Emerging mechanisms contributing to mast cell-mediated pathophysiology with therapeutic implications. *Pharmacol Ther* (2021) 220:107718. doi: 10.1016/j.pharmthera.2020.107718

25. West PW, Bulfone-Paus S. Mast cell tissue heterogeneity and specificity of immune cell recruitment. *Front Immunol* (2022) 13:932090. doi: 10.3389/fimmu.2022.932090

26. Frossi B, Mion F, Sibilano R, Danelli L, Pucillo CEM. Is it time for a new classification of mast cells? What do we know about mast cell heterogeneity? *Immunol Rev* (2018) 282(1):35–46. doi: 10.1111/imr.12636

27. Schulman ES, MacGlashan DW Jr., Peters SP, Schleimer RP, Newball HH, Lichtenstein LM. Human lung mast cells: purification and characterization. *J Immunol* (1982) 129(6):2662–7. doi: 10.4049/jimmunol.129.6.2662

28. Dvorak AM, Galli SJ, Schulman ES, Lichtenstein LM, Dvorak HF. Basophil and mast cell degranulation: ultrastructural analysis of mechanisms of mediator release. *Fed Proc* (1983) 42(8):2510–5.

29. Dvorak AM, Hammel I, Schulman ES, Peters SP, MacGlashan DW Jr., Schleimer RP, et al. Differences in the behavior of cytoplasmic granules and lipid bodies during human lung mast cell degranulation. *J Cell Biol* (1984) 99(5):1678–87. doi: 10.1083/jcb.99.5.1678

30. Dvorak AM, Schleimer RP, Schulman ES, Lichtenstein LM. Human mast cells use conservation and condensation mechanisms during recovery from degranulation. *In vitro* studies with mast cells purified from human lungs. *Lab Invest* (1986) 54 (6):663–78.

31. Dvorak AM, Schulman ES, Peters SP, MacGlashan DW Jr., Newball HH, Schleimer RP, et al. Immunoglobulin E-mediated degranulation of isolated human lung mast cells. *Lab Invest* (1985) 53(1):45–56.

32. Hammel I, Dvorak AM, Peters SP, Schulman ES, Dvorak HF, Lichtenstein LM, et al. Differences in the volume distributions of human lung mast cell granules and lipid bodies: evidence that the size of these organelles is regulated by distinct mechanisms. *J Cell Biol* (1985) 100(5):1488–92. doi: 10.1083/jcb.100.5.1488

33. Schulman ES, Kagey-Sobotka A, MacGlashan DW Jr., Adkinson NF Jr., Peters SP, Schleimer RP, et al. Heterogeneity of human mast cells. *J Immunol* (1983) 131 (4):1936–41. doi: 10.4049/jimmunol.131.4.1936

34. Schulman ES, Pollack RB, Post TJ, Peters SP. Histochemical heterogeneity of dispersed human lung mast cells. *J Immunol* (1990) 144(11):4195–201. doi: 10.4049/jimmunol.144.11.4195

35. Schulman ES, Post TJ, Vigderman RJ. Density heterogeneity of human lung mast cells. *J Allergy Clin Immunol* (1988) 82(1):78–86. doi: 10.1016/0091-6749(88)90055-3

36. Ishizaka T, Conrad DH, Schulman ES, Sterk AR, Ishizaka K. Biochemical analysis of initial triggering events of IgE-mediated histamine release from human lung mast cells. *J Immunol* (1983) 130(5):2357–62. doi: 10.4049/jimmunol.130.5.2357

37. Ishizaka T, Conrad DH, Schulman ES, Sterk AR, Ko CG, Ishizaka K. IgE-mediated triggering signals for mediator release from human mast cells and basophils. *Fed Proc* (1984) 43(13):2840–5.

38. Gonen B, O'Donnell P, Post TJ, Quinn TJ, Schulman ES. Very low density lipoproteins (VLDL) trigger the release of histamine from human basophils. *Biochim Biophys Acta* (1987) 917(3):418–24. doi: 10.1016/0005-2760(87)90121-4

39. Kelly SJ, Uri AJ, Freeland HS, Woods EJ, Schulman ES, Peters SP, et al. Effects of colchicine on IgE-mediated early and late airway reactions. *Chest* (1995) 107(4):985–91. doi: 10.1378/chest.107.4.985

40. MacGlashan DW Jr., Schleimer RP, Peters SP, Schulman ES, Adams GK, Sobotka AK, et al. Comparative studies of human basophils and mast cells. *Fed Proc* (1983) 42 (8):2504–9.

41. Peters SP, Schulman ES, Schleimer RP, MacGlashan DW Jr., Newball HH, Lichtenstein LM. Dispersed human lung mast cells. Pharmacologic aspects and comparison with human lung tissue fragments. *Am Rev Respir Dis* (1982) 126 (6):1034–9. doi: 10.1164/arrd.1982.126.6.1034

42. Schleimer RP, MacGlashan DW Jr., Schulman ES, Peters SP, Adams GK 3rd, Adkinson NF Jr., et al. Human mast cells and basophils–structure, function, pharmacology, and biochemistry. *Clin Rev Allergy* (1983) 1(3):327–41. doi: 10.1007/BF02991224

43. Schulman ES, Liu MC, Proud D, MacGlashan DW Jr., Lichtenstein LM, Plaut M. Human lung macrophages induce histamine release from basophils and mast cells. *Am Rev Respir Dis* (1985) 131(2):230–5. doi: 10.1164/arrd.1985.131.2.230

44. Schulman ES, Post TJ, Henson PM, Giclas PC. Differential effects of the complement peptides, C5a and C5a des Arg on human basophil and lung mast cell histamine release. *J Clin Invest* (1988) 81(3):918–23. doi: 10.1172/JCI113403

45. Schulman ES, Quinn TJ, Post TJ, O'Donnell P, Rodriguez A, Gonen B. Low density lipoprotein (LDL) inhibits histamine release from human mast cells. *Biochem Biophys Res Commun* (1987) 148(2):553–9. doi: 10.1016/0006-291X(87)90912-0

46. Glaum MC, Jaffe JS, Gillespie DH, Raible DG, Post TJ, Wang Y, et al. IgE-dependent expression of interleukin-5 mRNA and protein in human lung: modulation by dexamethasone. *Clin Immunol Immunopathol* (1995) 75(2):171–8. doi: 10.1006/clin.1995.1068

47. Jaffe JS, Glaum MC, Raible DG, Post TJ, Dimitry E, Govindarao D, et al. Human lung mast cell IL-5 gene and protein expression: temporal analysis of upregulation following IgE-mediated activation. *Am J Respir Cell Mol Biol* (1995) 13(6):665–75. doi: 10.1165/ajrcmb.13.6.7576704

48. Jaffe JS, Raible DG, Post TJ, Wang Y, Glaum MC, Butterfield JH, et al. Human lung mast cell activation leads to IL-13 mRNA expression and protein release. *Am J Respir Cell Mol Biol* (1996) 15(4):473–81. doi: 10.1165/ajrcmb.15.4.8879181

49. MacGlashan DW Jr., Schleimer RP, Peters SP, Schulman ES, Adams GK 3rd, Newball HH, et al. Generation of leukotrienes by purified human lung mast cells. *J Clin Invest* (1982) 70(4):747–51. doi: 10.1172/JCI110670

50. Meier HL, Heck LW, Schulman ES, MacGlashan DW Jr. Purified human mast cells and basophils release human elastase and cathepsin G by an IgE-mediated mechanism. *Int Arch Allergy Appl Immunol* (1985) 77(1-2):179–83. doi: 10.1159/000233779

51. Meier HL, Schulman ES, Heck LW, MacGlashan D, Newball HH, Kaplan AP. Release of elastase from purified human lung mast cells and basophils. Identification as a Hageman factor cleaving enzyme. *Inflammation* (1989) 13(3):295–308. doi: 10.1007/BF00914396

52. Peters SP, MacGlashan DW Jr., Schulman ES, Schleimer RP, Hayes EC, Rokach J, et al. Arachidonic acid metabolism in purified human lung mast cells. *J Immunol* (1984) 132(4):1972–9. doi: 10.4049/jimmunol.132.4.1972

53. Peters SP, Schulman ES, Liu MC, Hayes EC, Lichtenstein LM. Separation of major prostaglandins, leukotrienes, and monoHETEs by high performance liquid chromatography. *J Immunol Methods* (1983) 64(3):335–43. doi: 10.1016/0022-1759(83)90441-6

54. Proud D, MacGlashan DW Jr., Newball HH, Schulman ES, Lichtenstein LM. Immunoglobulin E-mediated release of a kininogenase from purified human lung mast cells. *Am Rev Respir Dis* (1985) 132(2):405–8. doi: 10.1164/arrd.1985.132.2.405

55. Thompson HL, Schulman ES, Metcalfe DD. Identification of chondroitin sulfate E in human lung mast cells. *J Immunol* (1988) 140(8):2708–13. doi: 10.4049/jimmunol.140.8.2708

56. Schleimer RP, Schulman ES, MacGlashan DW Jr., Peters SP, Hayes EC, Adams GK 3rd, et al. Effects of dexamethasone on mediator release from human lung fragments and purified human lung mast cells. *J Clin Invest* (1983) 71(6):1830–5. doi: 10.1172/JCI110938

57. Nishi H, Pelleg A, Schulman ES. IgE receptor-mediated histamine release in human lung mast cells: modulation by purinergic receptor ligands. *Ann Clin Lab Sci* (2016) 46(5):463–9.

58. Schulman ES, Glaum MC, Post T, Wang Y, Raible DG, Mohanty J, et al. ATP modulates anti-IgE-induced release of histamine from human lung mast cells. *Am J Respir Cell Mol Biol* (1999) 20(3):530–7. doi: 10.1165/ajrcmb.20.3.3387

59. Nishi H, Niyonsaba F, Pelleg A, Schulman ES. Enhancement of mast cell degranulation mediated by purinergic receptors' Activation and PI3K type delta. *J Immunol* (2021) 207(4):1001–8. doi: 10.4049/jimmunol.2001002

60. Gao ZG, Wei Q, Jayasekara MP, Jacobson KA. The role of P2Y(14) and other P2Y receptors in degranulation of human LAD2 mast cells. *Purinergic Signal* (2013) 9(1):31–40. doi: 10.1007/s11302-012-9325-4

61. Pelleg A. Extracellular adenosine 5'-triphosphate in pulmonary disorders. *Biochem Pharmacol* (2021) 187:114319. doi: 10.1016/j.bcp.2020.114319

62. Pelleg A, Schulman ES, Barnes PJ. Extracellular adenosine 5'-triphosphate in obstructive airway diseases. *Chest* (2016) 150(4):908–15. doi: 10.1016/j.chest.2016.06.045

63. Pelleg A, Schulman ES, Barnes PJ. Adenosine 5'-triphosphate's role in bradycardia and syncope associated with pulmonary embolism. *Respir Res* (2018) 19(1):142. doi: 10.1186/s12931-018-0848-2

64. Pelleg A, Sirtori E, Rolland J-F, Mahadevan A. DT-0111: a novel P2X3 receptor antagonist. *Purinergic Signalling* (2023) 19(3):469–79. doi: 10.1007/s11302-023-09930-5

65. Pelleg A, Xu F, Zhuang J, Undem B, Burnstock G. DT-0111: a novel drug-candidate for the treatment of COPD and chronic cough. *Ther Adv Respir Dis* (2019) 13:1753466619877960. doi: 10.1177/1753466619877960

66. Lazarowski ER, Boucher RC. Purinergic receptors in airway hydration. *Biochem Pharmacol* (2021) 187:114387. doi: 10.1016/j.bcp.2020.114387

67. Okada SF, Ribeiro CM, Sesma JI, Seminario-Vidal L, Abdullah LH, van Heusden C, et al. Inflammation promotes airway epithelial ATP release *via* calcium-dependent vesicular pathways. *Am J Respir Cell Mol Biol* (2013) 49(5):814–20. doi: 10.1165/rcmb.2012-0493OC

68. van Heusden C, Button B, Anderson WH, Ceppe A, Morton LC, O'Neal WK, et al. Inhibition of ATP hydrolysis restores airway surface liquid production in cystic fibrosis airway epithelia. *Am J Physiol Lung Cell Mol Physiol* (2020) 318(2):L356–l65. doi: 10.1152/ajplung.00449.2019

69. Nirody JA, Budin I, Rangamani P. ATP synthase: Evolution, energetics, and membrane interactions. *J Gen Physiol* (2020) 152(11). doi: 10.1085/jgp.201912475

70. Trautmann A. Extracellular ATP in the immune system: more than just a "danger signal". *Sci Signal* (2009) 2(56):pe6. doi: 10.1126/scisignal.256pe6

71. Drury AN, Szent-Györgyi A. The physiological activity of adenine compounds with especial reference to their action upon the mammalian heart. *J Physiol* (1929) 68(3):213–37. doi: 10.1113/jphysiol.1929.sp002608

72. Hopkins SV. The action of ATP in the Guinea-pig heart. *Biochem Pharmacol* (1973) 22(3):335–9. doi: 10.1016/0006-2952(73)90414-0

73. Schrader J, Gerlach E. Compartmentation of cardiac adenine nucleotides and formation of adenosine. *Pflugers Arch* (1976) 367(2):129–35. doi: 10.1007/BF00585148

74. Cheek DJ, McHugh JM, Blood-Siegfried J, McFetridge JF, Turner BS. A historical perspective on the discovery of adenyl purines. *Biol Res Nurs* (2000) 1(4):265–75. doi: 10.1177/109980040000100403

75. Taruno A. ATP release channels. *Int J Mol Sci* (2018) 19(3). doi: 10.3390/ijms19030808

76. Vultaggio-Poma V, Sarti AC, Di Virgilio F. Extracellular ATP: A feasible target for cancer therapy. *Cells* (2020) 9(11). doi: 10.3390/cells9112496

77. Bodin P, Bailey D, Burnstock G. Increased flow-induced ATP release from isolated vascular endothelial cells but not smooth muscle cells. *Br J Pharmacol* (1991) 103(1):1203–5. doi: 10.1111/j.1476-5381.1991.tb12324.x

78. Mills DC, Robb IA, Roberts GC. The release of nucleotides, 5-hydroxytryptamine and enzymes from human blood platelets during aggregation. *J Physiol* (1968) 195(3):715–29. doi: 10.1113/jphysiol.1968.sp008484

79. Day HJ, Holmsen H. Concepts of the blood platelet release reaction. *Ser Haematol* (1971) 4(1):3–27.

80. Holmsen H. Platelet metabolism and activation. *Semin Hematol* (1985) 22(3):219–40.

81. Dean BM, Perrett D. Studies on adenine and adenosine metabolism by intact human erythrocytes using high performance liquid chromatography. *Biochim Biophys Acta* (1976) 437(1):1–5. doi: 10.1016/0304-4165(76)90342-1

82. Bergfeld GR, Forrester T. Release of ATP from human erythrocytes in response to a brief period of hypoxia and hypercapnia. *Cardiovasc Res* (1992) 26(1):40–7. doi: 10.1093/cvr/26.1.40

83. Ellsworth ML, Forrester T, Ellis CG, Dietrich HH. The erythrocyte as a regulator of vascular tone. *Am J Physiol* (1995) 269(6 Pt 2):H2155–61. doi: 10.1152/ajpheart.1995.269.6.H2155

84. Zhang H, Shen Z, Hogan B, Barakat AI, Misbah C. ATP release by red blood cells under flow: model and simulations. *Biophys J* (2018) 115(11):2218–29. doi: 10.1016/j.bpj.2018.09.033

85. Pearson JD, Gordon JL. Vascular endothelial and smooth muscle cells in culture selectively release adenine nucleotides. *Nature* (1979) 281(5730):384–6. doi: 10.1038/281384a0

86. Ralevic V, Milner P, Kirkpatrick KA, Burnstock G. Flow-induced release of adenosine 5'-triphosphate from endothelial cells of the rat mesenteric arterial bed. *Experientia* (1992) 48(1):31–4. doi: 10.1007/BF01923600

87. Yang S, Cheek DJ, Westfall DP, Buxton IL. Purinergic axis in cardiac blood vessels. Agonist-mediated release of ATP from cardiac endothelial cells. *Circ Res* (1994) 74(3):401–7. doi: 10.1161/01.res.74.3.401

88. Bodin P, Burnstock G. ATP-stimulated release of ATP by human endothelial cells. *J Cardiovasc Pharmacol* (1996) 27(6):872–5. doi: 10.1097/00005344-199606000-00015

89. Katsuragi T, Tokunaga T, Ogawa S, Soejima O, Sato C, Furukawa T. Existence of ATP-evoked ATP release system in smooth muscles. *J Pharmacol Exp Ther* (1991) 259(2):513–8.

90. Katsuragi T, Soejima O, Tokunaga T, Furukawa T. Evidence for postjunctional release of ATP evoked by stimulation of muscarinic receptors in ileal longitudinal muscles of Guinea pig. *J Pharmacol Exp Ther* (1992) 260(3):1309–13.

91. Burnstock G, Boeynaems JM. Purinergic signalling and immune cells. *Purinergic Signal* (2014) 10(4):529–64. doi: 10.1007/s11302-014-9427-2

92. Junger WG. Immune cell regulation by autocrine purinergic signalling. *Nat Rev Immunol* (2011) 11(3):201–12. doi: 10.1038/nri2938

93. Di Virgilio F, Vuerich M. Purinergic signaling in the immune system. *Auton Neurosci* (2015) 191:117–23. doi: 10.1016/j.autneu.2015.04.011

94. Gov NS, Safran SA. Red blood cell membrane fluctuations and shape controlled by ATP-induced cytoskeletal defects. *Biophys J* (2005) 88(3):1859–74. doi: 10.1529/biophysj.104.045328

95. Begandt D, Good ME, Keller AS, DeLalio LJ, Rowley C, Isakson BE, et al. Pannexin channel and connexin hemichannel expression in vascular function and inflammation. *BMC Cell Biol* (2017) 18(Suppl 1):2. doi: 10.1186/s12860-016-0119-3

96. Forrester T. An estimate of adenosine triphosphate release into the venous effluent from exercising human forearm muscle. *J Physiol* (1972) 224(3):611–28. doi: 10.1113/jphysiol.1972.sp009915

97. Fredholm BB, Hedqvist P, Lindström K, Wennmalm M. Release of nucleosides and nucleotides from the rabbit heart by sympathetic nerve stimulation. *Acta Physiol Scand* (1982) 116(3):285–95. doi: 10.1111/j.1748-1716.1982.tb07142.x

98. Darius H, Stahl GL, Lefer AM. Pharmacologic modulation of ATP release from isolated rat hearts in response to vasoconstrictor stimuli using a continuous flow technique. *J Pharmacol Exp Ther* (1987) 240(2):542–7.

99. Katsuragi T, Tokunaga T, Ohba M, Sato C, Furukawa T. Implication of ATP released from atrial, but not papillary, muscle segments of Guinea pig by isoproterenol and forskolin. *Life Sci* (1993) 53(11):961–7. doi: 10.1016/0024-3205(93)90449-D

100. Tokunaga T, Katsuragi T, Sato C, Furukawa T. ATP release evoked by isoprenaline from adrenergic nerves of Guinea pig atrium. *Neurosci Lett* (1995) 186(2-3):95–8. doi: 10.1016/0304-3940(95)11290-D

101. Pelleg A, Katchanov G, Xu J. Purinergic modulation of neural control of cardiac function. *J Auton Pharmacol* (1996) 16(6):401–5. doi: 10.1111/j.1474-8673.1996.tb00063.x

102. Paddle BM, Burnstock G. Release of ATP from perfused heart during coronary vasodilatation. *Blood Vessels* (1974) 11(3):110–9. doi: 10.1159/000158005

103. Forrester T, Williams CA. Release of adenosine triphosphate from isolated adult heart cells in response to hypoxia. *J Physiol* (1977) 268(2):371–90. doi: 10.1113/jphysiol.1977.sp011862

104. Williams CA, Forrester T. Possible source of adenosine triphosphate released from rat myocytes in response to hypoxia and acidosis. *Cardiovasc Res* (1983) 17(5):301–12. doi: 10.1093/cvr/17.5.301

105. Baxter M, Eltom S, Dekkak B, Yew-Booth L, Dubuis ED, Maher SA, et al. Role of transient receptor potential and pannexin channels in cigarette smoke-triggered ATP release in the lung. *Thorax* (2014) 69(12):1080–9. doi: 10.1136/thoraxjnl-2014-205467

106. Bucchioni E, Csoma Z, Polkey M, Collins JV, Cramer D, Allegra L, et al. Adenosine 50-triphosphate (ATP) is increased in exhaled breath condensate in COPD. *Am J Respir Crit Care Med* (2002) 165:A599.

107. Mortaz E, Braber S, Nazary M, Givi ME, Nijkamp FP, Folkerts G. ATP in the pathogenesis of lung emphysema. *Eur J Pharmacol* (2009) 619(1-3):92–6. doi: 10.1016/j.ejphar.2009.07.022

108. Cicko S, Lucattelli M, Müller T, Lommatzsch M, De Cunto G, Cardini S, et al. Purinergic receptor inhibition prevents the development of smoke-induced lung injury and emphysema. *J Immunol* (2010) 185(1):688–97. doi: 10.4049/jimmunol.0904042

109. Jacobson KA, Pradhan B, Wen Z, Pramanik A. New paradigms in purinergic receptor ligand discovery. *Neuropharmacology* (2023) 230:109503. doi: 10.1016/j.neuropharm.2023.109503

110. Colgan SP, Eltzschig HK, Eckle T, Thompson LF. Physiological roles for ecto-5'-nucleotidase (CD73). *Purinergic Signal* (2006) 2(2):351–60. doi: 10.1007/s11302-005-5302-5

111. Knapp K, Zebisch M, Pippel J, El-Tayeb A, Müller CE, Sträter N. Crystal structure of the human ecto-5'-nucleotidase (CD73): insights into the regulation of purinergic signaling. *Structure* (2012) 20(12):2161–73. doi: 10.1016/j.str.2012.10.001

112. Schetinger MR, Morsch VM, Bonan CD, Wyse AT. NTPDase and 5'-nucleotidase activities in physiological and disease conditions: new perspectives for human health. *Biofactors* (2007) 31(2):77–98. doi: 10.1002/biof.5520310205

113. Zhao H, Bo C, Kang Y, Li H. What else can CD39 tell us? *Front Immunol* (2017) 8. doi: 10.3389/fimmu.2017.00727

114. Antonioli L, Pacher P, Vizi ES, Haskó G. CD39 and CD73 in immunity and inflammation. *Trends Mol Med* (2013) 19(6):355–67. doi: 10.1016/j.molmed.2013.03.005

115. Timperi E, Barnaba V. CD39 regulation and functions in T cells. *Int J Mol Sci* (2021) 22(15). doi: 10.3390/ijms22158068

116. Eckle T, Füllbier L, Wehrmann M, Khoury J, Mittelbronn M, Ibla J, et al. Identification of ectonucleotidases CD39 and CD73 in innate protection during acute lung injury. *J Immunol* (2007) 178(12):8127–37. doi: 10.4049/jimmunol.178.12.8127

117. Li J, Wang L, Chen X, Li L, Li Y, Ping Y, et al. CD39/CD73 upregulation on myeloid-derived suppressor cells *via* TGF-β-mTOR-HIF-1 signaling in patients with non-small cell lung cancer. *Oncoimmunology* (2017) 6(6):e1320011. doi: 10.1080/2162402X.2017.1320011

118. Burnstock G, Brouns I, Adriaensen D, Timmermans JP. Purinergic signaling in the airways. *Pharmacol Rev* (2012) 64(4):834–68. doi: 10.1124/pr.111.005389

119. Saul A, Hausmann R, Kless A, Nicke A. Heteromeric assembly of P2X subunits. *Front Cell Neurosci* (2013) 7:250. doi: 10.3389/fncel.2013.00250

120. Abbracchio MP, Burnstock G, Boeynaems JM, Barnard EA, Boyer JL, Kennedy C, et al. International Union of Pharmacology LVIII: update on the P2Y G protein-coupled nucleotide receptors: from molecular mechanisms and pathophysiology to therapy. *Pharmacol Rev* (2006) 58(3):281–341. doi: 10.1124/pr.58.3.3

121. Waldo GL, Harden TK. Agonist binding and Gq-stimulating activities of the purified human P2Y1 receptor. *Mol Pharmacol* (2004) 65(2):426–36. doi: 10.1124/mol.65.2.426

122. Alexander SPH, Christopoulos A, Davenport AP, Kelly E, Mathie A, Peters JA, et al. THE CONCISE GUIDE TO PHARMACOLOGY 2019/20: G protein-coupled receptors. *Br J Pharmacol* (2019) 176 Suppl 1(Suppl 1):S21–s141. doi: 10.1111/bph.14748

123. Burnstock G. Introduction and perspective, historical note. *Front Cell Neurosci* (2013) 7:227. doi: 10.3389/fncel.2013.00227

124. Pellegrino R, Wilson O, Jenouri G, Rodarte JR. Lung mechanics during induced bronchoconstriction. *J Appl Physiol (1985)* (1996) 81(2):964–75. doi: 10.1152/jappl.1996.81.2.964

125. Pelleg A, Hurt CM. Mechanism of action of ATP on canine pulmonary vagal C fibre nerve terminals. *J Physiol* (1996) 490(Pt 1):265–75. doi: 10.1113/jphysiol.1996.sp021142

126. Katchanov G, Xu J, Schulman ES, Pelleg A. ATP causes neurogenic bronchoconstriction in the dog. *Drug Dev Res* (1998) 45(3-4):342–9. doi: 10.1002/(SICI)1098-2299(199811/12)45:3/4<342::AID-DDR34>3.0.CO;2-P

127. Pelleg A, Schulman ES. Adenosine 5'-triphosphate axis in obstructive airway diseases. *Am J Ther* (2002) 9(5):454–64. doi: 10.1097/00045391-200209000-00014

128. Arzola-Martínez L, Benavente R, Vega G, Ríos M, Fonseca W, Rasky AJ, et al. Blocking ATP-releasing channels prevents high extracellular ATP levels and airway hyperreactivity in an asthmatic mouse model. *Am J Physiol Lung Cell Mol Physiol* (2021) 321(2):L466–l76. doi: 10.1152/ajplung.00450.2020

129. Straus DB, Pryor D, Haque TT, Kee SA, Dailey JM, Jackson KG, et al. IL-33 priming amplifies ATP-mediated mast cell cytokine production. *Cell Immunol* (2022) 371:104470. doi: 10.1016/j.cellimm.2021.104470

130. Bennett JP, Cockcroft S, Gomperts BD. Rat mast cells permeabilized with ATP secrete histamine in response to calcium ions buffered in the micromolar range. *J Physiol* (1981) 317:335–45. doi: 10.1113/jphysiol.1981.sp013828

131. Osipchuk Y, Cahalan M. Cell-to-cell spread of calcium signals mediated by ATP receptors in mast cells. *Nature* (1992) 359(6392):241–4. doi: 10.1038/359241a0

132. Tatham PE, Cusack NJ, Gomperts BD. Characterisation of the ATP4- receptor that mediates permeabilisation of rat mast cells. *Eur J Pharmacol* (1988) 147(1):13–21. doi: 10.1016/0014-2999(88)90628-0

133. Ye F, Lv J, Shen X, Zhang J, Zong Y, Zhu C, et al. Rutin ameliorates inflammatory pain by inhibiting P2X7 receptor in mast cells. *J Physiol Biochem* (2022) 79(2):287–95. doi: 10.1007/s13105-022-00938-w

134. Peachell PT, Columbo M, Kagey-Sobotka A, Lichtenstein LM, Marone G. Adenosine potentiates mediator release from human lung mast cells. *Am Rev Respir Dis* (1988) 138(5):1143–51. doi: 10.1164/ajrccm/138.5.1143

135. Hughes PJ, Holgate ST, Church MK. Adenosine inhibits and potentiates IgE-dependent histamine release from human lung mast cells by an A2-purinoceptor mediated mechanism. *Biochem Pharmacol* (1984) 33(23):3847–52. doi: 10.1016/0006-2952(84)90050-9

136. Abbracchio MP, Burnstock G. Purinoceptors: are there families of P2X and P2Y purinoceptors? *Pharmacol Ther* (1994) 64(3):445–75. doi: 10.1016/0163-7258(94)00048-4

137. Lambrecht G, Friebe T, Grimm U, Windscheif U, Bungardt E, Hildebrandt C, et al. PPADS, a novel functionally selective antagonist of P2 purinoceptor-mediated responses. *Eur J Pharmacol* (1992) 217(2-3):217–9. doi: 10.1016/0014-2999(92)90877-7

138. Di Virgilio F, Ferrari D, Falzoni S, Chiozzi P, Munerati M, Steinberg TH, et al. P2 purinoceptors in the immune system. *Ciba Found Symp* (1996) 198:290–302; discussion -5. doi: 10.1002/9780470514900.ch17

139. Dasari VR, Jin J, Kunapuli SP. Distribution of leukotriene B4 receptors in human hematopoietic cells. *Immunopharmacology* (2000) 48(2):157–63. doi: 10.1016/S0162-3109(00)00201-0

140. Feng C, Mery AG, Beller EM, Favot C, Boyce JA. Adenine nucleotides inhibit cytokine generation by human mast cells through a Gs-coupled receptor. *J Immunol* (2004) 173(12):7539–47. doi: 10.4049/jimmunol.173.12.7539

141. Wareham K, Vial C, Wykes RC, Bradding P, Seward EP. Functional evidence for the expression of P2X1, P2X4 and P2X7 receptors in human lung mast cells. *Br J Pharmacol* (2009) 157(7):1215–24. doi: 10.1111/j.1476-5381.2009.00287.x

142. von Kügelgen I. Molecular pharmacology of P2Y receptor subtypes. *Biochem Pharmacol* (2021) 187:114361. doi: 10.1016/j.bcp.2020.114361

143. Mellor EA, Maekawa A, Austen KF, Boyce JA. Cysteinyl leukotriene receptor 1 is also a pyrimidinergic receptor and is expressed by human mast cells. *Proc Natl Acad Sci U S A.* (2001) 98(14):7964–9. doi: 10.1073/pnas.141221498

144. Communi D, Janssens R, Robaye B, Zeelis N, Boeynaems JM. Rapid up-regulation of P2Y messengers during granulocytic differentiation of HL-60 cells. *FEBS Lett* (2000) 475(1):39–42. doi: 10.1016/S0014-5793(00)01618-5

145. Communi D, Robaye B, Boeynaems JM. Pharmacological characterization of the human P2Y11 receptor. *Br J Pharmacol* (1999) 128(6):1199–206. doi: 10.1038/sj.bjp.0702909

146. Inoue K, Hosoi J, Denda M. Extracellular ATP has stimulatory effects on the expression and release of IL-6 *via* purinergic receptors in normal human epidermal keratinocytes. *J Invest Dermatol* (2007) 127(2):362–71. doi: 10.1038/sj.jid.5700526

147. van der Weyden L, Adams DJ, Luttrell BM, Conigrave AD, Morris MB. Pharmacological characterisation of the P2Y11 receptor in stably transfected haematological cell lines. *Mol Cell Biochem* (2000) 213(1-2):75–81. doi: 10.1023/A:1007168215748

148. Kuang Y, Liu H, Guo S, Wang Y, Zhang H, Qiao Y. The antagonist of P2Y11 receptor NF157 ameliorates oxidized LDL-induced vascular endothelial inflammation. *Artif Cells Nanomed Biotechnol* (2019) 47(1):1839–45. doi: 10.1080/21691401.2019.1610412

149. Ullmann H, Meis S, Hongwiset D, Marzian C, Wiese M, Nickel P, et al. Synthesis and structure-activity relationships of suramin-derived P2Y11 receptor antagonists with nanomolar potency. *J Med Chem* (2005) 48(22):7040–8. doi: 10.1021/jm050301p

150. Bekhite MM, Finkensieper A, Binas S, Müller J, Wetzker R, Figulla HR, et al. VEGF-mediated PI3K class IA and PKC signaling in cardiomyogenesis and vasculogenesis of mouse embryonic stem cells. *J Cell Sci* (2011) 124(Pt 11):1819–30. doi: 10.1242/jcs.077594

151. Pritchard RA, Falk L, Larsson M, Leinders M, Sorkin LS. Different phosphoinositide 3-kinase isoforms mediate carrageenan nociception and inflammation. *Pain* (2016) 157(1):137–46. doi: 10.1097/j.pain.0000000000000341

152. Antonioli L, Fornai M, Blandizzi C, Pacher P, Haskó G. Adenosine signaling and the immune system: When a lot could be too much. *Immunol Letters* (2019) 205:9–15. doi: 10.1016/j.imlet.2018.04.006

153. Church MK, Holgate ST, Hughes PJ. Adenosine inhibits and potentiates IgE-dependent histamine release from human basophils by an A2-receptor mediated mechanism. *Br J Pharmacol* (1983) 80(4):719–26. doi: 10.1111/j.1476-5381.1983.tb10063.x

154. Feoktistov I, Polosa R, Holgate ST, Biaggioni I. Adenosine A2B receptors: a novel therapeutic target in asthma? *Trends Pharmacol Sci* (1998) 19(4):148–53. doi: 10.1016/S0165-6147(98)01179-1

155. Ott I, Lohse MJ, Klotz KN, Vogt-Moykopf I, Schwabe U. Effects of adenosine on histamine release from human lung fragments. *Int Arch Allergy Immunol* (1992) 98(1):50–6. doi: 10.1159/000236163

156. Ryzhov S, Zaynagetdinov R, Goldstein AE, Novitskiy SV, Dikov MM, Blackburn MR, et al. Effect of A2B adenosine receptor gene ablation on proinflammatory adenosine signaling in mast cells. *J Immunol* (2008) 180(11):7212–20. doi: 10.4049/jimmunol.180.11.7212

157. Barnes PJ. Asthma as an axon reflex. *Lancet* (1986) 1(8475):242–5. doi: 10.1016/S0140-6736(86)90777-4

158. Basoglu OK, Pelleg A, Kharitonov SA, Barnes PJ. Contrasting effects of ATP and adenosine on capsaicin challenge in asthmatic patients. *Pulm Pharmacol Ther* (2017) 45:13–8. doi: 10.1016/j.pupt.2017.04.004

159. Barnes PJ. Neuropeptides and asthma. *Am Rev Respir Dis* (1991) 143(3 Pt 2): S28–32. doi: 10.1164/ajrccm/143.3_Pt_2.S28

160. Tsai SH, Takeda K. Regulation of allergic inflammation by the ectoenzyme E-NPP3 (CD203c) on basophils and mast cells. *Semin Immunopathol* (2016) 38(5):571–9. doi: 10.1007/s00281-016-0564-2

161. Niyonsaba F, Ushio H, Hara M, Yokoi H, Tominaga M, Takamori K, et al. Antimicrobial peptides human beta-defensins and cathelicidin LL-37 induce the secretion of a pruritogenic cytokine IL-31 by human mast cells. *J Immunol* (2010) 184(7):3526–34. doi: 10.4049/jimmunol.0900712

162. Irani AM, Goldstein SM, Wintroub BU, Bradford T, Schwartz LB. Human mast cell carboxypeptidase. Selective localization to MCTC cells. *J Immunol* (1991) 147 (1):247–53.

163. Irani AM, Schwartz LB. Human mast cell heterogeneity. *Allergy Proc* (1994) 15 (6):303–8. doi: 10.2500/108854194778816472

164. Müller T, Vieira RP, Grimm M, Dürk T, Cicko S, Zeiser R, et al. A potential role for P2X7R in allergic airway inflammation in mice and humans. *Am J Respir Cell Mol Biol* (2011) 44(4):456–64. doi: 10.1165/rcmb.2010-0129OC

165. Matsuoka I, Yoshida K, Ito MA. Purinergic regulation of mast cell function: P2X4 receptor-mediated enhancement of allergic responses. *J Pharmacol Sci* (2022) 150 (2):94–9. doi: 10.1016/j.jphs.2022.07.005

166. Yoshida K, Tanihara S, Miyashita Y, Obayashi K, Ito MA, Yamamoto K, et al. P2X4 receptor stimulation enhances MrgprB2-mediated mast cell activation and pseudoallergic reactions in mice. *Sci Rep* (2022) 12(1):18613. doi: 10.1038/s41598-022-21667-6

167. Bonvini SJ, Birrell MA, Dubuis E, Adcock JJ, Wortley MA, Flajolet P, et al. Novel airway smooth muscle-mast cell interactions and a role for the TRPV4-ATP axis in non-atopic asthma. *Eur Respir J* (2020) 56(1). doi: 10.1183/13993003.01458-2019

168. Alberto AV, Faria RX, de Menezes JR, Surrage A, da Rocha NC, Ferreira LG, et al. Role of P2 receptors as modulators of rat eosinophil recruitment in allergic inflammation. *PloS One* (2016) 11(1):e0145392. doi: 10.1371/journal.pone.0145392

169. Gruenbacher G, Gander H, Rahm A, Dobler G, Drasche A, Troppmair J, et al. The human G protein-coupled ATP receptor P2Y(11) is associated with IL-10 driven macrophage differentiation. *Front Immunol* (2019) 10:1870. doi: 10.3389/fimmu.2019.01870

170. Alsaleh NB, Persaud I, Brown JM. Silver nanoparticle-directed mast cell degranulation is mediated through calcium and PI3K signaling independent of the high affinity igE receptor. *PloS One* (2016) 11(12):e0167366. doi: 10.1371/journal.pone.0167366

171. Huber M, Cato ACB, Ainooson GK, Freichel M, Tsvilovskyy V, Jessberger R, et al. Regulation of the pleiotropic effects of tissue-resident mast cells. *J Allergy Clin Immunol* (2019) 144(4s):S31–s45. doi: 10.1016/j.jaci.2019.02.004

172. Munoz I, Danelli L, Claver J, Goudin N, Kurowska M, Madera-Salcedo IK, et al. Kinesin-1 controls mast cell degranulation and anaphylaxis through PI3K-dependent recruitment to the granular Slp3/Rab27b complex. *J Cell Biol* (2016) 215(2):203–16. doi: 10.1083/jcb.201605073

173. Nishida K, Yamasaki S, Hasegawa A, Iwamatsu A, Koseki H, Hirano T. Gab2, *via* PI-3K, regulates ARF1 in FcεRI-mediated granule translocation and mast cell degranulation. *J Immunol* (2011) 187(2):932–41. doi: 10.4049/jimmunol.1100360

174. Santos Mde S, Naal RM, Baird B, Holowka D. Inhibitors of PI(4,5)P2 synthesis reveal dynamic regulation of IgE receptor signaling by phosphoinositides in RBL mast cells. *Mol Pharmacol* (2013) 83(4):793–804. doi: 10.1124/mol.112.082834

175. Nishida K, Wang L, Morii E, Park SJ, Narimatsu M, Itoh S, et al. Requirement of Gab2 for mast cell development and KitL/c-Kit signaling. *Blood* (2002) 99(5):1866–9. doi: 10.1182/blood.V99.5.1866

176. Siraganian RP, Hazard KA. Mechanisms of mouse mast cell activation and inactivation for IgE-mediated histamine release. *J Immunol* (1979) 122(5):1719–25. doi: 10.4049/jimmunol.122.5.1719

177. Chalhoub N, Zhu G, Zhu X, Baker SJ. Cell type specificity of PI3K signaling in Pdk1- and Pten-deficient brains. *Genes Dev* (2009) 23(14):1619–24. doi: 10.1101/gad.1799609

178. Lee-Rivera I, López E, Parrales A, Alvarez-Arce A, López-Colomé AM. Thrombin promotes the expression of Ccnd1 gene in RPE cells through the activation of converging signaling pathways. *Exp Eye Res* (2015) 139:81–9. doi: 10.1016/j.exer.2015.08.001

179. Tsuchiya A, Kanno T, Nishizaki T. PI3 kinase directly phosphorylates Akt1/2 at Ser473/474 in the insulin signal transduction pathway. *J Endocrinol* (2014) 220(1):49–59. doi: 10.1530/JOE-13-0172

180. Nishi H, Arai H, Momiyama T. NCI-H295R, a human adrenal cortex-derived cell line, expresses purinergic receptors linked to Ca^{2+}-mobilization/influx and cortisol secretion. *PloS One* (2013) 8(8):e71022. doi: 10.1371/journal.pone.0071022

181. Le TT, Berg NK, Harting MT, Li X, Eltzschig HK, Yuan X. Purinergic signaling in pulmonary inflammation. *Front Immunol* (2019) 10:1633. doi: 10.3389/fimmu.2019.01633

182. Zhang M, Sykes DL, Sadofsky LR, Morice AH. ATP, an attractive target for the treatment of refractory chronic cough. *Purinergic Signal* (2022) 18(3):289–305. doi: 10.1007/s11302-022-09877-z

Frontiers in Immunology

Explores novel approaches and diagnoses to treat immune disorders.

The official journal of the International Union of Immunological Societies (IUIS) and the most cited in its field, leading the way for research across basic, translational and clinical immunology.

Discover the latest Research Topics

See more →

Frontiers

Avenue du Tribunal-Fédéral 34
1005 Lausanne, Switzerland
frontiersin.org

Contact us

+41 (0)21 510 17 00
frontiersin.org/about/contact